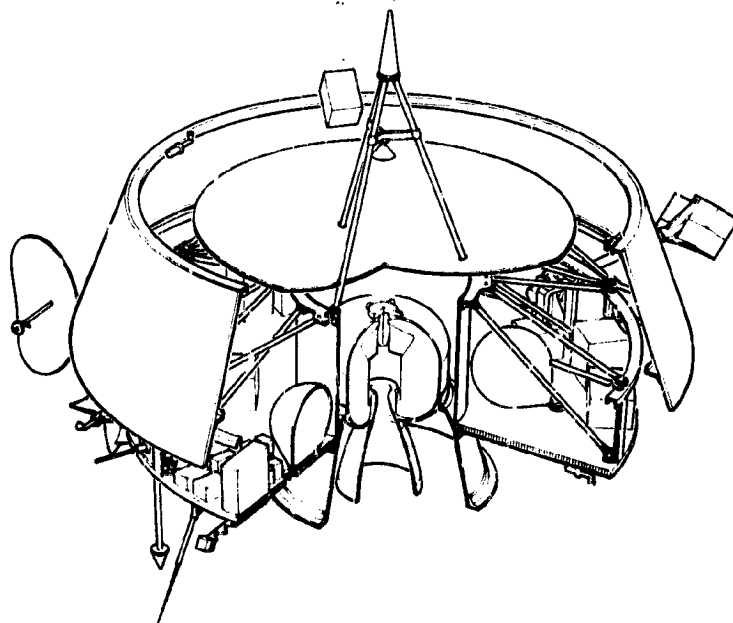
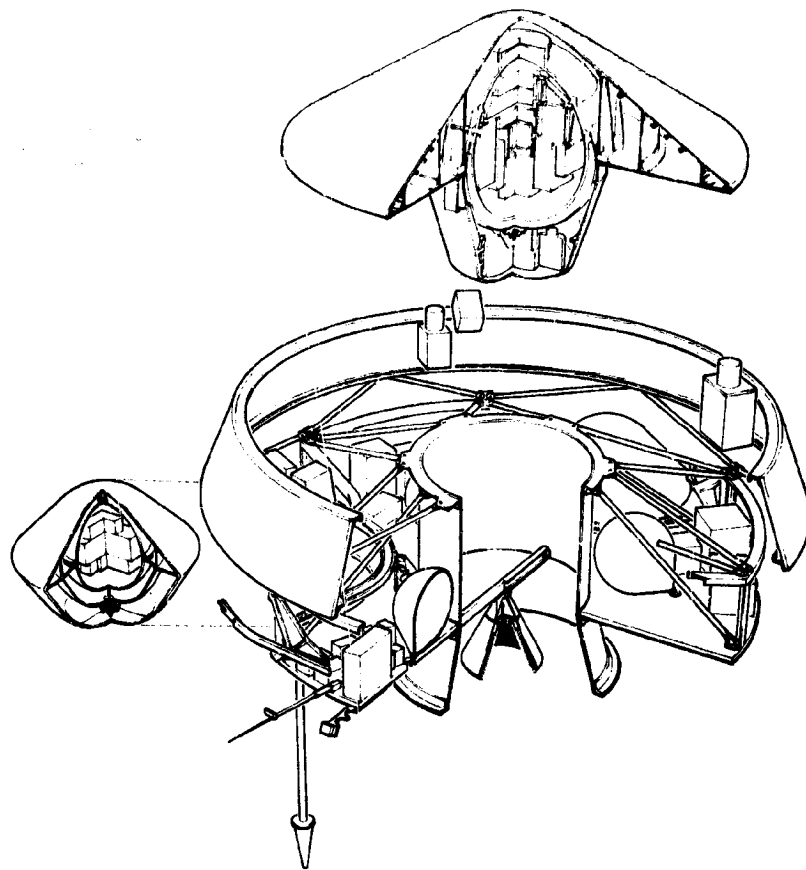


Systems Design Study of Pioneer Venus Spacecraft

Final Study Report

(NASA-CR-137506) SYSTEMS DESIGN STUDY OF
THE PIONEER VENUS SPACECRAFT. VOLUME 1.
TECHNICAL ANALYSES AND TRADEOFFS, SECTION
7 (PART 3 OF 4) Final Study (TRW
Systems Group) 342 p HC \$20.25 CSCL 22B G3



LIST OF VOLUMES

VOLUME I. TECHNICAL ANALYSES AND TRADEOFFS

SECTIONS 1-4 (PART 1 OF 4)

1. Introduction
2. Summary
3. Science Analysis and Evaluation
4. Mission Analysis and Design

VOLUME I. TECHNICAL ANALYSES AND TRADEOFFS

SECTIONS 5-6 (PART 2 OF 4)

5. System Configuration Concepts and Tradeoffs
6. Spacecraft System Definition

VOLUME I. TECHNICAL ANALYSES AND TRADEOFFS

SECTION 7 (PART 3 OF 4)

7. Probe Subsystem Definition

VOLUME I. TECHNICAL ANALYSES AND TRADEOFFS

SECTIONS 8-12 (PART 4 OF 4)

8. Probe Bus and Orbiter Subsystem Definition and Tradeoffs
9. NASA/ESRO Orbiter Interface
10. Mission Operations and Flight Support
11. Launch Vehicle-Related Cost Reductions
12. Long Lead Items and Critical Areas

VOLUME I APPENDICES

SECTIONS 3-6 (PART 1 OF 3)

VOLUME I APPENDICES

SECTION 7 (PART 2 OF 3)


VOLUME I APPENDICES

SECTIONS 8-11 (PART 3 OF 3)

VOLUME II. PRELIMINARY PROGRAM DEVELOPMENT PLAN

VOLUME III. SPECIFICATIONS

CR 137506


TRW Document No. 2291-6007-RJ-00

Systems Design Study of the Pioneer Venus Spacecraft

Final Study Report

Volume I. Technical Analyses and Tradeoffs Section 7 (Part 3 of 4)

29 July 1973

Contract No. NAS2-7249

Prepared for

AMES RESEARCH CENTER
NATIONAL AERONAUTICS AND SPACE ADMINISTRATION

TRW
SYSTEMS GROUP

MARTIN MARIETTA

CONTENTS

	<u>Page</u>
7. PROBE SUBSYSTEM DEFINITION	7.1-1
7.1 Aerodynamics and Aerophysics	7.1-1
7.1.1 Introduction and Summary	7.1-1
7.1.2 Requirements	7.1-4
7.1.3 Trades	7.1-6
7.1.4 Preferred Aerodynamic Configuration, Atlas/Centaur	7.1-10
7.1.5 Preferred Aerodynamic Configuration, Thor/Delta	7.1-15
7.1.6 Aerodynamics Analyses and Tests	7.1-16
7.1.6.1 Aerodynamic Coefficients	7.1-16
7.1.6.2 Dynamic Stability	7.1-16
7.1.6.3 Descent Capsule Sensor Environment	7.1-22
7.1.6.4 Wind Tunnel Test Results for Preferred Configurations	7.1-25
7.1.7 Aerothermodynamic Studies	7.1-30
7.1.7.1 Analysis Procedures	7.1-30
7.1.7.2 Environmental Results	7.1-32
7.1.7.3 Heating Correlations	7.1-43
7.2 Heat Shield	7.2-1
7.2.1 Introduction	7.2-1
7.2.2 Requirements	7.2-2
7.2.3 Trades	7.2-3
7.2.3.1 Analytical Evaluation of Heat Shield Materials	7.2-3
7.2.3.2 Experimental Evaluation of Candidate Materials	7.2-6
7.2.3.3 Heat Shield Test Costs Versus Ablator System and Design Margins	7.2-9
7.2.4 Preferred Heat Shield, Atlas/Centaur	7.2-9
7.2.4.1 Material Selection	7.2-9
7.2.4.2 Heat Shield Design	7.2-10
7.2.4.3 Design Margin	7.2-14
7.2.4.4 Fabrication Techniques	7.2-15
7.2.4.5 Preliminary Test Requirements	7.2-17
7.2.5 Preferred Heat Shield, Thor/Delta	7.2-19
7.2.6 Supporting Analyses and Tests	7.2-27
7.3 Structures and Mechanisms	7.3-1
7.3.1 Introduction and Summary	7.3-1
7.3.1.1 Large Probe Description	7.3-1
7.3.1.2 Small Probe Description	7.3-7

CONTENTS (CONTINUED)

	<u>Page</u>
7.3.2 Requirements	7.3-7
7.3.3 Tradeoffs	7.3-8
7.3.3.1 Parachute and Antenna Location	7.3-8
7.3.3.2 Selection of Large Probe Aeroshell Skin Design	7.3-8
7.3.3.3 Design of Aerodynamic Stabi- lizing Ring Structure for the Descent Capsule Sphere	7.3-13
7.3.3.4 Staging Separation System	7.3-13
7.3.3.5 Science Instrument Staging Clearance Cover Location	7.3-13
7.3.3.6 Aeroshell Afterbody Configuration	7.3-14
7.3.3.7 Cost Consideration Relative to Pressure Shell Materials	7.3-14
7.3.3.8 Shape of Pressure Vessel	7.3-16
7.3.3.9 Selection of Pressure Shell Subassemblies	7.3-17
7.3.3.10 Aeroshell Separation Design Approaches	7.3-17
7.3.4 Atlas/Centaur - Preferred Subsystem	7.3-22
7.3.4.1 Large Probe	7.3-22
7.3.5 Thor/Delta - Preferred Subsystem	7.3-37
7.3.5.1 Large Probe Interfaces	7.3-38
7.3.5.2 Large Probe Configuration Description	7.3-38
7.3.5.3 Parachute Installation	7.3-41
7.3.5.4 Small Probe Interfaces	7.3-42
7.3.5.5 Small Probe Configuration	7.3-42
7.3.5.6 GSE Provisions	7.3-43
7.3.6 Supporting Analysis and Tests	7.3-44
7.3.6.1 Pressure Vessel Design	7.3-46
7.3.6.2 Aeroshell Analysis	7.3-51
7.3.6.3 Structural Dynamics	7.3-52
7.4 Thermal Control	7.4-1
7.4.1 Introduction and Summary of Selected Design	7.4-1
7.4.2 Requirements	7.4-2
7.4.3 Tradeoffs	7.4-7
7.4.3.1 Pressure-Protected vs Nonpressure-Protected Designs	7.4-7
7.4.3.2 Pressure Shell Material and Insulation Material Tradeoffs - Large Probe	7.4-9

CONTENTS (CONTINUED)

	<u>Page</u>
7.4.3.3 Small Probe Thermal Design Tradeoffs	7.4-11
7.4.3.4 Other Tradeoffs	7.4-12
7.4.4 Preferred Thermal Control Subsystem, Atlas/Centaur	7.4-14
7.4.4.1 Large Probe	7.4-14
7.4.4.2 Small Probe	7.4-17
7.4.5 Preferred Thermal Control Subsystem, Thor/Delta	7.4-19
7.4.6 Supporting Analysis and Tests	
7.4.6.1 Atlas/Centaur Design Calculations	7.4-21
7.4.6.2 Insulation Thermal Performance	7.4-21
7.4.6.3 Insulation Outgassing and Interaction with Venus Trace Compounds	7.4-33
7.4.6.4 Insulation Mechanical Performance	7.4-34
7.4.6.5 Phase Change Device Development	7.4-35
7.4.6.6 Power Requirements for Science Window Heaters	7.4-36
7.5 Decelerator	7.5-1
7.5.1 Introduction and Summary	7.5-1
7.5.2 Requirements	7.5-2
7.5.3 Tradeoffs	7.5-3
7.5.3.1 Single versus Multistage Systems	7.5-4
7.5.3.2 Parachute Location, Packaging, and Deployment Method Tradeoff Studies	7.5-4
7.5.3.3 Canopy Configuration	7.5-9
7.5.3.4 Materials	7.5-12
7.5.3.5 Use of Existing Parachutes versus New Designs	7.5-13
7.5.4 Preferred Subsystem, Atlas/Centaur	7.5-13
7.5.5 Preferred Subsystem, Thor/Delta	7.5-15
7.5.6 Analyses and Special Studies	7.5-16
7.5.6.1 Parachute Deployment Dynamics	7.5-16
7.5.6.2 Small Probe Stabilizing Drogue Study	7.5-22
7.5.6.3 Parachute Sizing Analyses	7.5-25

CONTENTS (CONTINUED)

	<u>Page</u>
7.6 Probe Communication	7.6-1
7.6.1 Introduction and Summary	7.6-1
7.6.2 Requirements of Probe Communications Subsystems	7.6-2
7.6.2.1 Requirements, Atlas/Centaur (with Version IV Updated Payload)	7.6-2
7.6.2.2 Requirements, Thor/Delta (Version III Payload)	7.6-4
7.6.3 Communications Analyses and Tradeoffs	7.6-4
7.6.3.1 Channel Model	7.6-5
7.6.3.2 Modulation Trades	7.6-7
7.6.3.3 Coding Tradeoffs	7.6-8
7.6.3.4 One-Way versus Two-Way Links	7.6-13
7.6.3.5 Probe Communications Hardware Tradeoffs	7.6-15
7.6.4 Preferred Probe Subsystem Description, Atlas/Centaur	7.6-21
7.6.4.1 Large Probe Hardware, Atlas/Centaur	7.6-24
7.6.4.2 Small Probe Hardware, Atlas/Centaur	7.6-29
7.6.5 Preferred Subsystem Description, Thor/Delta	7.6-31
7.6.5.1 Large Probe Hardware, Thor/Delta	7.6-32
7.6.5.2 Small Probe Hardware, Thor/Delta	7.6-34
7.6.6 Supporting Analyses and Tests	7.6-34
7.7 Data Handling and Command	7.7-1
7.7.1 Introduction and Summary	7.7-1
7.7.2 Requirements	7.7-3
7.7.2.1 Large Probe Requirements Analysis	7.7-3
7.7.2.2 Small Probe Requirements Analysis	7.7-6
7.7.2.3 Probe/Bus Interface Requirements Analysis	7.7-7

CONTENTS (CONTINUED)

	<u>Page</u>
7.7.3 Tradeoffs	7.7-8
7.7.3.1 Probe Data Storage Requirements (for Blackout)	7.7-8
7.7.3.2 Probe Multiplexer and A/D Converter Requirements	7.7-13
7.7.3.3 Probe Digital Interface	7.7-14
7.7.3.4 Probe Multiple and Nonbinary Bit Rate Study	7.7-16
7.7.3.5 Synchronization and Time Reference Word Minimization	7.7-20
7.7.3.6 Programmer Design Concept	7.7-22
7.7.3.7 Large Probe Data/Descent Rate	7.7-23
7.7.4 Atlas/Centaur Data Handling and Command Subsystem Preferred Design	7.7-23
7.7.4.1 Programmer Board Design	7.7-26
7.7.4.2 Analog Subframe Board Design	7.7-27
7.7.4.3 Main Frame, Digital Subframe, and Output Logic Boards	7.7-28
7.7.4.4 Descent Timer/Programmer (DTP)	7.7-28
7.7.4.5 Coast Timer	7.7-31
7.7.4.6 Memory	7.7-32
7.7.5 Thor/Delta Data Handling and Command (DHC) Subsystem Preferred Design	7.7-33
7.7.5.1 Descent Timer/Programmer (DTP)	7.7-33
7.7.5.2 Data Buffer/Memory	7.7-33
7.7.5.3 Timing and Format Generator	7.7-38
7.7.5.4 Multiplexer	7.7-39
7.7.5.5 Data Framing for Probe Communications	7.7-39
7.8 Electrical Power	7.8-1
7.8.1 Introduction and Summary	7.8-1
7.8.2 Requirements	7.8-2
7.8.3 Tradeoff Studies	7.8-3
7.8.3.1 Probe Battery Analysis and Selection	7.8-3
7.8.3.2 Regulated versus Unregulated Bus	7.8-7
7.8.3.3 Cell Bypass versus No Bypass	7.8-8
7.8.3.4 Inflight Charging versus No-Flight Charging	7.8-9
7.8.3.5 Relays versus Solid State Switching	7.8-10
7.8.3.6 Capacitor versus Direct Battery Pyro Firing	7.8-10

CONTENTS (CONTINUED)

	<u>Page</u>
7.8.4 Preferred Electrical Power Subsystem, Atlas/Centaur	7.8-11
7.8.4.1 Battery	7.8-11
7.8.4.2 Power Control Unit (PCU)	7.8-11
7.8.5 Preferred Electrical Subsystem, Thor/Delta	7.8-15
7.8.5.1 Battery	7.8-15
7.8.5.2 Power Control Unit	7.8-17
7.8.5.3 Battery	7.8-17
7.8.5.4 Power Control Unit	7.8-19
7.9 Electrical Integration	7.9-1
7.9.1 Introduction and Summary	7.9-1
7.9.2 Requirements	7.9-2
7.9.3 Electrical Integration, Atlas/Centaur	7.9-2
7.9.4 Electrical Integration, Thor/Delta	7.9-6

ILLUSTRATIONS

	<u>Page</u>
7.1-1 Sketch of Atlas/Centaur Descent Capsule, Large Probe, and Small Probe	7.1-3
7.1-2 Large and Small Probe Attitude Variations Due to 0.05 mps/m Wind Shear	7.1-5
7.1-3 Estimated Static Aerodynamic Coefficients for the Large Probe	7.1-11
7.1-4 Estimated Dynamic Coefficients for the Large Probe	7.1-12
7.1-5 Estimated Static Aerodynamic Coefficients for the Small Probe	7.1-13
7.1-6 Small Probe Average Damping Derivative for Mach Number 0.05 Deduced from Spin Tunnel Tests	7.1-14
7.1-7 Descent Capsule Pitch Damping Coefficients as a Function of Angle of Attack at Mach ≈ 0.05	7.1-14
7.1-8 Sketch of Thor/Delta Descent Capsule, Large Probe, and Small Probe	7.1-15
7.1-9 Estimated Aerodynamic Coefficients for 55-Deg Cone	7.1-17
7.1-10 Comparison of Estimated Aerodynamic Coefficients for 45, 55 and 60 Degrees Conical Probes	7.1-18
7.1-11 Atlas/Centaur Small Probe Stability Boundaries as Functions of Pitch Damping Derivative, Roll Rate, and Altitude	7.1-20
7.1-12 Large Probe Entry Trajectory Parameters	7.1-21
7.1-13 Small Probe Entry Trajectory Parameters	7.1-22
7.1-14 Subsonic Smoke Flow About a Sphere	7.1-23
7.1-15 Streamlines About Sphere Showing Relation to Science Sensors	7.1-23
7.1-16 Reynolds Number for Descent Capsule	7.1-24
7.1-17 Boundary Layer Transition Point on a Sphere	7.1-24
7.1-18 Boundary Layer Thickness in Vicinity of Science Sensors	7.1-24
7.1-19 Configurations Tested in the NASA Langley Spin Tunnel	7.1-27
7.1-20 Comparisons of Inviscid Analysis Results for Several Configurations	7.1-31
7.1-21 Atlas/Centaur Large Probe Cold Wall No-Blowing Convective and Radiative Heating Rates	7.1-33

ILLUSTRATIONS (CONTINUED)

	<u>Page</u>
7.1-22 Distribution of Cold Wall No-Blowing Convective and Radiative Heating Rates on the Atlas/Centaur Large Probe	7.1-33
7.1-23 Effect of Entry Angle on the Atlas/Centaur Small Probe Cold Wall No-Blowing Stagnation Point Convective and Radiative Heating Rate	7.1-34
7.1-24 Effect of Entry Angle on the Atlas/Centaur Small Probe Cold Wall No-Blowing Off-Stagnation Convective and Radiative Heating Rates	7.1-34
7.1-25 Distribution of Cold Wall No-Blowing Convective and Radiative Heating Rates on the Atlas/Centaur Small Probe	7.1-35
7.1-26 Effect of Configuration on the Large Probe Cold Wall No-Blowing Convective and Radiative Stagnation Point Heating Rate	7.1-38
7.1-27 Effect of Configuration on the Large Probe Cold Wall No-Blowing Convective and Radiative Off-Stagnation Point Heating Rate	7.1-38
7.1-28 Effect of Configuration on the Large Probe Cold Wall No-Blowing Convective and Radiative Stagnation Point	7.1-39
7.1-29 Effect of Configuration on the Large Probe Cold Wall No-Blowing Convective and Radiative Off-Stagnation Point Heating Rate	7.1-40
7.1-30 Effect of Entry Angle on the Small Probe Cold Wall No-Blowing Convective and Radiative Stagnation Point Heating Rate	7.1-41
7.1-31 Effect of Entry Angle on the Small Probe Cold Wall No-Blowing Convective and Radiative Off-Stagnation Point Heating Rate	7.1-41
7.1-32 Spectral Distribution of the Continuum Processes and Molecular Band Radiative Heating	7.1-42
7.2-1 Atlas/Centaur '78 Heat Shield Configuration	7.2-1
7.2-2 Thor/Delta Large Probe Calculated Heat Shield Material Comparison	7.2-4
7.2-3 Thor/Delta Small Probe Calculated Heat Shield Material Comparison	7.2-5
7.2-4 Heat Shield Material Tests, $\dot{q}_{\text{Conv}} \sim 1500 \text{ W/CM}^2$	7.2-8
7.2-5 Heat Shield Material Tests, $\dot{q}_{\text{Conv}} \sim 3300 \text{ W/cm}^2$	7.2-8
7.2-6 Atlas/Centaur '78 Large Probe Nominal Thickness Versus Structure Temperature	7.2-11

ILLUSTRATIONS (CONTINUED)

	<u>Page</u>
7.2-7 Atlas/Centaur '78 Small Probe Nominal Thickness Versus Structure Temperature	7.2-12
7.2-8 Thermal Response of Atlas/Centaur '78 Large Probe Heat Shield	7.2-12
7.2-9a Thermal Response of Atlas/Centaur '78 Small Probe Heat Shield, Shallow Entry	7.2-13
7.2-9b Thermal Response of Atlas/Centaur '78 Small Probe Heat Shield, Steep Entry	7.2-13
7.2-10 Selected Heat Shield Materials and Fabrication Processes (Atlas/Centaur)	7.2-15
7.2-11 Aeroshell Cone Edge Ablator Cloth Layup	7.2-16
7.2-12 Thor/Delta '77 Heat Shield Configuration	7.2-19
7.2-13 Selected Heat Shield Materials and Fabrication Processes (Thor/Delta)	7.2-20
7.2-14 Thor/Delta Large Probe 1/4 Scale Heat Shield Mockup	7.2-20
7.2-15 Thor/Delta Large Probe Ablator Thicknesses Versus Structure Temperature	7.2-21
7.2-16 Thor/Delta Small Probe Ablator Thicknesses Versus Structure Temperature ($\gamma_e = -40^\circ$)	7.2-21
7.2-17 Thor/Delta Small Probe Nominal Ablator Thicknesses Versus Structure Temperature ($\gamma_e = -40^\circ$)	7.2-22
7.2-18 Thermal Response of Thor/Delta '77 Large Probe Heat Shield	7.2-23
7.2-19a Thermal Response of Thor/Delta '77 Small Probe Heat Shield, Shallow Entry	7.2-24
7.2-19b Thermal Response of Thor/Delta '77 Small Probe Heat Shield, Medium Entry	7.2-24
7.2-20 Performance of Ablators with Dummy Pressure Probes	7.2-28
7.2-21 Comparison of Low Density Quartz Nitrile Phenolic with Quartz Nitrile Phenolic and ESA 5500 Mz	7.2-29
7.3-1 Plan and Elevation of Large Probe	7.3-3
7.3-2 Mechanical Details of Large Probe	7.3-4
7.3-3 Descent Capsule Details Large Probe	7.3-5
7.3-4 Equipment Arrangement of Large Probe	7.3-6
7.3-5 General Arrangement of Small Probe	7.3-9

ILLUSTRATIONS (CONTINUED)

		<u>Page</u>
7.3-6	Optional Large Probe Shapes	7.3-14
7.3-7	Cost versus Shell Temperature	7.3-16
7.3-8	Thermal/Structural Mass versus Insulation Thickness	7.3-16
7.3-9	Configuration for Separation Design Tradeoff Study	7.3-19
7.3-10	Separation, Concept A1	7.3-19
7.3-11	Separation, Concept A2 (Tension Cone with Segmented Marman Ring Clamp)	7.3-20
7.3-12	Separation, Concept A-3	7.3-21
7.3-13	Parachute and Base Cover Release Concept	7.3-21
7.3-14	Door Mechanism	7.3-33
7.3-15	Thor/Delta Large Probe Structures and Separation Mechanism	7.3-39
7.3-16	Thor/Delta Structural/Mechanical Arrangement Small Probe	7.3-43
7.3-17	Boss Dimensional Parameters	7.3-47
7.3-18	Design Chart, External Bosses	7.3-47
7.3-19	Design Chart - Symmetrical Bosses	7.3-48
7.3-20	Weight of 55.9 cm (22.0 in.) Diameter Aluminum Shell (Spherical) Exclusive of Flanges, Bosses, Etc., kg (lb)	7.3-49
7.3-21	Weight of 55.9 cm (22.0 in.) Diameter Titanium Shell (Spherical) Exclusive of Flanges, Bosses, Etc., kg (lb)	7.3-50
7.3-22	Weight of 55.9 cm (22.0 in.) Diameter Shell (Spherical) Exclusive of Flanges, Bosses, Etc., kg (lb)	7.3-50
7.3-23	Large Probe Thermal Stress and Skin Buckling Allowable vs Back Face Skin Temperatures	7.3-52
7.3-24	Stress Strain Curve for MIN-K TE 1400	7.3-52
7.3-25	Estimated Pyrotechnic Shock Response at Large Probe Equipment Shelf/Descent Capsule	7.3-54
7.4-1	Atlas/Centaur Large Probe	7.4-3
7.4-2	Atlas/Centaur Small Probe	7.4-4
7.4-3	Atmospheric Pressure and Temperature Versus Time During Descent	7.4-6

ILLUSTRATIONS (CONTINUED)

	<u>Page</u>
7.4-4 Solar Aspect Angles, Large and Small Probes	7.4-7
7.4-5 Nonpressure-Protected Concepts	7.4-8
7.4-6 Large Probe Tradeoff Study	7.4-11
7.4-7 Small Probe Tradeoff Study	7.4-12
7.4-8 Thermal Control Approaches	7.4-13
7.4-9 Atlas/Centaur Large Probe Design Calculations	7.4-15
7.4-10 Atlas/Centaur Large Probe Payload Temperature History	7.4-15
7.4-11 Thermal/Structural Mass Sensitivity to Insulation Penetrations	7.4-16
7.4-12 Atlas/Centaur Small Probe Design Calculations	7.4-17
7.4-13 Atlas/Centaur Small Probe Payload Temperature History	7.4-18
7.4-14 Thor/Delta Large Probe	7.4-19
7.4-15 Thor/Delta Small Probe	7.4-20
7.4-16 Thor/Delta Large Probe	7.4-20
7.4-17 Thor/Delta Small Probe	7.4-21
7.4-18 Thermal Conductivity Versus Temperature at Various Pressures	7.4-23
7.4-19 Thermal Conductivity Versus Pressure at Mean Temperature of 322°K	7.4-24
7.4-20 Mini Descent Simulation Chamber	7.4-25
7.4-21 Midi Descent Simulation Chamber	7.4-25
7.4-22 Descent Simulation Test Results With and Without Water Vapor in CO ₂ Atmosphere	7.4-27
7.4-23 Effective Thermal Conductivities Derived from Test Data	7.4-27
7.4-24 Comparison of Test Results with Analytical Predictions	7.4-28
7.4-25 Thermal Response of Insulation to CO ₂ Filling Process	7.4-31
7.4-26 Thermal Response of Insulation to Nitrogen Filling Process	7.4-31
7.4-27 Thermal Response of Insulation to Helium Filling Process	7.4-32
7.4-28 Correlation of Transient Test Data with Free Convection Effects	7.4-32

ILLUSTRATIONS (CONTINUED)

	<u>Page</u>
7.4-29 Attachment Scheme for MIN-K TE 1400	7.4-34
7.4-30 Vibration Test Specimen	7.4-35
7.4-31 Science Window Configuration	7.4-37
7.4-32 Time-Temperature Profiles for One-Inch Sapphire Window with 15 Watt Heater	7.4-37
7.5-1 Sequence of Operations	7.5-1
7.5-2 Ballast Requirements Plotted as Function of Parachute Mass Offset Distance (r)	7.5-5
7.5-3 Capsule Oscillation Amplitude Due to Offset and Lateral Parachute Deployment	7.5-6
7.5-4 Parachute Lateral Displacement During Inflation ($\theta = 60^\circ$)	7.5-7
7.5-5 Candidate Atlas/Centaur Parachute Configurations	7.5-8
7.5-6 Comparison of Stability, Lift, and Oscillation of Parachute Canopy Types	7.5-10
7.5-7 Main Parachute Container	7.5-14
7.5-8 Mortar Configuration and Characteristics	7.5-14
7.5-9 Thor/Delta Parachute System	7.5-15
7.5-10 Thor/Delta Large Probe Dynamics at Parachute Deployment	7.5-17
7.5-11 Selected Atlas/Centaur Pilot Deployed Deceleration Sequence of Events	7.5-18
7.5-12 Atlas/Centaur Large Probe Dynamics at Parachute Deployment	7.5-19
7.5-13 Atlas/Centaur Capsule and Aeroshell Motions after Parachute Deployment	7.5-20
7.5-14 Small Probe Stabilizer	7.5-23
7.5-15 Stabilizer Canopy	7.5-24
7.6-1 Atlas/Centaur Two-Way Coherent Communications, Large Probe	7.6-3
7.6-2 Simplest Telecommunication System Model	7.6-5
7.6-3 Frame Deletion Rate for Sequential Decoding with No Synchronization or Fading Losses	7.6-12
7.6-4 Frame Deletion Probability for Sequential Decoding with Receiver Losses and Lognormal Fading Effects Included	7.6-12
7.6-5 Typical Antenna Pattern and Required Coverage Area	7.6-16

ILLUSTRATIONS (CONTINUED)

	<u>Page</u>
7.6-6 Turnstile Cone Antenna	7.6-16
7.6-7 Atlas/Centaur Two-Way Coherent Communications, Large Probe	7.6-24
7.6-8 Functional Diagram S-Band Receiver Portion of Large Probe Transponder	7.6-27
7.6-9 Functional Diagram S-Band Transmitter/Driver Portion of Large Probe Transponder	7.6-27
7.6-10 Atlas/Centaur One-Way Coherent Communications, Small Probes	7.6-29
7.6-11 Thor/Delta Two-Way Coherent Communications, Large Probe	7.6-32
7.6-12 Thor/Delta One-Way Coherent Communications, Small Probe	7.6-34
7.6-13 Antenna Gain Requirements	7.6-35
7.7-1 Data Handling and Command (DHC) Subsystem Boundaries	7.7-1
7.7-2 Large Probe Data Requirements, December Science List	7.7-10
7.7-3 Large Probe Data Transmission Rates	7.7-10
7.7-4 Small Probe Data Requirements, December Science List	7.7-12
7.7-5 Small Probe Data Transmission Rates	7.7-12
7.7-6 Experiment Interface Circuit	7.7-15
7.7-7 Experiment Interface Options	7.7-17
7.7-8 Non-Binary Data Acquisition Bit Rate	7.7-21
7.7-9 Non-Binary Frame Selection Circuit	7.7-21
7.7-10 Non-Binary Bit Rate Selection Circuit	7.7-21
7.7-11 DHC Functional Diagram	7.7-25
7.7-12 Location and Replacement of Pioneer 10 and 11 Boards	7.7-26
7.7-13 Atlas/Centaur Large Descent Probe Timer/Programmer	7.7-29
7.7-14 Descent Timer/Programmer Timing Diagram	7.7-30
7.7-15 Coast Timer Interface	7.7-32
7.7-16 Block Diagram Data Handling and Command (DHC) Unit, Thor/Delta	7.7-36
7.7-17 Data Buffer/Memory	7.7-37

ILLUSTRATIONS (CONTINUED)

	<u>Page</u>
7.7-18 Timing and Format Generator Interface, Large Probe	7.7-38
7.7-19 Large Probe Multiplexer Block Diagram	7.7-41
7.8-1 Probe Electrical Power Subsystem, Simplified Block Diagram	7.8-2
7.8-2 Power Profile, Large Probe	7.8-4
7.8-3 Power Profile, Small Probe	7.8-4
7.8-4 Atlas/Centaur Probe Battery Configuration	7.8-5
7.8-5 Ag-Zn Discharge Voltage Characteristic	7.8-6
7.8-6 Atlas/Centaur Power Control Unit Configuration	7.8-12
7.8-7 Power Transfer Control	7.8-13
7.8-8 Pyro Firing Bus and Current Limiting Resistor Grouping	7.8-14
7.8-9 Thor/Delta Small Probe Power Profile	7.8-16
7.8-10 Thor/Delta Large Probe Power Profile	7.8-17
7.8-11 Small Probe Battery, Thor/Delta Configuration	7.8-18
7.8-12 Large Probe Battery, Thor/Delta Configuration	7.8-18
7.8-13 Integrated Electronics	7.8-19
7.8-14 Equipment Mounting Shelf	7.8-19
7.8-15 Cut Away View of Thor/Delta Small Probe	7.8-20
7.9-1 Atlas/Centaur Small Probe System Interface Connections	7.9-3
7.9-2 Atlas/Centaur Large Probe System Interface Connections	7.9-4
7.9-3 RF Cable, Large Probe	7.9-6
7.9-4 RF Cable, Small Probe	7.9-6
7.9-5 Equipment Mounting Shelf, Thor/Delta Small Probe	7.9-7
7.9-6 Cut Away View of Thor/Delta Small Probe	7.9-8

ACRONYMS AND ABBREVIATIONS

A	ampere analog
abA	abampere
AC	alternating current
A/C	Atlas/Centaur
ADA	avalanche diode amplifier
ADCS	attitude determination and control subsystem
ADPE	automatic data processing equipment
AEHS	advanced entry heating simulator
AEO	aureole/extinction detector
AEDC	Arnold Engineering Development Corporation
AF	audio frequency
AGC	automatic gain control
AgCd	silver-cadmium
AgO	silver oxide
AgZn	silver zinc
ALU	authorized limited usage
AM	amplitude modulation
a. m.	ante meridian
AMP	amplifier
APM	assistant project manager
ARC	Ames Research Center
ARO	after receipt of order
ASK	amplitude shift key
at. wt	atomic weight
ATM	atmosphere
ATRS	attenuated total refractance spectrometer
AU	astronomical unit
AWG	American wire gauge
AWGN	additive white gaussian noise
B	bilevel
B	bus (probe bus)
BED	bus entry degradation

ACRONYMS AND ABBREVIATIONS (CONTINUED)

BER	bit error rate
BLIMP	boundary layer integral matrix procedure
BPIS	bus-probe interface simulator
BPL	bandpass limiter
BPN	boron potassium nitrate
bps	bits per second
BTU	British thermal unit
C	Canberra tracking station - NASA DSN
CADM	configuration administration and data management
C&CO	calibration and checkout
CCU	central control unit
CDU	command distribution unit
CEA	control electronics assembly
CFA	crossed field amplifier
cg	centigram
c.g.	center of gravity
CIA	counting/integration assembly
CKAFS	Cape Kennedy Air Force Station
cm	centimeter
c.m.	center of mass
C/M	current monitor
CMD	command
CMO	configuration management office
C-MOS	complementary metal oxide silicon
CMS	configuration management system
const	constant construction
COSMOS	complementary metal oxide silicon
c.p.	center of pressure
CPSA	cloud particle size analyzer
CPSS	cloud particle size spectrometer

ACRONYMS AND ABBREVIATIONS (CONTINUED)

CPU	central processing unit
CRT	cathode ray tube
CSU	Colorado State University
CTRF	central transformer rectifier filter
D	digital
DACS	data and command subsystem
DCE	despin control electronics
DDA	despin drive assembly
DDE	despin drive electronics
DDU	digital decoder unit
DDULBI	doubly differenced very long baseline interferometry
DEA	despin electronics assembly
DEHP	di-2-ethylhexyl phthalate
DFG	data format generator
DGB	disk gap band
DHC	data handling and command
DIO	direct input/output
DIOC	direct input/output channel
DIP	dual in-line package
DISS REG	dissipative regulator
DLA	declination of the launch azimuth
DLBI	doubly differenced very long baseline interferometry
DMA	despin mechanical assembly
DOF	degree of freedom
DR	design review
DSCS II	Defense System Communications Satellite II
DSIF	Deep Space Instrumentation Facility
DSL	duration and steering logic
DSN	NASA Deep Space Network
DSP	Defense Support Program
DSU	digital storage unit
DTC	design to cost
DTM	decelerator test model

ACRONYMS AND ABBREVIATIONS (CONTINUED)

DTP	descent timer/programmer
DTU	digital telemetry unit
DVU	design verification unit
E	encounter entry
EDA	electronically despun antenna
EGSE	electrical ground support equipment
EIRP	effective isotropic radiated power
EMC	electromagnetic compatibility
EMI	electromagnetic interference
EO	engineering order
EOF	end of frame
EOM	end of mission
EP	earth pointer
ESA	elastomeric silicone ablator
ESLE	equivalent station error level
ESRO	European Space Research Organization
ETM	electrical test model
ETR	Eastern Test Range
EXP	experiment
FFT	fast Fourier transform
FIPP	fabrication/inspection process procedure
FMEA	failure mode and effects analysis
FOV	field of view
FP	fixed price frame pulse (telemetry)
FS	federal stock
FSK	frequency shift keying
FTA	fixed time of arrival

ACRONYMS AND ABBREVIATIONS (CONTINUED)

G	Goldstone Tracking Station - NASA DSN
	gravitational acceleration
g	gravity
G&A	general and administrative
GCC	ground control console
GFE	government furnished equipment
GHE	ground handling equipment
GMT	Greenwich mean time
GSF	ground support equipment
GSFC	Goddard Space Flight Center
H	Haystack Tracking Station - NASA DSN
HFFB	Ames Hypersonic Free Flight Ballistic Range
HPBW	half-power beamwidth
htr	heater
HTT	heat transfer tunnel
I	current
IA	inverter assembly
IC	integrated circuit
ICD	interface control document
IEEE	Institute of Electrical and Electronics Engineering
IFC	interface control document
IFJ	in-flight jumper
IMP	interplanetary monitoring platform
I/O	input/output
IOP	input/output processor
IR	infrared
IRAD	independent research and development
IRIS	infrared interferometer spectrometer
IST	integrated system test
I&T	integration and test
I-V	current-voltage

ACRONYMS AND ABBREVIATIONS (CONTINUED)

JPL	Jet Propulsion Laboratory
KSC	Kennedy Space Center
L	launch
LD/AD	launch date/arrival date
LP	large probe
LPM	lines per minute
LPTTL	low power transistor-transistor logic
MSI	medium scale integration
LRC	Langley Research Center
M	Madrid tracking station - NASA DSN
MAG	magnetometer
max	maximum
MEOP	maximum expected operating pressure
MFSK	M'ary frequency shift keying
MGSE	mechanical ground support equipment
MH	mechanical handling
MIC	microwave integrated circuit
min	minimum
MJS	Mariner Jupiter-Saturn
MMBPS	multimission bipropellant propulsion subsystem
MMC	Martin Marietta Corporation
MN	Mach number
mod	modulation
MOI	moment of inertia
MOS LSI	metal over silicone large scale integration
MP	maximum power
MSFC	Marshall Space Flight Center
MPSK	M'ary phase shift keying
MSI	medium scale integration
MUX	multiplexer
MVM	Mariner Venus-Mars

ACRONYMS AND ABBREVIATIONS (CONTINUED)

NAD	Naval Ammunition Depot, Crane, Indiana
N/A	not available
NiCd	nickel cadmium
NM/IM	neutral mass spectrometer and ion mass spectrometer
NRZ	non-return to zero
NVOP	normal to Venus orbital plane
OEM	other equipment manufacturers
OGO	Orbiting Geophysical Observatory
OIM	orbit insertion motor
P	power
PAM	pulse amplitude modulation
PC	printed circuit
PCM	pulse code modulation
PCM- PSK-PM	pulse code modulation-phase shift keying- phase modulation
PCU	power control unit
PDA	platform drive assembly
PDM	pulse duration modulation
PI	principal investigator proposed instrument
PJU	Pioneer Jupiter-Uranus
PLL	phase-locked loop
PM	phase modulation
p.m.	post meridian
P-MOS	positive channel metal oxide silicon
PMP	parts, materials, processes
PMS	probe mission spacecraft
PMT	photomultiplier tube
PPM	parts per million pulse position modulation
PR	process requirements
PROM	programmable read-only memory
PSE	program storage and execution assembly

ACRONYMS AND ABBREVIATIONS (CONTINUED)

PSIA	pounds per square inch absolute
PSK	phase shift key
PSU	Pioneer Saturn-Uranus
PTE	probe test equipment
QOI	quality operation instructions
QTM	qualification test model
RCS	reaction control subsystem
REF	reference
RF	radio frequency
RHCP	right hand circularly polarized
RHS	reflecting heat shield
RMP-B	Reentry Measurements Program, Phase B
RMS	root mean square
RMU	remote multiplexer unit
ROM	read only memory rough order of magnitude
RSS	root sum square
RT	retargeting
RTU	remote terminal unit
S	separation
SBASI	single bridgewire Apollo standard initiator
SCP	stored command programmer
SCR	silicon controlled rectifier
SCT	spin control thrusters
SEA	shunt electronics assembly
SFOF	Space Flight Operations Facility
SGLS	space ground link subsystem
SHIV	shock induced vorticity
SLR	shock layer radiometer
SLRC	shock layer radiometer calibration

ACRONYMS AND ABBREVIATIONS (CONTINUED)

SMAA	semimajor axis
SMIA	semiminor axis
SNR	signal to noise ratio
SP	small probe
SPC	sensor and power control
SPSG	spin sector generator
SR	shunt radiator
SRM	solid rocket motor
SSG	Science Steering Group
SSI	small scale integration
STM	structural test model
STM/TTM	structural test model/thermal test model
STS	system test set
sync	synchronous
TBD	to be determined
TCC	test conductor's console
T/D	Thor/Delta
TDC	telemetry data console
TEMP	temperature
TS	test set
TTL MSI	transistor-transistor logic medium scale integration
TLM	telemetry
TOF	time of flight
TRF	tuned radio frequency
TTM	thermal test model
T/V	thermo vacuum
TWT	travelling wave tube
TWTA	travelling wave tube amplifier
UHF	ultrahigh frequency
UV	ultraviolet

ACRONYMS AND ABBREVIATIONS (CONTINUED)

VAC	volts alternating current
VCM	vacuum condensable matter
VCO	voltage controlled oscillator
VDC	volts direct current
VLBI	very long baseline interferometry
VOI	Venus orbit insertion
VOP	Venus orbital plane
VSI	Viking standard initiator
VTa	variable time of arrival
XDS	Xerox Data Systems

7.1 Aerodynamics and
Aerophysics

7. PROBE SUBSYSTEM DEFINITION

7.1 AERODYNAMICS AND AEROPHYSICS

7.1.1 Introduction and Summary

Considerations of aerodynamic drag, stability and heating; roll-to-pitch moment of inertia ratios; internal packaging; and integration with the bus have led to the selection of blunted cones for the Pioneer Venus probes. Because these probes must be passively stable, great care must be given to the details that affect aerodynamic stability, i. e., cone angle, nose radius, edge radius, base cover shape, c. g. location, and moment of inertia. The small probe must perform throughout the entire Mach number range from hypersonic entry to the subsonic velocity condition, whereas the large probe entry vehicle flight is terminated when the parachute is deployed, at which time the Mach number is 0.7. It is well known that large angle cones exhibit unstable aerodynamic pitch damping in the low supersonic/transonic Mach number range (References 1 through 8). References 1, 3, and 5 indicate that shaping of the base cover can have a significant effect on this coefficient; however, to date no blunt shape has been discovered for which there is no region of unstable damping. Fortunately, for a wide variety of base shapes, the instability is limited to small angles of attack, and only a slight divergence occurs for a very short period of time during entry.

Thus, the major aerodynamic design problems for the Pioneer Venus mission are to determine a small probe shape that will enter satisfactorily and then exhibit good stability during the lengthy subsonic portion of the mission.

For the large probe descent capsule, which is essentially a sphere with several protuberances, the major design problem is to provide a device that will increase the drag and also stabilize the sphere. The erratic behavior of spheres in free flight has been reported by several authors, with various stabilizing devices having been studied (References 9 and 10). The simplest device, suggested by ARC, consists of a ring of some finite thickness located near the equator of the sphere with a single peripheral row of holes which, if canted, also serve to produce a well controlled roll rate. In the case of the small probe, the most effective design involves a modification to the PAET concept, using a spherical base centered at

the mass center. The modification introduces a conical section aft of the maximum diameter to fix the point of flow separation.

In the present study, major attention has been devoted to the subsonic problems insofar as new experimental work has been concerned. Tests have been carried out in a parallel IRAD task in conventional subsonic wind tunnels at MMC Denver and Colorado State University, and, with NASA cooperation, in the LRC Spin Tunnel and ARC HFFB Water Facility. Force and moment, one degree of freedom, and six degree of freedom tests have been conducted.

In addition to the experimental efforts, flight dynamics studies have been made using six degree of freedom computer programs and analytical methods, in particular the method of Coakley, Reference 11. Aerodynamic heating analyses have been made using sophisticated real gas viscous and radiative computational methods for a number of entry vehicle shapes and initial trajectory conditions.

The preferred aerodynamic configurations for the probes are shown in Figure 7.1-1. The entry configurations and the stabilization ring for the descent capsule have been selected based on the tests and analyses mentioned earlier. These analyses have indicated that the small probe during entry with an initial angle of attack of 10 degrees and a spin rate of 10 rpm will damp to 0.5 degree by the time peak heating and peak deceleration occur. The spin tunnel tests have indicated that the preferred small probe, in contrast to a large number of other shapes tested, does not exhibit a limit cycle behavior but trims to zero angle of attack and can withstand an angular perturbation of about 45 degrees without tumbling. The three small probes enter the atmosphere with different flight path angles, .25, .45 and .60 degrees. The 60 degree entry produces maximum heating rates and shear stresses. Significant values are tabulated.

Location	$q_m^c, \frac{MW}{m^2}$	$q_m^r, \frac{MW}{m^2}$	$\int q^c dt, \frac{MJ}{m^2}$	$\int q^r dt, \frac{MJ}{m^2}$	$\tau_m, \frac{KN}{m^2}$
Stagnation Point	36.0	27.1	79.4	37.5	--
Cone	67.0	10.3	78.1	14.1	6.7

The integrated heat input values apply at a point 70 percent back on the cone.

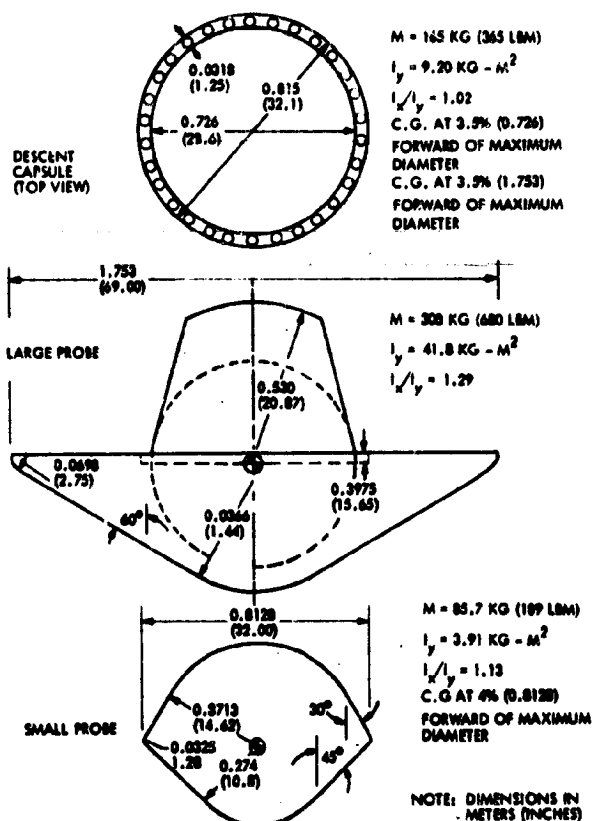


Figure 7.1-1. Sketch of Atlas/Centaur Descent Capsule, Large Probe, and Small Probe

The large probe afterbody shape, strongly influenced by mechanical integration considerations, was selected on the basis of analytical studies, data in the literature, including the Viking Program pitch damping data (References 7 and 8) which represent a very comprehensive study of the effects of various afterbody shapes on 60- and 70-degree half-angle blunted cones, and the tests conducted during the present study. These data and studies have indicated that the large probe during entry with an initial angle of attack of 10 degrees will damp to <0.5 degree before peak heating and deceleration are reached. The large probe is not intended to fly at the low Mach number obtained in the spin tunnel. Nevertheless, in the spin tunnel the configuration did exhibit 5-degree limit cycle behavior and the ability to withstand a disturbance of about 60 degrees without tumbling. During nominal entry, heating and shear values for the large probe are as tabulated.

Location	$q_m^c, \frac{MW}{m^2}$	$q_m^r, \frac{MW}{m^2}$	$\int q^c dt, \frac{MJ}{m^2}$	$\int q^r dt, \frac{MJ}{m^2}$	$\tau_m, \frac{KN}{m^2}$
Stagna - tion Point	19.0	11.3	65.1	22.5	--
Cone	38.5	10.8	83.5	22.1	2.9

In the following paragraphs, the topics covered are requirements; trades; preferred configurations, Atlas/Centaur; preferred configurations, Thor/Delta; aerodynamic analyses and tests; and aerothermodynamic studies.

7.1.2 Requirements

The fundamental requirements of the aerodynamic design of each of the Pioneer Venus probes are to provide (1) a specified ballistic coefficient, and (2) a stable platform for the science instruments. Because both the large probe and small probes are spin stabilized at 10 rpm during preentry coast, care must be taken to ensure that no roll resonance effects are encountered during entry with these initial roll rates. The probes transmit data directly to earth with very limited power. This, coupled with the antenna pattern characteristics, results in a limitation on communication angle increment due to probe attitude disturbances of ± 15 degrees during descent from 70 to 35 km, and then varying linearly to 0 degree at the surface.

The sequential release strategy for the probes is designed specifically to restrict the initial angles of attack at entry to less than 10 degrees; therefore, there is no requirement that the probes be capable of recovering from a backward or tumbling entry. Angular perturbations due to gusts are expected to be small. For example, the response to a wind shear of 0.05 mps/m of the probes in terminal descent is shown in Figure 7.1-2, which depicts the steady-state angle acquired when a probe is subjected to the specified shear until the maximum wind velocity is reached. Thus, if the small probe were subjected to the shear until a horizontal velocity of 100 m/s were reached, the trim angle relative to vertical would be about 27 degrees. If the wind shear were then terminated, the probe would be at an angle of attack of 27 degrees. This appears to be the

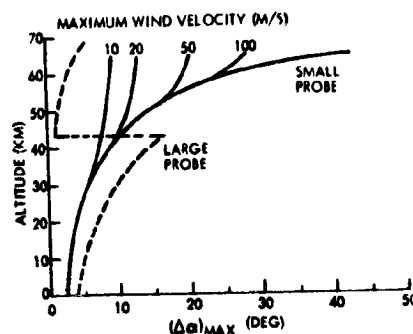


Figure 7.1-2. Large and Small Probe Altitude Variations Due to 0.05 mps/m Wind Shear

maximum angular disturbance from which the small probe must recover. Figure 7.1-2 also shows that the maximum disturbance angle for the large probe is about 17 degrees.

Assessment of instrumentation requirements indicates that a roll rate corresponding to approximately 5 revolutions per km may be required for the large probe subsequent to parachute deployment.

These requirements may be summarized by saying that the probes must exhibit "good" dynamic stability characteristics including the ability to recover from an angular perturbation rather quickly. However, the atmospheric reconstruction experiment probably calls for the most precise understanding and control of the aerodynamic characteristics of the probes. Ideally, this experiment would require zero angle of attack (i. e., zero lift and constant drag) throughout the flight. However, realistically, it is desirable and feasible to provide:

- 1) Small variation of lift and drag with angle of attack over a moderate range;
 - 2) Zero limit cycle behavior; and
 - 3) For a rolling probe, a pure spiral behavior in the α, β plane.
- The first two requirements are largely shape dependent and the third, additionally, requires that pitch and yaw moments of inertia be equal and that roll rate be controlled.

7.1.3 Trades

On the basis of systems analysis of the probes involving trajectory, heat shielding, and packaging requirements, it appeared very early in the study that blunted nose cone half-angles of 60 and 45 degrees were optimum for the large and small probes, respectively. Therefore, effort was devoted toward developing optimum base cover shapes for these forebodies. Subsequently, however, as a cost savings, it was suggested that a common aerodynamic shape for the two probes would result in reducing the development phase wind tunnel test program by a factor approaching 50 percent. Therefore, a compromise nose cone half-angle of 55 degrees was considered with several afterbody shapes. Consideration was also given to use a 70-degree cone angle in order to take more advantage of the available Viking aerodynamic data. The aerodynamics activities involved both analytical and experimental studies of aerodynamic characteristics, and included consideration also of c.g. location, d/σ , and roll rate.

Because the design problem for the large probe descent capsule is to develop a drag amplification/stabilization device for a sphere, experimental programs were undertaken to test parametric variations on several types of devices in order to develop design data for use as requirements varied during the design process. Devices tested were split flare type fins, vented flares, thin rings, and finite thickness, perforated rings. Also tested in conjunction with the above devices were several roll-fin configurations and protuberance arrangements simulating antenna configurations and science instruments.

In addition to the tests, analytical studies were made relating to the flight dynamics of the various configurations. Both six degree of freedom trajectory computer programs and the method of Coakley (Reference 11) have been used to study the effects of variations in the static and dynamic aerodynamic coefficients, mass properties, such as c.g. offset and principle axis angularity, and initial conditions at entry, especially roll rate.

Aerodynamic heating computations including both viscous and radiative heating were made using real gas flow field and boundary layer digital computer programs. A large number of configurations and entry flight conditions as indicated in Tables 7.1-1 and 7.1-2, were investigated.

Table 7.1-1. Atlas/Centaur Entry Trajectory and Geometry Conditions

CASE	V_E KM/S	γ_E DEG	β KG/M ²	θ_C DEG	R_N M	R_B M	P_{O_m} MN/M ²	q_m^c MW/M ²	q_m^r MW/M ²	τ_m KN/M ²
LARGE PROBE										
1	11.34	-35.0	86.40	60	0.3975	0.8763	0.55	38.5	11.3	2.9
2	11.34	-40.5	90.72	60	0.3975	0.8763	0.65	42.5	14.0*	3.3
3	11.34	-40.5	90.72	55	0.5080	0.8763	0.65	45.0	14.9	4.3
4	11.16	-40.0	78.54	60	0.5525	0.9906	0.54	23.0	10.6*	2.2
5	11.16	-40.0	78.54	55	0.5080	0.8763	0.54	35.0	8.3	3.4
6	11.16	-40.0	78.54	AP	2.378	0.9906	0.54	14.5	18.6	0.8
SMALL PROBE										
7	11.34	-25.0	141.4	45	0.2753	0.4064	0.63	32.0	11.1	3.7
8	11.34	-45.0	141.4	45	0.2753	0.4064	1.08	52.5	22.0	4.4
9	11.34	-60.0	141.4	45	0.2753	0.4064	1.31	67.0	27.1	6.0
10	11.34	-45.0	119.6	55	0.2355	0.4064	0.92	71.0	15.7	6.7
11	11.34	-45.0	119.6	55	0.2753	0.4064	0.92	54.0	17.4	4.5
*NOTE: THE MAXIMUM CONVECTIVE VALUES q_m^c AND τ_m OCCUR AT AN OFF-STAGNATION LOCATION AFTER TRANSITION. THE MAXIMUM RADIATIVE HEATING q_m^r OCCURRED AT THE STAGNATION POINT EXCEPT FOR THE VALUES DENOTED WITH										

Table 7.1-2. Thor/Delta Entry Trajectory and Geometry Conditions

CASE	V_E KM/S	λ_E DEG	β KG/M ²	θ_C DEG	R_N M	R_B M	P_{O_m} MN/M ²	q_m^c MW/M ²	q_m^r MW/M ²	τ_m KN/M ²
LARGE PROBE										
1	11.16	-40.0	78.54	60	0.3683	0.6604	0.54	26.0	8.8*	2.6
2	11.16	-40.0	78.54	70	0.3683	0.6604	0.54	19.0	13.2*	1.2
3	11.16	-40.0	78.54	AP	1.585	0.6604	0.54	17.0	15.5	1.1
SMALL PROBE										
4	11.16	-20.0	125.7	45	0.1346	0.2248	0.41	17.0	3.4	2.1
5	11.16	-40.0	125.7	45	0.1346	0.2248	0.83	39.0	8.2	4.1
6	11.16	-55.0	125.7	45	0.1346	0.2248	0.99	48.0	9.4	5.2
7	11.16	-20.0	125.7	AP	0.5734	0.2248	0.41	13.0	6.7	0.6
*NOTE: THE MAXIMUM CONVECTIVE VALUES q_m^c AND τ_m OCCUR AT AN OFF-STAGNATION LOCATION AFTER TRANSITION, EXCEPT FOR CASE 7 WHERE TRANSITION OCCURRED LATE IN THE TRAJECTORY. THE MAXIMUM RADIATIVE HEATING q_m^r OCCURRED AT THE STAGNATION POINT EXCEPT FOR THE VALUES DENOTED WITH *.										

The results of these trade studies and tests have been used in conjunction with the overall systems requirements to arrive at the preferred probe configurations. These probes meet all of the requirements discussed in Section 7.1.2.

The 30-degree half-angle cone afterbody terminating with a spherical cap has been shown to exhibit the most favorable stability characteristics out of the large variety of shapes tested within the range of c. g. location and d/σ values practically attainable for the Pioneer Venus probes. Of all the afterbody shapes tested, the full hemisphere was the only one that would not tumble. However, as indicated in Section 7.1.2, this feature is not required. Therefore, the 30-degree cone/spherical cap shape, which performs better than the full hemisphere in terms of limit cycle behavior, was selected for the small probes. For the Thor/Delta version of the large probe, which incorporated the large flare stabilizer for the descent capsule, packaging, and integration considerations, suggested selection of the 45-degree cone/spherical cap afterbody which, aerodynamically, is almost as good as the 30-degree afterbody. For the Atlas/Centaur large probe, selection of the perforated ring for stabilization of the descent capsule, instead of a flare, led to selection of the smaller, stepped back afterbody, which is similar to shapes for which transonic and supersonic data are available in the literature (References 5, 7, and 8). This afterbody shape greatly simplified the problems of afterbody staging and mounting the large probe to the bus. If the probes should be required to recover from very large perturbations or from tumbling, either the hemispherical afterbody as used on the PAET vehicle, or a deployable drogue device such as the Yee anchor (Sections 7.1.6 and 7.5.6.2), can be implemented. At the present time, this is not a requirement.

Spin tunnel tests on dynamically scaled models of the three probes have been conducted in order to document their subsonic stability characteristics. These tests involved perturbing the models with a stick and photographing their dynamic behavior. Thus, the degree of angular disturbance which the models would sustain without tumbling, as well as the steady-state behavior, was determined.

The perforated, equatorial ring was shown to be a very simple and effective device for increasing the drag and stabilizing the descent capsule. Canted holes in the ring were shown to control the roll rate very efficiently. Tests conducted with a representative arrangement of science experiment protuberances showed them to have an insignificant effect on the behavior of the descent capsule; however, modeling of the wind/altitude radar antenna plate directly on the bottom of the descent capsule and of two fairing arrangements resulted in an undesirable trim angle of attack. It is believed that a fairing can be developed to eliminate the trim angle, but it is recommended that consideration be given to curving the radar element and/or adapting a round versus square configuration to simplify its integration.

The following table summarizes the test results for the preferred configurations.

Model	Steady-State Behavior	Angle Without Tumbling	Angle for Tumbling
Large probe	Limit Cycles (a) <5 degrees	Approximately 50 degrees	Approximately 60 degrees
Descent Capsule	Trims to zero angle of attack	Approximately 90 degrees	90 degrees
Small probe	Trims to zero angle of attack	45 degrees	50 degrees

(a) Similar behavior was initially observed for the small probe configuration but disappeared when the model size was increased from 10- to 23-inch diameter. Only 10-inch diameter models of the large probe have been tested. It is very difficult in spin tunnel testing to determine whether model angular excursions less than about 10-degrees are truly limit cycle behavior or due to flow turbulence.

The idea of using a common entry configuration was discarded largely because the small afterbody shape adopted for the large probe would not accommodate the small probe pressure sphere and the benefits derived from this large probe design were greater than those afforded by the common probe shape approach. It then appeared rational to use the optimum 45- and 60-degree forebodies for the small and large probes, respectively, and the 55-degree cone was dropped from contention. The 70-degree cone was eliminated because it could not be packaged with the c.g. far enough forward to ensure satisfactory passive stability.

7.1.4 Preferred Aerodynamic Configuration, Atlas/Centaur

The external shapes of the large and small probe entry vehicles and the large probe descent capsule selected for the Atlas/Centaur option are shown in Figure 7.1-1. The mass properties are also shown for reference in the figure.

The aerodynamic coefficients for the entry configurations are given in Figures 7.1-3 through 7.1-6. The static coefficients are based upon values obtained from the literature (References 13 through 18) and from MMC subsonic wind tunnel tests conducted during the present study. The damping coefficients are based on forced oscillation and free oscillation type tests conducted at AEDC (References 8 and 9) for the Viking Program and on tests carried out in the LRC spin tunnel during the present study.

Static aerodynamic coefficients and derivatives for the descent capsule have been derived from tests in the MMC subsonic wind tunnel. The values are applicable for $-30 \text{ degrees} < \alpha < 30 \text{ degrees}$ and are:

$$C_D = 0.72$$

$$C_{N_\alpha} = 0.80 \text{ per rad}$$

$$C_{M_\alpha} = -0.091 \text{ per rad}$$

The reference area is $\frac{\pi d^2}{4}$, and reference length = sphere diameter = d , and $c_{g_{ref}}$ is at 3.5 percent d forward of the maximum diameter station. Pitch damping coefficients ($C_{m_q} + C_{m_{\dot{\alpha}}}$) for the perforated ring versions of the descent capsule have been deduced from the motion pictures obtained in the spin tunnel tests. From this type of test, "average" values of the coefficient are deduced. The values are given in Figure 7.1-7 which also shows a curve of "instantaneous" damping coefficient deduced from the "average" curve by means of the method of Reference 12.

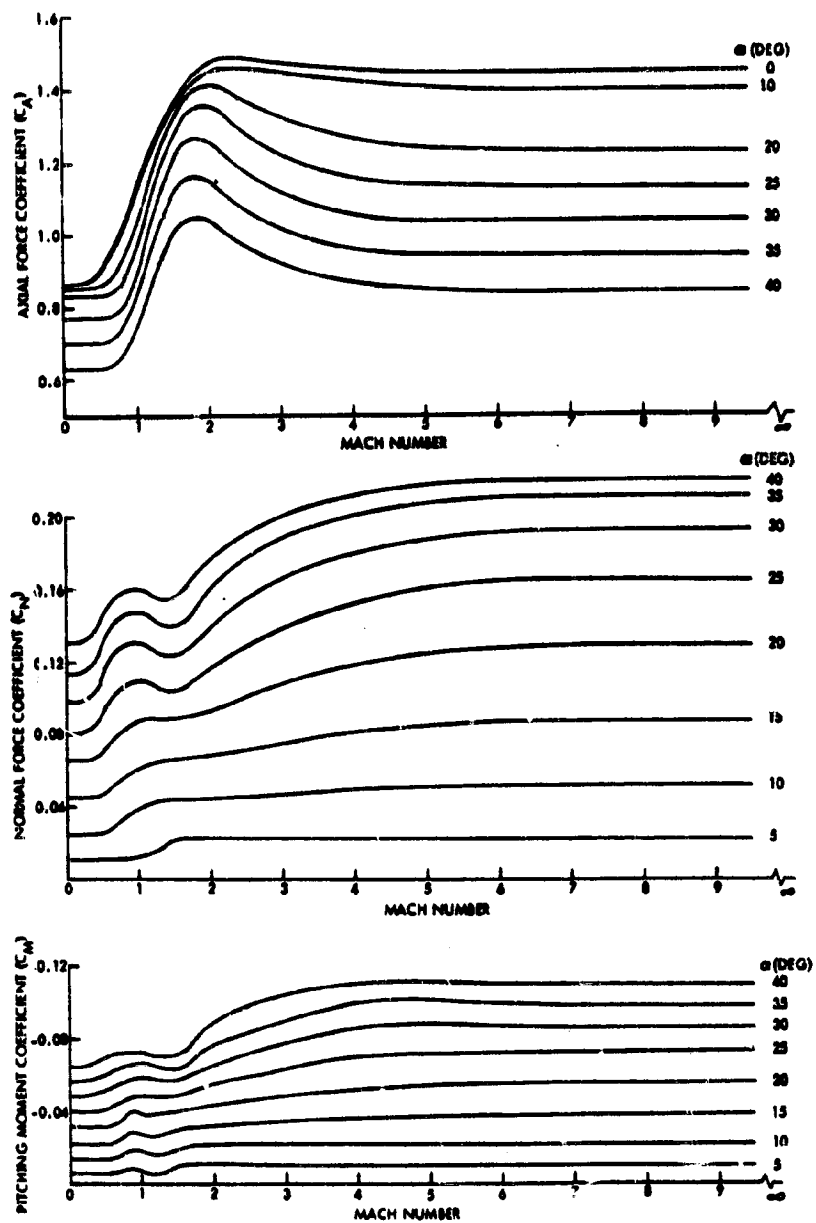
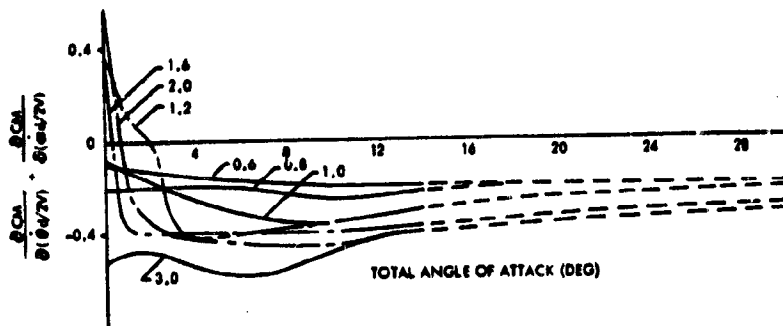
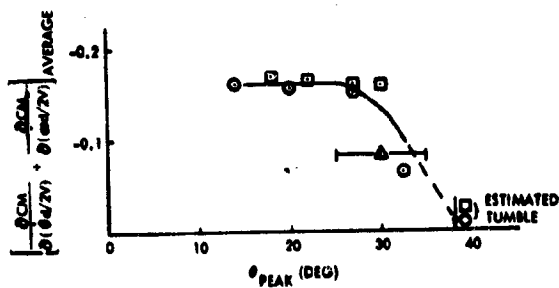


Figure 7.1-3. Estimated Static Aerodynamic Coefficients for the Large Probe



A. INSTANTANEOUS PITCH DAMPING

RUN	C.G. (%)	d	4/8	SERIES	V	M _A	FACILITY
119	-2.6		4.04	II	48	0.043	SPIN TUNNEL
278	-2.2		4.50	III	54	0.043	SPIN TUNNEL
	0		4.23		50	0.046	CSU



B. AVERAGE PITCH DAMPING

Figure 7.1-4. Estimated dynamic Coefficients for the Large Probe

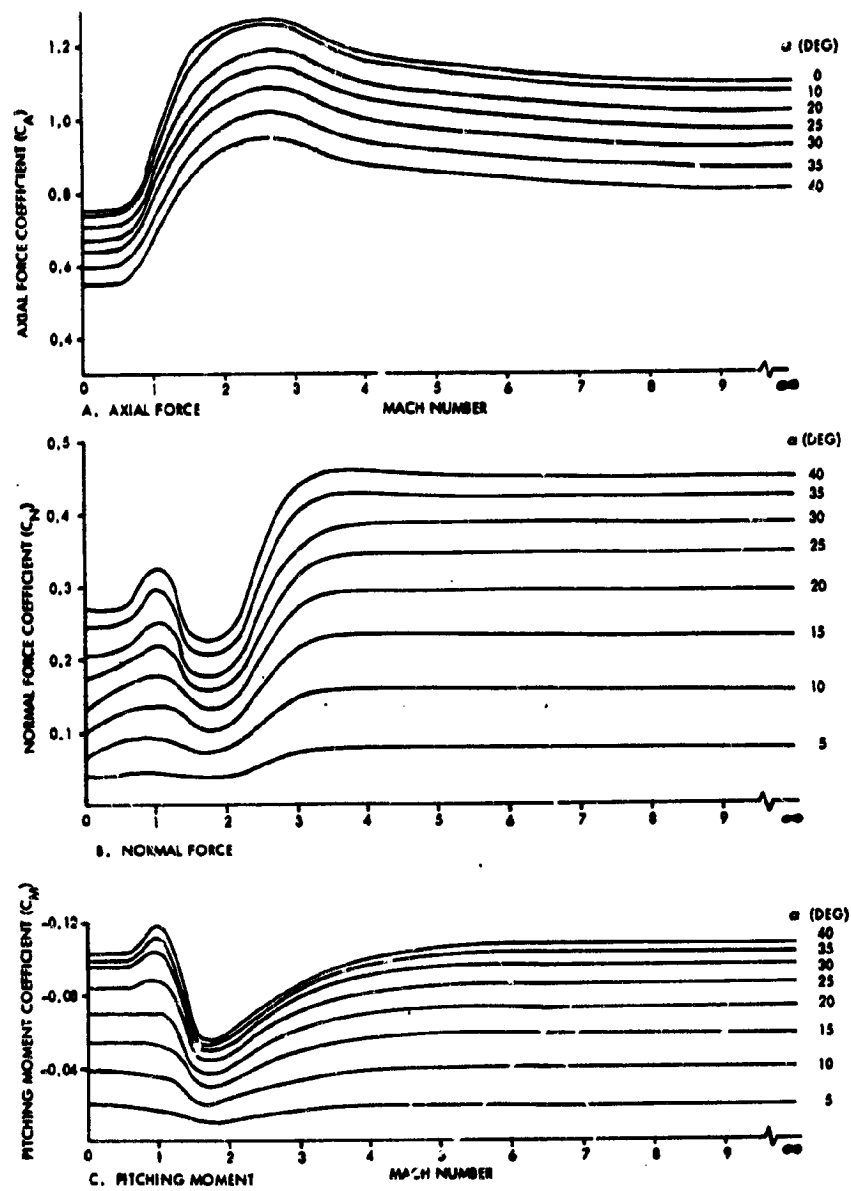


Figure 7.1-5. Estimated Static Aerodynamic Coefficients for the Small Probe

NOTE: INSTANTANEOUS DAMPING FOR SMALL PROBE
ASSUMED IDENTICAL TO THAT FOR LARGE PROBE (SEE FIG. 7.1-4A)

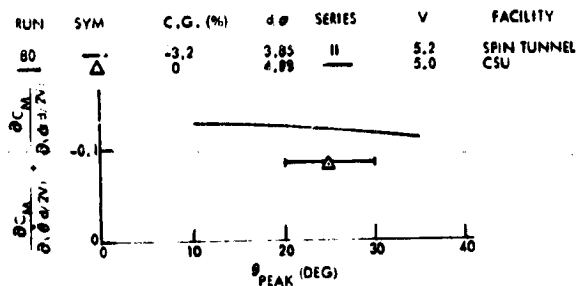


Figure 7.1-6. Small Probe Average Damping Derivative for Mach Number 0.05 Deduced from Spin Tunnel Tests

FACILITY	SYM	RUN	d/ø	C.G. (%d)	D/d	RING POROSITY (%)
SPIN TUNNEL	○	260	2.79	-3.5	1.125	19.7
SPIN TUNNEL	△	268	2.76	-3.1	1.125	39.7
SPIN TUNNEL	□	271	2.74	-3.5	1.115	43.4
SPIN TUNNEL	▽	273	2.73	-3.0	1.105	47.7

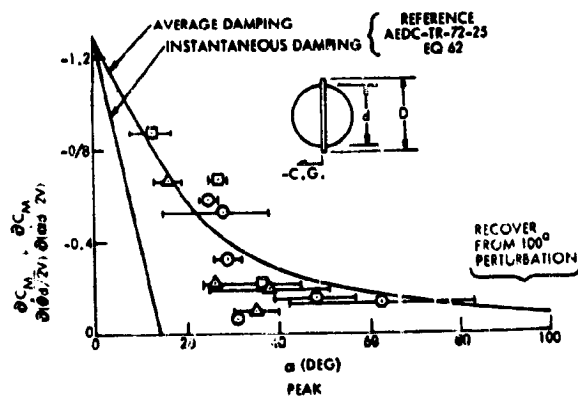


Figure 7.1-7. Descent Capsule Pitch Damping Coefficients as a Function of Angle of Attack at Mach 0.05

7.1.5 Preferred Aerodynamic Configuration, Thor/Delta

The external configurations for the large probe, small probe and descent capsule for the Thor/Delta option are shown in Figure 7.1-8. Because the small probe entry vehicle shape and large probe entry vehicle forebody configurations are identical to those for the Atlas/Centaur option, the aerodynamic coefficients given in Figures 7.1-3 through 7.1-6 are assumed to be applicable up to $\alpha \approx 40$ degrees. The difference in the Thor/Delta large probe afterbody shape will probably cause some transonic/subsonic pitch damping coefficient differences, but these will not affect the convergent α behavior.

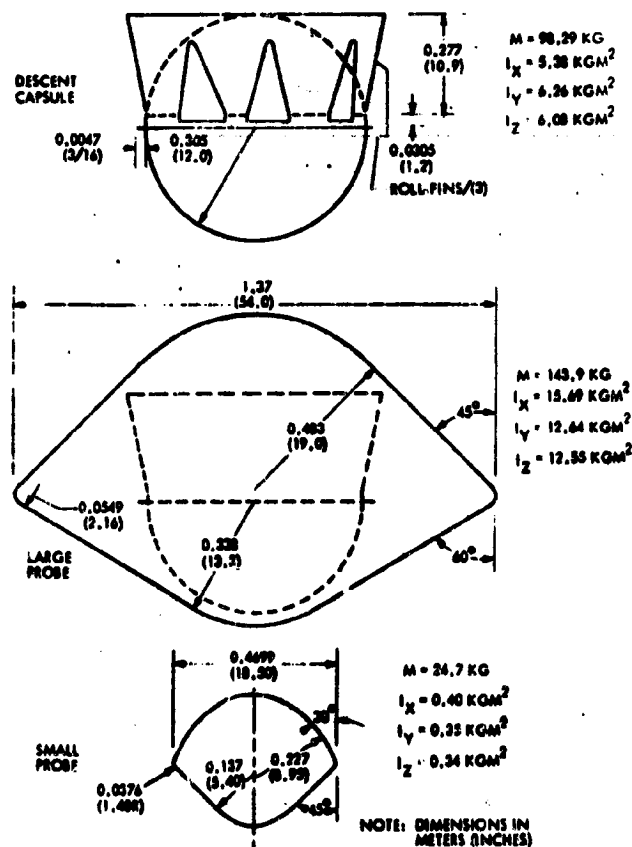


Figure 7.1-8. Sketch of Thor/Delta Descent Capsule, Large Probe, and Small Probe

The descent capsule stabilization flare for the Thor/Delta, however, is different from the perforated ring shown on the Atlas/Centaur version. The flare was designed for a drag coefficient of 0.8. This configuration was demonstrated to be stable in the spin tunnel, i. e., it exhibited a low limit cycle ≈ 6 degrees, and a relatively small amount of translation (lift).

Although possibly amenable to improvement by design modifications, the somewhat erratic nature of the oscillations, apparently deriving from alternating vortex shedding, was deemed to be undesirable. This led to the adoption for the Atlas/Centaur option of the very effective and simple perforated ring. This ring would be compatible with the Thor/Delta probe and also would currently be the choice for that probe system design as well.

7.1.6 Aerodynamics Analyses and Tests

Analyses carried out during the present study have involved:

- 1) Estimating static and dynamic aerodynamic coefficients for the three probe configurations.
- 2) Dynamic stability studies involving limited sensitivity studies of the effects of aerodynamic coefficients, mass properties, and roll rates.
- 3) Descent capsule sensor environment.

Aerodynamic test programs have been conducted in a number of facilities on a large number of conical shapes with various afterbodies and on spheres with various drag amplification/stabilization devices and roll producing devices.

7.1.6.1 Aerodynamic Coefficients

Aerodynamic coefficients for use in six degree of freedom digital computer studies of 45-, 55-, and 60-degree semi-angle cones have been developed using data from the literature (References 13 through 18) and from the IRAD tests conducted during the present study. These coefficients are shown in Figures 7.1-3 through 7.1-6 for the 60- and 45-degree cones, and Figure 7.1-9 for the 55-degree cone. C_D , C_{L_α} , C_{N_α} , C_{m_α} , and x_{cp} values for the three cone angles are compared in Figure 7.1-10.

7.1.6.2 Dynamic Stability

Analysis of the dynamic stability characteristics of an entry vehicle for varying initial conditions, mass properties, and aerodynamic coefficients through use of a digital six degree of freedom trajectory program can be an extremely time consuming and costly process. Thus, before undertaking such a study, preliminary work should be done with simpler methods in order to minimize the scope of the study. One such method has been presented by Coakley in Reference 11, where he develops a criterion that

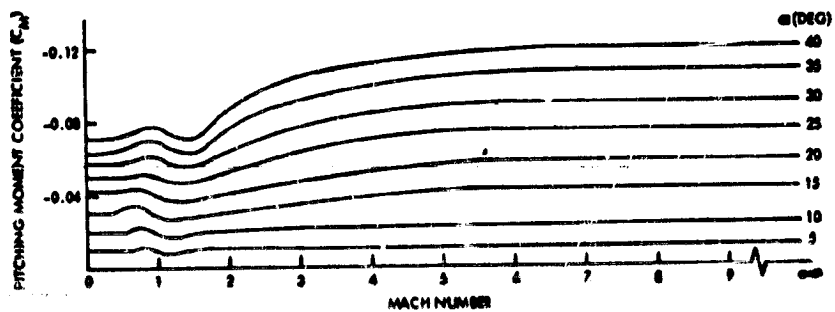
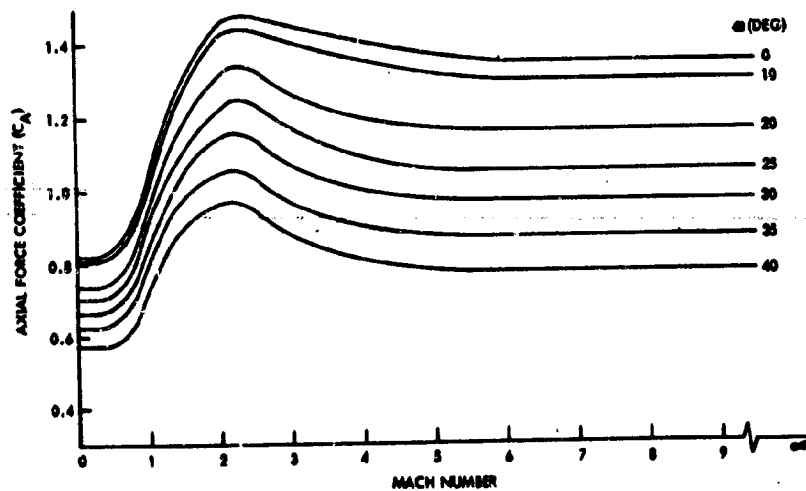
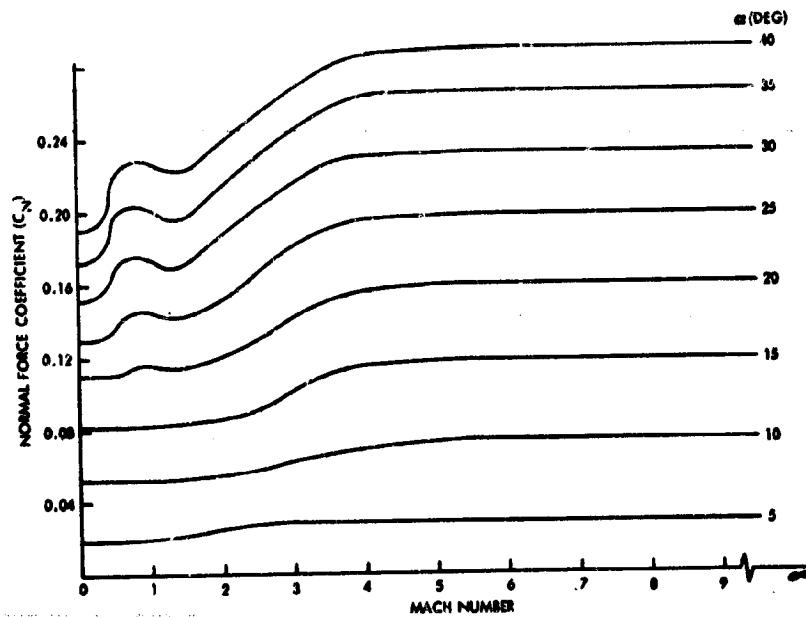


Figure 7.1-9. Estimated Aerodynamic Coefficients for 55-Deg Cone

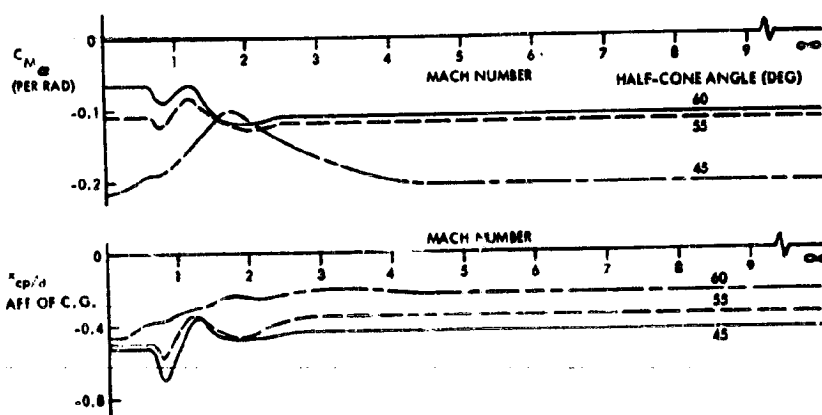
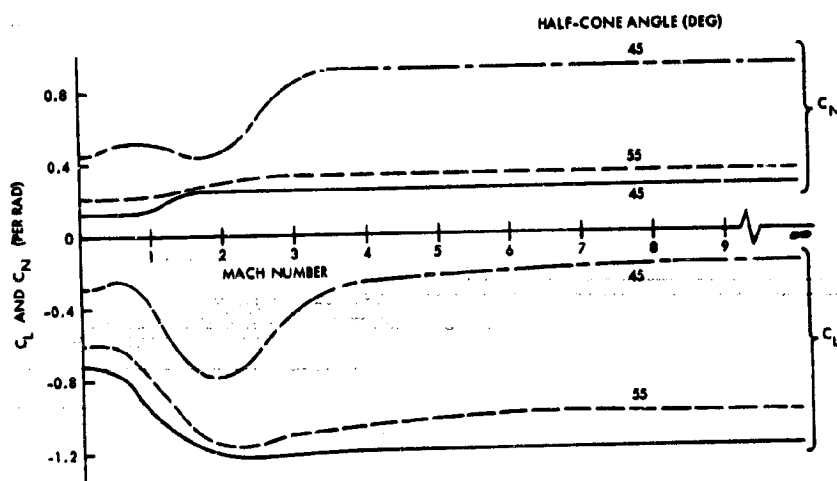
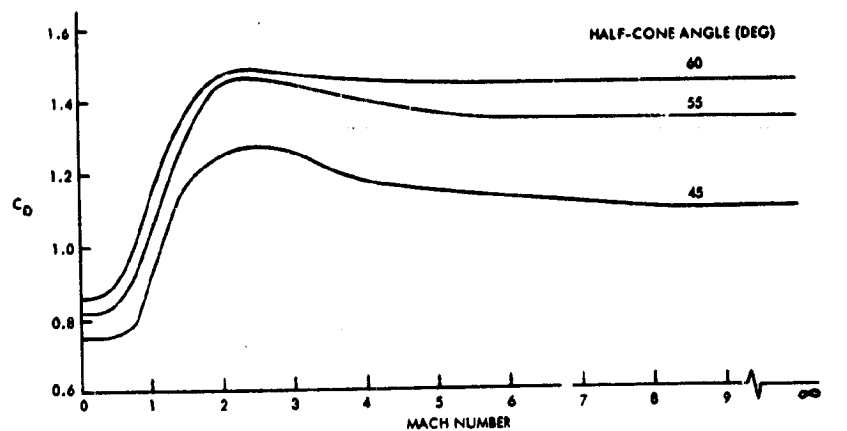


Figure 7.1-10. Comparison of Estimated Aerodynamic Coefficients for 45, 55, and 60 Degrees Conical Probes

indicates whether the angle of attack envelope of a rolling entry vehicle is divergent or convergent. This formula represents a significant improvement on the well known Allen formula in that roll rate, gravity, variable density, and variable flight path angle are all accounted for.

Stability Criterion Analysis

In Reference 19, Shirley and Misselhorn presented a study of the Coakley criterion by comparison with numerical trajectory results, with Allen's criterion and with criteria developed by Murphy in Reference 20 and Jaffe in Reference 19. The bulk of their study showed that the angle of attack behavior was largely determined by the pitch damping coefficient. However, for the blunted, 60-degree cone vehicle of their study, it was also shown that, at subsonic speeds, even with a negative pitch damping coefficient, a roll related divergence was indicated at about 4 rad/s.

In order to gain some understanding of how this phenomenon might relate to the proposed Pioneer Venus probes, a study has been carried out using the Coakley criterion. The complete analysis is given in Appendix 7.1B. The mass properties of the present preferred probes are somewhat different than those used in the study; nevertheless, the results are believed to be informative.

In summary the results of the analysis were:

Large Probe

- 1) The roll related divergence computed by Shirley and Misselhorn was found to result from the large value of roll-to-pitch moment of inertia, 1.8, whereas our large probe value is 1.32.
- 2) The large probe entry vehicle stability characteristics were strongly related to the pitch damping derivative. The probe was stable at the time of parachute deployment.
- 3) The descent capsule was found to be stable for terminal descent velocities and roll rates and the stability was found not to be significantly influenced by changes in ballistic coefficient.

Small Probe

- 1) The small probe was likewise found not to suffer a roll related divergence.
- 2) The small probe was stable above 77 km, primarily due to the atmosphere scale height term during the period of increasing dynamic pressure.

- 3) Between approximately 60 and 77 km, the indicated instability (Figure 7.1B-10 Appendix 7.1B) was dependent on the interaction of the drag, gravity, and density terms, corresponding to the period of rapidly decreasing dynamic pressure, and strongly influenced by the pitch damping coefficient.
- 4) In terminal flight the small probe was stable even for very small values of the pitch damping coefficient.

Stability boundaries for the preferred Atlas/Centaur small probe based on these studies are shown in Figure 7.1-11. It is significant that the small probe is stable throughout the trajectory with roll rates up to four times the 1 rad/s planned, even with very low values of $C_{m\dot{q}} + C_{m\dot{\delta}}$ relative to those it is estimated to possess (Figure 7.1-6). This indicates an insensitivity to the accuracy of the current estimates for this critical parameter. Comparison of this figure with the comparable figure for the Thor/Delta small probe (Figure 7.1B-7) in Appendix 7.1B shows that the preferred Atlas/Centaur small probe is slightly more sensitive to roll rate. This is the same effect mentioned earlier, since the Atlas/Centaur probe has a larger rolling moment of inertia. See equation 1 of Appendix 7.1B. However, this increased roll sensitivity is not of any significance for the planned roll rates of the descent.

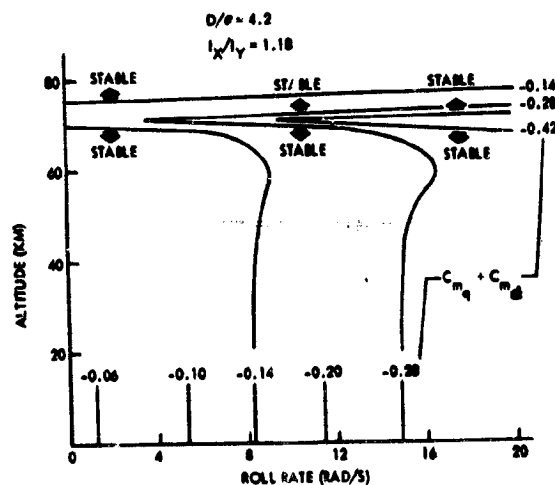


Figure 7.1-11. Atlas/Centaur Small Probe Stability Boundaries as Functions of Pitch Damping Derivative, Roll Rate, and Altitude

Six Degrees of Freedom Simulation

Trajectory parameters from six degrees of freedom digital computer runs for the large and small probes are shown in Figure 7.1-12 and 7.1-13 in terms of total angle of attack and dynamic pressure as functions of time, Mach number, and altitude. It is seen in these figures that the angle of attack, from an initial value of 10 degree at entry, converges throughout the trajectory except for a very slight tendency to diverge in the transonic range when the pitch damping coefficients go positive over a small angle of attack range (Figure 7.1-4a).

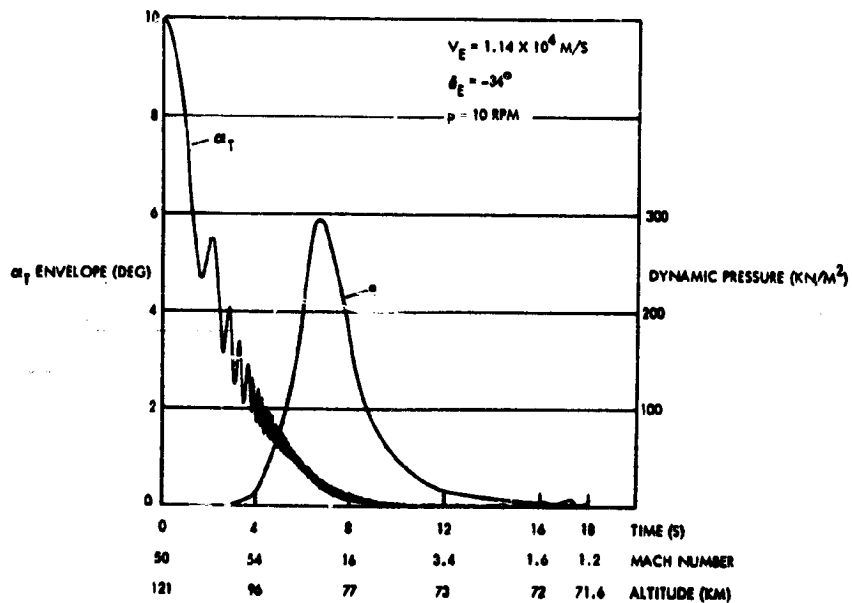


Figure 7.1-12. Large Probe Entry Trajectory Parameters

The small oscillations on the total angle of attack curves indicate the ellipticity of the motion in the α, β plane. The ellipticity, < 1 degree for the large probe and < 0.5 degree for the small probe, results from the moment of inertia in pitch being arbitrarily given a value equal to 1.02 times the moment of inertia in yaw.

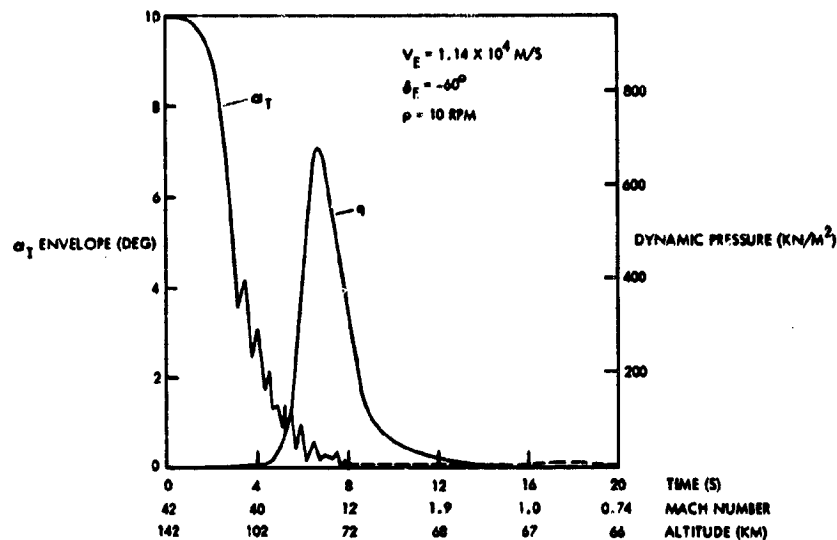


Figure 7.1-13. Small Probe Entry Trajectory Parameters

7.1.6.3 Descent Capsule Sensor Environment

The flow environment in the vicinity of the desired location for the science sensors on the descent capsule has been examined through study of a smoke flow photograph for a sphere in supercritical Reynolds number flow (Figure 7.1-14), and through calculation of the boundary layer transition point and thickness on the sphere. Figure 7.1-15 shows a tracing of the smoke filaments (streamlines) with the sensor ring and sensor axes indicated. It is seen that the flow is very nearly normal to the sensor axes. Figure 7.1-16 shows the Reynolds number variation during the descent capsule flight that was used in the boundary layer computations. Figure 7.1-17 shows the location of the boundary layer transition point (based on the method of Reference 21), and Figure 7.1-18 shows the boundary layer thickness at the sensor ring location. This thickness was assumed to be 7.54 (Blasius profile) times the momentum thickness, given also by Reference 21. These figures indicate that the boundary layer in the vicinity of the sensors is laminar and very thin throughout the descent.

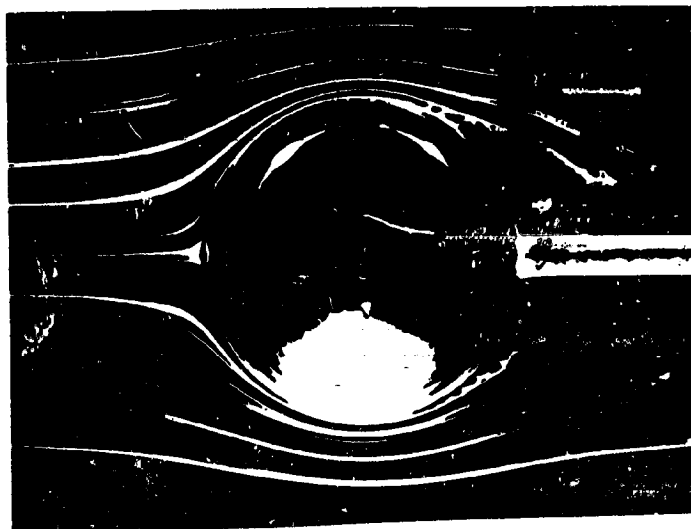


Figure 7.1-14. Subsonic Smoke Flow About a Sphere

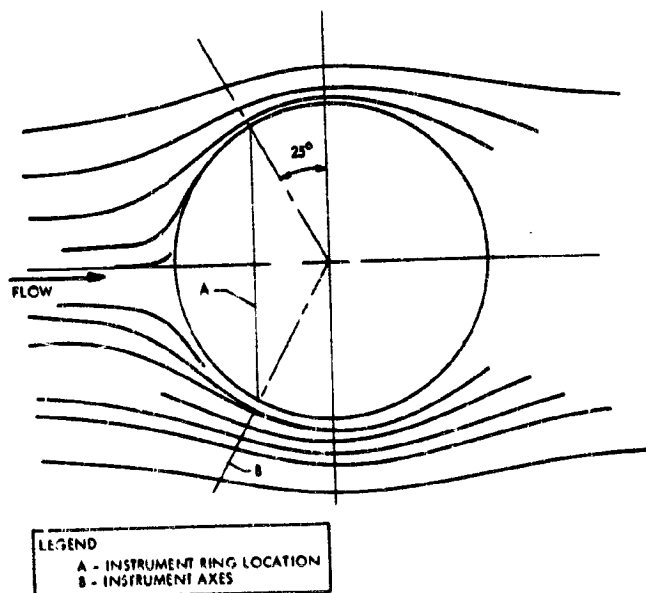


Figure 7.1-15. Streamlines About Sphere Showing Relation to Science Sensors

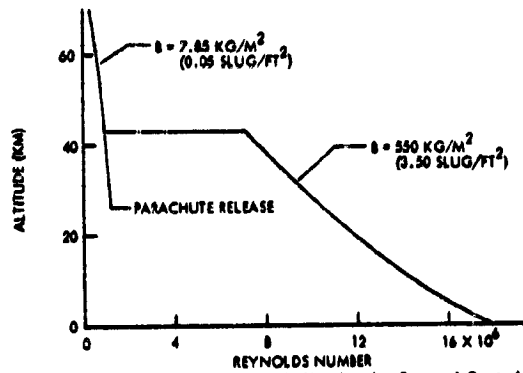


Figure 7.1-16. Reynolds Number for Descent Capsule

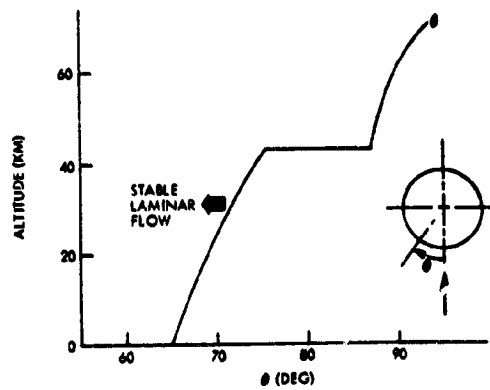


Figure 7.1-17. Boundary Layer Transition Point on a Sphere

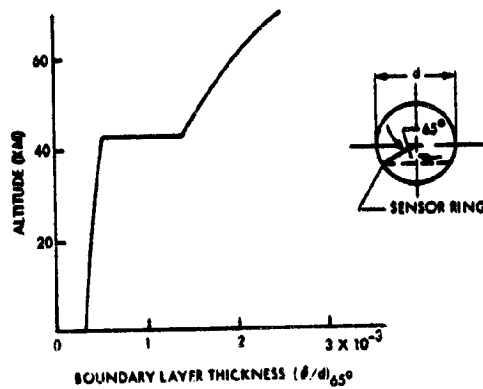


Figure 7.1-18. Boundary Layer Thickness in Vicinity of Science Sensors

It might be expected that a flow separation region will be produced ahead of the stabilization ring. However, it is believed that the holes in the ring will vent off most of the boundary layer and minimize the size of the separated region to the extent that it will not influence the sensors.

Local pressure on the sphere in the region of attached flow is given by the classical potential theory formula:

$$C_p = 1 - 9/4 \sin^2 \phi$$

where C_p is the pressure coefficient. At the location of the sensor ring $\phi = 65$ degree.

7.1.6.4 Wind Tunnel Test Results for Preferred Configurations

Extensive use was made of wind tunnel test results in evaluating candidate probe configurations. The test programs were carried as part of MMC's Planetary Entry Probes IRAD Program with NASA cooperation, starting prior to the Phase B Proposal and continuing into the present time. The test facilities used and the types of tests conducted in each follow.

Facility	Type of Test
MMC Low Speed Wind Tunnel	Static force and moment
Army Meteorological Wind Tunnel at Colorado State University	Single degree of freedom dynamic stability
NASA ARC HFFB Water Facility	Six degree of freedom dynamic stability
NASA LRC Vertical Spin Tunnel	Six degree of freedom dynamic stability.

Considerable data were gathered on various configurations of large probe, descent capsule and small probe in support of the Thor/Delta and Atlas/Centaur design and trade studies. Only low speed data were obtained in all facilities. Figures 7.1-19 and 7.1C-7, 7.1C-8 and 7.1C-10 of Appendix 7.1C show all of the model configurations tested. The major results pertaining to the preferred configurations are discussed below.

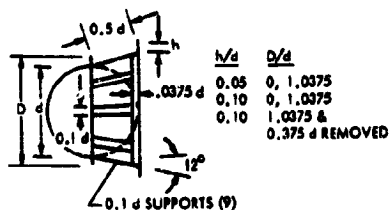
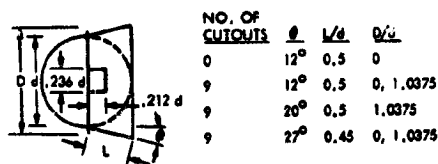
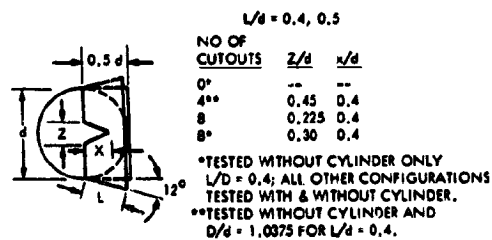
Small Probe Results

Aerodynamic considerations in the selection of the preferred small probe configuration were based largely upon the behavior of the 45-degree cone model with various afterbodies in the Langley Spin Tunnel. These results are summarized in Tables 7.1C-6 in Appendix 7.1C, where the preferred configuration is identified as A-F with c.g. at -4.0 percent d and d/σ equal to 4.0. The table shows that the 10-inch diameter model exhibited a small (4 degrees) limit cycle, whereas the 24-inch diameter model (75 percent full scale) trimmed at zero angle of attack. The difference is believed to be due to the scale of turbulence in the spin tunnel. It is also shown in Table 7.1C-6 that the configuration would recover from disturbances close to 50 degrees but with a disturbance of 50 degrees would tumble. In the ARC water facility tests, the A-F configuration with $d/\sigma = 3.8$ exhibited a limit cycle of about 15 degrees and with $d/\sigma = 4.6$, trimmed to zero angle of attack. The static coefficients obtained in the MMC wind tunnel, Figure 7.1C-1 of Appendix 7.1C show very little differences between the 60- and 45-degree cones and virtually no effect of afterbody shape except for the hemispherical afterbody. This difference is discussed in the Appendix.

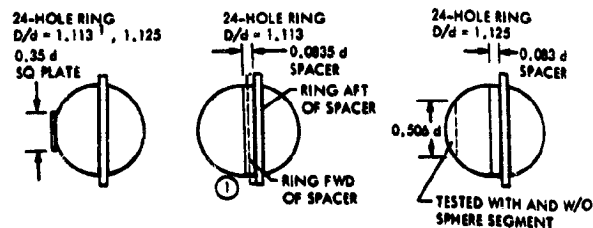
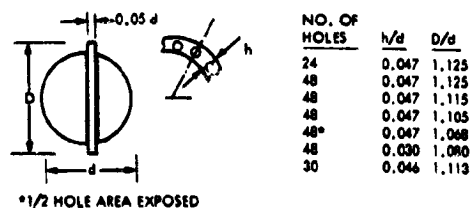
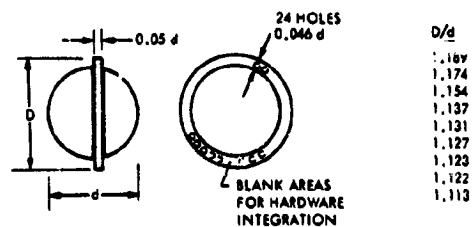
Large Probe Results

The large probe aerodynamic configuration selection was based largely upon the available data in the literature. Although the large probe will not encounter the low speeds obtained in the spin tunnel, it is believed that such tests are indicative of what might be expected in the Mach number range (0.7) just before parachute deployment. Therefore, the preferred configuration was tested in the spin tunnel with representative values of c.g. location and d/σ , i.e., -3.5 percent d and 4.9 respectively. The results are summarized in Table 7.1C-8 (Appendix 7.1C) with configuration code B-H₂. The table shows that the configuration (10-in. model) exhibited a small limit cycle, about 5 degrees, would recover from a disturbance of at least 52 degrees, and would tumble from a 58-degree disturbance. No tests were conducted with this configuration in either the MMC wind tunnel or the ARC water facility.

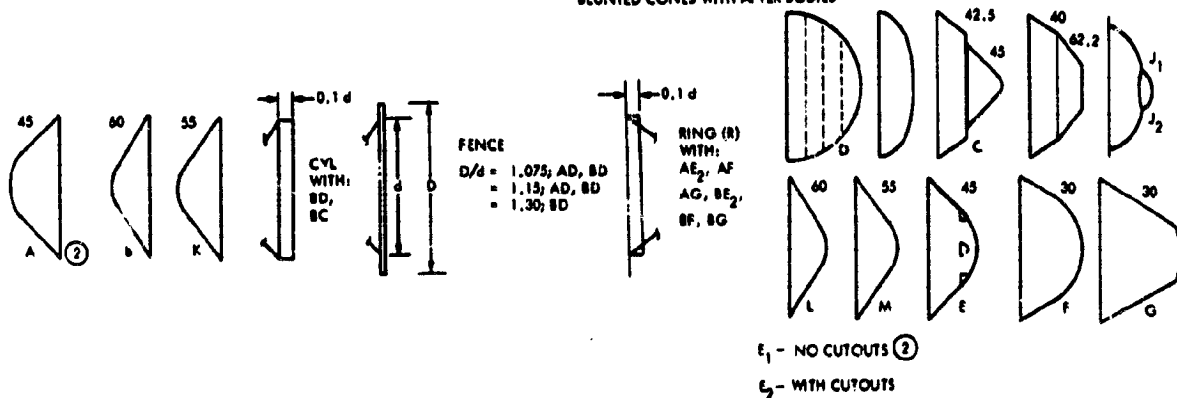
SPHERE/FLARES



SPHERE/PERFORATED RINGS



BLUNTED CONES WITH AFTER BODIES

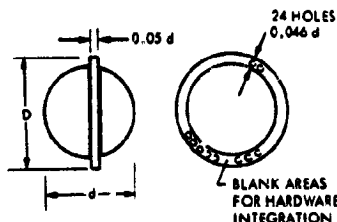


SPHERE/PERFORATED RINGS

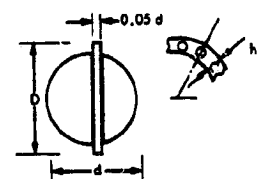
$d = 0.4, 0.5$

z/d	r/d
0.45	0.4
0.225	0.4
0.30	0.4

WITHOUT CYLINDER ONLY
; ALL OTHER CONFIGURATIONS
WITH & WITHOUT CYLINDER,
WITHOUT CYLINDER AND
0.075 FOR $L/d = 0.4$.

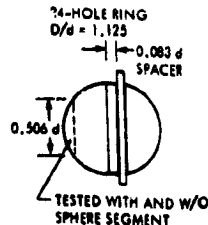
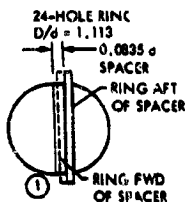
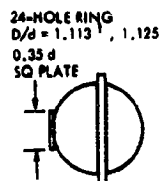


D/d
1.189
1.174
1.154
1.137
1.131
1.127
1.123
1.122
1.113



NO. OF HOLES	h/d	D/d
24	0.047	1.125
48	0.047	1.125
48	0.047	1.115
48	0.047	1.105
48	0.047	1.068
48	0.030	1.080
30	0.046	1.113

*1/2 HOLE AREA EXPOSED



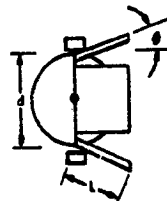
D/d
3, 1.0375
5, 1.0375
1.0375 &
0.375 d REMOVED

SPHERE/THIN RINGS



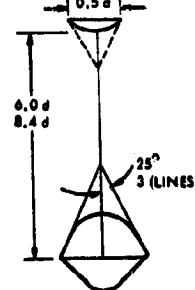
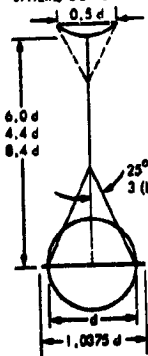
$D/d = 1.2; \theta = 30^\circ, 45^\circ$
 $= 1.3; \theta = 45^\circ$
 $= 1.4; \theta = 30^\circ, 45^\circ$

FINNED SPHERES

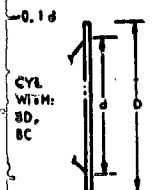


$L/d = 0.25; \theta = 30^\circ, 40^\circ, 45^\circ$
 $= 0.40; \theta = 40^\circ, 45^\circ$
 $= 0.50; \theta = 20^\circ, 30^\circ, 40^\circ, 45^\circ$

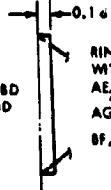
SPHERE/CONES WITH DROGUE



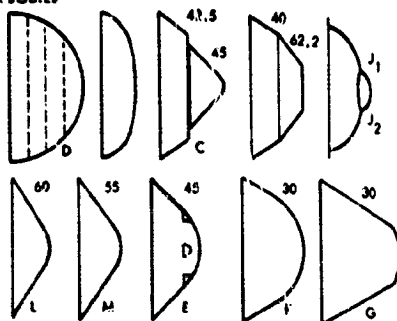
BLUNTED CONES WITH AFTER BODIES



FENCE
 $D/d = 1.075; AD, BD$
 $= 1.15; AD, BD$
 $= 1.30; BD$

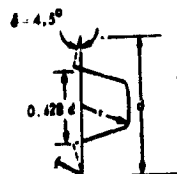


RING (R)
WITH:
AE₂, AF
AG, BE₂,
BF, BG



E₁ - NO CUTOUTS ②
E₂ - WITH CUTOUTS

NOTE:
① $d = 23$ (IN.)
② $d = 10$ (IN.) AND 23 (IN.)
ALL OTHERS $d = 10$ (IN.)



CONFIG	L/d	θ
H ₁	0.310	4.5°
H ₂	0.310	6°
I	0.232	0°

Figure 7.1-19. Configurations Tested in the NASA Langley Spin Tunnel

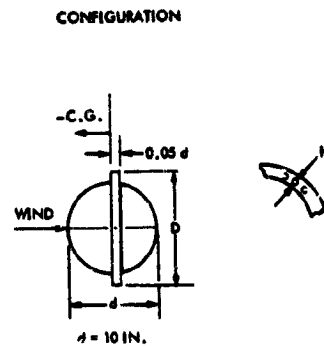
Descent Capsule Results

The preferred Atlas/Centaur descent capsule is basically a sphere with a thick perforated ring to provide the required drag and stability. Tests were performed with both 10-inch and 23-inch diameter sphere models in which the width and porosity (ratio of hole area to ring area) of the ring were varied. Other variables included c.g. location, protuberances (science instruments, pyro nut containers, aft antenna), and the wind/altitude radar antenna. The test results are summarized in Table 7.1-3. From the tabulated drag data it is apparent that the drag coefficient can readily be tailored by variations in ring geometry. With respect to stability, all configurations (except for certain configurations of the radar antenna) were stable. Limit cycle behavior was observed only at the lowest ring porosity tested, ≈ 13 percent, and reducing the ring width below 3.4 percent of the sphere diameter resulted in introducing a low trim angle. Neither of these limits imposes any problems in achieving the desired ballistic coefficient for the flight article. All of the models experienced some degree of low amplitude perturbations.

The influence on stability of various combinations of simulated science sensor protuberances in the equipment ring area was found to be negligible as was the effect of these sensors on the drag coefficients inferred from the tests.

The wind/altitude radar antenna protuberance, however, is a 10-inch square flat plate tangent to the sphere at its forward stagnation point. Tests were made on this configuration and on two faired configurations. To simulate a fully faired antenna, a cylindrical section was inserted between the fore and aft hemispheres. A partly faired configuration was achieved by cutting a sector off the fore hemisphere. These configurations are shown in Table 7.1-3. The fully faired model was statically unstable for aft c.g. locations. As the c.g. was moved forward, the model became stable and trimmed out at a successively decreasing angle of attack. This behavior indicates that inserting the cylindrical section between the two hemispheres results in moving the center of pressure, which is at the geometric center, of the forward hemisphere forward of the model c.g. It further implies that the pressure on the forward hemisphere dominates the static stability characteristics. The partly faired model exhibited

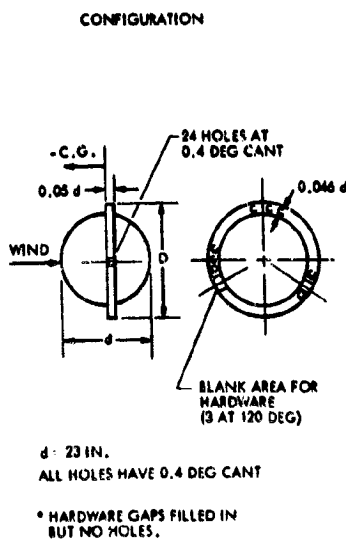
Table 7.1-3. Summary of Results of Sphere/Thick, Perfora



NOTES (a) ONLY SEMICIRCULAR HOLES REMAIN; PERIMETER OF RING WRAPPED WITH TAPE TO ENCLOSE HOLE.
(b) $d = 23 \text{ IN.}$

(a) RING VARIATIONS

HOLE CONFIGURATION	D/d	h/d	C.G. % d	POROSITY % RING AREA	REF. D C_D	TEST OBSERVATIONS
24 AT 0.8°	1.125	0.047	-5.0	19.9	0.62	0° TRIM, 2° PERTURBATIONS
24 AT 0.8°	1.125	0.047	-3.5	19.9	0.58	0° TRIM, 4° PERTURBATIONS
24 AT 0.8°	1.125	0.047	0	19.9	0.62	0° TRIM, 6° PERTURBATIONS
24 AT 0.8° 24 AT 0°	1.125	0.047	-3.5	39.7	0.44	0° TRIM, 4° PERTURBATIONS
24 AT 0.8° 24 AT 0°	1.115	0.047	-3.5	43.4	0.48	0° TRIM
24 AT 0.8° 24 AT 0°	1.105	0.047	-3.5	47.7	0.45	0° TRIM, 3° PERTURBATIONS
24 AT 0.8° 24 AT 0°	1.068	0.047	-3.5	37.5	0.35	4° LIMIT CYCLE
24 AT 0.4° 24 AT 0°	1.080	0.030	-3.5	26.0	0.49	0° TRIM, 2° PERTURBATIONS
24 AT 0.4°	1.125	0.47	-3.5	19.9	0.58	0° TRIM, 3° PERTURBATIONS
30 AT 0.4°	1.113	0.46	-3.5	27.6	0.54	3° TRIM



(a) RING VARIATIONS (CONTINUED)

D/d	C.G. % d	POROSITY % RING AREA	C_D REF. D	TEST OBSERVATIONS
1.189	-3.5	12.8	0.71	6° LIMIT CYCLE
1.174*	-3.5	13.9	0.70	0° TRIM, 7° PERTURBATIONS
1.154	-3.5	15.9	0.68	0° TRIM, 5° PERTURBATIONS
1.137	-3.5	18.0	0.68	0° TRIM, 6° PERTURBATIONS
1.131	-1.5	18.8	0.64	0° TRIM, 6° PERTURBATIONS, WEAK DAMPING
1.131	-5.0	18.8	0.64	0° TRIM, 4° PERTURBATIONS
1.131	-6.5	18.8	0.64	0° TRIM, 2° PERTURBATIONS
1.127	-3.5	19.5	0.63	0° TRIM, 5° PERTURBATIONS
1.123	-3.5	20.1	0.62	0° TRIM, 6° PERTURBATIONS
1.122	-3.5	20.4	0.62	0° TRIM, 4° PERTURBATIONS
1.113	-3.5	22.1	0.60	5° TRIM, 7° PERTURBATIONS

Summary of Results of Sphere/Thick, Perforated Ring Model Tests in the Spin Tunnel

ATIONS
Y-CYCLE
1 st PERTURBATIONS
5 th PERTURBATIONS
6 th PERTURBATIONS
6 th PERTURBATIONS, WEAK DAMPING
4 th PERTURBATIONS
2 nd PERTURBATIONS
-5 th PERTURBATIONS
6 th PERTURBATIONS
4 th PERTURBATIONS
7 th PERTURBATIONS



• MODELS WERE NOT BALANCED AFTER ATTACHING ANTENNAS. NO SIGNIFICANT EFFECT OF ANTENNAS ON AERODYNAMICS.

(c) WIND/ALTITUDE RADAR ANTENNA VARIATIONS					
C.G. % d	d, IN.	RING POSITION	POROSITY % RING AREA	C _D REF, D	TEST OBSERVATIONS
-2.5	23	RING FORWARD OF AFT SPLIT LINE	22.1	-	STATICALLY UNSTABLE
-3.5	23	RING AFT OF AFT SPLIT LINE	22.1	-	STATICALLY UNSTABLE, SOME IMPROVEMENT OBVIOUS
-5.0	23	RING AFT OF AFT SPLIT LINE	22.1	-	MARGINALLY STABLE, LARGE TRANSVERSE MOTION
-10.0	23	RING AFT OF AFT SPLIT LINE	22.1	0.59	12° TRIM, TRANSVERSE MOTION
-4.1	10	RING AFT OF AFT SPLIT LINE	20.0	0.52	10° TRIM, TRANSVERSE MOTION
-5.6	10	RING AFT OF AFT SPLIT LINE	20.0	0.50	6° TRIM, 11° PERTURBATIONS
-11.2	10	RING AFT OF AFT SPLIT LINE	20.0	0.50	0° TRIM, 6° PERTURBATIONS
-4.5	10	RING AFT OF AFT SPLIT LINE	20.0	0.52	10° - 15° TRIM, TRANSVERSE MOTION
-6.3	10	RING AFT OF AFT SPLIT LINE	20.0	0.50	5° TRIM, 10° PERTURBATIONS, WEAK TRIM POINT
-11.3	10	RING AFT OF AFT SPLIT LINE	20.0	0.50	5° TRIM, 8° PERTURBATIONS, STRONGER THAN ABOVE
-3.5	23	RING AFT OF AFT SPLIT LINE	22.1	0.58	15° TRIM
-3.5	10	RING AFT OF AFT SPLIT LINE	20.0	0.60	6° TRIM



similar trim angle behavior, but was stable in the c.g. location range where the fully faired model was unstable, indicating that the flat face was stabilizing. The antenna-alone configuration also had a finite trim point, but seemed to be better behaved in terms of random perturbations than the two faired models and not significantly worse than the same ring geometry version of the 23-inch sphere without the antenna. In the 10-inch sphere tests, the antenna-alone configuration definitely caused a degradation in behavior over the no-antenna case.

From these initial tests it is concluded that the descent capsule without the wind/altitude radar antenna will be adequately stabilized by a perforated ring. However, aerodynamic accommodation of the radar antenna has not been resolved. The tests also demonstrated that the canted holes in the ring are an effective means for producing a controlled spin rate.

7.1.7 Aerothermodynamic Studies

Cold wall, no-blowing entry convective and radiative environments have been calculated for the eleven Atlas/Centaur trajectory and geometry combinations shown in Table 7.1-1 and the seven Thor/Delta combinations given in Table 7.1-2. The 1978 launch entry velocity of 11.34 km/s was emphasized in the Atlas/Centaur analysis. However, three large probe configurations were considered at the lower entry velocity of 11.16 km/s encountered with a 1977 launch. All Thor/Delta calculations were for the 1977 launch.

7.1.7.1 Analysis Procedures

Details of the procedures used in the present entry environment calculations are presented in Appendix 7.1A. For the parametric study of configuration and trajectory influences, a completely uncoupled solution procedure was selected, i.e., convective and radiative phenomena were computed independently and the effect of ablation products on the environment considered in a separate material response analysis. A comparison is made (Appendix 7.1A) of the results from this procedure with those results available from the fully coupled analysis performed by LRC at one trajectory point for both a large and a small Thor/Delta probe. Reasonably good agreement is shown between the two results giving added confidence in the analysis technique used here.

For the chosen procedure, a separate inviscid analysis is required; in particular, the body pressure distribution and bow shock shape are necessary. The hypersonic pressure distribution and shock standoff distance at zero angle of attack for five of the configurations considered in the present study are depicted in Figure 7.1-20. If the cone angle is greater than about 51 degrees for the assumed Venus atmospheric gas composition, the body sonic point occurs at the aft corner. In this case the pressure and shock standoff distance distributions then also depend on the base-to-nose radius ratio. These detailed differences were accounted for in the configuration studies. For each configuration, however, the distributions were held constant throughout the heating period. The probes were assumed at zero incidence throughout the entry heat pulse and all calculations made for thermochemical equilibrium.

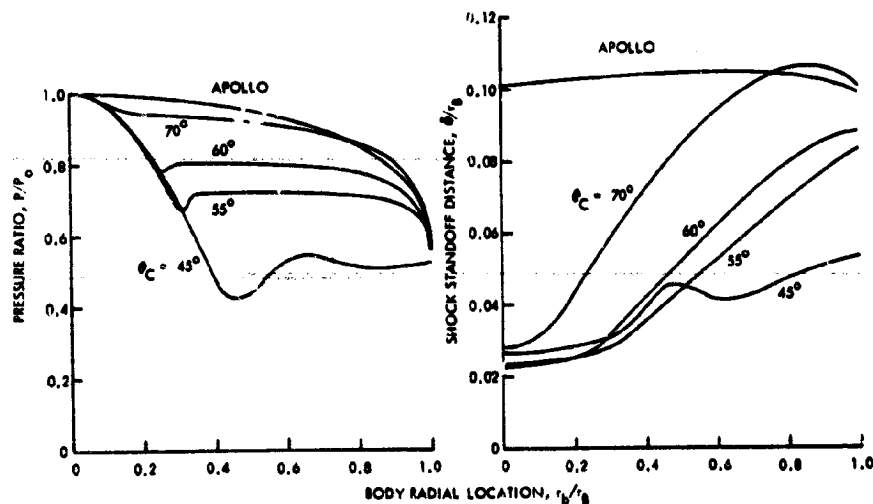


Figure 7.1-20. Comparisons of Inviscid Analysis Results for Several Configurations

Convective heating and shear stress have been obtained with the computer program SHIV. It is important to note that the effects of bow shock induced vorticity are included in the formulation. The stagnation point heating is from the correlation of Hoshizaki, the laminar heating distribution is that described by Lees, the turbulent heating procedure is that of

Bromberg, Fox, and Ackermann, with the wall shear stress found from the modified Reynolds analogy. For the lower entry velocity cases, transition was assumed to be instantaneous at a laminar momentum thickness Reynolds number of 250. For the 1978 launch cases, a transitional heating region was included with the start of transition determined from a momentum thickness Reynolds number/boundary layer edge Mach number correlation.

In calculating the radiation environment, initially the radiative heat flux to the wall from an isothermal, constant pressure slab was determined. The temperature and pressure of the slab at each body location were taken to be the local boundary layer edge values and its thickness equal to that determined in the inviscid analysis. This procedure approximately accounts for the entropy layer effect at locations away from the stagnation point. Nonadiabatic effects are then included by multiplying the slab results by a radiation cooling factor. The effect of ablation products in reducing the radiative heat flux to the wall was ignored because of the modest mass loss rates encountered with the present entry conditions.

No specific analysis of the base region was made. As discussed in Appendix 7.1A, the base heating environment was defined as a fraction of the cone environment immediately preceding the aft corner. This was done recognizing the close relation between the cone and base flow, in particular, regarding transition and turbulence. For flat base probes, the fraction specified was 0.03 of the sum of cone convective and radiative heating. For boat-tailed probes the fraction was taken to be 0.05.

7.1.7.2 Environmental Results

Atlas/Centaur '78 Mission

Results for the preferred Atlas/Centaur configurations with the 1978 launch entry velocity are depicted in Figures 7.1-21 through 7.1-25. The convective and radiative cold wall, no-blowing heating rate histories for the large probe at the nominal entry angle of -35 degrees are given in Figure 7.1-21 for two body locations. Transition occurs for the cone location shown near the time of peak stagnation point heating and leads to peak convective heating rates of nearly 40 MW/m^2 . Stagnation point convective and radiative heating maximize at about 19 and 11.3 MW/m^2 , respectively. Although not depicted, the maximum no-blowing wall shear

stress (the value to be simulated in materials tests) during the trajectory is about 2.9 kN/m^2 . The maximum convective and radiative heating rates and shear stress experienced by each of the probes as well as the maximum stagnation pressure are given in Tables 7.1-1 and 7.1-2.

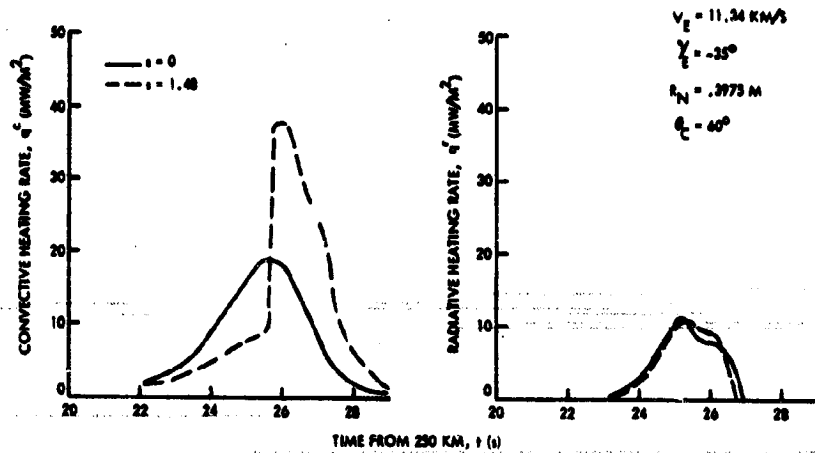


Figure 7.1-21. Atlas/Centaur Large Probe Cold Wall No-Blowing Convective and Radiative Heating Rates

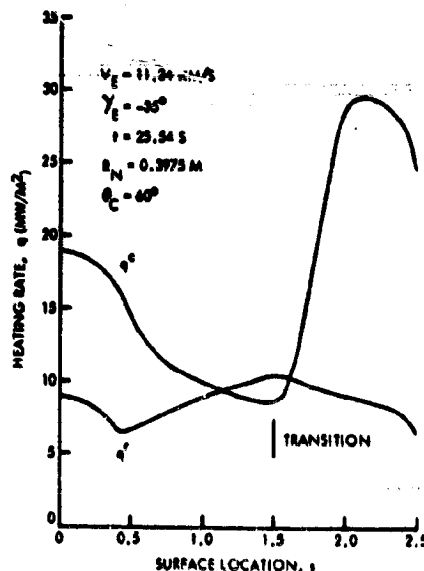


Figure 7.1-22. Distribution of Cold Wall No-Blowing Convective and Radiative Heating Rates on the Atlas/Centaur Large Probe

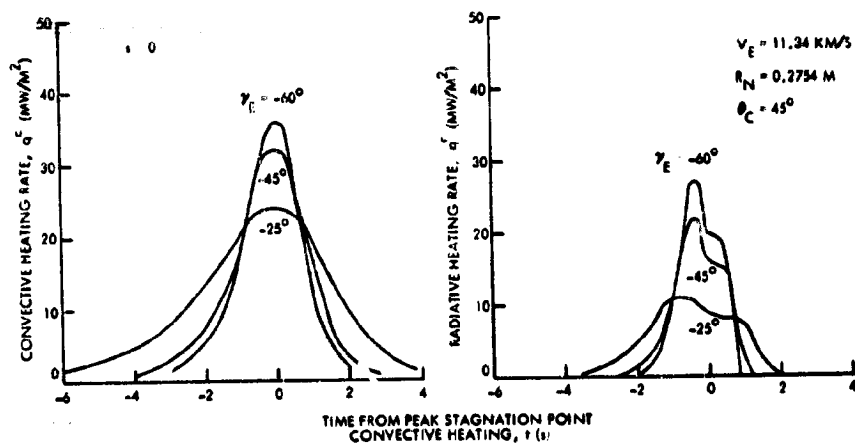


Figure 7.1-23. Effect of Entry Angle on the Atlas/Centaur Small Probe Cold Wall No-Blowing Stagnation Point Convective and Radiative Heating Rate

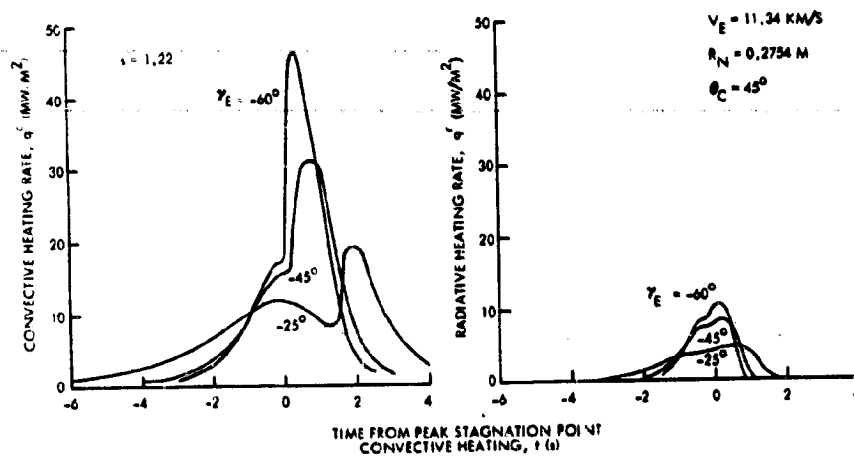


Figure 7.1-24. Effect of Entry Angle on the Atlas/Centaur Small Probe Cold Wall No-Blowing Off-Stagnation Convective and Radiative Heating Rates

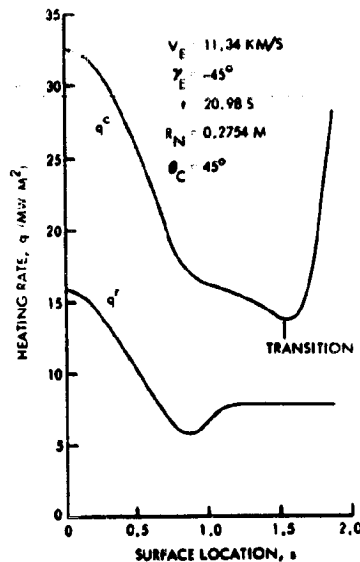


Figure 7.1-25. Distribution of Cold Wall No-Blowing Convective and Radiative Heating Rates on the Atlas/Centaur Small Probe

The double peak evident in the radiative heating pulse in Figure 7.1-22 is caused by the changing chemical composition of the shock layer. Early in the trajectory, the shock layer gas is at high temperature and low pressure, leading to large populations of atomic and ionized species. A large fraction of the radiation is from atomic line and continuum processes. As the probe decelerates, the pressure continues to rise and the temperatures drop, leading to an increase in the molecular population and the associated radiation. For the particular trajectories of interest, this transition in radiation processes occurs near the time of peak heating. Note that maximum radiative values for both locations shown occur at the first peak.

The distribution of both convective and radiative heating rates over the large probe is shown in Figure 7.1-22. At the particular time chosen, i. e., at peak stagnation point convective heating, the transition location is at the 60 percent surface location and is moving forward on the body. The radiation distribution displays two maxima. At the stagnation point the high temperature leads to high radiative heating despite the thin shock layer. With a nearly constant shock layer thickness on the spherical section (Figure 7.1-20), the radiation drops off as the flow expands and

cools. With the relatively constant temperature on the cone section, however, the radiative heat flux increases along the cone as the shock layer thickens. After transition the effective radiating temperature lowers as the entropy layer is entrained. This effect, combined with the drop in pressure along the body, serves to decrease the radiation.

The effect of the entry angle on the stagnation point convective and radiative heating rates for the preferred small probe configuration is shown in Figure 7.1-23 with similar results for a cone location in Figure 7.1-24. The peak radiative and convective heating rates increase and the total convective heating decreases with increasing entry angle as expected. However, because of the extreme sensitivity of the radiative heating to velocity at any given altitude, integrated radiative heating may increase with increasing entry angle. Of importance on the cone is the effectively earlier time of transition as the entry angle increases. The maximum convective heating and shear stress occur after transition. Note that maximum radiative results for the stagnation point occur at the first radiative peak, but at the second peak for the cone location. Thus, atomic line and continuum processes dominate in the stagnation region, but molecular band radiation dominates on the cone with the lower temperatures.

The heating rate distribution for the small probe near the time of peak stagnation point convective heating for $\gamma_E = -45$ degrees is depicted in Figure 7.1-25. Because of the smaller scale and lower cone angle of the small probe bodies, their entry environment is dominated by convective processes. At the time for which results are shown, transition has just occurred on the body and maximum heating rates have not yet been experienced. In contrast to the large probe, the maximum radiative heating occurs at the stagnation point and the radiation level is approximately constant on the conical section. This reflects the lower temperatures and shock layer thicknesses associated with lower angle cones.

Although the heating histories are not presented, Table 7.1-1 indicates the additional calculations made in selecting a preferred configuration for the 1978 Atlas/Centaur probes. Of particular interest are the results for a shape common to both the large and small probes, i.e., a cone angle of 55 degrees and a nose-to-base radius ratio of 1.725, cases 3 and 10. Comparing the maximum heating and shear results in Table 7.1-1

for the preferred and common large probe (cases 2 and 8), it is seen that the most significant effect is the 30-percent increase in shear stress for the 55-degree sphere cone. In addition, similar results are seen for the small probe, i.e., comparing cases 8 and 10, the small common probe experiences a maximum shear stress and convective heating rate increase of over 50 and 35 percent above the preferred small probe configuration, this despite a smaller ballistic coefficient. The main cause of these effects is the small nose radius required to obtain the necessary base-to-nose radius ratio for commonality with the large probe. With this constraint relaxed and the nose radius allowed to increase to the preferred configuration value, the results for case 11 are obtained. No significant differences between the maximum environment values for cases 8 and 11 are noted.

Atlas/Centaur '77 Mission

For the 1977 Atlas/Centaur mission, the cold wall, no-blowing entry heating environments have been calculated for the three large probe configurations shown in Table 7.1-1. A single trajectory was considered. The convective and radiative heating histories of the three probes for the stagnation point and an off-stagnation point location are shown respectively in Figures 7.1-26 and 7.1-27. The nose radii differences account for the stagnation point heating variations between the configurations with an increase in nose radius decreasing the convective and increasing the radiative heating. The higher boundary layer edge velocities on the 55-degree sphere cone lead to earlier transition and a much higher convective heating rate than for the other two configurations at the off-stagnation locations shown. Correspondingly, the lower temperatures reduce the radiative heating component for the more slender bodies.

Thor/Delta '77 Mission

For the Thor/Delta mission, cold wall, no-blowing entry heating environments for a number of trajectory combinations for three large probe geometries and two for the small probe have been calculated. Sphere cones of 60 and 70 degrees and the Apollo shape have been analyzed for the large probe; a 45-degree sphere cone and the Apollo shape for the small probe. The trajectory conditions considered for each configuration are noted in Table 7.1-2.

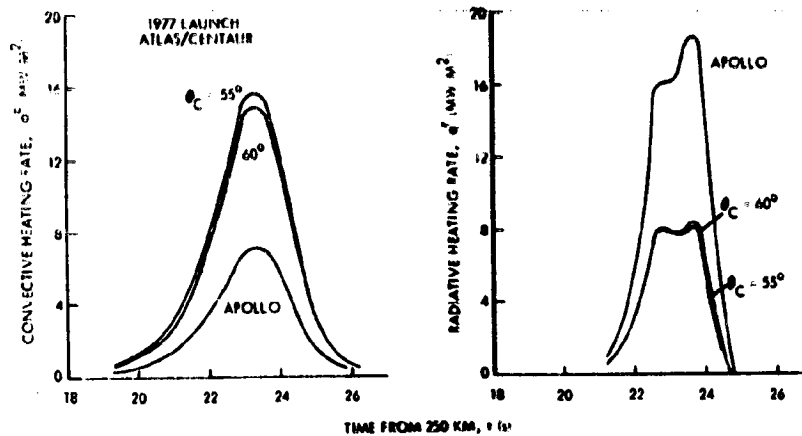


Figure 7.1-26. Effect of Configuration on the Large Probe Cold Wall No-Blowing Convective and Radiative Stagnation Point Heating Rate

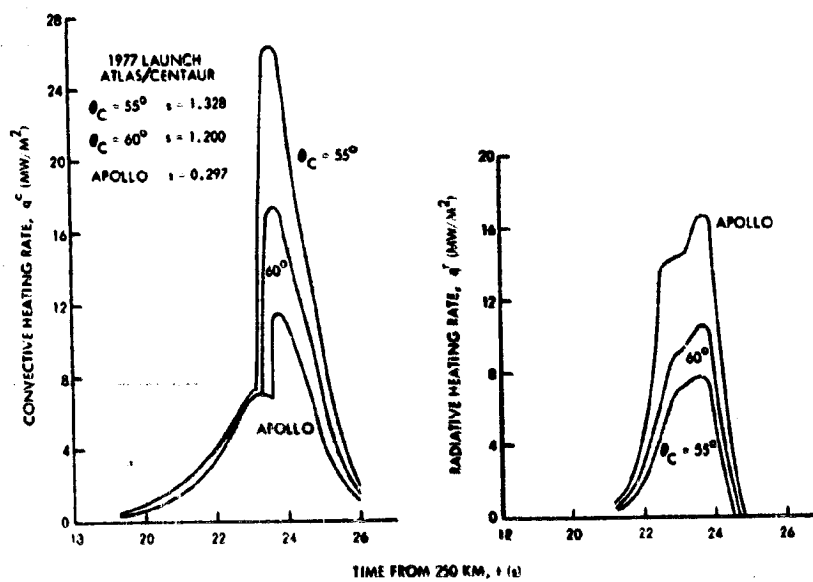


Figure 7.1-27. Effect of Configuration on the Large Probe Cold Wall No-Blowing Convective and Radiative Off-Stagnation Point Heating Rate

Large probe convective and radiative heating results are shown in Figures 7.1-28 and 7.1-29 where results for both the stagnation point and a selected off-stagnation point location are shown respectively. The 60-degree sphere cone experiences the highest stagnation point convective heating followed by the 70-degree sphere cone and Apollo shape. This results since the Apollo nose radius is much larger than that for the 60- and 70-degree sphere cones and the 70-degree sphere cone stagnation point velocity gradient is reduced from that for the 60-degree body because of the influence of the entirely subsonic forebody. The stagnation point shock standoff distance variation between geometries accounts for the radiative heating differences. The transition order for the three bodies is 60- and 70-degree sphere cones and then the Apollo shape. This order is due primarily to the higher boundary layer edge velocities and thus higher Reynolds numbers associated with more slender bodies. Note that for both body locations depicted, the maximum radiation occurs during the second peak. This is in contrast to the results for the 1978 launch and reflects the generally lower temperatures encountered in the 1977 launch.

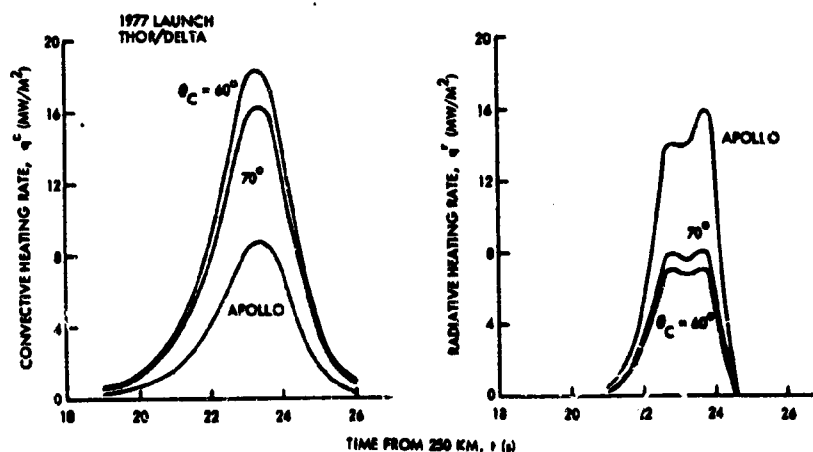


Figure 7.1-28. Effect of Configuration on the Large Probe Cold Wall No-Blowing Convective and Radiative Stagnation Point Heating Rate

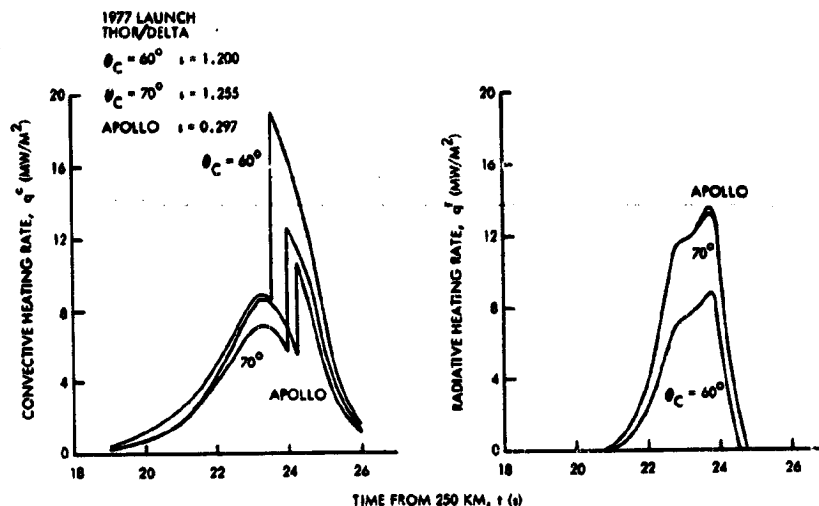


Figure 7.1-29. Effect of Configuration on the Large Probe Cold Wall No-Blowing Convective and Radiative Off-Stagnation Point Heating Rate

Entry heating results for the small probe are shown in Figures 7.1-30 and 7.1-31. The effect of entry angle is depicted for the 45-degree sphere cone at the stagnation point and an aft body location, respectively. The expected increase in peak rates as the trajectory steepens is apparent. A second small probe configuration was also considered at the lowest entry angle, 20 degrees. These results are also shown in the two illustrations. Boundary layer transition did not occur at the off-stagnation location for this blunt configuration; however, transition time is most important for the 45-degree sphere cone, with effectively earlier transition times as the entry angle is increased. Because of the smaller scale of the small probe bodies and low cone angle for the sphere cone, the entry environment is dominated by the convective heating.

From Tables 7.1-1 and 7.1-2 it is seen that the most critical entry environment experienced by the probes for either the 1977 or 1978 launch is the turbulent shear stress encountered on the small probe. This parameter is critical to selection of the heat shield material. The maximum value attained for the preferred configuration (45-degree sphere cone) is 6.0 kN/m^2 for the 1978 Atlas/Centaur mission at an entry angle of -60 degrees.

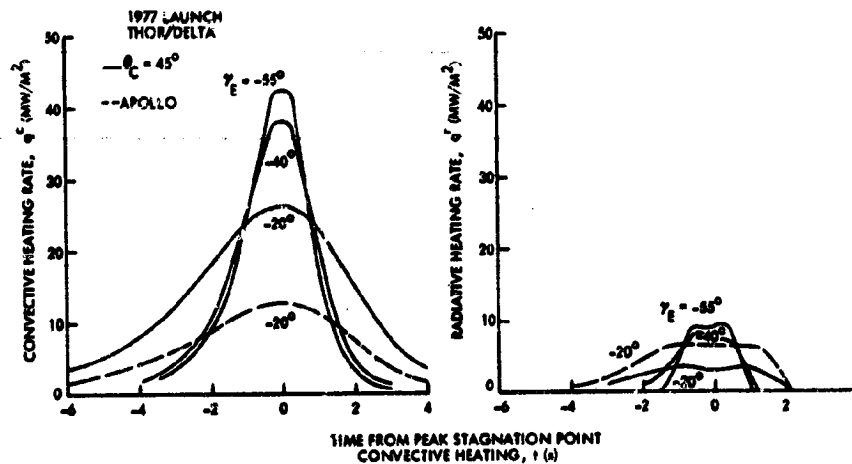


Figure 7.1-30. Effect of Entry Angle on the Small Probe Cold Wall No-Blowing Convective and Radiative Stagnation Point Heating Rate

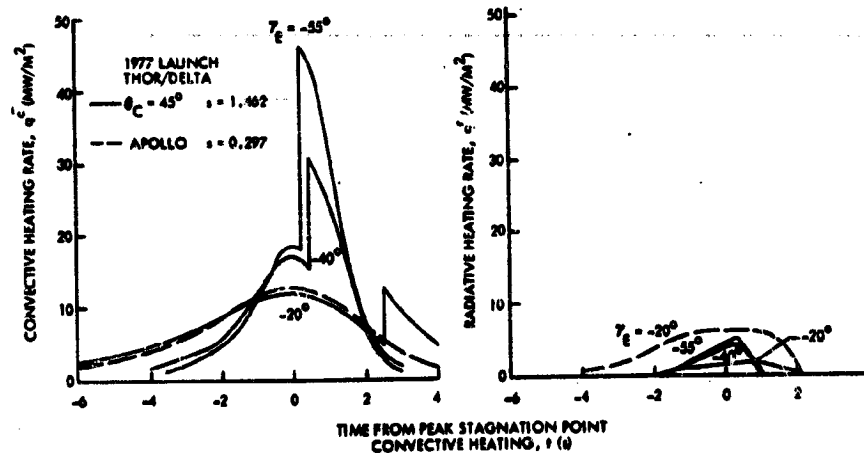


Figure 7.1-31. Effect of Entry Angle on the Small Probe Cold Wall No-Blowing Convective and Radiative Off-Stagnation Point Heating Rate

To aid in the evaluation of the reflecting, ablating heat shield, a spectral distribution of the radiative flux is required. Results from such a calculation for the Thor/Delta large probe 60-degree sphere cone are depicted in Figure 7.1-32. Shown is the spectral distribution of the continuum and molecular band transitions at three times near peak heating. The results are from the stagnation point isothermal slab analysis and do not include the cooling factor correction. The times shown bracket the period mentioned earlier where the chemical makeup of the shock layer is changing. The corrections for atomic line radiation to the total are 45, 16, and 4 percent, respectively, for the three times shown, indicating the increasing dominance of the molecular processes through the trajectory. Examination of the illustration shows a shift in radiation to the lower frequencies as the probe enters.

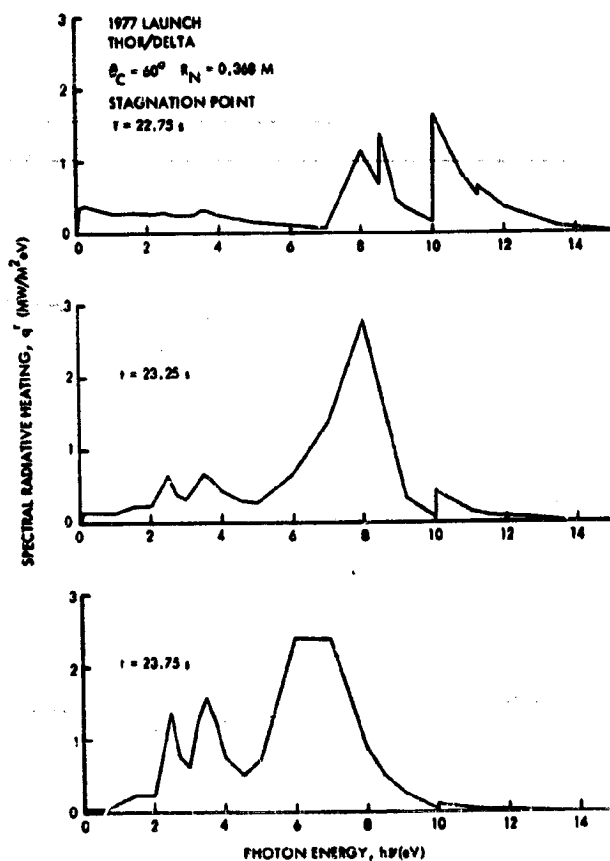


Figure 7.1-32. Spectral Distribution of the Continuum Processes and Molecular Band Radiative Heating

7.1.7.3 Heating Correlations

With the wide range of entry parameters considered in the study, the results lend themselves to correlation in terms of nose radius, R_N , ballistic coefficient, β , entry angle, γ_E and cone angle, θ_c . In particular, the maximum stagnation point convective heating rate, q_{om}^c , radiative heating rate, q_{om}^r and the maximum cone radiative heating rate, q_{cm}^r , were successfully correlated. The proper convective stagnation point parameters and powers are of course known and the following correlation was obtained;

$$q_{om}^c = K_o^c \left(\frac{\beta \sin \gamma_E}{R_N} \right)^{1/2}$$

with

$$\begin{aligned} K_o^c &= 1.54 \text{ (1977 launch)} \\ &= 1.71 \text{ (1978 launch)} \end{aligned}$$

For the maximum stagnation point radiative heating rate

$$q_{om}^r = K_o^r R_N^{0.497} (\beta \sin \gamma_E)^{1.18}$$

with

$$\begin{aligned} K_o^r &= 0.115 \text{ (1977 launch)} \\ &= 0.175 \text{ (1978 launch)} \end{aligned}$$

For the maximum cone radiative heating rate we obtained:

$$q_{cm}^r = K_c^r R_N^{0.497} (\beta \sin \gamma_E)^{1.18}$$

with

$$\begin{aligned} K_c^r &= 0.272 \text{ (1977 launch)} \\ &= 0.325 \text{ (1978 launch)} \end{aligned}$$

With one exception these correlations provided results well within 10 percent of the calculated values. The exception was the 70-degree sphere cone where the influence of the entirely subsonic forebody; leads to a lower stagnation point velocity gradient but larger standoff distance. Thus, the correlation overpredict the convective and underpredict the

radiative heating rates. The stagnation point convective and radiative heating rates as calculated by LRC (Appendix 7.1A) also fell well within a 10 percent error band. Note the large effect of cone angle on cone radiative heating. Increasing the cone angle from 45 to 55 degrees with other parameters remaining the same, increases the cone radiative heating by over 95 percent. The effect of entry velocity can be estimated by ratioing the coefficients K. The 1978 launch raises the stagnation point convective and radiative heating rates and the cone radiative heating rate by 11, 52, and 19 percent, respectively.

NOMENCLATURE

B	ballistic coefficient
c. g.	center of gravity
C_A	axial force coefficient
C_D	drag coefficient
C_L	lift coefficient
C_{L_α}	lift curve slope
C_m	pitching moment coefficient
C_{m_α}	pitching moment slope
$C_{m_q} + C_{m_{\dot{\alpha}}}$	pitch damping coefficient, $\frac{\partial C_m}{\partial \left(\frac{\dot{\theta} d}{2V}\right)} + \frac{\partial C_m}{\partial \left(\frac{\dot{\alpha} d}{2V}\right)}$
C_N	normal force coefficient
d, D	diameter
I_x, I_y, I_z	moment of inertia about roll, pitch and yaw axes, respectively
m	mass
M	Mach number
q	dynamic pressure
q_m^c	maximum convective heating
q_m^r	maximum radiative heating
R_e	Reynolds number

R_B	radius at base of cone
R_N	nose radius
S	maximum cross sectional area
V	velocity
x_{cp}	distance from c. g. to center of pressure
α	angle of attack
β	angle of sideslip
γ_E	flight path angle at entry
$\dot{\theta}$	pitch rate
θ_c	semi-angle of cone
σ	radius of gyration in pitch
τ_m	maximum shear stress

REFERENCES

1. R. I. Sammonds, "Dynamics of High-Drag Probe Shapes at Transonic Speeds," NASA TN D-6489 (September 1971).
2. Wayne J. Marko, "Transonic Dynamic and Static Stability Characteristics of Three Blunt-Cone Planetary Entry Shapes," JPL TR32-1357 (September 1969).
3. L. E. Ericsson and J. P. Reding, "Reentry Capsule Dynamics," J. Spacecraft (June 1971).
4. R. J. Bendura and C. H. Whitlock, "Preliminary Results of Low Subsonic Dynamic Stability Tests of Three Blunted 55 degree Half-Angle Cone Configurations with Various Afterbodies." Paper presented at Third Technical Workshop on Dynamic Stability Problems, Moffet Field, California (November 1968).
5. M. V. Krumins, "Drag and Stability of Mars Probe/Lander Shapes," J. Spacecraft (August 1967).
6. F. W. Gibson and James E. Carter, "Free-Flight Measurements of Dynamic Stability Derivatives of a Blunted 120 degree cone in Helium at Mach Number 15.4," NASA TM X-207 (October 1970).
7. B. L. Uselton, T. O. Shadow and A. C. Mansfield, "Damping-in-Pitch Derivatives of 120- and 140-degree. Blunted Cones at Mach Numbers from 0.6 through 3," AEDC-TR-70-49 (April 1970).

8. B. L. Uselton and A. R. Wallace, "Damping-in-Pitch and Drag Characteristics of the Viking Configuration at Mach Numbers from 1.6 through 3," AEDC-TR-72-56 (May 1972).
9. B. J. Short, "Dynamic Flight Behavior of a Ballasted Sphere at Mach Numbers from 0.4 to 14.5," NASA TN D-4198 (October 1967).
10. J. E. Marte and R. W. Weaver, "Low-Subsonic Dynamic Stability Investigation of Several Planetary-Entry Configurations in a Vertical Wind Tunnel - Parts I and II," JPL TR-32-743 (May 1965).
11. T. J. Coakley, "Dynamic Stability of Symmetric Spinning Missiles," AIAA J. Spacecraft (October 1968).
12. J. P. Billingsley and W. S. Norman, "Relationship Between Local and Effective Aerodynamic Pitch - Damping Derivatives as Measured by a Forced-Oscillation Balance for Preliminary Viking Configurations," AEDCTR-72-25 (May 1972).
13. B. Walker and R. W. Weaver, "Static Aerodynamic Characteristics of Blunted Cones in the Mach-Number Range from 2.2 to 9.5," JPL TR-32-1213 (December 1967).
14. W. J. Marko, "Static Aerodynamic Characteristics of Three Blunted Sixty-Degree Half-Angle Cones at Mach Numbers from 0.60 to 1.30," HPL TR-32-1298 (July 1968).
15. R. V. Owens, "Aerodynamic Characteristics of Spherically Blunted Cones at Mach Numbers from 0.5 to 5.0," NASA TN-D-3088 (December 1965).
16. J. O. Nichols and E. A. Nierengarten, "Aerodynamic Characteristics of Blunt Bodies," JPL TR-32-677 (November 1964).
17. J. F. Campbell, "Longitudinal Aerodynamics Characteristics of Several High-Drag Bodies at Mach Numbers from 1.50 to 4.63," NASA-TN-D-3915 (April 1967).
18. Charles D. Harris, "Transonic Aerodynamic Investigation of Tension Shell and Blunted 100 degree Conical Shapes for Unmanned Entry Vehicles," NASA TN-D-3700 (November 1966).
19. D. L. Shirley and J. E. Misselhorn, "Instability of High-Drag Planetary Entry Vehicles at Subsonic Speeds," AIAA J. Spacecraft (October 1968).
20. C. H. Murphy, "Free Flight Motion of Symmetric Missiles," BRL Report 1216 (July 1963).
21. N. Tetervin, "Theoretical Distribution of Laminar-Boundary-Layer Thickness, Boundary-Layer Reynolds Number and Stability Limit, and Roughness Reynolds Number for a Sphere and Disk in Incompressible Flow," NACA TN 4350 (September 1958).

7.2 Heat Shield

7.2 HEAT SHIELD

7.2.1 Introduction

Venus entry is significantly different from entry into the Earth's atmosphere as experienced to date. The mission requires high entry angles which, coupled with the high entry velocity and blunt configuration, result in substantial radiant heating (on the order of 20 percent of the total cold wall nonablating heat input and up to 40 percent of peak total heating rate). In addition, turbulent flow and high viscous shear exist over a substantial fraction of the entry body. Despite this unique combination of entry conditions, conventional heat shield materials and fabrication techniques are applicable to the Pioneer Venus heat shield system.

With the greater weight capability of the Atlas/Centaur configuration, cost savings relative to the Thor/Delta heat shield program can be achieved by selecting ablative materials which, although not weight optimized, do have high performance reliability and flight history. This allows reducing the scope of tests in the design-development and qualification, as well as reducing tests by specifying a single material for the forebody instead of tailoring the material to the environment distribution. The heat shield system selected for the Atlas/Centaur entry probes is composed of ablative materials that have been developed through years of ground and flight tests. Figure 7.2-1 shows the general configuration, thicknesses, and weights.

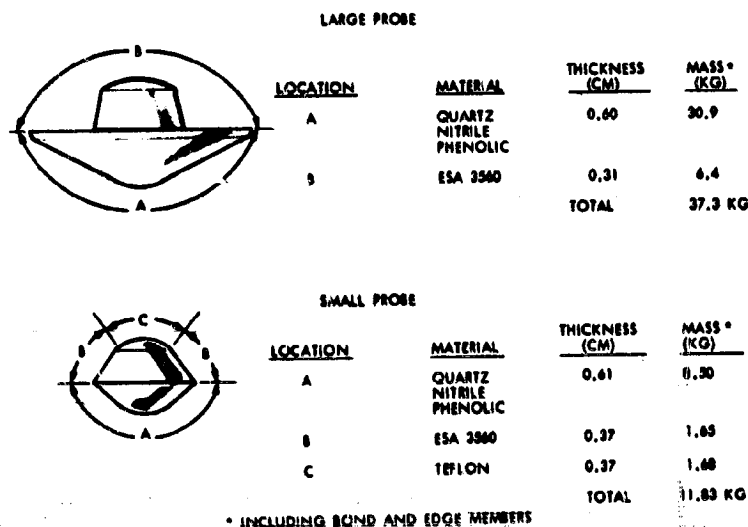


Figure 7.2-1. Atlas/Centaur '78 Heat Shield Configuration

Quartz nitrile phenolic, which is derived from the silica nitrile phenolics and quartz phenolic flight proven on the Sprint interceptor missile, has been selected for the forebody of both the large and small probes. For the afterbody regions of both probes, which are exposed to much lower heating conditions than the forebody, an elastomeric silicone material, ESA 3560, has been selected. This MMC proprietary material has been flight proven on the Air Force PRIME and NASA/Ames PAET reentry vehicles and will be flown on the Viking entry probe. Due to stringent attenuation requirements, the preferred antenna radome ablator for the small probe will be TFE Teflon, which has been flight proven on numerous entry systems. ESA 3560 is used on the large probe radome since this material is RF transparent prior to entry heating and the radome will be removed before transmission of data begins after entry. This results in a lower cost and lighter large probe radome heat shield design than a material such as TFE Teflon permits.

7.2.2 Requirements

The heat shield subsystem for the entry probes is attached to and supported by the aeroshell. It must provide protection from the aerothermal heating environment during entry. The heat shield must accommodate penetrations such as science sensors, engineering measurements sensors, electrical and mechanical attachment penetrations, and covers.

The material selection and design thicknesses are derived from detailed entry ablation analyses, based on the entry environment described in Section 7.1. The temperature limits of the ablator-structure interface used in defining the heat shield thicknesses and weights are summarized in Table 7.2-1. The RF attenuation of the heat shield and supporting structure protecting the antenna should not exceed 0.2 dB. The ablation of the heat shield material should provide an even mass loss and surface erosion so as not to cause significant perturbations in the aerodynamic characteristics. Special consideration has to be given to the heat shield, as well as to thermal control and science sensor design, to control outgassing to avoid contamination of the science sensors. In addition, the selected heat shield subsystem must have a storage life capability of 36 months, must be on-site repairable, and use known, reliable fabrication and bonding techniques which can be tested by nondestructive techniques.

Table 7.2-1. Heat Shield Design
Limit Temperatures

	ATLAS/CENTAUR LIMIT BONDLINE TEMPERATURE (°K) (°F)		THOR/DELTA LIMIT BONDLINE TEMPERATURE (°K) (°F)	
LARGE PROBE FOREBODY AEROSHELL	422	300	422	300
$P_{STAG} > 1 \times 10^5 \text{ N/M}^2$	542	515	584	600
$P_{STAG} < 1 \times 10^5 \text{ N/M}^2$				
LARGE PROBE AFTERBODY	422	300	581	600
SMALL PROBE FOREBODY AEROSHELL				
$P_{STAG} > 1 \times 10^5 \text{ N/M}^2$	478	400	422	300
$P_{STAG} < 1 \times 10^5 \text{ N/M}^2$	756	900	756	900
SMALL PROBE AFTERBODY PRIOR TO INSTRUMENT DEPLOY- MENT	422	300	422	300
SMALL PROBE AFTERBODY AFTER INSTRUMENT DEPLOY- MENT	756	900	756	900

7.2.3 Trades

7.2.3.1 Analytical Evaluation of Heat Shield Materials

The Pioneer Venus heat shield materials were analyzed using T-CAP III, an explicit finite difference digital thermo-chemical ablation program. Reflecting ablative materials were analyzed with a modified version of T-CAP III, dubbed RADSCAT. In this program, Kubelka-Munk radiation scattering theory is coupled with the basic ablator program. The radiant energy absorbed by each thermal element is combined with the enthalpy transitions due to temperature changes, pyrolysis reactions, and transpiring pyrolysis vapors to determine the heat shield thermal conduction and internal temperature response. Transmission and reflection are included as boundary conditions on the outer surface of the ablator and at the ablator-substructure interface. A detailed description of the RADSCAT version of the T-CAP III is presented in Appendix 7.2A.

The analytical models consisted of finite ablator slabs of varying thicknesses over the structural skin construction representative of several locations on the forebody and afterbody.

A number of materials were considered for use on the forebody of the entry probes, the primary candidates being:

<u>Material</u>	<u>Density (g/cm³)</u>	<u>Construction</u>
ESA 5500 M3	1.14	Carbon fiber reinforced silicone resin
Quartz Nitrile Phenolic	1.55	Astroquartz cloth reinforced butadiene acrylonitrile modified phenyl silane resin.
Carbon Phenolic	1.46	Carbon cloth reinforced phenolic resin.
TFE Teflon	2.15	Unfilled polytetrafluoroethylene resin.

The calculated unit weights of the candidate heat shield materials in a typical large probe entry are shown in Figure 7.2-2. These unit weights were computed for a point on the cone of the large probe at $r/r_b \sim 0.7$, for the following entry conditions:

$$\gamma_E \sim 40 \text{ deg}$$

$$\gamma_E \sim 11.16 \text{ km/s}$$

$$\beta \sim 78.54 \text{ kg/m}^2$$

The unit weights shown for carbon phenolic and Teflon were taken from preliminary data *. Martin Marietta calculations confirm these data.

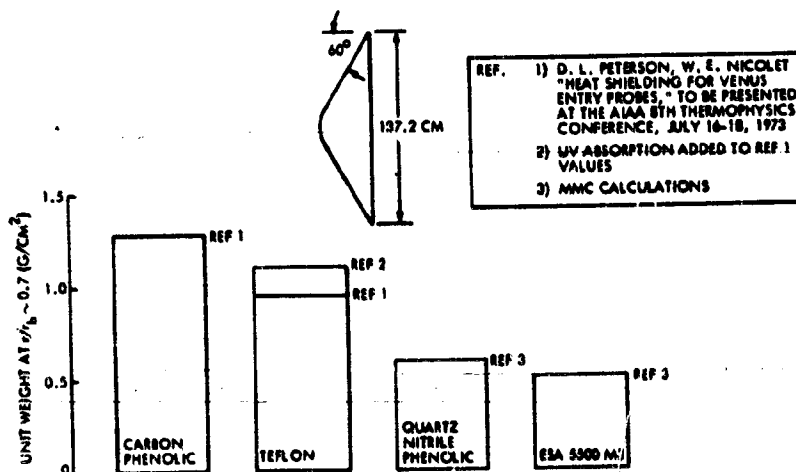


Figure 7.2-2. Thor/Delta Large Probe Calculated Heat Shield Material Comparison

*D. L. Peterson, W. E. Nicolet, "Heat Shielding for Venus Entry Probes," to be presented at the AIAA 8th Thermophysics Conference, July 16-18, 1973.

Carbon phenolic is an inefficient ablator for Venus entry, due to its high thermal conductivity. A high unit weight of Teflon is also required due to its low heat of sublimation and resultant high mass loss. The calculations of Peterson and Nicolet assumed total reflection of incident radiation by Teflon, while the slightly higher unit weights which we have computed indicate the increase in weight required to accommodate the absorption of the vacuum UV radiation by the Teflon. Additional analyses of the performance of Teflon as a reflecting ablator are presented in Appendix 7.2A.

Quartz nitrile phenolic has good performance due to its low thermal conductivity and high heat of sublimation; however, it is 20 to 35 percent heavier than ESA 5500 M3. ESA 5500 M3 performs well as a result of its low conductivity, high surface temperature (high reradiation), and good convective blocking.

For the small probe, the relative heat shield unit weights are consistent with large probe calculations, as shown in Figure 7.2-3. These calculations were for a point on the cone at $r/r_b \sim 0.7$ for a shallow entry at the following conditions:

$$\gamma_E \sim 25 \text{ deg}$$

$$\gamma_E \sim 11.16 \text{ km/s}$$

$$\beta \sim 125.7 \text{ kg/m}^2$$

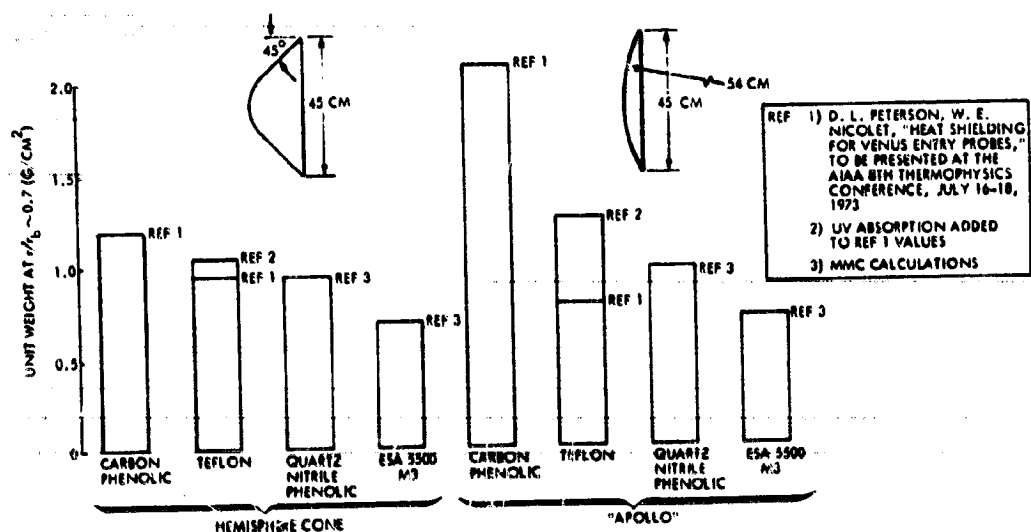


Figure 7.2-3. Thor/Della Small Probe: Calculated Heat Shield Material Comparison

A comparison is made in Figure 7.2-3 between a blunter, Apollo shape entry vehicle and the baseline 45-degree small probe sphere-cone configuration. For the blunter entry vehicle, the high conductivity of the carbon phenolic again results in very high heat shield unit weight. Teflon's performance, if a perfect reflector, is improved by the blunter Apollo shape, which reduces the convective input but significantly increases the radiation. When absorption of the vacuum UV radiation is included, the efficiency of Teflon is reduced by the blunter entry shape. Quartz nitrile phenolic and ESA 5500 M3 are fairly insensitive to entry shape.

With respect to reflective ablators other than Teflon, attempts to date to improve their reflectance have only been marginally successful. Analyses and experiments indicate that a very high purity silica reflective ablator will be the most efficient in high radiant heating. However, the analyses also show that for Venus entry, the reflective silica heat shield unit weights are significantly greater than for ESA 5500 M3 or quartz nitrile phenolic. A unit weight on the order of 2 g/cm^2 is required, compared to less than 1 g/cm^2 for quartz nitrile phenolic and ESA 5500 M3. The major problem with reflective ablators in Venus entry is the high fraction of vacuum UV, which is predicted to reach the ablator surface and be absorbed rather than reflected.

7.2.3.2 Experimental Evaluation of Candidate Materials

A large number of tests were conducted on the candidate heat shield materials for Venus entry with major emphasis on the higher density charring ablatives. All of these tests were designed to explore a particular aspect of the entry environment incurred on the entry probes. Table 7.2-2 summarizes the plasma arc tests conducted over the past 18 months. The tests in Ames Research Center's AEHS facility provide the best simulation of combined radiation and convective heating in the stagnation region, while the best simulation for cone regions is achieved in a shear-type test with radiant heating added. Consequently a 5-MW constricted arc shear-radiation facility, designed specifically for Venus entry simulation, has recently been activated at Martin Marietta and is being used to test the candidate materials.

Table 7.2-2. Test Summary of Heat Shield Materials Screening

MATERIALS	FACILITY	RANGE OF CONDITIONS	NUMBER OF MODELS	WHEN TESTED
M3, CP, CNP, SP, QP, QNP, M10, TFE	MMC 50 KW RAD SOURCE	800 - 1700 W/CM ² RAD 1 X 10 ⁵ N/M ² PRESSURE	81	SEPT - DEC 1971
M3, CP, CNP, QNP, M10, TFE, 104	MMC COMBINED SHEAR - RAD 1.5 MW	0 - 800 W/CM ² RAD 1500 W/CM ² CONV 2 - 3 X 10 ⁵ N/M ² PRESSURE 2800 - 4800 N/M ² SHEAR 4 - 7 MJ/KG ENTHALPY	91	JUNE - AUG 1972
M3, CP, QNP, TFE, 104, LDQNP	MMC COMBINED SHEAR - RAD 5 MW	0 - 1000 W/CM ² RAD 1000 - 4000 W/CM ² CONV 1 - 6 X 10 ⁵ N/M ² PRESSURE 2400 - 6000 N/M ² SHEAR 18 - 35 MJ/KG ENTHALPY	100	IN PROGRESS
M3, CP, QNP	MMC HIGH PRESSURE	800 - 1761 W/CM ² CONV 3 - 9 X 10 ⁵ N/M ² PRESSURE	23	MARCH 1972
M3, CP, QNP, TFE, FILLED TFE, 104	AMES AEHS	0 - 2000 W/CM ² RAD 1400 W/CM ² CONV 1 X 10 ⁵ N/M ² PRESSURE	46	NOV - DEC 1972
M3, CP, QNP, TFE, LDQNP	AMES HTT	3200 W/CM ² CONV 4 X 10 ⁵ N/M ² PRESSURE	24	MARCH 1973
MATERIALS GLOSSARY				
M3 - ESA 5500 M3	CP - CARBON PHENOLIC	CNP - CARBON NITRILE PHENOLIC	SP - SILICA PHENOLIC	QP - QUARTZ PHENOLIC
				LDQNP - LOW DENSITY QUARTZ
				QNP - QUARTZ NITRILE PHENOLIC
				M10 - ESA 5500 M10
				TFE - TEFLON
				104 - DC 93 - 104
				FILLED - TEFLON FILLED WITH PIGMENTS

Figures 7.2-4 and 7.2-5 compare the results of tests in several test configurations, including stagnation convective, stagnation convective combined with radiant, convective shear, and convective shear combined with radiant. The data show similar relative backface temperature rise in all modes of test, and confirm the results of the analyses. For Teflon, most of the predominantly visible and near UV radiant energy from the inert gas radiant sources is reflected, but a significant fraction is still transmitted to raise the backface temperature. The high conductivity carbon phenolic conducts a significant fraction of the heat into the substructure, raising the backface temperature. Both quartz nitrile phenolic and ESA 5500 M3 exhibit efficient thermal performance. The thermochemical surface recession of the charring ablators is a small fraction of the thickness of the samples (as is predicted for Venus entry), and is not a primary consideration. On the other hand, resistance to high viscous shear and spallation is important to maintain uniform and controlled surface erosion.

TEST FACILITY	CONV (W/CM ²)	RAD (W/CM ²)	PRESSURE (N/M ²)	ENTHALPY (MJ/KG)	SHEAR (N/M ²)	TEST TIME (S)	ABLATOR WEIGHT (G/CM ²)	SUBSTRUCTURE
AMES AEHS, STAGNATION	1400	1150	1×10^5	23.0	0	2.7	1.15	0.24 CM ALUMINUM
MMC 5 MW SHEAR	1600	0	1.6×10^5	18.6	2700	3.0	0.86	5.1 CM ASBESTOS PHENOLIC

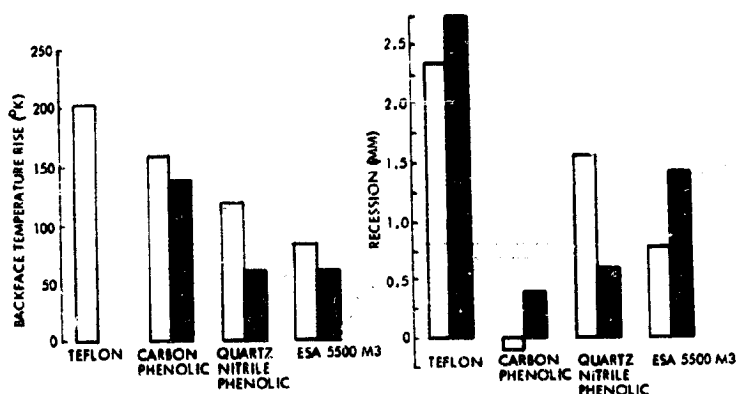


Figure 7.2-4. Heat Shield Material Tests, $q_{\text{Conv}} \sim 1500 \text{ W/CM}^2$

TEST FACILITY	CONV (W/CM ²)	RAD (W/CM ²)	PRESSURE (N/M ²)	ENTHALPY (MJ/KG)	SHEAR (N/M ²)	TEST TIME (S)	ABLATOR WEIGHT (G/CM ²)	SUBSTRUCTURE
AMES HIT, STAGNATION	3200	0	4×10^5	19	0	2	1.15	0.16 CM STAINLESS STEEL
MMC 5 MW SHEAR	3400	0	3×10^5	19	4600	2	0.86	5.1 CM ASBESTOS PHENOLIC
MMC 5 MW SHEAR, RADIATION	3400	800	3×10^5	10	4600	2	0.86	5.1 CM ASBESTOS PHENOLIC

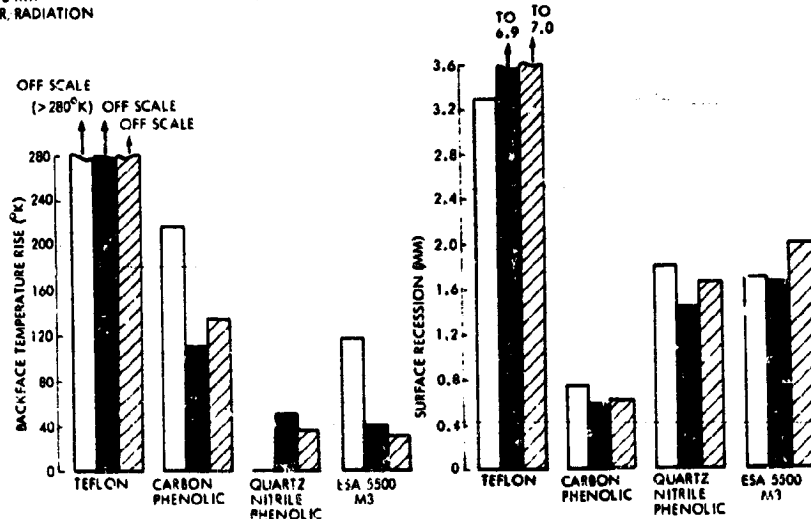


Figure 7.2-5. Heat Shield Material Tests, $q_{\text{Conv}} \sim 3300 \text{ W/cm}^2$

The best of the materials in appearance after test was the quartz nitrile phenolic, with a thin, uniform char layer, and no evidence of cracking or other thermal stress problems. ESA 5500 M3 and carbon phenolic both developed relatively thick char zones. ESA 5500 M3 did not recede as uniformly as quartz nitrile phenolic, with some evidence of spallation or shear erosion in some tests. Carbon phenolic receded uniformly, but exhibited cracks and swelling in the char zone in some tests. Teflon receded uniformly, but at a very high rate.

In summary, the tests to date show ESA 5500 M3 as the most efficient of the conventional reradiative ablators, with quartz nitrile phenolic as a close second. From test data and post-test appearance, quartz nitrile phenolic is the most reliable and repeatable ablator.

7.2.3.3 Heat Shield Test Costs Versus Ablator System and Design Margins

With the greater weight capability of the Atlas/Centaur configuration, cost savings relative to the Thor/Delta heat shield program can be achieved by selecting ablative materials which, although not weight optimized, do have high performance reliability and flight history. This not only allows reducing the scope of tests in the design-development and qualification, but permits specifying a single material of uniform thickness for the forebody, instead of tailoring the material and thickness to the environment distribution. The direct heat shield test cost savings are shown by comparing the preliminary test programs defined for the Atlas/Centaur and Thor/Delta configurations, (see Sections 7.2.4.5 and 7.2.5, respectively).

Over all, approximately 400 test samples are planned for the Atlas/Centaur probe heat shield system, versus approximately 650 for the Thor/Delta, a reduction of 40 percent in quantity of tests. Breakdown of tests costs indicate that the 40 percent reduction in number of tests results in approximately a 25 percent savings in test costs. These figures do not include reductions in the testing to support the determination of the aero-heating environment.

7.2.4 Preferred Heat Shield, Atlas/Centaur

The heat shield subsystem for both the large and small probes for the Atlas/Centaur are similar in configuration. Figure 7.2-1 presented the general configuration, design thicknesses, and weights.

7.2.4.1 Material Selection

With the greater weight capability of the Atlas/Centaur launch vehicle, cost savings are achieved by selecting a single material with proven reliability for the forebody. Use of a single material reduces the scope of tests required in the design-development, and qualification, at the expense of increased nominal weight. Still further reductions in the test program become possible due to the increased design margins provided. This is valid when the ablative material is well behaved (no catastrophic "step functions")

occur in its performance) as is the case with the selected material, quartz nitrile phenolic. Carbon reinforced ablators, on the contrary, are susceptible to mechanical erosion when certain limits (which are difficult to define except through extensive testing) are exceeded. Based upon available test data, the carbon-reinforced ESA 5500 M3 would accommodate the Pioneer Venus entry environment, and afford minimum weight design; however, an extensive test program would be required to qualify it, particularly for the more severe entry conditions and viscous shear of the 1978 mission.

In the tests discussed in Section 7.2.3, quartz nitrile phenolic has been shown to recede by sublimation. The high mass injection rate results in low net viscous shear at the wall. At the high heating of Venus entry, the melt layer is very thin, and when combined with the high viscosity of quartz and low net viscous shear at the wall, little or no melt flow occurs. Based upon its reliability and repeatability in plasma-arc tests, and the excellent performance of quartz phenolic and silica nitrile phenolics on the Sprint vehicle, quartz nitrile phenolic has been chosen as the ablative material for the forebody of the Atlas/Centaur large and small probes. Tests can be reduced to a minimum with this material, while maintaining a high confidence level in its performance.

7.2.4.2 Heat Shield Design

Extensive analyses were conducted to determine the nominal ablator thickness and the sensitivity of selected heat shield materials to structure design temperature, and uncertainties in entry conditions and material performance.

For the large probe, the selection of an aluminum aeroshell as the most cost effective and lightest structure for the forebody dictates that the ablator-aeroshell interface be maintained below 422°K during entry when the stagnation pressure exceeds $1 \times 10^5 \text{ N/m}^2$. Prior to aeroshell separation, and after the stagnation pressure decreases below $1 \times 10^5 \text{ N/m}^2$, the forebody critical load is the thermal stress in the aeroshell skin, and the ablator-aeroshell interface must be maintained below 542°K to prevent interframe buckling. On the large probe afterbody, the critical load/temperature occurs near parachute deployment when the structure temperature is near maximum and the base pressure is rising exponentially with time.

To prevent collapse of the base structure requires a limit temperature of 422°K .

The small probe maximum structural temperature is 478°K during entry when the stagnation pressure exceeds $1 \times 10^5 \text{ N/m}^2$. After the stagnation pressure decreases below $1 \times 10^5 \text{ N/m}^2$, the maximum small probe structure temperature on the forebody must not exceed 756°K , to prevent buckling of the aeroshell skin. As on the large probe afterbody, the small probe afterbody structure temperature rise due to entry heating must be maintained below 422°K to prevent collapse by the rapidly increasing base pressure. After instrument cover deployment vents the structure, however, the afterbody structure may go to 756°K .

The results of the parametric studies conducted to determine ablator thickness versus structure temperature limit for the Atlas/Centaur probes are shown in Figures 7.2-6 and 7.2-7. Table 7.2-3 summarizes the nominal thicknesses for the large and small probes. For the reradiative materials analyzed here, the highest temperature limit designed the ablator thickness on the forebody, due to the time lag between entry heating (and high stagnation pressure) and structure temperature response. The small probe afterbody heat shield, however, was designed by the 422°K limit due to the delay of instrument deployment until about 16 seconds after peak heating. Typical time varying structure temperature and surface recession response is shown in Figures 7.2-8 and 7.2-9.

$$\theta_c = 60^{\circ}; \gamma_c = -35^{\circ}; \beta = 90.72 \text{ KG/M}^2; V_c = 11.33 \text{ KM/S}$$

SYMBOL	ABLATOR	STRUCTURE (CM)	LOCATION	RECESSION (CM)
●	QUARTZ NITRILE PHENOLIC	0.127 ALUMINUM	STAG	0.16
■	QUARTZ NITRILE PHENOLIC	0.191 ALUMINUM	STAG	0.16
□	QUARTZ NITRILE PHENOLIC	0.203 ALUMINUM	CONE	0.28
△	QUARTZ NITRILE PHENOLIC	0.303 ALUMINUM	CONE EDGE	0.19
◇	ESA 3560	0.0635 POLYIMIDE	AFTERBODY	

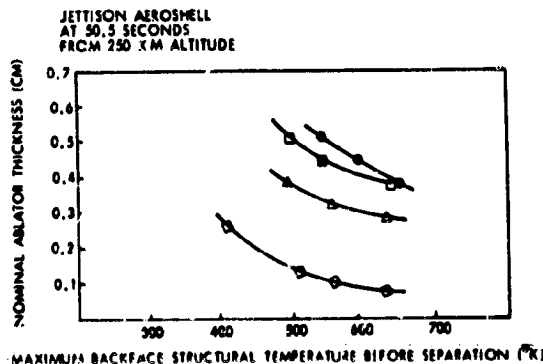


Figure 7.2-6, Atlas/Centaur 78 Large Probe Nominal Thickness Versus Structure Temperature

$\theta_c = 45^\circ$; $\gamma = -25^\circ$; $\beta = 141.4 \text{ KG/M}^2$; $V_\infty = 11.33 \text{ KM/S}$

SYMBOL	ABLATOR	STRUCTURE (CM)	LOCATION	RECESSION (CM)
●	QUARTZ NITRILE PHENOLIC	.0508 TITANIUM	STAG	0.29
■	QUARTZ NITRILE PHENOLIC	.1524 TITANIUM	STAG	0.29
□	QUARTZ NITRILE PHENOLIC	.0508 TITANIUM	CONE	0.16
◇	QUARTZ NITRILE PHENOLIC	.1524 TITANIUM	CONE EDGE	0.25
○	ESA 3560	.0635 TITANIUM	AFTERBODY	0.00
○	TEFLON	.1016 POLYIMIDE	RADOME	0.03

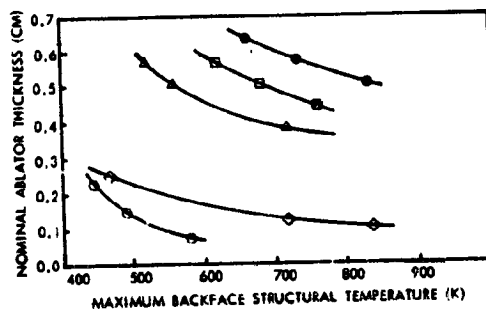


Figure 7.2-7. Atlas/Centaur '78 Small Probe Nominal Thickness Versus Structure Temperature

Table 7.2-3. Ablator Thickness for Atlas/Centaur Large and Small Probes

LOCATION	BACKFACE STRUCTURE (CM)	ABLATOR NOMINAL THICKNESS (CM)	DFSIGN MARGIN (CM)	DESIGN THICKNESS (CM)
LARGE PROBE, $\gamma = 35^\circ$				
STAGNATION	0.178 ALUMINUM	0.445 QUARTZ NITRILE PHENOLIC	0.150	0.60
CONE	0.203 ALUMINUM	0.445 QUARTZ NITRILE PHENOLIC	0.150	0.60
CONE EDGE	0.305 ALUMINUM	0.325 QUARTZ NITRILE PHENOLIC	0.275 (a)	0.60
AFTERBODY	0.064 ALUMINUM	0.229 ESA 3560	0.076	0.31
RADOME	0.102 POLYIMIDE	0.229 (a) ESA 3560	0.076	0.31
SMALL PROBE, $\gamma = -25^\circ$				
STAGNATION	0.127 TITANIUM	0.445 QUARTZ NITRILE PHENOLIC	0.163	0.61
CONE	0.051 TITANIUM	0.445 QUARTZ NITRILE PHENOLIC	0.163	0.61
CONE EDGE	0.152 TITANIUM	0.368 QUARTZ NITRILE PHENOLIC	0.242 (a)	0.61
AFTERBODY	0.065 TITANIUM	0.292 ESA 3560	0.076	0.37
RADOME	0.102 TITANIUM	0.292 (a) TEFLON	0.076	0.37

(a) EXCESS MATERIAL ADDED TO PRODUCE UNIFORM ABLATOR THICKNESS

LOCATION, $R/R_b = 0.7$ $\gamma = -35^\circ$

0.44 CM QUARTZ NITRILE PHENOLIC OVER
0.20 CM ALUMINUM

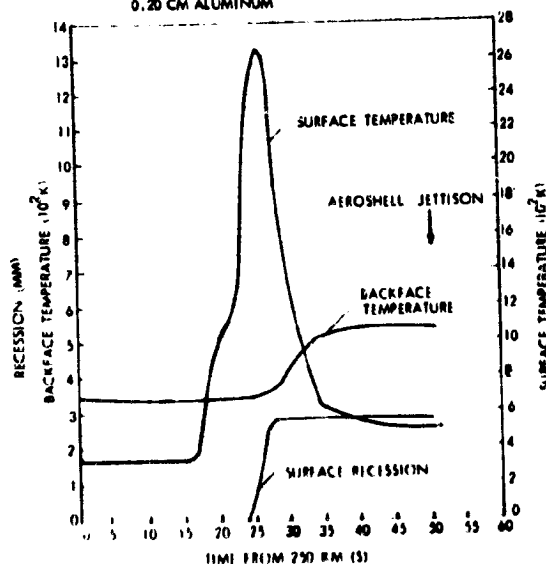


Figure 7.2-8. Thermal Response of Atlas/Centaur '78 Large Probe Heat Shield

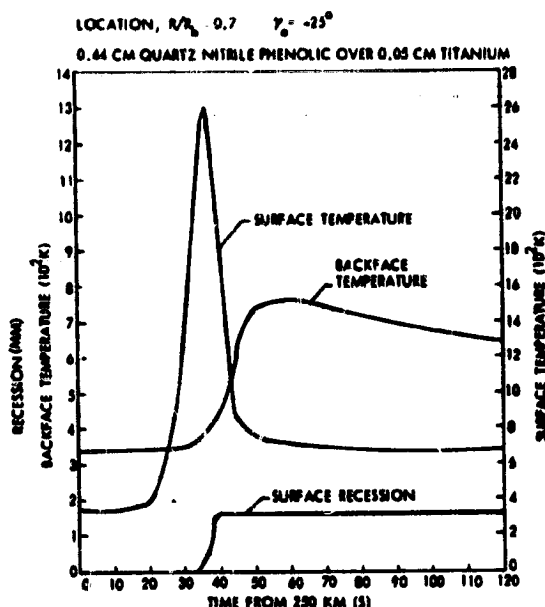


Figure 7.2-9a. Thermal Response of Atlas/Centaur '78 Small Probe Heat Shield, Shallow Entry

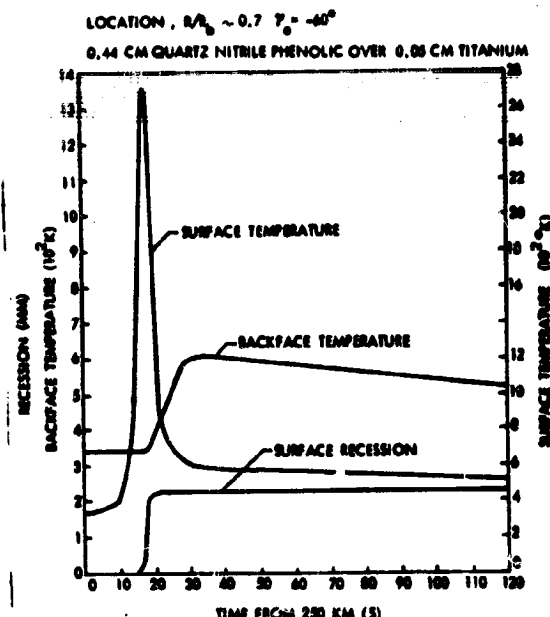


Figure 7.2-9b. Thermal Response of Atlas/Centaur '78 Small Probe Heat Shield, Steep Entry

Penetrations in the heat shield require special considerations in their design to maintain the integrity of the ablative heat shield. On the Atlas/Centaur large probe, there are no penetrations in the forebody. Penetrations do exist (access, electrical, etc) in the large probe afterbody, but are not considered serious problems. Baseline designs for the penetrations are shown in Section 7.3. On the small probe, however, there exists a pressure probe and a temperature probe cover in the forebody, as well as several penetrations in the afterbody. A graphite tube, backed up by copper to soak up the conducted energy, has been selected for the pressure probe. The temperature probe cover will be a plug of quartz nitrile phenolic bonded to the deployable plunger. Details of the pressure probe and temperature probe cover are presented in Figure 7.3-33. Preliminary tests (see Section 7.2.6) have shown that penetrations similar to the baseline pressure and temperature probe designs perform satisfactorily with no adverse effects in quartz nitrile phenolic. Further analyses and tests are required to refine and qualify the selected design concepts. As in the large probe, penetrations in the small probe afterbody require special consideration, but are not considered to be any real problem since the base heating environment is relatively mild. Baseline designs for the small probe afterbody penetrations are shown in Section 7.3.

7.2.4.3 Design Margin

In designing the heat shield subsystem, the uncertainties that exist in entry conditions, material performance, and manufacturing tolerances are accounted for by adding a design margin to the nominal thickness required to maintain the structure below its design limit temperature. The design margin thickness is obtained by combining the individual increments in heat shield thickness required to meet 3σ dispersions in entry conditions, material performance, and manufacturing tolerances. These increments, except the manufacturing tolerance, are root sum squared and added to the manufacturing tolerance to yield the design margin thickness.

The results of sensitivity studies for quartz nitrile phenolic on the cone ($r/r_b \sim 0.7$) of the Atlas/Centaur large probe are summarized in Table 7.2-4. This table exemplifies a typical design margin calculation, and shows that the most significant uncertainties are in: (1) the temperature prediction accuracy; (2) convective heating; and (3) radiant heating. In addition to these parameters, the vapor pressure is a significant parameter in the low entry angle small probe design margin. The quoted 3σ deviations in material performance are based upon preliminary data and estimates, and will be refined using the test results to be obtained during the design development.

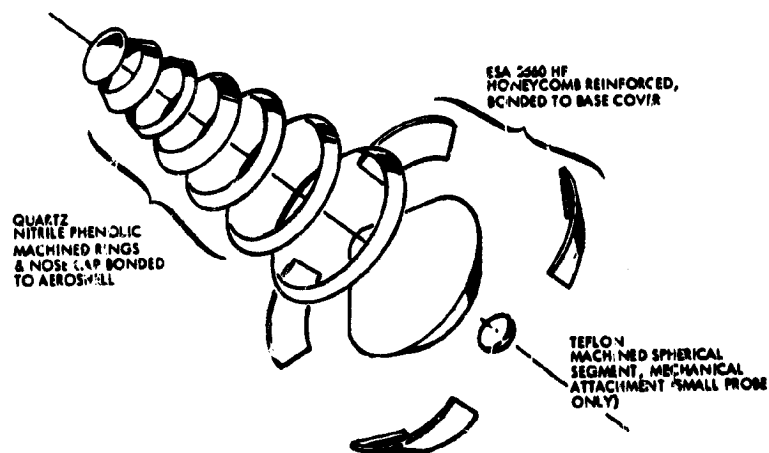
Table 7.2-4. Typical Design Margin Calculation, Atlas/Centaur Large Probe

UNCERTAINTY PARAMETER	3σ DEVIATION	Δ THICKNESS (CM)
ENTRY ENVIRONMENT:		
ENTRY ANGLE, γ_e	$35^\circ \pm 3^\circ$	0.0099
ENTRY VELOCITY, V_e	$11.25 \text{ KM/S} \pm 0.0043$	0.0000
SCALE HEIGHT, Δ	$4.25 \text{ KM} \pm 0.3$	0.0089
BALLISTIC COEFFICIENT, β	$90.75 \text{ KG/M}^2 \pm 5\%$	0.0089
INITIAL ANGLE OF ATTACK, α	$0 \text{ RAD} \pm 0.175$	0.0196
COMPOSITION	$97\% - 99\% \text{ CO}_2$	0.0061
AEROSHELL SEPARATION TIME	$\pm 0.7 \text{ S}$	0.0003
INITIAL TEMPERATURE	$300^\circ\text{K} \pm 20$	0.0119
ENVIRONMENT PREDICTION:		
CONVECTIVE HEATING, q_c	$\pm 40\%$	0.0457
RADIANT HEATING, q_r	$\pm 60\%$	0.0612
MATERIAL PERFORMANCE:		
HEAT OF DESUBLIMATION	$\pm 50\%$	0.0000
CONVECTIVE BLOCKING	VARIABLE	0.0168
VAPOR PRESSURE	VARIABLE	0.0910
TEMPERATURE PREDICTION ACCURACY	$\pm 80^\circ\text{K}$	0.0000
ROOT SUM SQUARE		0.0991
ADD THE MANUFACTURING TOLERANCE		0.0000
DESIGN MARGIN		0.100 CM

The design margins computed for other locations on the Atlas/Centaur large probe and small probe are summarized in Table 7.2-3. To minimize fabrication effort, the heat shield has been designed as a constant thickness of quartz nitrile phenolic over the forebody, and a constant thickness of ESA 3560 and Teflon on the afterbody. To achieve this, excess ablator will be applied on certain areas (see Table 7.2-3), and the nose cap structure skin thickness has been increased above the design thickness (see Section 7.3.6.2).

7.2.4.4 Fabrication Techniques

To fabricate the forebody heat shield, the quartz nitrile phenolic will be machined in annular rings from flat molded (3.4 MN/m pressure at 422°K) billets, and the segments simultaneously bonded with American Cyanamid HT 424 to the forebody aeroshell under vacuum pressure and 422°K temperature (see Figure 7.2-10). This process results in optimum orientation of the reinforcing quartz cloth and minimizes manufacturing tolerances in the ablator. Two combined quartz nitrile phenolic heat shield and substructure panels were fabricated by the above process and delivered to NASA/Ames as part of this system design study.



Figures 7.2-10. Selected Heat Shield Materials & Fabrication Processes (Atlas/Centaur)

Two methods of fabricating the aeroshell cone edge were considered. One method considered was to tape wrap the quartz nitrile phenolic around a mandrel, maintaining the quartz cloth at a specific angle to the outer surface, and machining the outside surface to the required contour (see Figure 7.2-11). This would result in optimum orientation of the quartz cloth. A less expensive method of fabrication was selected, however. The aeroshell cone edge will be machined from the same flat billet as the rings for the conical area (see Figure 7.2-11). This will reduce tooling costs substantially. In bonding the quartz nitrile phenolic to the aeroshell, the thin sections and low elastic modulus will permit the ablator to follow the aeroshell contour. Therefore, to achieve a concentric and smooth aerodynamic external surface, the heat shield surface will be machined after assembly.

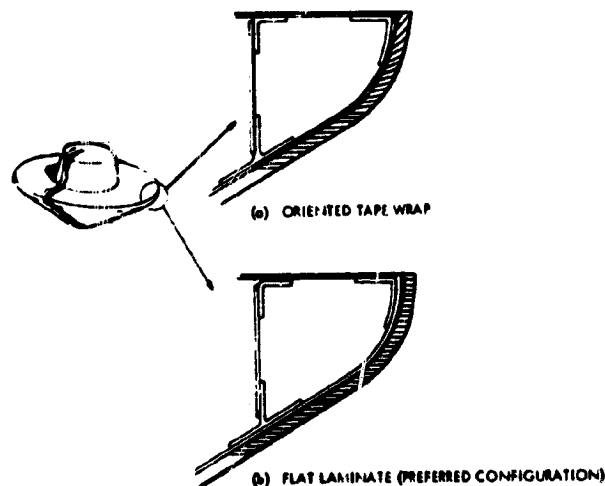


Figure 7.2-11. Aeroshell Cone Edge Ablator Cloth Layout

The ESA 3560 selected for the afterbody of the entry probes will be fabricated by a process developed for the Viking entry vehicle, which permits fabrication on complicated shapes with no new tooling required. Reinforcing honeycomb core, which is flexible, is cut to the design thickness from flat billets and bonded to the base cover structure. The ablative filler is troweled into the honeycomb core, and cured under vacuum pressure and 422°K temperature. The cured overfill is sanded down to the core level for final sizing. The ESA 3560 material can also be used in the radome area of the large probe, since it is RF transparent prior to entry heating, and during the period from the start of entry heating to parachute

deployment, no transmission is planned. The antenna radome is removed during parachute deployment, allowing reestablishment of the RF link. On the small probe the radome remains through descent to the surface, therefore its heat shield must be constructed of a material that remains RF transparent after entry heating. Teflon has been selected based upon its excellent RF characteristics and vast flight history as an antenna radome ablative material. The Teflon radome will be a machined unit and mechanically attached to the base cover structure.

Relative to field repair, the quartz nitrile phenolic is so tough as to be practically indestructable. In the unlikely event of damage greater than superficial cuts and scrapes, field repair can be accomplished by routing out the damaged area and bonding in a precured plug. The quartz nitrile phenolic ablators on each of the heat shield panels fabricated and delivered to NASA/Ames were field repaired by this process. ESA 3560 is less rugged, but is also easily repaired. The material in the damaged area is cut out down to the structure and a room temperature curing version of the same material is troweled in. On the small probe, the Teflon antenna radome will be replaced as a unit in the event of damage.

7.2.4.5 Preliminary Test Requirements

During the hardware phase of the Pioneer Venus Project, tests of the heat shield materials and components will be required to verify the performance of the selected materials; determine design properties and sensitivity to uncertainties; verify and qualify details of the design, including functional performance of the penetrations in the heat shield; and verify that the manufacturing process yields a product equivalent to that produced in the laboratory for development tests. The tests planned to meet the requirements of the Atlas/Centaur entry probe heat shields are shown in Table 7.2-5. Very early in the program a number of tests are required to substantiate the design properties and design margins of the ablative materials. This requires plasma arc tests (Test Set I, Table 7.2-5) and a number of thermophysical property tests (Test Set II).

Table 7.2-5. Heat Shield Design Development and Qualification Tests, Atlas/Centaur Entry Probes

TEST TITLE	NO. OF SAMPLES	TEST DESCRIPTION
ABLATION PERFORMANCE AND HEAT TRANSFER MODEL DEVELOPMENT:		
<ul style="list-style-type: none">• THERMOMECHANICAL SURFACE EROSION• THERMOCHEMICAL SURFACE EROSION• INTERNAL PYROLYSIS AND DEGRADATION• JOINTS, GAPS AND INTERFACES	<ul style="list-style-type: none">25103020	TEST SET I PLASMA ARC TESTS WITH COMBINED RADIANT, CONVECTIVE HEATING, AND SHEAR, USING CO ₂ AND AIR TEST MEDIA.
SUBTOTAL	85	
THERMOPHYSICAL PROPERTIES		
<ul style="list-style-type: none">• THERMAL CONDUCTIVITY• DEGRADATION KINETICS• SPECIFIC HEAT• THERMAL EXPANSION• SURFACE REFLECTANCE AND EMITTANCE• OUTGASSING STUDIES• BOND TENSILE & SHEAR STRENGTH• ABLATOR TENSILE & COMPRESSIVE STRESS-STRAIN	<ul style="list-style-type: none">66633404040	TEST SET II LABORATORY TESTS OF MATERIAL COUPONS, OVER A RANGE OF TEMPERATURE FROM 172 TO 751°K. BOTH VIRGIN ABLATORS AND CHAR SAMPLES WILL BE TESTED.
SUBTOTAL	147	
FABRICATION AND QC PROCESS DEVELOPMENT		
THERMOSTRUCTURAL COMPATIBILITY	3	TEST SET III FABRICATION AND QUALITY CONTROL EXPERIMENTS OF HEAT SHIELD MOCKUPS AND MATERIAL SAMPLES. PLASMA ARC TESTS WITH COMBINED RADIANT AND CONVECTIVE SHEAR IN CO ₂ .
PROCESS VARIABLES SENSITIVITY	20	
SUBTOTAL	35	
FABRICATION AND QC PROCESS VERIFICATION		
<ul style="list-style-type: none">• PLASMA ARC TESTS• MECHANICAL PROPERTY TESTS• REPAIR PROCESS VERIFICATION• OUTGASSING VERIFICATION	<ul style="list-style-type: none">1230516	TEST SET IV TESTS IN COMBINED RADIANT & CONVECTIVE SHEAR, ABLATIVE TENSILE STRESS-STRAIN, BOND TENSILE STRENGTH, PLASMA ARC TESTS IN COMBINED RADIANT AND SHEAR, LABORATORY TEST OF OUTGASSING CHARACTERISTICS.
SUBTOTAL	63	
PREENTRY EFFECTS VERIFICATION		
	40	TEST SET V PLASMA ARC TESTS AFTER CRUISE ENVIRONMENT EXPOSURE.
PENETRATIONS AND INTERFACE QUALIFICATION		
<ul style="list-style-type: none">• LARGE PROBE VENT• SMALL PROBE TEMPERATURE PROBE• SMALL PROBE PRESSURE PROBE• SMALL PROBE VENT	<ul style="list-style-type: none">1331	TEST SET VI PLASMA ARC TESTS AT QUALIFICATION LEVEL ENTRY ENVIRONMENT SIMULATION.
SUBTOTAL	8	
COMPATIBILITY VERIFICATION		
<ul style="list-style-type: none">• VENUS DESCENT• THERMOSTRUCTURAL COMPATIBILITY	<ul style="list-style-type: none">44	TEST SET VII SIMULATED DESCENT INTO VENUS ATMOSPHERE, CRUISE ENVIRONMENT EXPOSURE FOLLOWED BY PLASMA ARC TEST.
SUBTOTAL	8	

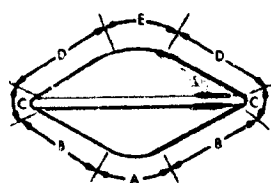
In parallel with these design development tests, experiments will be conducted (Test Set III) to determine the most cost-effective and reliable techniques for heat shield fabrication and quality control. During the hardware fabrication cycle, additional tests will be conducted to verify and qualify the heat shield component functional performance and adequacy of the fabricated hardware. Test Sets IV and V will use pieces and parts built in parallel with the hardware fabrication, to verify that full-scale fabrication produces a product equivalent to laboratory products. The component functional performance will be qualified through Test Sets VI and V.

7.2.5 Preferred Heat Shield, Thor/Delta

The Thor/Delta heat shield subsystem for both the large and small probes are similar in configuration. Figure 7.2-12 shows the general configuration, thicknesses, and weights.

Since the Thor/Delta system is very weight-sensitive, the most efficient ablators have been chosen for the forebody heat shield, and are tailored to the local environment. ESA 5500 M3 is machined in annular ring segments from molded (0.67 MN/m^2 at 422°K) billets and the rings simultaneously bonded with IIT-424 to the forebody aeroshell under vacuum pressure and 422°K temperature (see Figure 7.2-13). This process results in optimum orientation of the reinforcing carbon fibers and minimized manufacturing tolerances in ablator thickness. The quartz nitrile phenolic aeroshell cone edge ring is machined from a billet. This results in small manufacturing tolerances in the ablator thickness. The cone edge ring is also bonded to the aeroshell under vacuum pressure and 442°K temperature.

The ESA 3560 selected for the afterbody regions will be fabricated by the process developed for the Viking entry vehicle, as described in Section 7.2.4. The Teflon antenna radome (on both the small and large probes) is a machined unit, mechanically attached to the base cover structure. A 1/4 scale mockup of the large probe (Thor/Delta) heat shield has been fabricated recently by the processes summarized above, and is shown in Figure 7.2-14.



LARGE PROBE

LOCATION	MATERIAL	THICKNESS	MASS*
A	ESA 5500 M3	0.54 CM	0.6 KG
B	ESA 5500 M3	0.46 CM	0.5 KG
C	QUARTZ NITRILE PHENOLIC	0.43 CM	3.9 KG
D	ESA 3560	0.18 CM	2.9 KG
E	TEFLON	0.19 CM	1.0 KG
TOTAL			16.9 KG



SMALL PROBE

LOCATION	MATERIAL	THICKNESS	MASS*
A	ESA 5500 M3	0.69 CM	0.39 KG
B	ESA 5500 M3	0.61 CM	1.28 KG
C	QUARTZ NITRILE PHENOLIC	0.58 CM	0.54 KG
D	ESA 3560	0.27 CM	0.34 KG
E	TEFLON	0.27 CM	0.53 KG
TOTAL			3.08 KG

* INCLUDING BOND AND EDGE MEMBERS

Figure 7.2-12. Thor/Delta '77 Heat Shield Configuration

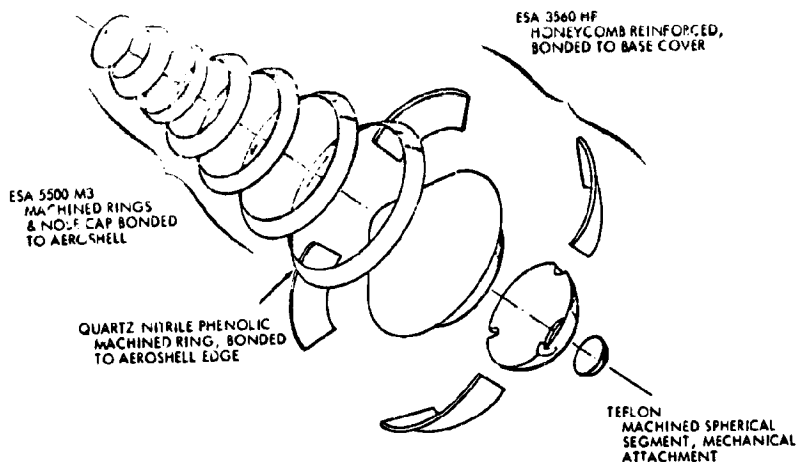


Figure 7.2-13. Selected Heat Shield Materials & Fabrication Processes (Thor/Delta)

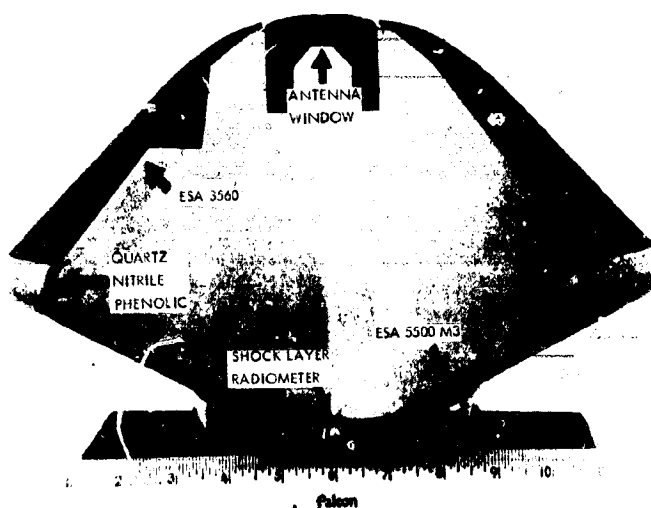


Figure 7.2-14. Thor/Delta Large Probe 1/4 Scale Heat Shield Mockup

Damage to the ESA 5500 M3 is not likely due to its toughness; however, should damage occur, it is easily repaired. The damaged area is removed down to the substructure, and a cured ESA 5500 M3 insert is bonded in place. The quartz nitrile phenolic and ESA 3560 would be repaired as described in Section 7.2.4. The Teflon antenna window would be replaced as a unit in event of damage.

The results of parametric studies conducted to determine ablator thickness versus structure temperature limit for the Thor/Delta mission are shown in Figures 7.2-15, 7.2-16, and 7.2-17.

$$\theta_c = 40^\circ, \gamma_c = -40^\circ, \beta = 78.54 \text{ KG/M}^2, V_c = 11.16 \text{ KM/S}$$

ABATOR	STRUCTURE (CM)	LOCATION	RECESSION (CM)
● ESA 3500 M3	0.102 ALUMINUM	STAG	0.03
■ ESA 3500 M3	0.152 ALUMINUM	CONE, $r/r_b \sim 0.7$	0.04
▲ QUARTZ NITRILE PHENOLIC	0.177 ALUMINUM	CONE EDGE	0.13
◇ ESA 3560	0.084 ALUMINUM	AFTERBODY	0.00
○ TEFLON	0.084 POLYIMIDE	RADOME	0.01

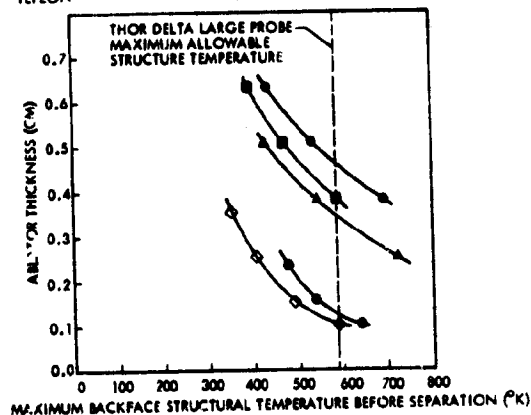


Figure 7.2-15. Thor/Delta Large Probe Ablator Thicknesses Versus Structure Temperature

$$\theta_c = 45^\circ, \gamma_c = -40^\circ, \beta = 125.7 \text{ KG/M}^2, V_c = 11.16 \text{ KM/S}$$

ABATOR	STRUCTURE (CM)	LOCATION	RECESSION (CM)
● ESA 3500 M3	0.064 TITANIUM	STAG	0.11
▼ ESA 3500 M3	0.051 TITANIUM	STAG	0.11
■ ESA 3500 M3	0.064 TITANIUM	CONE, $r/r_b \sim 0.7$	0.08
▽ ESA 3500 M3	0.051 TITANIUM	CONE, $r/r_b \sim 0.7$	0.08
▲ QUARTZ NITRILE PHENOLIC	0.144 TITANIUM	CONE EDGE	0.12
◇ QUARTZ NITRILE PHENOLIC	0.081 TITANIUM	CONE EDGE	0.12
○ ESA 3560	0.072 TITANIUM	AFTERBODY	0.00
● ESA 3560	0.081 TITANIUM	AFTERBODY	0.00
○ TEFLON	0.063 POLYIMIDE	RADOME	0.03
○ TEFLON	0.051 POLYIMIDE	RADOME	0.03

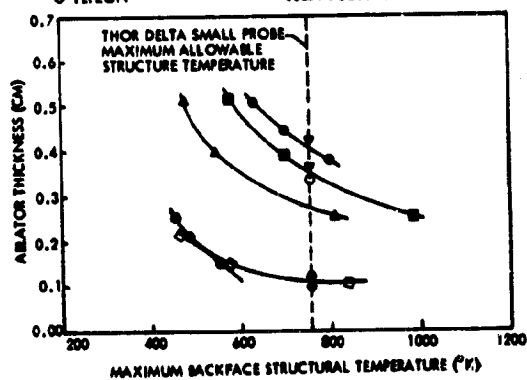


Figure 7.2-16. Thor/Delta Small Probe Ablator Thicknesses Versus Structure Temperature ($\gamma_c = -40^\circ$)

$$\theta_c = 45^\circ \quad \gamma_c = -20^\circ \quad \beta = 125.7 \text{ KG/M}^2 \quad V_c = 11.16 \text{ KM/S}$$

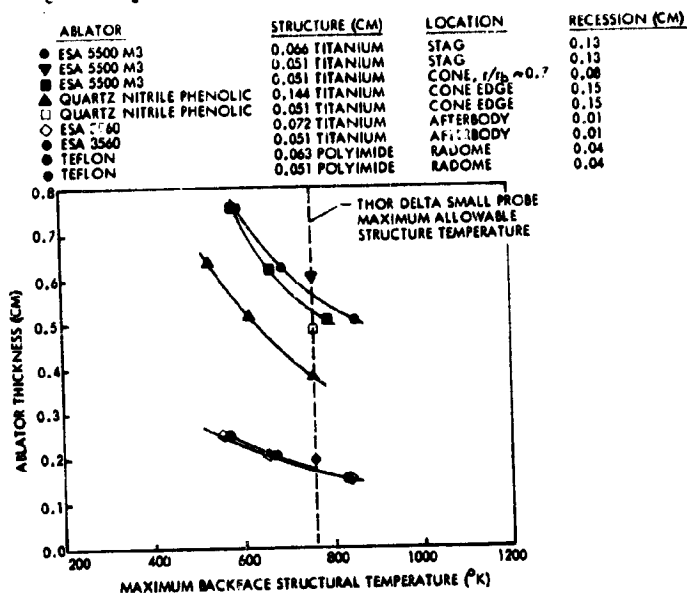


Figure 7.2-17. Thor/Delta Small Probe Nominal Ablator Thicknesses Versus Structure Temperature ($\gamma_c = -40^\circ$)

For the large probe, the use of an aluminum aeroshell structure on the forebody dictates that the ablator-aeroshell interface be maintained below 422°K during entry when the stagnation pressure exceeds $1 \times 10^5 \text{ N/m}^2$. Prior to aeroshell separation, and after the stagnation pressure decreases below $1 \times 10^5 \text{ N/m}^2$, the forebody critical load is the thermal stress in the aeroshell skin, and it was assumed the ablator-aeroshell interface must be maintained below 589°K to prevent interframe buckling. On the large probe afterbody, the critical load/temperature occurs near parachute deployment when the structure temperature is near maximum and the base pressure is rising exponentially with time. The vent would allow the structure temperature to go to 589°K prior to separation. The small probe maximum structural temperature is 478°K during entry when the stagnation pressure exceeds $1 \times 10^5 \text{ N/m}^2$. After the stagnation pressure decreases below $1 \times 10^5 \text{ N/m}^2$, the maximum small probe structure temperature on the forebody must not exceed 756°K , to prevent buckling of the aeroshell skin. Venting the small probe aeroshell allows the small probe afterbody and radome to reach a maximum of 756°K .

Table 7.2-6 summarizes the nominal design thicknesses derived from Figures 7.2-15 through 7.2-17, based upon the temperature criteria defined above. Typical time varying surface temperature, structure temperature, and surface recession for nominal ablator thicknesses and nominal heating are presented in Figures 7.2-18 and 7.2-19.

Table 7.2-6. Ablator Thicknesses for Thor/Delta Large and Small Probes

LOCATION	BACKFACE STRUCTURE (CM)	ABLATOR NOMINAL THICKNESS (CM)	DESIGN MARGIN (CM)	DESIGN THICKNESS (CM)
LARGE PROBE, $\gamma = -40^\circ$				
STAGNATION	0.1016 ALUMINUM	ESA 5300 M3/0.457	0.077	0.53
CONE	0.1524 ALUMINUM	ESA 5300 M3/0.381	0.077	0.46
CONE EDGE	0.127 ALUMINUM	QUARTZ NITRILE PHENOLIC/0.340	0.090	0.43
AFTERBODY	0.0635 ALUMINUM	ESA 3560/0.102	0.076	0.18
RADOME	0.0635 POLYIMIDE	TEFLON/0.117	0.076	0.19
SMALL PROBE, $\gamma = -20^\circ$				
STAGNATION	0.0508 TITANIUM	ESA 5300 M3/0.610	0.078	0.69
CONE	0.0508 TITANIUM	ESA 5300 M3/0.533	0.078	0.61
CONE EDGE	0.0508 TITANIUM	QUARTZ NITRILE PHENOLIC/0.485	0.090	0.58
AFTERBODY	0.0508 TITANIUM	ESA 3560/0.187	0.076	0.27
RADOME	0.0508 POLYIMIDE	TEFLON/0.188	0.076	0.27
SMALL PROBE, $\gamma = -40^\circ$				
STAGNATION	0.0508 TITANIUM	ESA 5300 M3/0.417	0.075	0.49
CONE	0.0508 TITANIUM	ESA 5300 M3/0.348	0.075	0.42
CONE EDGE	0.0508 TITANIUM	QUARTZ NITRILE PHENOLIC/0.322	0.090	0.41
AFTERBODY	0.0508 TITANIUM	ESA 3560/0.123	0.076	0.20
RADOME	0.0508 POLYIMIDE	TEFLON/0.109	0.076	0.19

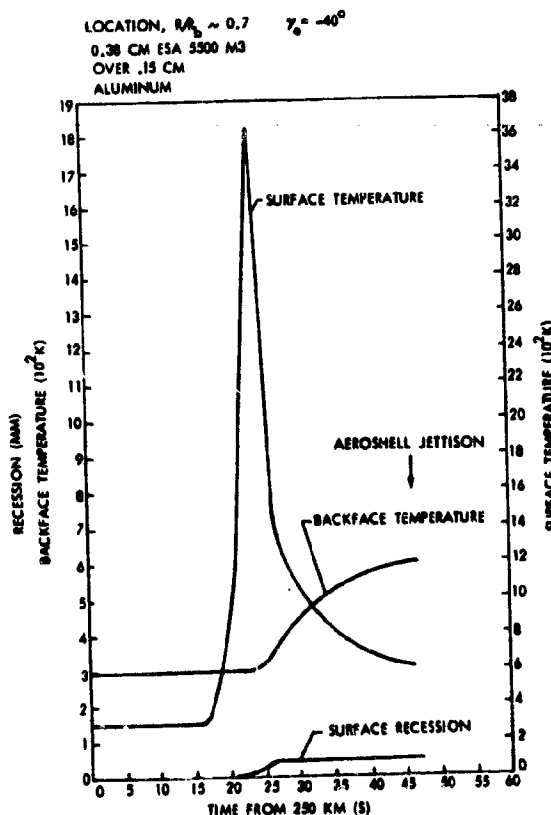


Figure 7.2-18. Thermal Response of Thor/Delta '77 Large Probe Heat Shield

LOCATION, $R/r_b \sim 0.7$ $\gamma = -20^\circ$
 0.53 CM ESA 5500 M3

OVER 0.05 CM TITANIUM

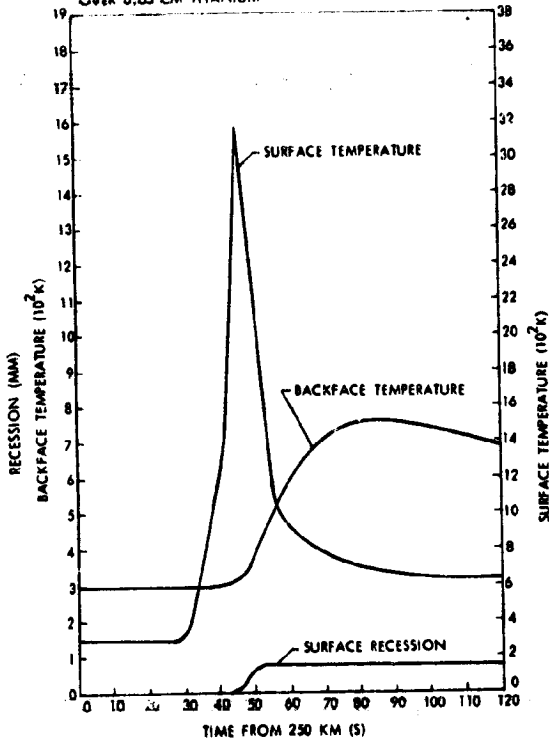


Figure 7.2-19a. Thermal Response of Thor/Delta '77 Small Probe Heat Shield, Shallow Entry

LOCATION, $R/r_b \sim 0.7$ $\gamma = -40^\circ$
 0.35 CM ESA 5500 M3

OVER 0.05 CM TITANIUM

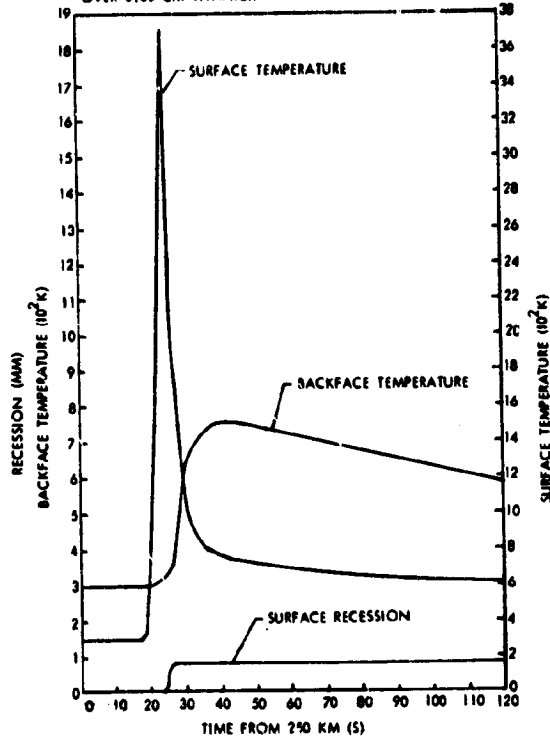


Figure 7.2-19b. Thermal Response of Thor/Delta '77 Small Probe Heat Shield, Medium Entry

In both the Thor/Delta and Atlas/Centaur, heat shield design uncertainties exist in the entry conditions, material performance, and manufacturing tolerances, and must be accounted for in determining the design thickness.

The results of sensitivity studies for ESA 5500 M3 on the cone ($r/r_b \sim 0.7$) of the Thor/Delta large probe are summarized in Table 7.2-7, an example of the design margin calculations conducted on the Thor/Delta heat shields. The quoted 3σ dispersions in material performance are based upon preliminary data and estimates. The design margins computed for other locations on the Thor/Delta large probe and small probe are summarized in Table 7.2-6, along with the total design thicknesses and weights.

Table 7.2-7. Typical Design Margin Calculation, Thor/Delta Large Probe

UNCERTAINTY PARAMETER	3 σ DEVIATION	Δ THICKNESS (CM)
ENTRY ENVIRONMENT:		
ENTRY ANGLE, γ	$40^\circ \pm 3^\circ$	0.00279
ENTRY VELOCITY, V_e	$11.123 \text{ KM/S} \pm 0.0043$	0.00102
SCALE HEIGHT, Δ	$4.25 \text{ KM} \pm 0.3$	0.00330
BALLISTIC COEFFICIENT, β	$78.54 \text{ KG/M}^2 \pm 2\%$	0.00147
ANGLE OF ATTACK, α	$0^\circ \pm 0.136^\circ$	0.00043
COMPOSITION	97% - 80% CO_2	0.00135
AEROSHELL SEPARATION TIME	$44.5 \pm 0.7 \text{ S}$	0.00008
ENVIRONMENTAL PREDICTION:		
CONVECTIVE HEATING, q_c	$\pm 20\%$	0.01118
RADIANT HEATING, q_r	$\pm 30\%$	0.00813
MATERIAL PERFORMANCE:		
BLOCKING FACTOR	VARIABLE	0.00762
HEAT OF SUBLIMATION	$\pm 30\%$	0.00076
VAPOR PRESSURE	VARIABLE	0.00051
SURFACE COMBUSTION	$\pm 30\%$	0.02794
TEMPERATURE PREDICTION ACCURACY	$\pm 35^\circ\text{K}$	0.03937
ROOT SUM SQUARE		0.0511
ADD THE MANUFACTURING TOLERANCE		0.0254
DESIGN MARGIN		0.077 CM

The penetrations in the Thor/Delta heat shield are similar to the penetrations in the Atlas/Centaur (see Section 7.3 for designs). The only significant penetrations are in the small probe, a graphite pressure probe and a temperature probe cover. Both of these penetrations would be surrounded with quartz nitrile phenolic (see Figure 3-80). With this type design, the optimum orientation of the carbon fiber reinforced ESA 5500 M3 can be maintained for maximum viscous shear resistance, while the more dense and less sensitive quartz nitrile phenolic is used as a transition section.

Tests of the heat shield materials and components will be required to verify the performance of the selected materials, determine design properties and sensitivity to uncertainties; verify and qualify details of the design, including functional performance of the penetrations in the heat shield; and to verify that the manufacturing process yields a product equivalent to the materials produced in the laboratory. The material selected for the forebody of the weight sensitive Thor/Delta probes is the lower density carbon reinforced ESA 5500 M3, and is inherently more susceptible to mechanical erosion than more dense quartz reinforced ablators. Therefore, more tests will be required to develop the design and to qualify this system than the Atlas/Centaur quartz nitrile phenolic forebody. The scope of the tests planned to meet the design requirements of the Thor/Delta probes is presented in Table 7.2-8. Almost all increases in numbers of tests above

Table 7.2-8. Heat Shield Design Development and Qualification Tests, Thor/Delta Entry Probes

TEST TITLE	NO. OF SAMPLES	TEST DESCRIPTION
ABLATION PERFORMANCE AND HEAT TRANSFER MODEL DEVELOPMENT:		
- THERMOMECHANICAL SURFACE EROSION	50	TEST SET I PLASMA ARC TESTS WITH COMBINED RADIATION, CONVECTIVE HEATING AND SHEAR; USING CO ₂ AND AIR TEST MEDIA.
- THERMOCHEMICAL SURFACE EROSION	40	
- INTERNAL PYROLYSIS AND DEGRADATION	60	
- JOINTS, GAPS AND INTERFACES	20	
SUBTOTAL	170	
THERMOPHYSICAL PROPERTIES		
- THERMAL CONDUCTIVITY	18	TEST SET II LABORATORY TESTS OF MATERIAL COUPONS, OVER A RANGE OF TEMPERATURE FROM 172 TO 754°K. BOTH VIRGIN ABLATORS AND CHAR SAMPLES WILL BE TESTED.
- DEGRADATION KINETICS	18	
- SPECIFIC HEAT	18	
- THERMAL EXPANSION	6	
- SURFACE REFLECTANCE AND EMITTANCE	6	
- OUTGASSING STUDIES	50	
- BOND TENSILE AND SHEAR STRENGTH	60	
- ABLATOR TENSILE AND COMPRESSIVE STRESS-STRAIN	60	
SUBTOTAL	236	
FABRICATION AND QC PROCESS DEVELOPMENT		
THERMOSTRUCTURAL COMPATIBILITY	6	TEST SET III FABRICATION AND QUALITY CONTROL EXPERIMENTS OF HEAT SHIELD MOCKUPS AND MATERIAL SAMPLES. PLASMA ARC TESTS WITH COMBINED RADIATION AND CONVECTIVE HEATING, IN CO ₂ .
PROCESS VARIABLES SENSITIVITY	24	
SUBTOTAL	46	
FABRICATION AND QC PROCESS VERIFICATION		
- PLASMA ARC TESTS	24	TEST SET IV TESTS IN COMBINED RADIANT AND CONVECTIVE SHEAR; ABLATOR TENSILE STRESS-STRAIN; BOND TENSILE STRENGTH; PLASMA ARC TESTS IN COMBINED RADIANT AND SHEAR; LABORATORY TESTS OF OUTGASSING CHARACTERISTICS.
- MECHANICAL PROPERTY TESTS	60	
- REPAIR PROCESS VERIFICATION	15	
- OUTGASSING VERIFICATION	24	
SUBTOTAL	123	
PREENTRY EFFECTS VERIFICATION		
	60	TEST SET V PLASMA ARC TESTS AFTER CRUISE ENVIRONMENT EXPOSURE.
PENETRATIONS AND INTERFACE QUALIFICATION		
- LARGE PROBE SHOCKLAYER RADIOMETER	3	TEST SET VI PLASMA ARC TESTS AT QUALIFICATION LEVEL ENTRY ENVIRONMENT SIMULATION.
- LARGE PROBE PARACHUTE LINE COVER	3	
- LARGE PROBE VENT	1	
- SMALL PROBE TEMPERATURE PROBE	3	
- SMALL PROBE PRESSURE PROBE	3	
- SMALL PROBE VENT	1	
SUBTOTAL	14	
COMPATIBILITY VERIFICATION		
- VENUS DESCENT	4	TEST SET VII SIMULATED DESCENT INTO VENUS ATMOSPHERE. CRUISE ENVIRONMENT EXPOSURE FOLLOWED BY PLASMA ARC TESTS.
- THERMOSTRUCTURAL COMPATIBILITY	4	
SUBTOTAL	8	

Atlas/Centaur occur in Test Sets I through III. These tests are increased in number through increase in the scope of the tests required to develop design data and design margins for ESA 5500 M3, as well as inclusion of tests to develop design data and margins for quartz nitrile phenolic. In the verification and qualification tests, Test Sets V through VII, essentially the same tests are required for Thor/Delta and Atlas/Centaur, since these tests are primarily component functional tests, which are independent of the ablative materials.

7.2.6 Supporting Analyses and Tests

During the system design study, a thermal protection system for a shock layer radiometer was evaluated. The shock layer radiometer was to be located at the stagnation point of the large probe, and required a "clean" heat shield surrounding it to prevent contamination of the boundary layer. Since the radiometer looks through a quartz window, which would ablate during entry, a clean heat shield can be obtained by using a high purity quartz around the radiometer window, backed up by a beryllium heat sink to accommodate the extra heat load due to transmitted and conducted energy at the backface. Details of the design are shown in Figure 3-78. If a quartz reflecting heat shield is developed, the shock layer radiometer heat shield could be used as a flight test to verify its performance. Additional tests and analyses beyond that described in Sections 7.2.4 and 7.2.5 would be required to develop and qualify a shock layer radiometer thermal protection system.

During the plasma arc tests in the Ames HTT, several models were tested with dummy pressure tap inserts of ATJ graphite at the model centerline. These dummy pressure taps were fabricated in two models each of quartz nitrile phenolic and ESA 5500 M3, to simulate the small probe stagnation point pressure sensor installation. The objective was to see if an insert would degrade the local ablator performance either through conduction of heat into the ablator or by protuberance heating. The appearance of the models after test is shown in Figure 7.2-20. As can be seen, quartz nitrile phenolic performed very well, with little in-depth charring. The ESA 5500 M3 did not perform quite as well, with some nonuniform recession around the graphite insert in the test of sample M3-6.

In addition to the tests of conventional medium to high-density ablators, a low-density quartz nitrile phenolic ($\rho \sim 0.96 \text{ g/cm}^3$) was developed and tested, and does show promise of being more efficient than either ESA 5500 M3 ($\rho \sim 1.12 \text{ g/cm}^3$) or quartz nitrile phenolic ($\rho \sim 1.55 \text{ g/cm}^3$). A comparison of its performance with ESA 5500 M3 and regular quartz nitrile phenolic is presented in Figure 7.2-21. Development cost considerations, however, precludes its use on the Pioneer Venus.

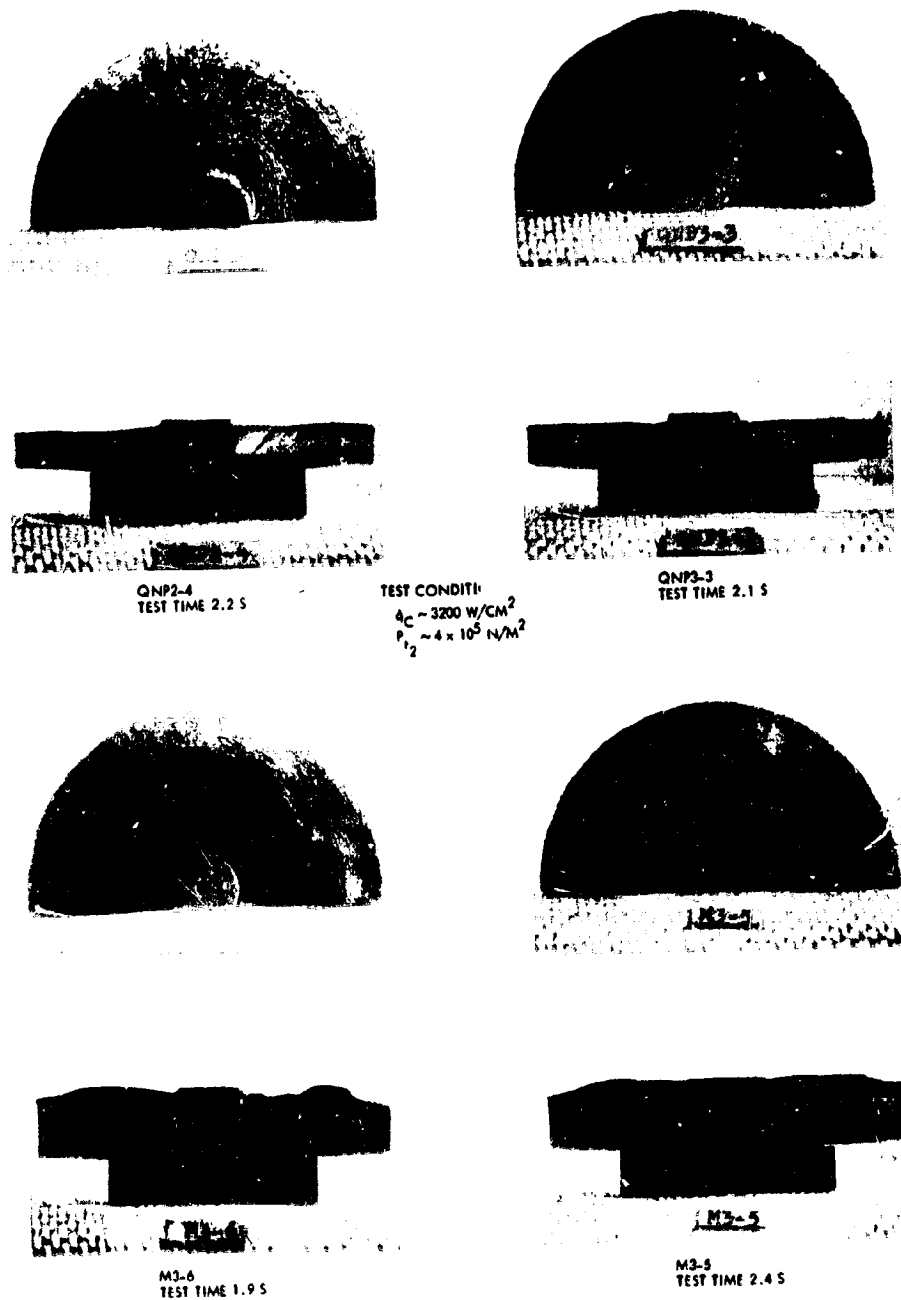


Figure 7.2-20. Performance of Ablators with Dummy Pressure Probes

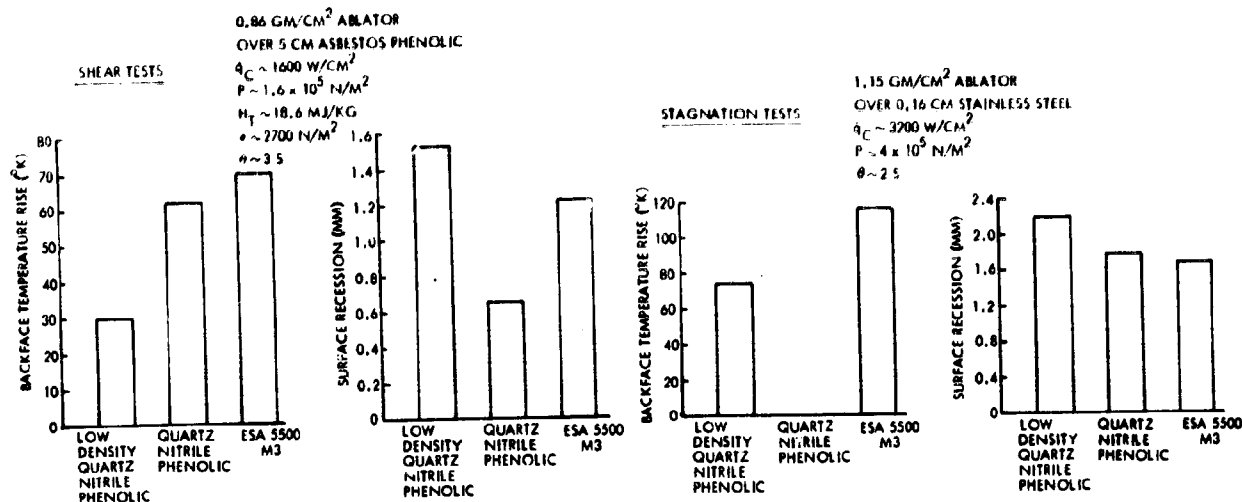


Figure 7.2-21. Comparison of Low Density Quartz Nitrile Phenolic with Quartz Nitrile Phenolic and ESA 5500 M3

In addition to the plasma arc tests, thermal and mechanical property and vacuum outgassing tests have been conducted on the more promising ablative materials, to derive preliminary design data. Table 7.2-9 presents the physical properties of quartz nitrile phenolic.

The properties of ESA 3560 are contained in MCR-70-170*. Since the ablator must be bonded to the aeroshell and remain attached at temperatures up to 756°K, preliminary constant temperature tests were conducted to determine the integrity of various ablative bonds at temperatures up to 756°K. The tests indicate that the HT-424 retains good adhesion between quartz nitrile phenolic or ESA 5500 M3 and a metal substrate at 756°K.

In addition to tests on the ablative materials that are candidates for the Pioneer Venus forebody, tests were conducted on several afterbody materials to confirm the selection of ESA 3560. The results of the tests are summarized in Table 7.2-10 and confirm that ESA 3560 performs well in Venus entry base heating environment, and remains bonded to the metal substructure at temperatures in excess of 756°K.

*D. L. Carlson, "Heat Shields for Planetary Atmospheric Experiments Test," Final Report, MCR-70-170, Vol. I (NAS 2-5538), Martin Marietta Corporation, Denver, Colorado (May 1970).

Table 7.2-9. Quartz Nitrile Phenolic Properties

TENSILE PROPERTIES, ASTM A30 TYPE 1, POST-CURED MATERIAL		TENSILE PROPERTIES, ASTM A30 TYPE 1, STANDARD CURE	
LAMINATE ORIENTATION	TEMPERATURE (K)	TEMPERATURE (K)	SECANT MODULUS (MN/M ²)
FLAT BIAS (DIR B)	300	300	216.5
30° SHINGLE (DIR A)	300	300	60
COMPRESSION STRENGTH, PERPENDICULAR TO SHINGLE (DIR C)			
TEST SET UP: 1.27 - CM - DIA STEEL CYLINDER SEARING ON 2.54-CM-DIA BY 1.27-CM-THICK ABULATOR SAMPLE			
INITIAL DEFLECTION RATE: 0.7005 CM/1.38 MN/M ²			
0.100 DEFLECTION AT 35.4 MIN PRESSURE (MAXIMUM LOAD), WITH 0.009 COMPRESSIVE SET			
VACUUM OUTGASING RATES			
STANDARD CURE: 5.04 x 10 ⁻³ %/DAY CONDENSIBLE WEIGHT LOSS RATE AT 325 K			
POST-CURED: 0.98 x 10 ⁻³ %/DAY CONDENSIBLE WEIGHT LOSS RATE AT 325 K (MEETS VIKING OUTGASING CRITERIA)			

Table 7.2-10. Plasma Arc Tests of Low Density Ablators

10 SECOND TEST		15 SECOND TEST	
MATERIAL	DENSITY (G/CM ³)	PEAK STRUCTURE TEMPERATURE (K)	COMMENTS
ESA 2800	0.48	878	HARD, SMOOTH, BLACK CHAR, EXCELLENT ADHESION AFTER TEST
ESA 4885	0.31	1082	HARD, SMOOTH, GLASSY CHAR, FAIRLY GOOD ADHESION AFTER TEST
SLA 220	0.25	1152	HARD, ROUGH, GLASSY CHAR, FAIRLY GOOD ADHESION AFTER TEST
MA 225	0.45	964	HARD, SMOOTH, BLACK CHAR, ADHESIVE FAILURE AFTER TEST

7.3 Structures and Mechanisms

7.3 STRUCTURES AND MECHANISMS

7.3.1 Introduction and Summary

The large and small probes are designed for their particular mission profiles and are distinctly different mechanical systems. Their external configurations are established largely on the basis of aerodynamic requirements, but in some cases structural design and mechanical integration factors also have had a major influence. For example, the benefits in cost, weight, and simplification of probe staging influenced the selection of the relatively small compact afterbody of the preferred large probe configuration; Structural efficiency had much to do with the decision to use spherical pressure vessels for the instrument containers.

Some features of the preferred structural/mechanical design that in particular enhance the low-cost, reliability, and flexibility aspects of the program are:

- Incorporation of all science sensors and electrical penetrations in a separate ring or segment of the large probe pressure shell to facilitate disassembly and accessibility of science and electronics system equipment;
- Avoidance, by virtue of the above feature, of any blind electrical connectors or use of service loops (high g problem areas);
- Sufficiently large internal volume to permit instrument design changes and use of common engineering electronics components in the large and small probes;
- Structural safety factors high enough, ~1.6, to permit qualification testing on flight units (deletion of structural test unit);
- Aeroshell construction patterned after existing Viking design;
- Use of Viking components in separation devices;

7.3.1.1 Large Probe Description

The large probe consists of two basic structural features, the aeroshell and the descent capsule, and mechanical devices associated with separation of the aeroshell from the descent capsule. (See Figure 7.3-1) The aeroshell is the outer housing of the probe during cruise and during

entry into the Venus atmosphere. It carries heat shielding to provide protection from entry heating, and its size and shape provide proper drag for the required entry trajectory. The forward shell of the forebody is very similar to Viking aeroshell construction and takes advantage of that experience. The aeroshell afterbody is compact to minimize weight and to interface with the bus load cylinder most efficiently. The base of this structure to the antenna ground plane is aluminum alloy, but aft of that plane all structure is nonmetal to provide RF transparency for efficient antenna functioning. In the separation sequence, this base cap or radome is released and finally, after completion of the parachute descent phase, the remainder of the afterbody is released with the main parachute.

The mechanical devices associated with separation are shown in Figure 7.3-2. Most of these are standard commercial items or applications of commonly used concepts. The separation nuts are the same as those used on the Viking program with minor adaptation for this program; Viking initiators are also used.

The descent capsule is a generally spherical body with an aerodynamic stabilizing ring at its equator and with radar and communication antennas at its fore and aft poles. The descent capsule, which provides mounting and environmental protection for science and electronic equipment throughout the mission, is particularly designed for flexibility in mounting science equipment and for ease of access to it. Figure 7.3-3 shows the main features of the capsule, and Figure 7.3-4 shows an equipment arrangement within it. Some of the significant features of the capsule are:

- Multiple, independent insulation/cover assemblies for easy disassembly with minimum disturbance of equipment installations;
- Three-segment pressure shell for easy access to equipment with least impact to probe and equipment assemblies;
- Heavy pressure shell mid-section for greatest flexibility in accommodating changes in science location;
- Dedicated science region to provide greatest freedom in integrating science equipment.

BASE COVER STIFFENERS
(TYP 45 PLACES EQUALLY SPACED)

BUS/PROBE AND GROUND
SERVICE UMBILICAL NOMINAL
LOCATION

PILOT CHUTE BRIDLE HARNESS STOWAGE

ACCESS DOOR
(2-EQUALLY SPACED)

HEATSHIELD

HEATSHIELD FILLER

SEAL RING

BASE COVER SEAL (VITON)

SECTION F-F
(FULL SIZE)

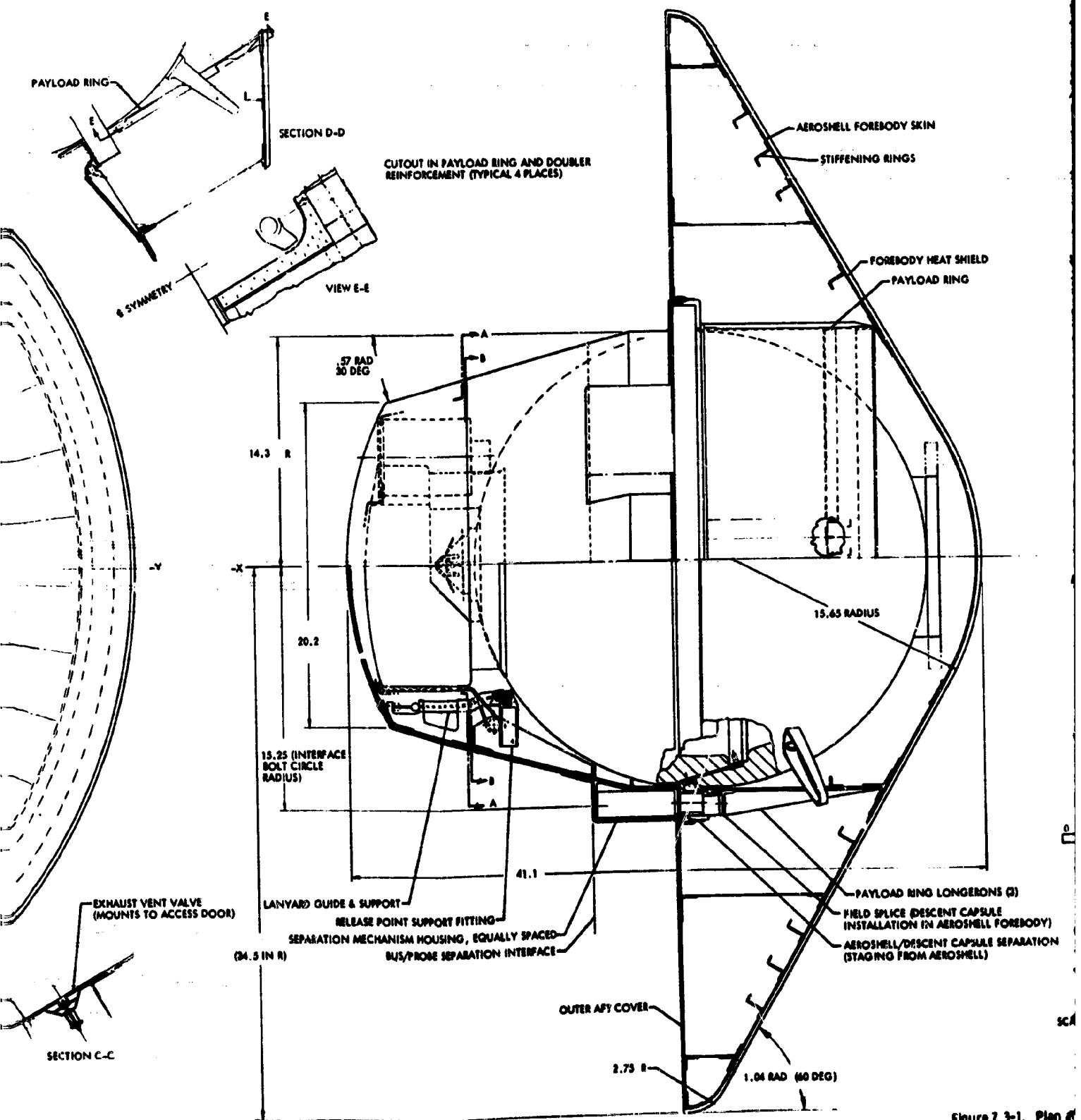


Figure 7.3-1. Plan of

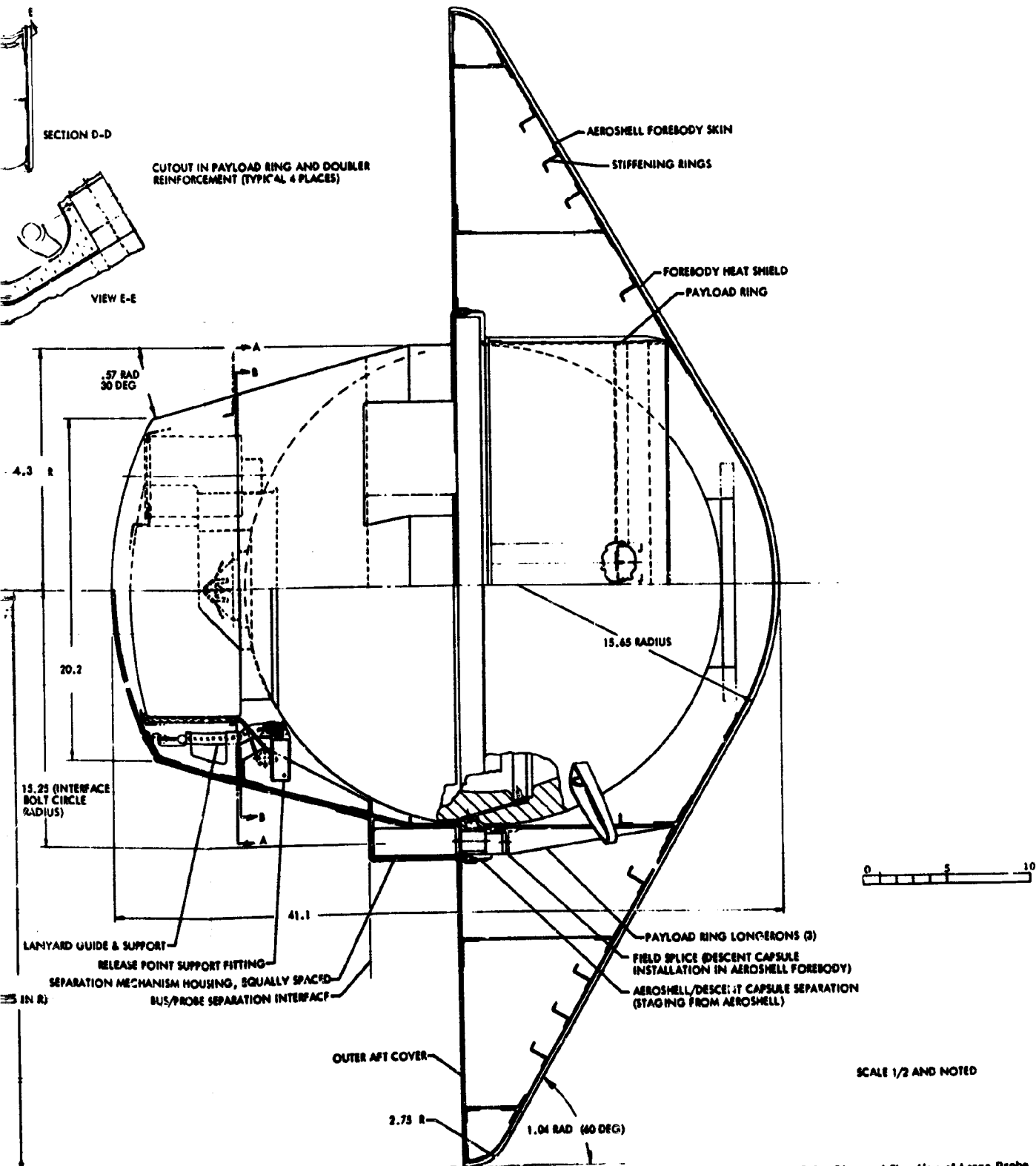
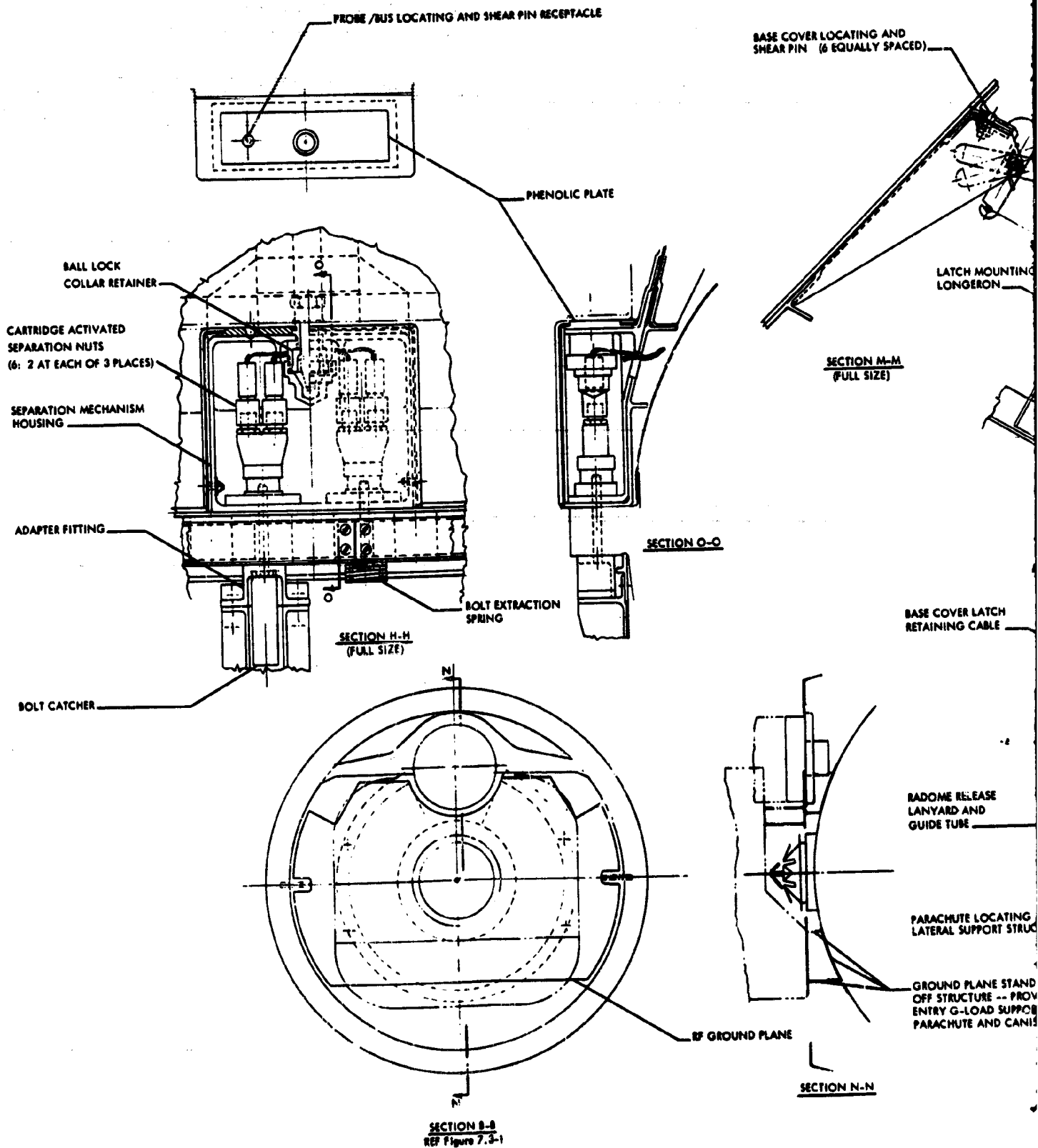


Figure 7.3-1. Plan and Elevation of Large Probe



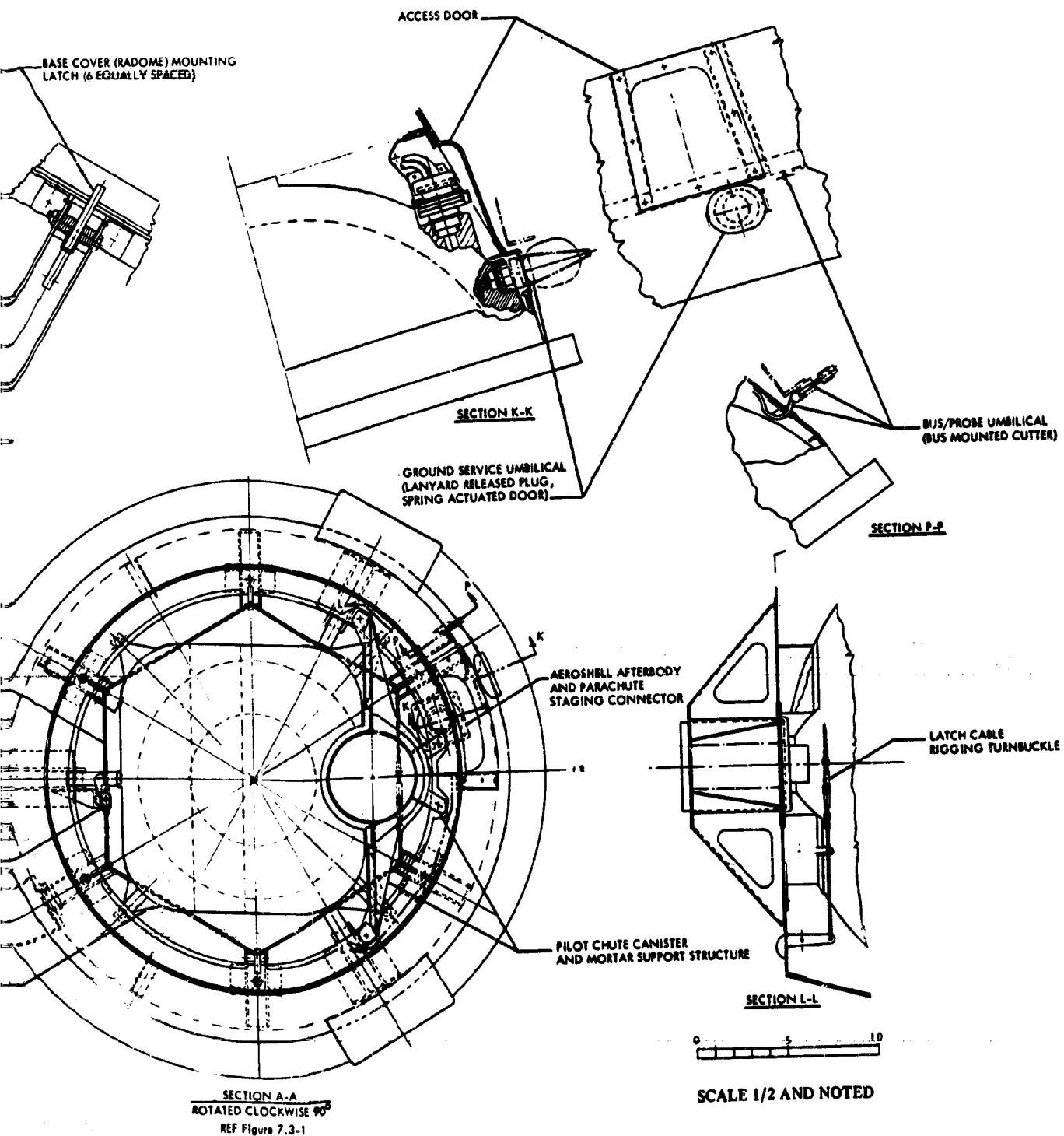


Figure 7.3-2. Mechanical Details of Large Probe

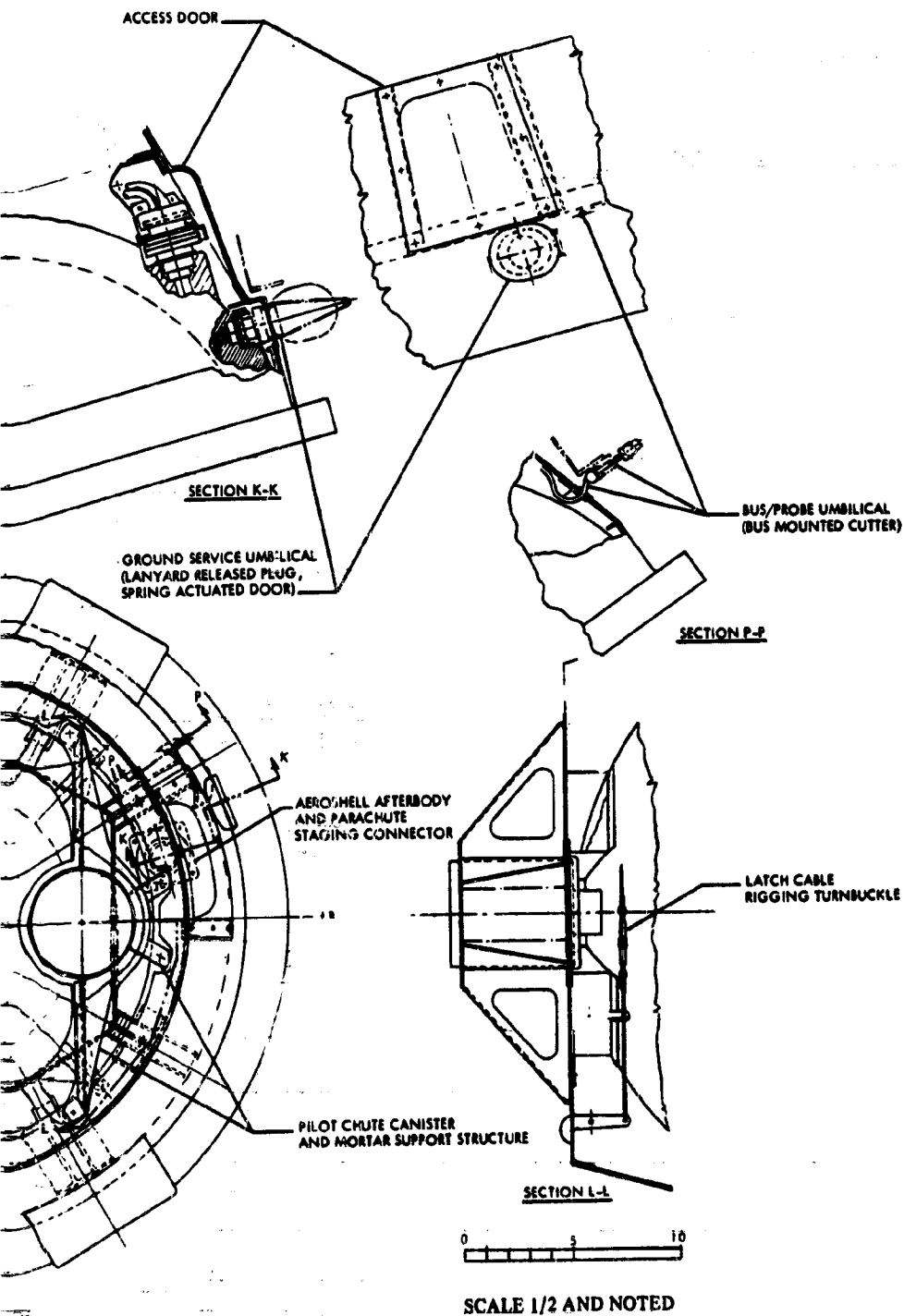
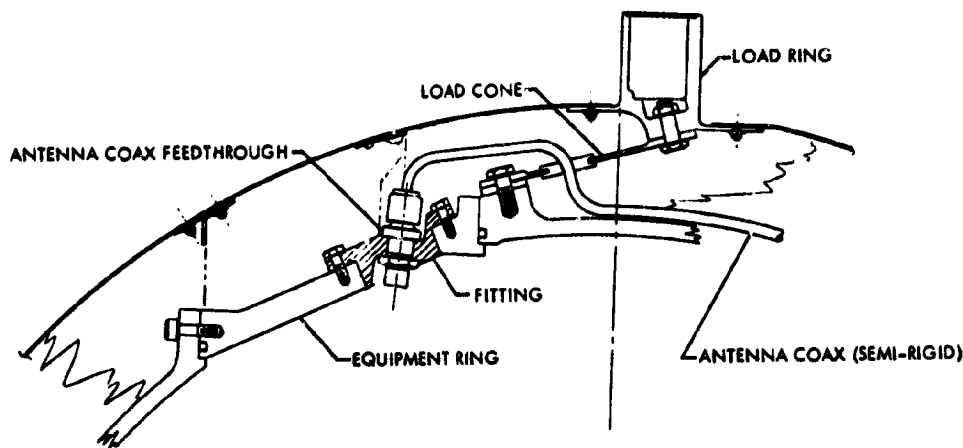
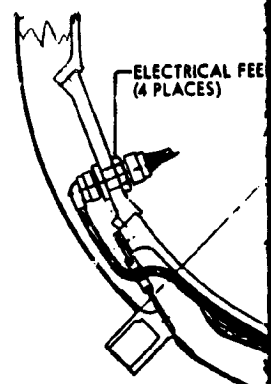


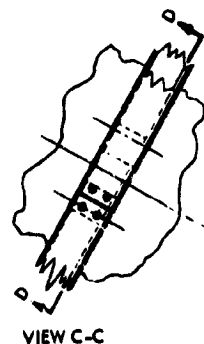
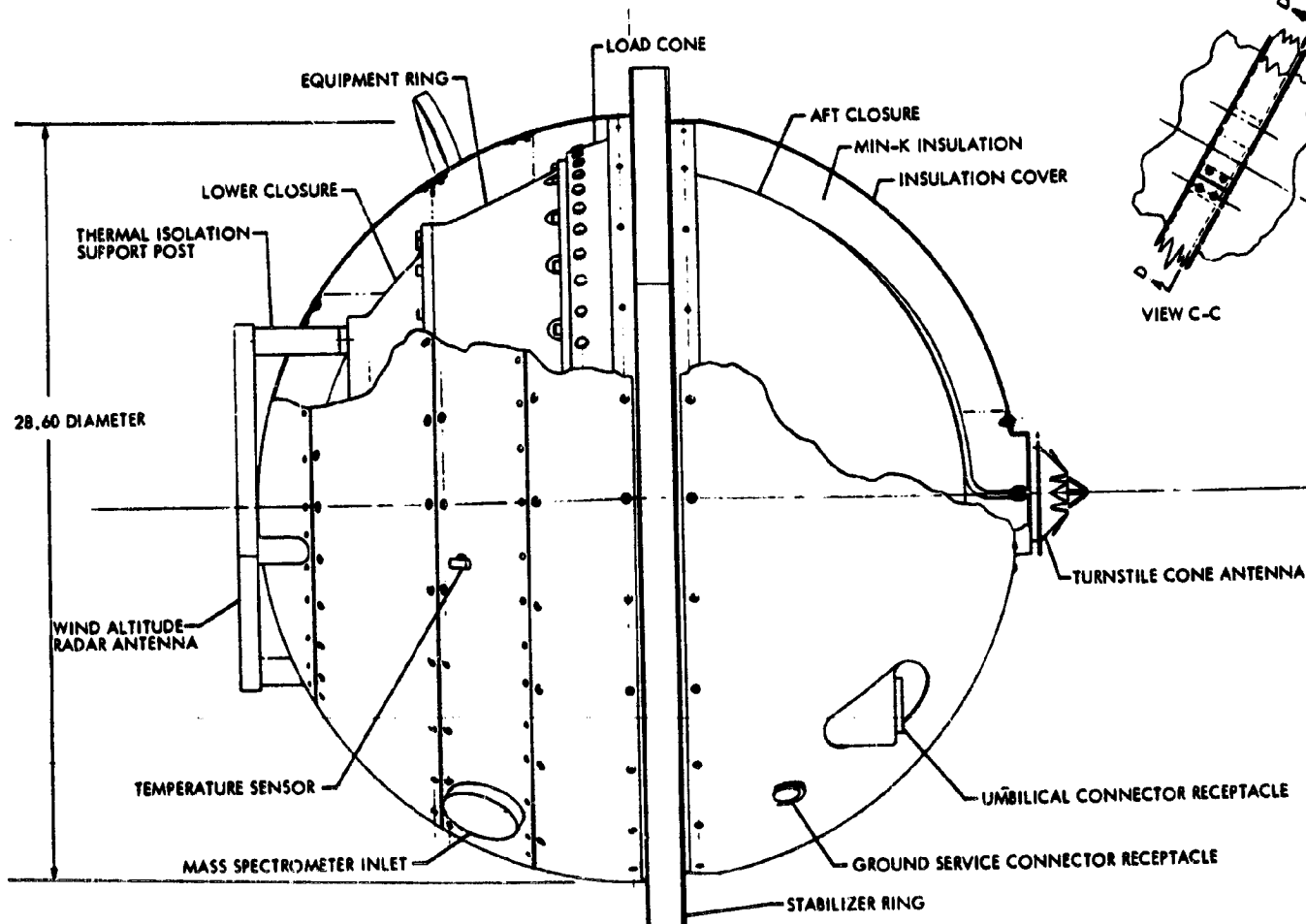
Figure 7.3-2. Mechanical Details of Large Probe



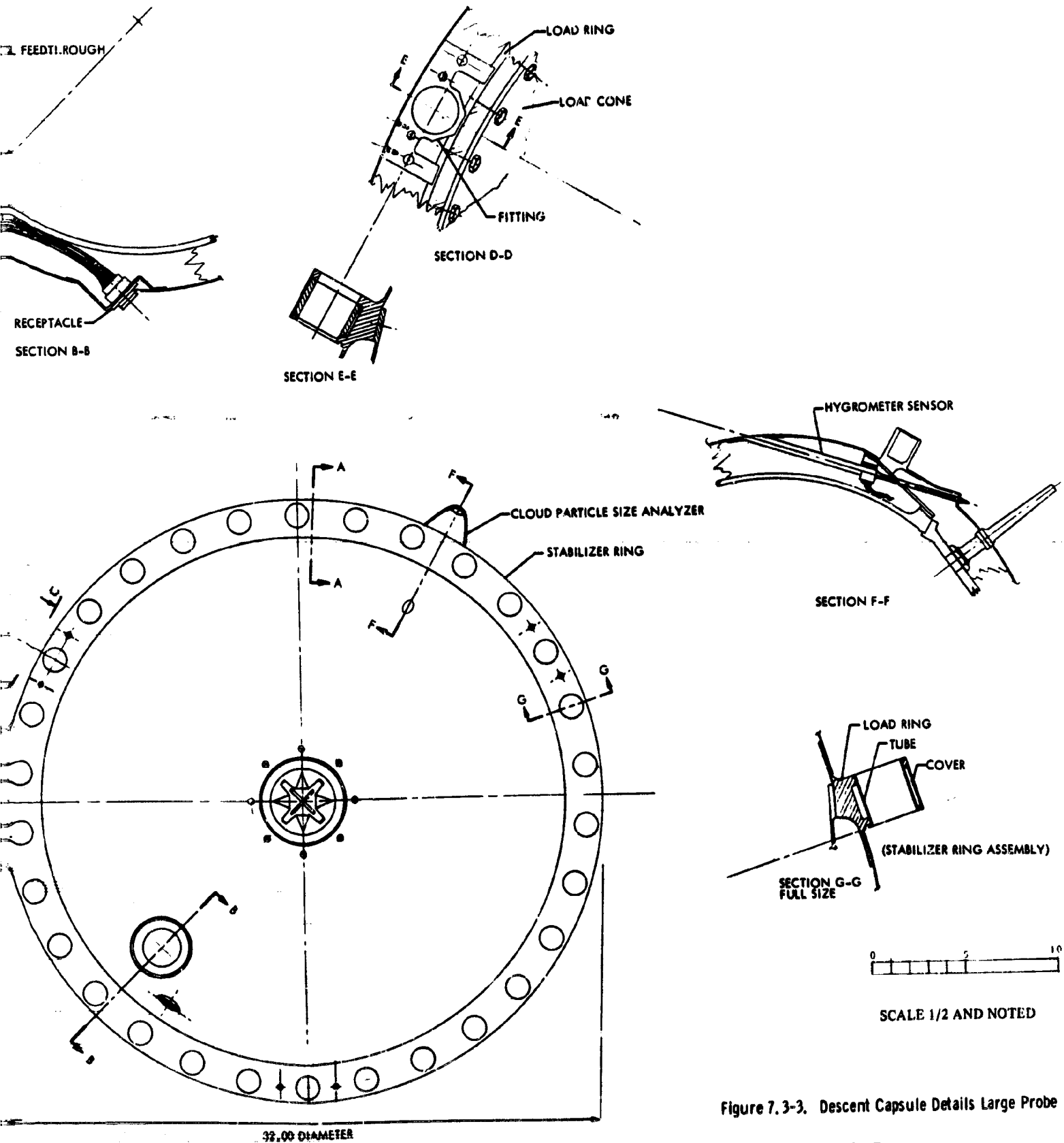
SECTION A-A FULL SIZE

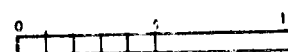
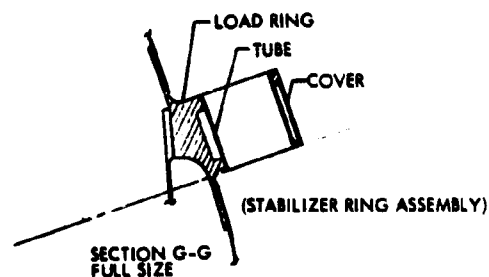
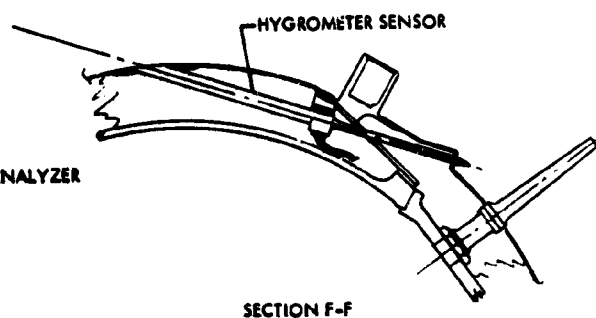
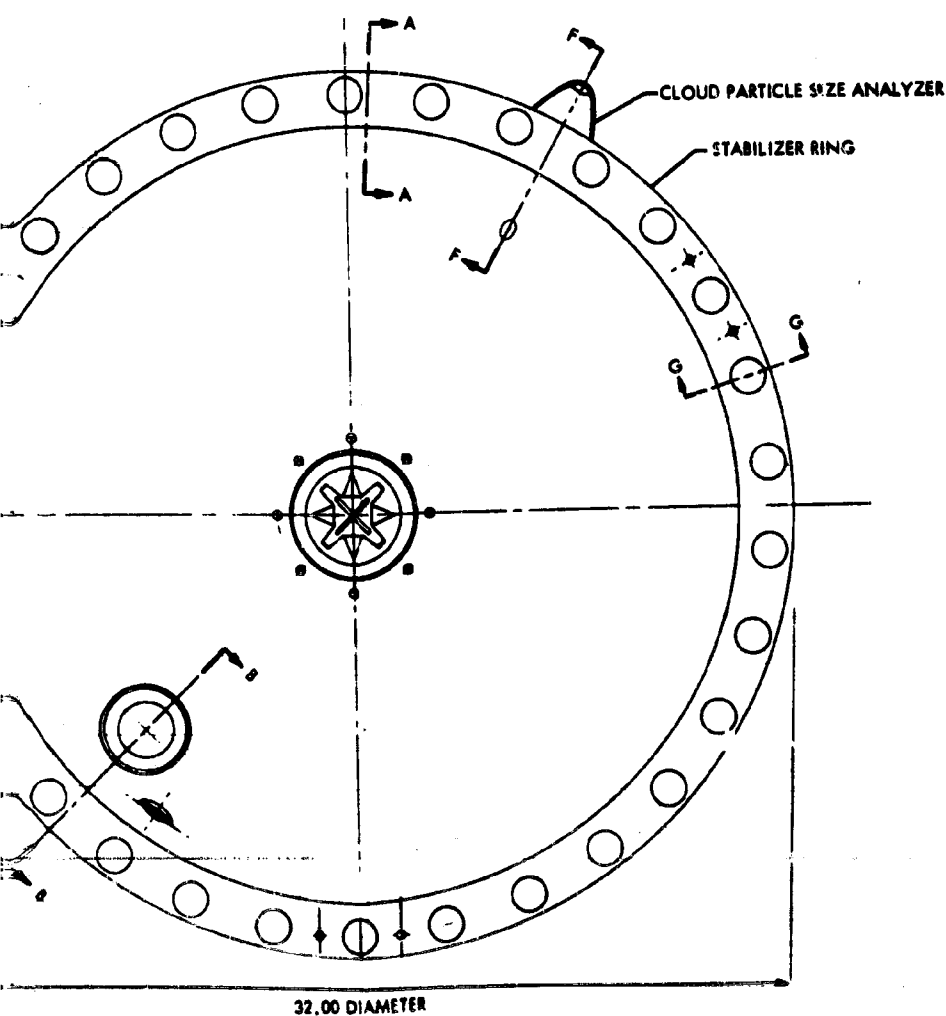
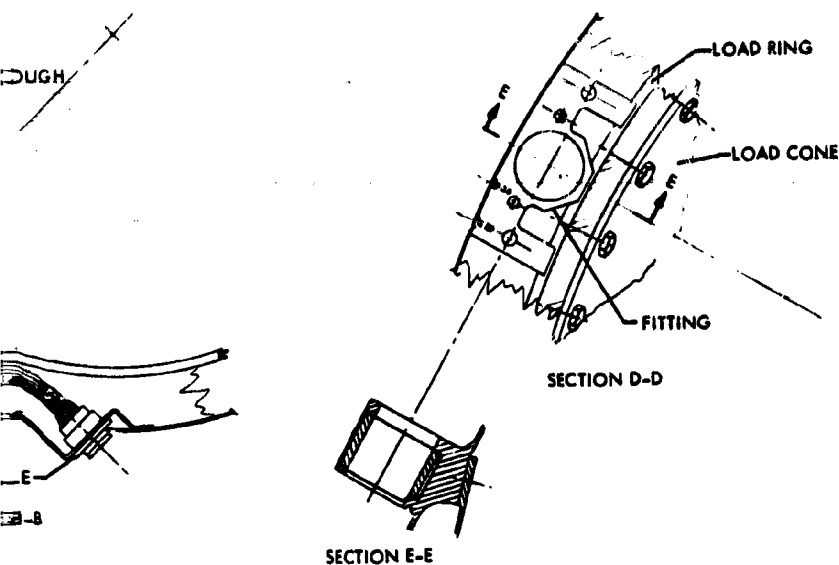


UMBILICAL CONNECTOR RECEPTACLE



VIEW C-C



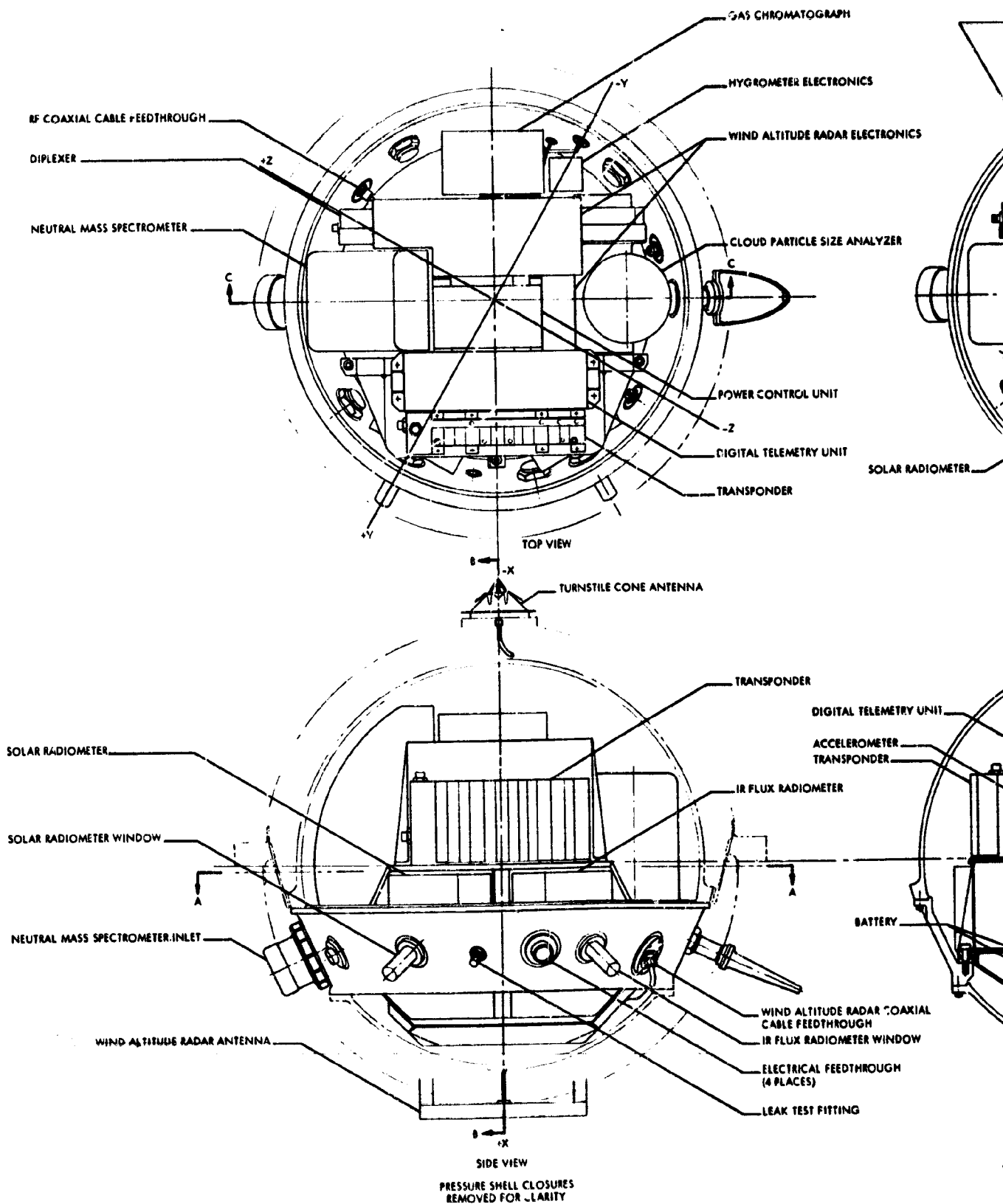


SCALE 1/2 AND NOTED

Figure 7.3-3. Descent Capsule Details Large Probe

7.3-5

FOLDOUT



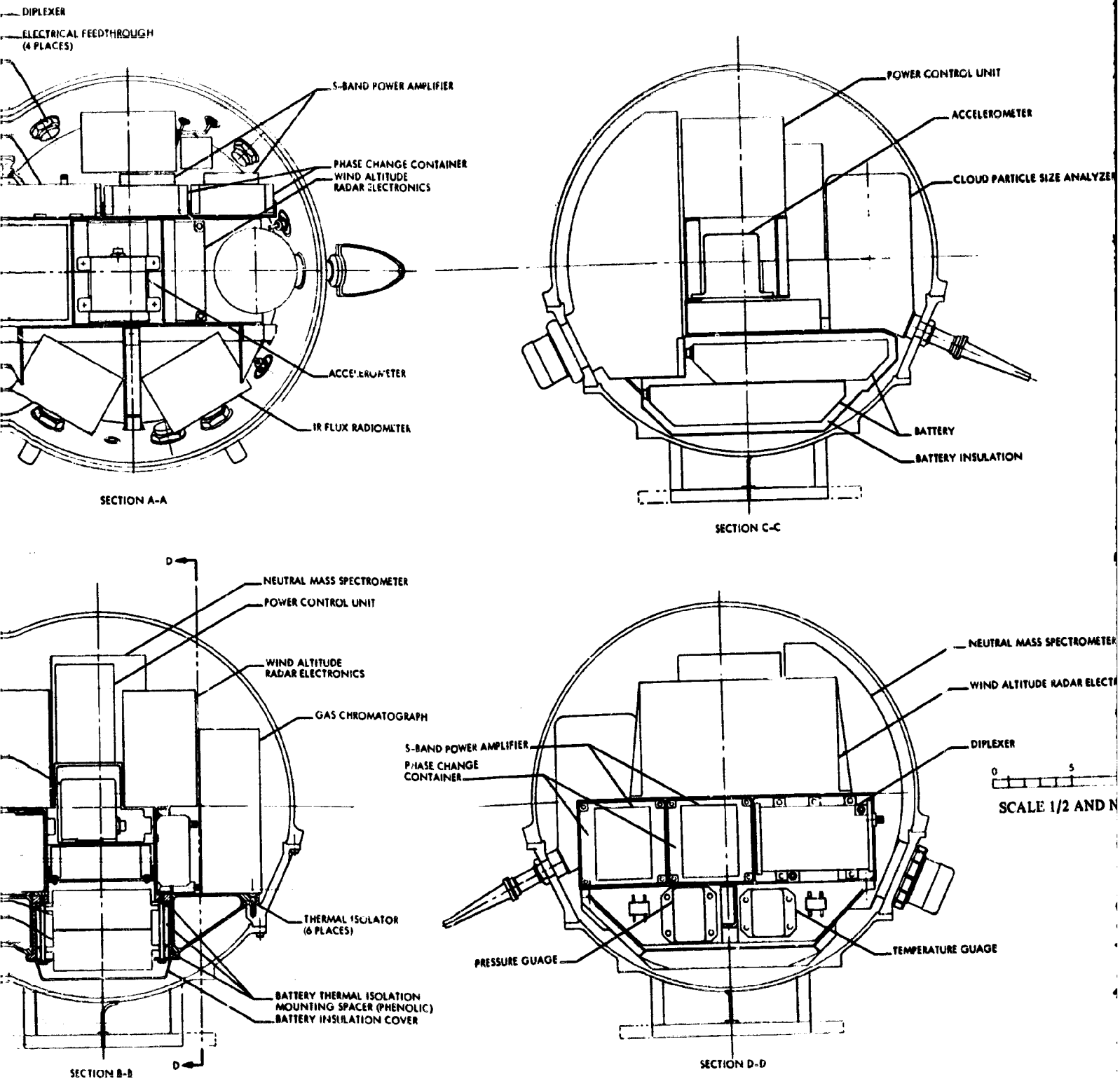


Figure 7.3-4. Equipment Arrangement of Large

7.3-6

FOLDOUT FR

FOLDOUT FRAME 2

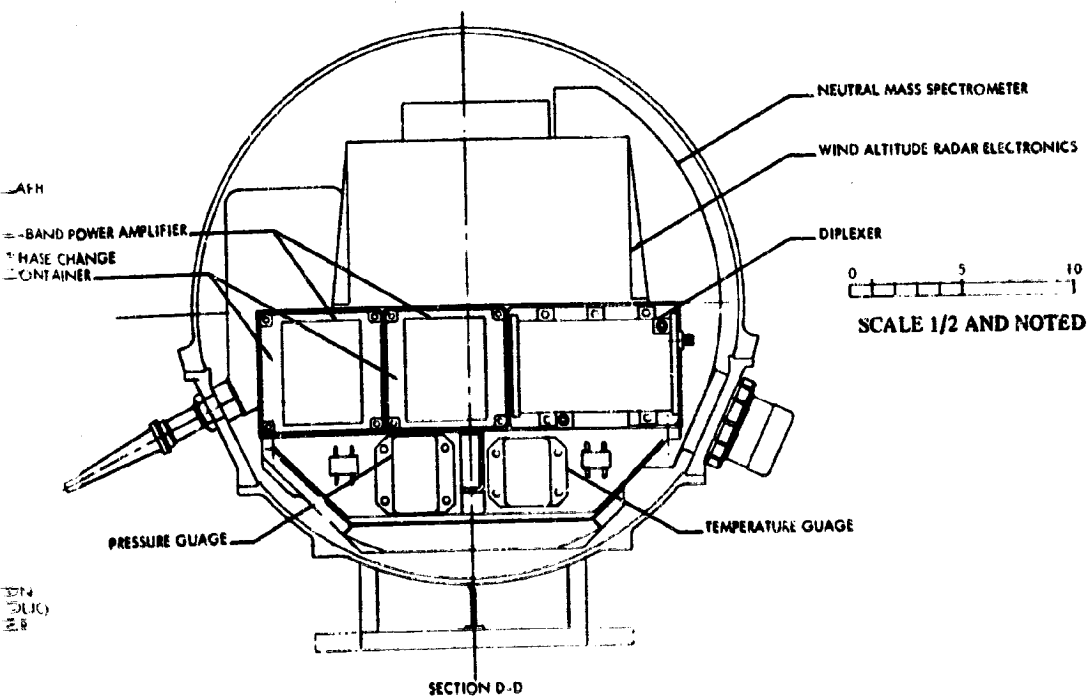
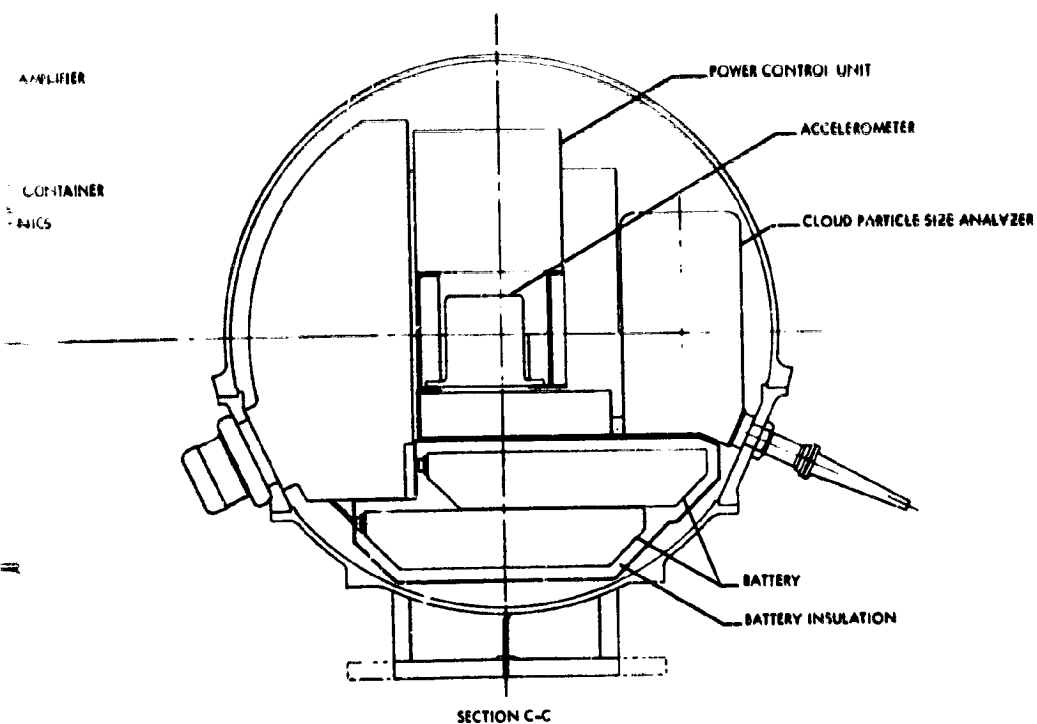


Figure 7.3-4. Equipment Arrangement of Large Probe

7.3.1.2 Small Probe Description

The small probe pressure vessel and aeroshell comprise an integral descent capsule as shown in Figure 7.3-5. The distinctive structural feature of the small probe is that the main load path for support of the pressure shell in the aeroshell is through the thermal insulation. This distributes load and minimizes skin thickness and also reduces insulation fabrication and installation costs due to the elimination of frames. Ease of access to science and electronic equipment is a primary consideration and the location of joints and penetrations is established with particular regard to that requirement.

Science sensors are exposed or deployed by ejecting cover segments in the aeroshell with simple adaptations of standard commercial release devices, as shown in Figure 7.3-5.

7.3.1.3 Arrangement of Structures and Mechanisms

Further information relative to study results of structure and mechanism design follows in the order given:

- 1) Requirements - a listing of requirements particularly pertinent to this section.
- 2) Tradeoffs - a description of alternatives considered and rationale for selection of preferred configurations, including tradeoffs directly related to the selected configuration, and related to earlier configurations.
- 3) Preferred Subsystem, Atlas/Centaur - a detailed description of structural and mechanical features of the preferred Atlas/Centaur large and small probe features.
- 4) Preferred Subsystem, Thor/Delta - a description similar to 3) for Thor/Delta.
- 5) Supporting Analyses and Tests - a report on the structural analyses and tests performed.

7.3.2 Requirements

The basic general requirements are to mount all science and electronics equipment and to provide environmental protection to assure functioning of all required systems until impact on the surface of the planet. Another basic requirement is to provide maximum ease of access for servicing or replacement of equipment and to assure successful operation.

One of the most significant requirements is to withstand the high entry deceleration. The implications of this requirement extend not only to sizing structure for high loads but to supporting wire bundles so connectors will not disconnect or coax cable so it will not kink. Some significant specific requirements are presented in Table 7.3-1.

7.3.3 Tradeoffs

In arriving at the preferred configuration, many alternative choices arose. In many of these cases the decision on selected configuration was quite clear and no real tradeoff was required, but in other cases the choice was not immediately obvious and systematic evaluation (tradeoff) was required. Cost, performance, and weight were the bases for evaluation of alternatives with weight a much more significant consideration on Thor/Delta than on Atlas/Centaur. The major tradeoff considerations for items where the choice is not obvious are presented here.

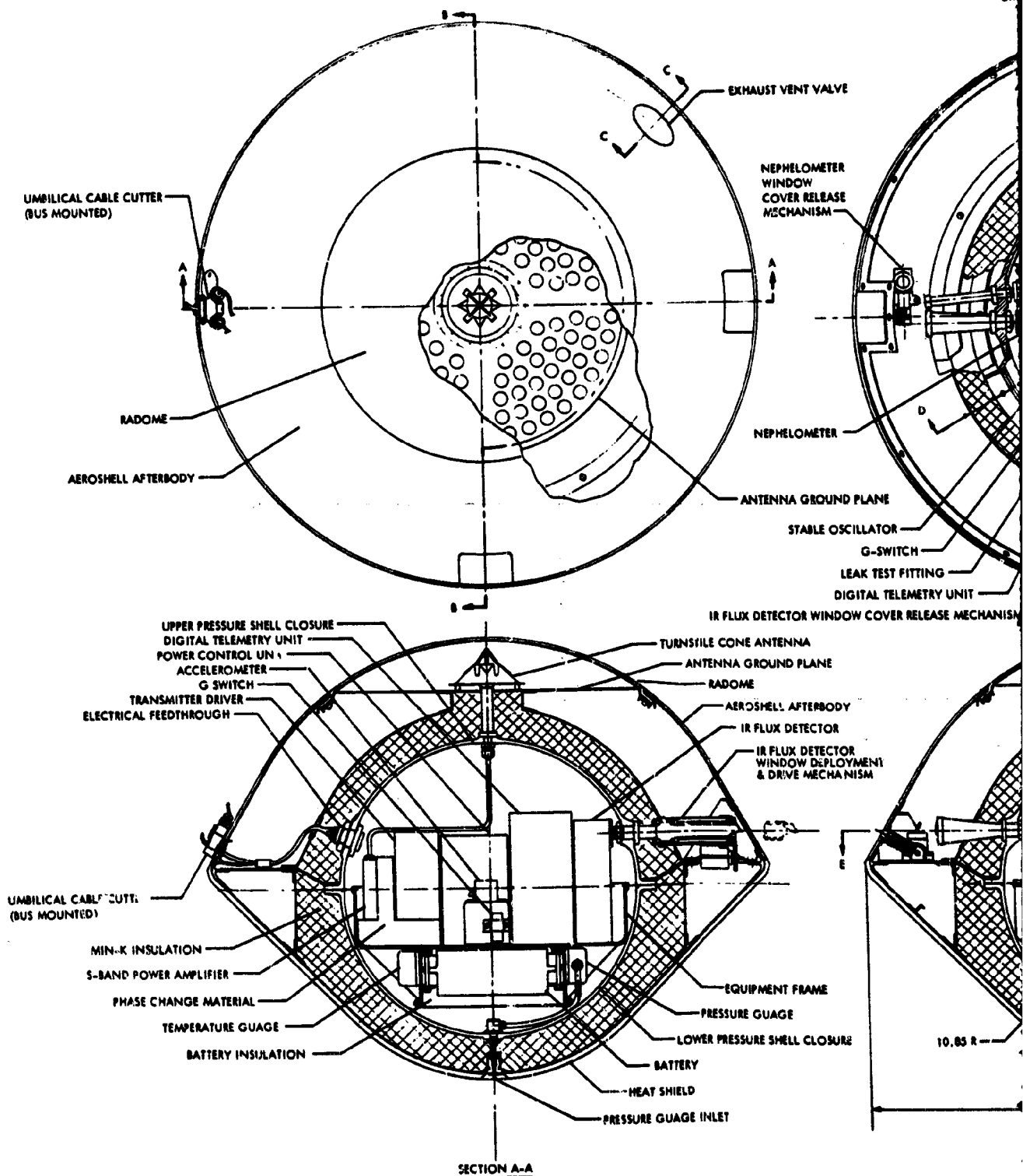
7.3.3.1 Parachute and Antenna Location

Selection of the configuration that best satisfied the demands of parachute deployment, RF transmission, aerodynamics, mass properties, and reliable staging of aeroshell, required the most extensive evaluation of alternatives in structures and mechanisms. It is not possible to adopt the obvious, first choice arrangements for each of these items because they conflicted. The principal configurations considered and their advantages and disadvantages are presented in Table 7.3-2.

7.3.3.2 Selection of Large Probe Aeroshell Skin Design

Aluminum and titanium material in honeycomb sandwich and in frame stabilized monocoque form were considered. A parametric weight study prepared by Martin Marietta for a broad range of planetary entries (Contract JPL 953311, "Outer Planet Entry Probe System Study, Aeroshell Parametric Weight Study") was used as a basis for evaluating these alternatives. The range of aeroshell pressures was between 34.47 and 413.68 N/cm² (50 and 600 psi) and the base diameters ranged from 0.762 to 1.219 m (2.5 to 4.0 ft).

For the lower range of pressures considered, the aluminum frame stabilized skin construction produces the lightest weight aeroshell. The titanium frame stabilized skin construction is relatively inefficient at



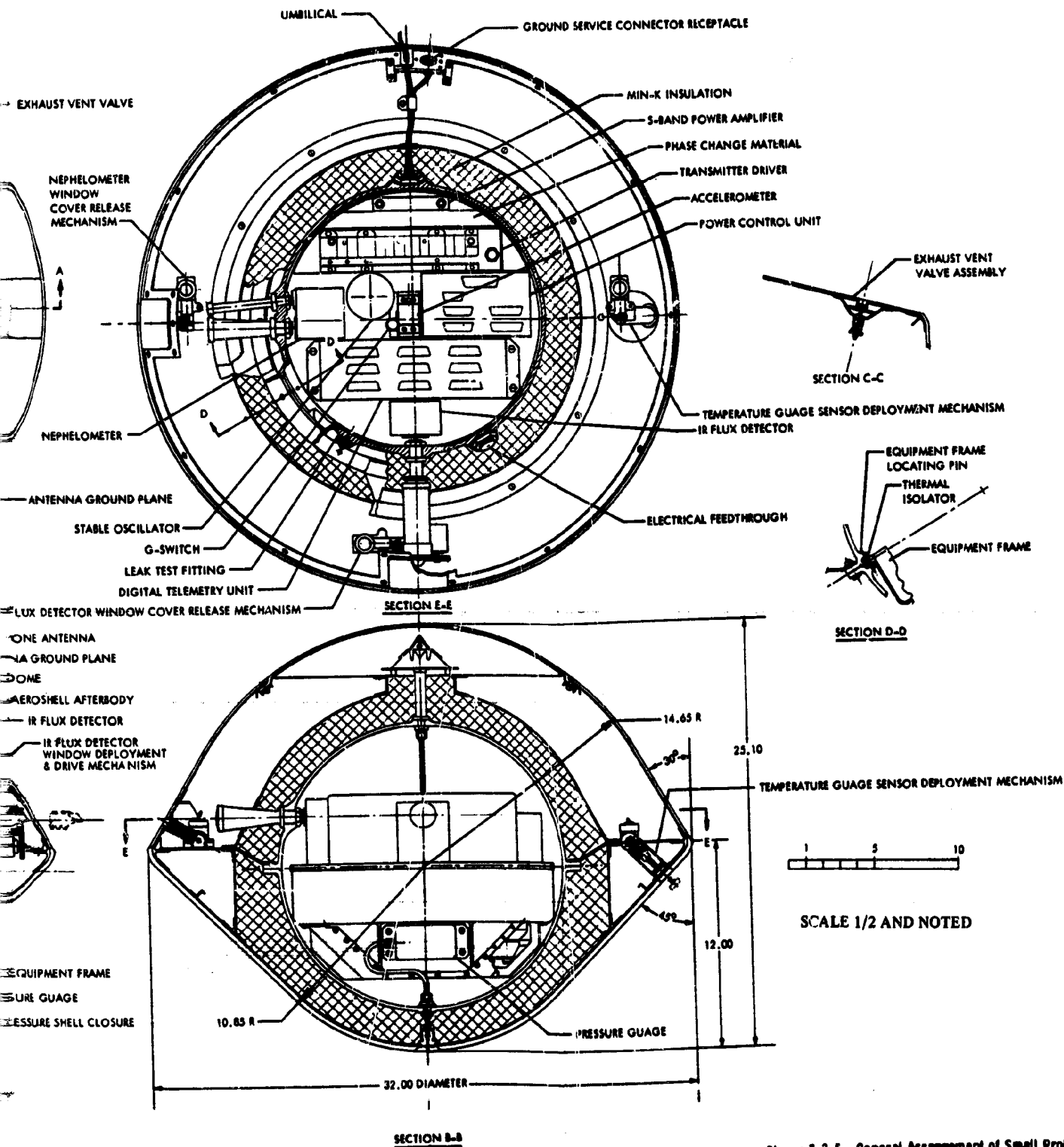


Figure 7.3-5. General Arrangement of Small Probe

Table 7.3-1. Significant Specific Design Requirements

ITEM	LARGE PROBE	SMALL PROBE
T/D PRESSURE VESSEL ULTIMATE COLLAPSE PRESSURE	93 ATMOSPHERES	93 ATMOSPHERES
T/D PRESSURE VESSEL ULTIMATE BURST PRESSURE	6 ATMOSPHERES	6 ATMOSPHERES
A/C PRESSURE VESSEL ULTIMATE COLLAPSE PRESSURE	116 ATMOSPHERES	116 ATMOSPHERES
A/C PRESSURE VESSEL ULTIMATE BURST PRESSURE	6 ATMOSPHERES	6 ATMOSPHERES
AEROSHELLAP (LIMIT)	0.689 N/CM ² (1.0 PSI)	0.689 N/CM ² (1.0 PSI)(a)
PARACHUTE RELEASE ALTITUDE	42.9 KM (140 748 FT)	N/A
PRESSURE VESSEL LEAKAGE RATE	0.005 CC/SEC	0.005 CC/SEC
SCIENCE SHELF FLATNESS	1.27 MM (0.005 IN.)	1.27 MM (0.005 IN.)
SCIENCE SHELF ANGULAR TOLERANCE	0.0087 RAD (0.5°)	0.0087 RAD (0.5°)
MAXIMUM INDIVIDUAL SCIENCE WEIGHT	12.2 KG (26 LB)	0.64 KG (1.4 LB)
MAXIMUM TOTAL	41.8 KG (92 LB)	3.45 KG (7.6 LB)
CG ACTUAL LOCATION LIMIT	3% OF MAJOR DIAMETER FORWARD OF MAJOR DIAMETER	2.5% OF MAJOR DIAMETER FORWARD OF MAJOR DIAMETER
RADIAL CG LOCATION TOLERANCE	± 2.54 MM (0.1 IN.)	± 2.54 MM (0.1 IN.)
T/D ENTRY DECELERATION	365 G'S	293 G'S (b)(c)
A/C ENTRY DECELERATION	358 G'S	488 G'S (c)
AFTERBODY RF ATTENUATION (MAX)	0.1 DB	0.1 DB
ENTRY ACOUSTICS A/C	141 DB	149 DB (d)
ENTRY ACOUSTICS T/D	140 DB	147 DB (d)
LAUNCH ACOUSTICS A/C	142 DB	142 DB (d)
LAUNCH ACOUSTICS T/D	140 DB	140 DB (d)
LAUNCH SUSTAINED ACCELERATION (A/C AND T/D)	LONGITUDINAL ± 20 G'S LATERAL ± 12 G'S	LONGITUDINAL ± 20 G'S LATERAL ± 10 G'S (e)
NOTES: (a) ASCENT AND DESCENT PRESSURE ON AEROSHELL. FOREBODY IS DESIGNED FOR ENTRY PRESSURE (b) 3-SIGMA ENTRY TRAJECTORY FOR '77 MISSION (c) 3-SIGMA ENTRY TRAJECTORY (d) ADD 4 DB TO GET TEST VALUES (e) LIMIT VALUES		
LARGE PROBE DESIGN QUALIFICATION RANDOM VIBRATION (THOR/DELTA)		
HZ	G ² /HZ	NOTE
20-300	±3 DB/OCTAVE	PSD LEVELS ARE 2.75 x EXPECTED 2 SIGMA FLT LEVELS.
300-2000	0.045	
OVERALL SPL	9.2 GRMS	
DURATION	2 MIN/AXIS (3 MUTUALLY PERPENDICULAR AXES)	
LARGE PROBE QUALIFICATION RANDOM VIBRATION (ATLAS/CENTAUR)		
20-130	0.00081 to 0.045 AT 608/OCTAVE	
150-2000	0.045	
OVERALL SPL	9.3 GRMS	
DURATION	4 MIN/AXIS (MUTUALLY PERPENDICULAR)	
LARGE PROBE DESIGN QUALIFICATION SINUSOIDAL VIBRATION ATLAS/CENTAUR		
AXIS	HZ	LEVEL (G, G-TO-PEAK)
AXIAL	5-8.5	1.2 IN. DA
	8.5-200	± 4.6 G
LATERAL	5-8	0.90 IN. DA
	8-7000	± 3.0 G
		SWEEP RATE (OCTAVES/MIN)
		2.0
		2.0
		2.0
		2.0
SMALL PROBE DESIGN QUALIFICATION RANDOM VIBRATION - ATLAS/CENTAUR AND THOR/DELTA		
20-60	0.05	
60-300	±308/OCTAVE	
300-1200	0.25	
1200-2000	±408/OCTAVE	
OVERALL	19.6 GRMS	
DURATION	1 MIN/AXIS (3 MUTUALLY PERPENDICULAR)	
SMALL PROBE DESIGN QUALIFICATION SINUSOIDAL VIBRATION - ATLAS/CENTAUR AND THOR/DELTA		
DIRECTION	HZ	G'S, G-TO-PEAK
AXIAL	3-15	±5" DOUBLE AMPLITUDE DISPLACEMENT (D.A.)
	15-21	15
	21-35	7.5
	35-50	5.0
	50-100	3.0
LATERAL	5-30	±5" D.A.
	30-100	3.0

Tabl

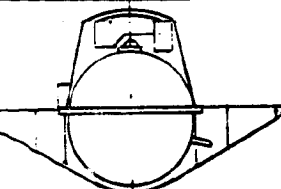
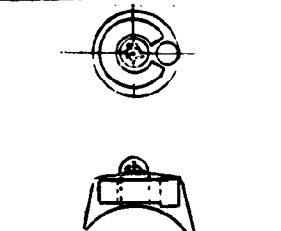
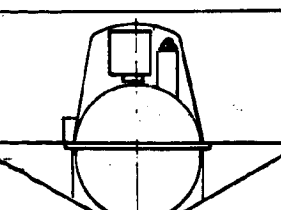
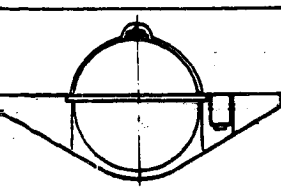
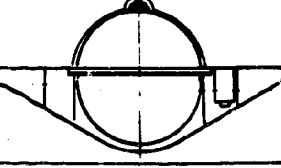
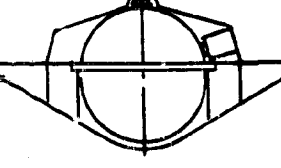
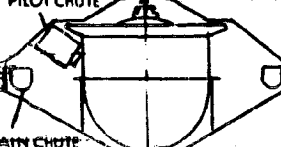
DESCRIPTION		EVALUATION OF EFFECT ON INDIVIDUAL CONSIDERA					
PICTORIAL	NARRATIVE	PRINCIPAL ADVANTAGE	PRINCIPAL DISADVANTAGE	PARACHUTE	RF TRANSMISSION	AERODYNAMICS	MASS
	ANTENNA UNDER PARACHUTE PACKAGE. MORTARED PILOT CHUTE.	REASONABLE SATISFACTION OF ALL REQUIREMENTS.	RF TRANSMISSION THROUGH PARACHUTE PACK.	NEARLY CONVENTIONAL PACK.	TRANSMISSION THROUGH PARACHUTE PACK DURING CRUISE/ENTRY. CLEAR FIELD AFTER STAGING.	CLEAN, SYMMETRICAL SHAPE.	NEARLY
	PARACHUTE AROUND ANTENNA. MORTARED PILOT CHUTE.	GOOD ANTENNA VIEW AT ALL TIMES.	UNKNOWN PARACHUTE DEVELOPMENT.	DEPLOYMENT FROM TORROIDAL TROUGH	GOOD	CLEAN AND SYMMETRICAL. MORE ANTENNA PROTRUSION THAN IS DESIREABLE.	NEARLY
	MORTARED MAIN PARACHUTE ON BACK OF AFTERBODY.	MOST SIMPLE AND RELIABLE PARACHUTE DEPLOYMENT.	LARGE AXIAL EXTENSION OF AFTERBODY. POOR ANTENNA GROUND PLANE.	SIMPLEST AND MOST RELIABLE DEPLOYMENT, BUT REQUIRES DEVELOPMENT OF LARGE MORTAR.	UNDESIREABLE. UNSYMMETRICAL, DEEP CAVITY BEHIND GROUND PLANE.	UNDESIREABLE. VERY LARGE AFTERBODY. LARGE UNSYMMETRICAL ANTENNA ON DESCENT CAPSULE.	UNDESIRABLE WAY TO BALANCE PHASES
	FOREBODY MAIN PARACHUTE MOUNT. MORTARED MAIN PARACHUTE.	SMALL CLEAN AEROSHELL AFTERBODY. RELATIVELY SIMPLE PARACHUTE DEPLOYMENT.	UNBALANCE - BALLAST REQUIRED.	SIMPLE DEPLOYMENT, BUT LARGE AMPLITUDE OSCILLATIONS. PROBLEM OF PACKAGING AND STRIPPING LINES ACROSS JOINT BETWEEN AEROSHELL HALVES AND AROUND AFTERBODY.	EXCELLENT THROUGHOUT.	CLEAN AND SYMMETRICAL. MORTAR IMPULSE TILTS CAPSULE MORE THAN IS DESIREABLE.	HIGHLY BALANCE. BALANCE REQUIRE NO FU
	FOREBODY MAIN PARACHUTE MOUNT. MORTARED PILOT CHUTE ADJACENT TO MAIN PARACHUTE PACK.	SMALL, CLEAN AEROSHELL AFTERBODY. RELATIVELY SIMPLE PARACHUTE DEPLOYMENT.	UNBALANCE. BALLAST REQUIRED.	NO OSCILLATION PROBLEM BUT OTHERWISE SAME AS 4A.	EXCELLENT THROUGHOUT.	CLEAN AND SYMMETRICAL.	SAME
	LOWER AFTERBODY MAIN PARACHUTE MOUNT. MORTAR DEPLOYED.	MORTAR IMPULSE THROUGH CG, SHORT AFTERBODY, SIMPLE PARACHUTE DEPLOYMENT.	UNBALANCE. BALLAST REQUIRED. TIME TO DAMP OUT CHUTE DEPLOYMENT OSCILLATIONS IS INCREASED. (SEE SECTION 7.3)	SIMPLE DEPLOYMENT BUT LARGEST PROBE OSCILLATIONS OF METHODS EVALUATED.	EXCELLENT THROUGHOUT.	CLEAN AND SYMMETRICAL AFTER STAGING. SOME UNBALANCE OF ENTRY CONFIGURATION.	VERY ASYMMETRICAL. NON BALANCE
	MAIN CHUTE IN TORROIDAL CONTAINER IN THE FOREBODY. PILOT CHUTE IN AFTERBODY.	GOOD WEIGHT DISTRIBUTION. GOOD ANTENNA VIEW AT ALL TIMES.	COST AND UNCERTAINTIES OF PARACHUTE DEVELOPMENT. PILOT DEPLOYMENT INDUCES LATERAL LOADS ON MAIN CHUTE DURING EXTRACTION.	NEW PACKAGING CONCEPT. NEW DEPLOYMENT CONCEPT. COST HARD TO PREDICT BUT EXPECTED TO BE HIGH.	EXCELLENT THROUGHOUT.	THE PARTICULAR ENTRY BODY SHOWN HAS RELATIVELY POOR LOW SPEED STABILITY CHARACTERISTICS. CHUTE CONCEPT, HOWEVER, COULD BE ADAPTED TO A BETTER AERO SHAPE.	GOOD BALANCE

Table 7.3-2. Parachute/Antenna Location Tradeoff

PRINCIPAL ADVANTAGE	PRINCIPAL DISADVANTAGE	EVALUATION OF EFFECT ON INDIVIDUAL CONSIDERATIONS					PRINCIPAL REASON FOR SELECTION OR REJECTION
		PARACHUTE	RF TRANSMISSION	AERODYNAMICS	MASS PROPERTIES	STAGING	
ENABLE SATISFACTION OF ALL REQUIREMENTS.	RF TRANSMISSION THROUGH PARACHUTE PACK.	NEARLY CONVENTIONAL PACK.	TRANSMISSION THROUGH PARACHUTE PACK DURING CRUISE/ENTRY. CLEAR FIELD AFTER STAGING.	CLEAN, SYMMETRICAL SHAPE.	NEARLY BALANCED.	AFT AEROSHELL CAP RELEASE MECHANISM REQUIRED. NO SEPARATION CLEARANCE PROBLEMS.	SATISFIES ALL CONSIDERATIONS WITHOUT SERIOUS SHORTCOMINGS. RESULTS IN LOWEST COST.
GOOD ANTENNA VIEW AT ALL TIMES.	UNKNOWN PARACHUTE DEVELOPMENT.	DEPLOYMENT FROM TORROIDAL TROUGH	GOOD	CLEAN AND SYMMETRICAL. MORE ANTENNA PROTRUSION THAN IS DESIREABLE.	NEARLY BALANCED.	SIMILAR TO 1, BUT SMALLER CAP FOR PILOT TO REMOVE.	SLIGHTLY LESS STANDARD PARACHUTE DEVELOPMENT. ALTERNATIVE 1 USED PROVEN CONCEPTS.
SIMPLE AND RELIABLE PARACHUTE DEPLOYMENT.	LARGE AXIAL EXTENSION OF AFTERBODY. POOR ANTENNA GROUND PLANE.	SIMPLEST AND MOST RELIABLE DEPLOYMENT, BUT REQUIRES DEVELOPMENT OF LARGE MORTAR.	UNDESIREABLE. UNSYMMETRICAL, DEEP CAVITY BEHIND GROUND PLANE.	UNDESIREABLE. VERY LARGE AFTERBODY. LARGE UNSYMMETRICAL ANTENNA ON DESCENT CAPSULE.	UNDESIREABLE. NO WAY TO HAVE BALANCE IN ALL PHASES OF STAGING.	SEPARATION CLEARANCE PROBLEM BETWEEN MORTAR AND ANTENNA. PROBABLY NEED GUIDE.	UNDESIREABLE FOR ALL CONSIDERATIONS EXCEPT PARACHUTE DEPLOYMENT. CHUTE SIZE CHANGES WILL REQUIRE REVIEW OF MORTAR DEVELOPMENT PROGRAM.
ALL CLEAN AEROSHELL AFTERBODY. RELATIVELY SIMPLE PARACHUTE DEPLOYMENT.	UNBALANCE - BALLAST REQUIRED.	SIMPLE DEPLOYMENT, BUT LARGE AMPLITUDE OSCILLATIONS. PROBLEM OF PACKAGING AND STRIPPING LINES ACROSS JOINT BETWEEN AEROSHELL HALVES AND AROUND AFTERBODY.	EXCELLENT THROUGHOUT.	CLEAN AND SYMMETRICAL. MORTAR IMPULSE TILTS CAPSULE MORE THAN IS DESIREABLE.	HIGHLY UNDESIREABLE. LARGE BALANCING MASSES REQUIRED THAT HAVE NO FUNCTION.	CLEAN EXCEPT FOR PROBLEMS OF STRIPPING PARACHUTE RISERS OUT OF HEAT SHIELD.	UNACCEPTABLY LARGE AMOUNT OF BALLAST.
ALL CLEAN AEROSHELL AFTERBODY. RELATIVELY SIMPLE PARACHUTE DEPLOYMENT.	UNBALANCE. BALLAST REQUIRED.	NO OSCILLATION PROBLEM BUT OTHERWISE SAME AS 4A.	EXCELLENT THROUGHOUT.	CLEAN AND SYMMETRICAL.	SAME AS 4A.	SAME AS 4A.	SAME AS 4A.
MORTAR IMPULSE THROUGH CG. SHORT AFTERBODY. SIMPLE PARACHUTE DEPLOYMENT.	UNBALANCE. BALLAST REQUIRED. TIME TO DAMP OUT CHUTE DEPLOYMENT OSCILLATIONS IS INCREASED (SEE SECTION 7.5)	SIMPLE DEPLOYMENT BUT LARGEST PROBE OSCILLATIONS OF METHODS EVALUATED.	EXCELLENT THROUGHOUT.	CLEAN AND SYMMETRICAL AFTER STAGING. SOME UNBALANCE OF ENTRY CONFIGURATION.	VERY UNDESIREABLE. LARGE, NONFUNCTIONAL BALANCING MASSES REQUIRED.	CLEAN AND SIMPLE.	UNACCEPTABLY LARGE AMOUNT OF BALLAST AND LARGE INDUCED OSCILLATIONS IN PROBE.
GOOD WEIGHT DISTRIBUTION. GOOD ANTENNA VIEW AT ALL TIMES.	COST AND UNCERTAINTIES OF PARACHUTE DEVELOPMENT. PILOT DEPLOYMENT INDUCES LATERAL LOADS ON MAIN CHUTE DURING EXTRACTION.	NEW PACKAGING CONCEPT. NEW DEPLOYMENT CONCEPT. COST HARD TO PREDICT BUT EXPECTED TO BE HIGH.	EXCELLENT THROUGHOUT.	THE PARTICULAR ENTRY BODY SHOWN HAS RELATIVELY POOR LOW SPEED STABILITY CHARACTERISTICS. CHUTE CONCEPT, HOWEVER, COULD BE ADAPTED TO A BETTER AERO SHAPE.	GOOD. NEARLY BALANCED.	PILOT CHUTE REQUIRED TO REMOVE LARGE AFTERBODY. OTHERWISE OK.	PARACHUTE COST AND UNCERTAINTY.

lower pressures but becomes more efficient at higher pressures. The aluminum structure reaches a working stress equal to its compressive yield strength at much lower pressures than do the titanium structures, thus aluminum is the more efficient material for either type of construction at the lower pressure range. As the pressure increases and the titanium reaches a working stress equal to its compressive yield strength then titanium becomes the more efficient of the two materials for both types of construction. The pressures at which aluminum and titanium curves cross each other are dependent on the base diameter of the aeroshell. This crossover point occurs at lower pressures for the larger diameter aeroshell since the larger diameter shells are more efficient, i. e., for a given design pressure, a larger percentage of the shell structure material is working to its compressive yield strength.

In general, the weight of sandwich construction was found not to be very competitive with frame-stabilized skin construction at higher design pressures. When design stresses of the frame/skin construction are equal to sandwich face skin stresses, sandwich construction carries a weight penalty because of additional components which are not really necessary to carry membrane loads, i. e., adhesive, core, and edge members. At lower design pressures, when frame/skin elements are in the instability range, sandwich face sheets are capable of working to the compressive yield strength of the material and, consequently, sandwich construction weight becomes much more competitive with that of the frame-stabilized skin construction. At very low design pressures [below the 34.47 N/cm^2 (50 psi) considered in this study], sandwich construction would prove to be the lighter weight method of construction.

Since the data from the JPL-sponsored study did not cover the 1.85 m (69 in.) diameter of the Atlas/Centaur large probe, additional data points were computed for aluminum ring stiffened monocoque and aluminum honeycomb to identify the trend for larger diameters. The results showed the ring stiffened monocoque to be more efficient at this size. Since the honeycomb construction is more costly because of tooling and heavier, the choice of ring stiffened monocoque was clear.

7.3.3.3 Design of Aerodynamic Stabilizing Ring Structure for the Descent Capsule Sphere

The requirements of light weight, ability to function at 755°K (900°F) temperature, maintenance of tight tolerances, and cost weighed in the choice between alternatives considered for fabrication of the stabilizing ring. Table 7.3-3 summarizes the facts considered in choosing the preferred machined titanium configuration.

7.3.3.4 Staging Separation System

The large probe requires three stages of separation to fulfill its mission, namely:

- 1) Separation of probe from bus,
- 2) Separation of aeroshell forebody,
- 3) Separation of aeroshell afterbody.

The first event, a bus function, not discussed here. Three arrangements were considered for accomplishing the second and third events for the preferred probe configuration; the evaluation of these alternatives is presented on Table 7.3-4.

7.3.3.5 Science Instrument Staging Clearance Cover Location

The protruding sensor of the cloud particle analyzer requires a cutout in the back face of the aeroshell forebody to provide clearance during forebody staging, (see Figure 7.3-1). This cutout must be covered during entry to keep hot gases away from structure. If the cover is in the aeroshell forebody it must be actuated open to allow staging clearance. This would leave a clean descent capsule, but a door opening failure could cause a separation failure or misalignment of the sensor. If the cover is mounted on the aeroshell afterbody, it would have to be actuated open to assure free flow of air through the cloud particle analyzer, but an actuation failure would not otherwise degrade the mission. In this mode the cover would remain on the afterbody as a folded up protrusion during parachute descent. The configuration of the door on the afterbody was selected because it was judged more desirable to have a fail-safe configuration than to optimize capsule aerodynamic shape during the flight regime when the parachute is providing a strong stabilizing influence.

7.3.3.6 Aeroshell Afterbody Configuration

Consideration was given to using a full afterbody design [Figure 7.3-6 (a)] on the large probe to achieve aerodynamic commonality with the small probe and to take advantage of the considerable amount of aero data that exists for these afterbody shapes. From the structural/mechanical standpoint, the tailored afterbody design (Figure 7.3-6b) offers advantages of lighter weight, greater staging clearances, and a compact spacecraft interface that allows greater bus/orbiter similarity. Decreased weight results from a reduced aeroshell afterbody surface area and from a smaller, shorter load structure between the spacecraft and the descent capsule load ring. Staging clearance with the full afterbody is critical between the science sensors and the afterbody rim and separation guide rails might well be required to assure staging success. The greater weight and the cost and uncertainties of ensuring separation with the full afterbody led to the choice of the tailored afterbody configuration from the structural/mechanical standpoint.

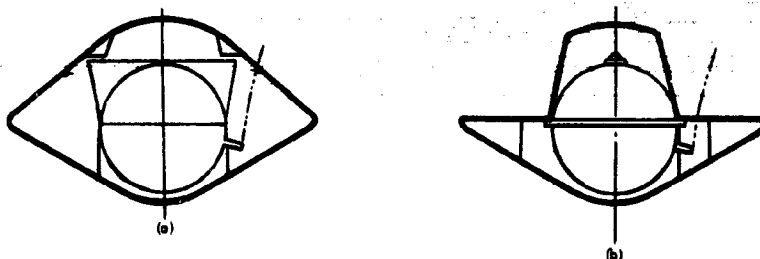


Figure 7.3-6. Optional Large Probe Shapes

7.3.3.7 Cost Consideration Relative to Pressure Shell Materials

Selection of pressure shell material involved consideration of the cost associated with the science/thermal interface, the total thermal structural mass, and the relative costs of fabricated pressure shells of different materials. A plot of the trend of estimated cost associated with science/thermal interface versus maximum shell temperature shows that, at temperatures much above the maximum equipment operating temperatures, costs start rising rapidly (Figure 7.3-7).

Taking 380°K (225°F) as cost effective temperature limit and imposing this as a limit on the plots of thermal/structural mass versus insulation thickness shows weights to be approximately equal for the three materials considered (see Figure 7.3-8).

Table 7.3-3.




DESCRIPTION		EVALUATION OF EFFECT ON INDIVIDUAL CONSIDERATIONS			
PICTORIAL	NARRATIVE	RELATIVE WEIGHT	THERMAL	TOLERANCES	FABRICATION
1 	MACHINED FROM TITANIUM FORGING WITH TI SLEEVES AND OUTER CLOSURE BAND.	9.07 KG (20 LB)	EXCELLENT THERMAL CHARACTERISTICS	CARE NEEDED TO ESTABLISH REQUIRED TOLERANCES BUT THEN WILL BE STABLE (0.0087 RAD (1/2°) HOLE ANGLE IS CRITICAL)	MODERATE COST RELATIVE TO OTHER CONFIGURATIONS
2 	ANGLE RING MACHINED FROM TI FORGING. FILLER BLOCK OF BERYLLIUM.	9.07 KG (20 LB)	EXCELLENT THERMAL CHARACTERISTICS	EASY TO ESTABLISH AND MAINTAIN TOLERANCES.	RELATIVELY EASY FOR FACILITY EQUIPPED TO HANDLE BERYLLIUM. HIGH MATERIAL COST.
3 SAME AS 2	SAME AS 2. EXCEPT FILLER BLOCK OF MAGNESIUM-THORIUM.	8.616 KG (19 LB)	MARGINAL. VERY LITTLE STRENGTH IN MG-TH AT (755° K)	SAME AS 2.	EASY FOR FACILITY WITH PERMIT TO MACHINE MG-TH. HIGH MATERIAL COST.
4 SAME AS 2	SAME AS 2. EXCEPT FILLER BLOCK OF ALUMINUM.	10.88 KG (24 LB)	MARGINAL. VERY LITTLE STRENGTH IN AL AT (755° K)	SAME AS 2.	EASY BUT EXTRA WORK OVER 2 AND 3 TO MACHINE LIGHTENING POCKETS.
5 SAME AS 2	FILLER BLOCK OF GLASS BEAD FILLED GLASS POLYIMIDE	7.71 KG (17 LB)	POOR. POLYIMIDE CHAR MAY CREATE UNACCEPTABLE AERODYNAMIC SURFACE	TOLERANCE EASY TO ESTABLISH BUT MAY BE LOST DUE TO CHAR.	EASY TO MACHINE. COSTLY PROCESS DEVELOPMENT FOR POLYIMIDE
6 	ANGLE RING MACHINED FROM TI FORGING. REMAINDER BUILT UP FROM TI SHEET AND TUBES.	6.35 KG (14 LB)	EXCELLENT THERMAL CHARACTERISTICS	MOST DIFFICULT TO ESTABLISH BUT THEN WILL BE STABLE.	VERY COSTLY MULTIPIECE ASSEMBLY.

Table 7.

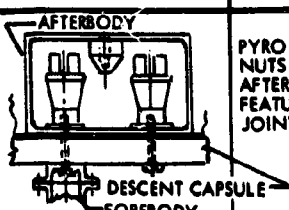
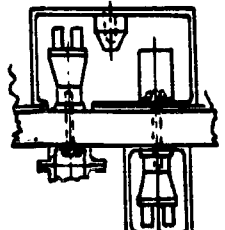
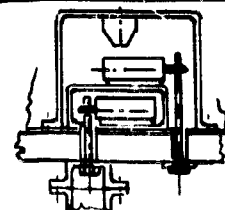
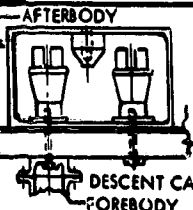
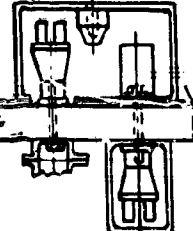
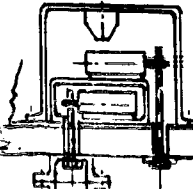
DESCRIPTION		ADVANTAGES	DISADVANTAGES
PICTORIAL	NARRATIVE		
	PYRO ACTUATED SEPARATION NUTS MOUNTED ON AEROSHELL AFTERBODY. BOLT EXTRACTION FEATURE PULLS BOLT OUT OF JOINT.	a. AERODYNAMICALLY CLEAN FINAL DESCENT CAPSULE CONFIGURATION. b. HIGHLY RELIABLE SEPARATION SYSTEM.	ORDNANCE FIRING CIRCUIT WIRES REQUIRE SEPARATION AFTER FIRING.
	PYRO ACTUATED SEPARATION NUTS MOUNTED ON AERODYNAMIC STABILITY FENCE. BOLT EXTRACTION FEATURE PULLS BOLT OUT OF JOINT.	a. ORDNANCE FIRING CIRCUIT WIRES DO NOT NEED TO BE CUT. b. HIGHLY RELIABLE SEPARATION SYSTEM.	SEPARATION NUT HOUSING REMAIN ON DESCENT CAPSULE MAY PERTURB AERODYNAMIC PERFORMANCE.
	PYRO ACTUATED PIN PULLERS MOUNTED ON AERODYNAMIC STABILITY FENCE. JOINING PIN PASSES THROUGH AERODYNAMIC HOLE.	SIMPLE RING STRUCTURE.	a. SIGNIFICANT LOAD MUST BE CARRIED BY PIN PULLER UNUSUAL APPLICATION b. LESS LIKELIHOOD OF OBTAINING LOW SHOCK PYRO ACTUATED DEVI

Table 7.3-3. Dynamic Stabilizing Ring Structure Tradeoff

	EVALUATION OF EFFECT ON INDIVIDUAL CONSIDERATIONS				RATIONAL FOR SELECTION OR REJECTION
	RELATIVE WEIGHT	THERMAL	TOLERANCES	FABRICATION	
	9.07 KG (20 LB)	EXCELLENT THERMAL CHARACTERISTICS	CARE NEEDED TO ESTABLISH REQUIRED TOLERANCES BUT THEN WILL BE STABLE (0.0087 RAD (1/2°) HOLE ANGLE IS CRITICAL)	MODERATE COST RELATIVE TO OTHER CONFIGURATIONS	SELECTED BECAUSE OF MODERATE COST AND CERTAINTY OF PERFORMANCE
	9.07 KG (20 LB)	EXCELLENT THERMAL CHARACTERISTICS	EASY TO ESTABLISH AND MAINTAIN TOLERANCES.	RELATIVELY EASY FOR FACILITY EQUIPPED TO HANDLE BERYLLIUM. HIGH MATERIAL COST.	REJECTED FOR COST REASONS
K	8.616 KG (19 LB)	MARGINAL. VERY LITTLE STRENGTH IN MG-TH AT (755°K)	SAME AS 2.	EASY FOR FACILITY WITH PERMIT TO MACHINE MG-TH. HIGH MATERIAL COST.	REJECTED FOR COST, MATERIAL AVAILABILITY AND MARGINAL PERFORMANCE REASONS.
K	10.88 KG (24 LB)	MARGINAL. VERY LITTLE STRENGTH IN AL AT (755°K)	SAME AS 2.	EASY BUT EXTRA WORK OVER 2 AND 3 TO MACHINE LIGHTENING POCKETS.	REJECTED BECAUSE OF MARGINAL PERFORMANCE AND DIFFERENTIAL EXPANSION PROBLEM.
LED	7.71 KG (17 LB)	POOR. POLYIMIDE CHAR MAY CREATE UNACCEPTABLE AERODYNAMIC SURFACE	TOLERANCE EASY TO ESTABLISH BUT MAY BE LOST DUE TO CHAR.	EASY TO MACHINE. COSTLY PROCESS DEVELOPMENT FOR POLYIMIDE	REJECTED FOR COST AND AERODYNAMIC UNCERTAINTY.
TI	6.35 KG (14 LB)	EXCELLENT THERMAL CHARACTERISTICS	MOST DIFFICULT TO ESTABLISH BUT THEN WILL BE STABLE.	VERY COSTLY MULTIPIECE ASSEMBLY.	REJECTED FOR COST REASONS

Table 7.3-4. Staging Separation Tradeoff

DESCRIPTION		ADVANTAGES	DISADVANTAGES	RATIONAL FOR SELECTION OR REJECTION
PICTORIAL	NARRATIVE			
	<p>PYRO ACTUATED SEPARATION NUTS MOUNTED ON AEROSHELL AFTERBODY. BOLT EXTRACTION FEATURE PULLS BOLT OUT OF JOINT.</p>	<p>a. AERODYNAMICALLY CLEAN FINAL DESCENT CAPSULE CONFIGURATION.</p> <p>b. HIGHLY RELIABLE SEPARATION SYSTEM.</p>	<p>ORDNANCE FIRING CIRCUIT WIRES REQUIRE SEPARATION AFTER FIRING.</p>	<p>ASSURANCE OF GOOD DESCENT PROFILE THROUGH CLEAN SHAPE. WIRE SEPARATION EASILY ACCOMPLISHED WITH SPRING ACTUATED CONNECTOR.</p>
	<p>PYRO ACTUATED SEPARATION NUTS MOUNTED ON AERODYNAMIC STABILITY FENCE. BOLT EXTRACTION FEATURE PULLS BOLT OUT OF JOINT.</p>	<p>a. ORDNANCE FIRING CIRCUIT WIRES DO NOT NEED TO BE CUT.</p> <p>b. HIGHLY RELIABLE SEPARATION SYSTEM.</p>	<p>SEPARATION NUT HOUSINGS REMAIN ON DESCENT CAPSULE, MAY PERTURB AERODYNAMIC PERFORMANCE.</p>	<p>REJECTED BECAUSE OF RISK OF UNSTEADY FINAL DESCENT.</p>
	<p>PYRO ACTUATED PIN PULLERS MOUNTED ON AERODYNAMIC STABILITY FENCE. JOINING PIN PASSES THROUGH AERODYNAMIC HOLE.</p>	<p>SIMPLE RING STRUCTURE.</p>	<p>a. SIGNIFICANT LOAD MUST BE CARRIED BY PIN PULLER. UNUSUAL APPLICATION.</p> <p>b. LESS LIKELIHOOD OF OBTAINING LOW SHOCK PYRO ACTUATED DEVICE.</p>	<p>REJECTED BECAUSE USAGE OF UNUSUAL APPLICATION OF PIN PULLER WOULD REQUIRE DEVELOPMENT, AND SHOCK INPUT MUST BE MINIMIZED.</p>

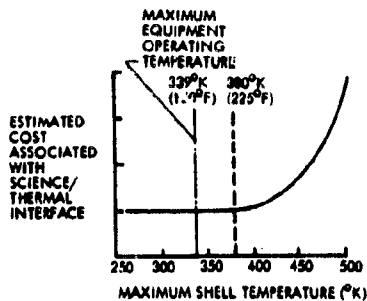


Figure 7.3-7. Cost versus Shell Temperature

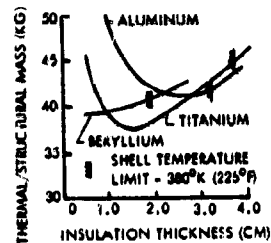


Figure 7.3-8. Thermal/Structural Mass versus Insulation Thickness

Relative costs of these materials are:

Aluminum	1.0 (preferred design)
Titanium	4.0
Beryllium	10.0

Through this analysis, aluminum was selected on the basis of cost.

7.3.3.8 Shape of Pressure Vessel

Spherical, ellipsoidal, and domed cylindrical shapes were considered as pressure vessel shapes. While a sphere might appear to be the obvious shape for a minimum weight pressure vessel of a given volume, the other shapes were considered as they might offer economy through commonality or ease of packaging, or might solve c. g. location problems. The domed cylindrical shape offered the added possibility that the domes could constitute the entire small probe ellipsoid. The ellipsoidal shape was necessary to attain required c. g. location on the "common aeroshell shape" versions of the small probe. For independent small and large probe shapes, the ellipsoid is not required for c. g. reasons and, as it is heavier and more costly to fabricate, it was therefore rejected. The common dome for a small probe vessel leads to an unsatisfactory large probe cylinder (too long for required c. g. location), so commonality is not feasible.

Although spherical shapes are not ideal from an equipment packaging standpoint, many arrangements of Pioneer Venus equipment have been successfully integrated into spheres in both probes. The structural efficiency of the sphere permits using more weight for increasing volume and design margins both of which are directly related to program cost reductions. Consequently, the spherical shapes have been chosen.

7.3.3.9 Selection of Pressure Shell Subassemblies

Four large probe pressure shell subassembly configurations were considered, two three segment and two two-segment configurations. Ease of access for servicing or replacing equipment was the prime consideration in selection. A description and comparison of the alternatives is presented in Table 7.3-5.

It should be noted that these tradeoffs were made before selection of the central, perforated aero-ring stabilizing device. Its selection further reinforces the choice of an equipment ring located forward of the equator.





7.3.3.10 Aeroshell Separation Design Approaches

An evaluation of aeroshell separation design approaches was performed for the Thor/Delta configuration early in the study. The preferred configuration has changed since that time, but the conclusions regarding selection of cartridge actuated nuts to effect forebody separation remain valid. The tradeoff study is presented here since it is still the basis for the preferred separation configuration shown in Figure 7.3-1. Conclusions relative to the base cover and parachute release design tradeoffs are not pertinent to the preferred Atlas/Centaur design (which uses cartridge actuated nuts, Figure 7.3-1), but are included to document the approaches evaluated. Figure 7.3-9 shows the capsule and aeroshell configuration at the time of the tradeoff.

Concept A1 - Forebody Separation

The pyrotechnic nut concept of aeroshell support, attachment, and separation is shown in the lower portion of Figure 7.3-10. Three pyrotechnic nuts located in equally spaced longerons provide secure restraint of the descent capsule in the aeroshell payload adapter ring. The longerons provide a direct load path between the bus interface and the descent capsule equipment canister. A continuous tension cone spans through the insulation from the cover at the equator to the pressure shell at the equipment shelf. It carries the high acceleration load applied at the adaptor flange through the insulation. A flange external to the insulation cover at the equator engages with a mating flange on the aeroshell payload ring. The aeroshell payload ring has a discontinuous mating flange. The nut secures the descent capsule within the payload ring for tension loads and provides a means of

Table 7.3-5. Pressure Shell Subassemblies Tradeoff

	NARRATIVE	ADVANTAGES	DISADVANTAGES	RATIONAL FOR SELECTION OR REJECTION
1	 <p>3-PIECE, NARROW EQUIPMENT RING BELOW LOAD CONE.</p>	<ol style="list-style-type: none"> 1. EASY ACCESS TO CRITICAL COMPONENTS. 2. EQUIPMENT RING CAN BE REMOVED WITHOUT DISTURBING AEROSHELL AFTER-BODY. 3. NARROW RING GIVES GREATEST ACCESS ON RING. 	<ol style="list-style-type: none"> 1. SHORT LOAD CONE PROVIDES SHORT HEAT AND SHOCK PATH. 2. MULTIPIECE INSULATION DISASSEMBLY REQUIRED TO GAIN ACCESS. 	EASIEST TOTAL ACCESSIBILITY.
2	 <p>2-PIECE, WIDE EQUIPMENT RING CENTERED, LOAD CONE BELOW PENETRATIONS.</p>	<ol style="list-style-type: none"> 1. EASY ACCESS TO CRITICAL COMPONENTS. 2. INSULATION ON EQUIPMENT RING DOES NOT HAVE TO BE DISTURBED FOR DISASSEMBLY. 	<ol style="list-style-type: none"> 1. COMPLETE PROBE DISASSEMBLY REQUIRED TO GAIN COMPLETE ACCESS. 2. EITHER SHORT LOAD CONE OR SENSORS PENETRATE CONE. 	NEED FOR AEROSHELL DIS-ASSEMBLY TO REMOVE EQUIPMENT RING.
3	 <p>2-PIECE, UNSYMMETRICAL LOAD CONE BELOW PENETRATIONS.</p>	<ol style="list-style-type: none"> 1. ONLY ONE JOINT TO SEAL. 	<ol style="list-style-type: none"> 1. COMPLETE PROBE DISASSEMBLY REQUIRED TO GAIN COMPLETE ACCESS. 2. SCIENCE ALIGNMENT AND CONNECTIONS BY TRIAL AND ERROR AND SPECIAL TOOLS. 	SAME AS CONFIGURATION 2 PLUS PRESSURE SHELL ASSEMBLY DIFFICULTY.
4	 <p>2-PIECE, SYMMETRICAL, LOAD CONE BELOW PENETRATIONS.</p>	<ol style="list-style-type: none"> 1. ONLY ONE JOINT TO SEAL. 2. ONE FORGING DESIGN. 	<ol style="list-style-type: none"> 1. SAME AS CONFIGURATION 3 PLUS SHORT LOAD CONE. 	SAME AS CONFIGURATION 3 PLUS SHORT LOAD CONE.

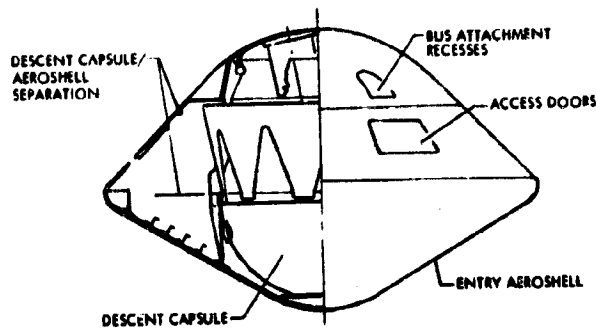


Figure 7.3-9. Configuration for Separation Design Tradeoff Study

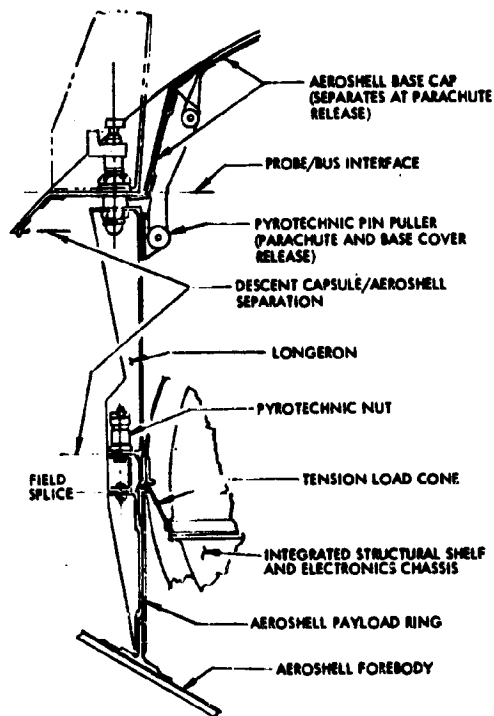


Figure 7.3-10. Separation, Concept A1

separation. The nuts were selected in preference to a segmented Marman clamp attachment (Figure 7.3-11) since they are more compatible than other concepts with a payload ring that has local cutouts to accommodate science instrument appendages, and they avoid potentially detrimental aerodynamic effects of the clamp flange. Separation reliability is provided by dual initiators on each nut. The continuity of the longerons to transmit compression boost loads through the load cone is provided by local stiffening of the cone. The aeroshell payload ring provides a partial means of guiding the separation by preventing lateral motion during the descent capsule's axial travel.

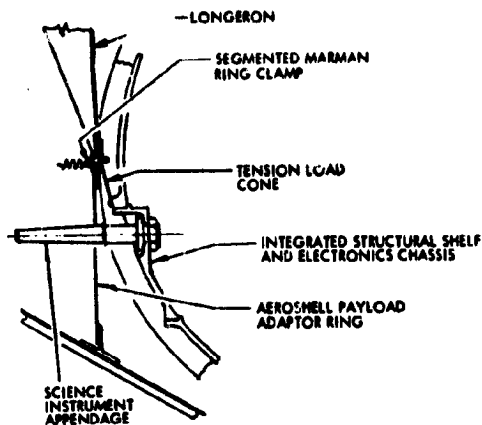


Figure 7.3-11. Separation, Concept A2 (Tension Cone with Segmented Marman Ring Clamp)

Concept A2 - Forebody Separation

In this approach (Figure 7.3-11) separation is achieved by pyrotechnically breaking a Marman ring clamp at locations coincident with the cutouts in the payload ring that accommodate the science appendages. This has the disadvantage that four break points are required because of the four cutouts for science instruments. An added disadvantage is that the clamp segments must retract adequately to ensure clearance of the projections. Also, the Marman clamp flange imposes an aerodynamic flow trip. An advantage is that much lower pyrotechnic shock levels are propagated to the electronics and science equipment.

Concept A3 - Forebody Separation

The shortest load path from the pressure shell flange to the aeroshell is a compression cylinder. This arrangement of descent capsule support in the aeroshell is shown in Figure 7.3-12. Attachment of the descent capsule to the aeroshell is provided by a continuous Marman clamp that is broken pyrotechnically to allow separation. An advantage of this system relative to concept A2 is that the aerodynamic flow around the equator is undisturbed because no external flange is needed. An annular recess is required at the adapter cylinder juncture to incorporate the clamp; however, its effects are negligible. Another advantage of this design is that the sensors, or protuberances, do not have to clear the payload support ring during separation.

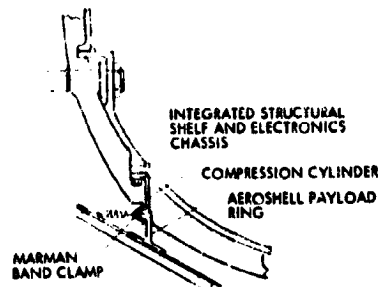


Figure 7.3-12. Separation, Concept A-3

The combined effect of the more direct structural load path and its impact on the thermal control was assessed relative to concept A2 and was found to result in essentially equal weight designs. However, because of inaccessibility for installation of the clamp deep in the aeroshell cap, this separation concept was not selected.

Base Cover Separation Concepts

Two arrangements of the base cover cap attachment to the descent capsule and separation mechanism are shown in the upper portion of Figure 7.3-10 and in Figure 7.3-13. Both incorporate a pyrotechnic pin puller for release of the cap. The main difference is in access to rig, install, and arm the pin puller in installation. Access to the pin puller in the first case is through the vents in the aerodynamic flare. (Figure 7.3-9). In the second case a door must be provided in the aerodynamic flare across the longeron. The flare vents required are adequate to provide access, however, more direct access is achieved in the second case.

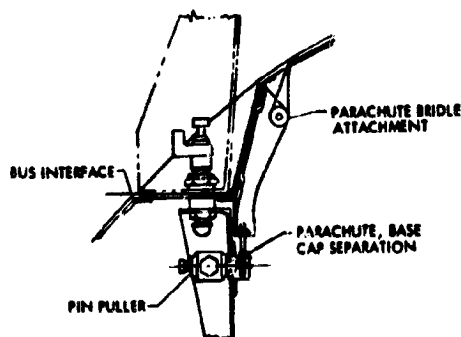


Figure 7.3-13. Parachute and Base Cover Release Concept

3.4 Atlas/Centaur - Preferred Subsystem

3.4.1 Large Probe

The large probe structural/mechanical subsystem is designed to carry loads and package equipment efficiently, to present a satisfactory aerodynamic configuration, and to allow easy access to science and electronic equipment. The compact frustum of a cone aeroshell afterbody nests into the bus central cylinder and accepts launch loads close to the descent capsule load ring. The aeroshell forebody transmits entry deceleration loads to the descent capsule load ring essentially in line with the launch load and close to the probe c.g. The descent capsule load ring also the aerodynamic stabilizer for the final descent configuration.

Access to equipment within the aeroshell is easily accomplished even after the probe is completely assembled. The aeroshell forebody can be removed without disturbing the cartridge actuated separation nut assemblies by removing six field splice bolts. Removal of the aeroshell forebody allows removal of the forward pressure vessel insulation and cover assembly and pressure shell assembly, providing direct access to batteries and other sensitive equipment located in the forward segment. Removal of the middle pressure vessel segment (the equipment ring) can also be accomplished without disturbing separation nuts or aeroshell afterbody and this allows access to all science equipment. The selected design avoids use of blind connectors and service loops in cabling to minimize harness and connector problems associated with high entry deceleration.

The large probe configuration and dimensions are shown in Figures 7.3-1 through 7.3-4. The total mechanical assembly includes thermal insulation and heat shielding as well as structure and mechanisms. The design and analysis of the heat shield is discussed in Section 7.2 and the thermal insulation in Section 7.4. The aerodynamic considerations of the external configuration are discussed in Section 7.1. A detailed discussion of structural and mechanical features follows.

Interfaces

The large probe attaches to the bus central cylinder with three equally spaced ball lock pins on a 77.5 cm (30.5 in.) diameter bolt circle. The probe is capable of withstanding all loads and environments associated with

the launch, boost, and cruise modes of operation at these points. A relative separation velocity of 0.3 m/s (1.0 ft/s) is imparted between the large probe and the bus at separation by three springs mounted on the bus and located at the probe/bus attach points. The umbilical from the bus to the probe passes through the aeroshell afterbody. A cartridge actuated cable cutter mounted on the spacecraft will sever the umbilical near the aeroshell surface before separation of the probe from the bus.

Descent Capsule

The descent capsule is basically a spherical body with a perforated annular ring with leading edge at the equator of the sphere. The principal elements of the capsule are:

- Pressure shell (in three segments),
- Equipment mounting beams and brackets,
- Insulation installation (in four assemblies),
- Outer shell (in four segments),
- Load ring/aerodynamic stabilizer.

Pressure Shell - The pressure shell is basically a spherical aluminum monocoque structure. Aluminum monocoque was selected over titanium monocoque, rib stiffened aluminum or titanium on the basis of cost and weight. The analytical and test basis for this decision is presented in Section 7.3.6. Fabrication of the sphere in three segments allows all equipment support and shell penetrations to be accomplished in one central segment and this, in turn, allows removal of that segment with minimum disturbance of the rest of the probe assembly. The foreward and aft pressure shell segments are simple spherical segments with no penetrations. They have bosses for mounting the antennas and provisions for electrical cable clips but are otherwise "clean." The central segment, also referred to as the equipment ring, is a frustum of a cone with wall thickness enveloping the spherical segment that would continue the geometry of the fore and aft segments. The conic shape is used to simplify penetrations and thereby provide flexibility in rearranging penetrations relatively late in the program. The thick wall and the fact that all penetrations are normal to the cone eliminates the need for special bosses, except for large mass spectrometer

penetration. Thus, procurement of the basic forging can proceed in the face of some uncertainty regarding final science penetrations, and changes can be accommodated with minimum cost up to the actual cutting of holes. Viton rubber seals fulfill leakage requirements.

Equipment Beams - The equipment mounting beams and brackets are an assembly separate from the pressure shell. This too provides flexibility to accommodate change at minimum cost since a change in mounting requirements will not directly affect the pressure shell. The basic beam structure, separate from the bracketry, allows capsule design and testing to proceed before detailed bracket design is determined. The separate beam structure introduces a joint where thermal and shock inputs can be attenuated. Figure 7.3-4 shows an arrangement for integration of science and electronic equipment that reserves the main equipment shelf for science instruments and thereby allows integration of science with minimal interaction with electronic equipment. Many arrangements with varying complements of equipment and sizes of equipment were investigated during the course of the study. In all cases a viable arrangement was achieved. There is, therefore, a basis for believing that the selected size and general arrangement of the pressure vessel is compatible with all foreseeable requirements. The accommodation of the alternative science instruments identified is documented and described in Section 3.1.2.2.

Insulation - The thermal insulation installation is external to the pressure shell for economy of cost and weight. Tradeoff between internal and external insulation is presented in Section 7.4. The insulation is installed in four assemblies, mounted on pressure shell segments consistent with the easy access plan of pressure vessel assembly. Installation on fore and aft pressure shell segments is relatively simple, cutouts for bosses and electrical cable runs being the only departure from uniform pieces. Installation on the central segment is relatively intricate in order to conform to various penetrations. Pieces in this segment are designed for disassembly without disturbing the penetrations so that access time will be minimized and only penetrations requiring service are disturbed.

To facilitate access, the outer shell (insulation cover), like the installation, is fabricated in four assemblies from titanium sheets because of need of a lightweight material with structural integrity at the

Venus surface temperature. The aft outer shell assembly incorporates mounting provisions for the communication antenna, for the electrical connector for lines to the afterbody, and for the ground service umbilical connector. The parachute pack entry load reaction is carried through the outer shell and the insulation, but there are no fasteners joining these assemblies. The central outer shell assembly has cutouts for the science penetrations and is designed for ease of assembly/disassembly. The lower outer shell assembly includes penetrations for supports for the wind drift radar antenna. The joints and splices in the shell act as vents to allow the atmosphere to permeate the insulation to the pressure shell.

Perforated Stabilizing Ring - This ring provides support of the descent capsule in the aeroshell, aerodynamic stability during final descent, and a controlled rate of rotation during final descent. The selected design for this assembly consists of a machined, U-shaped ring drilled to receive tubes for holes and inserts for separation fittings, and with a stub flange to attach the load cone. The ring and its fittings are titanium to provide a lightweight structure with good strength at Venus surface temperatures. The load cone is titanium to provide impedance to heat transfer to the pressure shell. Tolerances on the cant angle of the perforations were an important consideration in the tradeoff presented in Section 7.3.3 because of the small angle required, about $0.00873 \text{ rad } (1/2^\circ)$ and the short hole depth 36.32 mm, (1.43 in.) results in only 0.33 mm, (0.013 in.) offset between top and bottom edges. An error of only 0.025 mm, (0.001 in.) in location of the top of the hole relative to the bottom creates an 8% angle error. This virtually requires integral ring construction.

Load Cone - The load cone inboard of the ring supporting the pressure vessel is thin both for heat transfer and for weight reasons. The primary load is the tension load of entry, but the launch load governs design locally at the three spacecraft interface locations. Because the latter is a compression load, local rib stiffeners must be incorporated into the cone.

Aeroshell Forebody

The aeroshell forebody is a distinctly separate assembly from the aeroshell afterbody. The two are joined through the descent capsule stabilizing ring and interface directly at science protrusion clearance cutouts

(Figure 7.3-1) but are otherwise entirely separate. The principal elements of the aeroshell forebody are:

- Forward skin, stiffeners, and edge member,
- Payload ring,
- Back skin, stiffeners, and support cylinder,
- Heat shield installation

The conical structure of the aeroshell forebody is a ring stiffened monocoque essentially similar to the Viking aeroshell forebody but of heavier gage construction. The entire shell structure is aluminum for reasons of economy and weight. The structure temperature does not exceed 541°K (515°F) up to parachute deployment and the structure is not required after that time. The stiffening rings are spaced to preserve general structural stability. They can be heavy enough to preclude local crippling problems because they act with the shell in withstanding pressure. The edge member provides desired aerodynamic shape and stabilizes the edge of the shell.

The cylindrical payload ring is a rib stiffened titanium shell structure to provide high impedance to heat transfer. It has local cutouts to clear science instruments such as the cloud particle analyzer, the mass spectrometer, the solar flux sensor, and the planetary flux sensor. Three longerons are incorporated in the payload ring to provide a tension tie to the rest of the probe. The field splice for easy removal of the aeroshell forebody is incorporated into these longerons. Compression loads are transmitted by bearing the edge of the payload ring on the descent capsule load ring.

The forebody cavity is vented to relieve internal pressure differentials greater than 6895 N/m^2 (1 psi). This allows the flat, aft surface of the forebody to be a lightweight rib/skin structure with rib supports at the edge member and at an inner cylinder. The diameter of the inner cylinder is determined by the requirement for clearance for the cloud particle analyzer during staging of the forebody. The aft surface structure includes an annular recess with a flexibly mounted sealing ring that provides a closure over the forward end of the holes in the descent capsule stabilizing ring and a hollow Viton seal mounted in the recess bearing against the edge of the

ring to prevent circulation of hot gasses during entry. A cutout in the in-board portion of the aft face provides clearance for the cloud particle analyzer sensor during staging. Doors in the flat base surface provide access to field splice bolts for easy forebody removal.

Forebody Heat Shield - The heat shield installation consists of concentric, machined rings and nose cap. Details of heat shield fabrication and development are presented in Section 7. 2.

Aeroshell Afterbody

The aeroshell afterbody protects the aft part of the descent capsule and provides housing and support for the parachute system. The principal elements of the afterbody structure are:

- Base,
- Cap,
- Parachute system support,
- Heat shield.

The base of the afterbody is an aluminum alloy structure that extends from the descent capsule support ring to the communication antenna ground plane. The forward ring of this section covers the aft side of the descent capsule aerodynamic stability fence and has holes matching those in the fence so atmosphere can flow through and cause descent capsule rotation during parachute descent. This ring also serves as a mount for the separation fittings and for the cover for the cloud particle analyser clearance cutout in the aeroshell forebody. The cartridge actuated separation nuts for staging of aeroshell forebody and afterbody are housed in three separation fittings that provide protection for the nuts during entry. The top of these housings include phenolic plates that interface with the bus and shear pin receptacles and fittings for the cartridge actuated ball lock pin that joins the descent capsule to the bus. They also provide bases for the springs that separate the probe from the spacecraft after release. The cutout cover is spring-loaded to flip up against the afterbody after forebody separation to allow free flow of atmosphere through the sensor. The aft ring of the base reacts radial loads and provides a mounting surface for the cap. The structure between the rings is aluminum alloy sheet with three longerons

to react parachute loads and nine stringers to stabilize the cone structure, six of which support cap latching hardware. The three longerons coincide with spacecraft interface points. A door in the skin provides access to the staging connector so the connector can be mated and secured in place after the afterbody is mated to the probe.

The aft cap is a fiberglass polyimide structure, rather than a metal structure, to allow effective RF transmission. The cap is latched to the base and is released and removed by action of the pilot parachute to allow deployment of the main parachute. Release of the back of the cap only was considered but because carbon in the heat shield char on the conic part of the cap would interfere with RF transmission and because a simpler release mechanism was possible, the selected design removes the entire cap down to the antenna ground plane. The pilot parachute mortar is mounted with its cover insert, faired into, and forming part of the cap. Bridles legs from the pilot chute nest in small troughs in the cap. The gap between the mortar cover and the cap and the top part of the riser troughs over the bridles is filled with ESA 3560 heat shield repair material by troweling. The brittle repair material is easily stripped out by parachute deployment forces, but it provides a sound continuous heat shield prior to that time.

Afterbody Heat Shield - The afterbody is protected by an ESA 3560 honeycomb reinforced heat shield bonded to the structure. Joints are filled with ESA 3560 heat shield repair material. The heat shield design and development is described in detail in Section 7.2.

Parachute Support Structure - The parachute system support structure takes advantage of the ability of the descent capsule thermal insulation to accept distributed loads. A metal ground plane coincident with the antenna base has concentric rings bearing on the descent capsule insulation cover. The glass phenolic main chute container includes standoffs to transmit entry loads to this ring. Launch loads are reacted by tension fittings between the pack and the longerons. A fitting conforming to the base of the pilot mortar transmits mortar loads to the aeroshell afterbody through a bracket.

Mechanisms and Devices

Several mechanical devices are required to enable functioning of the large probe through its mission. These items and their purpose follow.

<u>Item</u>	<u>Purpose</u>
• Separation nuts	Enable aeroshell staging.
• Aeroshell afterbody separation connector	Disconnect electrical lines between descent capsule and aeroshell base cover at separation.
• Ground service separation connector	Disconnect accelerometer calibration and battery charging wires prior to launch.
• Aeroshell afterbody radome latch and release	Retain radome and release it during pilot parachute deployment.
• Ascent pressure relief valve	Relieve air pressure in aeroshell during launch to minimize structural loads.
• Cloud particle analyzer sensor clearance hole cover folding mechanism	Get cover out of flow path to allow undisturbed atmospheric flow through sensor.
• Ground service connector cover	Provide cover with heat shield for probe half of connector after disconnect.

Some of these are standard commercial items, some are modified standard items, and some must be designed. A description of the selected design and the rationale in choosing it over alternatives follows.

Separation Nuts - The basic Viking separation nut design will be used, but the design must be modified for Pioneer Venus separation usage. The Viking unit has the initiator ports on the side because of Viking peculiar mounting requirements. The Pioneer Venus separation devices must be mounted on the load ring of the descent capsule and the side ports would present an undesirable bulge on the afterbody. It is anticipated that rotating the ports would not adversely affect the performance of the existing design.

Due to the proximity of the separation devices to the internal equipment, it would be very desirable to use a low-shock output device to limit shock input to science and electronic equipment. Two ordnance manufacturing companies are developing low-shock separation nuts, and tests are now being performed by NASA on the devices of both companies. Qualification tests are scheduled to be run on one of these devices for another program in June or July 1973; it is therefore anticipated that by the time Pioneer Venus

equipment is to be purchased there will be a qualified low-shock nut available and possibly some usage data. Serious consideration will be given the low-shock design. The estimated cost for the low-shock nut was only 6% higher than the modified Viking design. Because there are small differences in cost with the possibility of substantial savings on electronic equipment, it is intended that the qualification testing requirements and results on the low-shock nut, when available, be thoroughly reviewed with Pioneer Venus requirements in mind to set up a limited qualification program to assure that the low-shock unit will perform successfully for Pioneer Venus.

Pin pullers were considered for use as separation devices; however, the anticipated loads are much higher than those for which the Viking pin puller was qualified. This concern, plus the relative difficulty in mating and demating with pin pullers and because no low-shock pin puller designs are available, were reasons for rejection of the pin pullers as staging devices.

Initiators - Two initiators for the separation nuts, both of which are qualified for space applications, were considered: the Viking Standard Initiator (VSI) and the Single Bridgewire Apollo Standard Initiator (SBASI). These initiators could almost be called interchangeable. Slight differences are present in these power sources; namely, the VSI output pressures center around $4\,826\,290\text{ N/m}^2$ (700 psi) and the SBASI center around $4\,481\,555\text{ N/m}^2$ (650 psi); there are more complete process, procedure, and material control on the VSI program and the epoxy used in the VSI is good to 436°K (325°F) whereas the SBASI epoxy is recommended to 394°K (250°F). Some degradation of the SBASI epoxy was experienced around the pins during tests at 422°K (300°F); however, this did not affect the performance of the unit tested. The sterilization requirements for the Viking necessitated the higher temperature resistant epoxy.

The above differences indicate that the VSI would be a slightly better device; however, the differences are not of such magnitude that selection could not be made based on cost. Preliminary cost and technical proposals have been received, and the VSI was 25% lower in program cost. Based on the slight technical and on the cost advantages of the VSI, it was selected for the Pioneer Venus program.

24

Separation Connector - The selected connector for separating wires between the descent capsule and the aeroshell afterbody is a 41 pin, spring-assisted connector manufactured by G&H Technology. This connector has been qualified for RMP-B on Atlas-launched reentry vehicles. This connector has no closing mechanisms; the halves are held together by the structure in which it is mounted. Upon release of the structure, a spring in the connector provides enough force to separate the connector halves. This connector was used successfully on the Viking Balloon Launch Decelerator Test Program.

An alternative separation method would be to use a pyro-activated wire cutter. The Viking PD5000010-001 cutter would easily cut the required number of wires (24). However, this cutter requires two initiators, two pressure cartridges, and two connectors, and it is neither lighter nor less expensive than the connector. The use of the cutter also presents a critical timing problem not experienced when the mechanical separation connector is used. These disadvantages more than offset the disadvantage of introducing another connector in the system. The G & H connector was therefore selected.

Ground Service Separation Connector - A connector is required to disconnect ground lines for battery charging and for accelerometer calibration before launch. The connector is mounted in the aeroshell afterbody to preserve the continuity of the forebody heat shield. At the time of disconnect, the connector is difficult to reach so a standard commercial manual lanyard pull disconnect was selected so the connector can be disconnected and removed through an opening in the payload fixing.

Aeroshell Afterbody Cap Latch and Release Mechanism - The aeroshell afterbody cap latch and release mechanism (Figure 7.3-2) will be actuated by a lanyard from a bridle leg of the pilot parachute. The latch and release mechanism will consist of six spring-loaded clamps held closed by a single 3.28 mm (1/8 in.) steel cable. The tension in the cable is released and the clamps rotate open when the lanyard pulls a pin holding the ends of the cable together. A turnbuckle will apply tension to the cable after assembly.

An alternative method of releasing the cable would be to use the Viking cable cutter. The advantage of the lanyard pull over the cable cutter is that no sequencing problem exists. The cutter would have to act after the pilot chute cleared the cap and before tension was achieved in pilot chute risers. The cap could be released before deployment of the pilot chute; however, this would require a positive means of assuring that the cap was clear of the probes. The lanyard release provides for such a way since the cap and the pilot chute risers are connected.

Pressure Relief Valve - The ascent pressure relief valve will be a simple check valve arrangement using a spring-loaded lip seal attached to a small circular opening in the aeroshell. When the atmospheric pressure decreases during boost the trapped ground ambient pressure will push open the seal and aeroshell relieving the internal pressure. The spring will be sized so that 0.345 N/cm^2 (1/2 psi) will open the valve and differential pressure $\leq 0.6895 \text{ N/cm}^2$ (1 psi) will be assured.

Cloud Particle Analyzer Cover Folding Mechanism - To allow the most favorable pattern of atmospheric flow through the cloud particle analyzer sensor before aeroshell afterbody separation, the sensor cover is flipped back against the afterbody after separation of the forebody. A glass phenolic cover with torsion springs, shown in Figure 7.3-14, will perform this function when released by separation of the forebody. The glass phenolic material will withstand entry heating conditions and will rotate smoothly over its hinge half. A pin in the tip of the cover engages a hole in a clip in the forebody to keep the cover closed. When the forebody separates, the cover hinges downward until the pin slips out of the clip. The cover then flips up, actuated by the torsion springs. Atmospheric flow would tend to open the cover, but two springs of about 39.8 cm N (3-1/2 in. -lb.) each are included to assure positive rotation of the cover.

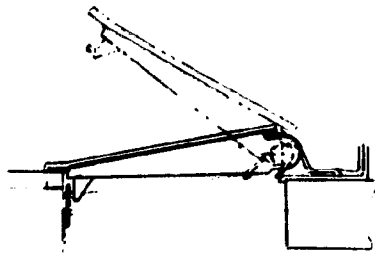


Figure 7.3-14. Door Mechanism

Ground Service Connector Cover - It is necessary to provide a cover over the ground service connector opening in the aeroshell afterbody. The opening is rather inaccessible at the time of disconnect so a spring-loaded cover will be provided. The cover will snap into place upon connector disconnect.

7.3.4.2 Small Probe.

The principal elements of the small probe are the aeroshell, pressure vessel, and devices that enable functioning of scientific experiments. Figure 7.3-5 shows the main features of these elements. This configuration operates as an aerodynamically stable body throughout entry and subsonic descent modes. The integration of structure, insulation, heat shielding, and science and electronic equipment has assured location of the c. g. sufficiently forward of the base diametral plane for aerodynamic stability.

Ease of access to scientific or electronic equipment is a prime consideration in the small probe structural design. There are no penetrations or attachments to the aeroshell afterbody, so it can be easily removed to gain access to fasteners joining the pressure shell to the forebody. The forebody is then removed to gain access to the fasteners joining pressure shell halves, the removal of which allows access to and removal of the equipment shelf for servicing or replacement of equipment on bench stands. Science sensor access to the Venus atmosphere is achieved by cover ejection or sensor deployment through the aeroshell after the entry phase.

Venus atmospheric entry loads are transmitted from the aeroshell to the pressure shell through the MIN-K thermal insulation. As explained in Section 7.3.6, this material has good load carrying capability. The selected design takes advantage of this to avoid concentrated loads and thereby achieve a lightweight aeroshell structure. Both structural and insulation fabrication costs are lessened due to the absence of closely spaced frames. Launch loads are also taken out in the bearing on the insulation on the aft side. This condition imposes a concentrated (ring) load on the aeroshell forebody but this is a relatively low loading condition. The support ring provides lateral stability and the pressure sensor port tube provides rotational stability for the pressure shell within the aeroshell.

Interfaces

The small probes are mounted equally spaced around the outer periphery of the equipment shelf on the bus. Each probe is held on the bus by four pairs of pads approximately 1.57 rad (90 deg) apart, each pair opposed in bearing on the aeroshell forebody and the afterbody to secure the rim of the major diameter. Two pair of pads are on the fixed bus structure and two are on hinged arms that are attached by an ordnance operated pin puller to allow probe release. The arrangement is described in Section 8.8.4.2. The probe structural frame and the interposing heat shield are designed for a maximum radial preload of 2225 N (500 lb) at each pair of pads. The umbilical cable penetrates the aeroshell afterbody. It is equipped with a connector for spacecraft attachment. A bus mounted cable cutter severs the umbilical close to the probe surface before separation of the probe from the bus.

The principal structural/mechanical elements of the small probe follow.

Pressure Vessel

The pressure vessel is a spherical, aluminum, monocoque structure fabricated in two halves. The basis for selection of this type of construction (same as the large probe pressure vessel) is presented in Section 7.3.6. The communication antenna penetration and all science sensor penetrations except the pressure sensor port are located in the aft shell half. This allows easy removal of the shell from the forebody because the forward insulation can remain undisturbed when the pressure shell is slipped out of it.

Four intermittent internal mating flanges with recesses to accommodate thermal isolators between the shell halves provide support for the equipment shelf.

The aft insulation retaining cover is part of the aft pressure shell assembly. This thin titanium shell retains the aft insulation, provides a mount for the antenna and its ground plane, and reacts pressure vessel loads through the insulation during launch.

Equipment Shelf

The equipment shelf is an integrally machined, pan shaped aluminum structure that supports science and electronic equipment such that the c. g. is well below the pressure vessel centerline, thus assuring required total probe c. g. location. As shown in Figure 7.3-5 the size of the Atlas/Centaur small probe provides ample room for integration of science and electronic equipment on the equipment shelf.

Aeroshell

Except for the radome the aeroshell skin is made of titanium because it is a functional part of the probe all the way to the surface and must therefore retain structural integrity at Venus surface temperatures. The radome must be RF transparent and it is made of fiberglass reinforced polyimide with a Teflon covering. The nose cap and part of the frontal cone are mainly protective covers over the insulation and have little structural function since they bear directly on the insulation. The outer frontal cone, outside the insulation retaining cylinder, functions as a ring stiffened conical shell similar to the large probe forebody. The forebody structure extends into the afterbody region locally at science sensor openings and at the umbilical penetration. This keeps all penetrations in the forebody so the afterbody can be slipped on or off most easily. Part of the edge member assembly (the outer ring) is titanium and part is aluminum. The part of the edge member that acts as a cylindrical retainer for the pressure shell insulation is aluminum to satisfy a need for a controlled heat path into the pressure vessel during cruise. During launch and entry when this cylinder carries significant load, the temperature is low and the aluminum has full strength. At the end of descent when temperature is high and the strength of the aluminum is very low, there is essentially no load. It would be possible to

Incorporate a thermal fuse into this cylinder should it prove necessary to further reduce heat inflow in the latter stages of the mission. Another alternative considered for this cylinder was to use titanium as basic structure and to add strips of highly conductive material such as copper to "tune" the heat conductance. This alternative would provide greater total structural integrity at termination of mission but this is not required. The alternative was not adopted because of greater cost than the aluminum concept.

Mechanisms and Devices

Mechanical devices are required to expose science sensors to the Venus atmosphere or to vent the probe. These are:

<u>Item</u>	<u>Purpose</u>
● Nephelometer window cover ejector	Expose nephelometer optics to Venus atmosphere after entry
● IR flux instrument cover ejector	Provide opening through which to extend instrument sensor
● Temperature sensor deployment mechanism	Deploy sensor beyond boundary layer.
● Pressure port	Transmit stagnation pressure to instrument, accommodating relative motion of pressure shell and aeroshell.
● Ascent pressure relief valve	Relieve air pressure in aeroshell during ascent to minimize structure weight.
● Ground separation connector and cover	Disconnect accelerometer calibration and battery charging wires and cover.

Ejectors. The nephelometer window cover ejector and the IR flux instrument cover ejector mechanisms will use the same design principal and basic parts. Essentially they will consist of a spring-loaded heat shield plug in the shell which is held in place with an electrically actuated pin puller. Upon receipt of the signal to open, the pin puller releases the spring that propels the plug with the spring mechanism away from the probe, providing the required viewing ports for the experiments.

The electrically actuated pin puller was selected for this application since it has a low-shock output compared to the pyro actuated devices used on Viking. This design, the electrically actuated pin puller, has been qualified by Martin Marietta for use on the Skylab Multiple Docking Adapter and should not present any problems when used on the small probes. The pin puller is made by G&H Technology and consists of a wire element wound around a split spool. This spool supports a spring-loaded pin. When current is applied to the wire, a prerduced section is heated and fails allowing the spool to separate and the pin is retracted. Reaction times are in the 6 to 10 millisecond ranges.

The temperature sensor will also be deployed with the electrically activated pin puller previously described. The mechanism will consist of a small spring loaded probe that when released will push out a small plug in the forebody shell and protrude from the release.

Pressure Port. A pressure port with a seal arrangement will be installed in the probe to accommodate any small relative movement between the aeroshell and pressure vessel which could damage the graphite pressure sensor pickup tube if the tube is not free to move at one end. A dynamic seal prevents hot ablation gases from entering the probe while allowing the movement. Relative movement can be caused by thermal and pressure loads and by compressibility of the insulation between the inner and outer structure.

Pressure Relief Valve. The ascent pressure relief valve will be the same concept as the large probe ascent pressure relief valve.

Ground Service Separation Connector and Cover - A connector is required to disconnect ground lines for battery charging and for accelerometer calibration before launch. This requirement is essentially the same as the large probe requirement except there are fewer accelerometer wires on the small probe. A standard commercial, manually operated, lanyard pull disconnect and a spring loader cover similar to those on the large probe are planned for use.

7.3.5 Thor/Delta - Preferred Subsystem

Thor/Delta studies were based on a large probe descent capsule configuration that included a vented flare aerodynamic stabilizer. The following

Discussion and associated illustrations are based on this configuration. However, the overall configuration is compatible with the perforated ring-stabilized descent capsule and the reduced volume afterbody adopted as the baseline for the Atlas/Centaur configuration. Consequently, these features would be incorporated in any future Thor/Delta probe activity. The large and small probes have similar aeroshell shapes; but, as in the Atlas/Centaur configuration, the requirements of staging of the large probe aeroshell lead to totally different structural systems.

3.5.1 Large Probe Interfaces

The large probe attaches to the bus central cylinder with three equally spaced ball lock pins on a 67.2 cm (26.5 inch) diameter bolt circle centered on the bus centerline. The probe is capable of withstanding all loads and environments associated with launch, boost, and cruise modes of operation at these points. A relative separation velocity of 0.3 m/s (1.0 ft/sec) is imparted between the large probe and the bus at separation by three springs mounted on the bus and located at the probe/bus attach points.

The preliminary loads that design the large probe at each ball lock attach point and probe carry-through structure are:

Axial	= 8900 N (2000 lb)
Radial	= 1335 N (300 lb)
Tangential	= 2225 N (500 lb)

The umbilical cable penetrates the probe base cap through a hole in a recess circle. The umbilical cable is equipped with a connector for bus attachment and has adequate length to allow rigging through a cable cutter that is mounted on the bus central cylinder.

7.3.5.2 Large Probe Configuration Description

The large probe structural/mechanical arrangement, shown in Figure 7.3-15b, includes the descent capsule, forebody aeroshell, base cover, and capsule parachute system as the major components.

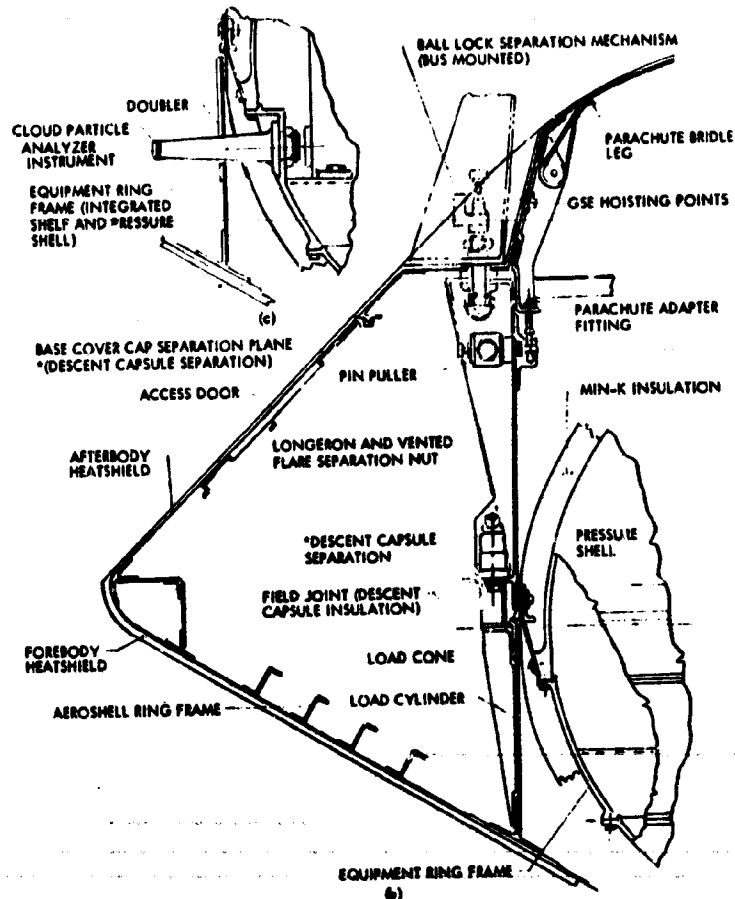


Figure 7.3-15. Thor/Delta Large Probe Structures and Separation Mechanism

The entry vehicle configuration is a 137.2 cm (54.0 in.) diameter 1.048 rad (60 deg) half angle blunted cone forebody with a 0.785 rad (45 deg) half cone afterbody, a 33.8 cm (13.3 in.) radius spherical nose cap and a 50.8 cm (20 in.) radius spherical base cap. The outer surface is covered with ablative heat shield material, described in Section 7.2.

The parachute is deployed by mortar at 70 km and extracts the descent capsule from the forebody aeroshell. After descent to 44 km, the descent capsule is released from the parachute and descends to impact. The base cap remains in place while the descent is on the parachute.

The descent capsule is basically a spherical body symmetrical about its spin axis with a vented aerodynamic flare extending above the sphere

equator. The vented flare provides aerodynamic drag to effect a terminal ballistic coefficient of 3.5 and to provide directional stability during the second descent stage. Three equally spaced longerons nest inside the flare to provide support for the boost loads at the bus separation interface, and to mount the collar for the ball lock mechanism that attaches the probe to the bus. The longerons extend down and exit the flare to provide a bathtub type fitting at their lower end for the cartridge actuated separation nut that attaches the descent capsule in the aeroshell.

The base cap is attached to the descent capsule by three equally spaced cartridge actuated pin pullers that engage lug fittings located in the longerons. The pin pullers are equipped with dual Viking standard initiators for redundancy. The machined fittings within the base cap that engage the pin puller also serve to attach the parachute bridle legs that extend through slots in the base cap. A continuous cone frustum shell within the base cap provides rigidity for maintaining the base cap shape and provides mounting for the parachute and staging fittings.

A pair of beams, located symmetrically about the probe centerline and straddling the antenna, span across the cone frustum to provide a mount for the parachute and mortar.

The base cap mounts three equally spaced local recesses for adapting to the bus interface. A fourth recess accommodates the bus/probe electrical umbilical and a battery recharge plug. The recess structural substrate is formed of glass phenolic to provide smooth faying surfaces within the complex curvature.

The base cap cover structure above the cone frustum is glass reinforced polyimide to provide RF transparency. It mounts the antenna aperture and the parachute canister cover. Two of the parachute bridle legs nest in slots imbedded in the base cap structure around the periphery of the aperture. The slots will be filled over the bridle with ESA 3560 heat shield repair material by troweling. The material is removed by parachute deployment forces. The antenna aperture is covered with a Teflon heat shield so that it remains RF transparent after entry heating. The surrounding elastomeric silicone ablator is RF transparent prior to entry; this, with the fiberglass structure, allows a wide view antenna angle before entry. After entry the parachute canister cover and protective heat shield are

removed. The teflon covered cap area with the open area caused by chute mortaring allow a 2.69 rad (160 deg) antenna cone view angle. A metallic screen above the parachute support beams at the top of the cone frustum provides an antenna ground plane. It is cut out to allow protrusion of the antenna and the parachute canister.

The descent capsule nests within the aeroshell payload ring and engages it through a ring flange at its equator to transmit the high entry deceleration loads. Local cutouts in the aeroshell payload ring accommodate the descent capsule science appendages that extend laterally below the equator. The descent capsule is secured within the aeroshell by three cartridge actuated separation nuts on equally spaced longerons that mate with an adapter fitting. Each separation nut is equipped with dual Viking standard initiators for redundancy.

The descent capsule includes a spherical, pressure protected equipment canister that is thermally insulated for protection through the atmospheric descent mode in a design similar to that described earlier for the Atlas/Centaur probe. The internal equipment arrangement and the main assembly joints of the pressure shell, the insulation cover, and the science mechanization concept are also similar to the Atlas/Centaur system and emphasis ease of access for assembly, checkout, and repair. The equipment ring through which science sensors and electrical feedthrough are mounted is machined from an aluminum plate. Its basic shape is that of a truncated spherical segment 12.7 cm (5.0 in.) deep that mates with a lower spherical segment closure and an upper hemisphere and cylinder to comprise the pressure shell. Internally, within the depth of the equipment ring are integrally machined beams configured to accommodate the major components of science and electronics equipment. Additional lugs, intercostals, or fittings will mount the various smaller components to the basic shelf.

7.3.5.3 Parachute Installation

The Thor/Delta parachute system is considerably smaller than that used for the Atlas/Centaur probe due both to the lesser probe weight and to

the more rapid descent profile which was baseline at the conclusion of Thor/Delta design studies. This smaller main chute is mortared directly instead of being deployed by a mortared pilot chute.

As received for installation in the probe base cover, the subsystem includes the parachute, packaged in a cylindrical canister, its mortar, and a cover attached to the canister with shear rivets. The parachute bridle legs extend from under the edge of the cover. The base cover structure supports the parachute canister, secures the bridle legs, and protects the system from the entry heating.

7.3.5.4 Small Probe Interfaces

The small probes are mounted equally spaced around the outer periphery of the equipment shelf on the bus. Each probe is held on the bus by four pairs of pads approximately 1.57 rad (90 deg) apart, as in the Atlas/Centaur design. The probe structural frame and heat shield are designed for a maximum radial preload of 2225 N (500 lb) at each pair of pads. For the launch, boost, cruise, and separation modes, the probe is designed for the following maximum additional loads at each pair of pads:

Axial	= 1335 N (300 lb)
Radial	= 668 N (150 lb)
Tangential	= 1335 N (300 lb)

The umbilical cable penetrates the aeroshell afterbody. It is equipped with a connector for spacecraft attachment. A cable cutter is rigged to sever the umbilical close to the probe surface before separation to the probe from the spacecraft.

7.3.5.5 Small Probe Configuration

The small probe structural/mechanical arrangement is shown in Figure 7.3-16. The aeroshell body is a 47.0 cm (18.5 in.) diameter 0.785 rad (45 deg) half angle 15.24 cm (6.0 in.) radius blunted cone forebody with a 0.523 rad (30 deg) half angle cone afterbody and a 21.2 cm (8.35 in.) radius spherical base cap. The outer surface is covered with ablative heat shield.

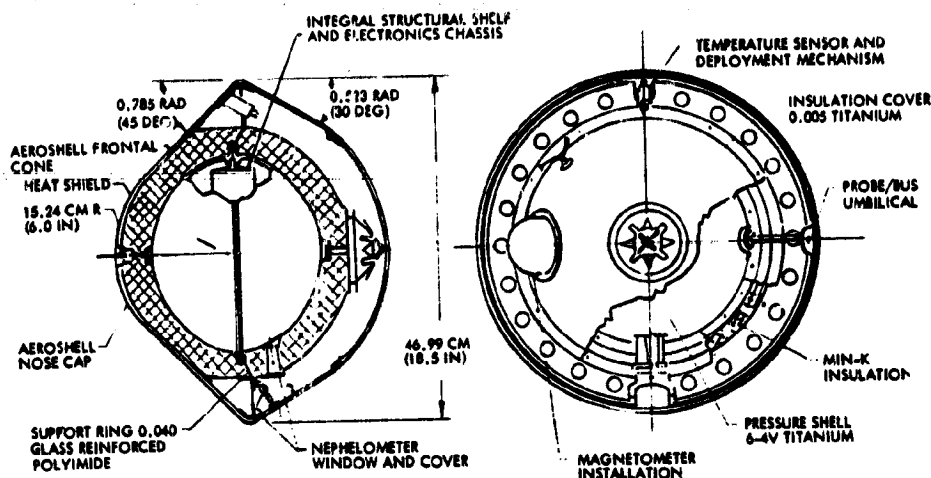


Figure 7.3-16. Thor/Delta Structural/Mechanical Arrangement Small Probe

An oblate spheroid shape for the pressure shell allows more efficient equipment packaging internally and results in a more forward center of gravity. However, a slight weight penalty results as compared to a sphere. The c. g. is sufficiently forward with respect to the base diametral plane to assure aerodynamic stability. The inertia load during entry deceleration is transferred from the pressure shell to the aeroshell by the MIN-K insulation. A circumferential support ring centrally locates and laterally supports the equipment canister. The base cover mounts to the forebody at the aft flange of the aeroshell edge ring.

Since the probe does not stage for the subsonic descent phase, mechanical functions similar to those described for the Atlas/Centaur probe are provided to expose science instruments.

7.3.5.6 GSE Provisions

The features or added parts that are required to make the probes compatible with ground handling equipment are minimal. The aeroshell major diameter ring frames with heat shield covering around the rim are inherently rigid and are suitable for clamping between mating surfaces of a handling ring. For handling and support of the inner assemblies, such as the descent capsule or the equipment shelf, the normal support points attached to handling rings or fixtures are acceptable because it is designed for the high

entry deceleration loads. For handling the descent capsule with the base cover cap in place, hoisting points are located in the base cap recesses provided for bus interface at mid-height of the cone frustum structure. A hole through the shell and heat shield allows installing a threaded eye bolt into a nut plate on each of the three parachute adapter fittings. The hole through the heat shield is rimmed with a glass phenolic shell. The hole will be plugged with a threaded stud with a glass phenolic cap after assembly.

7.3.6 Supporting Analysis and Tests

A preliminary structural analysis has been accomplished to support the design studies, establish the size requirements and assure structural integrity. For the Atlas/Centaur probes, a design ultimate factor of safety of 1.56 was selected for the launch, boost, cruise, entry, and descent conditions except for the pressure vessels that are designed by the pressure at the surface of Venus. A lower safety factor, 1.25, was selected for the pressure vessel because its critical load is not experienced until the end of the mission. By testing to structural loads 20% below these ultimate design levels, no yielding or degradation is anticipated and the tested article is still a flightworthy unit. Testing to this level is adequate to structurally qualify the design since it is still 1.25 times the limit load. Consequently the hardware cost of the program is reduced. In the case of Thor/Delta, the design is considerably more weight critical, and a lower design ultimate load factor, 1.25, was used for conditions other than terminal descent where the pressure vessel was designed for failure at the pressure corresponding to that at the nominal surface of Venus. For Thor/Delta, then, the structural qualification tests would have to be conducted at the ultimate design levels. This would likely result in some yielding or structural degradation and would preclude using the test article as a flight article.

The testing planned for the large and small probes has been designed to confirm the structural integrity consistent with a minimum cost by utilization of existing test facilities. The tests include critical loading conditions for launch and boost, Venus entry, and descent on the appropriate structural elements.

A discussion of the planned test program is covered in the Preliminary Project Development Plan, Volume III. Tables 7.3-6 and 7.3-7 summarize the anticipated structural tests and identify the facilities.

Table 7.3-6. Structural Test, Large Probe

PART	CRITICAL CONDITION	TYPE OF TEST	TEST FACILITY
PRESSURE VESSEL	TERMINAL DESCENT	PRESSURE (COLLAPSE)	HYPERTHERMOBARIC CHAMBER (1)
AEROSHELL	MAXIMUM ENTRY DECELERATION	STATIC TEST	STRUCTURAL TEST LAB (1)
LOAD CYLINDER	MAXIMUM ENTRY DECELERATION	STATIC TEST	STRUCTURAL TEST LAB (1)
LOAD CONE	MAXIMUM ENTRY DECELERATION	STATIC TEST	STRUCTURAL TEST LAB (1)
DECELERATOR ATTACHMENT FITTINGS	PARACHUTE OPENING	STATIC TEST	STRUCTURAL TEST LAB (1)
EQUIPMENT SUPPORT SHELF	MAXIMUM ENTRY DECELERATION	CENTRIFUGE TEST	CENTRIFUGE TEST FACILITY (2)
EQUIPMENT SUPPORT SHELF	LAUNCH VIBRATION	VIBRATION TEST	ENVIRONMENTAL TEST LAB (1)
MORTAR SUPPORT BEAMS	MAXIMUM ENTRY DECELERATION	CENTRIFUGE TEST	CENTRIFUGE TEST FACILITY (2)
MORTAR SUPPORT BEAMS	LAUNCH VIBRATION	VIBRATION TEST	ENVIRONMENTAL TEST LAB (1)
WIRE HARNESS ASSEMBLIES	MAXIMUM ENTRY DECELERATION	CENTRIFUGE TEST	CENTRIFUGE TEST FACILITY (2)
BASE COVER AFTERBODY	VENUS ENTRY	PRESSURE (COLLAPSE)	STRUCTURAL TEST FACILITY (1)
BASE COVER AFTERBODY	LAUNCH	ACOUSTIC	ACOUSTIC LAB (1)
SEPARATION NUT	AEROSHELL RELEASE	FUNCTION/SHOCK	STRUCTURAL TEST LAB (1)
SEPARATION NUT	DESCENT CAPSULE RELEASE	FUNCTION/SHOCK	STRUCTURAL TEST LAB (1)
CABLE CUTTER	DESCENT CAPSULE RELEASE	FUNCTION/SHOCK	ACOUSTICS LAB (1)
MASS SPECTROMETER	CARTRIDGE ACTUATED VALVES	FUNCTION/SHOCK	ACOUSTICS LAB (1)
COMPONENTS	MORTAR FIRING	FUNCTION/SHOCK	ACOUSTICS LAB (1)
COMPONENTS	SHOCK TEST BED	FUNCTION/SHOCK	ACOUSTICS LAB (1)

(1) MARTIN MARIETTA - DENVER
(2) MARTIN MARIETTA - ORLANDO

Table 7.3-7. Structural Test, Small Probe

STRUCTURAL TEST, SMALL PROBE			
PART	CRITICAL CONDITION	TYPE OF TEST	TEST FACILITY
PRESSURE VESSEL	TERMINAL DESCENT	PRESSURE (COLLAPSE)	HYPERTHERMOBARIC CHAMBER (1)
AEROSHELL	MAXIMUM ENTRY DECELERATION	STATIC TEST	STRUCTURAL TEST LAB (1)
EQUIPMENT SUPPORT SHELF	MAXIMUM ENTRY DECELERATION	CENTRIFUGE TEST	CENTRIFUGE TEST FACILITY (2)
EQUIPMENT SUPPORT SHELF	LAUNCH	VIBRATION TEST	ENVIRONMENTAL TEST LAB (1)
WIRE HARNESS ASSEMBLIES	MAXIMUM ENTRY DECELERATION	CENTRIFUGE TEST	CENTRIFUGE TEST FACILITY (2)
BUS INTERFACE	LAUNCH AND SEPARATION	STATIC TEST	STRUCTURAL TEST LAB (1)
BASE COVER AFTERBODY	VENUS ENTRY	PRESSURE (COLLAPSE)	STRUCTURAL TEST LAB (1)
WINDOW COVER	DEPLOYMENT	FUNCTION/SHOCK	ACOUSTICS LAB (1)
TEMPERATURE SENSOR	DEPLOYMENT	FUNCTION/SHOCK	ACOUSTICS LAB (1)

(1) MARTIN MARIETTA - DENVER
(2) MARTIN MARIETTA - ORLANDO

7.3.6.1 Pressure Vessel Design

The pressure vessels for Atlas/Centaur small and large probes are spherical shells made from 7049-T73 aluminum alloy forgings. This alloy has good strength properties and a low susceptibility to stress corrosion cracking. The Thor/Delta pressure vessels, a sphere on the large probe and an oblate spheroid on the small probes, are fabricated of 7049-T73 aluminum and 6A -4V titanium, respectively. The titanium alloy was selected since it retains good strength properties at the 532°K (498°F) experienced at the termination of descent.

The spherical pressure vessel design was based on results of a Martin Marietta initiated Research and Development Test Program conducted since mid-1970. The purpose of this program was to develop the technology required to design, fabricate, and test a structural thermal housing for a descent probe. The task accomplishments to date include fabrication and test of both titanium and aluminum simple monocoque hemispherical domes. Penetration bosses were included on three of the aluminum domes. Future tests to be conducted in 1973 include an aluminum and a titanium sphere with penetration bosses.

The results of the tests on metal hemispheres conducted to date are shown in Table 7.3-8 which includes the failing pressures, measured wall thicknesses and diameters, and material properties for the test articles. The presence of the penetration bosses was found not to reduce the collapse pressure load carrying capability of the aluminum monocoque hemispheres tested.

An analysis was performed to evaluate the design of penetration bosses in spherical shells. This resulted in the development of design curves that can be used for establishing the optimum dimensions for bosses in thin-walled shells. These curves are shown in Figure 7.3-17, 18, and 19. As noted earlier, the selected Atlas/Centaur pressure vessel design incorporated a thicker walled ring, or "belly band," for mounting the sensors and feedthroughs and thus avoids the need for individual bosses.

Table 7.3-8. Hemisphere Test Program Results

HEMISPHERE SERIAL NO.	INSIDE DIAMETER		ACTUAL WALL THICKNESS		ACTUAL COLLAPSE PRESSURE		MEMBRANE COMPRESSION STRESS AT COLLAPSE		COMPRESSIVE YIELD STRENGTH OF MATERIAL		MAXIMUM COLLAPSE PRESSURE BASED ON YIELD STRENGTH OF MATERIALS	
	CM	(IN.)	CM	(IN.)	N/CM ²	(PSI)	N/CM ²	(PSI)	N/CM ²	(PSI)	N/CM ²	(PSI)
9	50.2	19.75	0.411	0.162	1155	1675	35 728	51 100	41 364	60 000	1358	1970
10	50.2	19.75	0.403	0.159	1182	1715	36 745	53 300	41 364	60 000	1330	1930
11	50.2	19.75	0.414	0.163	1138	1630	34 470	50 000	41 364	60 000	1365	1980
15	50.2	19.75	0.457	0.180	1331	1930	36 469	52 900	41 364	60 000	1510	2190
12	50.2	19.75	0.509	0.232	1672	2425	35 573	51 600	41 364	60 000	1944	2820
13	50.2	19.75	0.594	0.234	1717	2490	36 194	52 500	41 364	60 000	1958	2840
14	50.2	19.75	0.587	0.231	1775	2575	37 917	55 000	41 364	60 000	1937	2810
5	50.2	19.75	0.650	0.256	1985	2880	45 018	66 300	41 364	60 000	2116	3070
6	50.2	19.75	0.635	0.240	1786	2590	37 198	53 900	41 364	60 000	1985	2880
7	50.2	19.75	0.559	0.220	1613	2340	36 607	53 100	41 364	60 000	1820	2640
23	54.9	21.60	0.478	0.188	2489	3610	72 111	104 600	89 208	129 400	3082	4470
24	54.9	21.60	0.460	0.181	2475	3595	74 455	108 000	89 208	129 400	2964	4300
25	54.9	21.60	0.467	0.184	2379	3450	70 388	102 100	89 208	129 400	3013	4370
38	54.9	21.60	0.307	0.121	1546	2245	49 423	108 700	97 550	141 500	2172	3150
39	54.9	21.60	0.328	0.129	1620	2350	48 251	99 000	97 550	141 500	2316	3360
41	54.9	21.60	TO BE TESTED IN 1973						104 099	151 000		
42	54.9	21.60	TO BE TESTED IN 1973						104 099	151 000		

NOTES:
1. DOME SERIAL NO. 5 THROUGH 15 ARE ALUMINUM 2014-T6 SIMPLE MONOCOQUE EXCEPT FOR NO. 5, 6, AND 7 WHICH INCLUDE PENETRATION BOSSES 0.4-INCH THICK.
2. DOME SERIAL NO. 23 THROUGH 25, 38 AND 39, 41 AND 42 ARE TITANIUM 6AL-4V SIMPLE MONOCOQUE.
3. DATA IS FROM MMC REPORT NO. D-72-48771-004.

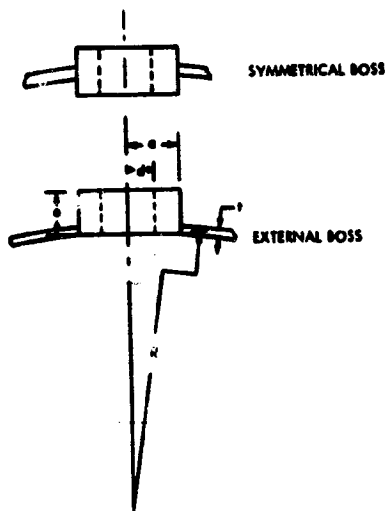


Figure 7.3-17. Boss Dimensional Parameters

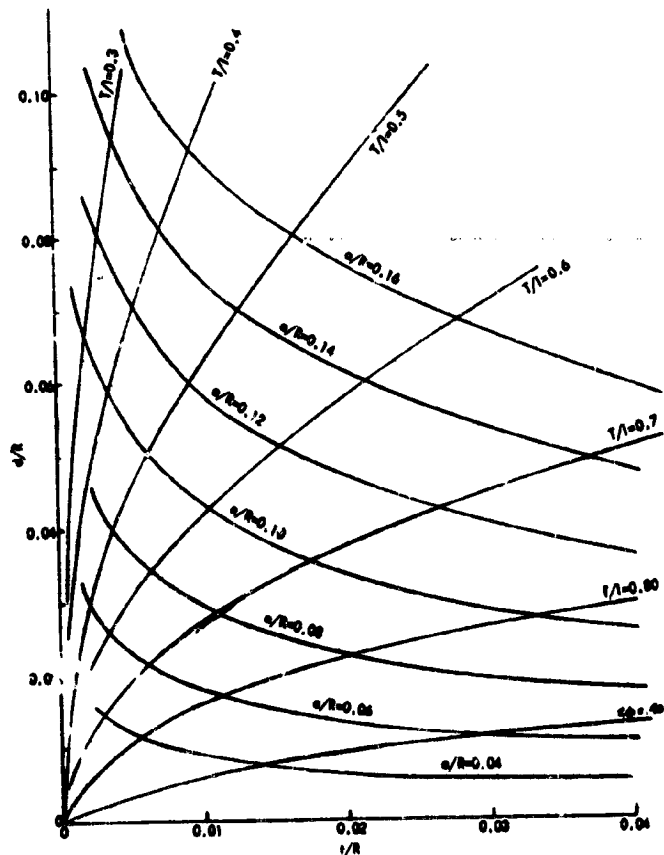


Figure 7.3-18. Design Chart, External Bosses

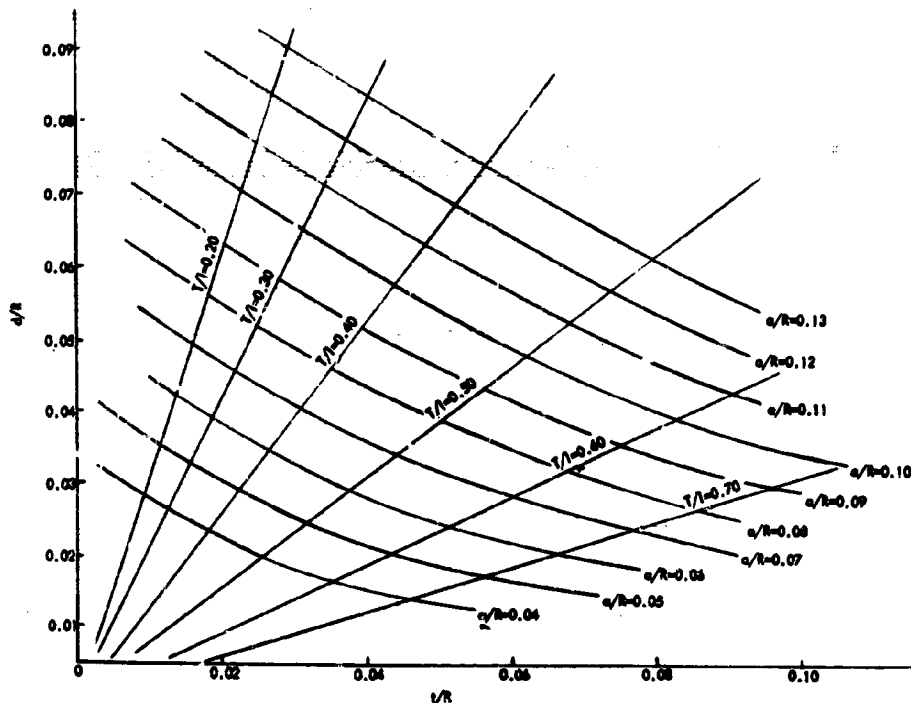


Figure 7.3-19. Design Chart - Symmetrical Bosses

Rib Stiffened versus Monocoque Design

Evaluation of rib stiffened shell designs showed that for a triangular rib stiffened aluminum shell a slightly greater weight was required than for a monocoque design. For titanium, which is thinner and is influenced more by buckling criteria, a rib stiffened design was found to result in approximately 6% weight reduction over the monocoque design at the 22 N/cm² (2250 psi) collapse pressure used. With the current design pressures, 945 N/cm² (1370 psi) a greater weight saving, approximately 17% would be possible in the rib stiffened titanium design over the monocoque design. In aluminum, however, the monocoque design is still lighter than the ribbed stiffened configuration. With either material, the monocoque designs have been selected because the cost of the intricate machining required for the rib stiffened shells is not warranted.

To use the design curves for design of penetration bosses, it is necessary to know (t/R) of the shell to be penetrated, and d , the radius

of the required hole. Simply locate the point whose abscissa is t/R and whose ordinate is d/R and estimate the associated values of a/R and $t/$ and calculate a and t . These are the required dimensions of the reinforcement ring which will elastically replace the shell material removed. Curves for symmetrical and external bosses are shown.

Design Curves for Monocoque Shells

Plots of the MMC test results on monocoque shells are shown in Figures 7.3-20 and 7.3-21. The aluminum tests were conducted on 19.75-inch inside diameter hemispheres. The data have been adjusted and plotted based on a 0.559 m (22.0 in.) diameter which is the baseline Thor/Delta large probe size. The results show relatively little scatter between test specimens. A literature survey of experimental results of monocoque spherical shells tested under external pressures showed that accurately machined or formed specimens showed close correlation with the MMC test results.

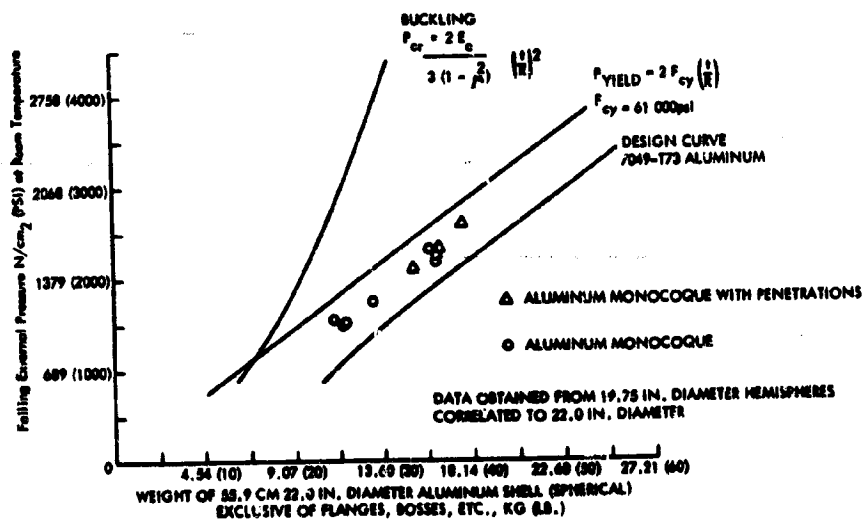


Figure 7.3-20. Weight of 55.9 cm (22.0 in.) Diameter Aluminum Shell (Spherical) Exclusive of Flanges, Bosses, Etc., kg (lb)

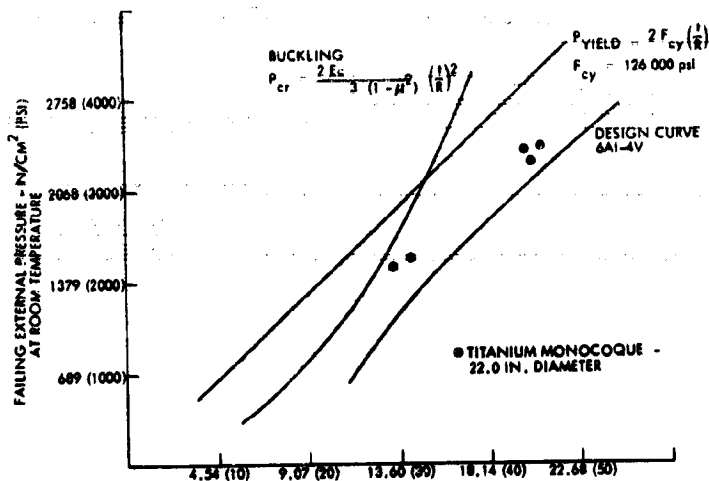


Figure 7.3-21. Weight of 55.9 cm (22.0 in.) Diameter Titanium Shell (Spherical) Exclusive of Flanges, Bosses, Etc., kg (lb)

Design curves based on the test data are also shown in Figures 7.3-20

and 7.3-21 along with the classic buckling equation $P_{cr} = \frac{2 E_c}{3 (1 - \mu^2)} \left(\frac{t}{R} \right)^2$,

and the strength critical equation, $P_{YIELD} = 2 F_{cy} \left(\frac{t}{R} \right)$. A comparison of the aluminum and titanium design curves is shown in Figure 7.3-22.

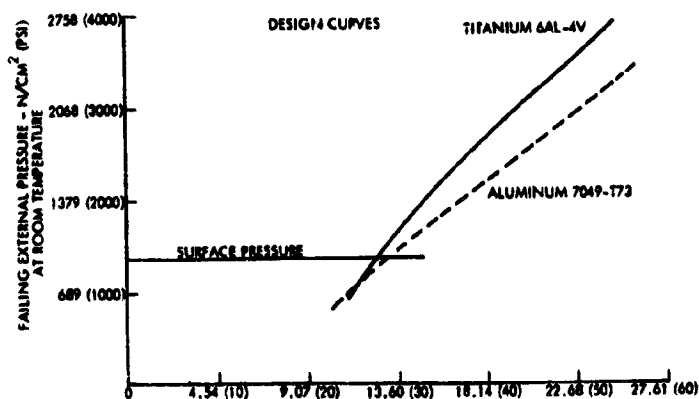


Figure 7.3-22. Weight of 55.9 cm (22.0 in.) Diameter Shell (Spherical) Exclusive of Flanges, Bosses, Etc., kg (lb)

In the externally insulated design concepts, the pressure vessel is subjected to moderately increasing temperatures as the probe descends through the Venus atmosphere. The resulting reduction in material properties is accounted for in the sizing calculations of Section 7.4.

A preliminary analysis indicates that the deflection of the shell caused by external pressure is nearly equal to the expansion due to the increased temperature; therefore, no thermal stress problem is anticipated.

7.3.6.2 Aeroshell Analysis

Analysis of the aeroshell forebody structure consisted of comparison of aluminum and titanium in both honeycomb and ring stiffened configurations. The general stability of the structure was included as well as local buckling of skin and crippling of flanges of the frames. The maximum loading condition results from the pressure loading at the maximum dynamic pressure entry condition at which time structural temperatures have not started to rise. Thermal stresses, however, do occur after soak-through of aerodynamic heating takes place. The frame spacing and skin thicknesses resulting from the maximum load condition were found to resist thermal stress buckling up to a temperature of 541.5°K (515°F). (See Figure 7.3-23) This temperature was thus established as the requirement on the heat shield design. A comprehensive tradeoff study increasing structural gages and requiring heat shield thickness to optimize the buckling temperature was not conducted. The 541.5°K (515°F) is near the maximum value that could be used with aluminum and is thus probably close to the optimum weight design.

The small probes are designed by the maximum dynamic pressure during entry, but also have to withstand buckling. The maximum temperature, 755°K (900°F), occurs at the end of the mission and also after entry heating soak-through. The small probe aeroshell is stabilized against buckling by the rigid insulation between the pressure vessel and the aeroshell. The MIN-K TE 1400 insulation used has a compression allowable higher than the maximum pressure resulting from the Venus entry environment. The stress strain curve for the material (Figure 7.3-24) indicates that the Thor/Delta insulation deflection is 0.20 cm (0.08 in.) for an entry

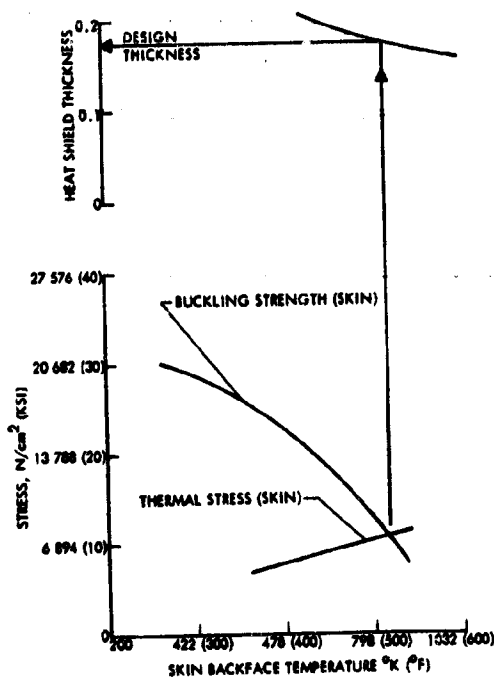


Figure 7.3-23. Large Probe Thermal Stress and Skin Buckling Allowable vs Back Face Skin Temperatures

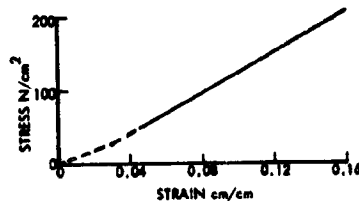


Figure 7.3-24. Stress Strain Curve for MIN-K TE 1400

pressure of 86 N/cm^2 (125 psi) and an insulation thickness of 3 cm (1.2 in.). Atlas/Centaur insulation thickness is 5 cm (2.0 in.) and corresponding deflection is 0.35 cm (0.13 in.).

7.3.6.3 Structural Dynamics

Dynamic events applicable to the probe were examined to assess their impact on structural and component design. The governing events for preliminary structural design were determined to be launch accelerations, entry accelerations, and entry pressures. In addition to analyses of these governing events, preliminary analyses were performed applicable to launch and boost acoustics and vibration, hooster, and shroud pyrotechnic shock levels at the probe interfaces, entry acoustics, and resulting induced random vibration, and pyrotechnic shock environments caused by probe devices. Considering the dynamic events previously described, a comprehensive test program has been defined for large and small probes.

By performing analyses on all dynamic events considered as possibly significant in terms of affecting design or reliability, analyses and/or tests have been defined which can encompass more than one mission event, and

yet be performed as one unit. For example, launch acoustics and entry acoustics can be combined in terms of one spectra envelope, for an analytically determined exposure period. Exposure times are significant in order to ensure that structural fatigue caused by acoustic loadings are considered.

Due to the proximity of probe components to the various pyrotechnic devices, shock was seen to be a significant environment to be considered. Pyrotechnic shock environments have been estimated at the large probe equipment shelf for several pyrotechnic configurations, two of which are indicated in Figure 7.3-25. The following pyrotechnic conditions were investigated: (1) chute deployment (drogue mortar), (2) aeroshell separation, (3) chute release (from descent capsule), and (4) shock due to the squibs on the spectrometer. At this time the shock associated with the descent capsule/aeroshell separation is estimated as a maximum shock response of 3100 g's at the equipment shelf. The shock level is due to the use of cartridge actuated separation nuts as the pyrotechnic source, and is considered to be the most severe shock environment estimated as an input to the equipment support structure at this time. Since the 3100 g-level would be approximately 5200 g's if the equipment beams were an integral part of the pressure vessel, the additional joint provided in the selected design is highly desirable.

Martin Marietta's considerable experience analyzing and testing pyrotechnic shock phenomena formed the basis for the preliminary shock environment estimates. In order to more accurately define these shock environments, however, because of the preliminary designs and generalized joint configurations available for this effort, a shock test bed fixture is planned for the implementation phase. The shock test bed fixture and supporting tests will enable flight-pyrotechnic devices, and realistic shock paths and joints to be combined, resulting in accurate shock environment acquisition. The shock test bed effort should result in minimum shock environments being defined at critical locations.

A preliminary dynamic model of the large probe has been developed and used to provide estimates of constrained mode shapes and frequencies. Initial results indicate a large probe fundamental frequency range greater

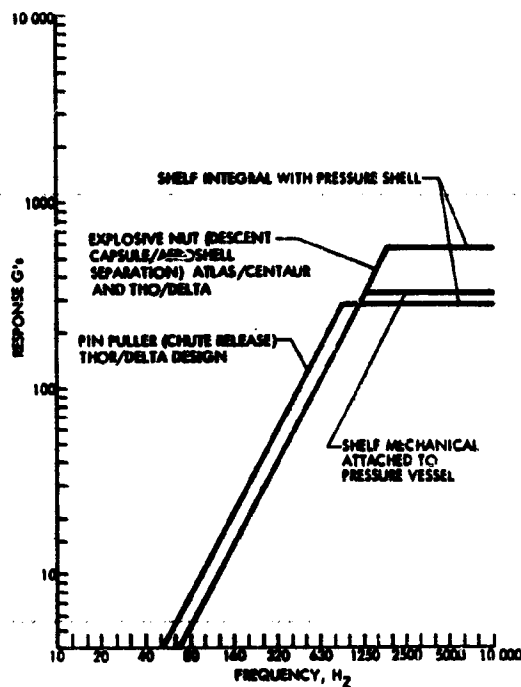


Figure 7.3-25. Estimated Pyrotechnic Shock Response at Large Probe Equipment Shelf/Descent Capsule

than 50 Hz. Probe mass and stiffness matrixes have also been provided for incorporation in the bus/probes modal analysis effort. Probe models with additional complexity will be generated early in the design and test phases to provide realistic estimates of loads and possible notching requirements.

7.4 Thermal Control

7.4 THERMAL CONTROL

7.4.1 Introduction and Summary of Selected Design

The thermal control subsystem must maintain all probe components within allowable temperature limits during all mission phases. This requirement was achieved using an essentially passive approach that provides a simple and reliable design. The probe thermal control subsystems are designed to bring payload temperature at entry near the lower end of its allowable operating temperature range. This minimizes the thermal system weight by maximizing available payload heat sink from entry to touchdown on the planet surface. Further, the structural components, e.g., the pressure vessel shell and the equipment support structure, are used as heat sinks in order to derive dual purpose from these elements.

Basic thermal characteristics of the mission allow the thermal insulation and thermal control coatings, the major thermal control subsystem components, to be designed essentially independent of one another. Thermal insulation requirements are totally dependent on descent through the Venus atmosphere. The thermal control coatings on the probe exterior are dependent on cruise conditions and design entry temperature, the coatings choice being somewhat insensitive to insulation configuration. Also, the entry payload temperature was found to be independent of the probe release temperature, thus providing an uncomplicated interface between the mission phases before and after probe release. For these reasons, the probe thermal design is divided into convenient independent parts.

The thermal control approach for the Atlas/Centaur and Thor/Delta missions is basically the same. In both cases, a pressure protected design is used with external insulation. The difference between the two designs is that the extra weight available for the Atlas/Centaur mission is used to increase thermal design margins. These increased margins, in turn, allow a decrease in required thermal testing and thus decreased program costs. These differences are discussed in Section 3 of Volume II.

The Atlas/Centaur large and small probe thermal control subsystems consist of MIN-K TE 1400 insulation, thermal control joint interface materials, battery and science window heaters, phase change material (eicosane), and thermal control coatings. Except for the window and battery heaters, the design is passive both for post-separation cruise and descent phases of the mission, as well as while attached to the bus. Thermal control coatings on the exterior of the heat shield provide the passive control during cruise while the thermal insulation and inherent heat sink of the structure, phase change material and payload passively control temperatures during descent.

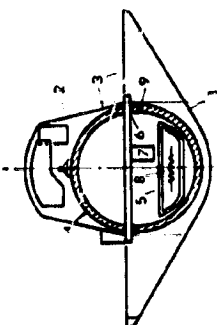
Figures 7.4-1 and 7.4-2 present the important design features of the thermal control subsystem for the large and small probes, respectively.

7.4.2 Requirements

Temperature limits and power dissipation for large probe components are given in Table 7.4-1; those for the small probe are given in Table 7.4-2.

Thermal boundary conditions for the descent and post-separation cruise phases of the mission are given in Figures 7.4-3 and 7.4-4. For descent, the boundary conditions are defined by ambient atmospheric temperature and pressure vs time. The solar aspect angle vs time from probe separation to entry provides the boundary conditions during the cruise phase of the mission. The power profile given in Section 7.8 shows the time lines for equipment operation.

Requirements other than temperature limits that influence thermal control subsystem design are accessibility of all probe components, compatibility with other subsystems, vibration, pyro-shock, and science window requirements. Compatibility requirements force the use of thermal materials on the probe exterior that do not outgas, thereby confusing mass spectrometer readings. Relative to the science windows, there is a requirement to maintain the exterior window surface temperatures above the local ambient so as to avoid condensation, and to inhibit thermally induced migration of solid particles to the window surface.



WEIGHT SUMMARY

	(KG)
ADHESIVES	1.0
SURFACE COATINGS	1.5
INSULATION, MIN-K	20.3
INSULATION, FA BATT	0.4
PHASE CHANGE DEVICE	2.4
HEATERS	0.3
SENSORS	0.4
INSULATION COVER	3.8
ANTENNA CABLE COVER	0.1
	30.2

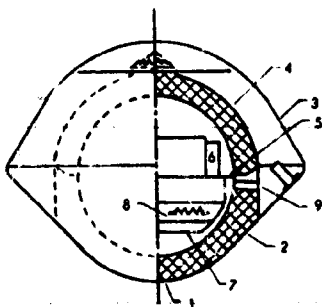
ID NO.	NAME OF ITEM	DESCRIPTION	PURPOSE	SURFACE PROPERTIES	
				ϵ	σ
1	EXTERNAL FORBODY SURFACE COATING	MOSAIC TO PRODUCE PRESCRIBED SOLAR ABSORPTIVITY (σ) TO EMISSIVITY (ϵ) RATIO 5-12-G WHITE AND 3M BLACK VELVET PAINT	MAINTAIN FORWARD SURFACE AND PAYLOAD WITHIN PRESCRIBED TEMPERATURE LIMITS DURING CRUISE AND POST-SEPARATION PHASES	0.35	0.88
2	EXTERNAL AFTERBODY SURFACE COATING ON TOP HALF CONICAL SECTION	3M BLACK VELVET PAINT	ABSORB SOLAR RADIATION TO MAINTAIN PAYLOAD WITHIN PRESCRIBED TEMPERATURE LIMITS PRIOR TO ENTRY	0.95	0.88
3	EXTERNAL AFTERBODY SURFACE COATING ON HORIZONTAL SURFACES AND LOWER HALF OF CONICAL SECTION	1 MIL SHEET OF ALUMINIZED MYLAR	PROVIDE LOW EMISSIVITY ON SURFACES THAT DO NOT RECEIVE SOLAR RADIATION	0.10	0.05
4	THERMAL INSULATION ON EXTERNAL SURFACE OF PRESSURE SHELL	4.5 CM LAYER OF MIN-K TE 1400 INSULATION	CONTROL TEMPERATURE OF PRESSURE SHELL AND PAYLOAD DURING DESCENT		
5	GLASS FIBER INSULATION	FA BATT AROUND BATTERY CASE AND IN MIN-K JOINTS	THERMALLY ISOLATE BATTERY FROM PAYLOAD AND FILL GAPS IN MIN-K INSULATION		
6	THERMAL ISOLATORS IN JOINT BETWEEN PRESSURE SHELL AND EQUIPMENT SHELL	0.43 CM LAYER OF MYKROY 750 IN BOLTED JOINT	REDUCE HEAT TRANSFER FROM PRESSURE SHELL TO EQUIPMENT SHELL DURING DESCENT		
7	PHASE CHANGE DEVICE	1.2 KG EICOSANE IN ALUMINUM CONTAINER WITH ALUMINUM MONEVCOMB FILLER	CONTROL PAYLOAD TEMPERATURE DURING DESCENT		
8	BATTERY HEATER	THERMOSTATICALLY CONTROLLED 20-WATT ELECTRICAL RESISTANCE HEATER PER BATTERY CASE	MAINTAIN MINIMUM BATTERY TEMPERATURE OF 20° DURING BATTERY OPERATION		
9	SCIENCE WINDOW HEATERS	15-WATT ELECTRICAL RESISTANCE HEATER ON EACH SCIENCE WINDOW	MAINTAIN SCIENCE WINDOW TEMPERATURE ABOVE LOCAL ATMOSPHERIC TEMPERATURE DURING DESCENT		

(a) SIMILAR TO VIERING LAMBER. ATTACHED ACCORDING TO MMC PROCESS STP-72206, "COATING, FILM, LOW EMISSIVITY, APPLICATION OF."

Figure 7.4-1. Atlas/Centaur Large Probe

ID NO.	NAME OF ITEM	DESCRIPTION	PURPOSE	SURFACE PROPERTIES	
				α	ε
1	EXTERNAL FOREBODY SURFACE COATING ON SPHERICAL NOSE SECTION	MOSAIC TO PRODUCE PRESCRIBED SOLAR ABSORPTIVITY (α) TO EMISSIVITY (ε) RATIO 5-13-G WHITE AND 3M BLACK VELVET PAINT	MAINTAIN FORWARD SURFACE AND PAYLOAD WITHIN PRESCRIBED TEMPERATURE LIMITS DURING POST-SEPARATION PHASE	0.35	0.88
2	EXTERNAL FOREBODY SURFACE COATING ON CONICAL SECTIONS	MOSAIC TO PRODUCE PRESCRIBED SOLAR ABSORPTIVITY (α) TO EMISSIVITY (ε) RATIO 5-13-G WHITE AND 3M BLACK VELVET PAINT	MAINTAIN FORWARD SURFACE AND PAYLOAD WITHIN PRESCRIBED TEMPERATURE LIMITS DURING POST-SEPARATION PHASE	0.48	0.88
3	EXTERNAL AFTERBODY SURFACE COATING ON CONICAL SECTION	1 MIL SHEET OF ALUMINIZED MYLAR	MAINTAIN PAYLOAD WITHIN PRESCRIBED TEMPERATURE LIMITS DURING POST-SEPARATION PHASE	0.10	0.05
4	THERMAL INSULATION ON EXTERNAL SURFACE OF PRESSURE SHELL	5 CM LAYER OF MIN-K TE 1400 INSULATION	CONTROL TEMPERATURE OF PRESSURE SHELL AND PAYLOAD DURING DESCENT PHASE		
5	THERMAL ISOLATORS IN JOINT BETWEEN PRESSURE SHELL AND EQUIPMENT SHELF	0.32 CM LAYER OF ASBESTOS REINFORCED PLASTIC 41 RPD LAMINATE	REDUCE HEAT TRANSFER FROM PRESSURE SHELL TO EQUIPMENT SHELF DURING DESCENT		
6	PHASE CHANGE DEVICE	1.4 KG EICOSANE IN ALUMINUM CONTAINER WITH ALUMINUM HONEYCOMB FILLER	CONTROL PAYLOAD TEMPERATURE DURING DESCENT		
7	GLASS FIBER INSULATION	FA BATT AROUND BATTERY CASE AND IN MIN-K JOINTS	THERMALLY ISOLATE BATTERY FROM PAYLOAD AND FILL GAPS IN MIN-K INSULATION		
8	BATTERY HEATER	THERMOSTATICALLY CONTROLLED 20-WATT ELECTRICAL RESISTANCE HEATER PER BATTERY CASE	MAINTAIN MINIMUM BATTERY TEMPERATURE OF 286°K DURING BATTERY OPERATION		
9	SCIENCE WINDOW HEATERS	15-WATT ELECTRICAL RESISTANCE HEATER ON EACH SCIENCE WINDOW	MAINTAIN SCIENCE WINDOW TEMPERATURE ABOVE LOCAL ATMOSPHERIC TEMPERATURE DURING DESCENT		

(c) SIMILAR TO VIKING LANDER. ATTACHED ACCORDING TO MMC PROCESS STP-72326, "COATING, FILM, LOW EMISSIVITY, APPLICATION OF."



WEIGHT SUMMARY	
	(KG)
ADHESIVES	0.6
SURFACE COATINGS	0.2
INSULATION, MIN-K	11.7
INSULATION, FA BATT	0.2
PHASE CHANGE DEVICE	2.8
HEATERS	0.1
SENSORS	0.4
INSULATION COVER	2.0
ANTENNA CABLE COVER	0.1
TOTAL	18.1

Figure 7.4-2. Atlas/Centaur Small Probe

Table 7.4-1. Temperature Limits,
Large Probe

INTERNAL COMPONENTS	OPERATING LIMITS (°K)	NONOPERATING LIMITS (°K)	POWER DISSIPATION (WATT)
TEMPERATURE ELECTRONICS	233 TO 363	233 TO 363	0.5
PRESSURE GAUGES AND ELECTRONICS	233 TO 353	233 TO 353	0.5
ACCELEROMETER	233 TO 363	233 TO 363	2.3
NEUTRAL MASS SPECTROMETER	255 TO 339	233 TO 339	12.0
CLOUD PARTICLE SIZE ANALYZER	255 TO 398	233 TO 398	20.0
SOLAR RADIOMETER	233 TO 339	233 TO 339	4.0
IR FLUX RADIOMETER	233 TO 339	228 TO 339	3.0
HYGROMETER ELECTRONICS	255 TO 339	253 TO 339	0.3
GAS CHROMATOGRAPH	(a) 255 TO 339	255 TO 339	6.0
WIND DRIFT RADAR	255 TO 339	255 TO 339	40.0
BATTERY	(b) 286 TO 355	255 TO 308	69.2
POWER CONTROL UNIT	255 TO 339	228 TO 367	30.0
DIPLEXER	255 TO 342	233 TO 355	2.1
TRANSPONDER	255 TO 342	242 TO 347	5.5
BATTERY HEATER	255 TO 355	255 TO 355	20.0 (2 HR)
TRANSMITTER POWER AMPLIFIER	255 TO 339	228 TO 339	126.0
ELECTRICAL HARNESS	255 TO 339	228 TO 339	3.1
RF CABLEING	255 TO 352	228 TO 339	0.4
DTU	255 TO 343	228 TO 367	5.0
G SWITCH	233 TO 367	233 TO 367	0.0
ENGINEERING INSTRUMENTATION	255 TO 339	228 TO 367	2.0
EXTERNAL COMPONENTS			
MORTAR	255 TO 339	172 TO 339	
PARACHUTE	228 TO 408	172 TO 339	
AEROSHELL ELECTRICAL CONNECTOR	200 TO 367	172 TO 367	
FOREBODY HEAT SHIELD		228 TO 367	
AFTERBODY HEAT SHIELD		172 TO 367	
ANTENNA RADOME		172 TO 367	
SEPARATION NUTS	200 TO 367	200 TO 367	
PYRO INITIATORS	200 TO 367	200 TO 367	
TEMPERATURE SENSOR	233 TO 798	172 TO 798	
ANTENNA	200 TO 772	200 TO 772	
RF CABLEING	200 TO 772	200 TO 772	
HYGROMETER SENSOR	(c) 233 TO 373	213 TO 373	
WIND ALTITUDE RADAR ANTENNA	200 TO 772	200 TO 772	
(a) LIMITS SHOWN ARE IN EXCESS OF TEMPERATURE ENVIRONMENTS REFERENCED IN INSTRUMENT PROPOSAL. THE INSTRUMENT CAN BE DESIGNED TO ACCOMMODATE THESE LIMITS WITH MINOR IMPACT. (b) OPERATING LIMITS SHOWN ARE FOR DESCENT. FOR CRUISE, THE OPERATING LIMITS ARE 286 TO 303°K. (c) INSTRUMENTS ARE NOT REQUIRED TO OPERATE AT TEMPERATURES IN EXCESS OF THOSE SHOWN.			

Table 7.4-2. Temperature Limits, Small Probe

INTERNAL COMPONENTS	OPERATING LIMITS (°K)	NONOPERATING LIMITS (°K)	POWER DISSIPATION (WATT)
TEMPERATURE ELECTRONICS	233 TO 363	233 TO 363	0.5
PRESSURE GAUGES AND ELECTRONICS	253 TO 353	253 TO 353	0.5
NEPHELOMETER	243 TO 339	243 TO 339	1.0
ACCELEROMETER	233 TO 363	233 TO 363	1.0
IR FLUX DETECTOR	255 TO 339	253 TO 339	1.0
BATTERY	(a) 286 TO 355	255 TO 305	25.0
TRANSMITTER DRIVER	255 TO 339	228 TO 339	4.0
TRANSMITTER POWER AMPLIFIER	255 TO 339	228 TO 339	63.0
BATTERY HEATER	255 TO 355	255 TO 355	20.0 (2.8 HR)
ELECTRICAL HARNESS ASSEMBLY	255 TO 339	228 TO 339	1.1
RF CABLEING	255 TO 552	228 TO 339	0.2
DTU	255 TO 343	228 TO 367	5.0
G SWITCH	233 TO 367	233 TO 367	0.0
ENGINEERING INSTRUMENTATION	255 TO 339	228 TO 367	2.0
STABLE OSCILLATOR	255 TO 339	228 TO 339	0.4
POWER CONTROL UNIT	255 TO 339	228 TO 367	20.0
EXTERNAL COMPONENTS			
FOREBODY HEAT SHIELD		228 TO 367	
AFTERBODY HEAT SHIELD		172 TO 367	
ANTENNA RADOME		172 TO 367	
NONEXPLOSIVE PIN PULLERS	200 TO 367	200 TO 367	
IR FLUX DETECTOR MIRROR	233 TO 772	200 TO 772	
TEMPERATURE SENSOR	233 TO 798	228 TO 798	
ANTENNA	200 TO 772	200 TO 772	

(a) OPERATING LIMITS SHOWN ARE FOR DESCENT. FOR CRUISE, THE OPERATING LIMITS ARE 286 TO 305°K.

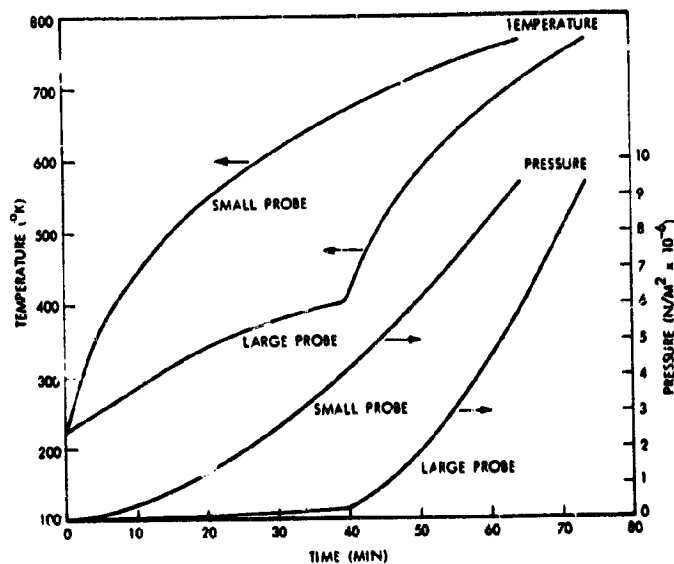


Figure 7.4-3. Atmospheric Pressure and Temperature Versus Time During Descent

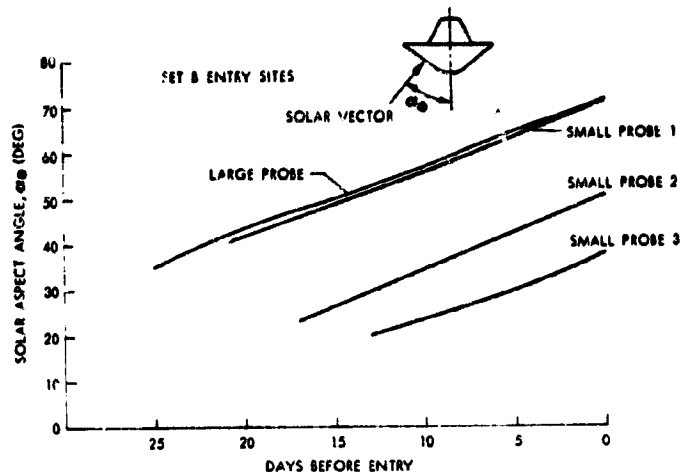


Figure 7.4-4. Solar Aspect Angles, Large and Small Probes

7.4.3 Tradeoffs

7.4.3.1 Pressure-Protected vs Nonpressure-Protected Designs

A tradeoff study was performed early in the program comparing pressure-protected designs, i. e., use of a pressure vessel to contain the science and electronic equipment, as opposed to nonpressure-protected or vented designs. The approaches that were investigated are given in the following study outline:

- I. Pressure-Protected Concepts
 - A) Insulation External to the Pressure Vessel
 - B) Insulation Internal to the Pressure Vessel
 1. Multilayer Insulation
 2. Fibrous Insulation
- II. Pre-Loaded Pressure Vessel
- III. Pressure Equalized Container
 - A) Atmospheric Venting
 - B) Voids Filled
 1. Phase Change Material as Filler
 2. 400 kg/m^3 (25 lb/ft^3) Filler Material
 - C) Cold Gas Pressurization

The pressure-protected approaches utilize a pressure vessel which is designed to resist the total Venus surface pressure. The pre-loaded approach is akin to the concept used in pre-stressed beams. Here, the

pressure vessel is pressurized on the launch pad to some fraction of the anticipated Venus surface pressure so that on the surface it must withstand a compressive pressure equal only to the difference between the internal probe pressure and the Venus surface pressure. The objective for the pressure equalized approaches is to fill the void spaces in the probes with a material or gas that is maintained at a pressure as close as possible to the atmospheric pressure. For this approach there will be some equipment components that will require pressure protection, and a small weight allocation is provided for this purpose.

The tradeoff study results are given in Figure 7.4-5 and Table 7.4-3. Even though the pressure-protected approach requires a relatively heavy pressure vessel, this weight is more than offset by reduced phase change material, insulation, or void filler material requirements. For example, the atmospheric venting approach requires a large quantity of phase change material to cool the incoming high pressure, high temperature atmospheric gases. This is due to the non-ideal gas behavior of high pressure CO_2 .

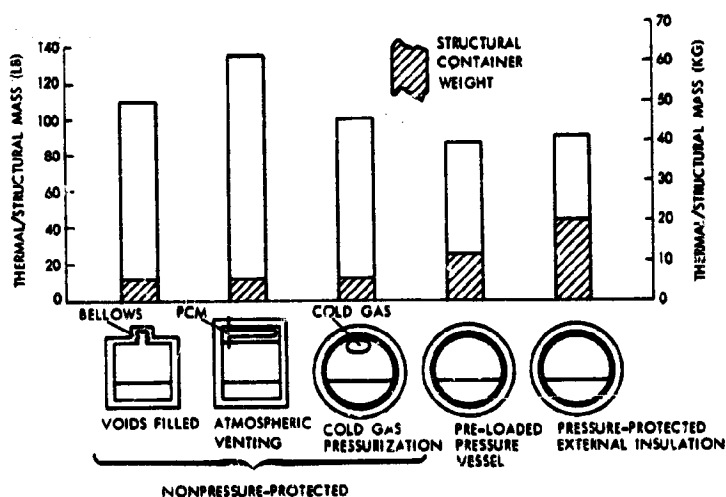


Figure 7.4-5. Nonpressure-Protected Concepts

The study results show that the pressure-protected approach is lighter than all the nonpressure-protected approaches except for one, the pre-loaded pressure vessel, and here the weight difference is small. When consideration is given to the requirement of testing science instruments and electronics to high pressure levels for nonpressure-protected designs, the program cost impact for high pressure component testing dictates the pressure-protected design.

Table 7.4-3. Weight Breakdown for 515.8 kg/m³ Packaging Density

	ATMOSPHERE VENTING	VOIDS FILLED PCM	VOIDS FILLED FILLER MATERIAL	PRESSURE-PROTECTED INTERNAL FIBEROUS INSULATION	PRESSURE-PROTECTED INTERNAL MULTILAYER INSULATION	PRESSURE-PROTECTED EXTERNAL MIN-K	COLD GAS	PRE-LOADED
SCIENCE	22.6	22.6	22.6	22.6	22.6	22.6	22.6	22.6
ELECTRONICS	21.3	21.3	21.3	21.3	21.3	21.3	21.3	21.3
INTERNAL EQUIPMENT SHELF	2.7	2.7	2.7	2.7	2.7	2.7	2.7	2.7
EXTERNAL INSULATION COVER, SUPPORTS, ETC.	8.6	8.6	8.6	8.6	8.6	8.6	8.6	8.6
PRESSURE SHELL				33.1	28.7	20.6		10.8
EQUIPMENT HOUSING (PRESSURE EQUALIZED)	7.7	5.0	5.0				4.7	
PRESSURE SHELL OR HOUSING CLOSURES, ETC.	4.1	4.1	4.1	8.2	8.2	8.2	4.1	6.1
THERMAL INSULATION	70.5	3.0	8.8	1.3	0.8	13.4	21.7	16.7
PCM (EQUIPMENT COOLING)	0.5		0.5	3.8	0.5	0.5	0.5	0.5
PCM (FILLER MATERIAL)		56.0						
PCM (ATMOSPHERE COOLING)	65.1							
T/C COATINGS	0.7	0.7	0.7	0.7	0.7	0.7	0.7	0.7
COLD GAS							1.6	0.7
COLD GAS BOTTLE							8.7	
FILLER MATERIAL			28.0					
COMPONENT PRESSURE PROTECTION	4.5	4.5	4.5				4.5	2.3
TOTALS	218.3	128.5	106.9	102.3	94.1	98.0	101.7	92.0

7.4.3.2 Pressure Shell Material and Insulation Material Tradeoffs - Large Probe

The pressure-protected descent tradeoff studies were performed using a special computer program described in detail in Technical Note P73-203434-064. This program provides a means for optimization of the thermal/structural design for planetary descent probes. Probe sizing is performed by coupling thermal, structural, and descent profile calculations within a single program to rapidly and accurately estimate probe weights.

The program incorporates the following features and options :

- 1) Pressure shell materials - aluminum, beryllium, or titanium
- 2) Pressure shell configuration - spherical or cylindrical mid-section with spherical domes
- 3) Fixed pressure shell weight or calculated from maximum pressure, maximum temperature, and internal dimensions
- 4) Thermal insulation materials - MIN-K TE 1400 or FA fiberglass
- 5) Thermal insulation configuration - external insulation only, internal insulation only, or a combination of internal and external insulation

- 6) Arbitrary insulation penetration conductance
- 7) Arbitrary equipment temperature limits
- 8) Phase change material weight fixed or based on amount required to keep payload temperature below the upper temperature limit
- 9) Descent profile computed based on arbitrary pre- and post-parachute ballistic coefficients arbitrary staging altitude and design survival altitude
- 10) Model atmospheres - options of three Venus atmospheres.

Using this program, a number of alternative pressure-protected designs were investigated.

Results of the portion of the study dealing with alternative pressure vessel and insulation designs is given in Figure 7.4-6. This study compares combinations of externally and internally insulated aluminum, titanium, and beryllium pressure shell materials with both MIN-K TE 1400 insulation (320 kg/m^3) and FA fiberglass insulation (160 kg/m^3 for external mounting, 64 kg/m^3 for internal mounting). Beryllium did not show a significant weight advantage and was therefore eliminated from further consideration because of cost; the cost of a beryllium shell compared to aluminum is approximately 10 to 1. In comparing aluminum and titanium it was found that if the shell temperature is permitted to rise to a maximum of about 500°K (440°F), the titanium provides a definite weight advantage relative to aluminum. Because shell temperatures of this magnitude would cause severe science integration problems, and consequently a significant cost impact, a decision was made to limit the shell temperature for large probes to below 422°K (300°F) for Thor/Delta and 380°K (225°F) for Atlas/Centaur. Inspection of Figure 7.4-6 shows that an aluminum shell with an external layer of MIN-K TE 1400 insulation provides a somewhat lighter design than a titanium shell with the same external insulation, when both are sized to meet the 422°K shell temperature limit. The use of aluminum does not provide as great a strength margin for local hot spots as does titanium; however, the high thermal conductivity of aluminum reduces the likelihood of such hot spots. This temperature spreading effect of aluminum is illustrated in Appendix 7.4A. Note also that an aluminum shell is approximately one-fourth the cost of a titanium shell.

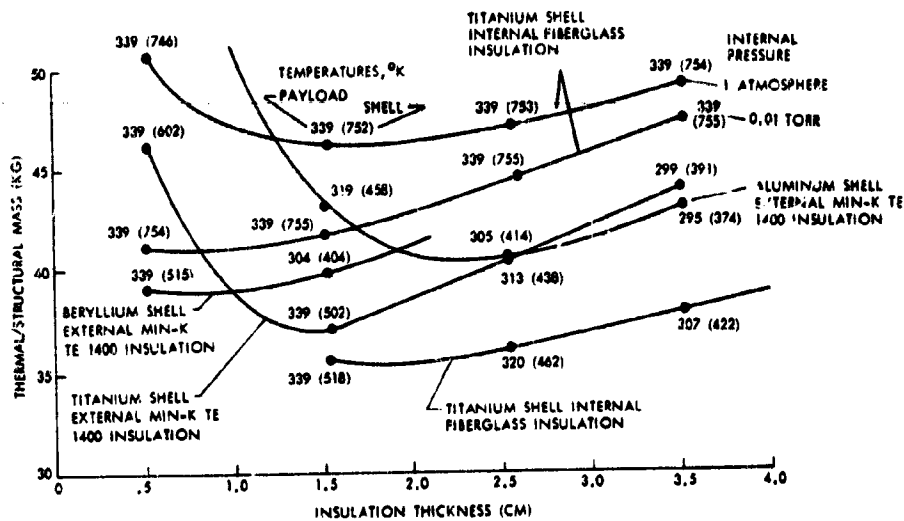


Figure 7.4-6. Large Probe Tradeoff Study

The main reason for selection of MIN-K is that it represents a lower cost, lower risk system than the fiberglass, because the molded fiberglass insulation requires a development program to eliminate outgassing during descent, whereas the MIN-K does not. This was shown in descent simulation tests we have conducted on both materials. The required development activity to preclude outgassing from the fiberglass is estimated to be considerably more costly than the somewhat higher fabrication cost of MIN-K. A detailed discussion of insulations is given in Section 7.4.6.

7.4.3.3 Small Probe Thermal Design Tradeoffs

Results of tradeoffs for the small probes are given in Figure 7.4-7. These tradeoffs illustrate the effect of pressure shell materials and inside vs outside insulation on thermal/structural weight. For both the Thor/Delta and Atlas/Centaur missions, the internal insulation approaches were rejected for the following reasons: (1) science integration problems associated with a pressure shell temperature just slightly less than the Venus atmospheric temperature; (2) inner surface-of-the-insulation temperatures considerably hotter than equipment operating temperatures; and (3) difficulties inherent in attaching insulation to the interior surfaces of the pressure shell. For the weight-critical Thor/Delta mission, the titanium shell with external insulation was chosen to save weight. An aluminum shell was again chosen for the Atlas/Centaur mission to save cost.

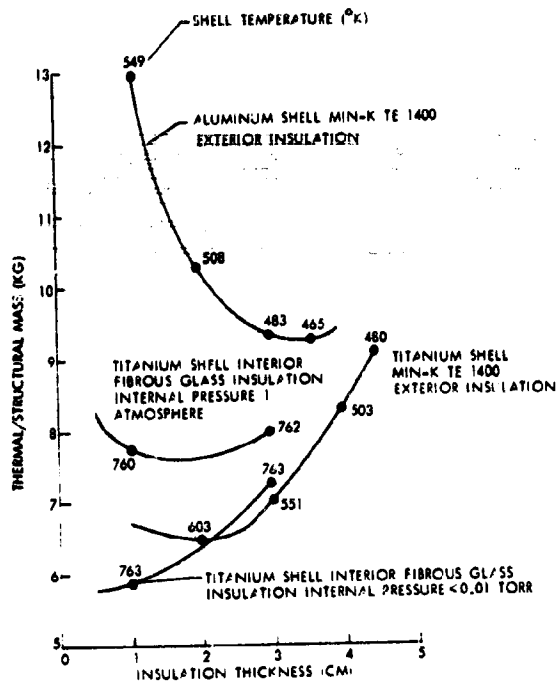


Figure 7.4-7. Small Probe Tradeoff Study

7.4.3.4 Other Tradeoffs

Consideration was given to alternative approaches relative to thermal control during the time period before entry. The preferred approach is thermal isolation of the battery and a thermostatically controlled battery heater to ensure that at entry the battery is equal to or greater than 286°K (55°F), its minimum operating temperature. The payload, other than the battery, is controlled passively, using external thermal control coatings to ensure an entry temperature equal to or greater than 255°K (0°F), but no higher than 305°K (90°F). Other approaches that could be used for entry thermal control are shown in Figure 7.4-8. These include a completely passive scheme, active control with the battery and payload thermally coupled, and active control with the battery and payload thermally decoupled.

The thermal isolation of the battery, which is consistent with the preferred design, prevents taking full advantage of the battery heat sink during descent. However, if the battery is not thermally isolated the entire payload would have to enter at 286°K (55°F). This would force a design approach as depicted in Figure 7.4-8 (b) and yield much smaller margins at

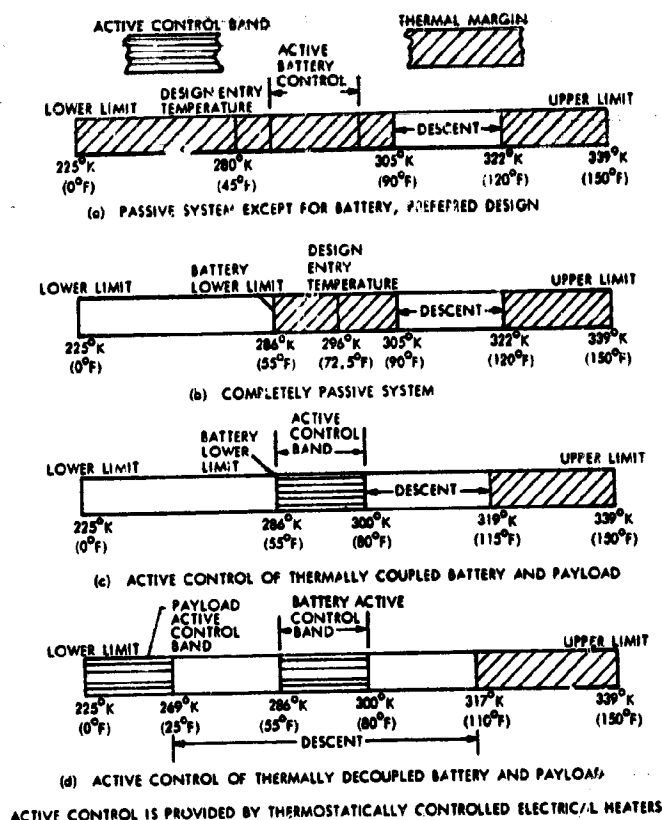


Figure 7.4-8. Thermal Control Approaches

entry. With these small margins increased post-separation cruise testing would be required. This cost is much greater than the cost of battery heaters. The approaches shown in Figure 7.4-8 (c) and (d) require that the entire payload be heated electrically. Even though those schemes provide larger thermal margins during descent than the preferred design, they were not chosen because of their excessive power requirements, which influence costs adversely.

Probe level tradeoff studies were conducted which examined the impact of varying the descent ballistic coefficients and the altitude to which the probe is designed to survive. The tradeoff results showed that increasing the post parachute-release ballistic coefficient from 550 to 1260 kg/m² yields a thermal/structural weight savings of ~2.3 kg (5%), and that designing the large probe for survival to 15 km above the nominal surface (6050 km) results in a weight savings of ~13.6 kg, or 32%. These options were not adopted since selection of the Atlas/Centaur significantly reduced the requirement for minimum weight.

7.4.4 Preferred Thermal Control Subsystem, Atlas/Centaur

7.4.4.1 Large Probe

The Atlas/Centaur large probe thermal control subsystem consists of insulation, thermal control joint conductance material, battery and science window heaters, phase change devices, and thermal control coatings. Figure 7.4-1 illustrates this design.

This thermal design is based on an entry nominal design temperature of 280°K (45°F) $\pm 25^{\circ}\text{K}$ ($\pm 45^{\circ}\text{F}$). This ensures that the initial descent temperature is higher than the lower equipment operating temperature, 255°K (0°F). For the descent phase, the initial design temperature is taken to be the upper side of the tolerance at entry or 305°K (90°F). An additional temperature rise of 16.6°K (30°F) is allowed during descent to the surface. This provides a $\pm 25^{\circ}\text{K}$ ($\pm 45^{\circ}\text{F}$) margin at entry, and a $+16.6^{\circ}\text{K}$ ($+30^{\circ}\text{F}$) margin at the planet surface where the nominal temperature is 322°K (120°F) compared to the upper equipment temperature limit of 338°K (150°F). Figure 7.4-8 (a) illustrates this approach.

With the choice of aluminum for the pressure vessel material and MIN-K TE 1400 for the insulation, the descent thermal control subsystem is designed as illustrated in Figure 7.4-9. First an optimum thermal-plus-structural weight point is found by allowing the structural shell weight to vary as dictated by its strength vs temperature characteristics, and providing sufficient insulation to limit the payload to 322.0°K (120°F) at impact. Then the shell weight is fixed, consistent with maximum temperature from the optimum weight point, and the insulation thickness is increased to determine an insulation thickness that reduces the maximum shell temperature approximately 28°K (50°F). This provides a temperature margin for both the payload and the pressure shell design, and permits the reductions in testing described elsewhere. These calculations were performed using the generalized probe thermal/structural design program described in Section 7.4.3.2.

A 21-node thermal model was developed for post-separation cruise studies of the large probe. Steady-state temperatures were calculated for this model at a number of selected times between separation and entry. Previous studies have shown that the thermal behavior is pseudo-steady-state. In order to effectively use the payload mass as a thermal heat sink

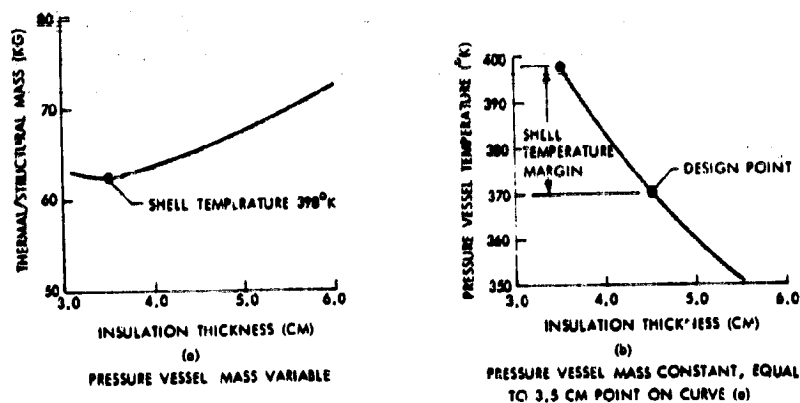


Figure 7.4-9. Atlas/Centaur Large Probe Design Calculations

during descent, a relatively low payload temperature was desired at entry. External surface radiation properties were selected to produce a payload entry temperature of 280.4°K (45°F) $\pm 25^{\circ}\text{K}$ ($\pm 45^{\circ}\text{F}$) and to maintain all other surfaces and components within their allowable temperature limits. Because the battery operating temperature is between 286°K (55°F) and 305°K (90°F), each battery is thermally isolated from the rest of the payload and its temperature is independently controlled by a 20-watt thermostatically controlled heater.

The temperature history of the probe payload from probe separation to touchdown on the planet surface is given in Figure 7.4-10. It is apparent that the payload is maintained well within temperature limits during this phase of the mission. Note also that a special analysis to investigate the effect of the entry thermal pulse on the payload was performed and found to be insignificant.

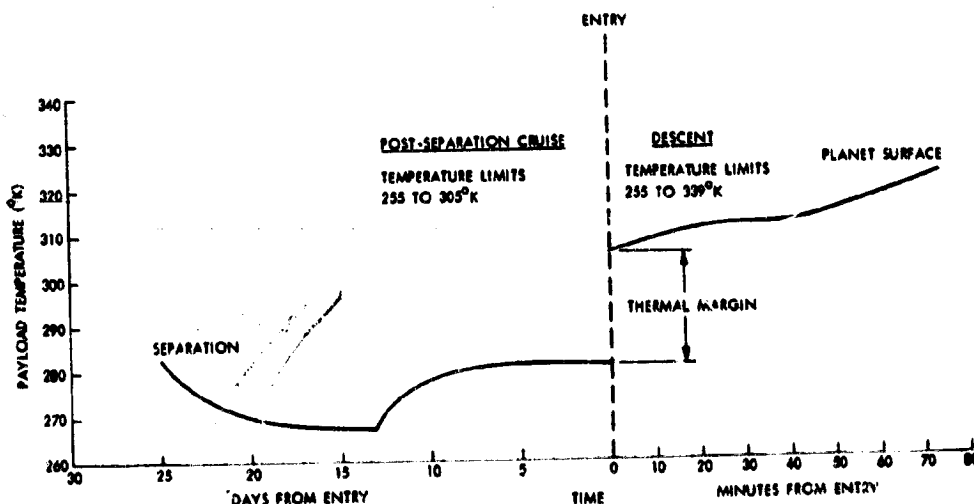


Figure 7.4-10. Atlas/Centaur Large Probe Payload Temperature History

The large probe thermal designs, both descent and cruise, are influenced by penetrations through the insulation. The thermal control coating selection, which controls cruise conditions, is a function of the penetrations. During descent, the penetrations influence the insulation and phase change weight as well as the pressure shell temperature. The penetration values are given in Table 7.4-4, and Figure 7.4-11 illustrates the influence of insulation penetrations on probe weight.

Table 7.4-4. Insulation Penetrations for Atlas/Centaur Large Probe

PENETRATION	CONFIGURATION	MATERIAL	TOTAL AREA (CM ²)	CONDUCTIVITY (WATT/CM-K)	K · A (WATT/CM-K)
PRESSURE GAUGE PORT	1.6 MM DIA TUBE, 0.13 MM WALL	INCONEL	0.0065	0.194	0.00126
CLOUD PARTICLE ANALYZER WINDOW	2.54 CM DIA TUBE, 0.51 MM WALL	INCONEL	0.405	0.194	0.0786
SOLAR RADIOMETER WINDOW	2.54 CM DIA TUBE, 0.51 MM WALL	INCONEL	0.405	0.194	0.0786
IR FLUX DETECTOR WINDOW	2.54 CM DIA TUBE, 0.51 MM WALL	INCONEL	0.405	0.194	0.0786
GAS CHROMATOGRAPH INLET PORT	1.6 MM DIA TUBE, 0.13 MM WALL	INCONEL	0.0097	0.194	0.0019
MASS SPECTROMETER INLET PORT	3.1 MM DIA TUBES (12), 0.2 MM WALL, IN 7.6 CM DIA TUBE, 0.76 MM WALL	INCONEL	2.06	0.194	0.400
WIND DRIFT RADAR ANTENNA MOUNTS	5.1 MM DIA POSTS (4) WITH 7.6 MM x 1.1 MM WEBS	TITANIUM	1.85	0.104	0.1925
STRUCTURAL LOAD CONE	15° CONE 6.1 CM LONG, 0.9 MM THICK	TITANIUM	18.97	0.104	1.641*
ELECTRICAL LEADS	22 GAUGE (4) 24 GAUGE (78) SHIELDS (20)	COPPER	0.013	3.86	0.0501
		COPPER	0.160	3.86	0.616
		COPPER	0.291	3.86	1.123

* ADJUSTED FOR 6.1 CM LENGTH

Σ KA = 4.262
(3.181 BELL-IN)
HR = °F

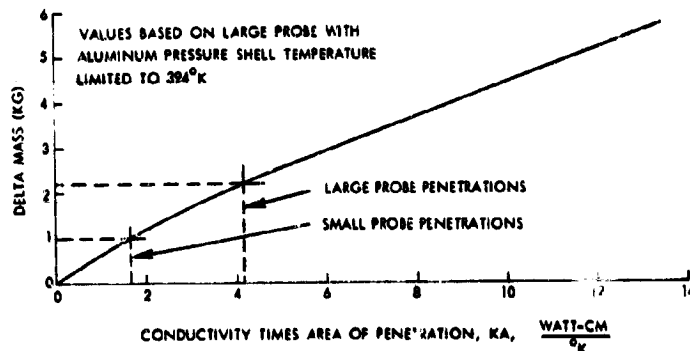


Figure 7.4-11. Thermal/Structural Mass Sensitivity to Insulation Penetrations

Other thermal control studies conducted include the effect of insulation performance on maximum pressure shell temperature. Here a 50% increase in the effective conductivity of the thermal insulation causes approximately a 25°K (45°F) increase in the shell temperature.

7.4.4.2 Small Probe

The Atlas/Centaur small probe thermal control subsystem consists of insulation, thermal control joint conductance material, battery and science window heaters, phase change devices, and thermal control coatings. Figure 7.4-2 illustrates this design. The basic approach (shown in Figure 7.4-8 (a)) for the small probes is identical to that for the Atlas/Centaur large probe. The determination of the insulation thickness and shell temperature margin was performed as described for the large probe. This result is given in Figure 7.4-12.

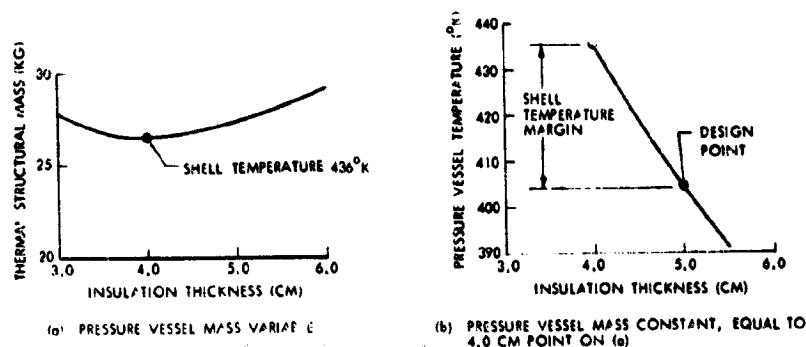


Figure 7.4-12. Atlas/Centaur Small Probe Design Calculations

The post-separation cruise phase design for the small probes is somewhat more complicated compared to the large probes. For the small probes, solar aspect angles for the various probes are unequal because of targeting them to different places on the planet and producing zero angle of attack at entry. With these unequal solar aspect angles and the requirement of identical small probes, a single thermal coating pattern must be found that minimizes the payload entry temperature spread. A coating pattern that meets this requirement and maintains all surfaces and components within their allowable temperature limits is given in Figure 7.4-2. This pattern is based on solar aspect angles consistent with target site B rather than the preferred mission to site A (see Section 4.2.2.1.) The site B angles were used since their spread at entry is larger than the site A angle spread, and therefore present a more difficult condition to meet. Previous studies have shown that the thermal behavior during probe cruise is pseudo-steady-state; therefore, steady-state analysis is used to establish the entry

temperature of each probe. Once a pattern that minimizes the entry payload temperature spread is established, then points are calculated between probe release to entry to ensure that temperature limits are met throughout the probe cruise phase of the mission. These calculations were performed using a 28-node thermal model.

The small probe temperature histories from separation to touchdown on the planet surface are shown in Figure 7.4-13. The penetrations through the small probe insulation are given in Table 7.4-5.

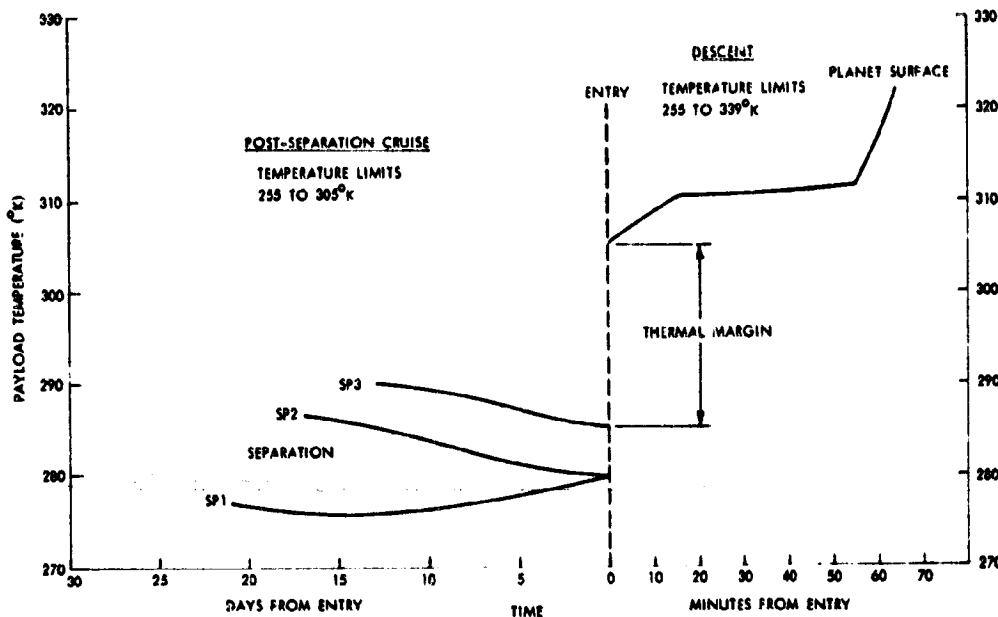


Figure 7.4-13. Atlas/Centaur Small Probe Payload Temperature History

Table 7.4-5. Insulation Penetrations for Atlas/Centaur Small Probe

PENETRATION	CONFIGURATION	MATERIAL	TOTAL AREA (CM ²)	CONDUCTIVITY (WATT/CM-K)	K · A (WATT-CM/K)
PRESSURE GAUGE FORT	1.6 MM DIA TUBE 0.13 MM WALL	INCONEL	0.0065	0.194	0.00126
NEPHELOMETER WINDOWS	CONICAL TUBE 1.63 CM DIA, 0.51 MM WALL	INCONEL	0.445	0.194	0.090
	STRAIGHT TUBE 1.27 CM DIA, 0.51 MM WALL				
IR FLUX DETECTOR WINDOW	1.9 CM DIA TUBE 0.51 MM WALL	INCONEL	0.304	0.194	0.059
ANTENNA SUPPORT	1.9 CM DIA TUBE 0.51 MM WALL 7.6 CM LONG	TITANIUM	0.304	0.104	0.0211 *
HORIZONTAL STABILIZER RING	DISC 0.52 MM THICK 53.4 CM O. D., 43.1 CM I. D.	TITANIUM	7.86	0.104	0.818
ELECTRICAL LEADS	24 GAUGE (42) SHIELDS (10)	COPPER	0.086	3.86	0.332
		COPPER	0.104	3.86	0.401

K · A = 1.722
(11.266 BTU-IN.)
HR-°F

* ADJUSTED FOR 7.6 CM LENGTH

7.4.5 Preferred Thermal Control Subsystem, Thor/Delta

The thermal control approach for the Thor/Delta is similar to that for the Atlas/Centaur, except that the design entry temperature was 263.7°K (15°F) to $+0$ -8.3°K ($+0$ -15°F), the allowable descent temperature rise was from 263.7°K (15°F) to 339°K (150°F), and titanium was chosen for the small probe shell material. All of the differences were chosen in order to save weight for the weight critical Thor/Delta mission.

The Thor/Delta large probe and small probe thermal subsystem designs are shown in detail in Figures 7.4-14 and 7.4-15, respectively. The temperature histories from separation to touchdown on the planet surface are shown in Figure 7.4-16 for the large probe and Figure 7.4-17 for the small probe. Descent calculations for Thor/Delta probes were performed using the thermal/structural computer program described in Section 7.4.3.2. Thermal models were developed for probe cruise analysis; the large probe model contained 34 nodes while the small probe model was made up of 28 nodes.

ID NO.	NAME OF ITEM	DESCRIPTION	PURPOSE	SURFACE POSITIONS	
				a	b
1	EXTERNAL FOREBODY SURFACE COATINGS	MOSAIC TO PRODUCE PRESCRIBED SOLAR ABSORPTIVITY (α) AND EMISSIVITY (ϵ) RATIO 5-13-G WHITE AND 3M BLACK VELVET PAINT	MAINTAIN FORWARD SURFACE AND PAYLOAD WITHIN PRESCRIBED TEMPERATURE LIMITS DURING CRUISE AND POST-SEPARATION PHASES	0.32	0.08
2	(a)EXTERNAL AFTERBODY SURFACE COATINGS	1 MIL SHEET OF ALUMINIZED MYLAR	MAINTAIN PAYLOAD WITHIN PRESCRIBED TEMPERATURE LIMITS DURING POST-SEPARATION CRUISE PHASE	0.10	0.05
3	THERMAL INSULATION ON EXTERNAL SURFACE OF PRESSURE SHELL	2.5 CM LAYER OF MIN-K T 1400 INSULATION	CONTROL TEMPERATURE OF PRESSURE SHELL AND PAYLOAD DURING DESCENT PHASE		
4	GLASS FIBER INSULATION	FA BATT AROUND BATTERY CASE AND IN MIN-K JOINTS	THERMALLY ISOLATE BATTERY FROM PAYLOAD AND FILL GAPS IN MIN-K INSULATION		
5	BATTERY HEATER	THERMOSTATICALLY CONTROLLED 20-WATT ELECTRICAL RESISTANCE HEATER PER BATTERY CASE	MAINTAIN MINIMUM BATTERY TEMPERATURE OF 286°K DURING POST-SEPARATION CRUISE PHASE		
6	SCIENCE WINDOW HEATERS	15-WATT ELECTRICAL RESISTANCE HEATERS ON EACH SCIENCE WINDOW	MAINTAIN SCIENCE WINDOW TEMPERATURE ABOVE LOCAL ATMOSPHERIC TEMPERATURE DURING DESCENT		

(a) SIMILAR TO VIKING LANDER. ATTACHED ACCORDING TO MMC MP-72326

WEIGHT SUMMARY	
	(KG)
SURFACE COATINGS	0.7
INSULATION, MIN-K	9.7
HEATERS	0.5
SENSORS	0.4
TOTAL	11.3

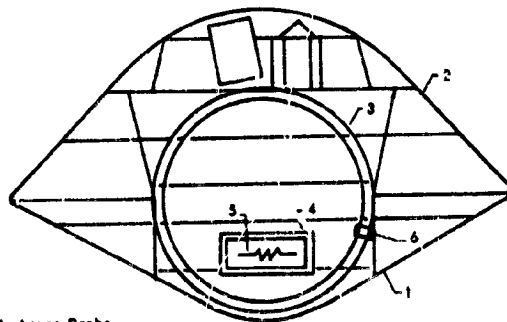


Figure 7.4-14. Thor/Delta Large Probe

ID NO.	NAME OF ITEM	DESCRIPTION	PURPOSE	SURFACE POSITIONS	
				α	ϵ
1	EXTERNAL FOREBODY SURFACE COATINGS SPHERICAL NOSE SECTION	Z-93 WHITE PAINT	MAINTAIN FORWARD SURFACE AND PAYLOAD WITHIN PRESCRIBED LIMITS DURING POST-SEPARATION PHASE	0.24	0.92
2	EXTERNAL FOREBODY SURFACE COATINGS ON LOWER CONICAL SECTION	MOSAIC TO PRODUCE PRESCRIBED SOLAR ABSORPTIVITY (α) AND EMISSIVITY (ϵ) RATIO Z-93 WHITE AND 3M BLACK VELVET PAINTS	MAINTAIN FORWARD SURFACE AND PAYLOAD TEMPERATURES WITHIN PRESCRIBED LIMITS DURING POST-SEPARATION PHASE	0.37	0.92
3	EXTERNAL FOREBODY SURFACE COATINGS ON UPPER CONICAL SECTION	MOSAIC TO PRODUCE PRESCRIBED SOLAR ABSORPTIVITY (α) AND EMISSIVITY (ϵ) RATIO Z-93 WHITE AND 3M BLACK VELVET PAINTS	MAINTAIN FORWARD SURFACE AND PAYLOAD TEMPERATURES WITHIN PRESCRIBED LIMITS DURING POST-SEPARATION PHASE	0.42	0.92
4	EXTERNAL AFTERBODY SURFACE COATING ON CONICAL SECTION	MOSAIC TO PRODUCE PRESCRIBED SOLAR ABSORPTIVITY (α) AND EMISSIVITY (ϵ) RATIO Z-93 WHITE AND 3M BLACK VELVET PAINTS	MAINTAIN AFT SURFACE AND PAYLOAD TEMPERATURES WITHIN PRESCRIBED LIMITS DURING POST-SEPARATION PHASE	0.78	0.92
5	EXTERNAL AFTERBODY SURFACE COATING ON AFT SPHERICAL SECTION	VACUUM DEPOSITED SILVER ON 1 MIL MYLAR	MAINTAIN PAYLOAD WITHIN PRESCRIBED LIMITS DURING POST-SEPARATION PHASE	0.06	0.04
6	THERMAL INSULATION ON EXTERNAL SURFACE OF PRESSURE SHELL	3.0 CM LAYER OF MIN-K TE 1400 INSULATION	CONTROL TEMPERATURE OF PRESSURE SHELL AND PAYLOAD DURING DESCENT PHASE		
7	GLASS FIBER INSULATION	FA BATT AROUND BATTERY CASE AND IN MIN-K JOINTS	THERMALLY ISOLATE BATTERY FROM PAYLOAD AND FILL GAPS IN MIN-K INSULATION		
8	THERMAL ISOLATORS IN JOINT BETWEEN PRESSURE SHELL AND EQUIPMENT SHELF	0.32 CM LAYER OF ASBESTOS REINFORCED PLASTIC 41 RPD LAMINATE	REDUCE HEAT TRANSFER FROM PRESSURE SHELL TO EQUIPMENT SHELF DURING DESCENT		
9	BATTERY HEATER	THERMOSTATICALLY CONTROLLED 20-WATT ELECTRICAL RESISTANCE HEATER PER BATTERY CASE	MAINTAIN MINIMUM BATTERY TEMPERATURE OF 286°K DURING POST-SEPARATION PHASE		
10	SCIENCE WINDOW HEATER	15-WATT ELECTRICAL RESISTANCE HEATER ON EACH SCIENCE WINDOW	MAINTAIN SCIENCE WINDOW TEMPERATURE ABOVE LOCAL ATMOSPHERIC TEMPERATURE DURING DESCENT		

WEIGHT SUMMARY	
	(KG)
SURFACE COATINGS	0.1
INSULATION, MIN-K	2.8
HEATERS	0.1
SENSORS	0.1
TOTAL	3.1

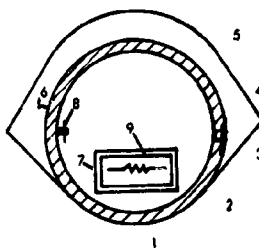


Figure 7.4-15. Thor/Delta Small Probe

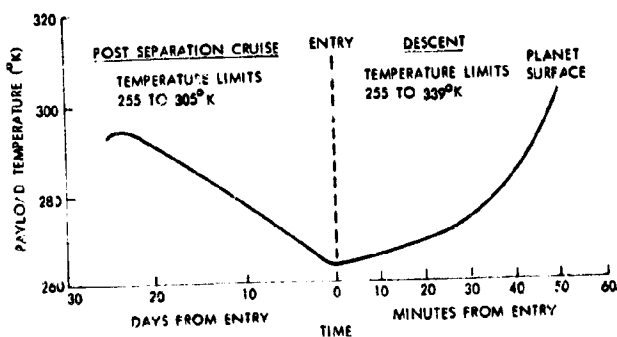


Figure 7.4-16. Thor/Delta Large Probe

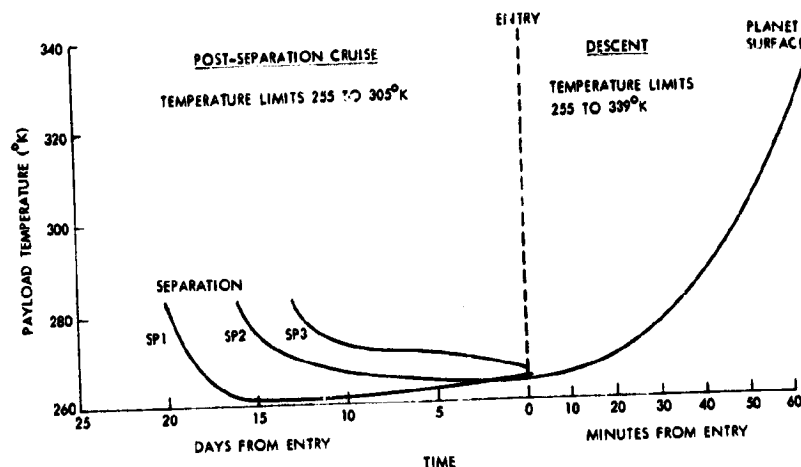


Figure 7.4-17. Thor/Delta Small Probe

7.4.6 Supporting Analysis and Tests

7.4.6.1 Atlas/Centaur Design Calculations

After having decided to use aluminum for the pressure vessel material and MIN-K TE 1400 insulation, the descent thermal control system was designed as follows. Identification of the optimum designs was made by varying insulation thickness which, in turn, affects the pressure shell weight and the required phase change material weight. An example of these calculations is given in Figure 7.4-9. In Figure 7.4-9 (a) the insulation thickness is varied and for each insulation thickness the pressure shell thickness is found consistent with its maximum temperature; phase change is added, as needed, to limit the payload temperature to less than the maximum allowable. From these calculations the pressure shell weight and maximum temperature are determined for the minimum weight design. This shell weight is held constant and insulation is added in order to reduce the maximum shell temperature approximately 28°K (50°F) to provide a thermal margin for the pressure shell design. This calculation is illustrated in Figure 7.4-9 (b). These calculations were performed using the generalized probe thermal/structural design program described in Section 7.4.3.2.

7.4.6.2 Insulation Thermal Performance

Summary. A coupled experimental/analytical study was conducted to establish the performance of thermal insulations in high pressure CO_2 . The experimental work consisted of steady-state guarded hot plate conductivity tests to 125 atmospheres and transient Venus descent simulation

tests. Permeability and adsorption tests were also conducted on candidate insulations. Analytical studies included the determination of effective conductivity values from transient test data, the thermal modeling of mass transfer effects, and the investigation of free convection within the porous insulation. The mass transfer is potentially an important consideration since energy will be transferred into the insulation as atmospheric pressure increases during a Venus descent, forcing high pressure, high temperature gas into the porous insulation.

Results of this activity have established that mass transfer effects are relatively unimportant, while free convection and probably adsorption are quite important. These effects have been found to degrade insulation conductivity by up to a factor of four; however, a factor of two is achievable with the preferred insulation, MIN-K TE 1400. This study also established that water vapor in a CO_2 environment has little effect on insulation performance, and established high vacuum conductivity data for MIN-K TE 1400. All design analyses performed in the final designs utilized effective conductivities derived from near full-scale descent simulation testing. The following paragraphs describe the insulation studies including testing conducted in parallel IRAD programs.

Steady-state Conductivity Tests. The thermal conductivity of several candidate insulations was determined by Dynatech R/D Corporation under contract to Martin Marietta. This test program consisted of screening tests in which five insulation materials were evaluated in CO_2 to a pressure of ~30 atmospheres. This was followed by high pressure tests, to ~125 atmospheres, with MIN-K TE 1400 being tested in CO_2 and helium environments, while FA fiberglass was tested in CO_2 only. The materials tested to 30 atmospheres were MIN-K TE 1400, MIN-K 1301, FA fiberglass, palarite, and silfrax.

Results of the guarded hot plate steady-state tests are given in Figure 7.4-18. For these tests, insulation samples were 2.54 cm (1.0 inch) thick and were tested in the horizontal position. The density of the MIN-K was 320 kg/m^3 (20 lbm/ft^3), while the FA fiberglass was 128 kg/m^3 (8.0 lbm/ft^3). The conductivity values are in the range to be expected considering the conductivities of the basic insulation and the CO_2 .

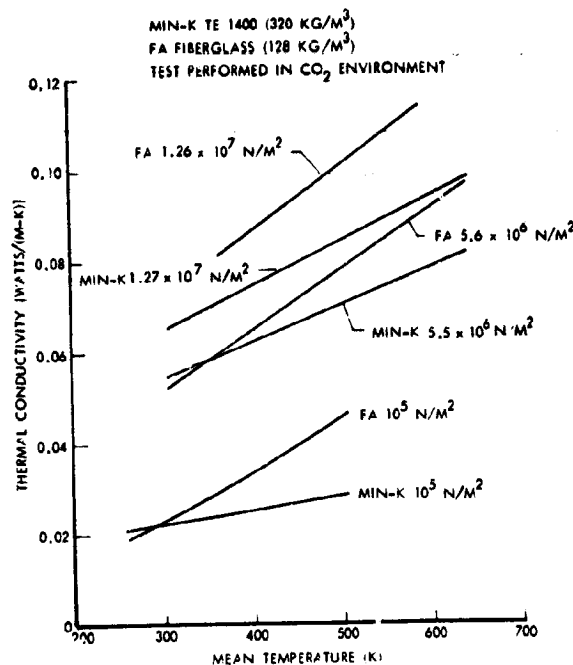


Figure 7.4-18. Thermal Conductivity Versus Temperature at Various Pressures

To provide an independent check on the Dynatech steady-state data, tests were also performed at Martin Marietta Denver Division on MIN-K TE 1400 and TG 15000 fibrous insulation. The TG 15000 is a FA fiberglass insulation with a binder added which allows forming the insulation in rigid shapes. These test results are shown in Figure 7.4-19. Included in these tests was a MIN-K TE 1400 sample configured so that the heat transfer is parallel rather than normal to the major plane of the as-received insulation slabs. The conductivity values for the "parallel" orientation are approximately 30 percent higher than the "normal" orientation. This is an important point because the fabrication of the MIN-K requires roughly 50% of the insulation to be installed with a parallel orientation on the pressure shell.

Tests were performed at Martin Marietta Denver Division on MIN-K TE 1400 at high vacuum, low temperature conditions. These tests were performed to provide data for cruise calculations, such data being unavailable in the literature. The results of these tests were conductivities of 0.0021 watts/m-K (0.0007 Btu/hr-ft-°F) at 228°K (-50°F) and 0.026 watts/m-K (0.0015 Btu/hr-ft-°F) at 283°K (+50°F), both test points at a pressure of 1.33×10^{-3} N/m² (10^{-5} torr).

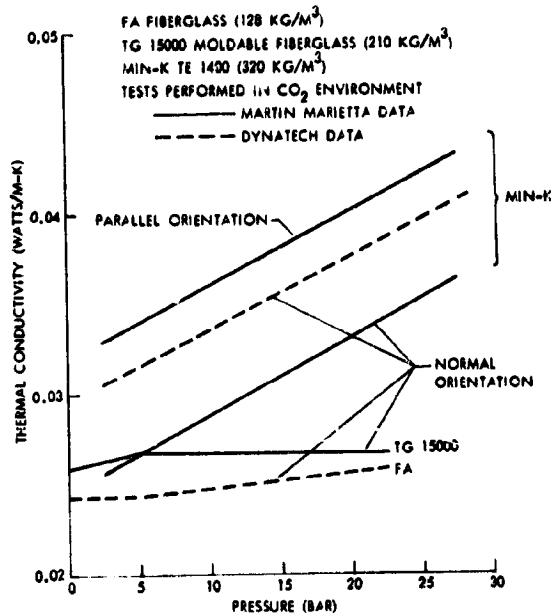


Figure 7.4-19. Thermal Conductivity Versus Pressure at Mean Temperature of 322°K

Transient Tests. Descent simulation tests have been performed on several insulations using a number of insulation/heat sink configurations. Table 7.4-6 lists the matrix of the transient tests. Figures 7.4-20 and 7.4-21 show the Martin Marietta descent simulation facilities used to perform these tests. The mini chamber shown in Figure 7.4-20 has a cylindrical test volume of approximately 25.4 cm (10 inches) diameter by 84 cm (33 inches) long. The Venus descent is simulated by manually controlled pressurization and heating systems. Heaters are provided both internally and externally to the chamber.

Table 7.4-6. Descent Simulation Tests

TEST NUMBER	INSULATION TYPE	INSULATION DENSITY KG/M ³ (LBM/FT ³)	INSULATION THICKNESS CM (IN.)	HEAT SINK DESCRIPTION	COMMENTS
1	MIN-K 1301	292 (18.2)	2.54 (1.00)	SOLID ALUMINUM CYLINDER 5.1 CM (2.0 IN.) DIA, 25.4 CM (10 IN.) LONG	MINI CHAMBER TEST WITH CO ₂ ATMOSPHERE
2	FA FIBERGLASS	117 (7.3)	2.54 (1.00)	SAME AS TEST 1	SAME AS TEST 1
3	FA FIBERGLASS	83 (5.2)	4.83 (1.90)	SOLID ALUMINUM CYLINDER 10.2 CM (4 IN.) DIA, 25.4 CM (10 IN.) LONG	SAME AS TEST 1
4	FA FIBERGLASS	83 (5.2)	4.83 (1.90)	SAME AS TEST 3	MINI CHAMBER TEST WITH 1 TO 25% WATER VAPOR INJECTED TO CO ₂ ATMOSPHERE
5	FA FIBERGLASS	69 (4.3)	3.97 (1.56)	SOLID CAST IRON SPHERE 12.5 CM (4.94 IN.) DIA	SAME AS TEST 1
6	FA FIBERGLASS	130 (8.1)	3.83 (1.51)	SAME AS TEST 5	SAME AS TEST 1
7	MIN-K TE 1400	320 (20)	2.54 (1.0)	SOLID COPPER SPHERE 15.2 CM (6.0 IN.) DIA	SAME AS TEST 1
8	MIN-K TE 1400	320 (20)	3.43 (1.35)	SPHERICAL PRESSURE VESSEL 53.5 CM (20.25 IN.) DIA, 0.433 CM (0.25 IN.) ALUMINUM WALL	MIDI CHAMBER TEST WITH CO ₂ ATMOSPHERE
9	MOLDED FIBERGLASS TG 15 000	210 (13.2)	3.56 (1.4)	SAME AS TEST 8	SAME AS TEST 8

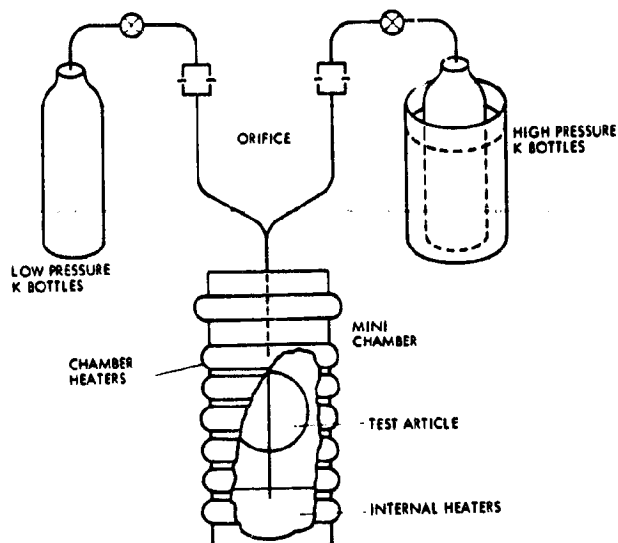


Figure 7.4-20. Mini Descent Simulation Chamber

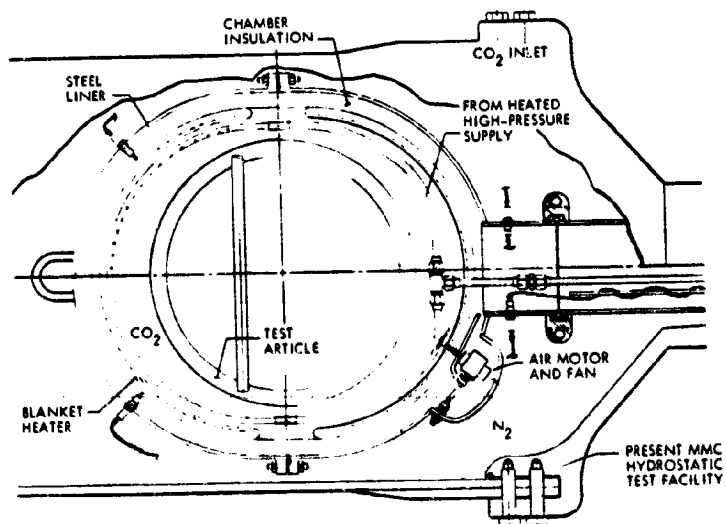


Figure 7.4-21. Midi Descent Simulation Chamber

The midi test facility is a modified hydrostatic test chamber in which Venus descent conditions, i.e., CO_2 gas rapidly increasing in temperature and pressure versus time, can be simulated for a full-scale test article. Figure 7.4-21 is a sketch of the midi facility. In order to protect the hydrostatic pressure vessel from high temperature and to minimize the CO_2 requirements, a steel liner is used with N_2 pressure controlled in concert with the CO_2 so that a relatively small pressure difference is maintained across the liner.

Inside the liner is a spherical blanket heater that heats the CO_2 to the descent profile temperature. Ceramic insulation behind the blanket heater insulation protects the liner from the high temperature CO_2 . The working volume available inside the blanket heater is spherical, 74 cm (29 inches) in diameter.

Because water vapor is believed to be a constituent of the Venus atmosphere, a test was performed to address the problem of condensation on and within the thermal insulation. For this test, water vapor was introduced into the CO_2 atmosphere during a simulated Venus descent insulation test. The test article was an aluminum heat sink insulated with fiberglass. The results of this test are contrasted to an identical test without water vapor in Figure 7.4-22. Even though approximately 25 percent by weight of water vapor was introduced into the atmosphere, the net heat transfer was the same for both tests. Because current estimates of the percent of water in the Venus atmosphere are ~1% and since water is the atmospheric trace compound that has the greatest potential for influencing insulation performance due to condensation, it is felt that condensation is not a problem.

Analysis

1) Computer Program to Determine Effective Thermal Conductivities from Transient Tests. This program is used to correlate transient test data. The heat sink temperature and insulation surface temperature from the transient testing is input to the program. With this information, the program computes the overall effective conductivity of the insulation. The thermal capacitance of the insulation is accounted for; however, mass transfer effects are ignored. These effects, therefore, are lumped into

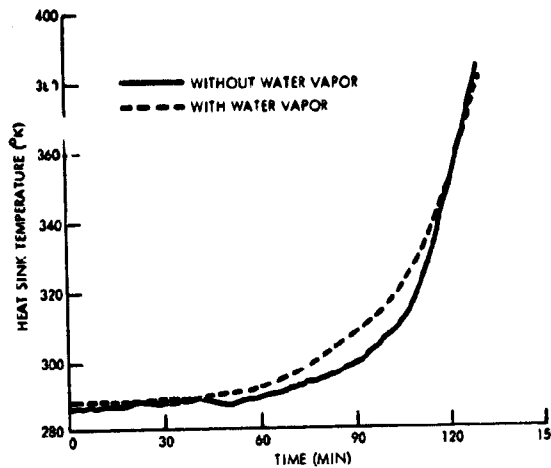


Figure 7.4-22. Descent Simulation Test Results With and Without Water Vapor in CO_2 Atmosphere

the overall effective conductivity. Applying this technique to the experimental data from Test 7 (Table 7.4-6) results in the conductivity values shown in Figure 7.4-23.

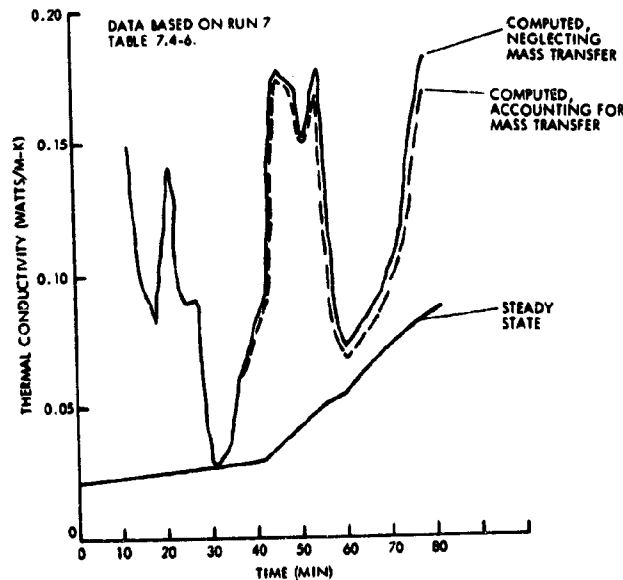


Figure 7.4-23. Effective Thermal Conductivities Derived From Test Data

2) Insulation Thermal Model Including Mass Transfer Effects. This computer program models a Venus probe insulation system including mass transfer effects. The mass transfer is caused by migration of atmospheric gases into the porous insulation as the ambient atmospheric pressure increases during descent. When these atmospheric gases enter the insulation system, they provide an input energy that must be accounted for in the overall insulation energy balance.

The model that has been developed is a generalized thermodynamic simulation of the overall insulation system. This model accounts for the internal energy associated with incoming gases, the compression and internal energy changes of the gases within the porous insulation, and heat transfer through the insulation/gas system. Real-gas properties are used for all aspects of the modeling along with the high pressure guarded hot-plate insulation conductivity data. An example of the results of this program is given in Figure 7.4-24.

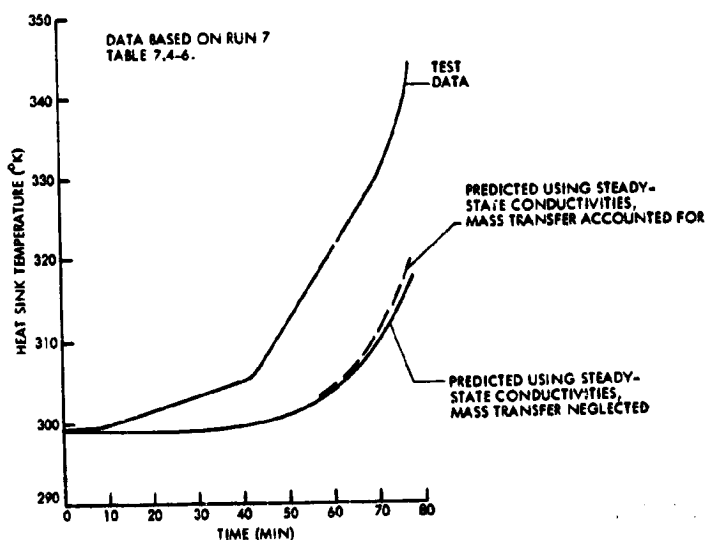


Figure 7.4-24. Comparison of Test Results With Analytical Predictions

3) Free Convection Within Porous Insulation. Free convection within the insulation at high pressure levels is a distinct possibility. If present, the free convection has a serious degrading effect on the insulation performance. This problem is unusual relative to insulation systems and, indeed, is not mentioned in twelve current heat transfer texts. Work in the area of free convection in porous media, however, has been performed in the oil and gas industry relative to reservoir engineering problems. The parameter which defines the onset of convection in a porous media is the Rayleigh number times the Darcy number and is given by:

$$R_a D_a = \frac{\rho^2 \beta g \Delta T L C_p K}{\mu k}$$

where

- ρ = density
- β = coefficient of volumetric expansion
- g = gravitational acceleration
- ΔT = characteristic temperature difference
- L = characteristic length
- C_p = specific heat
- K = permeability
- μ = viscosity
- k = thermal conductivity

Once the critical value of the Rayleigh-Darcy number has been reached, the free convection becomes stronger with increasing values of this number. It is interesting to note that the gas properties ($\rho^2 \beta C_p / \mu k$) are a strong function of temperature with this grouping, decreasing with increasing temperature, thus, to help avoid free convection the pressure shell (insulation interior) should be designed to run hot. A plot of ($\rho^2 \beta C_p / \mu k$) for CO_2 at constant pressure of 100 atmospheres shows that at about 422°K (300°F), the strong variation with temperature ceases; it is at the lower temperature that large values of the Rayleigh-Darcy numbers tend to exist. The other large contributor to the Rayleigh-Darcy number is the permeability. It is obvious that an insulation with as small a permeability as is possible should be used.

The permeability values used in the free convection correlations were obtained from tests performed by Core Laboratories for a Martin Marietta IRAD program. These tests were performed in air at room temperature. For the MIN-K TE 1400, cylindrical samples were cut with the axis of the sample normal, parallel, and at 45° to the major plane of the as-received insulation slab. The results of tests performed on these samples showed that permeability values are insensitive to orientation. These tests were confirmed by tests performed at Martin Marietta Denver using a specially fabricated test apparatus which allowed testing at high temperature with a CO_2 test fluid. The important result here is that the permeability of MIN-K

TE 1400 is approximately 0.01 Darcys, over an order of magnitude less than for fiberglass. Also, the permeability of the MIN-K is not a strong function of temperature.

Adsorption Effects

It is known that CO_2 is adsorbed by fibers similar to those of the candidate insulations. The adsorption process is exothermic and represents an energy release in the insulation during descent. In order to investigate this phenomenon tests were performed on 8.25 cm (3.25 inches) diameter by 8.25 cm (3.25 inches) long insulation samples fitted with thermocouples and placed in a 8.6 cm (3.4 inches) diameter by 15.2 cm (6 inches) long cylindrical pressure chamber. The chamber and insulation were first evacuated and then pressurized to 500 psia. Results of these tests with MIN-K TE 1400 insulation and CO_2 , N_2 , and He are shown in Figures 7.4-25, 7.4-26 and 7.4-27, respectively. For all of the gases a thermodynamic calculation of the filling process predicts a temperature rise of approximately 11°K (20°F) if adsorption effects are neglected. From low pressure adsorption data, the degree of adsorption increases from He to N_2 to CO_2 with the He yielding little or no adsorption. Inspection of the results shows that the He response is consistent with the thermodynamic analysis which neglected adsorption effects. The N_2 and CO_2 results are consistent with the assumption that adsorption occurs. The CO_2 results yield a temperature rise of approximately 16.6°K (30°F) above the rise expected due to the filling process (adiabatic compression). This magnitude of temperature rise suggests that adsorption is a significant factor relative to insulation performance. A CO_2 test with FA fiberglass showed similar results. With the awareness of this phenomenon, together with free convection and mass transfer, it is felt that all significant factors relative to insulation thermal performance are known.

Results and Conclusions

A comparison of the steady-state conductivities with the conductivities analytically derived from the transient tests showed that the conductivities from the transient tests were much larger than the steady-state values for a number of the tests. A special analysis, which accounted for mass transfer effects, migration of atmospheric gases in the porous insulation, failed to account for much of the differences; this result is shown in Figure 7.4-24.

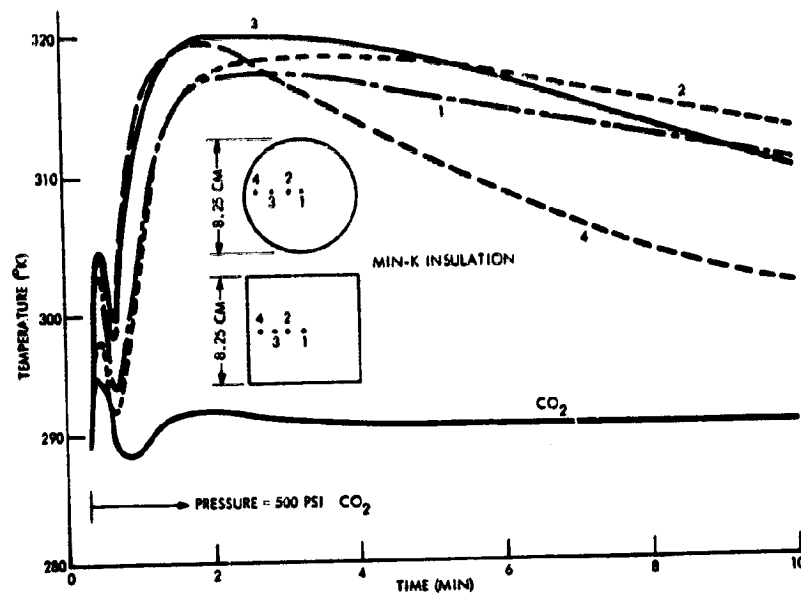


Figure 7.4-25. Thermal Response of Insulation to CO₂ Filling Process

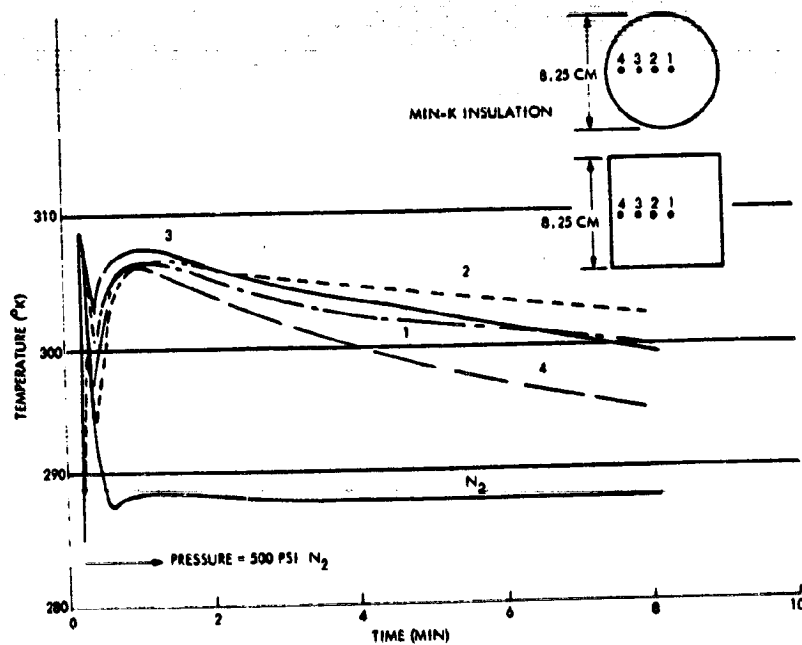


Figure 7.4-26. Thermal Response of Insulation to Nitrogen Filling Process

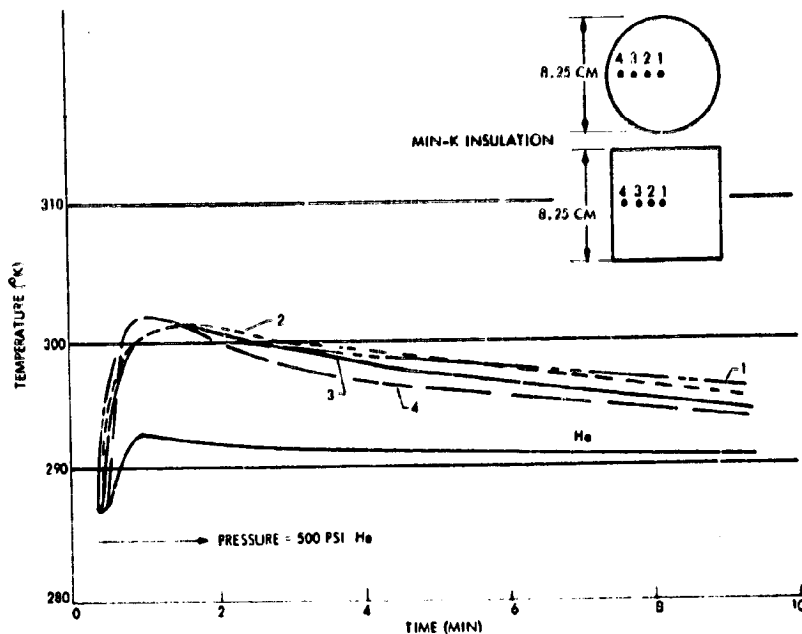


Figure 7.4-27. Thermal Response of Insulation to Helium Filling.

Factoring free convection effects in the analysis of the transient data provided an explanation for the FA fiberglass transient performance but failed to explain the MIN-K TE 1400 performance based on two descent tests. This result is shown in Figure 7.4-28. Here the solid curves are taken from a paper by B. K. C. Chan, *et al.*, "Natural Convection in Enclosed Porous Media with Rectangular Boundaries," *Journal of Heat Transfer*, February 1970, ASME.

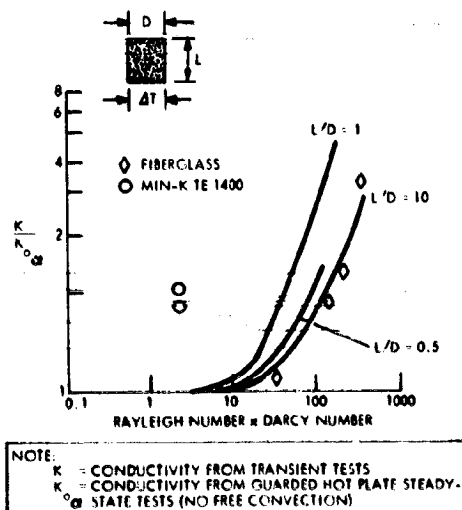


Figure 7.4-28. Correlation of Transient Test Data With Free Convection Effects

The MIN-K TE 1400 performance in the transient descent tests resulted in an effective conductivity of approximately twice the steady-state values. This difference is concluded to be due to the sum of three things; the insulation being oriented on the probe so that the heat transfer is parallel to the major plane of the as-received insulation slabs (Figure 7.4-19); the mass transfer contribution; and the adsorption of CO_2 in the insulation fibers. All the design calculations given in this report were based on conductivities derived from the transient testing.

7.4.6.3 Insulation Outgassing and Interaction with Venus Trace Compounds

Because outgassing of thermal insulation could influence mass spectrometer readings or produce products that could condense on the science windows, a test was conducted to investigate this potential problem area. The test setup consisted of a Venus descent simulation chamber with two mass spectrometers connected to the chamber. A descent simulation run was monitored by the mass spectrometers with the chamber empty in order to establish a "background" condition. Then insulation samples, run 1 MIN-K TE 1400 and run 2 moldable fiberglass TG 15000, were placed in the chamber along with a contamination source, NH_4HF_2 . This source was included since it reacts to form NH_3 and HF; the HF being the Venus atmospheric trace compound that would most likely interact with the insulation. The NH_3 also is considered as a potential Venus atmospheric trace compound. For the descent simulation runs, the concentration of HF was approximately 1000 times that anticipated in the Venus atmosphere (based on NASA SP-8011).

For the MIN-K test, absolutely no outgassing or interaction with the contaminants was observed; however, the TG 15000 evolved benzene in a concentration of a few parts per 1000 at Venus surface conditions. A thermogravimetric analysis on the TG 15000 moldable fiberglass also showed outgassing and a residual gas analysis of the materials released confirmed the benzene. For TG 15000 fiberglass to be considered as a viable insulation choice, a development program would be required to eliminate the outgassing problem.

7.4.6.4 Insulation Mechanical Performance

Both MIN-K TE 1400 and fiberglass TG 15000 have been fabricated and applied to near full-scale large probe pressure vessels. The MIN-K was only available in 7.6 cm (3 inches) thick slabs so a great deal of machining was required relative to the fiberglass that was procured in hemispherical sections. The MIN-K machining was performed by first rough cutting quarter-ring sections and then finish cutting on a lathe, using internal and external fixtures. The MIN-K rings were then bonded to a phenolic backface forming quarter hemispherical sections. These sections were then attached to the pressure vessel as shown in Figure 7.4-29. The fiberglass required minimum machining for fitting over the pressure shell and was attached to the shell by a thin metallic insulation cover.

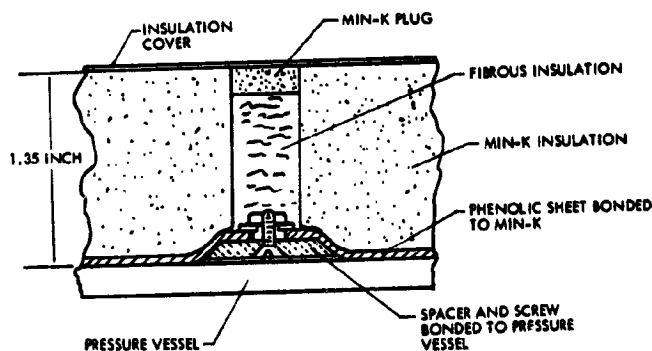


Figure 7.4-29. Attachment Scheme for MIN-K TE 1400

The anticipated configuration of the insulation system for both large and small probes is MIN-K TE 1400 insulation attached to the exterior surface of the pressure vessel by an adhesive with a thin metal cover over the exterior insulation surface. This configuration was simulated for vibration testing by the test article shown in Figure 7.4-30. Vibration tests were performed on this test article at levels of 9.1 g-rms for a duration of four minutes in each of three axes. The shape of the power spectrum was:

0.0029 to 0.045 g^2/Hz in the range 200-300 Hz

0.045 g^2/Hz in the range 300-2000 Hz

No mechanical damage of the insulation was detected after performing this test.

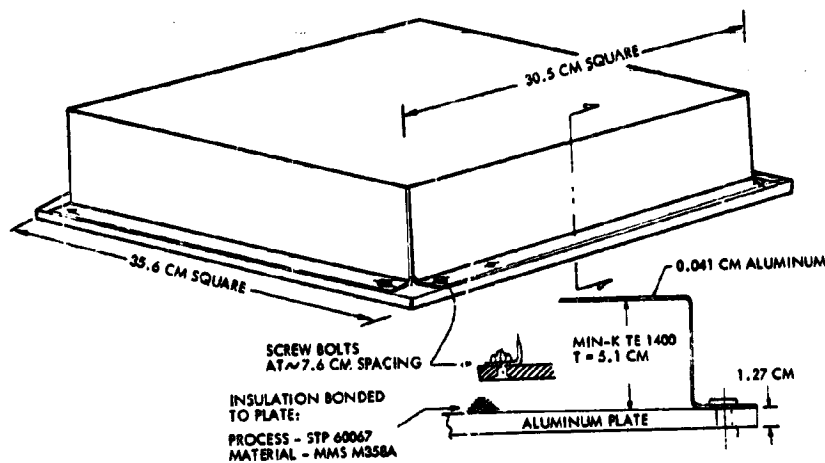


Figure 7.4-30. Vibration Test Specimen

7.4.6.5 Phase Change Device Development

Both the large and the small Atlas/Centaur probes include phase change material for control of payload temperatures during the descent phase. The Martin Marietta Denver Division has funded an IRAD phase change study program during 1971 and 1972. During 1972, phase change thermal control development was also performed under Contract NAS8-28360 for NASA-MSFC.

Under the IRAD tasks, several phase change cells were designed, fabricated, and tested with materials in the melting point range from 300 to 354°K. The cell designs include an aluminum rectangular cell 7.62 x 15.2 x 5.24 cm and a stainless steel cylindrical bellows cell 10.2 cm diameter x 7.1 cm long. Both cells were tested with and without metallic honeycomb fillers. Two types of fillers were used. One filler was constructed from aluminum honeycomb with hexagonal cells 4 mm on a side and with 0.076-mm wall thickness. A second filler was constructed from aluminum honeycomb cells with a 0.254-mm wall thickness.

The phase change materials tested in these cells included octadecane, docasane, lithium nitrate trihydrate, sodium hydrogen phosphate dodecahydrate, myristic acid, acetamide and Cerrobend. In the 1971 task, these materials were tested with the heater on the bottom of the cell. In 1972, a number of these materials were tested with the heater on the top of the cell to minimize the convection mechanism in the liquid phase and to simulate more closely conditions in a low-gravity environment.

These tasks also included the development of a computer program that analytically models the transient melting process. A model based on a conduction mechanism in the liquid phase provided a good correlation of the experimental data. This program provides a design procedure for new cell designs and facilitates integration of phase change devices in spacecraft thermal control systems.

Under the 1972 NASA contract, the phase change materials cited were subjected to thermal cycling tests, materials compatibility tests, and systems operation studies. Methods of preventing supercooling were studied. Also, candidate materials for low-temperature applications in the melting temperature range from 173 to 273°K were recommended for future investigation.

7.4.6.6 Power Requirements for Science Window Heaters

The minimum power required to maintain the temperature of a 2.54 cm (1-inch) diameter, cylindrical science window above the local atmospheric temperature during a large probe descent has been determined both analytically and experimentally to be 15 thermal watts. If less than 15 watts are applied to the window, the temperature will drop below the local atmospheric temperature before the probe reaches the planet surface.

Analytical Predictions. The thermal analytical model of the science window shown in Figure 7.4-31 contained three concentric ring window nodes, 14 cylindrical nodes along the barrel length, and a heater node. The transient temperatures of these nodes were calculated for defined atmospheric and pressure shell time-temperature profiles and a constant heater power of 15 watts. The transient temperature response of the center window node is shown in Figure 7.4-32 for the specified pressure shell and atmospheric temperature profiles.

Under these conditions, the temperature difference between the window and the local atmosphere increases to a maximum of 180°K at 0.25 hours while the probe is in the anticipated cloud layers. After a programmed parachute release at 0.25 hours, the temperature differences decreased rapidly to a steady value of about 10°K. A slight decrease in heater power would cause the window temperature to fall below the local atmospheric temperature before the probe reached the planet surface.

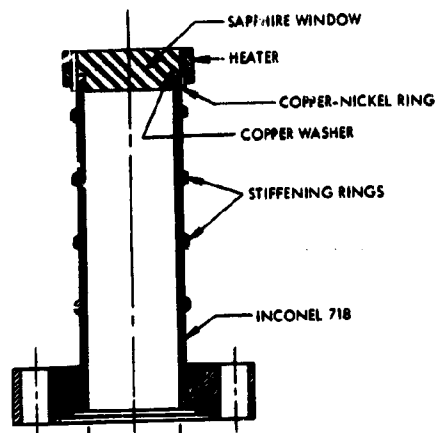


Figure 7.4-31. Science Window Configuration

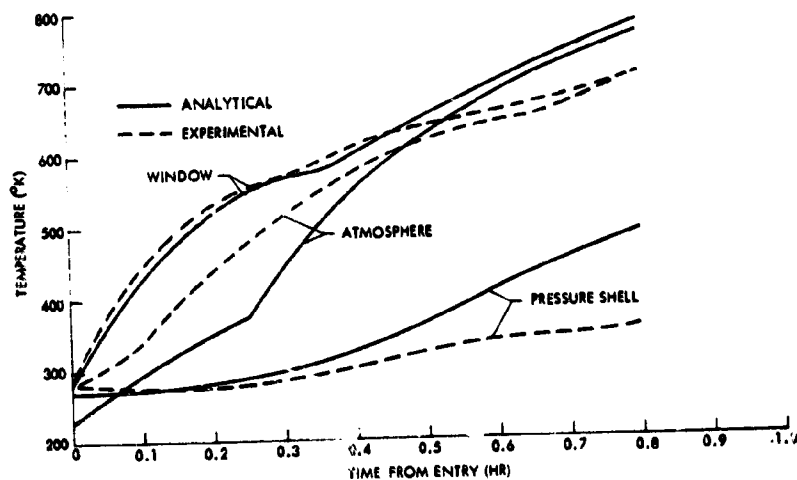


Figure 7.4-32. Time-Temperature Profiles for One-Inch Sapphire Window With 15 Watt Heater

Experimental Measurement. The cylindrical window shown in Figure 7.4-31 was mounted in a 8.6-cm (3.4-inch) diameter by 15.2 cm (6 inches) long cylindrical pressure chamber. The chamber atmospheric temperature was controlled by heaters on the chamber walls and the window mounting fixture temperature was controlled independently with gaseous nitrogen coolant. Carbon dioxide was admitted to the chamber according to a predetermined time-pressure profile and the atmospheric and mounting fixture temperatures were controlled according to the profiles shown in Figure 7.4-32. With 15 watts of thermal power applied around the circumference of the window, the temperature at the center of the window responded as shown in Figure 7.4-32.

For the first 0.5 hours, the measured window and pressure shell temperature closely followed the analytical predictions. After 0.5 hours, the measured temperatures fell below the analytical curves. After 0.8 hours, the measured window temperature fell slightly below the measured atmospheric temperature. The measured window temperature would have remained above the local atmospheric temperature if the pressure shell temperature had been allowed to increase at a faster rate.

Conclusion. A minimum of 15 watts of thermal power are required to maintain the temperature of the 2.54-cm (1-inch) cylindrical science window above the local atmospheric temperature throughout the entire descent phase.

7.5 Decelerator

7.5 DECELERATOR

7.5.1 Introduction and Summary

Decelerator subsystem design studies have been conducted on Thor/Delta and Atlas/Centaur launched probe systems for a number of variations in probe mechanical and aerodynamic configuration and for various descent rate requirements. The parameters considered in the studies included size and type of parachutes, methods of deployment, and methods of packaging the parachute in the probes.

The preferred configuration, based on the Atlas/Centaur launched probe, is composed of a 2.0-meter diameter mortar-deployed ribless guide surface pilot parachute which extracts a 6.6-meter diameter ribless guide surface main descent parachute. The sequence of operation is shown in Figure 7.5-1. Nylon is the principal textile material and all elements of the subsystem utilize nonmetallic materials to the maximum practicable extent to reduce interference with communications in view of the aft \mathcal{Q} location selected for the stowed main chute.

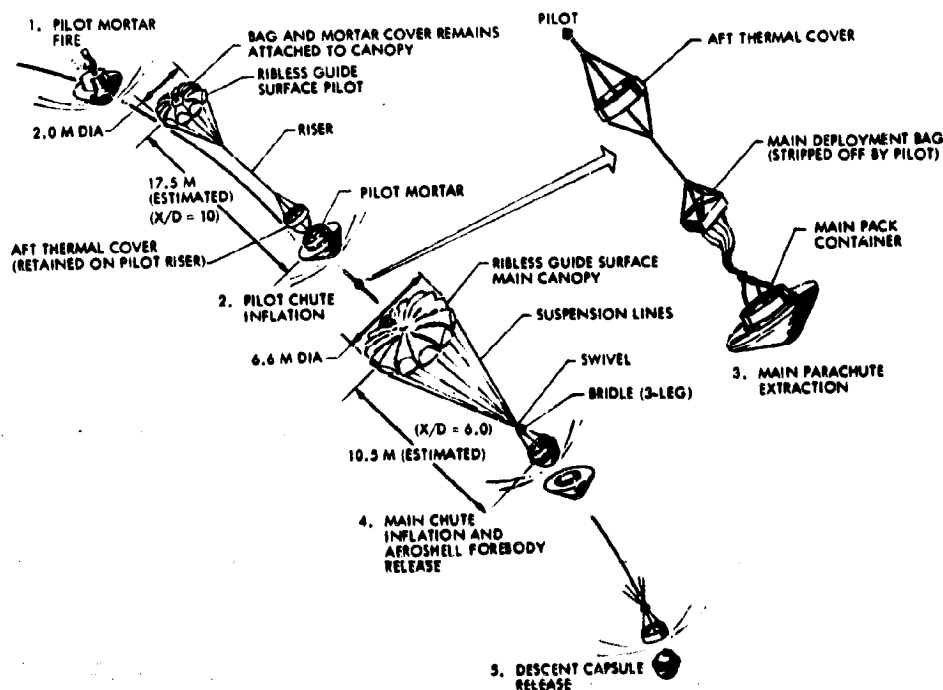


Figure 7.5-1. Sequence of Operations

The performance of the selected design is characterized by:

- Very low amplitude probe oscillations, $< 5^\circ$, induced by parachute deployment.
- High relative acceleration between descent capsule and aeroshell ensures a clean separation.
- Nominally zero parachute lift/glide behavior exists during descent.
- Oscillations induced by wind profile are rapidly damped.

The parachute stowed location and deployment method selected were chosen to provide a conventional arrangement, and thus to minimize development cost, as well as to preclude balance weight requirements and/or the excessive depth of aeroshell afterbody dictated by other methods of deploying the main chute. The canopy type provides the best nongliding performance of the known design parachutes. The following paragraphs discuss requirements, tradeoffs, system description for Atlas/Centaur and Thor/Delta, and special studies and analyses. The latter include parachute dynamics and a study of a drogue chute for the small probe.

7.5.2 Requirements

The requirements and criteria are summarized in Tables 7.5-1 for Atlas/Centaur and 7.5-2 for Thor/Delta. Of primary importance to Pioneer Venus mission science objectives and communications requirements is the overall stability, which in this case include not only the parachute's oscillating characteristics but also lift/glide characteristics in no-wind conditions. A zero-lift/glide configuration is a primary goal to minimize effects on science data; a configuration that meets this goal will also enhance communications.

Parachute system materials must be capable of operation in the presence of dilute concentrations of the various compounds of atmosphere constituents encountered in the descent. Functional requirements applicable to the decelerator system are:

- 1) Positive deployment on command from vehicle systems, e. g., timer based on g-level sensing during entry
- 2) Provision of sufficient drag force to a) separate the descent capsule from the aeroshell forebody; b) decelerate and stabilize the descent capsule in the range from high to low subsonic velocities; c) separate the aeroshell afterbody from the descent capsule at the conclusion of the parachute descent phase.
- 3) Drag characteristics that are predictable and repeatable within less than ± 7 percent.

Table 7.5-1. Atlas/Centaur Requirements

ITEM	VALUE
<u>MAIN PARACHUTE DEPLOYMENT (T = 215)</u>	
ALTITUDE	70.4 KM
MACH NO.	1.0
DYNAMIC PRESSURE	1800 N/M ² *
FLIGHT PATH ANGLE	-0.96 RAD
AMBIENT TEMPERATURE	224° K
<u>DESCENT</u>	
PARACHUTE BALLISTIC COEFFICIENT	7.85 KG/M ²
MAXIMUM OSCILLATION (NO-GUST)	.262 RAD
MAXIMUM LIFT/GLIDE CHARACTERISTIC	0 (GOAL)
MAXIMUM SPIN RATE	2.09 RAD/S
MAXIMUM SWIVEL TORQUE	0.27 N-M
<u>TERMINATION (T = 2358 S)</u>	
ALTITUDE	42.9 KM
VELOCITY	6.3 M/S
DYNAMIC PRESSURE	77 N/M ²
FLIGHT PATH ANGLE	-1.57 RAD
AMBIENT TEMPERATURE	407° K *
ABOVE DATA IS BASED ON: ENTRY FLIGHT PATH ANGLE = -0.558 RAD * ENTRY BALLISTIC COEFFICIENT = 90.7 KG/M ² * VEHICLE WEIGHT AT DEPLOYMENT = 328.9 KG * DESCENT WEIGHT = 215.4 KG * TIME = 0 IS BASED ON SENSING OF 50 G DURING ENTRY	

* WORST CASE

Table 7.5-2. Thor/Delta Requirements

ITEM	VALUE
<u>MAIN PARACHUTE DEPLOYMENT (T = 245)</u>	
ALTITUDE	70.5 KM
MACH NO.	0.80 *
DYNAMIC PRESSURE	1705 N/M ² *
FLIGHT PATH ANGLE	-0.96 RAD
AMBIENT TEMPERATURE	224° K
<u>DESCENT</u>	
PARACHUTE BALLISTIC COEFFICIENT	18.9 KG/M ²
MAXIMUM OSCILLATION (NO-GUST)	0.262 RAD
MAXIMUM FOREBODY SPIN RATE	2.09 RAD/S
MAXIMUM SWIVEL TORQUE	0.27 N-M
<u>TERMINATION (T = 8905)</u>	
ALTITUDE	49.75 KM
VELOCITY	13 M/S
DYNAMIC PRESSURE	163 N/M ²
FLIGHT PATH ANGLE	-1.57 RAD
AMBIENT TEMPERATURE	354° K *
ABOVE DATA IS BASED ON: ENTRY ANGLE = -0.602 RAD * ENTRY BALLISTIC COEFFICIENT = 86.4 KG/M ² * VEHICLE WEIGHT AT DEPLOYMENT = 143 KG DESCENT WEIGHT = 109 KG TIME = 0 IS BASED ON SENSING OF 0.5 G DURING ENTRY	

* WORST CASE

7.5.3 Tradeoffs

The principal tradeoff studies conducted in the design study consisted of:

- 1) Single versus multistage systems,
- 2) Packaging and deployment concepts,
- 3) Canopy configuration,
- 4) Materials,
- 5) Use of existing parachutes versus new designs.

7.5.3.1 Single versus Multistage Systems

The use of a supersonic/transonic drogue stage before deployment of the main chute was considered early in the study, and was examined relative to stabilizing the probe and also achieving suitably low Mach numbers for main chute deployment at a higher altitude than would be possible with a single stage system, i.e., 72 km instead of 70 km. This study revealed that a fairly large drogue chute would be required (~4-meters in diameter) to achieve the higher altitude, and the supersonic deployment required would result in a more costly development program. It was subsequently determined that altitudes of 70 km or less were acceptable from the science deployment standpoint, and also that the basic entry vehicle stability would suffice in the supersonic/transonic flight regime. Consequently, further tradeoff studies were limited to single-stage systems.

7.5.3.2 Parachute Location, Packaging, and Deployment Method Tradeoff Studies

The location of the chute package in the probe, the configuration of the package/container, and the method of deploying the chute are key elements of the system design. These items also are greatly dependent upon each other. The mass of the chute required to achieve the preferred descent profile, about 10 kg, suggests choosing a location near the axial centerline to avoid having to ballast to achieve an axisymmetric center of gravity, axisymmetric principal axes, and equal pitch and yaw moments of inertia. The ballasting weight requirements are given in Figure 7.5-2 as a function of the distance the parachute is located off-axis. From these curves, it can be determined that for situations where this mass asymmetry can be compensated for by weights located at a distance equal to only one to two times the distance that the parachute mass is offset from the axis (generally the case); the penalty is having to carry dead weight* equal to or greater than the parachute weight.

*"Dead weight" is indicated since only a very small amount of the compensation can be derived by relocating items of equipment already onboard. The descent capsule has to be independently spin-balanced eliminating use of its equipment.

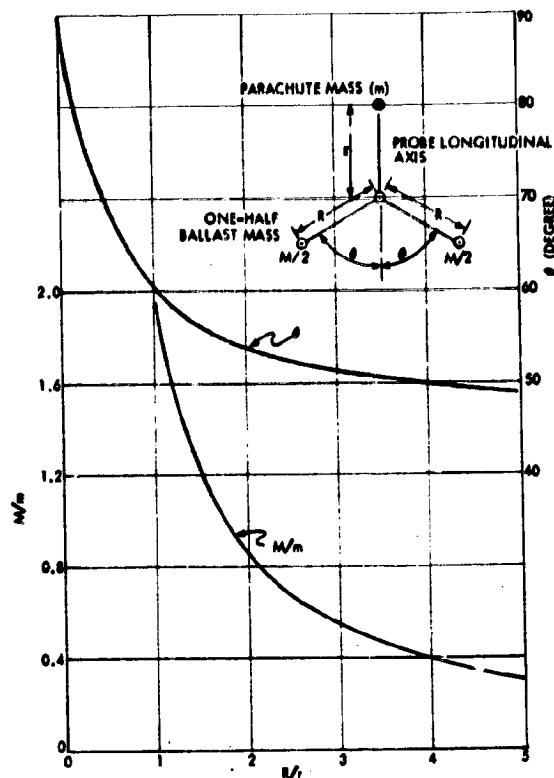


Figure 7.5-2. Ballast Requirements Plotted as Function of Parachute Mass Offset Distance (r)

Achieving this desired axisymmetric location, however, without resorting to annular or toroidal packaging conflicts with the antenna location requirements discussed in Section 7.3. Consequently, several off-axis parachute designs have been evaluated in spite of the ballasting problem to determine if they are feasible from the chute deployment standpoint. The space available in these off-axis locations, e. g., forebody aeroshell, permits a mortar-deployed main chute even for the large chute of the preferred design. Calculations were performed to determine the probe response to both a mortar located parallel to the centerline, designated Offset Deployment, and a mortar firing laterally at an angle but still having its reaction along a line through the c. g. designated Lateral Deployment. The vehicle response data are summarized in Figure 7.5-3. From this figure it can be seen that parachutes larger than about 4 meters have oscillations which exceed 10 to 15 degrees which will cause one bridle leg to go slack. When this occurs the damping of the capsule motion drops and hinders the aeroshell separation. The separation event must then be delayed until sufficient damping has occurred, resulting in the loss of considerable altitude.

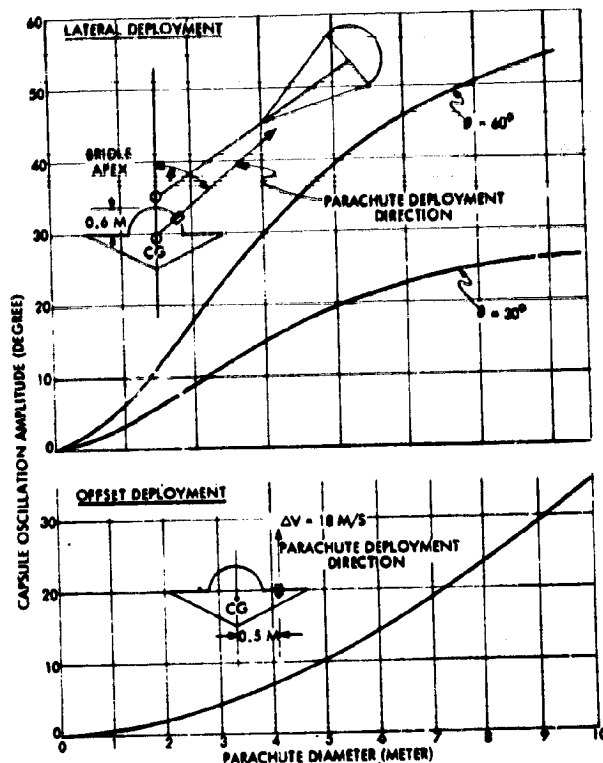


Figure 7.5-3. Capsule Oscillation Amplitude Due to Offset and Lateral Parachute Deployment

It is also of interest in Figure 7.5-3 that lateral deployment causes more severe probe motions than offset deployment, in spite of the absence of any initial pitching moment from the mortar reaction in the former. This is caused by the long moment arm and the finite duration of the drag forces on the chute just after its inflation. The moment arm results from the fact that drag forces on the parachute before its inflation are not sufficient to swing the parachute behind the probe due to the high drag of the probe. This is illustrated in Figure 7.5-4 where the effect of mortaring a 4-meter diameter parachute 60 degrees laterally from the probe axis shown.

It was concluded from the above calculations that for the required chute size, substantially off-axis locations are bad from the ballasting standpoint and from the induced probe oscillation standpoint. Although the latter factor can be overcome by use of a pilot chute (mortared parallel to the probe axis to avoid lateral main chute extraction loads), the ballasting required, ~ 1.0 to ~ 2.0 times the 10 kg chute mass, still makes this approach highly undesirable.

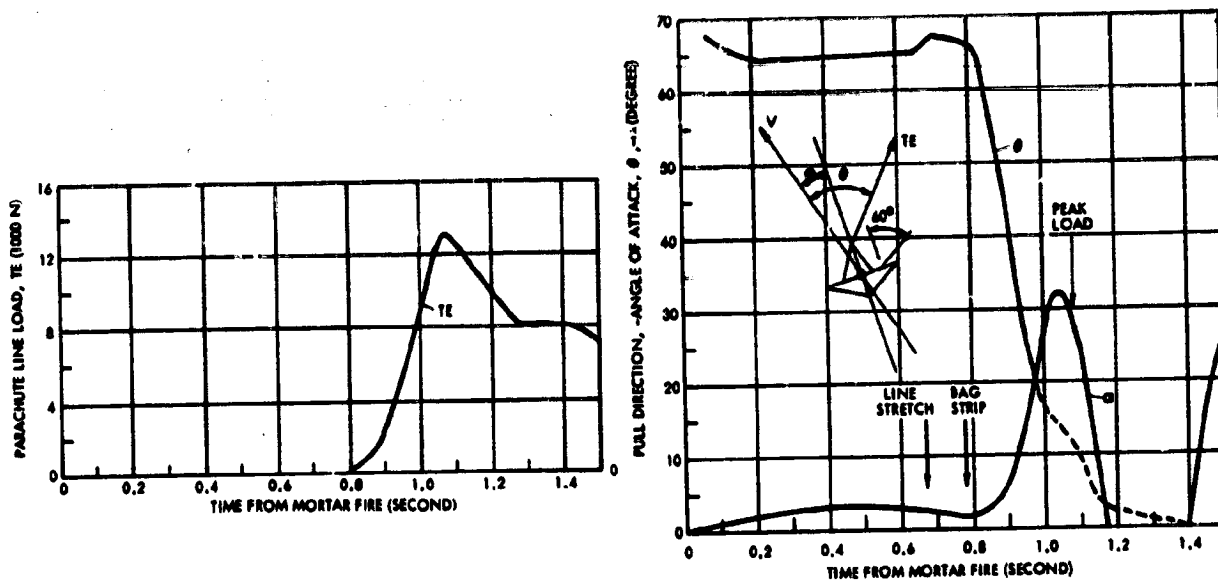


Figure 7.5-4. Parachute Lateral Displacement During Inflation
($\theta = 60^\circ$)

Based on these findings, the choice of chute location and deployment method for the preferred Atlas/Centaur mission profile was narrowed to three configurations, all of which meet the objective of a near-axisymmetric parachute location. These are shown in Figure 7.5-5. The advantages and disadvantages of each of these concepts relative to aeroshell shape and mechanical separation are also factors in their selection and are discussed in Section 7.3. From the parachute deployment and operation standpoint, either configuration A or B are preferred over C because of the more straightforward (thus, less costly) packaging and pull-out situations they afford. Between A and B there are no major differences estimated to exist in the basic parachute system development costs or reliability. However, one parachute cost-related factor does enter into the selection in concept B: the pilot chute and main chute can be developed somewhat independently and substantial changes can occur in main chute size requirements without affecting the pilot chute design. In concept A, mortar development work (thus, costs related to it) would be adversely impacted if the main chute were to grow very much in size. (Such a situation did, in fact, develop in the course of the Viking program decelerator development.)

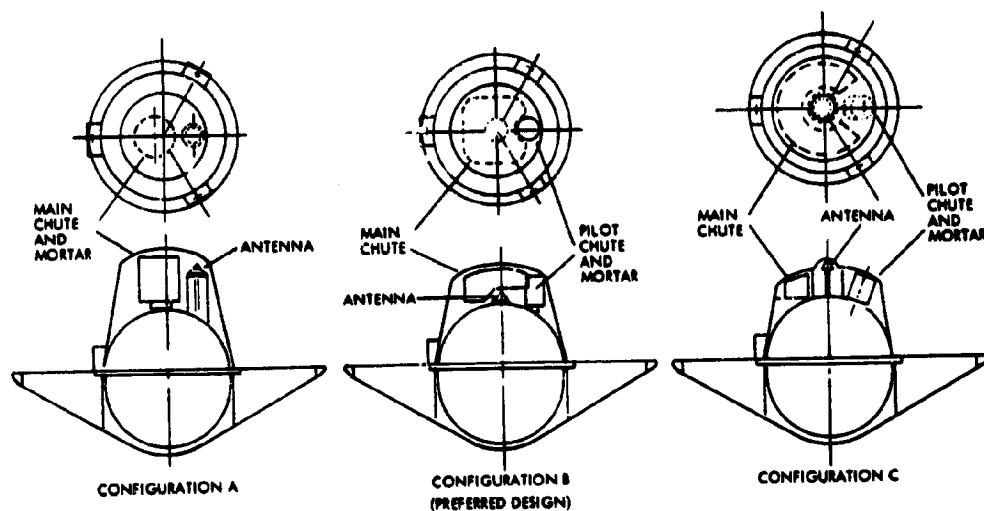


Figure 7.5-5. Candidate Atlas/Centaur Parachute Configurations

This factor and the shallower afterbody and antenna design advantages relative to afterbody separation discussed in 7.3 have led to the selection of configuration B of Figure 7.5-5 over configuration A. Relative to configuration C, which affords a slightly better antenna situation at the expense of simplicity of parachute deployment, configuration B was again selected, pending confirmation of antenna performance, due to the lower parachute development costs it affords. A mortar was selected as the means of deploying the pilot chute, based on an assessment of factors summarized in Table 7.5-3.

The performance of the selected design is discussed in Section 7.5.6 in which plots of probe motions resulting from parachute deployment are presented. These motions, much milder than for the off-axis versions considered, permit aeroshell separation within 5 seconds of parachute deployment.

Thor/Delta Chute Deployment

For the Thor/Delta large probe descent profile selected, a smaller main chute was required and this allowed selection of a parachute arrangement similar to that shown in Atlas/Centaur configuration A (Figure 7.5-5). The smaller chute package removed the main disadvantages of configuration A, that of requiring too great an afterbody depth and too asymmetric an antenna installation. Section 7.5.6 presents the separation performance data for this Thor/Delta design.

Table 7.5-3. Deployment Method Tradeoff Summary

MORTAR	<ul style="list-style-type: none"> • PYROTECHNICALLY ENERGIZED DEVICE, VERY WIDELY USED IN PARACHUTE SYSTEMS, WELL ADVANCED DEVELOPMENT • FUNCTIONS AS CHUTE CONTAINER AS WELL AS EJECTOR, AIDS IN MINIMIZING SYSTEM VOLUME AND WEIGHT • REACTION LOADS AND VELOCITIES READILY CONTROLLED BY DILATING ORIFICE • VERY RELIABLE
DROGUE SLUG GUN	<ul style="list-style-type: none"> • PYROTECHNICALLY EXPELLED MASS USED TO EXTRACT PARACHUTE DEVICES, CHUTE WEIGHT USUALLY LIMITED TO 1.5 LB • REQUIRES LONG LINE TO ATTACH TO CHUTE FOR EXTRACTION • SEPARATE CONTAINER REQUIRED FOR CHUTE • GENERATES HIGH SHOCK EFFECTS, OTHERWISE CAN BE READILY CONTROLLED • VERY RELIABLE
GAS EJECTOR	<ul style="list-style-type: none"> • USES INFLATING BAG TO EXPEL CHUTE PACK FROM CONTAINER • REQUIRES SEPARATE COLD OR HOT GAS SUPPLY • DEVICE RARELY USED, WOULD REQUIRE DEVELOPMENT FOR PIONEER VENUS • RELIABILITY SOMEWHAT QUESTIONABLE
CATAPULT	<ul style="list-style-type: none"> • TECHNIQUE GENERALLY SIMILAR TO MORTAR, BUT GAS GENERATION AND PROPULSION IS DONE IN CHAMBER IN TANDEM TO PARACHUTE CAVITY • LOW REACTION LOAD CHARACTERISTIC • REQUIRES ALMOST TWICE AS MUCH SPACE AS MORTAR • HEAVIER THAN OTHER DEVICES CONSIDERED • USED ON F-111 "ZERO/ZERO" ESCAPE SYSTEM
ROCKET EXTRACTION	<ul style="list-style-type: none"> • SMALL, SOLID FUEL ROCKET FIRES AND, WITH A LONG RISER LINE, EXTRACTS CHUTE FROM CONTAINER FOR DEPLOYMENT • TECHNIQUE IS USED ON STANLEY AVIATION'S "YANKEE" PERSONNEL ESCAPE SYSTEM • WOULD PROBABLY REQUIRE EXTENSIVE DEVELOPMENT FOR PIONEER VENUS • REACTION AND OTHER FORCES LEAST OF DEVICES CONSIDERED • ROCKET COULD BE USED TO ASSURE EJECTION OF COVERS FROM AFT AEROSHELL AS WELL AS EXTRACTING THE CHUTE
SELECTION:	MORTAR.

7.5.3.3 Canopy Configuration

Another factor that is of utmost importance is the type of canopy. The drag produced and size and weight of the device required are fundamental considerations. High drag/weight efficiency, normally a goal in parachute selection, becomes less critical when weight and volume are not tightly constrained and when emphasis is placed, as it is in PV requirements, on achieving zero-glide characteristics. The better zero-glide chutes, such as the ribless guide surface type, exhibit a 5 percent to ten percent weight penalty over types such as the disc-gap band. This magnitude of a weight penalty, however, is not a deterrent in the case of the Atlas/Centaur probe.

Achieving zero-lift/glide during descent can be related directly to certain parachute characteristics. The tendency of a parachute to glide is a function of two parameters, pitching moment and lift. The pitching moment causes the parachute to cock to one side and develop an angle of attack where a lift force is generated. With any particular parachute, these parameters are also influenced by the forebody wake. Normally, the lack of rigidity in the parachute allows the direction of the lift vector

to rotate in a random manner about the velocity vector, and thus average out to an essentially ballistic trajectory; however, selection of a canopy design with a stable trim at zero angle of attack eliminates the need to depend on such a random motion. The moment and lift of parachutes follow systematic behavior that agrees with the flight oscillation performance. A correlation of lift curve slope and moment curve slope (nondimensionalized by the drag) is shown in Figure 7.5-6. With typical flight oscillation data superimposed, these data indicate that the more stable canopy designs tend to have less oscillation and less lift during descent. The guide surface canopies are clearly superior to other canopy types, with ribbon design a possible alternative. Other canopy selection factors are summarized in Table 7.5-4. Final selection of the RGS-type was based primarily on performance since cost factors are not significantly different for the established design parachutes. (Use of existing hardware versus development of a new parachute is discussed in Section 7.5.3.5.)

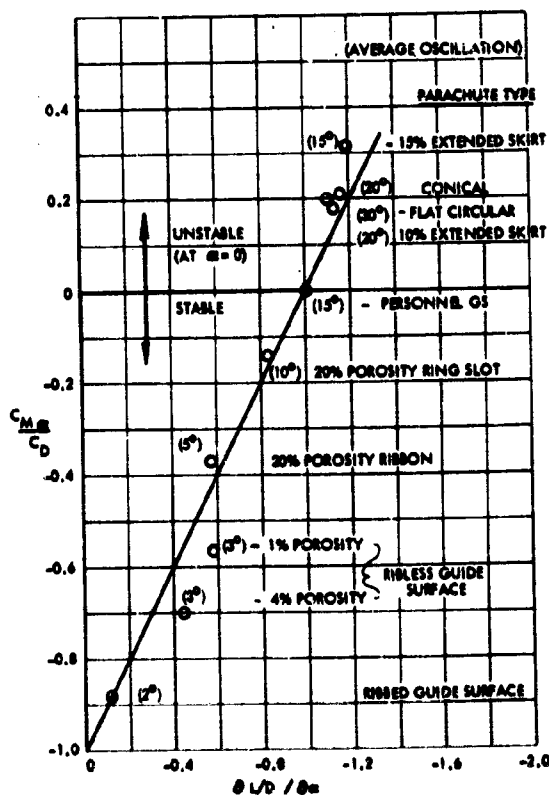


Figure 7.5-6. Comparison of Stability, Lift, and Oscillation of Parachute Canopy Types

Table 7.5-4. Parachute Canopy Type Tradeoff Summary

RIBBLESS GUIDE SURFACE (RGS)	<ul style="list-style-type: none"> • EXHIBITS BEST STATIC STABILITY CHARACTERISTICS OF TYPES CONSIDERED IN TERMS OF OSCILLATION AND NEAR-ZERO GLIDE CHARACTERISTICS • OPERATES EFFECTIVELY IN TRANSONIC-TO-LOW-SUBSONIC RANGE • DRAG/WEIGHT EFFICIENCY NOT QUITE AS HIGH AS SOME OTHER CONFIGURATIONS (E.G., RINGSLOT, CROSS) THAT COULD BE CONSIDERED • OPENING LOAD CHARACTERISTIC IS LOW TO MEDIUM • MANUFACTURE MORE COMPLEX THAN CROSS, RINGSLOT OR DGB, BUT COMPARES FAVORABLY WITH RINGSAIL OR RIBBON • TEST AND USE HISTORY MOSTLY INVOLVED WITH WEAPONS STABILIZATION, FREQUENTLY USED AS PILOT CHUTE BY USAF
RINGSLOT	<ul style="list-style-type: none"> • DRAG/WEIGHT EFFICIENCY SOMEWHAT BETTER THAN RGS FOR SAME APPLICATION • GOOD STABILITY IN TERMS OF LOW OSCILLATIONS BUT SHOWS MORE TENDENCY TO GLIDE THAN RGS OR RIBBON • OPERATION GENERALLY LIMITED TO LOW SUBSONIC SPEEDS • OPENING LOAD CHARACTERISTIC IS LOW • MANUFACTURE RELATIVELY SIMPLE AS COMPARED TO RGS OR RIBBON • PRIMARILY USED FOR CARGO DELIVERY AND AIRCRAFT DECELERATION
RIBBON (FLAT OR CONICAL)	<ul style="list-style-type: none"> • DRAG/WEIGHT EFFICIENCY COMPARABLE TO RGS • EXHIBITS GOOD STATIC STABILITY CHARACTERISTICS, BUT RGS HOLDS ADVANTAGE • OPERATES EFFECTIVELY AT HIGH SUBSONIC SPEEDS • OPENING LOAD CHARACTERISTIC IS LOW • MANUFACTURING COMPLEXITY MOSTLY INVOLVED WITH ACCURATE PLACEMENT OF RIBBONS • MOSTLY USED FOR CARGO DELIVERY OR AIRCRAFT DECELERATION, REQUIRES SPECIAL "SHAPING" FOR TRANSONIC OPERATION
CROSS	<ul style="list-style-type: none"> • DRAG/WEIGHT EFFICIENCY SOMEWHAT BETTER THAN RGS FOR SAME APPLICATION • VERY LOW OSCILLATION ANGLE, BUT TENDENCY TO GLIDE IS NOT WELL KNOWN EXCEPT FOR "CROSS-CONE" TYPE (EXPERIMENTAL) • INFLATION STABILITY AT HIGH SUBSONIC SPEEDS NOT AS GOOD AS OTHER TYPES (E.G., RGS OR RIBBON) • OPENING LOAD CHARACTERISTIC IS LOW TO MEDIUM • VERY SIMPLE MANUFACTURE AS COMPARED TO OTHER TYPES • PRIMARILY USED FOR FLARE DELIVERY
RINGSAIL	<ul style="list-style-type: none"> • HIGH DRAG/WEIGHT EFFICIENCY AS COMPARED TO MOST ALL TYPES • HAS STRONG TENDENCY TO GLIDE • HAS OPERATED AT TRANSONIC SPEEDS • OPENING LOAD CHARACTERISTIC IS LOW TO MEDIUM • MANUFACTURE IS COMPLEX COMPARED TO MOST OTHER TYPES • MOSTLY USED IN MANNED RECOVERY (APOLLO, F-111)
FLAT CIRCULAR	<ul style="list-style-type: none"> • HIGH DRAG/WEIGHT EFFICIENCY AS COMPARED TO MOST OTHER TYPES • POOR STABILITY IN TERMS OF OSCILLATION AND WILL GLIDE AT HIGH ANGLES OF ATTACK (E.G., 52 RAD) • USE LIMITED TO LOW SUBSONIC SPEEDS • OPENING LOAD CHARACTERISTIC IS HIGH • MANUFACTURE IS VERY SIMPLE AS COMPARED TO RGS, RINGSLOT, OR RIBBON • MAJOR USAGE IS PERSONNEL DESCENT AND CARGO DELIVERY
DISK-GAP-BAND (DGB)	<ul style="list-style-type: none"> • GOOD DRAG/WEIGHT EFFICIENCY AS COMPARED TO RGS • LOW OSCILLATION ANGLE, BUT VIKING DATA SHOWS STRONG TENDENCY TO GLIDE • HAS OPERATED IN MACH 2.7 RANGE AT VERY LOW Q • OPENING LOAD CHARACTERISTIC IS MEDIUM • MANUFACTURE IS SIMPLER THAN RGS OR RIBBON • PRIMARY USAGE IS FOR METEOROLOGICAL SOUNDING EFFORTS, USED ON VIKING DUE TO ABILITY TO OPERATE EFFECTIVELY AT MACH 2.0
OTHER	<ul style="list-style-type: none"> • CHUTES FROM VIKING, APOLLO, BIOSATELLITE, ETC. GENERALLY MUCH TOO LARGE AND HEAVY FOR PIONEER VENUS APPLICATION • VIKING: 14.2 M DGB, 41 KG • APOLLO: 25.8 M RINGSAIL, 59 KG • BIOSATELLITE: 9.7 M RINGSLOT, 15 KG • ALL HAVE TENDENCY TO GLIDE

For Thor/Delta, the disc-gap band canopy type was selected to achieve minimum weight and cost design. As indicated in the previous discussion, this selection would result in a science performance penalty relative to inferring wind velocities during descent and further consideration of the better performing ribless guide surface design should be undertaken in any future study involving Thor/Delta.

7.5.3.4 Materials

Materials considerations were mostly involved with the "normal" textile synthetics, Nylon, Dacron and Nomex. A new duPont product, Special Fiber B, was also considered as a candidate for part of the application. Nylon is the preferred choice, primarily due to its wide availability in products made under MIL specifications for parachutes and its ability to meet temperature environments. Various aspects of the materials considered are summarized in Table 7.5-5.

Table 7.5-5. Parachute Materials Tradeoff Summary

NYLON	<ul style="list-style-type: none"> • HIGHEST STRENGTH/DENSITY RATIO OF THOSE CONSIDERED • ADEQUATE RESISTANCE TO HEAT EFFECTS FOR PIONEER VENUS • READILY AVAILABLE IN PRODUCTS MADE UNDER MIL SPECIFICATIONS • MOST WIDELY USED SYNTHETIC IN PARACHUTES, WELL UNDERSTOOD • TEMPERATURE AT INFLATION SHOULD BE LIMITED TO 339° K • MELTS AT 523° K
DACRON	<ul style="list-style-type: none"> • MEDIUM STRENGTH/DENSITY RATIO, HIGHER WEIGHT THAN FOR SAME SIZE CHUTE MADE IN NYLON • GOOD RESISTANCE TO HEAT EFFECTS, PROVEN ON VIKING (411° K) • FOR PIONEER VENUS, WOULD PROBABLY HAVE TO HAVE PRODUCTS WOVEN OR BRAIDED TO SPECIAL ORDER • NOT QUITE AS ELASTIC AS NYLON • APPLICATION IN PARACHUTES GENERALLY WELL UNDERSTOOD • MELTS AT 523° K
NOMEX	<ul style="list-style-type: none"> • LOWER STRENGTH/DENSITY RATIO THAN NYLON OR DACRON • EXCELLENT RESISTANCE TO HEAT EFFECTS (RETAINS 60% TO 70% OF ORIGINAL STRENGTH AT 478° K) • FOR PIONEER VENUS, WOULD PROBABLY HAVE TO BE PRODUCED TO SPECIAL ORDER • ELASTICITY NOT NEARLY AS GOOD AS NYLON • ZERO-STRENGTH TEMPERATURE IS 700° K
OTHER	<ul style="list-style-type: none"> • DUPONT'S NEW SPECIAL FIBER B IS PROBABLY BEST CHOICE FOR BRIDLE LEGS: ZERO-STRENGTH OCCURS AT 728° K • FIBERGLASS, AND METAL CLOTHS NOT ADVANCED IN DEVELOPMENT FOR PARACHUTES, HIGH COSTS INVOLVED • NATURAL FIBRES NOT SUITED FOR PIONEER VENUS APPLICATIONS AS OPPOSED TO OTHERS CONSIDERED
SELECTION:	<p>NYLON FOR ALL BUT BRIDLE LEGS NOMEX OR FIBER B FOR BRIDLE LEGS</p>

7.5.3.5 Use of Existing Parachutes versus New Designs

Suppliers were consulted in the cost reduction aspects of using an available Federal Stock (FS) canopy. The answer has been that about 10 percent savings in developmental costs can be realized which is consistent with our estimate. Also, a change in the suspension line geometry may be advisable or required in the interests of overall performance. This would reduce the estimated cost savings. Finally, manufacturers note that canopies produced to FS specifications are not as closely controlled in terms of dimensions as those made in small quantities specifically for applications such as Pioneer Venus. This would affect achieving a known ballistic coefficient design.

Although, as previously indicated, the actual savings of using an existing parachute canopy are somewhat uncertain, a survey of existing hardware and design chutes was conducted. Some of those located are listed in Table 7.5-4. An existing aircraft decelerator chute was found that was the right size for the midterm version of the Atlas/Centaur probe (FS Ringslot Canopy). For the selected Atlas/Centaur probe descent profile no existing chutes were found that fit the drag requirements. In any case, the requirements for achieving extremely low glide characteristics and drag repeatability appear to be met fully only with a system designed specifically for Pioneer Venus.

7.5.4 Preferred Subsystem, Atlas/Centaur

As a result of the above tradeoff studies a configuration has been selected that uses a mortar-deployed pilot parachute to remove the after-body base cap and extract a main descent parachute. The general features of this design are:

- 1) Ribless guide surface type canopies are used for both the pilot and main parachutes. (See Figure 7.5-1)
- 2) The sabot and cover of the pilot mortar are retained to preclude damage. (See Figures 7.5-7 and 7.5-8)
- 3) The pilot chute will remove and carry away the base cap and extract the main parachute for deployment.
- 4) Packaging of main parachute will be in a separate nonmetallic container. (See Figure 7.5-7)

- 5) Nylon is the principal textile material.
- 6) A swivel is used in the main parachute suspension system but not in the pilot riser.
- 7) A lanyard on the pilot riser will release the latch mechanism holding the base cap in place.

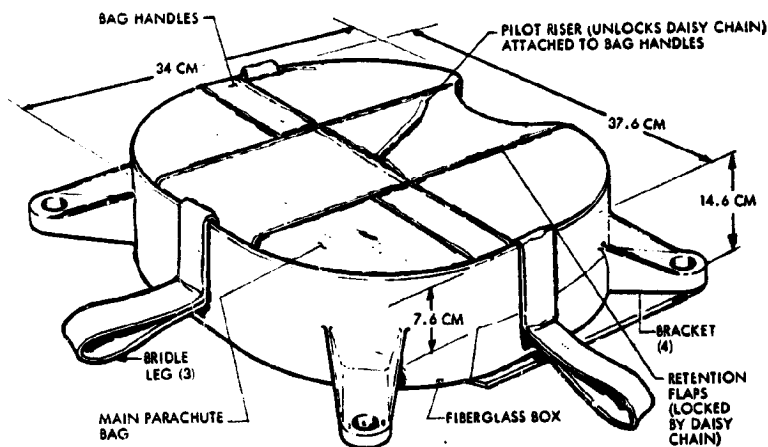


Figure 7.5-7. Main Parachute Container

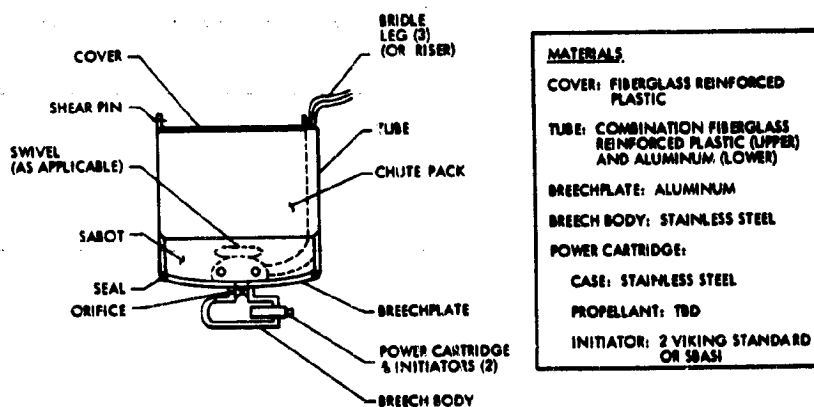


Figure 7.5-8. Mortar Configuration and Characteristics

The pilot chute sizing is based on attaining a ballistic coefficient of 0.6 times the ballistic coefficient of the main chute/descent capsule combination. This provides assurance that the pilot chute/aft thermal cover combination will not overtake the descending main parachute and capsule. The RGS parachute selected for the pilot has a long history with USAF for

similar applications. The estimated trailing distance requirements shown in Figure 7.5-1 are subject to wind tunnel test verification.

Nonmetallic construction, fiberglass-reinforced epoxy resin, will be used for the main chute container and mortar tube and cover. During the period when transmission through both parachute and container is required, a 2 dB attenuation is acceptable.

7.5.5 Preferred Subsystem, Thor/Delta

Figure 7.5-9 shows the selected Thor/Delta parachute design and sequence of events during operation.

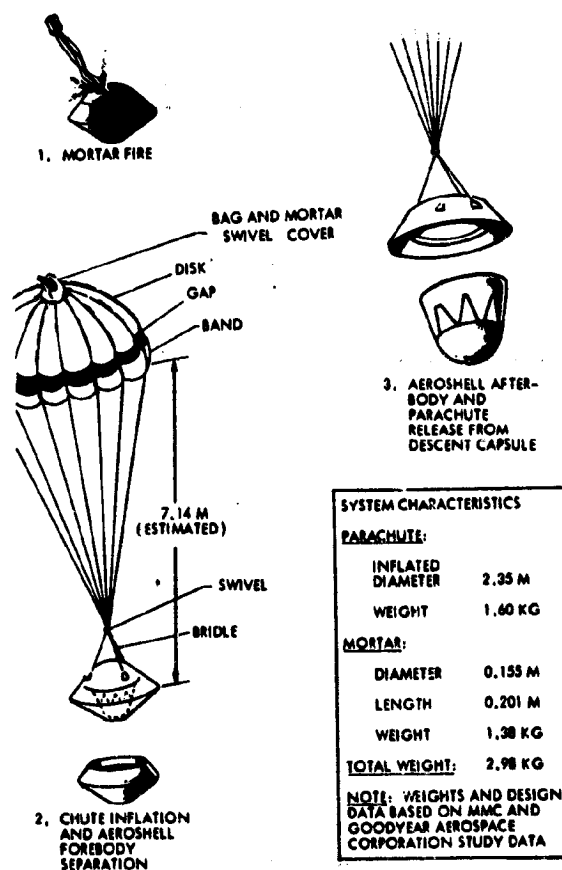


Figure 7.5-9. Thor/Delta Parachute System

The disk-gap band (DGB) type canopy was selected for application, largely because of its known performance behind blunt forebodies in the low subsonic through Mach 2.2 velocity range. Data from Viking wind tunnel and flight tests were the principal substantiating sources. The DGB has a high drag/weight efficiency.

7.5.6 Analyses and Special Studies

Specific analyses and studies performed during the course of the studies included:

- 1) Parachute dynamics during deployment and aeroshell separation,
- 2) Design of a stabilizing drogue device for the small probe,
- 3) Parachute size, weight, volume, and mortar performance calculations.

7.5.6.1 Parachute Deployment Dynamics

During parachute deployment, various bodies are separated and loosely coupled by forces that depend on aerodynamic characteristics of the bodies, their relative position, and the resilient connecting lines. The vehicle disturbance during this highly transient interval requires proper simulation of the various components and, in general, specialized tailoring of the simulation tool. The dominant behavior, however, can be normally scoped using more general models. The Viking decelerator deployment simulation model was therefore adapted to the Pioneer Venus deployment characteristics to study the capsule and parachute behavior during parachute deployment. In addition, closed form solutions for the dominant motions were employed to provide insight into the relative importance of the various parameters. Since the Viking dynamic model employs a mortared decelerator deployment, it was readily adapted to the proposed Thor/Delta system. Representative deployment dynamic parameters for the preferred Thor/Delta system are presented in Figure 7.5-10, and the system parameters used in the simulation are given in Table 7.5-6. It can be seen that the system quickly damps to low amplitudes.

The Atlas/Centaur decelerator uses a pilot parachute to extract the main parachute, the sequence of events being as shown in Figure 7.5-11. For this sequence, the dynamic simulation was begun when the pilot chute was fully inflated, and the main parachute was released from the probe. Representative dynamics of the capsule, aeroshell, and parachute are shown in Figures 7.5-12 and 7.5-13, and the system parameters are given in Table 7.5-7.

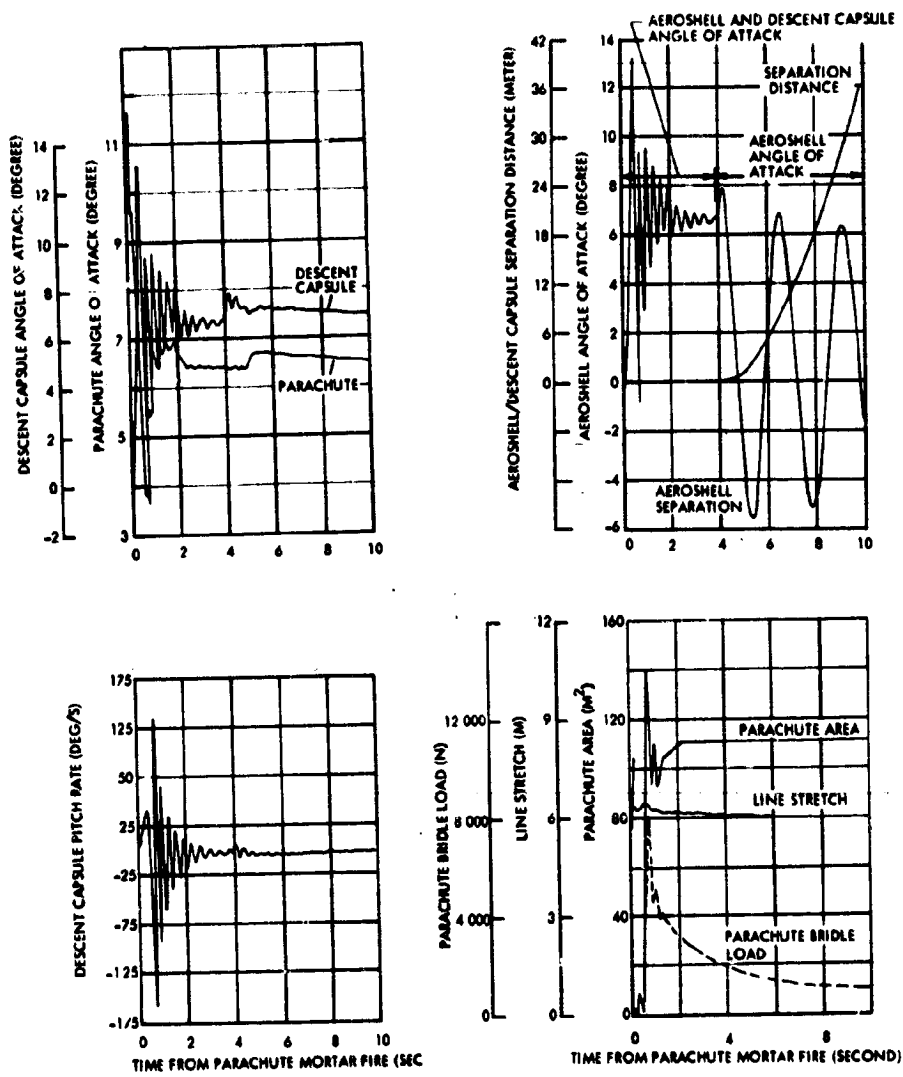


Figure 7.5-10. Thor/Delta Large Probe Dynamics at Parachute Deployment

Table 7.5-6. Thor/Delta Parachute
Deployment Simulation

<u>DGB PARACHUTE PROPERTIES</u>	
DIAMETER	3.62 M
TRAILING DISTANCE	8.1 M
EJECTED PARACHUTE MASS	2.1 KG
MORTAR VELOCITY	36.7 M/S
SUSPENSION LINE RESILIENCE	9650. N/M
SUSPENSION LINE DAMPING	87.5 N/M/S
<u>AEROSHELL/CAPSULE PROPERTIES</u>	
DIAMETER	1.33 M
MASS	194 KG
MOMENT OF INERTIA	12.8 KG-M ²
BRIDLE HEIGHT	1.15 M
<u>TRAJECTORY INITIAL CONDITION</u>	
ALTITUDE	70 KM
VELOCITY	161.5 MPS
FLIGHT PATH ANGLE	-47°
<u>DISTURBANCES</u>	
MORTAR OFFSET	0.004 M
INITIAL ANGLE OF ATTACK	-1.2°
WIND GUST	0.05 M/S/M

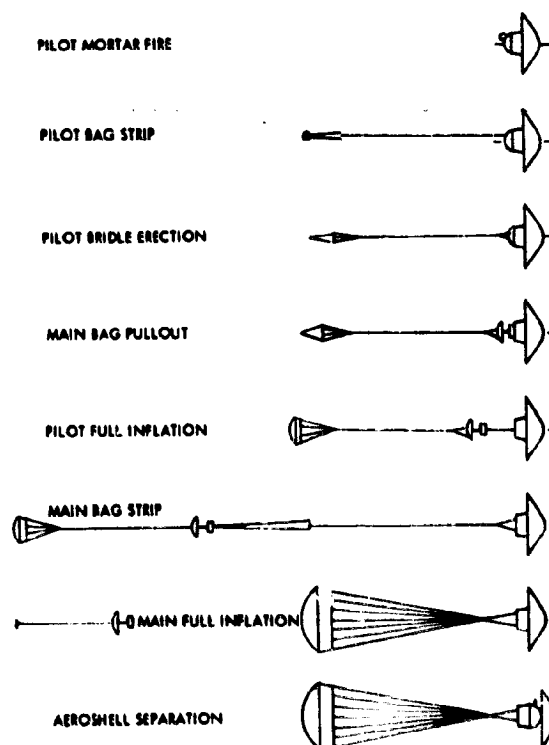


Figure 7.5-11. Selected Atlas/Centaur Pilot Deployed Deceleration
Sequence of Events

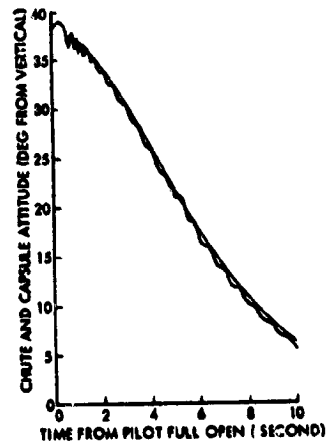
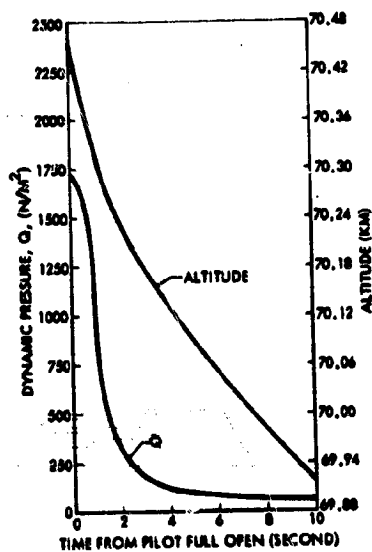
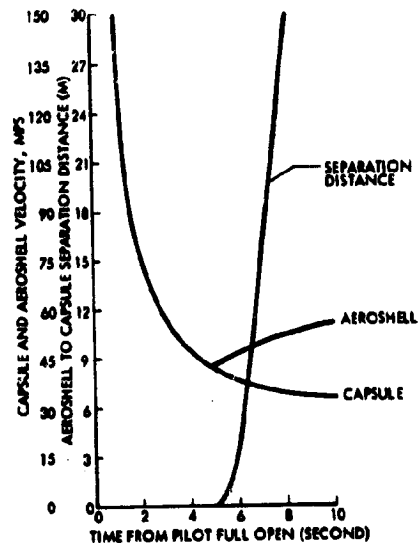
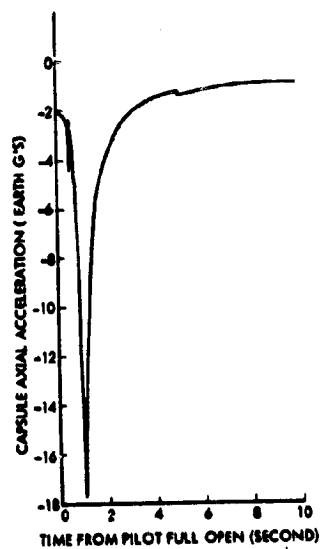


Figure 7.5-12. Atlas/Centaur Large Probe Dynamics at Parachute Deployment

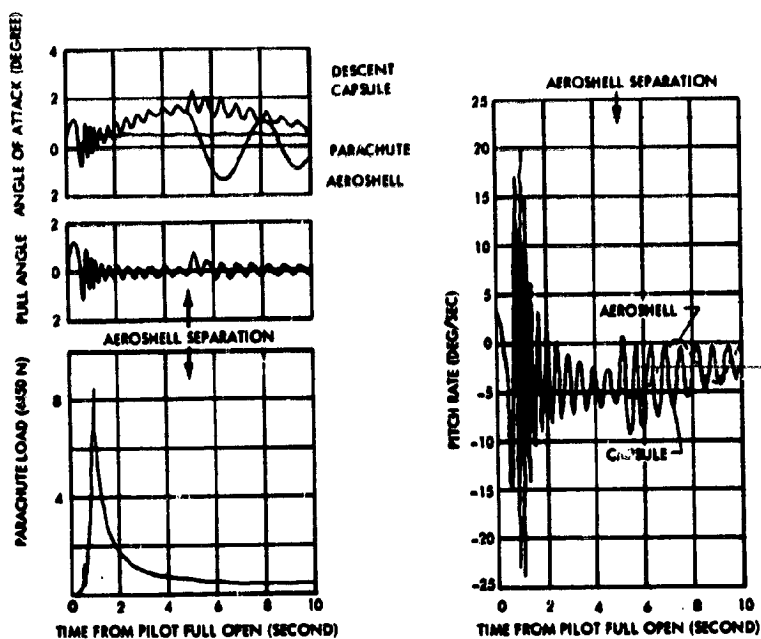


Figure 7.5-13. Atlas/Centaur Capsule and Aeroshell Motions After Parachute Deployment

Table 7.5-7. Atlas/Centaur Parachute Deployment Simulation

<u>RGS PILOT PARACHUTE PARAMETERS</u>	
DIAMETER	2M
TRAILING DISTANCE (DEPLOYED)	18 M
EJECTED PARACHUTE MASS	1 KG
MORTAR VELOCITY	18 MPS
TIME TO FULL INFLATION	1 SEC
<u>RGS MAIN PARACHUTE PARAMETERS</u>	
DIAMETER	6.6 M
TRAILING DISTANCE	14 M
PARACHUTE MASS	7.2 KG
SUSPENSION LINE RESILIENCE	43 800 N/M
SUSPENSION LINE DAMPING	44 N/M/S
<u>AEROSHELL/CAPSULE PROPERTIES</u>	
DIAMETER	1.76 M
MASS	242 KG
MOMENT OF INERTIA	30.4 KG-M ²
BRIDLE HEIGHT	1.13 M
AEROSHELL SEPARATION TIME	6 SEC
<u>TRAJECTORY INITIAL CONDITIONS</u>	
ALTITUDE	70.9 KM
VELOCITY	187 M/S
FLIGHT PATH ANGLE	-28.3°
<u>DISTURBANCES</u>	
INITIAL PITCH RATE	3.5 °/S

In contrast to the characteristic trimming of the DGB parachute at an angle of attack of about 6 degrees, which can be seen (Figure 7.5-10) to induce a like angle in the capsule and to cause a relative pitch rate at aeroshell separation, the relative motion in RGS (Atlas/Centaur) system at aeroshell separation is much less pronounced (Figure 7.5-13). The damping of the deployment disturbances appear to be comparable in both sequences; thus, a 5-second delay from parachute deployment to aeroshell separation is satisfactory for both designs. Note the higher separation acceleration of the Atlas/Centaur system which should result in a lesser clearance problem at separation.

Closed Form Dynamic Solutions

The dynamic behavior of a parachute/capsule system, elastically coupled, can be analyzed in terms of a number of dominant oscillation modes. A fundamental mode assumes a rigid system where the mass properties are evaluated about the center of gravity of the system and the aerodynamic forces of the total system are lumped together.

Due to the dominating influence of the parachute trailing distance, this mode is highly damped and can be characterized by the following dynamic equation.

$$M_p L^2 \ddot{\theta} + DL^2 \dot{\theta} + DL\theta = 0$$

where:

M_p = parachute mass

L = parachute trailing distance

D = parachute drag force

θ = parachute trailing angle.

The natural frequency and damping ratio are then given by

$$\omega^2 = \frac{D}{M_p L}$$

$$\delta = 2 D/M_p V$$

This mode of oscillation is excited when the parachute is deployed laterally from the vehicle and can be seen to describe the parachute motion shown in Figure 7.5-4.

The dominant capsule motion is due to the resilient suspension lines that couple the parachute and capsule. The restoring moment and damping which the lines give to capsule motions increase the normal aerodynamic frequency and damping by the following increments.

$$\Delta W_c^2 = L_B \cdot \frac{F}{I_c} \cdot \left(1 + \frac{L_B}{L_s}\right)$$

$$\Delta \delta = \frac{RK}{2 I_c} \left[\frac{L_B D_p}{L_s} \right]^2$$

where:

W_c = capsule natural frequency, rad/sec

δ = oscillation damping, per second

L_B = effective bridle moment center from c. g.

F = parachute riser force

I_c = capsule moment of inertia

L_s = suspension lines length

RK = suspension line damping

D_p = parachute suspension line diameter.

The bridle height, which so dominates both frequency and damping ratio, is limited primarily by potential slack line conditions that could be incurred during initial deployment of the parachute, especially off axis such as would occur with a lateral fired mortar system. The pilot-deployed main parachute is extremely effective in minimizing the lateral displacement of the parachute at peak load, thus minimizing the disturbing moments and simultaneously permitting the maximum damping potential of a high bridle height to be used without a slack line.

7.5.6.2 Small Probe Stabilizing Drogue Study

A brief study was performed to size a low-drag, stabilizing parachute to operate on the small probe all the way to impact. The principal problem in this design is that standard textiles cannot survive the very high temperature encountered at the lower altitudes on Venus; also, the available volume in the probe is somewhat constrained. Metal fabrics are one answer to the

problems of high temperature and packageability; however duPont has recently developed a textile called Fiber B whose zero-strength temperature is approximately 728°K , which makes it a possible candidate. Taking advantage of this material, a spring-deployed vane type canopy, very similar to those used as pilot chutes in personnel systems, was selected. The general configuration is shown in Figure 7.5-14. Using heavy cloth (680 gm/m^2) and cord to work the high temperature problem, the device shown, including a container, would weigh approximately 0.45 kg. A spring-loaded door on the aft aeroshell, released by a pin-puller or equivalent device, would be required also, but the weight of this part was not included in the estimate.

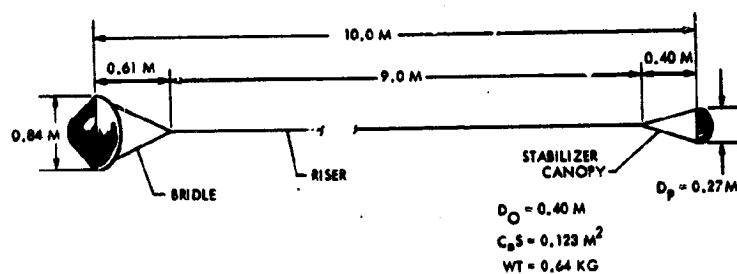


Figure 7.5-14. Small Probe Stabilizer

The objective in sizing the device was to reduce the ballistic coefficient as little as possible while still providing an effective stabilizer. The probe-alone ballistic coefficient is 198 kg/m^2 in the subsonic range and it was decided that any reduction should be limited to 15 percent, resulting in a combined value of 173 kg/m^2 . Figure 7.5-14 shows a 0.27m D_O chute located approximately 12 diameters behind the forebody. This represents what is believed to be an effective system.

Figure 7.5-15 shows the canopy in some detail to indicate how the spring is installed in a cloth cone in the canopy. When the chute is folded for packing, the spiral-wound spring stows flat and, when the aft aeroshell door is released, provides energy to deploy the canopy in the airstream.

The selected approach, using heavyweight Fiber B cloth and cords, should assure survival to altitudes approaching the Venus surface. Although some degradation of the drag surface is anticipated, there will not be a sudden or rapid destruction of the device, mainly due to the fact that the drag load will not exceed 245 N or 267 N.

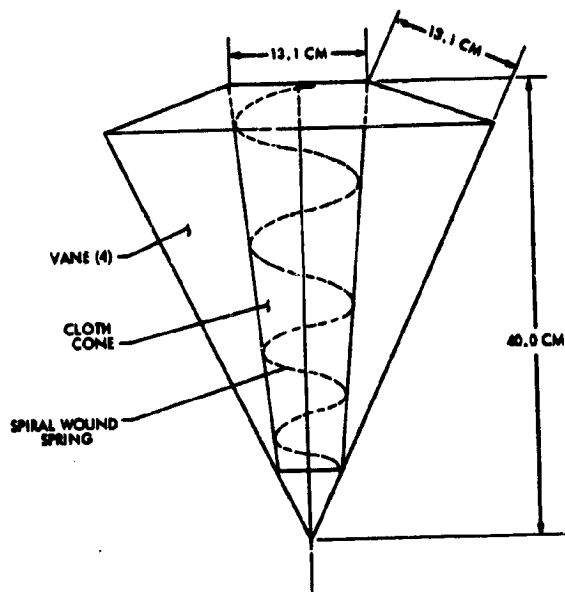


Figure 7.5-13. Stabilizer Canopy

In the Atlas/Centaur system a somewhat larger chute ($D_o = 0.40$ m) would be required and would weigh about 0.64 kg. This is based on an Atlas/Centaur small probe weight of 75 to 80 kg having the same ballistic coefficient as the Thor/Delta small probe.

As an alternative to the spring-deployed chute, a drogue-slug gun was considered, but an additional 0.57 to 0.68 kg would be added to the system. The space available for such an installation is extremely limited within the confines of the aft aeroshell and an unwanted "blister" might be required.

It has been suggested by Ames Research Center that trailing a portion of the aft aeroshell may be a more viable approach, particularly in terms of weight and volume required. Very limited testing with such a device has been accomplished by Martin Marietta with a subscale model in the Langley spin tunnel with inconclusive results; i. e., a strong stabilizing influence was afforded relative to damping large pitching motions, but with the one bridle/riser/drogue cap arrangement tried, some small amplitude motions were found to be induced by the presence of the drogue cap.

If a final assessment of science requirements and/or final determination of the detailed probe stability performance indicate that an auxiliary

stabilizing device is required on the small probes, development of a drogue anchor of the ARC-type appears to be a good choice with the Fiber B textile canopy design as an alternative.

7.5.6.3 Parachute Sizing Analyses

The criteria and calculations applicable to the pilot chute, main chute and pilot mortar size, weight and volume requirements determination are provided for the preferred Atlas/Centaur design in Appendix 7.5A-1. Viking program data was used in these calculations along with information provided by Goodyear Aerospace and the Pioneer Parachute Company, Inc. The requirements of Table 7.5-1 were applied in the cases shown.

7.6 Probe Communication

The probe communication is a critical component of the system, ensuring that the probe can effectively communicate with the host system. This section details the various communication protocols and methods used to facilitate this process.

The probe communication is implemented using a combination of hardware and software components. The hardware components include the probe itself, which is designed to interface with the host system's communication bus. The software components include the communication drivers and protocols that manage the data flow between the probe and the host.

The communication process involves several steps, including initialization, data transfer, and error handling. The probe must first establish a connection with the host system before any data can be exchanged. Once the connection is established, the probe can send and receive data from the host.

Error handling is a crucial part of the communication process, as it ensures that any data corruption or transmission errors are detected and handled appropriately. The probe and host system both implement error-checking mechanisms to ensure the integrity of the communication.

The probe communication is a complex process that involves many factors, including the quality of the hardware, the efficiency of the software, and the stability of the communication bus. By understanding the various components and steps involved in the process, users can optimize the performance of the probe communication system.

In conclusion, the probe communication is a vital part of the system, and its proper implementation is essential for the overall functionality of the probe. This section provides a comprehensive overview of the communication process, from initialization to error handling, and offers insights into how to optimize the system for better performance.

The probe communication is a complex process that involves many factors, including the quality of the hardware, the efficiency of the software, and the stability of the communication bus. By understanding the various components and steps involved in the process, users can optimize the performance of the probe communication system.

In conclusion, the probe communication is a vital part of the system, and its proper implementation is essential for the overall functionality of the probe. This section provides a comprehensive overview of the communication process, from initialization to error handling, and offers insights into how to optimize the system for better performance.

The probe communication is a complex process that involves many factors, including the quality of the hardware, the efficiency of the software, and the stability of the communication bus. By understanding the various components and steps involved in the process, users can optimize the performance of the probe communication system.

In conclusion, the probe communication is a vital part of the system, and its proper implementation is essential for the overall functionality of the probe. This section provides a comprehensive overview of the communication process, from initialization to error handling, and offers insights into how to optimize the system for better performance.

The probe communication is a complex process that involves many factors, including the quality of the hardware, the efficiency of the software, and the stability of the communication bus. By understanding the various components and steps involved in the process, users can optimize the performance of the probe communication system.

In conclusion, the probe communication is a vital part of the system, and its proper implementation is essential for the overall functionality of the probe. This section provides a comprehensive overview of the communication process, from initialization to error handling, and offers insights into how to optimize the system for better performance.

The probe communication is a complex process that involves many factors, including the quality of the hardware, the efficiency of the software, and the stability of the communication bus. By understanding the various components and steps involved in the process, users can optimize the performance of the probe communication system.

In conclusion, the probe communication is a vital part of the system, and its proper implementation is essential for the overall functionality of the probe. This section provides a comprehensive overview of the communication process, from initialization to error handling, and offers insights into how to optimize the system for better performance.

The probe communication is a complex process that involves many factors, including the quality of the hardware, the efficiency of the software, and the stability of the communication bus. By understanding the various components and steps involved in the process, users can optimize the performance of the probe communication system.

In conclusion, the probe communication is a vital part of the system, and its proper implementation is essential for the overall functionality of the probe. This section provides a comprehensive overview of the communication process, from initialization to error handling, and offers insights into how to optimize the system for better performance.

7.6 PROBE COMMUNICATION

7.6.1 Introduction and Summary

This study recommends and defines preferred communications subsystems for a Venus probe mission using Atlas/Centaur and Thor/Delta launch vehicles. Analyses, tradeoffs, and design tasks were performed first to define preferred subsystem configurations for both Atlas/Centaur and Thor/Delta missions, then to select the preferred mission. This phase was followed by additional tradeoffs and analyses to define the preferred configurations for the Version IV science payload redefinition for the Atlas/Centaur mission, the selected mission.

This section presents the highlights of the preferred probe communications subsystems for the recommended Atlas/Centaur mission, then the analyses and tradeoffs followed by detailed descriptions of the preferred configurations of the Atlas/Centaur and Thor/Delta missions. Finally tests of the probe antenna mounted on a probe mockup are described. Details of analyses, tradeoffs, and tests are presented in a series of appendices.

Impact of Version IV Science Payload Redefinition. The impact on the communications subsystems of the Version IV science redefinition was felt largely in Atlas/Centaur small probe configurations in that the data rate for the small probes was increased to 64 bps from the former 16 bps rate to accommodate the highest post-entry science sampling rate. This higher rate reduced the small probe link margin considerably, but was accommodated readily by the 20 watt transmitter.

Significant analytical accomplishments or new results from this study can be found in the development of a lognormal channel model, and assessment of planet atmospheric effects on both coded and noncoded channels, including MFSK channels.

Highlights of the preferred large and small probe configurations for the selected Atlas/Centaur mission are given in Table 7.6-1. Note that the communications links are compatible with the projected DSN capabilities for real-time communications links. A predetection recording capability is recommended at the DSN for backup of the real-time links, especially during high Doppler rate regimes at the initial post-entry acquisition period. Every effort has been made to use DSN compatible links and existing hardware or hardware requiring minimum modifications.

Table 7.6-1. Highlights of the Preferred Probe Communications Subsystem for the Atlas/Centaur Mission

	LARGE PROBE	SMALL PROBES
ANTENNA TYPE	TURNTILE/CONE	SAME
ANTENNA PATTERN & ON AXIS GAIN	CONICAL BEAM, 5.4 DBI	SAME
TRANSMITTER OUTPUT POWER	36 W (2-20 W UNITS PAKAL-LELED)	20 W
CHANNEL MODEL	LOGNORMAL	SAME
MODULATION	PCM/PSK/PM	SAME
DOPPLER TRACKING	2-WAY, TRANSPONDER	1-WAY, STABLE OSCILLATOR
BIT RATE	128 BPS	64 BPS
CODING TYPE & RATE	CONVOLUTIONAL, RATE 1/2	SAME
DECODING	SEQUENTIAL-SOFT DE- CISION	SAME
TRANSMISSION PERIODS - PREENTRY	10 MINUTES DURATION	6-2.7 OR 6-3.0 HOUR
POSTBLACKOUT	BEGINNING AT E-0.75 HR	
TOTAL NUMBER OF BITS TRANSMITTED	73.6 MINUTES, NOMINAL 642 048 BITS	63.4 MINUTES NOMINAL 281 856 BITS
SUBSYSTEM MASS	5.12 KG (11.3 LB)	2.39 KG (5.3 LB)
SUBSYSTEM POWER	175.5 W	87 W

A block diagram of the large probe is shown in Figure 7.6-1 to illustrate the hardware selections to date. Detailed descriptions of the subsystem are found following the requirements and tradeoff sections.

7.6.2 Requirements of Probe Communications Subsystems

The major requirements of the probe communications subsystem have changed as the study progressed to accommodate changing science payloads and changing requirements of the mission and other probe subsystems. The present requirements for the Atlas/Centaur mission with the Version IV updated science payload are given first, followed by requirements for the Thor/Delta mission, which has subsequently been dropped as the final option.

7.6.2.1 Requirements, Atlas/Centaur (with Version IV Updated Payload)

- Direct links to earth--range of 0.43 AU
- Compatible with DSN: frequencies, transmit/receive turnaround ratio, modulation, decoding
- Survive through space, entry and descent to Venus surface--not required to survive impact
- Return data at an error rate no greater than:

Bit error rate 10^{-3}
Word deletion rate 10^{-2}

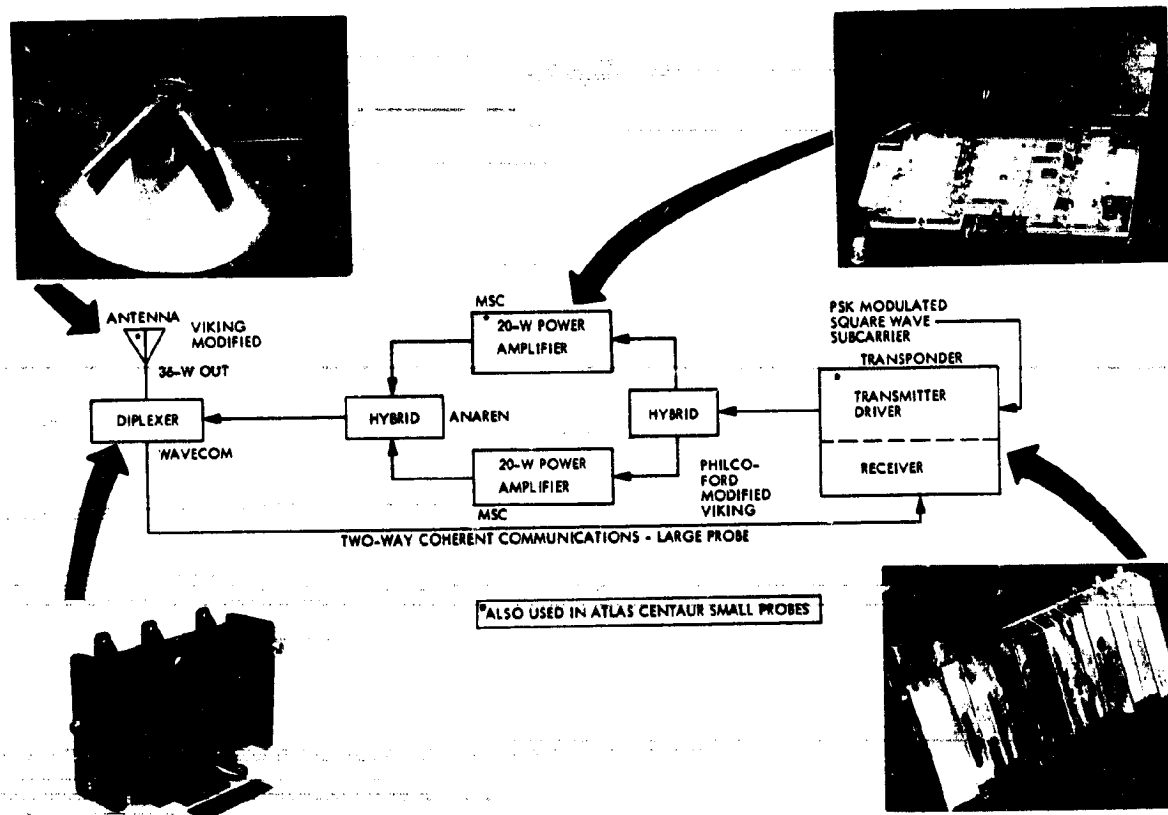


Figure 7.6-1. Atlas/Centaur Two-Way Coherent Communications, Large Probe

- Return data at a rate no less than:

Large probe	128 bps
Small probe	64 bps

- Data transmission periods:

- 1) 10 minutes duration within 1 hour prior to entry
- 2) From entry to end of mission on planet's surface

- Maintain Atlas/Centaur weight constraints

- Accomplish above at minimum program cost

7.6.2.2 Requirements, Thor/Delta (Version III Payload)

Same as for Atlas/Centaur except as follows:

- Direct links to earth--range of 0.48 AU

- Return data at a rate no less than:

Large probe--	102.4 bps above approximately 30 km altitude
	85.3 bps below approximately 30 km altitude
Small probe--	10 bps

- Maintain Thor/Delta weight constraints.

7.6.3 Communications Analyses and Tradeoffs

A series of communications analyses and tradeoffs were performed to arrive at recommended configurations and the Atlas/Centaur and Thor/Delta missions. Some of the key analyses were modeling of the channel and developing parameteric data representative of modulation and coding performance for unique Venus-to-earth fading channels. This entailed analyses of tracking loop performance, one-way and two-way tracking performance, evaluating MFSK, PSK/PM and PSK/SC, developing methods of estimating the combined effects of coding and noisy carrier losses under fading conditions, investigating methods of computing atmospheric absorption and defocusing losses, and investigating planet multipath parameters.

Other tasks included the tradeoff and selection of modulation, coding, decoding, and hardware specification and selection, the preparation of detail telecommunications design control tables showing tolerances for each item, and the design mockup and testing of a probe antenna.

The results of these analyses and tradeoffs follow in succeeding paragraphs. The antenna tests are reported in Section 7.6.6.

7.6.3.1 Channel Model

From the outset of this study, characterization of the channel turbulence, Doppler profile, planetary multipath, refractive defocusing, and atmospheric attenuation phenomenon was an important and tedious technical problem. Careful analysis and various study efforts were devoted to the problem of structuring a channel model that could be justified on the basis of compatible theoretical as well as experimental evidence (Figure 7.6-2).

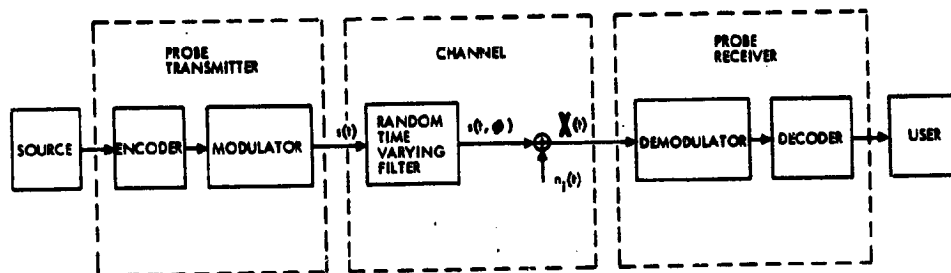


Figure 7.6-2. Simplest Telecommunication System Model

Channel turbulence is characterized by quantitatively establishing the amount of random fluctuation that the electromagnetic wave acquires in passing through a medium. This is accomplished by establishing the statistical parameters characterizing the probability distribution for the amplitude and phase of the wave. The lognormal probability distribution for the amplitude and normal distribution for the phase is recommended. Previous work to compute PSK performance used the Rician amplitude distribution. The Rician distribution also had previously been supported by deWolf in Venus propagation studies. However, the lognormal distribution gives a more accurate representation with regard to the physics underlying the scattering phenomenon in the case of weak fluctuations. The performance of the PSK system with lognormal fading was derived and is given in Appendix 7.6C, Figure 7.6C-1, using values for the variance computed by Woo at the surface of Venus. These values are based on Soviet Venera 7 data. The effect of the phase fluctuations, as expected for Venus probe channels on the coherent receiver, appears to be negligible. This area requires more investigation however, as does the tracking problem. Appendices 7.6A, 7.6B, and 7.6C present a detailed overview of the theory and experimental

data pertinent to modeling the channel turbulence, as well as explaining why the complex lognormal turbulence model is recommended.

Studies of the Doppler profile due to probe motion indicated early in the study that tracking using a second-order loop was not feasible during portions of the pre-entry, as well as post-entry period. This implies that data must be stored for a period of time after blackout before transmission begins or else one must rely on recovery of data from a DSN predetection magnetic tape.

In Appendix 7.6F a model is recommended for assessing the atmospheric attenuation and defocusing losses on up-link and down-link radio signals passing through the Venus atmosphere. Techniques for assessing the deleterious effects on link performance due to planetary multipath (backscatter) are given in Appendices 7.6A and 7.6G. Appendix 7.6A presents the necessary theory while Appendix 7.6G gives the geometry involved in applying the theory to assess the actual link degradations. The impact of channel effects on performance is given in the design control tables of Appendix 7.6H. Significant factors taken from these appendices are highlighted below:

Turbulence Fading (Appendices 7.6A, B and C)

Complex Lognormal Turbulence Model (Recommended)

- Amplitude characteristic (lognormal)
- Phase characteristic (Gaussian)
- Supporting theory - Tartarskii, Strohbehn, Woo, Ishimaru
- Weak amplitude fluctuations
- Single parameter amplitude distribution
- Parameterized by experimental data -- Veneras 4, 5, 6, 7 -- Mariner 5 flyby
- Slow fluctuations -- fading rate given in Appendix 7.6A
- Spurs development of new theory of tracking and data detection performance.

Rician Turbulence Model (not recommended)

- Amplitude characteristic (Rice-Nakagami)
- Phase characteristic (sine-wave plus Gaussian noise)

- Supporting theory -- deWolf
- Valid for strong fluctuations
- Two parametric amplitude distribution
- Slow fluctuations
- Denounced by Tartarskii for weak fluctuations
- Later denounced by deWolf in favor of lognormal model for amplitude.

Atmospheric Attenuation (Appendix 7.6F)

Absorption and Refractive Defocusing

- Loss theory developed by Croft, Eshleman, Marouf, and Tyler of SEL
- Loss theory also developed by Martin Marietta Corporation using planet model, SP-8011
- Recommended model for preparation of design control table is Martin Marietta Corporation model.

Planetary Backscatter (Appendix 7.6G)

- Model and theory given in Appendix 7.6A
- Probe geometry and velocities with respect to Venus are used to tabulate effects (see Appendix 7.6G)
- Conclusion -- planetary backscatter is not a first-order effect and can be assumed negligible in preparing design control tables.

7.6.3.2 Modulation Trades

During the course of the study four modulation techniques were considered for the probe communication links. These include:

- Phase-shift keying a subcarrier while retaining a carrier component for carrier tracking and coherent demodulation (PSK/PM)
- Phase-shift keying so as to suppress the carrier (PSK/SC)
- Amplitude shift keying (ASK or on-off keying) the carrier directly
- Multiple frequency shift keying (MFSK) with noncoherent detection.

Neglecting the application of coding and considering a perfectly synchronized white Gaussian noise channel, then PSK/SC is the most efficient among the

above modulation candidates; however, for probe communication links one must consider the following additional design constraints and factors:

- 1) Turbulence effects
- 2) Absorption and defocusing effects
- 3) Thermal noise
- 4) Planetary backscatter effects
- 5) DSN capability
- 6) Costs
- 7) Weight and power constraints
- 8) Mission Doppler profile
- 9) Signal acquisition time and range
- 10) Data handling constraints

Considering the above factors and design constraints, the advantages and disadvantages of each modulation technique are summarized in Table 7.6-2. The entries in this table are provided from the study results documented in Appendices 7.6A through H.

From Table 7.6-2 the modulation choice is PSK/PM for both the large and small probes. The rationale is primarily based on cost, compatibility with DSN hardware and software, existence of flight-qualified hardware, and communication efficiency provided by coherent detection and Doppler extraction tempered by the disadvantages of the other modulation candidates.

7.6.3.3 Coding Tradeoffs

The most suitable candidates for coding methods to be used on planetary entry probe communication channels are sequential and Viterbi. These coding techniques provide significant reduction in required E_b/N_0 at a specified probability of bit error from the uncoded PSK requirements. They also provide superior error rate performance to orthogonal codes, as well as block codes of equivalent complexity. Hybrid and bootstrap codes are too complex for this application. Which of the two methods, sequential or Viterbi, is more suitable is essentially dictated by the user data

Table 7.6-2. Comparison of Candidate Probe Modulation Techniques

MODULATION TECHNIQUE	ADVANTAGES	DISADVANTAGES
I. PSK/SUPPRESSED CARRIER MODULATION	<ol style="list-style-type: none"> 1) EFFICIENT USE OF TRANSMITTER POWER FOR DATA TRANSMISSION AND CARRIER SYNCHRONIZATION. 2) DOES NOT REQUIRE A SUB-CARRIER DEMODULATOR ASSEMBLY. 3) EFFICIENT USE OF CHANNEL BANDWIDTH. 4) PROVIDES FOR COHERENT DOPPLER EXTRACTION. 	<ul style="list-style-type: none"> - NOT DSN COMPATIBLE. - TRACKING LOOPS MUST TRACK TWICE THE DOPPLER AND DOPPLER RATES. - INTRODUCES 180° PHASE AMBIGUITY IN DATA STREAM. - REQUIRES DIFFERENTIAL ENCODING OR POWER ALLOCATED TO A RESIDUAL CARRIER. - INEFFICIENT DUE TO NOISY REFERENCE LOSS AT LOW DATA RATES. - COST IS HIGH TO IMPLEMENT IN DSN.
II. ASK (ON-OFF) MODULATION	<ol style="list-style-type: none"> 1) EFFICIENT USE OF TRANSMITTER PEAK POWER CAPABILITY. 2) SIMPLE TO IMPLEMENT IN THE SPACECRAFT. 	<ul style="list-style-type: none"> - NOT DSN COMPATIBLE. - REQUIRES IMPLEMENTATION OF A VARIABLE THRESHOLD IN RECEIVER OWING TO FADING. - INEFFICIENT USE OF AVERAGE TRANSMITTER POWER. - DOES NOT PROVIDE DOPPLER DATA DURING OFF PERIODS. - CREATES SIGNAL ACQUISITION PROBLEMS. - REQUIRES DEVELOPMENT OF FREQUENCY AND BIT SYNCHRONIZATION ALGORITHMS. - COST IS HIGH TO IMPLEMENT IN DSN.
III. MFSK MODULATION	<ol style="list-style-type: none"> 1) DOES NOT REQUIRE COHERENT DETECTION — THUS COHERENT CARRIER AND SUBCARRIER TRACKING LOOPS ARE NOT REQUIRED. 2) TOTAL TRANSMITTER POWER ALLOCATED TO DATA TRANSMISSION AS WELL AS SYNCHRONIZATION. 	<ul style="list-style-type: none"> - NOT DSN COMPATIBLE UNLESS RECORDING CAPABILITY IS IMPLEMENTED. - PROGRAM COST IS APPROXIMATELY \$3 MILLION > PSK/PM. - DUE TO OSCILLATOR INSTABILITIES, INEFFICIENT TO USE AT DATA RATES LESS THAN 6 TONES PER SECOND. - A FREQUENCY TRACKING ALGORITHM HAS NOT BEEN FULLY DEMONSTRATED TO TRACK DOPPLER AND DOPPLER RATES. - A TIME (BIT SYNC) ALGORITHM COMPATIBLE WITH A FREQUENCY TRACKING ALGORITHM HAS NOT BEEN DEVELOPED. - REQUIRES DEVELOPMENT OF A FLIGHT QUALIFIED FREQUENCY SYNTHESIZER. - OSCILLATOR INSTABILITIES DEGRADE DETECTION EFFICIENCY.
IV. PSK/PM MODULATION (RECOMMENDED FOR BOTH SMALL AND LARGE PROBS)	<ol style="list-style-type: none"> 1) DSN COMPATIBLE. 2) FLIGHT QUALIFIED HARDWARE EXISTS. 3) COST EFFECTIVE. 4) PROVIDES FOR COHERENT DOPPLER EXTRACTION. 5) MOST EFFICIENT FORM OF DATA DETECTION (EXCLUDING PSK/SC). 	<ul style="list-style-type: none"> - INEFFICIENT AT LOW DATA RATES. - INTRODUCES 180° PHASE AMBIGUITY IN SUBCARRIER.
NOTE: IT IS ASSUMED THAT PREDETECTION RECORDING IS REQUIRED WHATEVER TECHNIQUE IS CHOSEN.		

requirements, channel characteristics, system complexity considerations, and DSN hardware compatibility. The latter of these is a significant cost consideration. The choice is sequential decoding primarily based on compatibility with DSN and existing Pioneer spacecraft equipment. Interleaving is not presently recommended due to DSN noncompatibility.

To make the choice and design for the channel it was necessary to obtain the performances of the two coding methods for probe channels. Although the performances of each method have been previously computed by computer simulation for the additive white Gaussian noise (AWGN) channel, these results are inadequate because we are faced with significant receiver synchronization errors, as well as channel fading due to propagation effects. Therefore, we were required to develop the necessary theory and computer programs to compute the performance of the coded system using either sequential or Viterbi decoding in the presence of synchronization errors and multiplicative noise (fading). The corresponding performance for the uncoded PSK system was also computed. With these results we are able to compare the performances of the two coding methods, their coding gains, and the theoretically achievable benefits of interleaving. In addition, the results are used to construct the link design control tables. Table 7.6-3 summarizes the results for a 50-degree transmitting angle from the surface of Venus.

Table 7.6-3. Required E_b/N_0 with Lognormal Fading and Radio Losses

CODING METHOD, AT 50°, BER 10^{-3} , FOR 10^{-2}	IDEAL (ADDITIVE WHITE GAUSSIAN NOISE ONLY) (DB)	NOISY CARRIER REFERENCE EFFECTS INCLUDED (13 DB IN 28 10^0) (DB)	LOGNORMAL FADING EFFECTS INCLUDED (DB)	COMBINED NOISY CARRIER REF AND FADING EFFECTS INCLUDED (DB)	TOTAL RECEIVER CARRIER, SUBCARRIER AND FADING EFFECTS INCLUDED (DB)
VITERBI R - 13, K - 6	2.5	5.2	4.95	6.5	7.7
SEQUENTIAL R - 12, K - 32 128 BPS	2.25	5.15	4.7	6.1	7.3 (7.4 AT 64 BPS)
UNCODED PSK	6.9	7.5	0.2	8.9	9.9
SEQUENTIAL DECODING GAIN	4.65	2.35	3.5	2.8	2.6
VITERBI DECODING GAIN	4.4	2.3	3.25	2.4	2.2
THEORETICAL INTER- LEAVING GAIN OVER CODED SYSTEM WITH- OUT INTERLEAVING					2.0

The basic data used was the AWGN results for Viterbi decoding available in the literature, and the experimental AWGN sequential decoding results with and without receiver loss, obtained at JPL by NASA/Ames. The sequential decoding results without receiver losses are given in Figure 7.6-3. The effects of reference phase errors and amplitude fluctuations due to channel fading were included in the bit error or frame deletion probability, P_E , through the integral

$$P_E = \int_{\theta} \int_A P(E|\theta, A) P_{\theta, A}(\theta, A) d\theta dA.$$

The $P(E|\theta, A)$ represents the probability of bit error or frame deletion conditioned on a phase error value θ and an amplitude value A . In the computations we have assumed that the noisy carrier phase reference and the fluctuating signal amplitude due to fading are independent and remain constant over the decoder memory length. In the cases where subcarrier loss estimates were required, subcarrier losses were arrived at by the information available in the Telecommunications System Design Techniques Handbook with a 0.2 dB estimate added for Doppler effects. Using the NASA/Ames data for sequential decoding deletion rate with all receiver losses included and computing the fading effects on these data, the total loss was estimated. These results are given in Figure 7.6-4. To obtain more accurate results, elaborate simulation or experimentation is required. For details of the analysis and tradeoff, see Appendix 7.6D.

Based on the performance values, DSN compatibility, and commonality with existing Pioneer spacecraft encoding equipment, the sequential decoding technique is recommended for the Atlas/Centaur configuration for both the large and small probes. Interleaving cannot be recommended without further study because of complexity, storage requirements, DSN incompatibility, and possible loss of large amounts of data at impact because of the stored data. Even though the table lists a theoretical 2.0 dB interleaving gain it may be difficult to realize this gain.

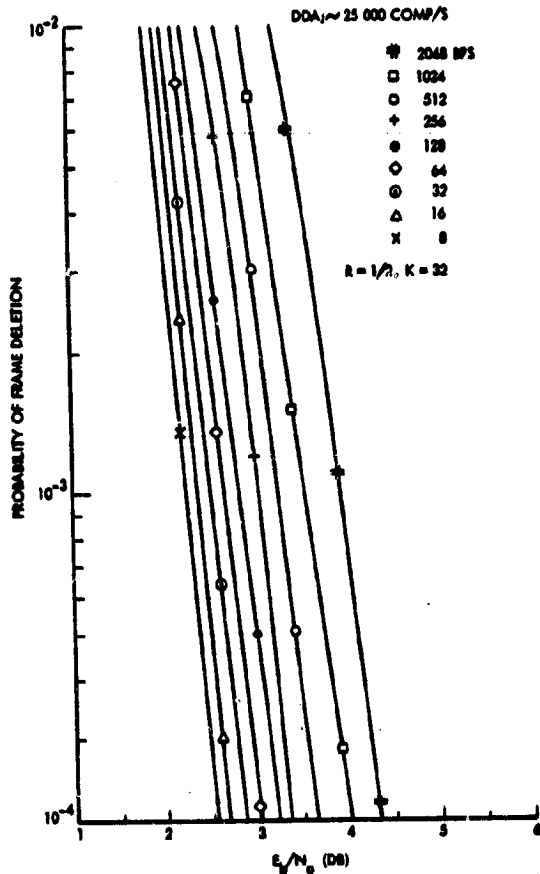


Figure 7.6-3. Frame Deletion Rate for Sequential Decoding with No Synchronization or Fading Losses

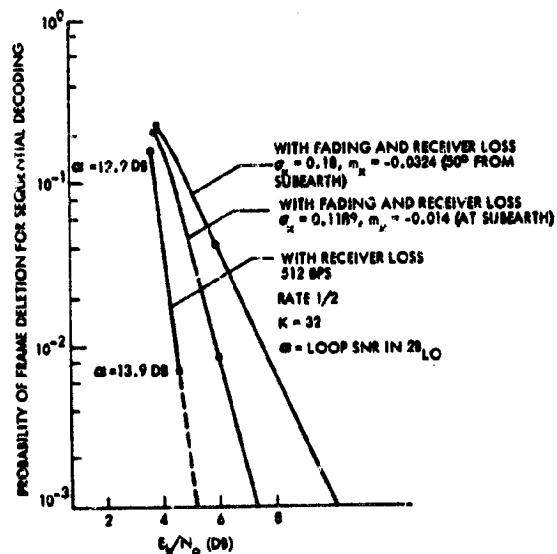


Figure 7.6-4. Frame Deletion Probability for Sequential Decoding with Receiver Losses and Lognormal Fading Effects Included

To compute the performance of an MFSK system with these codes, metric derivations and other analyses were required. Since PSK is the chosen modulation, MFSK results are not given here, but the performance results, as well as other pertinent material, are contained in Appendix 7.6E. The coding choice for the MFSK system with off-line processing is Viterbi decoding with constraint length 10.

7.6.3.4 One-Way versus Two-Way Links

A tradeoff study of one-way versus two-way links was performed to decide which type or types of links to use in the large and small probes. This study, reported in Appendix 7.6L, was done in conjunction with the modulation tradeoff studies and was strongly influenced by the projected capabilities of the DSN in order to effect a cost savings. A major factor influencing our decision was the requirement for a transponder established in the Version III science payload definition. The Version IV science payload deletes this requirement and reconsideration of the one-way link is recommended.

Requirements

Basic requirements are: (1) to provide some measure of Doppler to assess wind shear as the probes descend to the planet's surface; (2) provide downlink telemetry from each of the probes during the descent phase; (3) provide capabilities of performing both Doppler measurement and telemetry for a minimum of two probes and the bus simultaneously for a staggered arrival time of probes at the planet; and (4) alternatively, consider providing Doppler measurement and telemetry for four probes and the bus simultaneously for a nearly simultaneous arrival of probes at the planet. Additional requirements are given in Section 7.6.2.

Theory

Theoretical analysis of the predicted performance for the one-way and two-way links is presented in Appendices 7.6A, 7.6B and 7.6C. It has been concluded that the effects of fading on the tracking loops are relatively negligible and that one-way and two-way links are comparable when the uplink signal-to-noise ratio is high.

DSN Capability and Constraints

The DSN has the capability for a maximum of three uplink channels of 40 kW or greater (two at Goldstone, one at Madrid or Canberra) covering vehicles in a 64-meter antenna pattern.

For the case of two or more probes arriving at the planet at the same time and requiring high power uplinks for two-way Doppler, at least two uplinks are needed. Should the Goldstone transmitter be inoperative the two 40 kW channels would not be available, leaving only one uplink for two or more vehicles. Therefore, it is concluded that at least some one-way links are required unless one resorts to one probe at a time coverage or use of nonstandard DSN transponder turnaround ratios; this latter approach was deemed too costly. See Appendix 7.6L for details of this study.

Signal Acquisition in One-Way and Two-Way Links

An automatic frequency search capability in the transponder would provide the quickest uplink acquisition and two-way downlink acquisition with least loss of post-entry data as compared to ramping the ground transmitter. This is true because of the time of arrival uncertainty and the fact that for any reasonable uplink ramp rate (to search the uplink frequency uncertainty in a reasonable time) the rate is too high for downlink acquisition. Hence, one must delay ramping the uplink transmitter for the post-entry phase until the probe, even a late arriving one, will have entered. This results in probable loss of two-way Doppler for several minutes and possibly loss of data due to frequency jumping when the uplink does lock.

A comparison of acquisition times for one-way and two-way links for various Doppler predict accuracies and oscillator stabilities is given in Appendix 7.6L, Table 7.6L-2. For one-way links with probe oscillators having long-term stability of one part in 10^6 or better, the downlink acquisition time is comparable to a two-way link with auto search in the transponder.

Tracking Accuracy

Range rate errors due to frequency uncertainty alone need to be less than ± 10 mm/s (refer to Section 4.2.4). For the range rates experienced, this results in a need for an oscillator having a long-term design frequency stability of about ± 4 parts in 10^7 and ± 8 parts in 10^7 at the actual post-entry time. Refer to Figure 7.6L-3 of Appendix 7.6L.

Hardware Implications, Weight & Cost

A comparison of weight and cost of one-way and two-way links shows a weight savings of 1.7 kg (3.75 lb) for a one-way link for the Atlas/Centaur over that of a two-way link due to elimination of the receiver, diplexer, and some RF cabling even though the receiver is replaced by a stable oscillator. The savings is slightly less for the Thor/Delta. Also, there is a cost factor of about \$1/2 million in development and hardware costs for two-way links compared to one-way links.

Telemetry Degradation Effects

One-way and two-way links with high uplink signal-to-noise ratios are comparable in performance after uplink acquisition is effected; however, depending on the uplink acquisition method, the downlink transmissions can be degraded by delayed acquisition of the uplink. Malfunction of receivers, switchover circuitry, and other problems can contribute to loss of two-way downlink data; therefore, we conclude that the two-way link is more risky and the more expensive of the two.

Recommendation

A two-way link is recommended for the large probe primarily because it is included on the Version III science list. One-way links with stable oscillators (± 4 parts in 10^7) are recommended for the small probes due to lower cost, lack of sufficient DSN uplink capability, and some doubt as to the need for two-way tracking. A final review of use of the two-way link on the large probe is desirable before commitment to hardware.

7.6.3.5 Probe Communications Hardware Tradeoffs

Several hardware configuration tradeoffs were made in selecting baseline components to meet the basic mission requirements and assess relative weight and cost penalties. The latter, in many cases, consisted of engineering judgements on relative cost.

Probe Antenna Tradeoffs

The objective of the tradeoff study was to investigate and select a low-gain antenna for Pioneer Venus mission. The basic requirements considered in the tradeoff were:

- 1) Use a single antenna for both large and small probes
- 2) Obtain maximum gain over antenna communications coverage
(see Figures 7.6-5 and 7.6-6)
- 3) Minimize the antenna size, weight, and cost
- 4) Select a circularly polarized antenna whose pattern has acceptable axial ratio degradation over the coverage angles
- 5) Select material suitable for high temperatures and low cost construction.

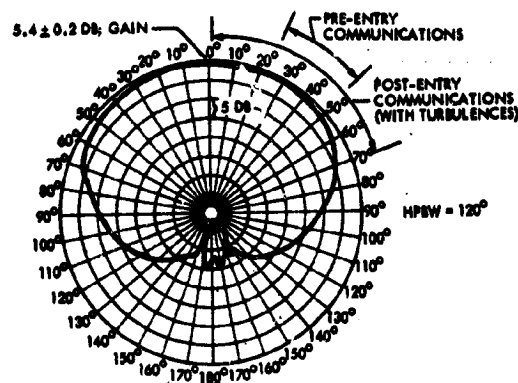
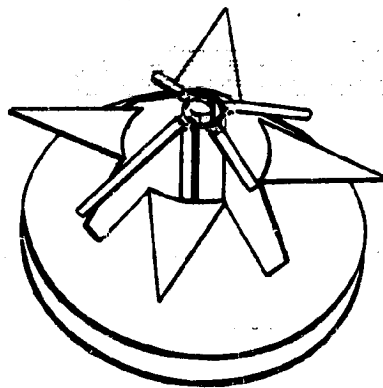


Figure 7.6-5. Typical Antenna Pattern and Required Coverage Area



ANTENNA CHARACTERISTICS
 PATTERN - CONICAL BEAM, HPBW = 120°
 ON-AXIS GAIN - 5.4 ± 0.2 DB, AT 2.1 TO 2.3 GHZ
 POLARIZATION - RHC
 MATERIAL - TITANIUM
 TEMPERATURE - 473°C (766 K)
 ENVELOPE - 11.5 CM DIA x 5.4 CM (4.5 IN. DIA x 2.1 IN.)
 MASS - 40.23 KG (89.0 LB)

Figure 7.6-6. Turnstile Cone Antenna

Two basic types of antenna patterns were considered, the conical beam and the split conical beam (butterfly). Four different small light-weight antennas were investigated that basically meet the above requirements. They are:

- 1) Turnstile over a conical cavity
- 2) Planar spiral
- 3) Conical spiral
- 4) Loop vee.

Antenna trade characteristics are shown in Table 7.6-4. For the Thor/Delta mission the butterfly and conic patterns were considered because both could meet the pattern coverage requirements. However, for the Atlas/Centaur mission the probes have a wider communications coverage area (from approximately 0 to 70 degrees on-axis due to targeting spread of the small probes), which eliminates the use of a butterfly pattern. This eliminates the loop vee antenna and the difference mode excitation of the planar and conical spiral. The turnstile/cone was selected for both Atlas/Centaur and Thor/Delta missions as the antenna which best meets the performance requirements listed above. A detailed description of the tradeoff study is presented in Technical Note P73-203434-076, Rev B, "Probe Antenna Selection," by G. R. Proctor, Martin Marietta Corporation, Denver, Colorado, February 22, 1973.

S-Band Power Amplifier Tradeoffs

Several suppliers of solid-state S-band power amplifiers have been contacted regarding their capabilities and product line items in the 5 to 40 watt power output range. A result of this survey, including interchange of data with TRW, is shown in Table 7.6-5. Of the companies contacted, Microwave Semiconductor Corporation's designs appear to come closest to meeting our requirements, although they must be repackaged to include an output filter and isolator. Traveling wave tubes amplifiers were never seriously considered due to the entry environment although Watkins Johnson does not anticipate problems in this area (with special orientation when mounted in the probe).

Baseline power amplifier nominal outputs for the Thor/Delta and Atlas/Centaur missions are as follows:

Thor/Delta	Nominal Output Power (W)
Large Probe	21.9
Small Probe	10.0
Atlas/Centaur	
Large Probe	36
Small Probe	20

Consideration was given to commonality of design between bus and probes to effect cost savings. For the Thor/Delta mission, probe weight and volume were critical. These factors ruled out the paralleling of single 6-watt packaged spacecraft units to provide the 10-watt small probe and 21.9-watt large probe units. Also ruled out for the same reasons was the paralleling of single 12-watt units to obtain 21.9-watts for the large probe.

For the Atlas/Centaur configuration the decision was to use a single 20-watt unit for the small probe and two parallel 20-watt units for the large probe as opposed to developing a 20-watt unit and a 36-watt unit or using two 11-watt units and four 11-watt units. However, when final detailed costs are developed this decision may be reversed to that of using individual 20 and 36 watt units for better performance.


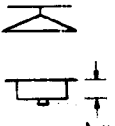

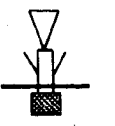
The method selected for paralleling the two 20-watt small probe Atlas/Centaur units is the simplest, namely the use of hybrids. Other methods considered were switched $1/4\lambda$ transmission lines to provide partial redundancy and diode switched Wilkerson hybrid combiner but both were rejected on the basis of added complexity and cost.

Transponder Receiver and Transmitter Driver Selection Tradeoffs

A transponder or combination of receiver and transmitter driver is required for the large probe and a transmitter driver is required for the small probes. For the Thor/Delta probe configurations, weight and volume restrictions are quite severe. Units considered for the large probe were a Viking transponder (modified), separate modified receiver and

REPRODUCIBILITY OF THE ORIGINAL PAGE IS POOR,

Table 7.6-4. Probe Antenna Trade Characteristics

CHARACTERISTICS CONCEPTS	ANTENNA GAIN AT 2.3 GHz (DBI)	3 DB BEAM- WIDTH (DEG)	POLAR- IZA- TION	FEED	AXIAL RATIO (DB)	MASS (KG) (LB)	MATERIAL	SIZE	POWER HANDLING CAPABIL- ITY (W)	BACK- LOBE (DBI)	PATTERN TYPE	DEVELOPMENT STATUS	COSTS
 TURNSTILE/CONE	5.4 ON AXIS	120	RHC	SINGLE SPLIT BALUN	4 BE- TWEEN 0° TO 70°	0.23 (0.5)	METAL AND DIELEC- TRIC	5.3 CM X 11.4 CM DIA (2.1 IN. X 4.5 IN. DIA)	GREATER THAN 60	-14	CONICAL BEAM	THE ANTENNA IS A MODIFIED VIKING LANDER RADAR ALTIMETER ANTENNA. A BREADBOARD MODEL HAS BEEN BUILT AND TESTED ON A THOR/DELTA LARGE PROBE MODEL (SEE REFERENCE 1* AND APPENDIX 7.6J). THE ANTENNA MET THE GAIN COVERAGE REQUIREMENTS EASILY AND THE SMALL SIZE IS COMPATIBLE FOR BOTH LARGE AND SMALL PROBES.	BEING A MODIFIED ANTENNA AND MADE OF METAL WHICH IS MAINTAINED, THE ANTENNA IS RELATIVELY LOW COMPARED TO DEVELOPMENT COSTS TO MAKE A CERAMIC ANTENNA.
 PLANAR SPIRAL	NO PAT- TERNS OR GAIN OBTAINED 2.7	50 5 - 40	RHC	SINGLE BALUN SUM MODE EXITATION SINGLE BALUN DIFFER- ENCE MODE EXITATION	5 BE- TWEEN 15° & 70°	0.27 (0.6)	METAL AND EPOXY FIBER- GLASS OR CERAMIC PLATE	ANTENNA TOO LARGE FOR PROBE WHEN HPBW IS ~ 120 DEG 3.3 CM X 11.4 CM DIA (1.5 IN. X 4.5 IN. DIA) WITH CAVITY UNDER AN- TENNA	HEATING DAMAGE AT 20	-14	CONICAL BEAM BUTTER- FLY BEAM	THE ANTENNA WAS CONSIDERED FOR PROBE USE IN REFERENCE 1*. IT WAS DETERMINED IN THAT STUDY THAT THE SIZE BECOMES TOO LARGE WHEN THE HPBW WAS LARGE ENOUGH TO MEET THE GAIN COVERAGE REQUIREMENTS. THE POWER HANDLING CAPABILITY WAS ALSO A PROBLEM AREA.	THE COST IN DEVELOPING A CERAMIC MOLD, TOLERANCES NEEDED TO PHOTOETCH THE ANTENNA CONFIGURATION, AND THE MORE COSTLY THAN METAL ANTENNA.
 CONICAL SPIRAL	3.8 ON AXIS 3.8 OFF AXIS AT 5 ANGLE	145 55 5 - 60	RHC RHC	SINGLE BALUN SUM MODE EXITATION SINGLE BALUN DIFFER- ENCE MODE EXITATION	4 BE- TWEEN 0° & 70° 4 BE- TWEEN 30° & 70°	0.23 (0.5) 0.32 (0.7)	METAL AND EPOXY FIBER- GLASS OR CERAMIC CONE	8.9 CM X 5.3 CM DIA (3.5 IN. X 2.1 IN. DIA) 10.2 CM X 9.4 CM DIA (4.0 IN. X 3.7 IN. DIA)	GREATER THAN 60	-7 -11	CONICAL BEAM BUTTER- FLY BEAM	A BREADBOARD MODEL WAS DESIGNED, BUILT, AND TESTED (SEE REFERENCE 1*) FOR PROBE USE. THE PERFORMANCE AND SIZE ARE ACCEPTABLE. HOWEVER THE HIGH TEMPERATURE CERAMIC CONE WOULD NEED MORE DEVELOPMENT.	THE COST IN DEVELOPING A CERAMIC CONE, TOLERANCES NEEDED TO PHOTOETCH THE ANTENNA, AND THE COSTS TO MAKE THE CERAMIC CONE WOULD BE CONSIDERABLY MORE THAN METAL ANTENNA.
 LOOP VEE	2.0 OFF AXIS AT 5 ANGLE	60 5 - 70	RHC	SINGLE BALUN	5 BE- TWEEN 40° & 90°	0.23 (0.5)	METAL AND DIELEC- TRIC	5.6 CM X 3.1 CM DIA (2.2 IN. X 1.2 IN. DIA)	BREAK- DOWN AT ~40	-9	BUTTER- FLY BEAM	THE ANTENNA WAS CONSIDERED FOR THE THOR/DELTA MISSION, HOWEVER THE PATTERN CHARACTERISTICS (BUTTERFLY) WILL NOT MEET THE COVERAGE REQUIREMENTS OF THE ATLAS/CENTAUR MISSION. THE ANTENNA WAS DESIGNED, BREADBOARDED AND TESTED IN REFERENCE 1*. THE ANTENNA HAD SERIOUS PROBLEMS WITH POWER BREAK-DOWN AND CIRCULARITY.	THE ANTENNA IS CONSIDERED FOR THE ATLAS/CENTAUR MISSION. THE PATTERN CHARACTERISTICS (BUTTERFLY) ELIMINATE THE ANTENNA FOR THE ATLAS/CENTAUR MISSION.

REPRODUCIBILITY OF THE ORIGINAL PAGE IS POOR,

istics

	COST	NOTES
MODIFIED R. ALTI- READ- EN BUILT OR DELTA SEE REFER- (X 7.6J) BE GAIN LIMITS EAS- Y IS H LARGE	BEING A MODIFIED VIKING ANTENNA AND MAINLY MADE OF METAL WHICH IS EASILY MAINTAINED, THE COST OF THE ANTENNA IS RELATIVELY LOW COMPARED TO THE DE- VELOPMENT COSTS NEEDED TO MAKE A CERAMIC MOLDED ANTENNA.	THE ANTENNA IS MACHINED FROM HIGH TEMPERATURE TITANIUM WITH A HIGH TEMPERATURE CERAMIC DI- ELECTRIC USED IN THE BALUN.
CONSIDERED REFERENCE 1. THAT BECOMES E HPBW TO MEET REQUIRE- HANDLING A PROB-	THE COST IN DEVELOPMENT OF A CERAMIC MOLD AND THE TOLERANCES NECESSARY TO PHOTOETCH THE ANTENNA ON THE CERAMIC. MAKES THIS AN- TENNA CONFIGURATION MUCH MORE COSTLY THAN A METAL ANTENNA.	THE ANTENNA IS PHOTO- ETCHED ON A HIGH TEMPER- ATURE CERAMIC DIELECTRIC. THE BASE IS MACHINED FROM HIGH PURITY TITANIUM.
EL WAS ND TESTED OR PROBE NCE AND HOW- TEMPERATURE ED NEED	THE COST IN DEVELOPMENT OF A CERAMIC CONE MOLD AND THE TOLERANCES NECESSARY TO PHOTOETCH THE ANTENNA ON THE CERAMIC CONE, WOULD MAKE THE COSTS INCREASE CONSIDERABLY OVER A METAL ANTENNA.	THE ANTENNA IS PHOTO- ETCHED ON A HIGH TEMPER- ATURE TRUNCATED CERAMIC CONE. THE BASE IS ALSO OF TITANIUM.
ON- OR DELTA THE ISTICS OT MEET RE- THE XNED, TESTED SE AN- PROB- EAK- RITY.	THE ANTENNA IS SIMPLE IN CONSTRUCTION, HOWEVER THE PATTERN CHARACTERISTICS (BUTTERFLY) ELIMINATES THIS ANTENNA FOR AN ATLAS CENTAUR MISSION.	THE ANTENNA IS MACHINED FROM TITANIUM WITH A CERAMIC DIELECTRIC USED IN THE BALUN. *REFERENCE 1 IS TECH NOTE P. 73-203434-076.

Table 7.6-5. Survey of Power Amplifiers

MANUFACTURER	PROGRAM	STATUS	MASS (KG) (LB)	DC POWER (W)	RF POWER (W)	COMMENTS
RADIATION INC.	TECHNOLOGY PROGRAM GSFC	DELIVERED	0.15 (0.3)	18	6	MUST MODIFY DESIGN TO REDUCE JUNCTION TEMP
TRW	DEFENSE SATELLITE PROGRAM (DSP)	ENGINEERING MODEL	0.34 (0.8)	15	4	30 DB GAIN
MSC	COMMERCIAL NEAR OFF SHELF	MUST QUALIFY	0.23 (0.5)	24	7	REPACKAGE TO INCLUDE FILTER AND ISOLATOR.
			0.45 (1)	52	12	
			0.9 (2)	80	17	
			0.9 (2)	100	22	
			0.9 (2)	150	30	
PHILCO FORD	PROPOSED		0.45 (1)	27	5	
			0.9 (2)	40	10	
			1.5 (3.3)	105	20	
MOTOROLA	PROPOSED		0.63 (1.4)	25	5	
			N/A	50	10	
			N/A	100	20	

NOTE: WEIGHTS DO NOT REFLECT HEAT SINK BASEPLATE FOR HIGH PROBE TEMPERATURE ENVIRONMENT.

transmitter driver of the Pioneer 10 and 11 design, and separate modified receiver, transmitter-drivers of the Skynet II design.

For the small probe, a modified Pioneer 10 and 11 and a modified Skynet II (or modified Viking transponder modules) were considered. Table 7.6-6 compares estimated power weight and status of these units.

Table 7.6-6. Transponder, Receiver, Transmitter Drivers

MANUFACTURER	PROGRAM	STATUS	UNIT	MASS (KG) (LB)	DC POWER (W)	COMMENTS
TRW	PIONEER 10/11	FLIGHT	REC XMTR	2.45 (5.4) 0.59 (1.3)	2.0 1.4	REQUIRES SPECIAL POWER INPUT (OTHER THAN 28VDC) AND OTHER MODIFICATIONS (SEE TEXT)
PHILCO FORD	VIKING LANDER	IN QUAL	TRANS- PONDER	2.0 (4.4)	4	NEED TO REDUCE MAGNETIC FIELD FOR CLEANLINESS (SEE TEXT FOR OTHER MODS).
PHILCO FORD	SKYNET II	FLIGHT	REC XMTR	0.99 (2.1) 0.64 (1.4)	1.5 4.0	WEIGHT & POWER ESTIMATED FROM PHILCO FORD DATA SHEETS.
PHILCO FORD	VIKING - SKYNET II COMBINED DESIGN (NOT ACCOMPLISHED)		REC XMTR	0.95 (2.1) 0.64 (1.4)	1.5 4.0	ESTIMATED FOR PIONEER VENUS THOR/DELTA MISSION
MOTOROLA	MARINER SERIES					TOO LARGE AND HEAVY.
MOTOROLA	THEIR MINIATURIZED VERSION	IN DESIGN MID-73 DEMON- STRATION	TRANS- PONDER			NO ESTIMATE OBTAINED ON PERFORMANCE.
TRW	THEIR MINIATURIZED VERSION	IN DESIGN 1973	REC XMTR			NO ESTIMATES OBTAINED ON PERFORMANCE.

Modifications required for the receivers, whether part of a transponder or separate units, include adding frequency search and acquisition capability, modifying the threshold tracking loop bandwidth to 250 Hz ($2B_{LO}$), eliminating the command channel (and ranging on the Viking receiver). Modification of the transmitter driver portions of the transponder or individual transmitter drivers is required to eliminate dual subcarrier inputs (only one subcarrier is used for the probes). The Pioneer units require a special power supply to provide both +12 volts and -12 volts DC for the receiver and -16 volts DC for the transmitter driver.

The baseline selection for the Thor/Delta large probe is Skynet II-type separate receiver and transmitter-driver units using Viking modules to get the $\frac{221}{240}$ frequency ratio. For the Thor/Delta small probes a transmitter-driver identical to the large probe is used.

For Atlas/Centaur a modified Viking transponder is used for the large probe and a transmitter-driver using Viking modules is used for the small probes.

Rationale for the Thor/Delta selection is savings in weight plus flexibility in having two smaller packages in the large probe.

Rationale for the Atlas/Centaur selection is potential cost savings from use of an existing design and desirability of the more up-to-date Viking design.

Diplexer Selection Tradeoff

The diplexer selection for the large probe for both Atlas/Centaur and Thor/Delta was based on data received from TRW and Wavecom. The Pioneer 10 and 11 model produced by Wavecom (their Type II) with a single antenna outlet can be used without modification. Other units considered, such as for the Viking Lander, included unneeded functions and were quite large and heavy.

Stable Oscillator Tradeoff

The stable oscillator for the small probes is carried on the science list for the small probe; however, it may not be a GFE item. Performance requirements for this item are based on tracking and acquisition studies in Appendix 7.6L, where it was concluded that long-term stability of ± 4 parts in 10^7 would be the minimum to provide good tracking and acquisition performance (less than 10 mm/s range rate error due to frequency uncertainty and about 100 seconds or less to acquire the downlink carrier after the Doppler rates drop to 6 Hz/s or less using a 10 Hz DSN receiver tracking loop.)

Use of a less stable oscillator, ± 1 part in 10^6 for example, would require an increased carrier acquisition time (189 seconds) for ± 1 percent Doppler shift prediction accuracy.

Potential sources for such an oscillator (see Table 7.6-13 in Section 7.6.4.2 for typical characteristics) are Frequency Electronics Incorporated, Philco Ford, and others (response from some potential sources is still expected).

7.6.4 Preferred Probe Subsystem Description, Atlas/Centaur

The communications subsystem designs are described for the large and small probes. They are based on use of standard DSN modulation/demodulation, decoding, and tracking techniques. Common hardware

designs between large and small probes are used where applicable. These include antenna, transmitter driver, and S-band power amplifiers.

A complete set of telecommunications design control tables is contained in Appendix 7.6H; however, Tables 7.6-7A and 7B of the downlinks when the probes are near the surface (altitude < 1 km) are provided here for insight into the overall link designs. Modulation is PSK/PM on the downlink with unmodulated carrier on the large probe uplink to provide a two-way Doppler tracking capability. Present design is based on margin equal to or greater than the sum of the adverse tolerances including 1 dB nominal loss for predetection recording. For other carrier and data channel losses see Appendix 7.6H.

Table 7.6-7A. Telecommunications Design Control Atlas/
Centaur Large Probe, Near Venus Surface

NO.	PARAMETER	NOMINAL VALUE	ADVERSE TOLERANCE	NOTES
1	TOTAL TRANSMITTING POWER (DBM) 36 W	+ 45.6	0.8	VOLTAGE & TEMP
2	TRANSMITTING CIRCUIT LOSS (DB)	- 1.6	0.4	
3	TRANSMITTING ANTENNA GAIN (DB) $\theta = 50^\circ$	+ 3.5	1.5	GAIN VARIATION
4	COMMUNICATIONS RANGE LOSS (DB) 0.43 AU	-255.9	0.0	
5	ATMOSPHERIC ABSORPTION & DEFOCUSING LOSSES (DB)	- 0.9	0.1	
6	POLARIZATION LOSS (DB)	- 0.2	0.1	
7	MULTIPATH & OTHER LOSSES (DB)	SEE NOTE 1		
8	RECEIVING ANTENNA GAIN (DB)	+ 61.7	0.4	JPL 810-5
9	RECEIVING CIRCUIT LOSS (DB)	0.0	0.0	JPL 810-5
10	NET LOSS (DB) (2+3+4+5+6+7+8+9)	-193.4	2.5	
11	TOTAL RECEIVED POWER (DBM) (1+10)	-147.8	3.3	
12	RECEIVER NOISE SPECTRAL DENSITY - (DBM/HZ)	-184.5	1.4	25.5 \pm 9.5°K
13	TOTAL RECEIVED POWER/NO (DBM/HZ) (11-12)	+ 36.7	SUM 4.7	
CARRIER TRACKING				
14	CARRIER POWER/TOTAL (DB)	- 5.4	0.4	NOTE 2
15	ADDITIONAL CARRIER LOSSES (DB)	- 1.5	0.2	
16	THRESHOLD TRACKING BANDWIDTH - $2B_{LO}$ (DB)	+ 10.0	0.8	
17	REQUIRED SNR (DB)	+ 13.0	0.0	
18	PERFORMANCE MARGIN (DB) (13+14+15-16-17)	+ 6.8	SUM 6.1	
DATA CHANNEL				
19	DATA POWER/TOTAL (DB)	- 1.5	0.2	NOTE 3
20	ADDITIONAL DATA CHANNEL LOSSES (DB)	- 6.0	0.5	
21	DATA BIT RATE - BPS (DB)	+ 21.1	0.0	128 BPS
22	THRESHOLD ENERGY PER DATA BIT - E_b/N_0 (Db)	+ 2.3	0.0	NOTE 4
23	PERFORMANCE MARGIN (DB) (13+19+20-21-22)	+ 5.8	SUM 5.4	

- NOTE: 1. MULTIPATH INCLUDED IN 15 & 20 BELOW.
2. 1.0 DB PREDTECTION RECORDING LOSS + 0.5 DB DOWNLINK SUPPRESSION & DOPPLER EFFECTS IN ITEM 15.
3. 1.0 DB PREDTECTION RECORDING LOSS + 3.8 DB NOISY CARRIER & FADING + 1.2 DB SUBCARRIER & DOPPLER.
4. K = 32, RATE 1/2 CONVOLUTIONAL CODING. FRAME DELETION RATE 10^{-2} .

Table 7.6-7B. Telecommunications Design Control Atlas/
Centaur Small Probe, Near Venus Surface

NO.	PARAMETER	NOMINAL VALUE	ADVERSE TOLERANCE	NOTES
1	TOTAL TRANSMITTING POWER (DBM) 20W	+ 43.0	0.8	VOLTAGE & TEMP
2	TRANSMITTING CIRCUIT LOSS (DB)	- 1.0	0.2	NOTE 3
3	TRANSMITTING ANTENNA GAIN (DB) AT $\theta = 55^\circ$	+ 3.0	1.5	$\Delta\theta \pm 0 \text{ DEG}$
4	COMMUNICATIONS RANGE LOSS (DB)	-255.9	0.0	0.43 AU
5	ATMOSPHERIC ABSORPTION & DEFOCUSING LOSSES (DB)	- 0.9	0.1	
6	POLARIZATION LOSS (DB)	- 0.2	0.1	
7	MULTIPATH & OTHER LOSSES (DB)	- SEE NOTE 4 -		
8	RECEIVING ANTENNA GAIN (DB)	+ 61.7	0.4	JPL 810.5
9	RECEIVING CIRCUIT LOSS (DB)	0.0	0.0	JPL 810.5
10	NET LOSS (DB) (2+3+4+5+6+7+8+9)	-193.3	2.3	
11	TOTAL RECEIVED POWER (DBM) (1+10)	-130.3	3.1	
12	RECEIVER NOISE SPECTRAL DENSITY - (DBM/MZ)	-184.0	0.9	$28.5 \pm 6.5^\circ\text{K}$
13	TOTAL RECEIVED POWER/NO (DBM/MZ) (11-12)	+ 33.7	SUM 4.0	
CARRIER TRACKING				
14	CARRIER POWER/TOTAL (DB)	- 5.2	0.5	
15	ADDITIONAL CARRIER LOSSES (DB)	- 1.5	0.2	NOTE 1
16	THRESHOLD TRACKING BANDWIDTH $-28 L_0$ (DB)	+ 10.0	0.8	
17	REQUIRED SNR (DB)	+ 11.0	0.0	
18	PERFORMANCE MARGIN (DB) (13+14+15+16-17)	+ 6.0	SUM 5.5	
DATA CHANNEL				
19	DATA POWER/TOTAL (DB)	- 1.6	0.2	
20	ADDITIONAL DATA CHANNEL LOSSES (DB)	- 6.6	0.5	NOTE 2
21	DATA BIT RATE - BPS (DB)	+ 18.1	0.0	64 BPS
22	THRESHOLD ENERGY PER DATA B'T - E_b/N_0 (DB)	+ 2.2	0.0	NOTE 5
23	PERFORMANCE MARGIN (DB) (13+19+20-21-22)	+ 5.2	SUM 4.7	

- NOTES: 1. 1.0 DB PREDETECTION RECORDING LOSS + 0.5 DB OSCILLATOR & DOPPLER EFFECTS INCLUDED IN ITEM 15.
2. 1.0 DB PREDETECTION RECORDING LOSS + 4.4 DB NOISY CARRIER & FADING + 1.2 DB SUBCARRIER & DOPPLER.
3. INCLUDES 0.4 DB RADOME LOSS.
4. MULTIPATH LOSSES INCLUDED IN ITEMS 15 AND 20.
5. $K = 32$, RATE 1/2 CONVOLUTIONAL CODING. FRAME DELETION RATE 10^{-2} .

Both RSS and a combination of antenna gain plus RSS of the rest of tolerances are shown. Use of these latter criteria for margin has some basis in fact and remains as a possible option in reducing transmitter power by about 3.1 to 2.3 dB respectively.

Transmission periods have been established at entry minus 45 minutes, or sooner, for a period of 10 minutes to affirm that the system is working prior to entry. This is followed by turning on the S-band power amplifier at 50 g increasing plus 10 seconds (9 seconds for small probes) for transmission until end of mission on the planet surface.

Use of the 400 kW transmitter at Goldstone or alternatively the 100 kW transmitter at Canberra to establish the uplink provides good signal-to-noise ratio in the transponder receiver for rapid uplink lock (the receiver has an automatic search capability for rapid acquisition).

Completion of the pre-entry transmission at least 0.5 hour prior to blackout avoids the high Doppler rates immediately prior to entry and allows time to change the DSN transmitter frequency to the best lock uplink frequency estimate for post-entry.

Use of narrowband tracking loops at the DSN limits the on-line downlink lockup operational periods to other than the high Doppler rates prior to parachute deployment. Downlink carrier lockup time is estimated to be 40 seconds after the parachute deployment based on uplink lock being accomplished in less than 10 seconds and initial use of the 30 Hz loop. For the 10 Hz loop this time increases to 139 seconds (see Appendix 7.6L).

The small probe link is a one-way PSK/PM link operating at a bit rate of 64 bps. Transmission periods are scheduled for pre-entry and post-entry as they are for the large probe. Downlink carrier acquisition is expected to be accomplished in less than 100 seconds based on use of the DSN 30 Hz receiver loop for initial acquisition. (This is after high Doppler rates have subsided to <6 Hz/s).

7.6.4.1 Large Probe Hardware, Atlas/Centaur

The preferred Atlas/Centaur large probe communications subsystem consists of an antenna, transponder, a pair of 20 watt power amplifiers coupled with 90-degree hybrids, and a diplexer. (Interconnecting RF cabling is described in the cabling discussion, Section 7.9). A functional block diagram is shown in Figure 7.6-7. Each of the hardware components is described in the following sections. Note that the data train encoding and modulation of the square wave subcarrier are performed by the data handling subsystem; the DSN configuration is discussed in Section 12.

Large Probe Antenna

The conical beam antenna selected for the large probe was described in Appendix 7.6L. Characteristics are given in Table 7.6-8.

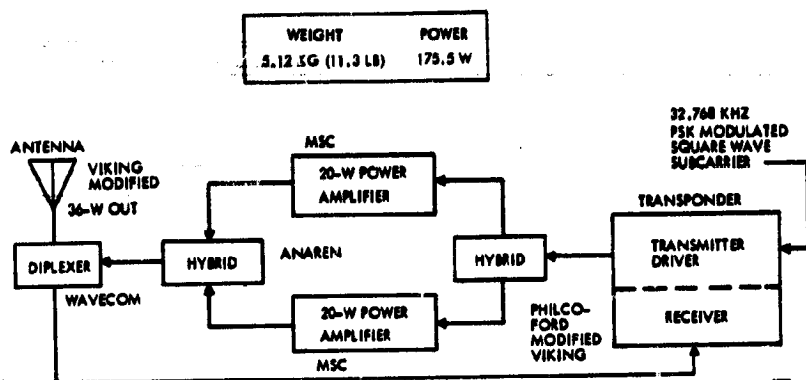


Figure 7.6-7. Atlas/Centaur Two-Way Coherent Communications, Large Probe

Table 7.6-8. Large Probe Antenna Characteristics

ANTENNA TYPE - TURNSTILE OVER A CONICAL CAVITY
PATTERN - CONICAL BEAM, HPBW = 120°
ON-AXIS GAIN - $+ 5.4 \pm .2$ DBI AT 2.1 TO 2.3 CHZ
POLARIZATION - RHCP
MATERIAL - TITANIUM
TEMPERATURE - 766°K
ENVELOPE - 11.5 CM DIA X 5.4 CM
MASS - 0.23 KG
BACK LOBES - 14 DB
POWER CAPABILITY - GREATER THAN 60 W

Atlas/Centaur Large Probe Transponder

The functions of the transponder are to provide a two-way coherent Doppler tracking capability and a probe-to-earth telemetry link directly to the DSN using a $\frac{240}{221}$ transmit-to-receive frequency ratio.

A summary of the characteristics for each of the units, which when operated in a two-way mode comprise a coherent transponder, is given in Tables 7.6-9 and 7.6-10. The receiver is a dual conversion super-heterodyne employing a phase lock carrier-tracking loop designed to search, acquire, and track the uplink frequency both prior to and following the high g entry. Ranging and uplink command channels are eliminated in this design. In the absence of coherent drive from the receiver, an auxiliary oscillator in the transmitter driver provides an output at the nominal transmit frequency. Mechanical design of both units is based on the Viking transponder modular building block construction. Thin and thick film substrates are used in each module. Typical functional block diagrams for the units are shown in Figures 7.6-8 and 7.6-9.

Atlas/Centaur Large Probe Diplexer

The S-band diplexer is required to allow use of a common antenna for transmit and receive and to provide added filtering for the transmitter output.

Table 7.6-9. Receiver Characteristics,
Large Probe

RECEIVING FREQUENCY RANGE	2110 - 2120 MHZ
NOISE FIGURE, MAXIMUM	7.5 DB
INPUT VSWR, MAXIMUM	1.7 TO 1
IMAGE RESPONSE	-60 DB
INPUT SIGNAL RANGE	NOISE TO -30 DBM
ACQUISITION THRESHOLD (15 DB ABOVE 28_{LO} THRESHOLD)	-127 DBM
ACQUISITION SWEEP PERIOD	7 S
LOOP NOISE BW AT THRESHOLD (SNR 0 DB IN 28_{LO})	250 HZ (28_{LO})
STRONG SIGNAL LOOP BANDWIDTH (20 DB ABOVE 28_{LO} SNR)	857 HZ
FREQUENCY OFFSET ACQUISITION AND TRACKING CAPABILITY	± 125 KHZ 4 DEG
STATIC PHASE ERROR, MAXIMUM	200 HZ/S
TRACKING RATE AT ACQUISITION THRESHOLD	100 DB
AGC RANGE	$\pm 10\%$
AGC LINEARITY OVER -150 TO -70 DBM RANGE	23 S
AGC LOOP TIME CONSTANT	$\pm 3/10^5$
VCXO FREQUENCY STABILITY (2 HR)	3 mW \pm 0.5 mW
TRANSMITTER DRIVE LEVEL (AT 27_{REC})	110.5
UNREGULATED POWER REQUIREMENT, 28 VDC	1.5 W
OPERATING TEMPERATURE	247°K TO 338°K
SIZE	2200 CM ³ (135 IN. ³) (a)
MASS	2.0 KG (4.4 LB) (a)

(a) TOTAL WEIGHT & VOLUME WHEN COMBINED WITH THE TRANSMITTER DRIVE SECTION INTO A TRANSPONDER

Table 7.6-10. Transmitter Driver
Characteristics

TRANSMITTER FREQUENCY RANGE	2290-2300 MHZ
POWER OUTPUT, MINIMUM	240 mW
POWER OUTPUT, MAXIMUM	289 mW
SPIRIOUS LEVEL, BELOW OUTPUT FREQUENCY	50 DB DOWN, MIN
OUTPUT VSWR, MAXIMUM	1.5 TO 1
LOAD VSWR, MAXIMUM SAFE	INFINITY
FREQUENCY STABILITY, AUXILIARY OSCILLATOR	± 1 PART 10^6
INITIAL FREQUENCY	± 1.5 PARTS 10^5
LONG-TERM DRIFT, MAXIMUM	± 0.5 PARTS 10^6
SHORT-TERM JITTER, 1.0 S AVG	2 DEG PEAK
VCXO/AUX OSC INTERACTION, MAXIMUM	3 mW \pm 0.5 mW
RF POWER INPUT FROM RECEIVER	
PHASE MODULATOR (TLM) (a)	0.5 RAD/VOLT \pm 5%
MODULATION SENSITIVITY	DC TO 1.0 MHZ
BANDWIDTH	2.0 RADIAN
MAXIMUM CAPABILITY	2.0% MAX
DEVIATION FROM STRAIGHT LINE TO 2.0 RAD	
POWER DISSIPATION, MAXIMUM	4.0 W
UNREGULATED 28 VDC	247°K TO 338°K
OPERATING TEMPERATURE	2200 CM ³ (135 IN. ³) (b)
SIZE	2.0 KG (4.4 LB) (b)
MASS	

(a) PARAMETER VALUES ARE REFERENCED TO THE S-BAND OUTPUT

(b) TOTAL WEIGHT & VOLUME WHEN COMBINED WITH RECEIVER SECTION OF TRANSPONDER

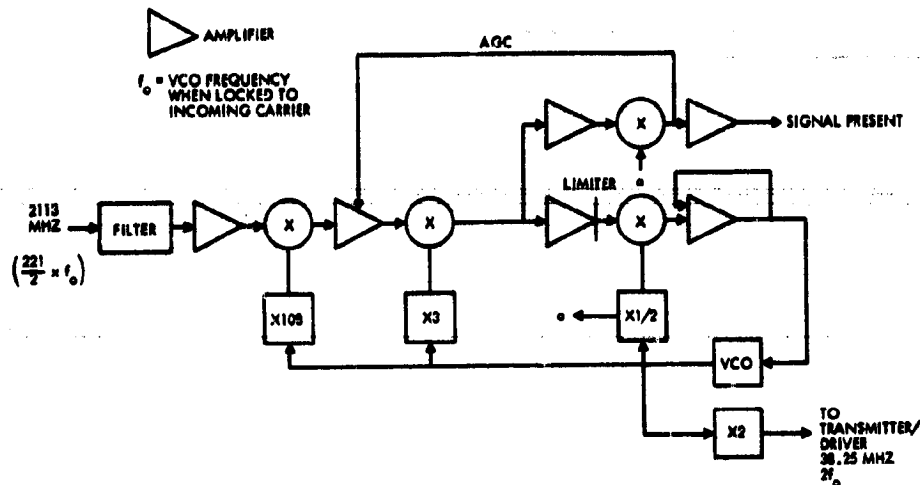


Figure 7.6-8. Functional Diagram S-Band Receiver Portion of Large Probe Transponder

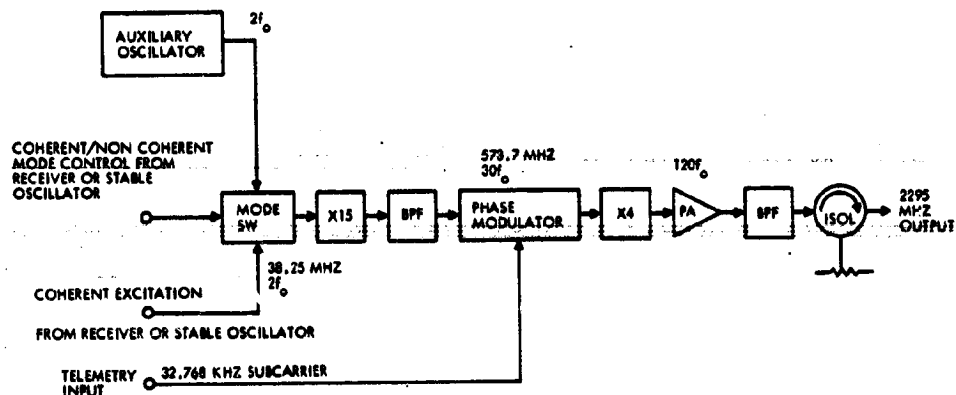


Figure 7.6-9. Functional Diagram S-Band Transmitter/Driver Portion of Large Probe Transponder

The unit is essentially identical to that used on the Pioneer 10 and 11 spacecraft. Its major characteristics are shown in Table 7.6-11.

Special features, if any, required for this unit are related to meeting the high g planet entry environment since the unit will handle the 36 watts for Pioneer Venus (Pioneer 10 and 11 power was approximately 8 watts).

Table 7.6-11. S-Band Diplexer Assembly Characteristics

PARAMETER	SPECIFICATION REQUIREMENT
RECEIVER CHANNEL:	
CENTER FREQUENCY	2115 \pm 5 MHZ TYPICAL
PASSBAND BANDWIDTH	10 MHZ MIN
PASSBAND INSERTION LOSS	0.75 DB MAX
PASSBAND VSWR	1.15:1 MAX
STOPBAND INSERTION LOSS	
1500 TO 2000 MHZ	65 DB MIN
2287 TO 2297 MHZ	85 DB MIN
2350 TO 3000 MHZ	65 DB MIN
TRANSMITTER CHANNEL:	
RF POWER HANDLING	40 W
CENTER FREQUENCY	2295 \pm 5 MHZ TYPICAL
PASSBAND BANDWIDTH	10 MHZ MIN
PASSBAND INSERTION LOSS	0.5 DB MAX
PASSBAND VSWR	1.15:1 MAX
STOPBAND INSERTION LOSS	
1500 TO 2000 MHZ	65 DB MIN
2110 TO 2120 MHZ	85 DB MIN
2550 TO 3000 MHZ	55 DB MIN
ISOLATION BETWEEN CHANNELS	
1500 TO 2000 MHZ	65 DB MIN
2106 TO 2116 MHZ	85 DB MIN
2290 TO 2300 MHZ	85 DB MIN
2350 TO 3000 MHZ	65 DB MIN

Baseline Atlas/Centaur Large Probe Power Amplifier

The large probe power amplifier selected for this program is an all transistorized microwave integrated circuit (MIC) power amplifier using hermetically sealed MSC 3005 transistors and alumina microstrip matching networks. The higher gain, more efficient 4005 transistors may eventually replace the 3005 units for this application when more history on these transistors is available. Networks are combined for efficient paralleling of output transistors in each amplifier. Major characteristics of the power amplifier are given in Table 7.6-12.

Table 7.6-12. 20 Watt S-Band Power Amplifier

FREQUENCY	2290 TO 2300 MHZ
POWER OUTPUT (MINIMUM)	20 W 255°K TO 311°K 18.2 W 311°K TO 339°K
BANDWIDTH	10 MHZ
PASSBAND OUTPUT RIPP L	0.2 DB
EFFICIENCY	24%
INPUT VOLTAGE	28 V \pm 10%
INPUT IMPEDENCE	50 OHMS
LOAD IMPEDENCE	50 OHMS
DRIVE POWER	135 TO 195 mW
INPUT VSWR	1.5 TO 1
HARMONICS	45 DB DOWN
OUTPUT STOP BAND (DSM RECEIVE FREQUENCIES)	60 DB DOWN
TEMPERATURE (OPERATING)	225°K TO 341°K (CASE)
OTHER ENVIRONMENT	MISSION LEVELS
SIZE	328 CM ³ (20 IN. ³)
MASS (NOT INCLUDING EXTERNAL HEAT SINKS)	0.91 KG (2 LB)

Two of these 20-watt units are paralleled by two 90-degree strip line hybrid couplers to provide a nominal output of 36 watts. Phase change material will be used to control the base plate temperature of these units.

7.6.4.2 Small Probe Hardware, Atlas/Centaur

The preferred small probe communications subsystem consists of a transmitter-driver, 20 watt S-band power amplifier, antenna, and a separate external stable oscillator. (Interconnecting RF cabling is described in the cabling discussion, Section 7.9). A functional diagram of the subsystem is shown in Figure 7.6-10. Each of the above RF components is described in the following sections. The DSN configuration is discussed in Section 12.

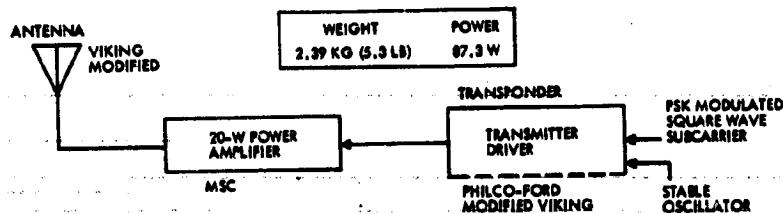


Figure 7.6-10. Atlas/Centaur One-Way Coherent Communications, Small Probes

As a subsystem the small probe communications equipment provides a one-way link directly between each small probe and the DSN at a fixed data rate of 64 bps during a 10-minute pre-entry transmission period beginning 60 minutes or more before entry, and again during the descent phase beginning a few seconds after entry, and ending after the probe impacts on the surface.

Error control encoding of the PCM data stream and PSK modulation of the 32.768 kHz subcarrier are accomplished by the small probe data handling subsystem.

Small Probe Antenna

The Atlas/Centaur small probe antenna is identical in design to the large probe antenna.

Small Probe Transmitter Driver, Atlas/Centaur

The small probe transmitter driver has the identical electrical characteristics of the transmitter driver portion of the large probe transponder, except that the output drive power is reduced to drive a single

20-watt power amplifier and the input frequency is supplied from an external stable oscillator rather than the receiver. Size and weight are given in the subsystem size, weight, and power table at the end of this section--Table 7.6-14.

Small Probe S-Band Power Amplifier, Atlas/Centaur

The small probe power amplifier is the same as one of the two identical 20-watt units used for the large probe.

Small Probe Stable Oscillator - A stable oscillator is required for the one-way links of the small probes to keep DSN signal acquisition times to a minimum and to provide good short-term stability and minimize error in range rate measurements.

Typical characteristics for this oscillator are shown in Table 7.6-13. Possible sources have been previously enumerated; however, in any case, some development work on this item remains in addition to that of the Applied Physics Laboratory of The Johns Hopkins University, which is currently under contract to NASA.

Table 7.6-13. Stable Oscillator Characteristics
(Small Probe)

FREQUENCY RANGE	38.0 TO 78.4 MHZ
POWER OUTPUT	3 mW + 1.2 mW
SPURIOUS OUTPUT	50 DB DOWN, MINIMUM
OUTPUT VSWR	1.5:1 MAXIMUM
FREQUENCY STABILITY	
INITIAL FREQUENCY	± 1 PART IN 10 ⁶
LONG TERM DRIFT, MAXIMUM (2 HR)	± 4 PARTS IN 10 ⁷
SHORT TERM STABILITY (0.1 S AVERAGING TIME)	± 3 PARTS IN 10 ¹¹
TEMPERATURE RANGE	247°K TO 338°K
POWER DISSIPATION MAXIMUM	300 mW
UNREGULATED 28 VDC ± 10%	(1 W OF HEATER POWER MAY BE USED FOR 1 HOUR INTERMITTENTLY)
MASS, MAXIMUM	0.341 KG (3/4 LB)
SIZE, MAXIMUM	7-CM-DIA SPHERE (OR EQUIVALENT VOLUME)
OUTPUT MONITOR	PROVIDE BILEVEL INDICATION OF POWER OUTPUT TO CONTROL TRANSMITTER DRIVER SOURCE

Small Probe Size, Weight, and Power Tables for Atlas/Centaur

The size, weight, and power for the Atlas/Centaur large and small probe communication subsystem are given in Table 7.6-14.

Table 7.6-14. Atlas/Centaur Probe Communications Weight, Power, and Volume

	LARGE PROBE			SMALL PROBE		
	MASS (KG) (LB)	POWER (W)	VOLUME (CM ³) (IN ³)	MASS (KG) (LB)	POWER (W)	VOLUME (CM ³) (IN ³)
RECEIVER	2.0 (4.4)	5.5	2200 (135)	--	--	--
TRANSMITTER/DRIVER	COMBINED			0.91 (2.0)	4.0	920 (56)
S-BAND POWER AMPLIFIER	1.8 (a) (4.0)	170.0	656 (40)	0.91 (2.0)	83.0	328 (20)
ANTENNA	0.23 (0.5)		11.5 CM DIA BY 5.4 CM HIGH	0.23 (0.5)		11.5 CM DIA BY 5.4 CM HIGH
HYBRID COUPLERS (2 TOTAL) (b)	0.18 (0.4)		32.8			
DIPLEXER	0.91 (2.0)		103.9			
STABLE OSCILLATOR	--	175.5	--	0.34 (0.8)	0.3	
TOTAL ATLAS/CENTAUR	5.12 (11.3)			2.39 (5.3)	87.3	
TOTAL THOR/DELTA (SEE TABLE 7.6-15)	3.6 (7.9)	95.5		1.37 (3.0)	46.3	
(a) SUM OF TWO POWER AMPLIFIERS						
(b) USED TO PARALLEL TWO S-BAND POWER AMPLIFIERS						

7.6.5 Preferred Subsystem Description, Thor/Delta

The preferred communications subsystems for the Thor/Delta mission are based on a 1977 arrival date as compared to 1978 for the Atlas/Centaur configuration and are designed for the Version III science payload.

These subsystems operate in the same manner as those for the Atlas/Centaur probes using the same modulation and tracking techniques. However, the convolutional coding constraint length is reduced to $K = 8$ for use of Viterbi decoding and the rate is reduced to $1/3$ instead of $1/2$ as used in the Atlas/Centaur configuration. This decision was based on Version III conclusions that a Viterbi, rate $1/3$, decoding capability would be available at the DSN and that this decoding approach would be less costly and show better performance under fading conditions. Bit rate for the large probe is switched from 102.4 to 85.3 bps at an altitude of 30 km as opposed to a constant bit rate for the Atlas/Centaur large probe.

A complete set of telecommunications design control tables for the Thor/Delta large and small probes is given in Appendix 7.6H along with detail justification for most parameters. However, a table (Table 7.6-15) is provided here for the large and small probes at an altitude near the planet surface.

Additional carrier and data channel losses including fading for a Rician channel, are used for Version III science prior to Version IV. The lognormal channel model has been used for Version IV links. For a comparison of Rician and lognormal channels, see Appendix 7.6C.

Table 7.6-15. Thor/Delta Link Analysis, Large and Small Probes

1 KM ABOVE SURFACE		LARGE	SMALL		
TRANSMITTER POWER (W-MIN)		20	9.1		
BIT RATE (BPS)		85.3	10		
		LARGE PROBE		SMALL PROBE	
NO.	PARAMETER	NOMINAL	ADVERSE	NOMINAL	ADVERSE
1	TOTAL TRANSMITTING POWER (DBW)	+ 13.4	-0.4	+ 10.0	-0.4
2	TRANSMITTING CIRCUIT LOSS (DB)	- 2.0	-0.2	- 1.0	-0.2
3	TRANSMITTING ANTENNA GAIN (DB)	+ 3.5	-1.2	+ 3.0	-1.2
4	COMMUNICATIONS RANGE LOSS (DB)	-236.78	0	-236.8	0
5	ATMOSPHERIC ABSORPTION & DEFOCUSING LOSSES (DB)	- 0.89	-0.11	- 0.9	-0.1
6	POLARIZATION LOSS (DB)	- 0.26	-0.1	- 0.2	-0.1
7	MULTIPATH & OTHER LOSSES (DB)	SEE NOTES		SEE NOTES	
8	RECEIVING ANTENNA GAIN (DB)	+ 61.70	-0.4	+ 61.7	-0.4
9	RECEIVING CIRCUIT LOSS (DB)	0	0	0	0
10	NET LOSS (DB) (2+3+4+5+6+7+8+9)	-194.67	-2.01	-194.2	-2.0
11	TOTAL RECEIVED POWER (DBW) (1+10)	-181.27	-2.41	-184.2	-2.4
12	RECEIVER NOISE SPECTRAL DENSITY - (DBW/HZ)	-214.30	+1.0	-214.5	+1.0
13	TOTAL RECEIVED POWER/NO (DBW · HZ) (11-12)	+ 33.73	-3.41	+ 30.3	-3.4
CARRIER TRACKING					
14	CARRIER POWER/TOTAL (DB)	- 4.72	-0.4	- 1.6	-0.2
15	ADDITIONAL CARRIER LOSSES (DB)	- 0.7	-0.2	- 0.6	-0.4
16	THRESHOLD TRACKING BANDWIDTH - $2B_{LO}$ (DB)	+ 10.0	-0.8	+ 10.0	-0.8
17	THRESHOLD SNR (DB)	+ 13.0	0	+ 11.0	0
18	PERFORMANCE MARGIN (DB) (13+14+15-16-17)	+ 4.81	-4.81	+ 7.1	-4.8
DATA CHANNEL					
19	DATA POWER/TOTAL (DB)	- 1.76	-0.2	- 5.1	-0.5
20	ADDITIONAL DATA CHANNEL LOSSES (DB)	- 5.25	-0.5	- 5.6	-0.8
21	DATA BIT RATE - BPS (DB)	+ 19.3	0	+ 10.0	0
22	THRESHOLD ENERGY PER DATA BIT - E_b/N_0 (DB)	+ 2.5	0	+ 2.5	0
23	PERFORMANCE MARGIN (DB) (13+19+20-21-22)	+ 4.42	-4.11	+ 7.1	-4.7
1. MULTIPATH LOSSES ITEM 7 ARE INCLUDED IN ITEMS 15 & 20.		LARGE PROBE		SMALL PROBE	
2. $K = 6$, RATE 1/3 CONVOLUTIONAL VITERBI SOFT DECISION DECODING.		SUM	RSS	SUM	RSS
		S/NO. CARRIER	3.41 1.68	S/NO. CARRIER	3.4 1.68
		DATA	4.81 1.91	DATA	4.8 1.91

Note that the margins equal or exceed the sum of the adverse tolerances, which were the criteria used in the link designs.

7.6.5.1 Large Probe Hardware, Thor/Delta

The preferred Thor/Delta large probe communications subsystem consists of an antenna, receiver, transmitter-driver, 20-watt S-band power amplifier, and a diplexer. (Interconnecting RF cabling is described in the cabling discussion, Section 7.9). A functional subsystem block diagram is shown in Figure 7.6-11. Each of the hardware components is described in the following sections. The DSN configuration is discussed in Section 12.0. Convolutional encoding of the PCM data stream and PSK modulation of the 16.384 kHz subcarrier are accomplished in the data handling subsystem. Size, weight, and power for the subsystem are contained in Table 7.6-16.

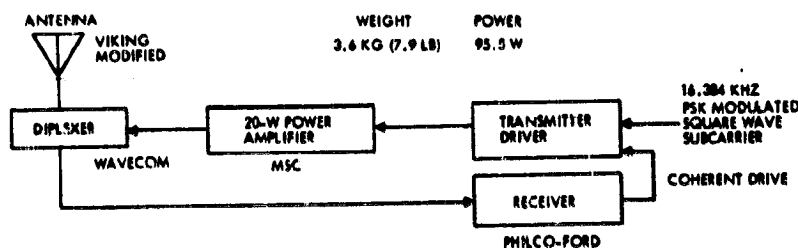


Figure 7.6-11. Thor/Delta Two-Way Coherent Communications, Large Probe

Table 7.6-16. Thor/Delta Probe Communications Weight, Power, and Volume

	LARGE PROBE			SMALL PROBE		
	MASS (KG) (LB)	POWER (W)	VOLUME (CM ³)	MASS (KG) (LB)	POWER (W)	VOLUME (CM ³)
RECEIVER	0.96 (2.1)	1.5	785	--	--	--
TRANSMITTER/DRIVER	0.64 (1.4)	4.0	523	0.64 (1.4)	4.0	523
S-BAND POWER AMPLIFIER	0.91 (2.0)	90.0	193	0.5 (1.1)	42.3	129.5
ANTENNA	0.23 (0.5)		11.5 CM DIA BY 5.4 CM HIGH	0.23 (0.5)		11.5 CM DIA BY 5.4 CM HIGH
DIPLEXER	0.86 (1.9)		1039			
TOTAL THOR/DELTA	3.6 (7.9)	95.5		1.37 (3.0)	46.3	
TOTAL ATLAS/CENTAUR (SEE TABLE 7.6-14)	5.12 (11.3)	175.5		2.39 (5.3)	87.3	

NOTE: STABLE OSCILLATOR IN THOR/DELTA SMALL PROBE IS PART OF SCIENCE PAYLOAD AND NOT SHOWN HERE

Large Probe Antenna

The large probe antenna design is identical to that of the Atlas/Centaur large probe antenna described in Section 7.6.4.1, and is also identical to the Thor/Delta small probe antenna.

Large Probe Receiver and Transmitter/Driver

The functions of the receiver and transmitter driver are to provide a two-way coherent Doppler tracking capability and a probe-to-earth telemetry link directly to the DSN using a $\frac{240}{221}$ transmit-to-receive frequency ratio. A summary of the characteristics for each of the units except for size and weight, which when operated in a two-way mode makes up a coherent transponder, is given in Table 7.6-9 and 7.6-10.

The receiver is a dual-conversion superheterodyne unit employing a phase lock carrier-tracking loop designed to search, acquire, and track the uplink frequency before and following the high gentry. Ranging and uplink command channels are eliminated in this design. In the absence of coherent drive from the receiver, an auxiliary oscillator in the transmitter driver provides an output at the nominal transmit frequency. Mechanical design of both units is based on Viking and Skynet II transponder modular building block construction. Thin and thick film substrates are used in each module. Typical functional block diagrams for the two units are the same as for the Atlas/Centaur, Figures 7.6-8 and 7.6-9.

Large Probe Diplexer

The large probe diplexer is identical to the unit described previously for the Atlas/Centaur configuration (see Section 7.6.4.1 and Table 7.6-11).

Large Probe Power Amplifier

The large probe power amplifier is identical to the single 20-watt unit described for the Atlas/Centaur small probe which in turn is identical to the basic 20-watt unit identified in Table 7.6-12. (Two of these are paralleled for the Atlas/Centaur large probe).

7.6.5.2 Small Probe Hardware, Thor/Delta

The Thor/Delta small probe communications subsystem consists of a transmitter-driver, 10-watt S-band power amplifier, antenna, and a separate external stable oscillator. (Interconnecting RF cabling is described in the cabling discussion, Section 7.9). A functional diagram of the subsystem is shown in Figure 7.6-12. Each of the above RF components is described below.

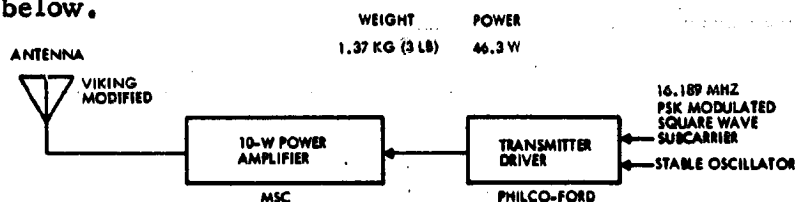


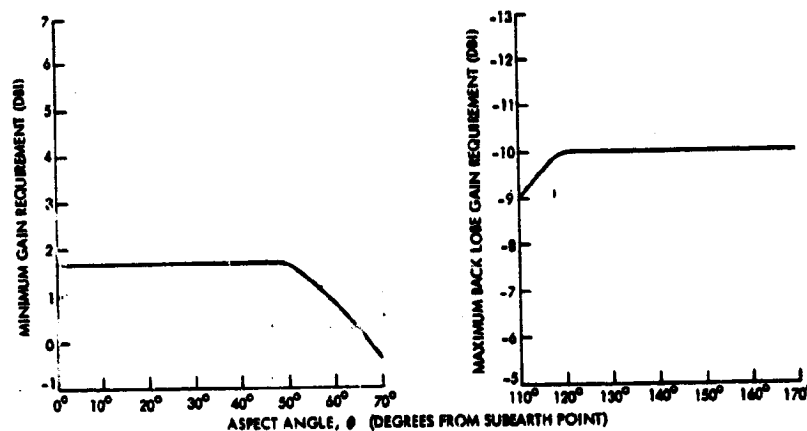
Figure 7.6-12. Thor/Delta One-Way Coherent Communications,
Small Probe

The small probe antenna and transmitter driver are identical to the large probe units. The stable oscillator is identical to the Atlas/Centaur unit described in Section 7.6.4.2. The only remaining unit, the 10-watt power amplifier is identical to the large probe power amplifier with the following exceptions: (1) weight is reduced to 0.5 kg (1.1 lb); (2) output power is 9.1 watts minimum for a temperature range of -48°C to $+38^{\circ}\text{C}$ and 8.3 watts minimum for the temperature range of $+38^{\circ}\text{C}$ to $+66^{\circ}\text{C}$.

7.6.6 Supporting Analyses and Tests

Antenna Performance Test - A test program was conducted to investigate the perturbations on the radiated antenna pattern resulting from the mounting arrangement on the aft body (basecover) of the Thor/Delta large probe. A full-scale mockup of the aft body of the Thor/Delta large probe was built and the proposed Pioneer Venus antenna (turnstile/cone) was mounted and tested. A summary of the test configurations and antenna patterns is shown in Appendix 7.6J.

As a result of the testing, it was determined that the antenna pattern was critically degraded by the presence of a large open cavity directly under the antenna. The antenna's half power beam width (HPBW) was reduced from approximately 100 degrees (free space) to approximately 60 degrees and the ripple increased 6.8 dB. The solution to the problem was a metal screen or plate placed over the cavity and around the parachute canister. The resulting antenna patterns meet the gain and ripple requirements shown in Figure 7.2-13.



THE PROBES WILL BE SPINNING, THEREFORE THE COMMUNICATION COVERAGE WILL BE SYMMETRICAL ABOUT THE PROBE SPIN AXIS (0 DEGREE). GAIN VARIATION (PATTERN RIPPLE) OVER THE ± 70 DEGREE VIEWING ANGLE SHALL NOT EXCEED 4 DB. THE MINIMUM GAIN REQUIREMENT AND MAXIMUM BACK LOBE REQUIREMENT ARE AS SHOWN ABOVE.

Figure 7.6-13. Antenna Gain Requirements

The information obtained during Thor/Delta configuration testing is currently being incorporated in the Atlas/Centaur large and small probe configurations. An Atlas/Centaur antenna test program, for both large and small probes, is currently under way and will be completed before the next program phase. Preliminary results show that the small probe antenna and afterbody configuration is compatible, whereas mounting a parachute container above the large probe antenna creates problems. This latter problem can be corrected by raising the antenna on a pedestal and mounting the parachute in a pack partially surrounding the antenna pedestal.

7.7 Data Handling and
Command

7.7 DATA HANDLING AND COMMAND

7.7.1 Introduction and Summary

The data handling and command subsystem supplies timing and commands to the scientific instruments and the other subsystems, acquires data from these instruments and subsystems, quantizes and arranges these data into the desired format, and codes and processes the data into a form suitable for modulating the RF downlink. In addition, memory is provided to store information during periods of RF blackout and to buffer high speed data bursts from the scientific instruments. The data handling subsystem and its functional interfaces are depicted in Figure 7.7-1.

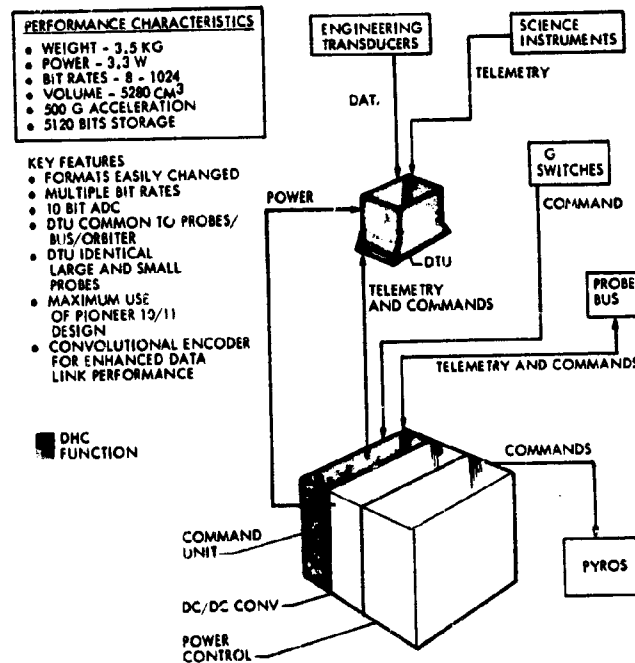


Figure 7.7-1. Data Handling and Command (DHC) Subsystem Boundaries

During the Phase B study, preferred subsystem approaches were synthesized for the Thor/Delta and the Atlas/Centaur launch vehicles. In general the requirements and interfaces were identical for both launch vehicle designs. However, the weight limitations of the Thor/Delta configuration severely constrained design and packaging while the Atlas/Centaur design realized additional cost savings at the expense of increased weight.

A survey of candidate data handling equipment, including new light-weight designs as well as existing flight-qualified units, was conducted. A summary of the trade parameters for the off-the-shelf equipment is given in Table 7.7-1. None of the existing units contained the flexibility to fulfill the Pioneer Venus mission requirements without modifications. In addition, all units were too large and required too much power for use on the Thor/Delta configuration.

Table 7.7-1. Potential DHC Subsystem Survey Results

SYSTEM	VOLUME (CC)	MASS (KG)	POWER (W)	CHANNELS SAMPLED	GENERAL
THOR/DELTA (PIONEER VENUS)	2 360	6.1	3	256	NEW DESIGN 10-BIT ADC
MVM '73	20 500	77.0	35	?	
PIONEER 10 & 11	7 300	15.0	3.8	290	6-BIT ADC NEW PROGRAMMER NEW MEMORY
VIKING DAPU	9 100	10.5	6	246	8-BIT ADC NEW PROGRAMMER NEW MEMORY
OSO	5 700	16.5	9	132	8-BIT ADC NEW PROGRAMMER NEW MEMORY

The preferred Atlas/Centaur DHC subsystem design for the probes uses a modified Pioneer 10/11 Digital Telemetry Unit (DTU) to perform the data handling functions. The circuit design modifications to the existing printed wiring boards are identical to those required by the probe bus and orbiter. Significant cost savings accrue from the common usage of this design for all mission applications. Circuit boards which are devoted exclusively to probe and orbiter functions will be removed and the probe package size reduced accordingly. Both large and small probes use the identical DTU configuration which simplifies spares provisioning.

The command functions are performed by the command unit which is packaged in a compartment of the power control unit (PCU). Included in this unit are the coast timer, descent timer, discrete events format generator and memory unit. The command unit provides all power transfer, pyro firing, bit rate, format change, and memory mode select commands. Information defining the sequence and time at which each command signal is initiated is stored in read-only-memories (ROM) and is readily changeable by replacement of a few parts. The command requirements are all derived requirements needed to implement the science and engineering

mission requirements. The large probe derived command requirements are given in Figure 7.7-13. The small probe requirements are similar, but more limited in number.

The system functional block diagram is given in Figure 7.7-1. A detailed discussion of the preferred Atlas/Centaur configuration is given in paragraph 7.7.4.

Subsequent paragraphs of this section describe the requirements, the trades and analyses, and define the preferred configurations. Unless otherwise specified, the Atlas/Centaur launch vehicle configuration and Version IV (April 1973) science payload definition is described.

7.7.2 Requirements

Several categories of requirements were imposed on the data handling and command subsystem. Those requirements associated with timing determination are derived from error budget allocations with the other subsystems. The number and type of engineering measurements and data inputs are taken from the compiled telemetry lists. Downlink coding requirements are set in inter-subsystem tradeoffs and format and coding constraints are imposed by the deep space network (DSN) capability. Since science and engineering telemetry requirements are not firm, we allocated a reasonable amount of growth commensurate with the program cost constraints. The resultant conceptual designs are adequate, however, to permit subsystem tradeoffs and sizing. The principal functional requirements are examined below.

7.7.2.1 Large Probe Requirements Analysis

The data handling subsystem acquires engineering data for subsequent telemetry. The engineering analog measurements will be quantized to at least 64 levels (6 bits). Science analog housekeeping will be quantized to 7, 8, or 10 bits as required. A telemetry list summary gives the measurement requirements shown in Table 7.7-2.

The scientific data acquisition requirements for terminal descent are given in Table 7.7-3. The quantization levels are defined in the science requirements document as "bit size." The 7-, 8-, and 10-bit words require the words to be quantized to 128, 256, and 1024 level, respectively.

Table 7.7-2. Large Probe Engineering Measurements Summary

Measurement	Analog	Bilevel	Digital
Electrical Power & Pyrotechnics	6	7	0
Data Handling	3	15	11
Communications	19	1	0
Thermal	11	0	0
Science	<u>6</u>	<u>1</u>	<u>0</u>
Total Required	45	24	11

Table 7.7-3. Large Probe Terminal Descent (Nominal) Experiment Data Sampling Requirement

INSTRUMENT	MEASUREMENT			MINIMUM SAMPLING INTERVAL	
	DESCRIPTION	ANALOG, BILEVEL, DIGITAL	SIZE (BITS)	ALTITUDE (M.)	TIME (S)
TEMPERATURE	ATM TEMP THERMISTOR	A	10	200	NA
		A	7	NA	140
PRESSURE	ATM PRESSURE THERMISTOR	A	10	200	NA
		A	7	NA	140
ACCELERATION (SEE NOTE a)	TURBULENCE	A	7	100	NA
	AXIAL	A	10	NA	20
	AXIAL B.U.	A	10	NA	20
	LATERAL	A	10	NA	10
	LATERAL THERMISTOR	A	10	NA	40
		A	7	NA	140
HYGROMETER	HUMIDITY RANGE	A	10	300 (b)	NA
	RANGE	B	1	500 (b)	NA
	HOUSEKEEPING	A	10	1 PER EVERY 10 HUMIDITY MEASUREMENTS	NA
PARTICLE SIZE SPECTROMETER	SCIENCE AND HOUSEKEEPING	D	240	200	NA
SOLAR RADIOMETER	SCIENCE AND HOUSEKEEPING	D	240 (c) 72 (d)	750	NA
IR FLUX	SCIENCE AND HOUSEKEEPING	D	100	750	NA
WIND-ALTITUDE RADAR	SCIENCE	D	37	NA	20
	VOLTAGE	A	7	NA	60
	TEMPERATURE	A	7	NA	60
MASS SPECTROMETER	SEE "SPECIAL SAMPLING REQUIREMENTS"				
GAS CHROMATOGRAPH	SEE "SPECIAL SAMPLING REQUIREMENTS"				
(a) A TOTAL OF 1000 BITS OF DATA RECORDED DURING ENTRY ARE TO BE READ OUT DURING THE PROBE DESCENT					
(b) NO MEASUREMENTS REQUIRED BELOW 44 KM					
(c) 66 KM TO 44 KM					
(d) 44 KM TO THE SURFACE					
SPECIAL SAMPLING REQUIREMENTS					
MASS SPECTROMETER - A MINIMUM OF 80 000 BITS OF DATA WILL BE GENERATED BETWEEN 66 KM AND 44 KM. THESE DATA ARE TO BE SAMPLED AT ONE CONSTANT RATE. DATA READOUT ABOVE 66 KM SHALL BE SAMPLED AT THIS SAME RATE. THE NUMBER OF BITS PER COMPLETE MEASUREMENT WILL VARY. HOWEVER, ALL FORMATTING IS DONE WITHIN THE INSTRUMENT.					
FROM 44 KM TO THE SURFACE A MINIMUM OF 80 000 BITS ARE GENERATED. THESE DATA ARE TO BE SAMPLED AT A CONSTANT RATE.					
GAS CHROMATOGRAPH - THIS INSTRUMENT WILL MAKE ONE MEASUREMENT EVERY 20 MINUTES REGARDLESS OF ALTITUDE INTERVAL. DURING THE FIRST 10 MINUTES, THE INSTRUMENT WILL GENERATE AND STORE 13 200 BITS IN A BUFFER MEMORY. NO DATA ARE TO BE READ OUT BY THE PROBE DURING THIS PERIOD. DURING THE LAST 10 MINUTES THE INSTRUMENT IS NOT IN A MEASUREMENT TAKING MODE. IT IS REQUIRED THAT THE 13 200 BITS BE READ OUT BY THE SPACECRAFT DURING THIS TIME.					

Except for the accelerometer, all data will be acquired after the probe enters the atmosphere. Only the accelerometers are on during blackout (high g entry); all others are turned on during terminal descent.

Other candidate instruments are given in Table 7.7-4. The memory size and the number of data channels could be significantly impacted if these instruments are included.

Table 7.7-4. Large Probe Terminal Descent (Other Candidate)
Experiment Data Sampling Requirements

INSTRUMENT	MEASUREMENT			MINIMUM SAMPLING INTERVAL	
	DESCRIPTION	ANALOG OR DIGITAL	SIZE (BITS)	ALTITUDE (M)	TIME (S)
X-RAY FLUORESCENCE	SCIENCE	D	2560	NA	300
	HOUSEKEEPING	A	8	NA	100
	HOUSEKEEPING	A	8	NA	100
	HOUSEKEEPING	A	8	NA	100
ATR SPECTROMETER	SCIENCE AND HOUSEKEEPING	D	3600	NA	100
AUREOLE DETECTOR	SCIENCE AND HOUSEKEEPING	D	400	500	NA
SHOCK LAYER RADIOMETER	SCIENCE AND HOUSEKEEPING	17 ANALOG	84 TOTAL BITS PER SCAN	NA (a)	NA
(a) A TOTAL OF 3360 BITS OF DATA RECORDED DURING ENTRY ARE TO BE READ OUT DURING THE PROBE DESCENT					

The data handling subsystem provides the probe timing source. The timing requirement is paced by the subcarrier frequency and stability necessary for the telemetry downlink. The frequency should be synchronized and in phase with the telemetry data at all bit rates, and must be compatible with the ground stations (DSN). The resultant characteristics, which are compatible with Pioneer 10 and 11, design are:

Frequency	32.768 kHz \pm 0.02%
Jitter	0.5% between any two cycles
Stability	200 ppm long term

This source provides a number of timing signals to the instruments and other subsystems; however, very few have been specifically defined by the users.

To improve the RF downlink communication efficiency, we recommend data coding. The selected coding, together with format design must be compatible with the DSN.

The data handling subsystem should be capable of relaying probe data to the probe bus during preseparation checkout for transmission to ground via the probe bus telemetry link.

7.7.2.2 Small Probe Requirements Analysis

The engineering data acquisition requirements are summarized in Table 7.7-5

Table 7.7-5. Small Probe Engineering Measurements Summary

Measurement	Analog	Bilevel	Digital
Electrical Power	3	5	0
Data Handling	3	15	11
Communication	6	0	1
Thermal	10	0	0
Science	<u>3</u>	<u>0</u>	<u>3</u>
Total	25	20	15

The scientific data acquisition requirements for terminal descent are given in Table 7.7-6. Only the accelerometer is required to be on prior to and during entry. The data are to be quantized to 64, 128, and 1024 levels respectively for the 6, 7, and 10 bit words lengths. Additional housekeeping data are anticipated, but not yet defined.

Table 7.7-6. Small Probe Terminal Descent (Nominal) Experiment Data Sampling Requirement

INSTRUMENT	MEASUREMENT			MINIMUM SAMPLING INTERVAL	
	DESCRIPTION	ANALOG OR DIGITAL	SIZE (BITS)	ALTITUDE (M)	TIME (S)
TEMPERATURE	ATM TEMP THERMISTOR	A	10	200	NA
		A	7	NA	140
PRESSURE	ATM PRESS THERMISTOR	A	10	200	NA
		A	7	NA	140
ACCELEROMETER (SEE NOTE a)	TURBULENCE	A	7	100	NA
	AXIAL	A	10	NA	20
	THERMISTOR	A	7	NA	140
NEPHELOMETER	SCIENCE CALIBRATION	D	43	200	NA
		D	10	NA	900
FLUX RADIOMETER	NET FLUX	D	8	NA	30
	DETECTOR TEMP	D	8	NA	60
	WINDOW TEMP	D	8	NA	60
(a) A TOTAL OF 250 BITS OF DATA RECORDED DURING ENTRY ARE TO BE READ OUT DURING THE PROBE DESCENT					

Other candidate instruments are shown in Table 7.7-7. No significant impact on data channels, bit rate, or memory size would result from their inclusion.

Table 7.7-7. Small Probe Terminal Descent (Other Candidate)
Experiment Data Sampling Requirements

INSTRUMENT	MEASUREMENT			MINIMUM SAMPLING INTERVAL	
	DESCRIPTION	ANALOG OR DIGITAL	SIZE (BITS)	ALTITUDE (M)	TIME (S)
RF ALTIMETER (SEE NOTE a)	SCIENCE AND HOUSEKEEPING	D	10	NA	10
MAGNETOMETER (SEE NOTE b)	SCIENCE AND HOUSEKEEPING	D	40	NA	24
(a) INSTRUMENT TO OPERATE FROM ~50 KM TO THE SURFACE					
(b) A TOTAL OF 1200 BITS OF DATA RECORDED DURING ENTRY ARE TO BE READ OUT DURING THE PROBE DESCENT					

7.7.2.3 Probe/Bus Interface Requirements Analysis

The probe/bus interface requirements are derived from the prelaunch and preseparation test requirements. To minimize hardware change in the bus the same interface identified for the Pioneer 10/11 command interface configuration has been used, i. e., the three input lines are (1) command data; (2) command clock; and (3) execute. The output lines are (1) data; (2) clock; and (3) enable.

The circuits used are standard 5400 series logic buffers and Schmitt triggers for transmitters and receivers respectively.

The command word is composed of two 8-bit words received from the EGSE or bus. The first eight bits are used to set the "events counter" (see Figure 7.7-15) to a state that will decode to provide the command or sequence of events that is desired. The first bit of the second word is used to inhibit the counter so prevent any other events in the sequence. The last seven bits are spares.

The hardware required for the interface circuitry is minimized by using the descent timer circuitry to do all the decoding necessary for the command word to perform a command function. Any command not desired for the normal descent function can be driven by the bits presently identified as spares.

7.7.3 Trades

We conducted several trade studies during the study period. They were:

- 1) Probe data storage requirements;
- 2) Probe multiplexer and A/D converter requirements;
- 3) Probe digital interface;
- 4) Small probe 'blackout' memory feasibility;
- 5) Probe multiple and nonbinary bit rate;
- 6) Synchronization and time reference word minimization;
- 7) Probe/processor/programmer analysis;
- 8) Large probe data/descent rate;
- 9) Probe data system preliminary design.

Some of the studies are discussed together because of the overlapping content. The preferred design reflects the results of the studies as applied to fulfilling the Version IV science requirements.

Since the power and weight constraint differences were significant between the Thor/Delta and Atlas/Centaur systems, different trade study results were reached in some cases.

7.7.3.1 Probe Data Storage Requirements (for Blackout)

This task is concerned with storing sufficient data to fill the scientific information gaps caused by the periods of RF blackout when no data can be successfully transmitted. In addition to the blackout periods, we considered these periods of time before and after blackout when high Doppler rates exist or DSN lock up is questionable.

For the Thor/Delta system, probe angle of entry, Doppler rates, descent velocity, and spare transmission capability for later transmission of stored data were considered. Only the November and December 1972 science definitions were studied, since the Atlas/Centaur decision preceded the April 1973 requirements issuance.

For the Atlas/Centaur system, and the Version IV science definition, a specific storage requirement is defined, since the ballistic coefficient and entry angles were assumed. The best method of using the stored bits was studied.

Probe Data Storage Requirements (Atlas/Centaur)

Presently identified blackout science requirements for the large probe are 1000 bits for the accelerometer data. The small probe requires 250 bits for accelerometer data storage during blackout. At least twice the specified amount is provided for each probe since no data rate is specified and the DTU is limited to binary data rate steps. Both large and small probes could use data storage at times other than during blackout, because of poor probe-to-Earth communication link periods or for short collection bursts when it is not feasible to turn on the transmitter. The memory is the 2560 bit hybrid used in the orbiter data storage unit (DSU).

The Version IV science definition requires a maximum bit rate of 101 and 50 bps of science data for the large and small probe, respectively. The communication link can support 128 bps for the large probe and 64 bps for the small probe. Therefore, both large and small probes can transmit all data, after blackout, in a real-time mode. Surplus transmission rate capability at low altitudes could be utilized to empty several kilobits of stored data if it were determined that data should be stored for a period of time below 70 km to ensure ground station acquisition. However, the preferred approach does not incorporate this feature because of the additional cost impact.

Thor/Delta Configuration

The maximum transmission bit rate is limited to 105 and 10 bps for large and small probes respectively, because of transmitter limitations. Consequently, multiple collection and transmission bit rates were required; the added storage capability was a negligible cost consideration. The following study results evolved from an analysis of the Thor/Delta requirements.

The upper profile in Figure 7.7-2 depicts the specified Version III large probe science data collection rates for the various mission phases. The data collection rates obtained with the baseline design are shown in Figure 7.7-3. These include engineering and housekeeping data. The

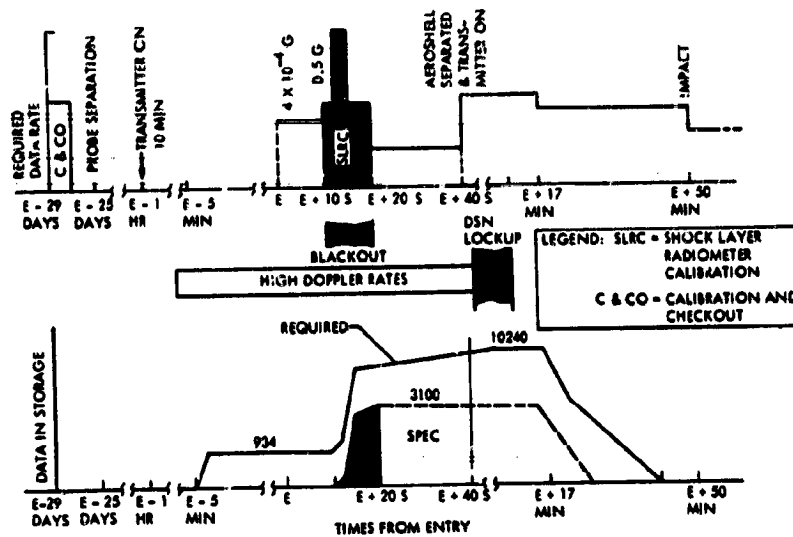


Figure 7.7-2. Large Probe Data Requirements, December Science List

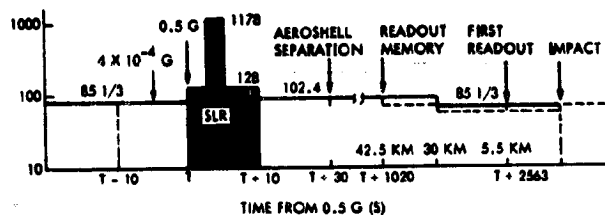


Figure 7.7-3. Large Probe Data Transmission Rates

64 bps specified for the cloud particle size analyzer (CPSA) has been reduced to 24 bps to be consistent with the candidate principal investigator's (PI) proposed instrument. All other instrument data rate requirements are met. The baseline design data rate can be increased to accommodate the additional 40 bps specified for the CPSA by minor trades on the descent profile as discussed later.

An entry data storage capability of at least 3100 bits is specified for the shock layer radiometer (SLR) and accelerometers. However, the high Doppler rates during the preentry through post blackout phases necessitate storing all data during those periods as shown in the lower figure (Figure 7.7-2). At E-5 minutes, SLR calibration data (84 bits) are stored and sampling of the primary axial accelerometer at 80 bps is begun. The

850 bits of accelerometer and engineering data are stored and updated at 85 1/3 bps until 0.5 g increasing ($T = 0$) is sensed. The last 850 bits of data are then held in storage and four-axis accelerometer and engineering data are stored at 128 bps. Within 2 to 4 seconds after 0.5 g, 2100 bits of SLR data are stored upon sensing peak radiance. Storage of accelerometer and engineering data at 128 bps is continued through blackout to $T + 10$ seconds. Accelerometer data are then stored at 102.4 bps, giving a total of 6362 bits in storage by $T + 30$ seconds. Data from all descent instruments are then transmitted at 102.4 bps. A total of 10 240 bits (4×2560) of stored data can be transmitted between 42.5 km and 5 km. This permits storage of eight frames of data (3872 bits) during the high altitude, pre-DSN lockup phase. The first eight frames of data cover 2.5 km and contain four measurements from the pressure, temperature, aureole, hygrometer, CPSA, and turbulence instruments; two measurements from the solar and IR flux, nephelometer, and accelerometer instruments; and 3200 bits of mass spectrometer data.

Readout of the stored data at 10.97 bps begins at ~ 42.5 km ($T + 1020$ seconds) when the hygrometer and aureole detector are turned off. The transmission rate is reduced to 85 1/3 bps at 30 km due to atmospheric losses and continues at this rate through impact. The memory is read out once by $T + 2563$ seconds or 5.5 km.

The small probe Version III science data rate requirements are summarized in the upper figure of Figure 7.7-4. The accelerometers require 10 bps through the blackout phase and 1.55 bps thereafter. The total data rate requirement during terminal descent is 4.82 bps until impact. The postimpact seismic mode requires 10.05 bps. The baseline design data rate capabilities are illustrated in the Figure 7.7-5. All instrument data rate requirements are met or exceeded.

For the large probe, the high Doppler rates necessitate storage of all data during the preentry through postblackout phases rather than just during blackout. The baseline design storage profile is shown in the lower half of Figure 7.7-4.

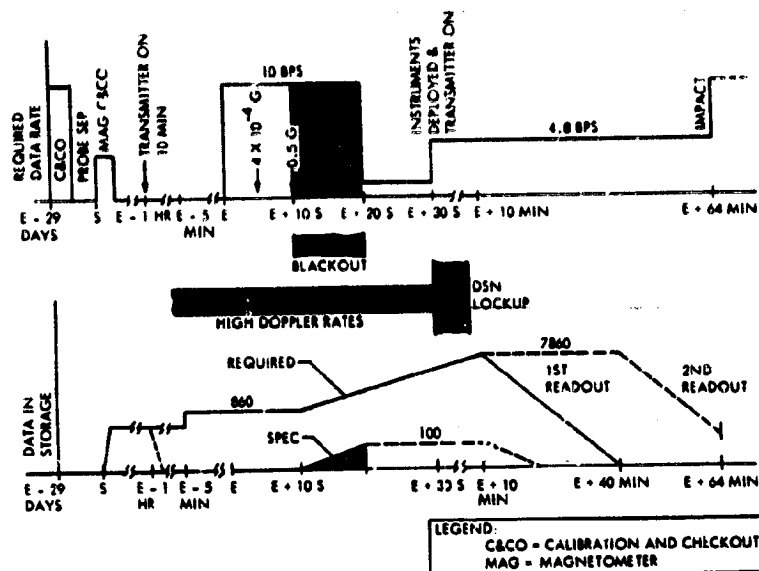


Figure 7.7-4. Small Probe Data Requirements, December Science List

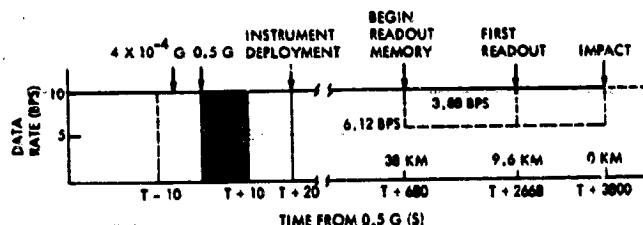


Figure 7.7-5. Small Probe Data Transmission Rates

Magnetometer calibration data (768 bits) are stored within 3 minutes after probe separation and is read out (nondestructively) during the 10-minute transmission period at E - 1 hour. Accelerometer data (100 bits) are placed in storage at E - 5 minutes and updated at 10 bps until 0.5 g increasing is sensed. The latest 100 bits are then locked in storage and subsequent accelerometer measurements are stored at 10 bps until T + 20 seconds when the other instruments are deployed and the transmitter is turned on. At this point, there are 1068 bits of data in storage. All data are then both stored and transmitted at 10 bps until T + 680 seconds (~38 km) resulting in a total of $1068 + 6600 = 7668$ bits of data in the 7680 bit storage.

The stored data are then interleaved at 3.88 bps with the real-time data at 6.12 bps. The first readout of memory occurs at ~ 9.6 km ($T + 2668$ seconds); 58 percent of the data are read out a second time by impact.

The main memory is composed of static random access memory circuits of 256 bits per chip. They are packaged in groups of ten chips and are accessed as a 256 by 10 by N matrix, where N is determined by the total storage size. The chips are CMOS for low quiescent power (nominally $0.2 \mu W$ per bit) and high noise threshold.

7.7.3.2 Probe Multiplexer and A/D Converter Requirements

We analyzed the requirements for probe multiplexers and A/D converters considering the number of data sources, how they are grouped, and what timing problems may exist between them. If two data sources require analog-to-digital conversion simultaneously, or if one source is asynchronous to the main system, two or more ADCs are required. Probe multiplexer requirements were based on the assumption that the largest impact on the probe system is the number of wires required to interconnect boxes. (Tradeoffs indicate that the data bus method of interface is not optimum for the probe mission.) The interface list is given in Table 7.7-8. Column 2 lists the number of interface wires assuming all multiplexing is done in the DTU, and column 3 assumes that all multiplexing is done in the instruments listed in column 1. The recommended location for the multiplexer for each instrument is given in column 4. A similar chart for the December science list is given in Table 7.7-9.

Table 7.7-8. Central Versus Remote Signal Conditioning, Large Probe, Version IV Science Definition

INSTRUMENT	NUMBER OF WIRES (a)		RECOMMENDED LOCATION	
	MULTIPLEXER IN DTU	MULTIPLEXER IN SCIENCE	MULTIPLEXER	A/D CONVERTER
TEMPERATURE	3	3	DTU	DTU
PRESSURE	3	3	DTU	DTU
ACCELEROMETER	3	3	DTU	DTU
HYGROMETER	4	4	DTU	DTU
PARTICLE SIZE SPECTROMETER	1	1	DTU	DTU
SOLAR RADIOMETER	1	1	DTU	DTU
IR FLUX	1	1	DTU	DTU
W/A RADAR	4	3	DTU	DTU
MASS SPEC	1	1	DTU	DTU
GAS CHROM	1	1	DTU	DTU

(a) DOES NOT INCLUDE ANY CLOCK LINES COMMON TO ALL CONFIGURATIONS

Table 7.7-9. Central Versus Remote Signal Conditioning, Large Probe, Version III, December 1972 Science Definition

INSTRUMENT	NUMBER OF WIRES		RECOMMENDED LOCATION	
	MULTIPLEXER IN DHC	MULTIPLEXER IN SCIENCE	MULTIPLEXER	A/D CONVERTER
ACCELEROMETER	5	5	DHC	DHC
TEMPERATURE	5	5	DHC	DHC
PRESSURE	5	5	DHC	DHC
CLOUD PARTICLE	30	6	SCIENCE (a)	N/A
SOLAR FLUX	14	8	SCIENCE	DHC
PLAN FLUX	14	8	SCIENCE	DHC
HYGROMETER	6	7	DHC	DHC
SHOCK LAYER RAD	17	11	SCIENCE	DHC
MASS SPEC	7	8	DHC	N/A
AUREOLE	5	6	SCIENCE	SCIENCE (b)
NEPHELOMETER	9	10	DHC	N/A

(a) MAY BE PARALLEL TO SERIAL REGISTER OR MULTIPLEXER
(b) A/D CONVERSION ASYNCHRONOUS TO BASIC CLOCK

Probe ADC requirements were determined by the ability of the instrument to be controlled in sampling time by the central data system clock. Our primary assumption was that it was less expensive in hardware to have all conversion in a single converter than to have multiple units throughout the system. The penalty of a single ADC is the decreased accuracy of transferring low-level analog signals over longer lines prior to the conversion. This is less serious when the settling times are long, allowing system capacitance to charge to steady-state values. This will be the case at the slow data rates at which the probe system operates.

Five instruments (cloud particle size and mass spectrometers, nephelometer, solar radiometer and IR flux) have no analog outputs now identified. We recommend that the analog conversion for all instruments be performed in the central data system (Column 5, Table 7.7-8).

For the December science definition (Table 7.7-9) all but three instruments have some analog outputs. Of those with analog outputs only the aureole/extinction detector (AED) must be operated asynchronously to the main clock. For that mission, we recommend that an A/D converter be in the AED and all other conversion be done in the DHC.

7.7.3.3 Probe Digital Interface

We analyzed various interfaces between the data handling system and the science instruments while considering experiment and other subsystem characteristics, as well as data subsystem operation. We coordinated the

design between the bus and orbiter to achieve any possible standardization. A joint study was conducted to consider a data bus approach, but this proved to be more complex than a unique design.

Two basic configurations were considered with several iterations of each. The first assumes the use of a standard "interface module" and its various possible locations. The second considers various locations for the multiplexers, A/D converters, and address logic as they relate to the DTU configuration.

Interface Module

The interface module contains all the circuitry necessary to monitor the instrument science and housekeeping signals, both analog and digital, and convert them to a digital bit stream for use by the DTU. The block diagram is given in Figure 7.7-6.

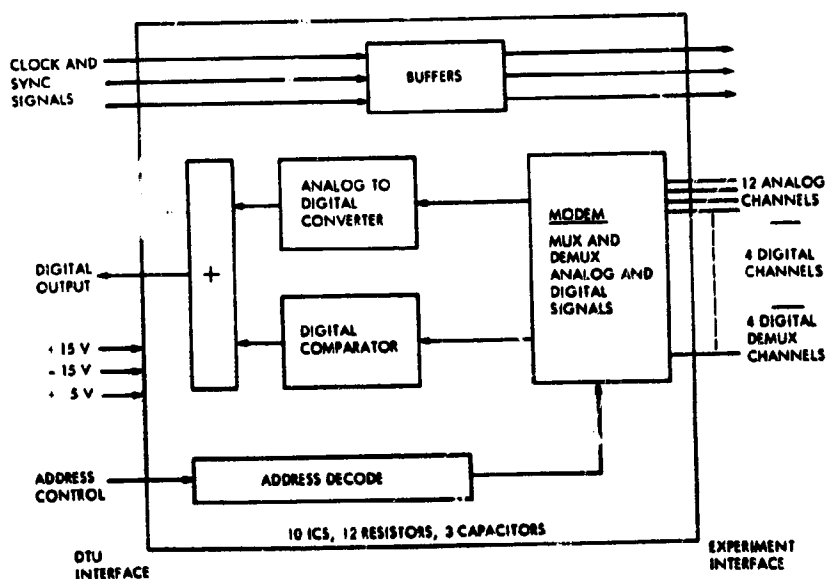


Figure 7.7-6. Experiment Interface Circuit

All parts necessary for this interface will fit on two 2 x 3-inch boards. The ADC has 10-bit resolution and is used for all analog-to-digital conversion even when less resolution is required. An input buffer is included to provide multimegohm input impedance. The multiplexer is partitioned in groups of four channels and any combination of groups can be connected as analog or digital channels. Four channels are used as demultiplex

channels to provide enable signals for the digital channels. Buffers are provided to isolate all clock and sync signals and fix interface impedances.

Each experimenter would be provided an interface module to use as a breadboard tool and a flight unit to install in the flight hardware.

Location configuration trades are shown in Figure 7.7-7 with configuration description and remarks given in Table 7.7-10.

Digital Telemetry Unit (DTU) Configuration

We considered several configurations of the DTU with respect to the total system impact. The basic DTU was assumed to be the Pioneer 10/11 unit with and without modifications to the existing boards.

The trades considered and remarks about each are given in Table 7.7-11. Configuration 7 is the recommended approach because it allows common systems, except for format programmable read-only memories (PROMs), to be used for probes, orbiter, and bus.

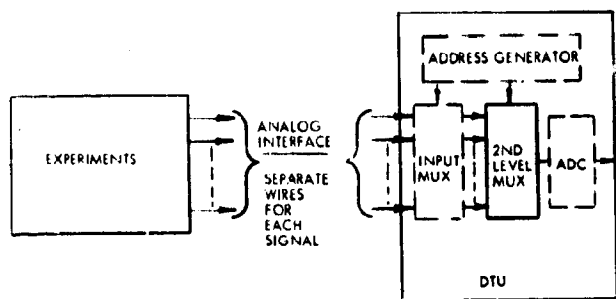
7.7.3.4 Probe Multiple and Nonbinary Bit Rate Study

In terms of scientific value, desired bit rate profiles have been established for the probes. We also evaluated the hardware impact of providing multiple bit rates for data acquisition in the probes (not constrained to binary steps) to more closely match the desired science profiles.

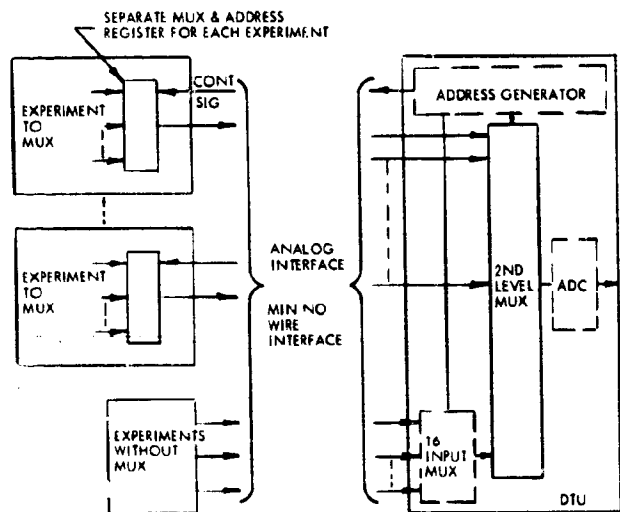
A capability to provide data profile matching is required in a system when the communication link is limited both in time and power and if the data acquisition requirement exceeds the transmission capability for significant time periods. Binary step changes are acceptable if no limitation is required on memory size and sufficient time is available to transmit the excess data.

For the Atlas/Centaur configuration with the Version IV science definition the data acquisition rates are continuously variable, but in no case are in excess of the transmission rate capability; therefore a nonbinary data system is not required.

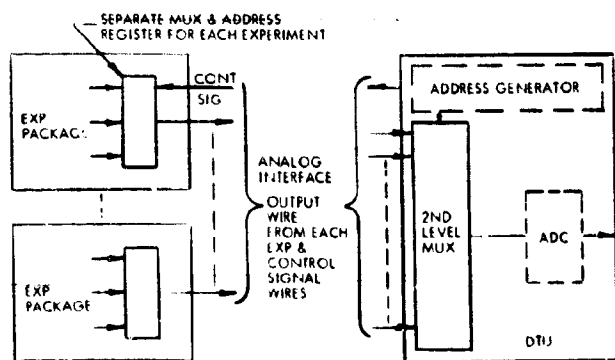
For the Version III science definition, or Thor/Delta booster, the data rates are greater than the transmission rate for a portion of the mission and less for the remainder of the mission; thus a nonbinary system is



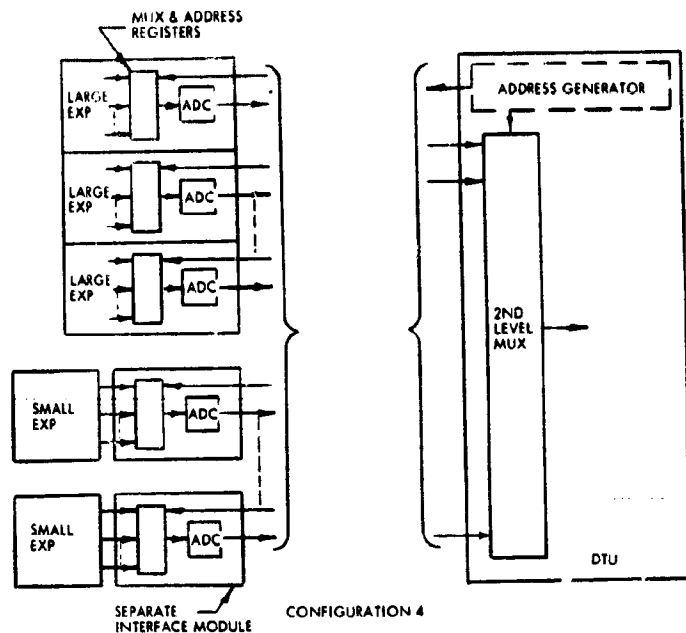
CONFIGURATION 1



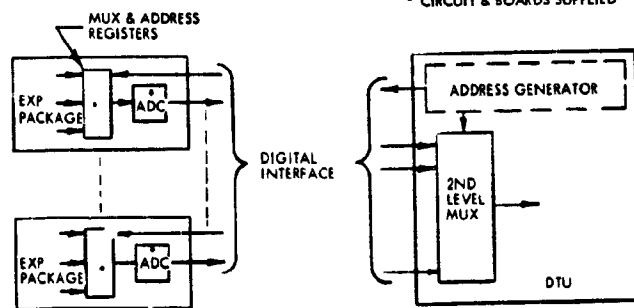
CONFIGURATION 2



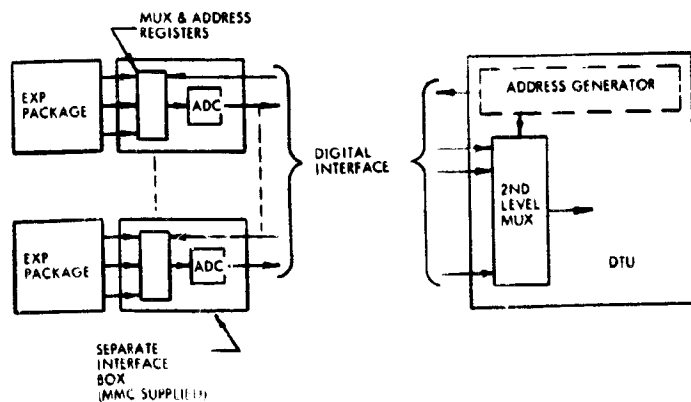
CONFIGURATION 3



CONFIGURATION 4



CONFIGURATION 5



CONFIGURATION 6

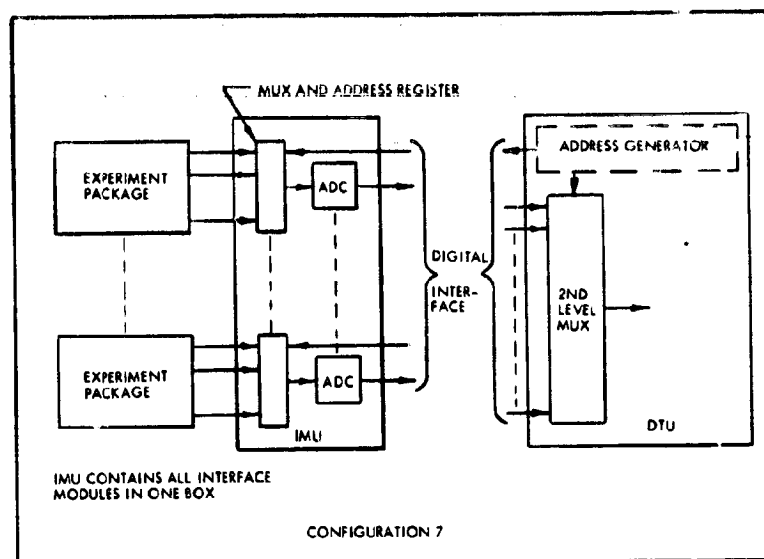
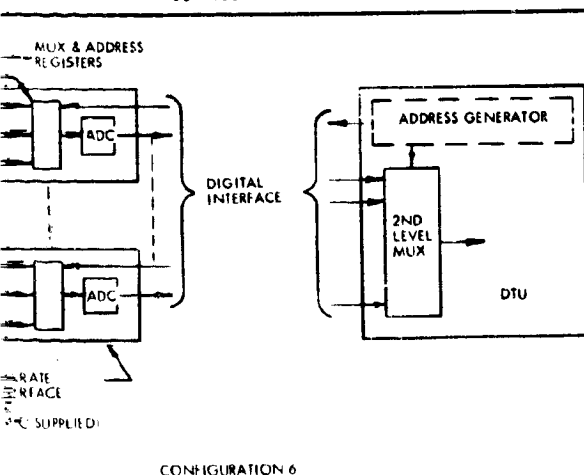
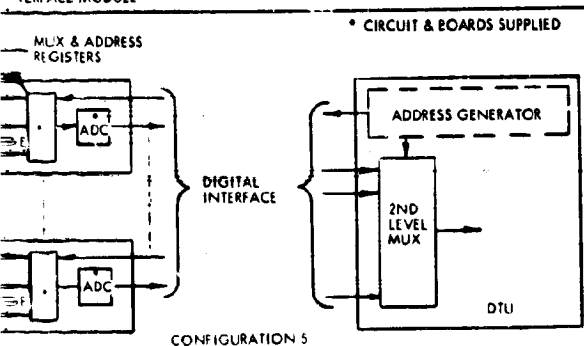
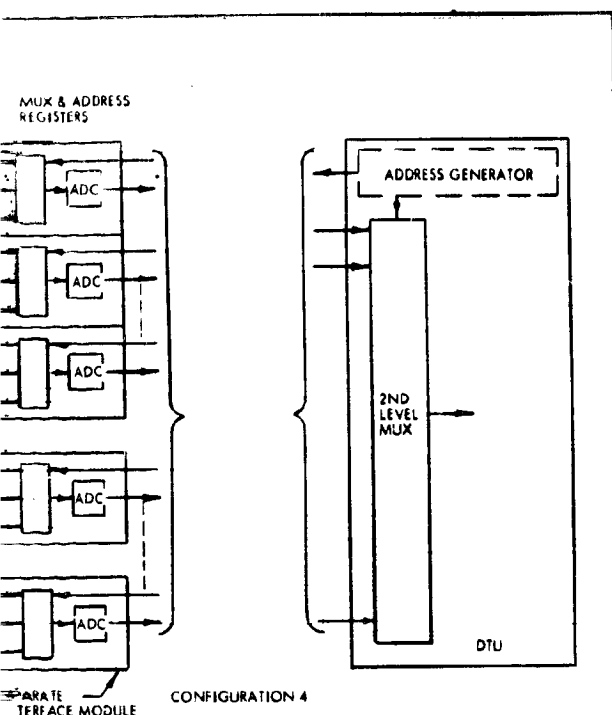


Figure 7.7-7. Experiment Interface Options

Table 7.7-10. Interface Module Configuration Impact

CONFIGURATION	ADVANTAGES	DISADVANTAGES	MASS	POWER
1. ALL MULTIPLEXING IN CENTRAL UNIT. (DTU)	ELIMINATE NEED FOR INTERFACE UNIT.	LONGEST RUN FOR ANALOG SIGNALS WITH INCREASED INACCURACY. MULTIPLEXERS AND ADC MUST BE ADDED TO DTU. MAXIMUM NO. WIRES BETWEEN EXPERIMENT AND DTU.	BASELINE (≈ 450 G)	BASELINE (≈ 3 W)
2. SOME MULTIPLEXING IN EXPERIMENTS.	REDUCES NO. OF WIRES BETWEEN EXPERIMENTS AND DTU.	ADDS COUNTER FOR EACH REMOTE MUX. EXPERIMENTER MUST ADD COMPONENTS TO HIS EQUIPMENT. SOME MULTIPLEXING AND ADC MUST BE ADDED TO DTU. LONG RUNS FOR ANALOG SIGNALS.	DECREASED BY REDUCTION IN NO. OF WIRES.	SAME AS BASELINE
3. ALL MULTIPLEXING IN EXPERIMENTS.	NO CHANGE TO DTU MULTIPLEXING. MINIMIZES NO. OF WIRES BETWEEN EXPERIMENTS AND DTU.	ADC MUST BE ADDED TO DTU. INEFFICIENT USE OF MULTIPLEXERS. LONG RUNS FOR ANALOG SIGNALS.	SLIGHTLY OVER BASELINE	SLIGHTLY OVER BASELINE
4. MULTIPLEXING AND ADC IN LARGER EXPERIMENTS AND IN SEPARATE OUTSIDE BOX FOR SMALLER EXPERIMENTS. INTERFACE MODULE PROVIDED TO EACH EXPERIMENTER.	GOOD CONFIGURATION FOR MEASUREMENT ACCURACY. EXPERIMENTER HAS SAME INTERFACE DURING DESIGN AND TEST AS HE WILL HAVE FOR MISSION. LOW IMPACT ON EXPERIMENT ENVELOPE.	INEFFICIENT USE OF MULTIPLEXERS. REQUIRES EXTRA ADC'S. INCREASE WEIGHT AND POWER DISSIPATION. SOME EXPERIMENTS MUST ADD EXTRA COMPONENTS.	+110 G/EXP (6 LARGE) +340 G/EXP (4 SMALL) +BATTERY WT (+370 G) TOTAL = 2.4 KG	2.2 W/EXP = 22 W
5. MULTIPLEXING AND ADC WITH ALL EXPERIMENTS. INTERFACE MODULE PROVIDED TO EACH EXPERIMENTER.	GOOD CONFIGURATION FOR MEASUREMENT ACCURACY. EXPERIMENTER HAS SAME INTERFACE DURING DESIGN AND TEST AS HE WILL HAVE FOR MISSION. DON'T NEED DESIGN FOR SEPARATE BOX.	INEFFICIENT USE OF MULTIPLEXERS. REQUIRES EXTRA ADC'S. INCREASES WEIGHT AND POWER DISSIPATION. PROVIDES SIGNIFICANT INCREASE TO SIZE OF SMALLER EXPERIMENTS. ALL EXPERIMENTS MUST ADD COMPONENTS.	+110 G/EXP + BATTERY WT (+370 G) TOTAL = 1.5 KG	2.2 W/EXP = 22 W
6. SEPARATE MULTIPLEXER AND ADC FOR EACH EXPERIMENT BUT PACKAGED IN SEPARATE EXTERNAL BOXES. INTERFACE MODULE PROVIDED TO EACH EXPERIMENTER.	GOOD CONFIGURATION FOR MEASUREMENT ACCURACY. EXPERIMENTER HAS SAME INTERFACE DURING DESIGN AND TEST AS HE WILL HAVE FOR MISSION. EXPERIMENTER DOES NOT NEED TO PACKAGE DHC COMPONENTS.	INEFFICIENT USE OF MULTIPLEXERS. REQUIRES EXTRA ADC'S. INCREASE WEIGHT AND POWER DISSIPATION. LARGEST WEIGHT AND SIZE PENALTY.	+340 G/EXP + BATTERY WT (370 G) TOTAL = 3.76 KG	2.2 W/EXP = 22 W
7. SEPARATE MULTIPLEXER AND ADC FOR EACH EXPERIMENT ALL PACKAGED IN ONE BOX. INTERFACE MODULE PROVIDED TO EACH EXPERIMENTER.	GOOD CONFIGURATION FOR MEASUREMENT ACCURACY. EXPERIMENTER HAS SAME INTERFACE DURING DESIGN AND TEST AS HE WILL HAVE FOR MISSION. EXPERIMENTER DOESN'T NEED TO PACKAGE INTERFACE CIRCUITS. INTERFACE PACKAGING IS DONE IN ONE BOX FOR EFFICIENCY.	INEFFICIENT USE OF MULTIPLEXERS. REQUIRES EXTRA ADC'S. INCREASES WEIGHT AND POWER DISSIPATION. SEPARATE UNIT WILL NEED TO BE SUPPLIED TO EXPERIMENTER DURING DESIGN AND CHECKOUT.	TOTAL = 2.27 KG	2.2 W/EXP = 22 W
NOTE: ASSUMES LARGE PROBE WITH SIX LARGE EXPERIMENTS AND FOUR SMALL EXPERIMENTS. SMALL PROBE FOLLOWS SAME PHILOSOPHY WITH FOUR SMALL EXPERIMENTS ASSUMED.				

required. A method for implementing the nonbinary data acquisition was designed for minimum memory and for hardware simplicity.

The concept for providing multiple bit rates uses a stepwise variable frame rate and constant bit rate within the frames to achieve the effect of a variable bit rate. Each frame is started by the time counter at predetermined intervals that have been stored in a field programmable read-only memory (PROM).

Table 7.7-11. DTU Configuration Studies

CONFIGURATION NO.	SCIENCE INSTRUMENT CONTAINS	DIGITAL TELEMETRY UNIT CONTAINS	COMMAND/CONTROL UNIT CONTAINS	REMARKS
1.	PRIMARY MULTIPLEXERS BUFFER AMPLIFIER ANALOG-TO-DIGITAL CONVERTER ADDRESS COUNTERS	DIGITAL MAINFRAME MULTIPLEXERS, PROGRAMMER BOARD SUBFRAME MULTIPLEXERS (ANALOG AND DIGITAL) CONVOLUTIONAL ENCODER BIPHASE MODULATOR DESCENT CLOCK OSCILLATORS	SEQUENCER COAST TIMER MEMORY	USES PIONEER DTU WITH REDUNDANCY AND SP5G BOARDS REMOVED. SCIENCE INSTRUMENTS MUST OPERATE WITH TWO FIXED FORMATS EITHER OF WHICH IS SELECTABLE FROM THE SEQUENCER.
2.	PRIMARY MULTIPLEXERS ADDRESS COUNTERS	DIGITAL MAINFRAME MULTIPLEXERS PROGRAMMER BOARD SUBFRAME MULTIPLEXERS ENCODER MODULATOR DESCENT CLOCK OSCILLATORS	SEQUENCER COAST TIMER MEMORY A/D CONVERTER BUFFER AMPLIFIER	USES PIONEER DTU WITH REDUNDANCY AND SP5G BOARDS REMOVED. ISOLATION RESISTORS MUST BE REMOVED FROM MAINFRAME MULTIPLEXER BOARDS TO ALLOW THEM TO HANDLE ANALOG SIGNALS. SAVES ON NUMBER OF A/D CONVERTERS USED BUT ANALOG SIGNALS MUST TRAVEL LONG PATH FROM SCIENCE INSTRUMENT TO DTU TO COMMAND/CONTROL UNIT WITH CONSEQUENT REDUCTION IN ACCURACY -- OR A/D CONVERTER MAY BE PLACED IN DTU, REQUIRING A NEW BOARD DESIGN IN THE DTU. SCIENCE FORMATS STILL FIXED AS IN CONFIGURATION 1 ABOVE.
3.	NO ADDITIONAL CIRCUITRY	DIGITAL MAINFRAME MULTIPLEXERS PROGRAMMER BOARD SUBFRAME MULTIPLEXERS ENCODER MODULATOR DESCENT CLOCK OSCILLATORS	SEQUENCER COAST TIMER MEMORY A/D CONVERTER BUFFER AMPLIFIER PRIMARY MULTIPLEXERS ADDRESS COUNTERS	SAME AS CONFIGURATION 2 ABOVE, EXCEPT THAT SCIENCE INSTRUMENTS ARE NOT REQUIRED TO DO MULTIPLEXING. REQUIRES MORE WIRES BETWEEN SCIENCE AND COMMAND/CONTROL UNIT.
4.	SAME AS CONFIGURATIONS 1, 2, AND 3	DIGITAL MAINFRAME MULTIPLEXERS MODIFIED PROGRAMMER BOARD SUBFRAME MULTIPLEXERS ENCODER MODULATOR DESCENT CLOCK OSCILLATORS	SAME AS CONFIGURATIONS 1, 2, AND 3	TO OBTAIN FLEXIBLE FORMAT CHANGES, A MAJOR PROGRAMMER REDESIGN IS REQUIRED. THIS CAN BE DONE BY EXTENSIVELY MODIFYING THE PROGRAMMER BOARD IN THE DTU. OTHERWISE SAME AS CONFIGURATIONS 1, 2, AND 3
5.	NO ADDITIONAL CIRCUITRY	SUBFRAME MULTIPLEXERS ENCODER MODULATOR DESCENT CLOCK OSCILLATORS	SEQUENCER COAST TIMER MEMORY A/D CONVERTER BUFFER AMPLIFIER PRIMARY MULTIPLEXERS ADDRESS COUNTER SECOND LEVEL MULTIPLEXERS PROGRAMMER	USES THE DIGITAL AND ANALOG SUBFRAME MULTIPLEXER BOARDS AND THE OUTPUT LOGIC BOARDS FROM THE PIONEER DTU. PROVIDES FORMAT FLEXIBILITY; REDUCES LENGTH OF PATH ANALOG SIGNALS MUST TRAVEL BY REMOVING DTU FROM THE CIRCUIT; REQUIRES GREATEST COMMAND/CONTROL UNIT DESIGN EFFORT.
6.	NO ADDITIONAL CIRCUITRY	NOT USED	SEQUENCER COAST TIMER MEMORY A/D CONVERTER BUFFER AMPLIFIER ALL MULTIPLEXERS & ADDRESS COUNTER ENCODER PROGRAMMER MODULATOR DESCENT CLOCK OSCILLATORS	REQUIRES REPACKAGING OF ENGINEERING MEASUREMENT MULTIPLEXERS, CONVOLUTIONAL ENCODER, BI-PHASE MODULATOR, AND CLOCK OSCILLATORS. (3 BOARDS IN DTU) ALLOWS ALL MULTIPLEXING, COMMAND, AND CONTROL LOGIC TO BE GROUPED TOGETHER WITH RESULTANT SAVINGS IN SIZE AND WEIGHT. ALLOWS ALL CIRCUITS TO BE PACKAGED UNDER SAME DESIGN CONCEPT WITH ONLY ONE PACKAGE NEEDING TO BE QUALIFIED. INCREASES RELIABILITY BECAUSE OF REDUCTION IN NUMBER OF WIRES AND CONNECTORS INVOLVED AND BECAUSE OF REPLACEMENT OFSSI CIRCUITS USED IN DTU WITH CURRENT MSI CIRCUITS.
7.	NO ADDITIONAL CIRCUITRY	SAME AS CONFIGURATION 4 WITH ANALOG BOARD MODIFIED	SEQUENCER COAST TIMER MEMORY	PROVIDES FORMATS COMPATIBLE WITH BOTH PROBES, BUS, AND ORBITER. CHANGE TO ANALOG BOARD ALLOWS RESPONSE TO 7 AND 10 BIT ANALOG SCIENCE AND HOUSEKEEPING REQUIREMENTS.

In Figure 7.7-8 the smooth curve is indicative of the bit rate versus time requirements of data acquisition for the large probe science experiments, assuming a fixed number of samples per kilometer. The steps shown are representative of discrete changes in the time between the acquisition of a frame of data. At the two points shown, frames are started at 2 1/2- and 7 1/2-second intervals, respectively. In both cases, it takes less than 2 seconds to acquire the data to fill a frame. The result is an effective bit rate change while holding the sampling time for each instrument constant throughout the mission. This technique allows all measurements within a frame to be taken in a minimum descent distance interval and provides consistency in settling time for measurements. The circuitry of Figure 7.7-9 implements the variable nonbinary frame rate data collection. Figure 7.7-10 shows the circuitry required to provide nonbinary bit rate changes. Appendix 7.7A discusses this in more detail.

7.7.3.5 Synchronization and Time Reference Word Minimization

We have reviewed the requirements for frame synchronization and the minimization of frame sync bits. For the Atlas/Centaur preferred configuration housekeeping word size is not critical and the 24-bit sync word used in Pioneer 10/11 will be used. Time reference is common to both systems and will be discussed below. For the Thor/Delta system, Viterbi decoding, which requires no sync word for decoding, is recommended. Frame sync after decoding can be done by a seven-bit Barker sequence code.

For all probes, mission time is referenced to the initialization of the descent timer by redundant g switches. The maximum mission duration is 1 1/4 hours or 4200 seconds. If each frame were time tagged to the nearest second, 13 bits and a separate counter would be required. If timing resolution exceeding 1 second were desired, additional bits would be required.

A maximum of 700 frames of data will be transmitted for the large probe and less than 330 frames of data for the small probes. Because all event times are fixed with respect to the timer (including the start of each frame) frame count contains as much time information as would a time word. In addition, subcommutated data are also locked into a given position with respect to the start of each defined major frame, so no subcommutator identification tag is required. Since the frame count contains all timing information necessary for the mission, the 10-bit count for the large and small probes is recommended as the only time reference data requirements.

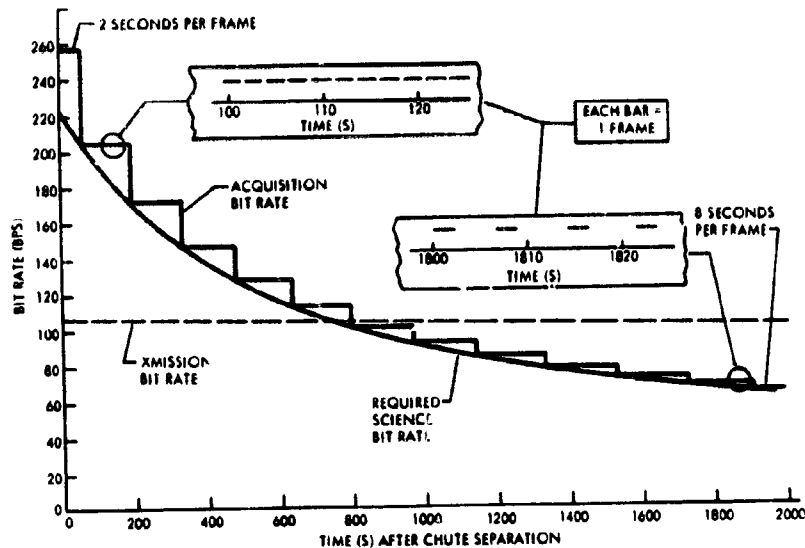


Figure 7.7-8. Non-Binary Data Acquisition Bit Rate

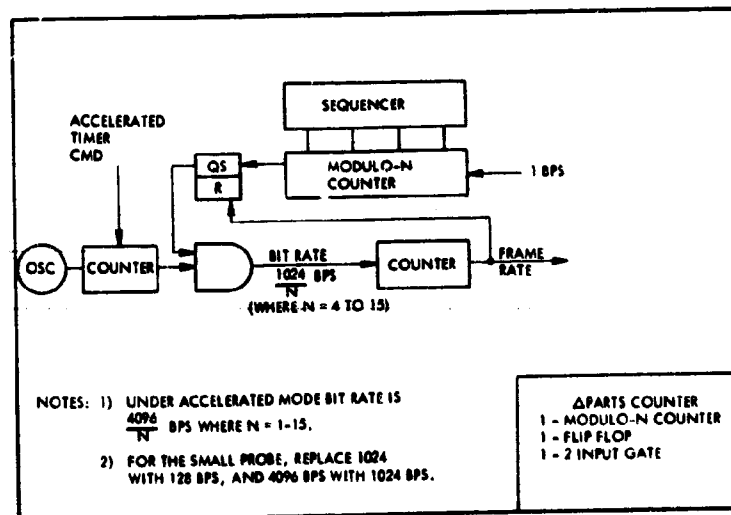


Figure 7.7-9. Non-Binary Frame Selection Circuit

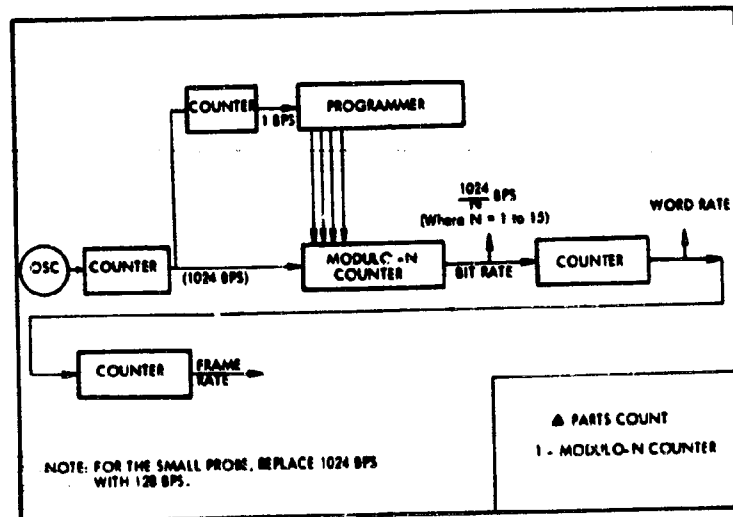


Figure 7.7-10. Non-Binary Bit Rate Selection Circuit

7.7.3.6 Programmer Design Concept

The merits of a central programmable processor in the probes versus conventional programmers in the subsystem have been considered. The relative simplicity and fixed mission concept of the probes would not justify putting a programmer in each experiment. The selection of different programmers in the probe was based on power requirements during the two distinct mission phases, coast and descent.

Two programmers, coast and descent, are used for both large and small probes. The first programmer is used during coast from separation to entry minus 3 hours and initiates the required events. The purpose is to transfer to main battery power and start the second, or descent mode, programmer. The descent programmer provides all timing controls for the final 4 hours before impact. Two programmers are required, since the 1-second resolution required for the descent phase would impose an unacceptable decode requirement if used over a 25-day period. No reason was found to separate the descent programmer into subprogrammers for format, pyro, power, or any other block of event sequences.

The coast phase programmer is driven by a crystal controlled oscillator, with an accuracy of 1 part in 10^4 , has an output resolution of 1 hour, and uses less than 100 microwatts of power. It is initiated prior to separation by the probe bus via the command umbilical, through the DHC. Two days prior to entry it turns on the IR detector heaters. Two hours before entry it turns on the main battery heater. Prior to entry it turns on the main battery power, presets the sequencer to a predetermined state, and has no further function during the mission. The transfer to the main battery must be done with an uncertainty of less than ± 300 seconds to perform the required preentry operations.

The descent phase programmer is driven by a crystal controlled oscillator in the DTU with an accuracy of 1 part in 10^4 , has an output resolution of 1 second, and uses less than 7.5 mW of average power by using power switching on the read-only memories. To reduce the complexity of the time decode hardware, the time between events is measured and compared to a preprogrammed time code.

The PROMs store 255 usable addresses, allowing that many distinct event times to occur. However, since the maximum time allowable on the time counter is 255 seconds, a dummy command must be given before the timer times out. Only 40 discrete command times and less than 60 dummy commands are required to cover the last 4 hours before impact. Any desirable sequence of events can be preprogrammed into the remaining 155 command times available for prelaunch and preseparation checkout. This greatly simplifies acceptance and cruise checkout software and hardware.

Addresses 1 through 128 in the event counter are assigned to flight operations. Addresses 129 through 192 are assigned to the preseparation checkout. Addresses 193 through 255 are available for any unique ground checkout sequences on a routine performance basis. Any given condition may be programmed and held by disabling the time counter.

7.7.3.7 Large Probe Data/Descent Rate

We performed an overall system tradeoff to select the optimum combination of power, weight, transmitter power, and thermal control allocations for the specified mission. For the early Phase B contract science requirements, (bits/km), 24 k bit memory storage was required for the large probe, and 4.2 k bit memory storage for the small probe.

However, the Version IV science definition specified the memory size to be provided. The utilization of this memory size is discussed in paragraph 7.7.3.1.

7.7.4 Atlas/Centaur Data Handling and Command Subsystem Preferred Design

We selected the telemetry unit for the Atlas/Centaur system based on minimum cost, and maximum commonality and interchangeability. The extra weight allowances of the Atlas/Centaur booster make this possible. The added weight allows the use of an existing design with minimum modifications.

All mission science requirements defined in paragraph 7.7.2 are exceeded by the capability of the data system. A more detailed description of the modified DTU is given in paragraph 8.3.4.1.

The DHC subsystem is packaged in two boxes. One component is the modified digital telemetry unit as used on the bus and orbiter and contains the functions described in paragraphs 7.7.4.1 through 7.7.4.3. The remaining command, timing, and memory functions described in paragraphs 7.7.4.4 through 7.7.4.6 are packaged in a compartment of the power control unit box in order to avoid modifications to the DTU and to reduce the weight and cost of separate packages. The DHC functional block diagram showing the interrelationships of the two units is given in Figure 7.7-11.

The telemetry unit used in the Pioneer 10/11 spacecraft will be used in both large and small probes. Since no attitude control systems are on the probe, the spin period sector generator boards are of no value and will be removed. Since no uplink commands or self-check are available after probe separation, decision-making circuitry on board the redundant main frame and programmer boards will be removed to save weight and power. In addition, to meet the science requirements in terms of format, bit rate, and word length, the programmer and analog subframe boards will be redesigned. Changes are shown in Figure 7.7-12. If the probes alone were involved in the programmer and analog board changes, it would be cost effective to either adapt these functions by the additions of external circuitry or develop the Thor/Delta new design described in paragraph 7.7.5. However, the requirements imposed on the bus and orbiter also require changes to the same two boards.

The five boards used in the probes are:

- 1) **Mainframe Multiplexer** - This board contains multiplexers, demultiplexers, and drivers for 32 digital channels. Selection is under control of the programmer.
- 2) **Programmer** - The modified programmer controls the addressing of all data channels and controls the bit rate and mode. All formatting is done by PROMs and enough are used to contain both large and small probe formats.
- 3) **Analog** - The analog board contains two 10 bit ADCs and the related analog multiplexers and drivers. One ADC is scheduled for use by engineering, but may be used for science. Six-, seven-, eight-, or ten-bit words are extracted from the output register as needed, under control of the programmer. All analog words, mainframe and subframe are channeled through this board.

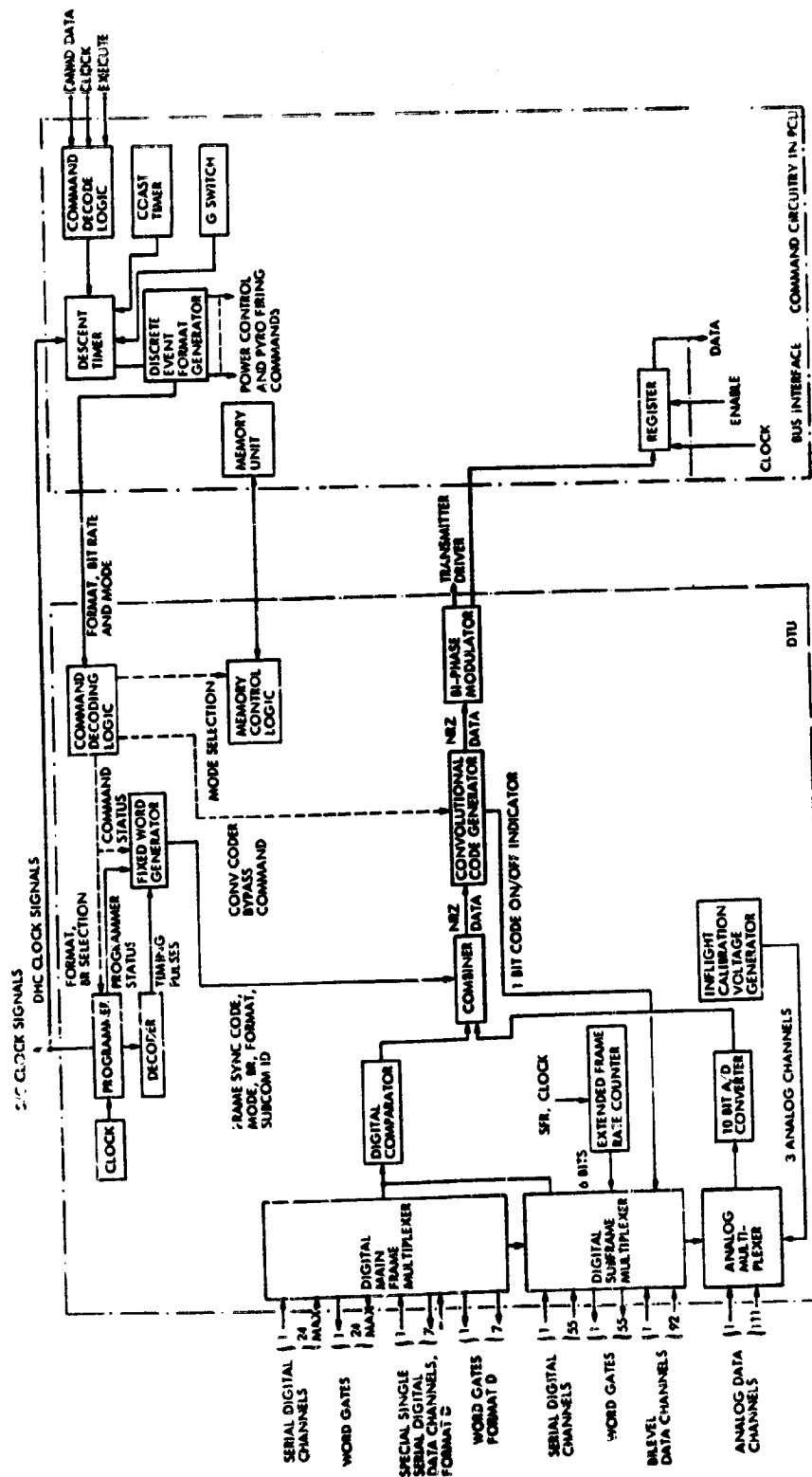


Figure 7-7-11. DHC Functional Diagram

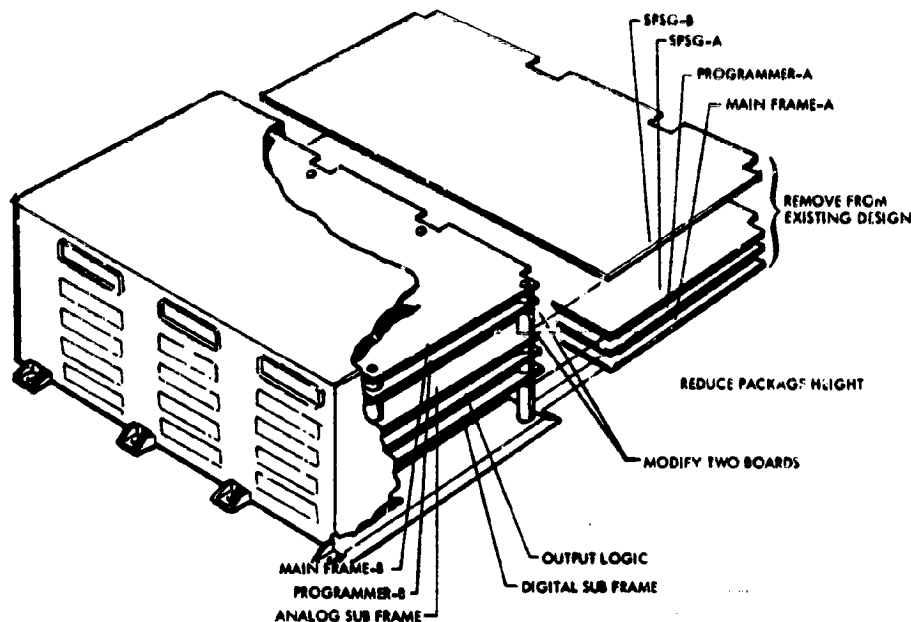


Figure 7.7-12. Location and Replacement of Pioneer 10 and 11 Boards

- 4) Digital Subframe - All digital channels used for subcommutated data are channeled through this board. All the necessary multiplexers, demultiplexers, and drivers are available.
- 5) Output Logic - The convolutional encoder, biphase modulator, and miscellaneous logic is provided by this board.

With the board modification, the five nonredundant boards are common to bus, orbiter, and both probes. Further cost reduction is achieved because the telemetry units have enough PROMs to cover both large and small probe formats, making them interchangeable and reducing the spares problem. DTU characteristics for the preferred design are given in Table 7.7-12.

The Version IV science requirements are the basis for the design.

7.7.4.1 Programmer Board Design

The programmer board design follows the basic concepts of the Thor/Delta design. Formats are controlled and changeable by the use of PROMs. The word length is changeable by the use of a programmable countdown counter whose address is supplied by two outputs from the format PROM.

The main difference between the Atlas/Centaur programmer and that used in Thor/Delta is that the Atlas/Centaur design uses only binary steps in bit rate selection. In fact, both large and small probes use only one bit

Table 7.7-12. Modified DTU Characteristics - Atlas/Centaur,
Large and Small Probes

1. BASIC CLOCK FREQUENCY	4.194304 MHZ STABILITY: 0.02%
2. TYPE	PCM
3. BIT RATES	2048 BPS 1024 BPS 512 BPS 256 BPS 128 BPS 64 BPS 32 BPS 16 BPS
4. DATA INPUT CHANNELS	
MAIN FRAME	32 DIGITAL CHANNELS 24 BASIC SCIENCE FORMAT A&B 8 SPECIAL SCIENCE FORMATS D-1 THROUGH D-8 16 ANALOG CHANNELS
SUBFRAME	55 DIGITAL 92 BILEVEL 95 ANALOG
5. INPUT VOLTAGE RANGE	0 to + 5 VOLTS ANALOG (MAIN FRAME) DIGITAL AND BILEVEL COMPARATOR THRESHOLD + 2.0 VOLTS
6. A/D RESOLUTION	10 BITS
7. DATA OUTPUT	BIPHASE MODULATED NRZ-L
8. SUBCARRIER FREQUENCY	32.768 KHZ \pm 0.02% SQUAREWAVE
9. DATA CODING	CONVOLUTIONAL CODED DATA OUTPUT
10. OPERATING MODES	REAL TIME TELEMETRY STORE MEMORY READOUT REAL TIME PLUS MEMORY READOUT
11. DATA FORMATS, SCIENCE (ALL REPROGRAMMABLE BY REPLACING APPROPRIATE READ ONLY MEMORY)	A ENTRY D ₁ DESCENT D ₂ DESCENT D ₃ DESCENT E-1 & E-2 64 WORD SCIENCE SUBFRAME (NOT SELECTABLE BY GROUND COMMAND)
ENGINEERING (SELECTABLE BY GROUND COMMAND)	C - ACCELERATE FORMATS C-1 THRU C-2 AS TWO 64 WORD MAIN FRAMES IN SEQUENCE C-1 ACCELERATE ONLY C-1 IN MAIN FRAME C-2 ACCELERATE ONLY C-2 IN MAIN FRAME
12. FRAME SIZE	
MAIN FRAME	768 BITS, 6, 7, 8 OR 10 BIT WORD GROUPS
SUBFRAME	SCIENCE - 64, 10 BIT WORDS ENGINEERING - 128, TWO 6 BIT WORDS/FRAME
13. MAIN FRAME LENGTH	
SCIENCE	FORMAT A - 768 BITS FORMAT D-1 THRU D-3 768 BITS
ENGINEERING	FORMAT C - 128 BITS FORMAT C-1 AND C-2 - 64 BITS
14. EXTENDED FRAME COUNTER	IDENTIFIES 1024 UNIQUE DATA FRAMES
15. POWER REQUIREMENTS	3.3 W
16. SIZE	7.4 x 11 x 3-1/2 (IN.)

rate each during descent; 128 bps in the large probe and 64 bps in the small probe. Other bit rates, as shown in Table 7.7-12, are available as required and are under control of external command or the sequencer. This board differs from the bus and orbiter only in the internal program of the PROMs.

7.7.4.2 Analog Subframe Board Design

The analog subframe board now has two 10-bit ADCs and associated multiplexers. The change of both the analog and programmer boards allow

the ADCs to be used in both main frame and subframes. All words will be converted to 10-bit resolution and any unused bits will be dropped. This board is identical to the bus and orbiter board.

7.7.4.3 Main Frame, Digital Subframe, and Output Logic Boards

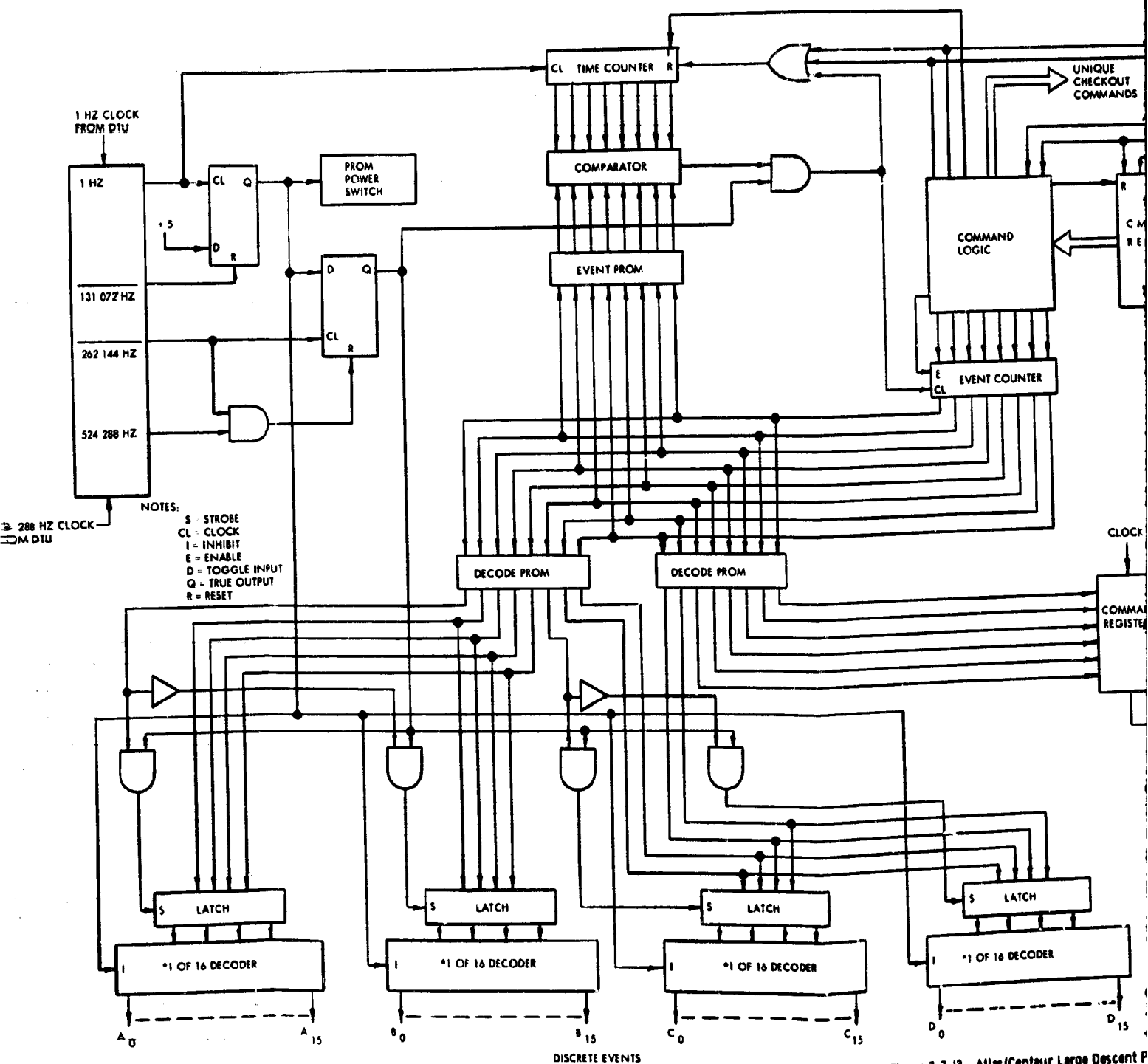
These boards are all identical to the Pioneer 10/11 boards and are unchanged in probes, bus, and orbiter.

7.7.4.4 Descent Timer/Programmer (DTP)

The DTP provides memory storage for commands and time intervals between commands. It contains the circuitry for discrete event signal decoding and provides latching circuits where long-term outputs are required. It also contains a register for receiving external real-time commands. A block diagram of the DTP is shown in Figure 7.7-13.

A signal from the coast timer at E-3 hours, and a signal from either of two g switches at entry, set the event counter to different predetermined counts that are used as addresses by the PROMs. Information defining the time intervals between events are stored in a 256 word by 8 bit PROM. Two PROMs are used to define which event occurs at each event time, providing 256 words of 16 bits each. These PROMs use 300 mW of power each, so at the beginning of each 1 second clock pulse, power is applied to the PROMs for approximately an 8-microsecond period, as shown in Figure 7.7-14. At the same time, the Δ time counter is incremented by one count. The time interval stored in the time PROM is compared to the Δ time count. If they agree a match signal is generated. This signal increments the event counter, causing a new address to be supplied to the time PROM. The maximum time interval that can be stored is 255 seconds. When longer time intervals occur between events, they must be stored in a sequence of intervals no longer than 255 seconds each. The time PROM has sufficient capacity to allow this type of programming for several hours.

The match signal causes a new 16-bit discrete event word to be read out of the event decode PROMs and entered into the decoders. Four 16-output decoders are used, providing a total output capability of 64 discrete events. The rejection of an all-zeros command as an acceptable state reduces the usable events to 60. The decoders contain latches that can



*0000 CODE NOT USED

Figure 7.7-13. Atlas/Contaur Large Descent F

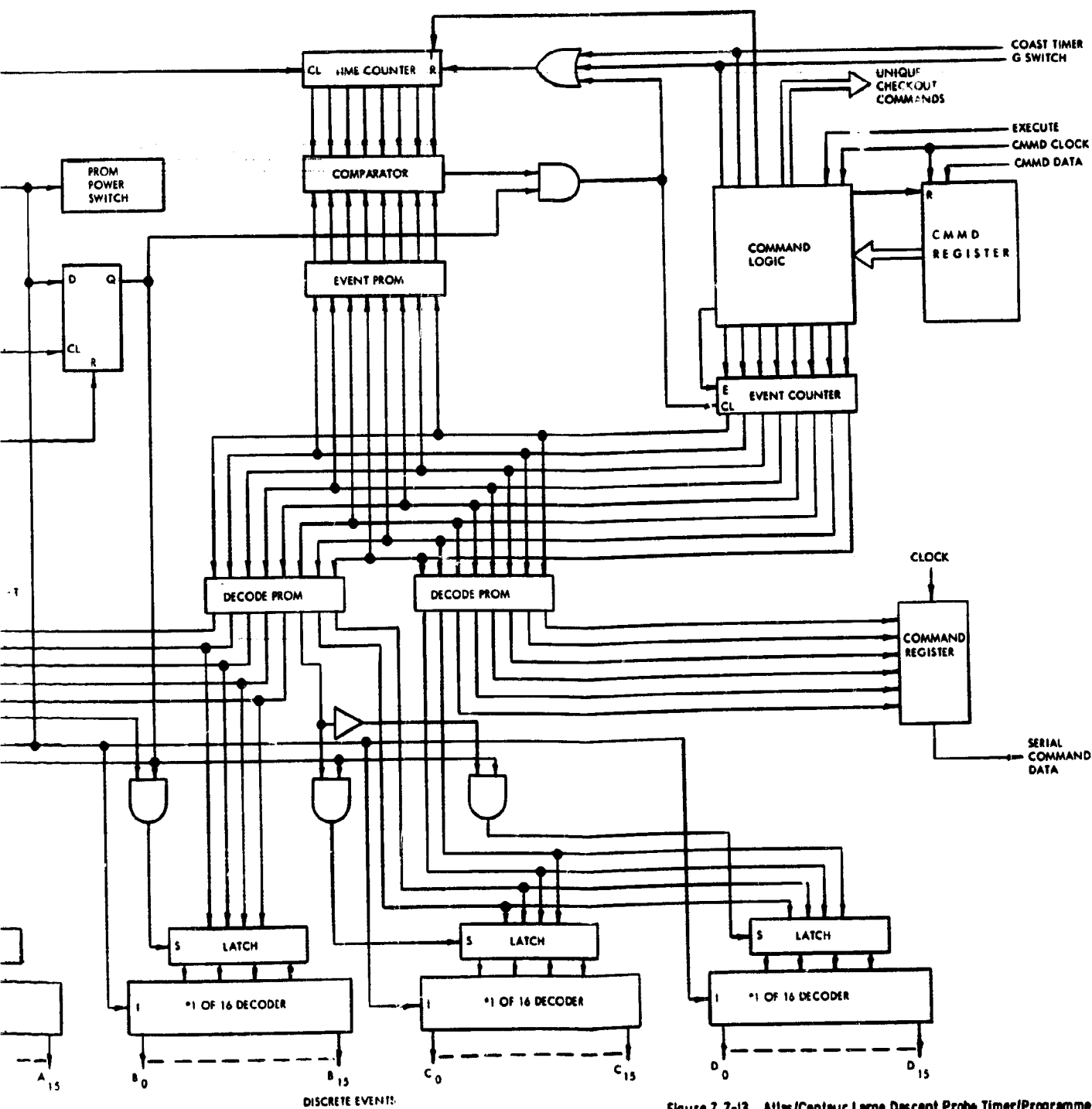


Figure 7.7-13. Atlas/Centaur Large Descent Probe Timer/Programmer

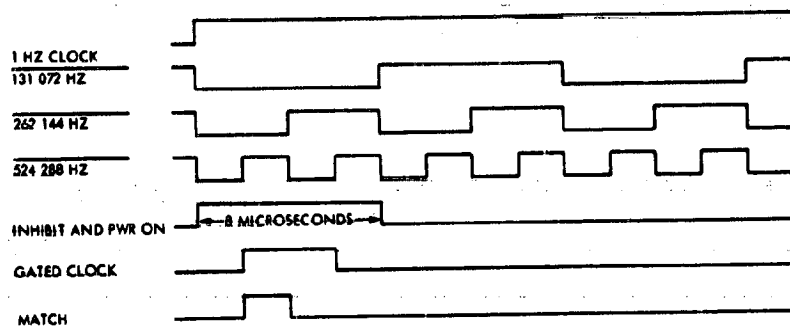


Figure 7.7-14. Descent Timer/Programmer Timing Diagram

store the command until the next 1 second clock signal occurs. If momentary commands are required they may be dropped by external circuitry. (Pyro firing signals are 250 milliseconds long.) For long-duration commands, additional latch circuits are provided at the decoder outputs. Each decoder is enabled by a separate bit of the event word. This permits up to four unique commands to be issued at the same time which is sufficient for probe requirements. Presently assigned output commands for the large probe are given in Table 7.7-13.

The DTP can also receive external commands in the form of a 16-bit word via the probe umbilical. These may be unique checkout commands that are not used during the mission. In this case, they are not issued as discrete events from the decoders, but are generated directly from the command register outputs. This economizes on the memory storage capacity and decoder capacity required. A disable function is provided that permits the Δ time count to be inhibited when responding to an external command.

The PROMs also contain a checkout sequence that can be entered via external command. In this case the external command presets the event counter to the correct address to start the checkout sequence. The counter then steps the probe through the checkout sequence with no additional external commands.

The relationship between the descent timer and the coast timer is significant. It is a function of the coast timer to turn on the descent timer sometime prior to entry. In case the coast timer fails to turn on the descent timer, the g switches turn on everything at entry and only pre-entry data and warmup time are lost.

Table 7.7-13. Large Probe Sequencer Discrete Event Channel Assignments, Atlas/Centaur (Version IV Science Definition)

<p>A. 0 (NOT USED)</p> <p>1 BATTERY HEATER <u>ON</u></p> <p>2 BATTERY HEATER <u>OFF</u></p> <p>3 IR HEATER <u>ON</u></p> <p>4 IR HEATER <u>OFF</u></p> <p>5 TEMPERATURE GAGE POWER <u>ON</u></p> <p>6 TEMPERATURE GAGE POWER <u>OFF</u></p> <p>7 MAIN POWER <u>ON</u></p> <p>8 PARACHUTE DEPLOYMENT <u>FIRE</u></p> <p>9 MASS SPEC - TUBE 1 <u>OPEN</u></p> <p>10 MASS SPEC - TUBE 1 <u>CLOSE</u></p> <p>11 MASS SPEC - TUBE 2 <u>OPEN</u></p> <p>12 MASS SPEC - TUBE 2 <u>CLOSE</u></p> <p>13 MASS SPEC - TUBE 4 <u>OPEN</u></p> <p>14 MASS SPEC - TUBE 4 <u>CLOSE</u></p> <p>15 MAIN POWER <u>OFF</u></p>	<p>B. 0 (NOT USED)</p> <p>1 TRANSMITTER DRIVER, RECEIVER, AND ENGINEERING XDUCE POWER <u>ON</u></p> <p>2 TRANSMITTER DRIVER, RECEIVER AND ENGINEERING XDUCE POWER <u>OFF</u></p> <p>3 PRESSURE GAGE POWER <u>ON</u></p> <p>4 PRESSURE GAGE POWER <u>OFF</u></p> <p>5 COAST TIMER POWER <u>ON</u></p> <p>6 COAST TIMER POWER <u>OFF</u></p> <p>7 PYRO'S <u>DISARM</u></p> <p>8 PYRO'S <u>ARM</u></p> <p>9 ACCELEROMETER POWER <u>ON</u></p> <p>10 ACCELEROMETER POWER <u>OFF</u></p> <p>11 MASS SPEC HEATER HIGH <u>ON</u></p> <p>12 MASS SPEC HEATER HIGH <u>OFF</u></p> <p>13 AEROSHELL FOREBODY JETTISON <u>FIRE</u></p> <p>14 NEUTRAL MASS SPECTROMETER POWER <u>ON</u></p> <p>15 NEUTRAL MASS SPECTROMETER POWER <u>OFF</u></p>
<p>C. 0 (NOT USED)</p> <p>1 MODE 1 (TRANSMIT REAL TIME DATA)</p> <p>2 MODE 2 (TRANSMIT AND STORE)</p> <p>3 MODE 3 (STORE ONLY)</p> <p>4 SOLAR RADIOMETER POWER <u>ON</u></p> <p>5 SOLAR RADIOMETER POWER <u>OFF</u></p> <p>6 CLOUD PARTICLE SIZE ANALYZER POWER <u>ON</u></p> <p>7 FOREBODY ELECTRICAL CABLE CUTTER <u>FIRE</u></p> <p>8 MASS SPEC - TUBE 6 <u>OPEN</u></p> <p>9 MASS SPEC HEATER LOW - <u>ON</u></p> <p>10 MASS SPEC HEATER LOW - <u>OFF</u></p> <p>11 HUMIDITY POWER <u>OFF</u></p> <p>12 MASS SPEC - TUBE 3 <u>OPEN</u></p> <p>13 MASS SPEC - TUBE 3 <u>CLOSE</u></p> <p>14 CLOUD PARTICLE SIZE SPECTROMETER POWER <u>OFF</u></p> <p>15 HUMIDITY POWER <u>ON</u></p>	<p>D. 0 (NOT USED)</p> <p>1 TRANSMITTER POWER AMPLIFIER, POWER <u>ON</u></p> <p>2 TRANSMITTER POWER AMPLIFIER, POWER <u>OFF</u></p> <p>3 IR FLUX RADIOMETER POWER <u>ON</u></p> <p>4 IR FLUX RADIOMETER POWER <u>OFF</u></p> <p>5 GAS CHROMATOGRAPH POWER <u>ON</u></p> <p>6 GAS CHROMATOGRAPH POWER <u>OFF</u></p> <p>7 WINDOW HEATER POWER <u>ON</u></p> <p>8 WINDOW HEATER POWER <u>OFF</u></p> <p>9 MASS SPEC INLET CAP EJECTION <u>FIRE</u></p> <p>10 AFTER BODY ELECTRICAL CABLE CUTTER <u>FIRE</u></p> <p>11 AFTER BODY PARACHUTE <u>RELEASE</u></p> <p>12 MASS SPEC - TUBE 5 <u>OPEN</u></p> <p>13 MASS SPEC - TUBE 5 <u>CLOSE</u></p> <p>14 WIND ALTITUDE RADAR POWER <u>ON</u></p> <p>15 WIND ALTITUDE RADAR POWER <u>OFF</u></p>

Another failure mode is possible in the coast timer that may turn on the descent timer hours or even days early. If this were the case, the batteries could be completely discharged at entry and the g switch backup would be unusable. To prevent this, the descent timer will shut off the main power if an excessive time lapse occurs after turn on and if no g switch signal has occurred. The probe then remains dormant until the g switches activate and put the probes in the descent mode. Once again some or all of the pre-entry data may be lost but the bulk of the mission is protected.

7.7.4.5 Coast Timer

The coast timer is powered from the main battery but is isolated by a high impedance resistor to protect the battery in case of a low impedance

short in the timer. The timer contains a crystal controlled oscillator with an accuracy of >1 part in 10^4 over the temperature range of interest. Count-down circuitry is supplied to give outputs with 1 hour resolution. Relay outputs turn on the IR and battery heaters and the main power switch. The coast timer interface is shown in Figure 7.7-15.

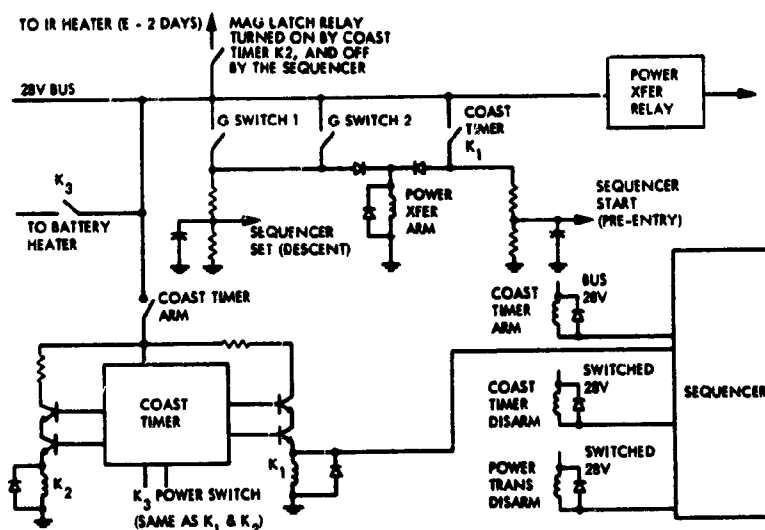


Figure 7.7-15. Coast Timer Interface

7.7.4.6 Memory

The memory unit is packaged with the descent timer/programmer to avoid additional changes to the DTU. The memory is required to store entry data prior to establishing the communication link. To obtain maximum commonality, the same memory unit is used on the large and small probe.

The memory uses the same memory element used on the orbiter-- a 2560 bit hybrid. Science storage requirements are 1000 bits for the large probe and 250 bits for the small probe, but no bit rate is defined. Since any bit rate may be needed, the binary steps in data acquisition rates put a restriction on the efficiency of the storage system. To provide for this contingency twice the specified storage is provided. Engineering data are required, in addition, and will use the other remaining bits.

7.7.5 Thor/Delta Data Handling and Command (DHC) Subsystem Preferred Design

A preliminary design has been completed on the DHC subsystem for the Thor/Delta booster configuration. The design is in sufficient detail to allow part selection and count. All system requirements are implemented at the block diagram level and feasibility of function capability has been verified by analysis. Power, volume, and weight requirements have been confirmed and a preliminary packaging concept has been determined for each probe size. The DHC characteristics are given in Tables 7.7-14 and 7.7-15.

The basic design concepts are common to the large and small probes. The changes occur in the stored programs in the PROMs used for the sequencer and format generators and in the number of formats and data channels. A block diagram of the DHC is presented in Figure 7.7-16. A detailed functional description of key blocks is discussed in the following paragraphs.

7.7.5.1 Descent Timer/Programmer (DTP)

The DTP designed for Atlas/Centaur (Figure 7.7-13) with slight changes will be used to supply all the discrete event commands and to decode the command word. It differs from the Atlas/Centaur design in that format, bit rate and mode select are discrete commands rather than a serial bit stream. The discrete events command assign events are listed in Table 7.7-16.

7.7.5.2 Data Buffer/Memory

The data buffer/memory (Fig. 7.7-17) receives serial data, converts it into four-bit parallel bytes, and stores it in a COSMOS memory. An address counter is incremented by one count for every byte stored. When data are to be read out, the address counter is cleared and the first datum stored is the first read out.

The memory for the probes is composed of four hybrid packages, each containing ten 256-bit COSMOS integrated circuit memories. Each package can be viewed as a 2560 word by one bit memory. These four hybrids are addressed in parallel to form a 2560 word by four-bit memory. The address counter is composed of an eight-stage binary counter which,

Table 7.7-14. Large Probe DHC Characteristics, Thor/Delta

1. BASIC CLOCK FREQUENCY	4.194304 MHZ STABILITY = 0.01%
2. TYPE OF DATA AND MODULATION	PCM/PSK/PM
3. BIT RATES	1024 BPS 170.7 BPS 93 BPS 512 BPS 146.3 BPS 85.3 BPS 341.3 BPS 128 BPS 78.8 BPS 256 BPS 113.9 BPS 73.2 BPS 205 BPS 102.4 BPS 68.3 BPS
4. DATA INPUT CHANNELS	
MAIN FRAME	ANALOG - 64 DIGITAL - 16 BILEVEL - 8
SUBFRAME	ANALOG - 40 DIGITAL - 0 BILEVEL - 16
5. INPUT VOLTAGE RANGE	0 TO +5 VOLTS ANALOG, DIGITAL AND BILEVEL COMPARATOR THRESHOLD = +2.0 VOLTS
6. A/D ACCURACY	10 BITS ($\pm .05\% \pm 2.5$ mV)
7. DATA OUTPUT	BIPHASE MODULATED NRZ-L
8. SUBCARRIER FREQUENCY	16.384 KHZ $\pm 0.02\%$ SQUARE WAVE
9. DATA CODING	CONVOLUTIONAL RATE 1/3, K = 6
10. OPERATING MODES	1. REAL TIME 2. TELEMETRY STORE 3. REAL TIME WITH MEMORY READOUT
11. DATA FORMATS	A - PREENTRY, SEISMIC B - BLACKOUT D ₁ - DESCENT, HIGH ALTITUDE D ₂ - DESCENT, LOW ALTITUDE
12. FRAME SIZE	
MAIN FRAME	A ₁ 504 BITS, 8 AND 10 BIT WORDS D ₁ 504 BITS, 8 AND 10 BIT WORDS D ₂ 480 BITS, 8 AND 10 BIT WORDS B ₁ 504 BITS, 8 AND 10 BIT WORDS, STORED DATA ONLY
13. FRAME COUNTER	IDENTIFIES UP TO 1024 FRAMES
14. POWER REQUIREMENTS	3.0 W
15. SIZE	2620 CM ³
16. WEIGHT	1.4 KG

Table 7.7-15. Small Probe DHC Characteristics, Thor/Delta

1. BASIC CLOCK FREQUENCY		4.194304 MHZ STABILITY = 0.01%	
2. TYPE OF DATA AND MODULATION		PCM/PSK/PM	
3. BIT RATES	128 BPS	21.3 BPS	11.6 BPS
	64.0 BPS	18.3 BPS	10.7 BPS
	42.7 BPS	16.0 BPS	9.85 BPS
	32.0 BPS	14.2 BPS	9.15 BPS
	25.6 BPS	12.8 BPS	8.53 BPS
4. DATA INPUT CHANNELS			
MAIN FRAME		ANALOG	- 16
		DIGITAL	- 8
		BILEVEL	- 8
SUBFRAME		ANALOG	- 32
		DIGITAL	- 8
		BILEVEL	- 24
5. INPUT VOLTAGE RANGE		0 TO +5 V ANALOG, +2.0 V THRESHOLD ON BILEVEL AND DIGITAL	
6. A/D RESOLUTION		10 BITS	
7. DATA OUTPUT		BIPHASE MODULATED NRZ-L	
8. SUBCARRIER FREQUENCY		16.384 KHZ \pm 0.02% SQUARE WAVE	
9. DATA CODING		CONVOLUTIONAL RATE 1/3, K = 3	
10. OPERATING MODES		1. REAL TIME 2. TELEMETRY STORE 3. REAL TIME WITH MEMORY READOUT	
11. DATA FORMATS		A - PREENTRY & SEISMIC B - BLACKOUT D - DESCENT	
12. FRAME SIZE			
MAIN FRAME		A - 264 BITS, 7 AND 10 BIT WORDS B - 264 BITS, 7 AND 10 BIT WORDS, STORAGE ONLY D - 264 BITS, 7 AND 10 BIT WORDS	
13. FRAME COUNTER		IDENTIFIES UP TO 1024 FRAMES	
14. POWER REQUIREMENTS		2.2 W	
15. SIZE		1980 CM ³	
16. WEIGHT		0.9 KG	

Table 7.7-16. Large Probe Sequencer Discrete Event Channel Assignments, December 1972 Science

<p>A. 0 (NOT USED) 1 FORMAT A 2 FORMAT B 3 FORMAT D1 4 FORMAT D2 5 SCIENCE POWER A <u>ON</u> 6 SCIENCE POWER A <u>OFF</u> 7 COAST TIMER POWER <u>OFF</u> 8 PARACHUTE DEPLOYMENT <u>FIRE</u> 9 MASS SPEC - TUBE 1 <u>OPEN</u> 10 MASS SPEC - TUBE 1 <u>CLOSE</u> 11 MASS SPEC - TUBE 2 <u>OPEN</u> 12 MASS SPEC - TUBE 2 <u>CLOSE</u> 13 MASS SPEC - TUBE 4 <u>OPEN</u> 14 MASS SPEC - TUBE 4 <u>CLOSE</u> 15 SPARE</p>	<p>B. 0 (NOT USED) 1 TRANSMITTER DRIVER, RECEIVER, AND ENGINEERING XDUCE POWER <u>ON</u> 2 TRANSMITTER DRIVER, RECEIVER, AND ENGINEERING XDUCE POWER <u>OFF</u> 3 SHOCK LAYER RADIOMETER CALIBRATION <u>ON</u> 4 SHOCK LAYER RADIOMETER CALIBRATION <u>OFF</u> 5 SCIENCE POWER C <u>ON</u> 6 SCIENCE POWER C <u>OFF</u> 7 PYRO'S <u>DISARM</u> 8 PYRO'S <u>ARM</u> 9 SHOCK LAYER RADIOMETER THRESHOLD SENSOR <u>ARM</u> 10 SHOCK LAYER RADIOMETER THRESHOLD SENSOR <u>DISARM</u> 11 MASS SPEC HEATER HIGH <u>ON</u> 12 MASS SPEC HEATER <u>OFF</u> 13 AEROSHELL FOREBODY JETTISON <u>FIRE</u> 14 INTERNAL POWER <u>OFF</u> 15 SPARE</p>
<p>C. 0 (NOT USED) 1 MODE 1 (TRANSMIT REAL TIME DATA) 2 MODE 2 (TRANSMIT AND STORE) 3 MODE 3 (STORE ONLY) 4 SPARE 5 SCIENCE POWER B <u>ON</u> 6 SCIENCE POWER B <u>OFF</u> 7 FOREBODY ELECTRICAL CABLE CUTTER <u>FIRE</u> 8 MASS SPEC - TUBE 6 <u>OPEN</u> 9 MASS SPEC HEATER LOW - <u>ON</u> 10 COAST TIMER POWER <u>ON</u> 11 HYGROMETER POWER <u>OFF</u> 12 MASS SPEC - TUBE 3 <u>OPEN</u> 13 MASS SPEC - TUBE 3 <u>CLOSE</u> 14 AUREOLE/EXTINCTION DETECTOR POWER <u>OFF</u> 15 SPARE</p>	<p>D. 0 (NOT USED) 1 TRANSMITTER POWER AMPLIFIER, POWER <u>ON</u> 2 TRANSMITTER POWER AMPLIFIER, POWER <u>OFF</u> 3 DATA BIT CLOCK <u>START</u> 4 DATA BIT CLOCK <u>STOP</u> 5 SCIENCE POWER D <u>ON</u> 6 SCIENCE POWER D <u>OFF</u> 7 WINDOW HEATER POWER <u>ON</u> 8 WINDOW HEATER POWER <u>OFF</u> 9 MASS SPEC INLET CAP EJECTION <u>FIRE</u> 10 AFTER BODY ELECTRICAL CABLE CUTTER <u>FIRE</u> 11 AFTER BODY PARACHUTE <u>RELEASE</u> 12 MASS SPEC - TUBE 5 <u>OPEN</u> 13 MASS SPEC - TUBE 5 <u>CLOSE</u> 14 SPARE 15 SPARE</p>

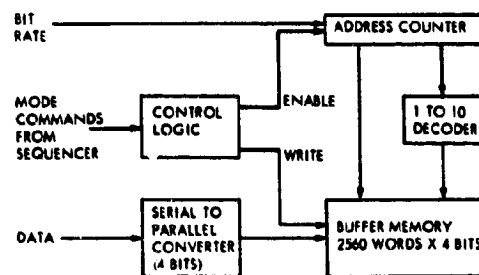


Figure 7.7-17. Data Buffer/Memory

in turn, feeds a decade counter. The output of the decade counter drives a 1 of 10 decoder. The output of the decoder selects the particular IC chip in a hybrid package into which data are stored.

Costs are reduced by using the same hybrids used in the orbiter.

7.7.5.3 Timing and Format Generator

The timing and format generator generates all timing pulses for the DHC by counting down the output from a crystal oscillator. The bit rate is variable through the use of a programmable counter that is controlled by the descent timer/programmer (DTP). Four separate formats are stored in the format generator composed of four PROMs. Format selection is controlled by the DTP. A block diagram of the timing and format generator is given in Figure 7.7-18.

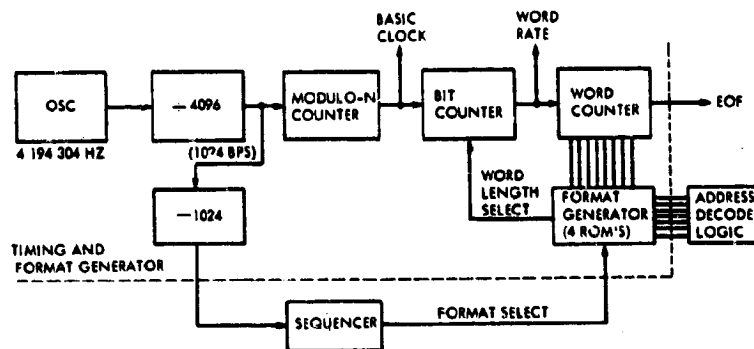


Figure 7.7-18. Timing and Format Generator Interface, Large Probe

The oscillator runs at 4 194 304 Hz. This frequency was selected so that the 1-second sequence clock could be obtained by dividing the oscillator frequency by an integral multiple of 2 (2^{24}).

A high clock rate (1024 for the large probe and 128 for the small probe) is fed into the modulo-N counter, which can be commanded to divide by any integer between 1 and 15. In this way the system bit rate can be varied as required throughout the mission. This bit rate is then divided by 7, 8, or 10, under control of the format generator, to generate word rate pulses. The word pulses, in turn, are counted in a word counter to provide an end of frame (EOF) indication. The parallel outputs from the word counter are used to provide an eight-bit address to the format generator. Each PROM in the format generator is 256 words by 8 bits. Power is applied to the PROMs for 8 μ s at the beginning of each word pulse. The eight-bit word read from a PROM is stored in a low power IC register and is used to control the word length and to provide an address to the multiplexer.

7.7.5.4 Multiplexer

The multiplexer performs the functions of address decoding, signal multiplexing, and analog-to-digital conversion. A block diagram of the multiplexer is shown in Figure 7.7-19.

The multiplexer receives an eight-bit address from the format generator. Six address bits are used to select a measurement, and one bit is used to determine whether it is an 8- or 10-bit measurement (large probe) or a 7- or 10-bit measurement (small probe). The address detector determines whether the address is multiplexed locally, or remotely in the experiment, and if it is a subcommutated address. Control signals are then issued to the proper multiplexer. Several engineering and instrument temperature measurements require a current source for the thermistors and this demultiplexing is done in parallel with the multiplexing operation. Timing pulses are also supplied as required. Separate analog ground returns from each experiment are multiplexed along with the signal leads.

The temperature measurements are low-level signals (approximately 1-40 mV) and are fed through a low-level amplifier to raise them to the standard 0-5 volt range. The outputs from the various multiplexers are then selected by a second-level multiplexer, fed through a differential to single-ended amplifier and into a ten-bit ADC. Digital and bilevel words are fed through a digital comparator. The outputs of the comparator and ADC are combined and fed out to the data storage unit as a continuous bit stream.

7.7.5.5 Data Framing for Probe Communications

For the Thor/Delta configuration, the Viterbi algorithm is the preferred decoding method for the probe channels. This is discussed in the communications section (paragraph 7.6). This decoding method requires no frame synchronization so that framing techniques need only be concerned with attaining correct data blocking. The data frame synchronization can be done entirely after decoding, i. e., on the decoded data that gives error protection to the framing sequence and simplifies the decoding procedure.

A framing sequence must be chosen that has satisfactory correlation properties in a noiseless environment to separate it from data, and which

will also give acceptable probabilities for correct data framing with noise present. The bit error rates (BER) on the typical probe channels will be about 10^{-4} and data framing must be achieved in this noise environment. Frame synchronization can be accomplished by using either a prefix method (insertion of a known sequence called a prefix or comma), or a comma-free method. Only the prefix method will be considered at this time with concentration on Barker sequences.

Barker sequences are limited in length to 13, three of which are given below,

$$N = 3, \quad 110$$

$$N = 7, \quad 1110010$$

$$N = 11, \quad 11100010010.$$

For p (bit error probability) = 10^{-4} , the probability of making an error within a frame sequence of length $N = 11$ is approximately 10^{-3} ; and the probability of two frames each containing a bit error is approximately 10^{-6} . Hence, the number of repetitions, M , of the sequence required to attain synchronization due to noise errors is small. To establish frame synchronization the following decision variable can be used:

$$Z_v = p^{d_v} (1 - p)^{Mn - d_v}$$

where n is the number of bits in the synchronizing sequence, d_v is the Hamming distance (number of bit value differences) between the observed sequences hypothesized to give frame synchronization and the actual sequence, and v is the epoch or the index of the frame synchronization being considered. For frame synchronization, Z_v is maximized with respect to v . For $p < 1/2$ the decision variable can be simplified to:

$$Z_v = d_v$$

For Barker-type sequences the number of repetitions, M , of the sequence required for synchronization can be approximated by:

$$M \approx \left[\frac{p(1-p) + \frac{q-1}{2}}{N\left(1 - \frac{1}{q} - p\right)} \right] \cdot \left[2 \ln \left(\frac{1}{p_e} \right) \right]$$

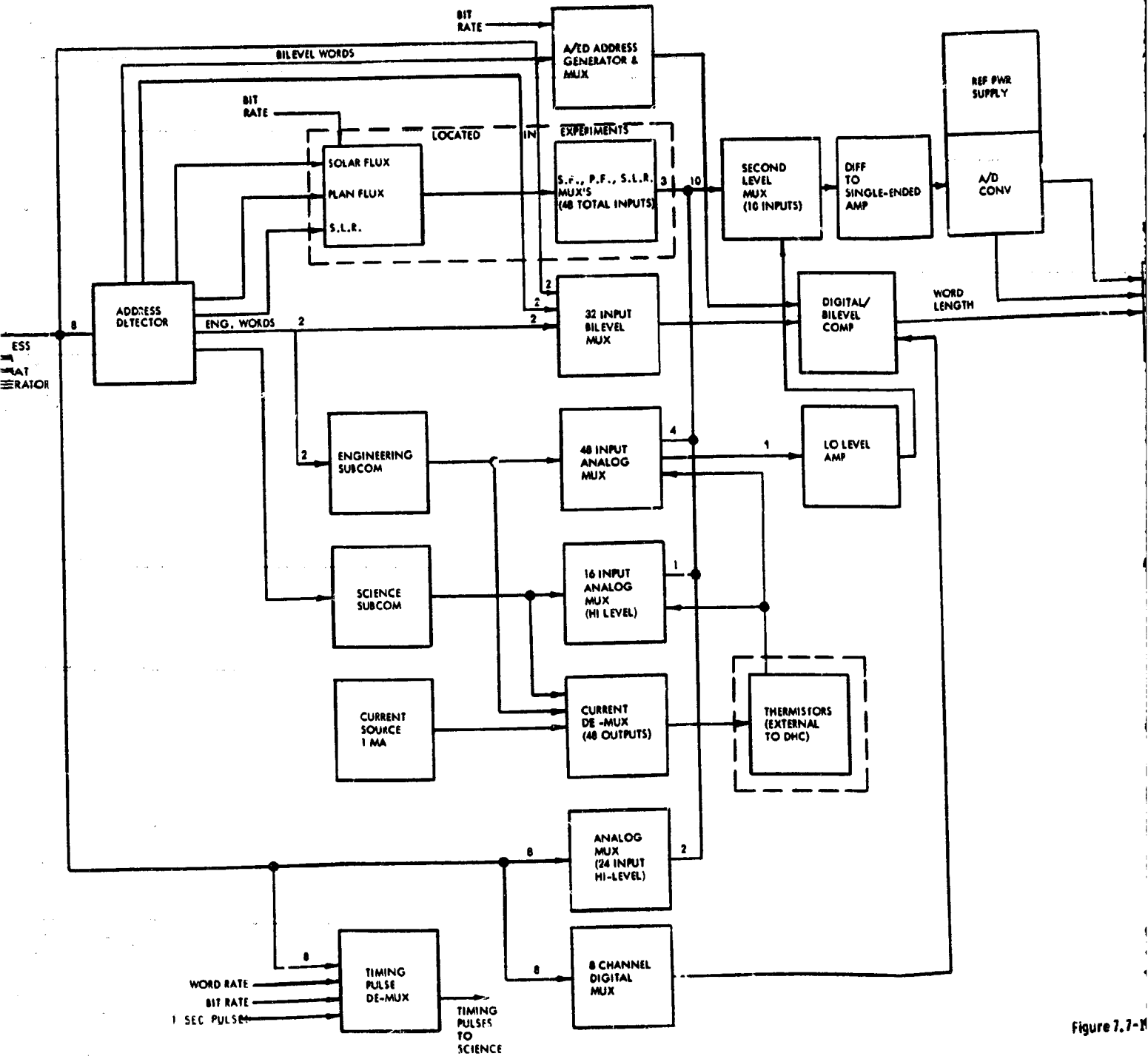


Figure 7.7-M

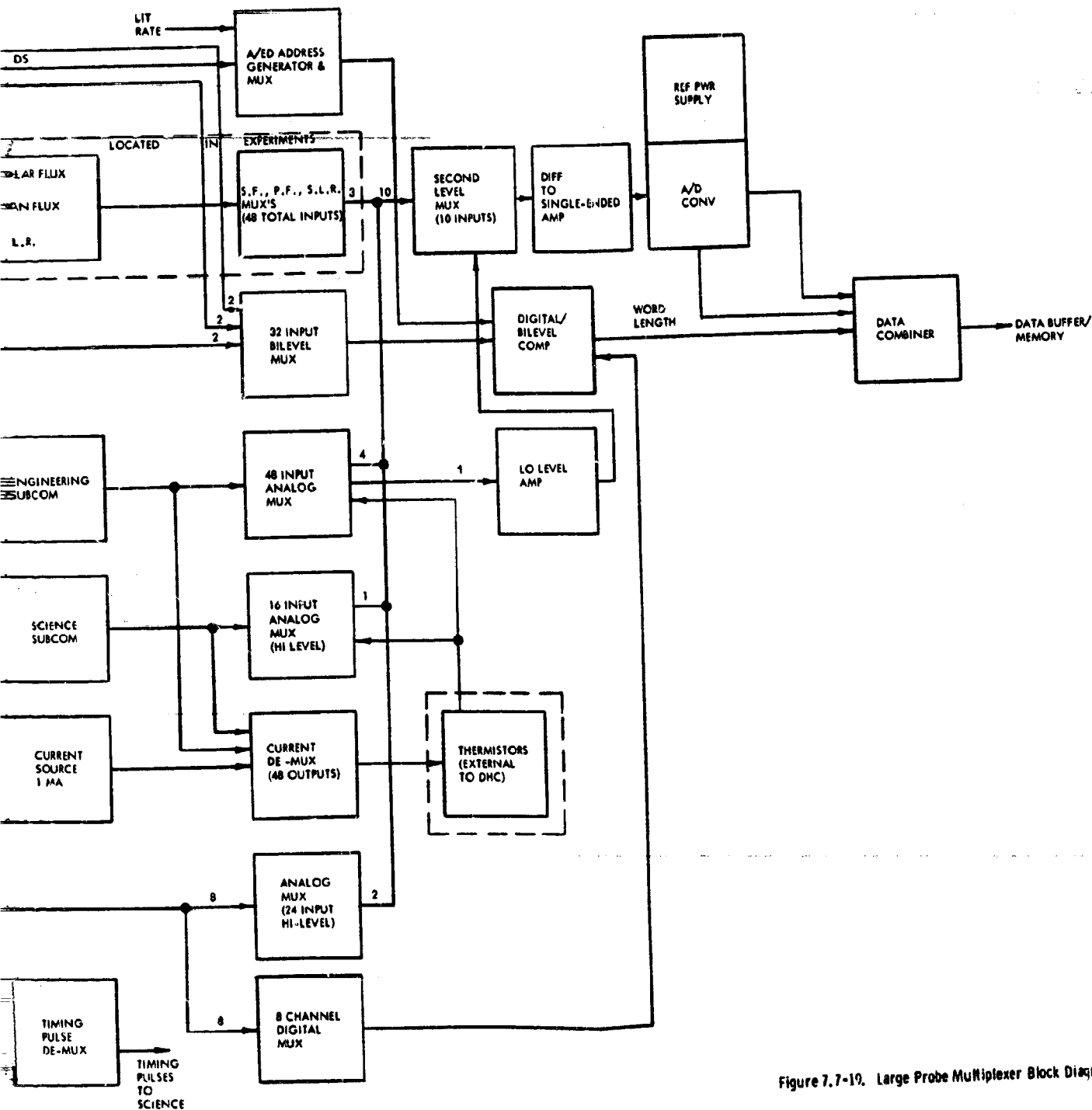


Figure 7.7-10. Large Probe Multiplexer Block Diagram

where $q = 1-p$ and P_e is the probability of incorrect synchronization. For example, with $N = 11$, $p = 10^{-1}$, and a desired $P_e = 10^{-2}$, $M = 13.8$ while for $p = 10^{-3}$, $P_e = 10^{-2}$,
 $M = 1.38 \times 10^{-3}$

Since $M < 1$, only one iteration is required. Results are, of course, better for a $p = 10^{-4}$ or better BER.

7.8 Electrical Power



7.8 ELECTRICAL POWER

This section contains requirements, power profiles, and battery sizing data for the Atlas/Centaur and Thor/Delta probes.

7.8.1 Introduction and Summary

The probe electrical power subsystem consists of the battery, which is the primary source of power for all independent probe operations, and the Power Control Unit (PCU). A simplified block diagram is shown in Figure 7.8-1. The PCU controls the power to all using subsystems, contains the fault isolation circuits and provides the firing circuits for pyrotechnic initiators. In addition, portions of the Data Handling and Command (DHC) subsystem such as the coast timer, descent sequencer, and data storage unit are packaged in the PCU to eliminate the need to design and qualify another separate box. In arriving at the preferred design for the electrical power subsystem, a number of trade studies were conducted, including:

- Probe battery analysis and selection
- Regulated versus unregulated bus
- Cell bypass versus no bypass
- Inflight charge versus no-flight charging
- Relays versus solid state switching
- Capacitor versus direct battery pyro firing.

The results of these studies, discussed in the paragraphs that follow, combined with the mission requirements and the derived load profiles led to the preferred subsystem design for each mission option. For the 1978 mission with Atlas/Centaur launch vehicle and the Version IV (April 1973) science payload and descent profile, the subsystem description follows.

Silver Zinc Battery. This battery was selected because of its long life with high energy density (83 W-hr/kg), its minimum charge stand losses, because it has successfully passed 750-g acceleration tests and is capable of providing 526 W-hr of energy as required for the mission with ± 10 percent regulation.

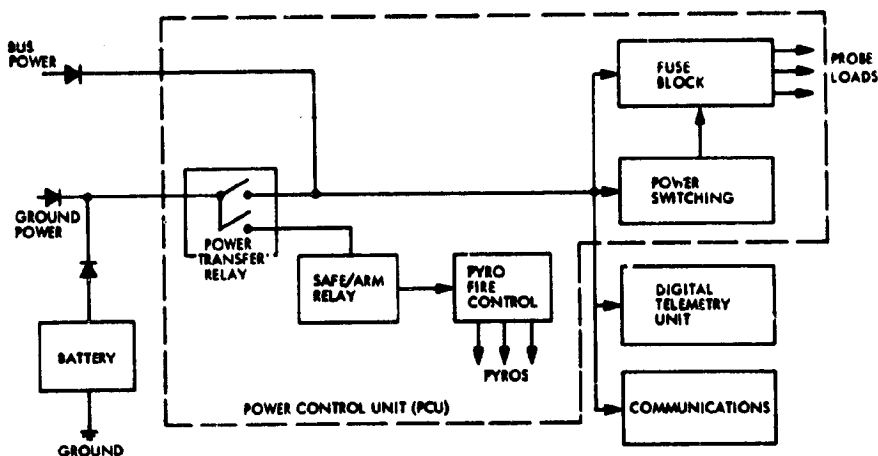


Figure 7.8-1. Probe Electrical Power Subsystem, Simplified Block Diagram

Power Control Unit. This unit provides the timing, sequencing, command, control functions, fault isolation, and pyrotechnics ignition.

7.8.2 Requirements

The Atlas/Centaur probe battery requirements are summarized in Table 7.8-1 for the large and small probes.

Table 7.8-1. Battery Requirements Summary, Atlas/Centaur Configuration

	LARGE PROBE	SMALL PROBE
WET STAND TIME	16 MONTHS	16 MONTHS
MISSION DURATION	133 DAYS	133 DAYS
DISCHARGE TIME (ENTRY)	1.20 HR	1.10 HR
MAXIMUM ACCELERATION (QUAL LEVEL)	600 G	600 G
TOTAL ENERGY	526 W-HR	246 W-HR
MAXIMUM ORDNANCE FIRING CURRENT	36 AMP	--
BATTERY TEMPERATURE RANGE	-18 TO 85°C	-18 TO 85°C
VOLTAGE TO USERS		
A) SCIENCE	28 VDC \pm 10%	28 VDC \pm 10%
B) SUBSYSTEMS	28 VDC \pm 10%	28 VDC \pm 10%
BATTERY HEATER POWER (PREENTRY)	80 W-HR	40 W-HR

The time-phased load profiles for the Atlas/Centaur large and small probes are shown in Figures 7.8-2 and 7.8-3. During probe checkout before separation, probe battery power is used only for the transmitter and required telemetry. Science, DHC, and transducer checkout power is supplied by the probe bus.

7.8.3 Tradeoff Studies

7.8.3.1 Probe Battery Analysis and Selection

The key parameters imposed by the probe requirements are weight, volume, dynamic environment, life, mission reliability, and cost.

The majority of sources can be immediately eliminated by the major probe constraints of battery volume allocation, 0.175 W-hr/cm^3 ($2.87 \text{ W-hr-hr/in.}^3$) and low cost. Typical of those considered and rejected on these bases were Ni-Cd and Ag-Cd.

Systems satisfying both volume and cost were Ag-Zn, Hg-Zn, and Hg-Cd. All systems have satisfactory energy density considerations (W-hr/kg) but both mercuric oxide couples are extremely sensitive to load variations and would need to be significantly oversized to satisfy the voltage criteria. The Ag-Zn system, of course, is not without its limitations. The following study compares the Ag-Zn cell performance characteristics with the operational requirements.

Silver-Zinc Battery Study

Martin Marietta has been developing a high energy density long-life battery specifically for use in planetary probes. This task has been performed under the auspices of IRAD number 48705 and is described in Appendix 7.8A. Results to date demonstrate that a probe battery with an end-of-life energy density of 92.4 W-hr/kg is attainable for the Venus mission. Subsequent to the issuance of this report, significant changes have occurred in the baseline design of the Pioneer Venus battery. The IRAD task has been redirected to include these changes and at the same time some improvement has been incorporated into newly designed cells.

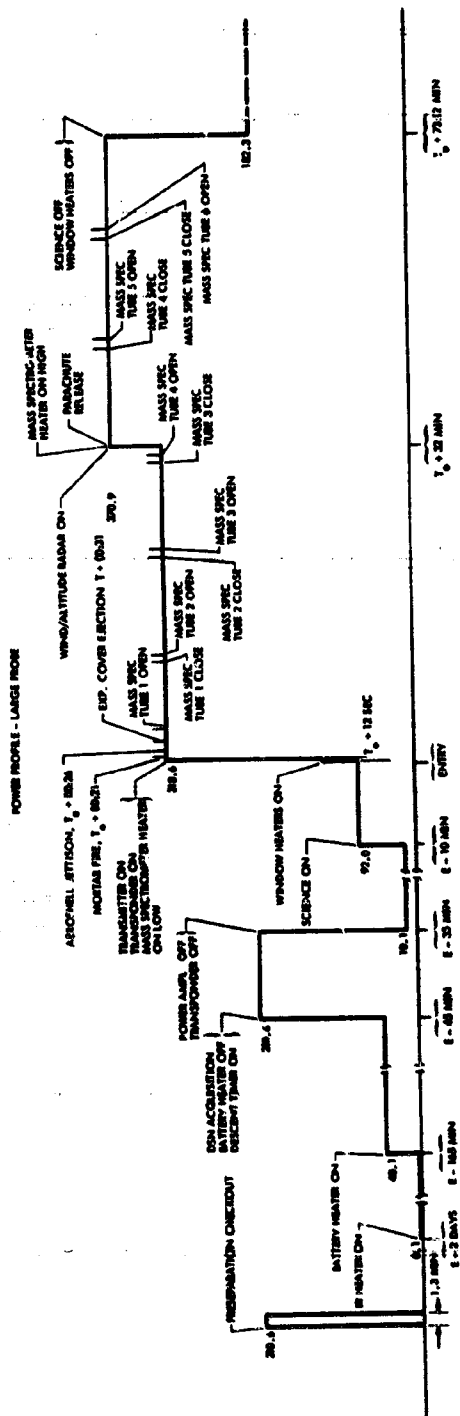


Figure 7.9-2 Power Profile, Large Probe

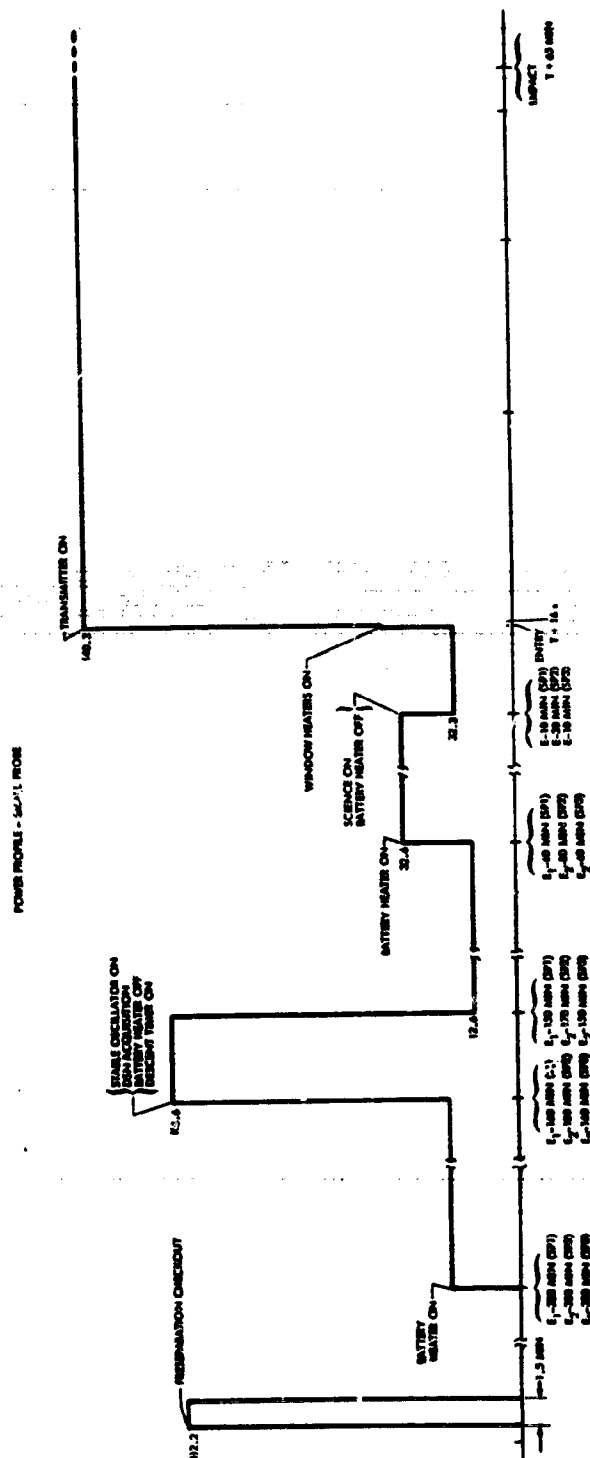


Figure 7.8-3. Power Profile, Small Probe

Cell Design Improvements

- 1) Positive plate manufacturing process revised to ensure closer tolerances on plate porosity.
- 2) Negative plate width increased to positive plate width.
- 3) One layer of polyvinyl alcohol film (PVA) placed between permion separators to reduce separator oxidation and increase cell life.

These changes have increased the original cell capacity by 25 percent within the same volume constraints.

Redirected Studies

The IRAD task has been modified to include the following studies: (1) sealed cells, (2) monoxide charge, (3) passivation (charge open circuit stand), (4) passivation (discharge open circuit stand), (5) pulse loads.

Preliminary results to date show that the IRAD cell design meets all the Pioneer Venus additional requirements specified above. The final report (to be published in December 1973) will document this data.

Standard aerospace Ag-Zn cells were considered for use in the Atlas/Centaur application to reduce costs. It was determined, however, that the increased weight and volume required did not justify the small parts cost saving. A cost saving was realized as a result of commonality in use of two parallel connected small probe batteries to supply the large probe power requirements. A sketch of the Atlas/Centaur battery is shown in Figure 7.8-4.

ENERGY STORAGE CAPACITY	343 W-HR
A-HR CAPACITY MONOVALENT	12.8 A-HR
MASS	4.64 KG
SIZE	31.6 X 14.8 X 6.4 CM
NO. OF CELLS	20
VOLUME	2800 CM ³
BATTERY HEATERS	20 W

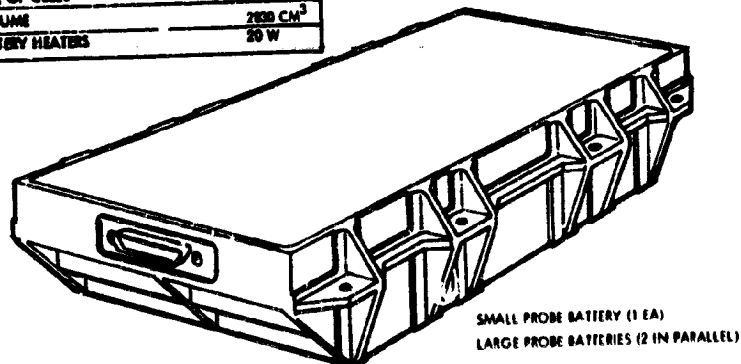


Figure 7.8-4. Atlas/Centaur Probe Battery Configuration

The flat monovalent discharge characteristic results from limiting the voltage on charge to 1.92 volts/cell. By limiting the formation of the more active divalent silver oxide (AgO), a capacity penalty of 25 percent results, while wet stand capacity retention is improved. The divalent charge method requires a discharge regulator to meet ± 10 percent voltage regulation because of the wider voltage variation during discharge.

Sizing of the power system to include a regulator for the required power increases the total probe mass by 7.6 kg. This includes two 13-cell batteries and a 340-watt regulator with an efficiency of 85 percent. Although the battery has fewer cells, they are larger in weight and volume to meet the total power requirement. Appendix 7.6B shows that the monovalent operation of the battery results in a lighter weight system with smaller volume and lower costs. Secondary voltages (which are a small portion of the total power) are provided by power conditioning within the user subsystem.

We concluded that regulation was unnecessary since only 2 watts of small probe unit power and 8 watts of large probe unit power required ± 2 percent regulation; the remaining demand was unregulated (± 10 percent) power. This small amount of regulated power for experiments can be supplied by the user requiring it, with a series regulator. The ± 10 percent regulation is achieved through control of the battery discharge voltage characteristic as shown in Figure 7.8-5.

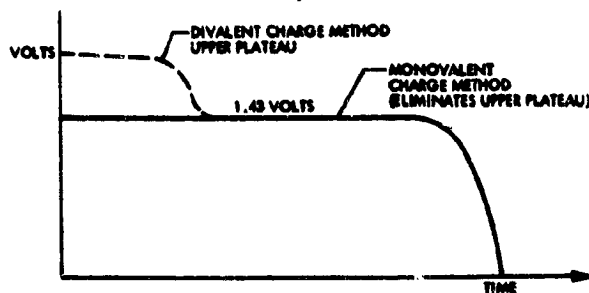


Figure 7.8-5. Ag-Zn Discharge Voltage Characteristic

The battery temperature must be controlled between 12 and 28°C while discharging to maintain ± 10 percent regulation (Appendix 7.8A). Both the small and large probes have a battery heater that is activated

3 hours before entry to raise the battery temperature. (Appendix 7.8A provides detailed information for battery heater calculation and design.)

Advantages of monovalent operation in addition to a flat discharge characteristics are as follows:

- Charged stand losses during cruise are reduced.
- The lower oxidizing potential reduces attack on integrity of separation material.
- Transient load performance is better.
- Open circuit voltage measurement becomes viable indication of full charge.
- Requirement for discharge regulator eliminated; weight, volume, and cost savings. Each battery consists of 20 series-connected cells contained in a fiberglass wrap structure with associated thermistors, heater, thermostatic switch, and a Cannon series DMA connector. The configuration of the preferred battery design is shown in Figure 7.8-4. For the Atlas/Centaur, the large probe uses two small probe batteries connected in parallel to the power bus; the small probe uses a single battery. The increased weight capability of the Atlas/Centaur allows a common battery to be used for both the large and small probe. This commonality reduces cost.

7.8.3.2 Regulated versus Unregulated Bus

The regulated versus unregulated power bus study, Appendix 7.8B identifies losses and margins that apply to the Atlas/Centaur design. An unregulated power bus was chosen for the Atlas/Centaur probe because of lower weight, volume, and cost, and an improvement in reliability. The tradeoff between regulated versus unregulated bus discussed in Section IV of Appendix 7.8B differs in that redundant regulators were used in sizing the power system. This comparison was updated for a nonredundant regulator and the tradeoff between alternative approaches is shown in Table 7.8-2.

There is a substantial savings in volume and weight for the large probe. By deleting the boost regulator, a substantial cost savings would also be realized by eliminating the design and development of an additional component.

The reliability of two 20-cell silver zinc batteries in parallel through isolation diodes for the large probe is 0.9967 while the small probe with a single 20-cell battery has a reliability of 0.9985. This gives a baseline

probe reliability of 0.945 for the large probe and 0.964 for the small probe. A discharge regulator and two 13-cell silver zinc batteries in the large probe has a reliability of 0.9369 and the reliability of the small probe is 0.9666. The total probe reliability with two 13-cell batteries and a regulator is 0.888 while the small probe reliability falls to 0.933.

Table 7.8-2. Bus Regulation Trade Summary

	BATTERY		BOOST REGULATOR		TOTAL	
	MASS (KG)	VOLUME (CM ³)	MASS (KG)	VOLUME (CM ³)	MASS (KG)	VOLUME (CM ³)
LARGE PROBE						
WITH REGULATOR	14.5	12 220	2.56	5 900	17.06	18 100
WITHOUT REGULATOR	9.28	5 550	-	-	9.28	5 550
SMALL PROBE						
WITH REGULATOR	7.36	6 150	0.594	1 188	7.954	7 338
WITHOUT REGULATOR	4.64	2 830	-	-	4.64	2 830

Since a regulator increased the weight and reduced the reliability of the probes, direct discharge battery system providing ± 10 percent regulation was chosen.

7.8.3.3 Cell Bypass versus No Bypass

The Pioneer 10 and 11 type bypass electronic circuitry in the large probe battery was omitted from the baseline design because of excessive battery power consumption. During the 133-day period before entry, the bypass circuits would require approximately 90 W-hr (28 milliwatt load on the battery).

The use of silicon diodes for bypass protection (open circuits only) would result in a minimal weight increase (diode + heat sink) and 12 W-hr of power drain.

The reliability of the large probe battery with diodes is increased to 0.99889 from a reliability of 0.9984 without diodes. This results in a probe reliability of 0.9455 with diodes, from a reliability of 0.9456 without diodes. Only the fifth significant figure changes due to the addition of diodes. The bypass diodes do not increase the reliability sufficiently to warrant the extra parts and weights.

7.8.3.4 Inflight Charging versus No-Flight Charging

The proposed Phase B Pioneer Venus, bus/probe, electrical power subsystem included an inflight probe battery charging capability. This capability was provided to restore the following battery capacity losses.

Planned capacity losses

- Cruise charge stand losses,
- Preseparation checkout power consumption.

Non-planned capacity losses

- Battery cell failure (shorting),
- Parasitic loads,
- Extended discharge duration.

Planned Capacity Loss

The basic design of the battery uses the more conservative, monovalent conversion of the positive plate (silver) during charge. This results in a substantial reduction in charge stand losses during cruise. During charge stand, the electrodes self discharge. This discharging varies with temperature. The reaction proceeds more slowly at room temperature and below. Throughout the cruise the battery temperature is between -18°C and 4°C (0 and 40°F); thus the losses will be low.

Preseparation power will be supplied from the bus except for one minute maximum of operation on the probe battery to verify battery and RF transmitter function.

It can be seen that a minimal amount of capacity will have to be restored because of charge stand losses and preseparation checkout.

Non-Planned Capacity Losses

Loss of a cell due to a short would reduce the battery voltage by 5 percent. Trying to restore this capacity would involve an elaborate control system for the ground crew to eliminate over-charging. Without this charge control system, the battery would charge to the divalent state and create gas thus increasing the degradation of the battery and a possibility of rupturing a cell, thus causing the total loss of the battery and probe.

Loss of capacity due to the parasitic load of a shorted coast timer is minimized by use of an isolation resistor of approximately 500 k ohms, and a magnetic latching relay contact that activates the timer from a command in the sequencer unit.

The probe battery has been sized to provide a regulation of ± 10 percent for the total mission duration, with a 5 percent capacity loss in 4 months from launch.

Based on the considerations that (1) a minimal amount of capacity would have to be restored because of charge stand losses and preseparation checkout, (2) the bus would have to supply logic for automatic and ground override charge control and termination with switching for sequencing the 4 batteries plus tracking station surveillance with a specialized crew for up to 72 hours of charging of a shorted cell battery, and (3) the bus would require a special converter/charger that could supply 40 volts of high accuracy voltage and current telemetry, no inflight charging is planned for the probe mission.

7.8.3.5 Relays versus Solid State Switching

Selection of magnetic latching relays over solid state switching was based primarily on their low power losses. Relays in the open state have a zero power drain and no voltage drop in the closed state. Solid state switching devices, on the other hand, have leakage drain in the open state and have from 0.5 to 1.0 volts drop in the closed state. The high current demand of the pyro firing system (36 amperes, or higher) which are transient in nature prohibits the use of solid state switch as the main power transfer. Also, the use of solid state devices would require a larger battery to supply the additional energy requirement. Since relay contact contamination is a major failure mode, redundant contacts or redundant relays will be used in all relay switching circuits.

7.8.3.6 Capacitor versus Direct Battery Pyro Firing

Firing of pyro devices directly from the probe battery and controlling the current flow to each bridgewire to reduce the transient effect on the bus was selected over the capacitor bank firing method. A magnetic latching relay is used as the pyro bus arming switch. Each bridgewire is fired by triggering a silicon controlled rectifier. A current limiting resistor is inserted in each bridgewire circuit and is sized to provide a minimum of amperes at the minimum bus voltage. The bus voltage will not drop below 20 volts during the maximum pyro current transient.

Recycling the safe/arm relay after each pyro firing event will interrupt any leakage current due to low impedance leakage paths in the ordnance devices and allow the silicon controlled rectifiers to turn off. Using the probe battery reduces the weight and volume problem of packaging and qualifying a separate capacitor firing system.

The capacitor bank pyro firing system does eliminate the transient load changes on the bus; however, the complexity and the volume of space required to package this system requires twelve 82- μ f capacitors, connected in parallel and charged to between 36 and 40 volts to fire a pyro bridgewire. The Pioneer Venus probe would require a maximum of six capacitor banks to meet the ordnance redundancy requirement and the number of bridgewires fired simultaneously. The volume required to package one capacitor bank is 53.3 cm³.

7.8.4 Preferred Electrical Power Subsystem, Atlas/Centaur

7.8.4.1 Battery

A 20-cell silver-zinc rechargeable battery designed and conditioned to operate in the flat monovalent silver discharge voltage characteristic was chosen for the Pioneer Venus probe. The silver zinc battery was chosen for its high energy density, low charged stand losses and low cost of manufacturing in that both probes use identical batteries.

7.8.4.2 Power Control Unit (PCU)

The PCU is the central sequencing, timing control, and distribution point for the overall power subsystem. It is shown in Figure 7.8-6 and implements in the following functions:

- Descent sequencer and coast timer
- DC-DC converter
- Power transfer function and switching
- Pyro firing functions
- Fault isolation
- Power subsystem status (telemetry).

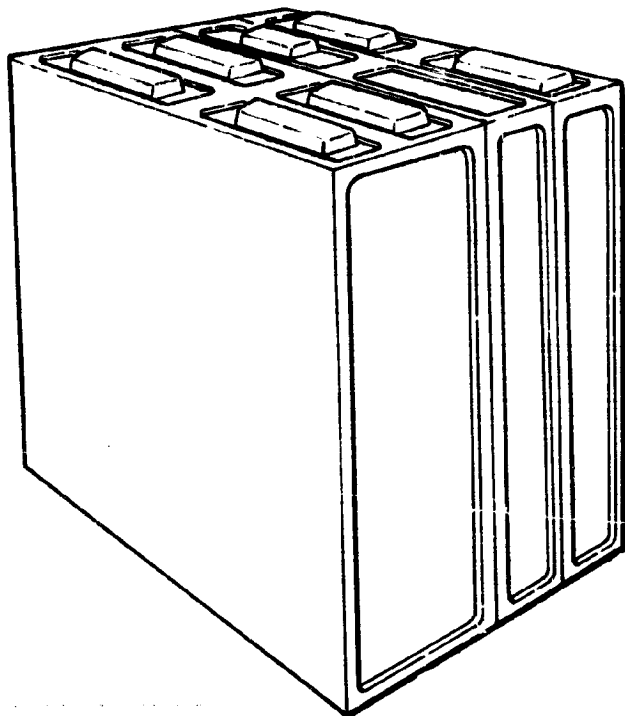


Figure 7.8-6. Atlas/Centaur Power Control Unit Configuration

PCU Functional Description

The PCU will be packaged in a rectangular chassis (15.4 x 15.4 x 9.6 cm). The assembly is comprised of seven "slices" of electronics. Double-sided printed circuit boards will be sufficient for this design. Relays are to be mounted such that their least sensitive axis will be parallel to the direction of deceleration. The chassis is aluminum. The mounting hardware, Cannon DMA connectors #24 hook-up wire STME 742 lightweight high strength copper wire developed for the Viking Project, will be used to reduce weight.

Two of the slices in the PCU comprise the timing sequencer and coast timer. A more detailed description of these two functions can be found in Section 7.7.4, the data handling and command section of this report. Basically, the sequencer and timer operate as follows.

Power Switching Function

[illegible]

Figure 7.8-7. Power Transfer Control

The capability to operate through the anticipated high sustained deceleration of entry has been demonstrated by tests at Martin Marietta in excess of 600 g's. All power switching is controlled by command signals from the DHC.

Pyro Firing Circuits

The ordnance firing and control functional diagram is presented in Figure 7.8-8. Standard initiators used on Viking have been selected. The safe and arming relay is controlled by command signals from the DHC. The relay is armed just before initiation of the firing signal and then returned to safe within 250 milliseconds after the pyro firing signal. This clears any shorts that may have developed as a result of pyro bridge short to ground by removal of voltage across the SCR. A current limiting resistor is employed to provide a minimum of 5 amperes per bridgewire at the expected battery voltage. With the relay in the safe condition the contacts provide a short across the SCR through the pyro bridge. The shorted bridge, SCR loop is also returned to single point power ground preventing static charge build up. The trigger circuit SCR combination is used on the VO-75 system. A trigger circuit module cast in epoxy contains eight firing circuits with mounting provisions and solder connections. The pyros are ignited in redundant groups of three for the fore- and afterbody release; the remaining pyros are redundant and activated separately.

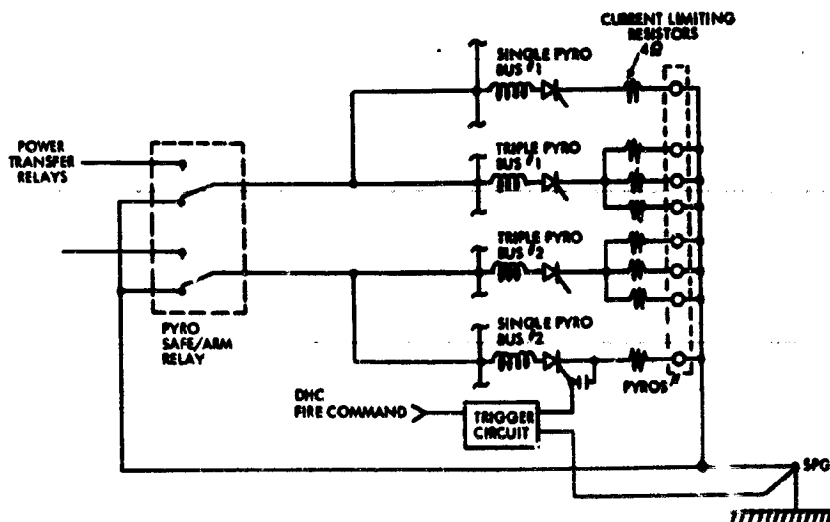


Figure 7.8-8. Pyro Firing Bus and Current Limiting Resistor Grouping

Overload and Fault Protection

Overload Protection. The probe electrical power system feeds both critical and noncritical loads. Critical loads are those loads necessary to maintain the probe subsystems operation while noncritical loads could fail without affecting the operation of other subsystems. Experiments were classified as noncritical loads since the loss of one or more experiments could be tolerated with the remaining experiments still supplying data.

Both overload protection and fault protection were considered for the noncritical loads. Overload protection requires the use of sophisticated bus monitoring techniques and a control scheme that would permit detection of overload conditions on an individual load basis with the capability to isolate each load from the distribution bus, when failures are detected. Both cost and weight penalties are incurred when using this type of system.

Fault Protection. Our alternative to using overload protection is to use a Hughes fault protection design. This technique has been used in the past and has been proven acceptable. Both the cost and weight impact as compared to the overload protection system are minimal. Only nonessential loads would be fused. This approach does result in a lower quality power bus since the fault load would be seen on the power bus until the fuse opened and cleared the fault. Since the battery selected for the probe power source is designed to deliver high peak or surge currents, the fault current during the fuse opening time would not appreciably affect the power quality.

7.8.5 Preferred Electrical Subsystem, Thor/Delta

The power requirement for the Thor/Delta must meet the same operational mission objectives and constraints as stated in Section 7.8.1 for the Atlas/Centaur approach. Cost reduction versus weight and volume was considered in the design approach. The systems power demand required resizing of the probe batteries.

7.8.5.1 Battery

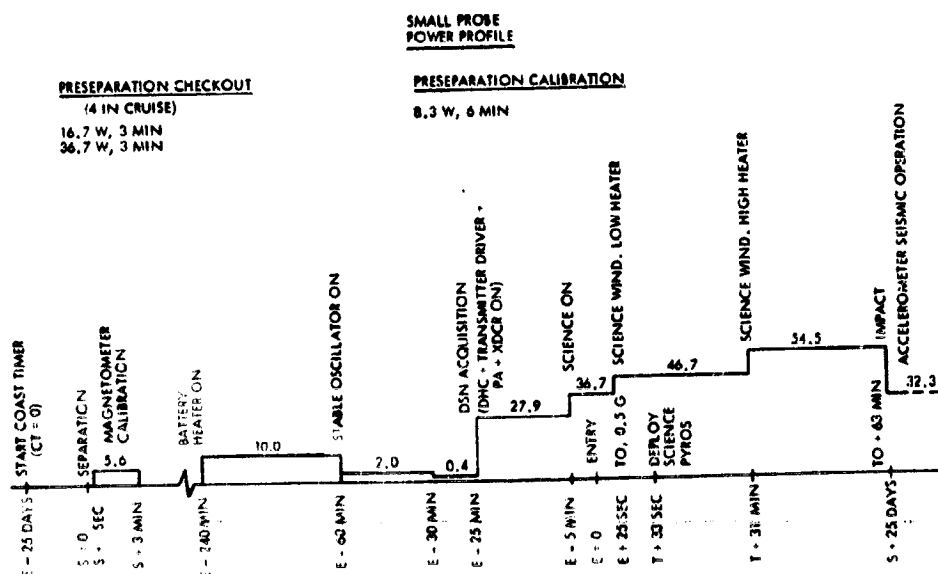
The Thor/Delta probe uses silver-zinc batteries in the monovalent mode of operation, but the power profile requirements for the large and small probe are such that they required two separately designed battery

packages. Cost reduction versus weight and volume was considered in the design with the primary emphasis on low weight because of the limited launch vehicle capability.

The Thor/Delta battery requirements are summarized in Table 7.8-3. The power profiles for the large and small probes are shown in Figures 7.8-9 and 7.8-10.

7.8-3. Thor/Delta Requirements Summary

	LARGE PROBE	SMALL PROBE
WET STAND TIME	16 MONTHS	16 MONTHS
MISSION DURATION	133 DAYS	133 DAYS
DISCHARGE TIME (ENTRY)	1.0 HR	1.0 HR
MAXIMUM DECELERATION	500 G	500 G
MAGNETIC PROPERTIES (AT 31 CM)	40 GAMMA	30 GAMMA
TOTAL ENERGY TO LOAD	182 W-HR	114.9 W-HR
MAXIMUM ORDNANCE FIRING CURRENT	5 AMP	5 AMP
BATTERY TEMPERATURE RANGE	-18 TO 85°C	-18 TO 85°C
VOLTAGES TO USERS		
A) SCIENCE	28 VDC \pm 10%	28 VDC \pm 10%
B) SUBSYSTEMS	28 VDC \pm 10%	28 VDC \pm 10%
BATTERY HEATER POWER (PREENTRY)	15 W-HR	30 W-HR



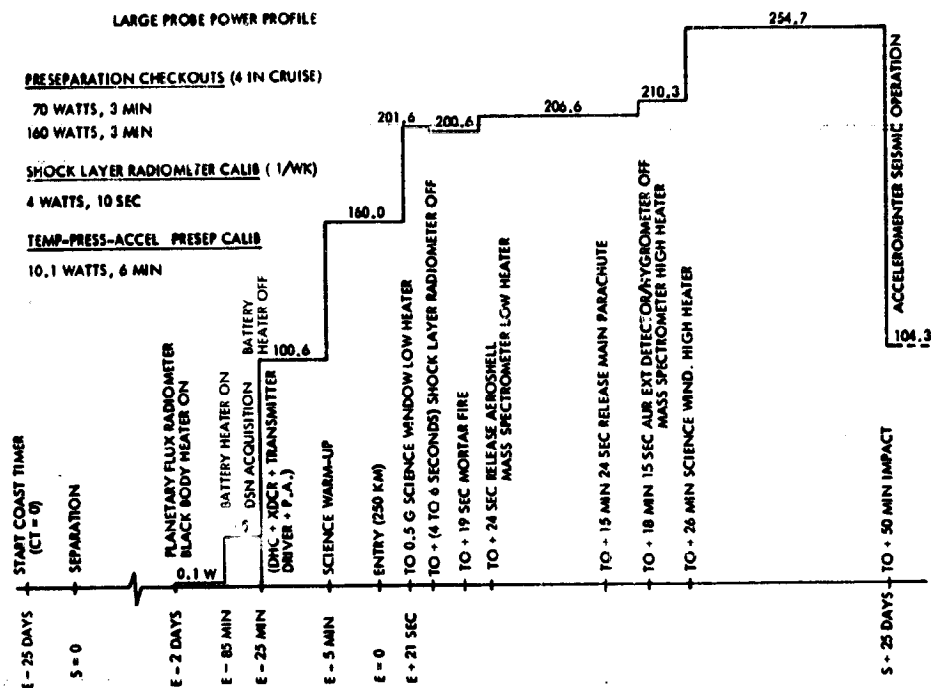


Figure 7.8-10. Thor/Delta Large Probe Power Profile

7.8.5.2 Power Control Unit

Thor/Delta - Large Probe

Packaging requirements for the Thor/Delta large probe lend themselves to a more conventional approach than do those of the small probe. The PCU will be packaged in a rectangular chassis (7.6 x 8.9 x 21.6 cm). Double-sided boards should be sufficient for this design. Relays will be mounted so that their least sensitive axes will be parallel to the direction of deceleration forces. The chassis will be magnesium and mounting hardware and connectors will be the cannon DMA series.

7.8.5.3 Battery

The battery pack will be fabricated using an impregnated fiberglass wrap design reinforced with magnesium structure at various stress locations. The pack size will be (8.3 x 9.9 x 13.7 cm).

Sketches of the small and large probe batteries are shown in Figures 7.8-11 and 7.8-12.

SIZING FACTORS	VALUE, %
LINE AND CONTACT LOSS	1
CHARGED STAND LOSS	5
CONTINGENCY	5
MONOVALENT OPERATION	25
MANUFACTURING TOLERANCE	12

ENERGY STORAGE CAPACITY	143 W-HR
A-HR CAPACITY (MONOVALENT)	5.1 A-HR
MASS	3.7 KG
SIZE	20 X 8.85 X 7.9 CM
NO OF SERIES CELLS	20
BATTERY HEATER POWER	10.0 W FOR 3 HR
VOLUME	1398 CM ³

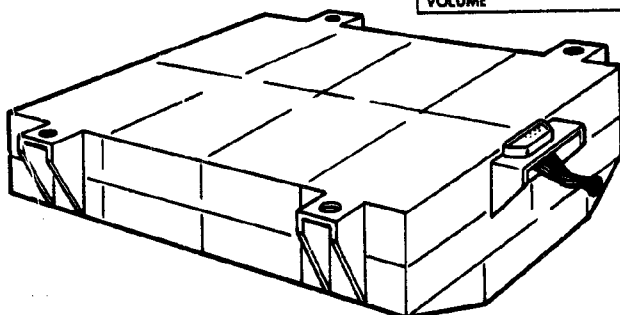


Figure 7.8-11. Small Probe Battery, Thor/Delta Configuration

ENERGY STORAGE CAPACITY	238 W-HR
A-HR CAPACITY (MONOVALENT)	9.2 A-HR
MASS	3.7 KG
SIZE	20 X 8.85 X 10.3 CM
VOLUME	1823 CM ³
NO OF SERIES CELLS	20
BATTERY HEATER POWER	15 W FOR 1 HR

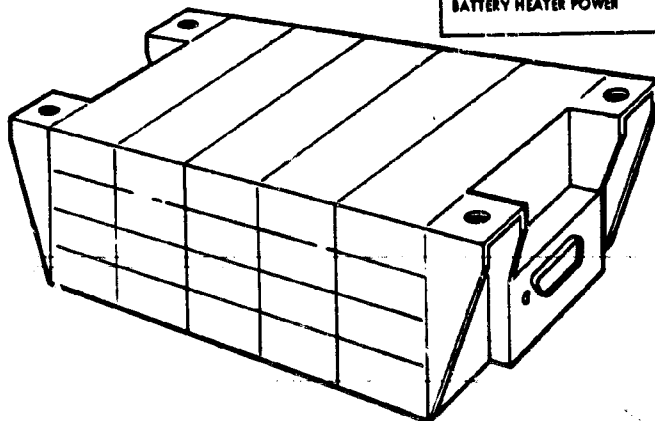


Figure 7.8-12. Large Probe Battery, Thor/Delta Configuration

7.8.5.4 Power Control Unit

Thor/Delta - Small Probe

The proposed packaging concept for the Thor/Delta small probe is an evolution based on many design requirements. The probe size and shape were the main determining factors. The efficient utilization of allotted volume resulted in a cylindrical housing and an integrated electronics assembly which contains the DHC, PCU, accelerometer, pressure, temperature, and magnetometer electronics. (Figure 7.8-13). This housing also acts as the equipment mounting shelf for the battery pack, stable oscillator, transmitter driver, nephelometer and the power amplifier. (Figure 7.8-14). Using this approach, all of the equipment is mounted to the pressure shell separation plane at three locations. Thermal isolators are used at these locations to minimize heat transfer from the pressure shell to the electronic assemblies. With removal of the jam nut on the pressure transducer fitting, and the lower pressure shell, all electrical connectors are accessible for disconnection and removal of the entire electronics assembly, excluding the antenna and its coax cable, which are mounted to the upper pressure shell. Thermal isolators are used to support

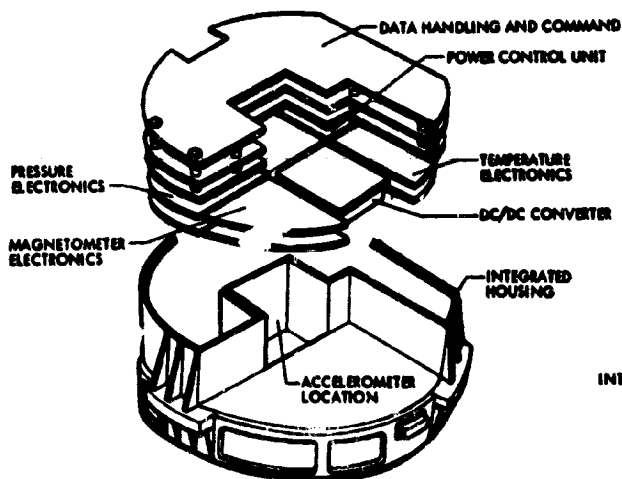


Figure 7.8-13. Integrated Electronics

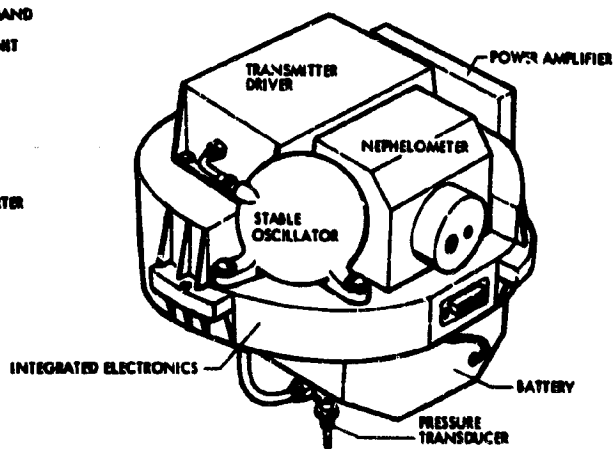


Figure 7.8-14. Equipment Mounting Shelf

the coax cable from the pressure shell (Figure 7.8-15). Cannon Series, DMA connectors are used for interface connections between the battery pack and all other probe equipment units.

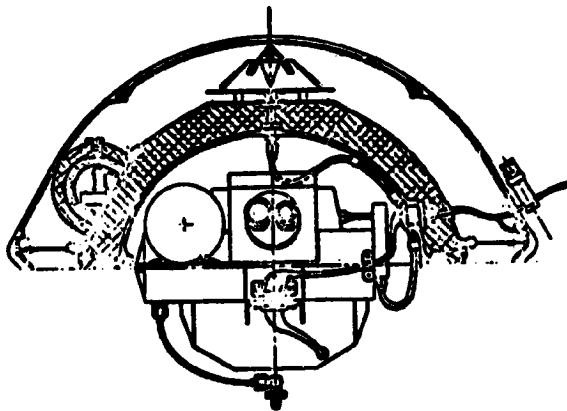


Figure 7.8-15. Cut Away View of Thor/Delta Small Probe

The battery pack housing will be fabricated using an impregnated fiberglass wrap design, reinforced with magnesium structure at various stress locations.

Experiment electronics (pressure, temperature, acceleration and magnetometer) and the power control circuitry will be packaged in individual cavities located in the bottom half of the integrated electronics housing. These printed wiring boards should be primarily two-sided boards.

All boards will be mounted to the housing with #4-40 titanium torque set screws with #4-40 Helicoil inserts (phosphor bronze or beryllium copper) installed in the housing. Boards will be spaced using magnesium spacers.

7.9 Electrical Integration

7.9 ELECTRICAL INTEGRATION

7.9.1 Introduction and Summary

The probe electrical integration involved solutions to a number of problems not normally encountered on previous planetary missions. Among these were the grounding, interconnection, and EMI techniques to permit the multiple probes to function as integrated subsystems, while attached to the probe bus, and yet function as completely autonomous spacecraft after separation. Allied with these problems was the need to minimize potential drain on the probe batteries during cruise. Other problems included the electrical penetrations to withstand the high temperatures and high pressures to be encountered at the surface of Venus, the selection of an electrical separation device, and the design of interconnections to withstand the high entry deceleration of the order of 600 g. Although packaging is not normally considered an electrical integration function or responsibility, in the probes it is heavily influenced by the need for accessibility to connectors and to cable routing and attachment to survive the environment. A particular case is the Thor/Delta small probe where most of the electronics were to be packaged in a single, integrated structure to minimize size, weight, and interconnecting cables.

The Atlas/Centaur, 1978 mission with the Version IV science has also impacted the electrical integration. Removal of the magnetometers from the primary payload has eased the problem of magnetic cleanliness. However, addition of the wind drift radar to the large probe may cause some new EMI problems. The preferred electrical integration for this mission is a subsystem with the primary power single point ground at the RF power amplifiers in the communications subsystem (the power amplifiers have the output stages tied to ground). Secondary power returns and signal returns may be connected to a common chassis point. The chassis connection will be brought out to a pin on the umbilical connector to tie back to the bus single point ground. Interface connections to the bus will consist of three command lines, three data lines, +28 volt DC power, and the ground connection described above. All experiments will be fault isolated from the +28 volt power bus by fuses. Power will be switched by relays. A 20-cell silver-zinc battery will provide primary 28 volt ± 10 percent power throughout the descent phase of the mission. There will be no auxiliary

batteries for the timers or pyrotechnic firing. All functions will be powered from the primary battery. All pyros will be fired directly from the battery, without energy storing capacitor banks. The umbilical will be separated by a cable cutter. All timing, sequencing, and command and control functions are performed by circuits within the power conditioning unit (PCU). Figures 7.9-1 and 7.9-2 show the system interface connections for both large and small probe preferred designs.

7.9.2 Requirements

There are two primary requirements for probe electrical integration. The first is that each probe, while operating as a separate, autonomous spacecraft, will provide the capability for each science experiment to collect and have data transmitted to earth without interference or degradation due to the operation of other experiments or subsystems within the probe. The second requirement is that, while attached and electrically connected to the probe bus, the probes will not interface with, nor degrade the performance of the bus electrical subsystems. Here it may be possible to tolerate some interference during short, predetermined periods, such as prelaunch and/or preseparation checkout where the effects are known and controllable.

An ancillary problem is to provide the capability to test, check out, and calibrate the experiments and electrical subsystems within the probes after they are closed and sealed.

7.9.3 Electrical Integration, Atlas/Centaur

Electrical integration of the Atlas/Centaur probes is heavily influenced by the selection of existing design hardware for most of the electrical subsystems. This dictates a need to use these designs without modifications such as changing grounding methods, external connectors, or connector locations. This establishes the primary power, single-point ground at the RF power amplifiers because they are built with the output transistors connected directly to the chassis to provide a good thermal conduction path. The secondary power returns and signal returns are connected to a common chassis point. The chassis connection is routed through the bus/probe umbilical to the single point ground located in the bus. Ground battery charging and accelerometer check out is accomplished through a separate connector located on the descent capsule bulkhead up to the time



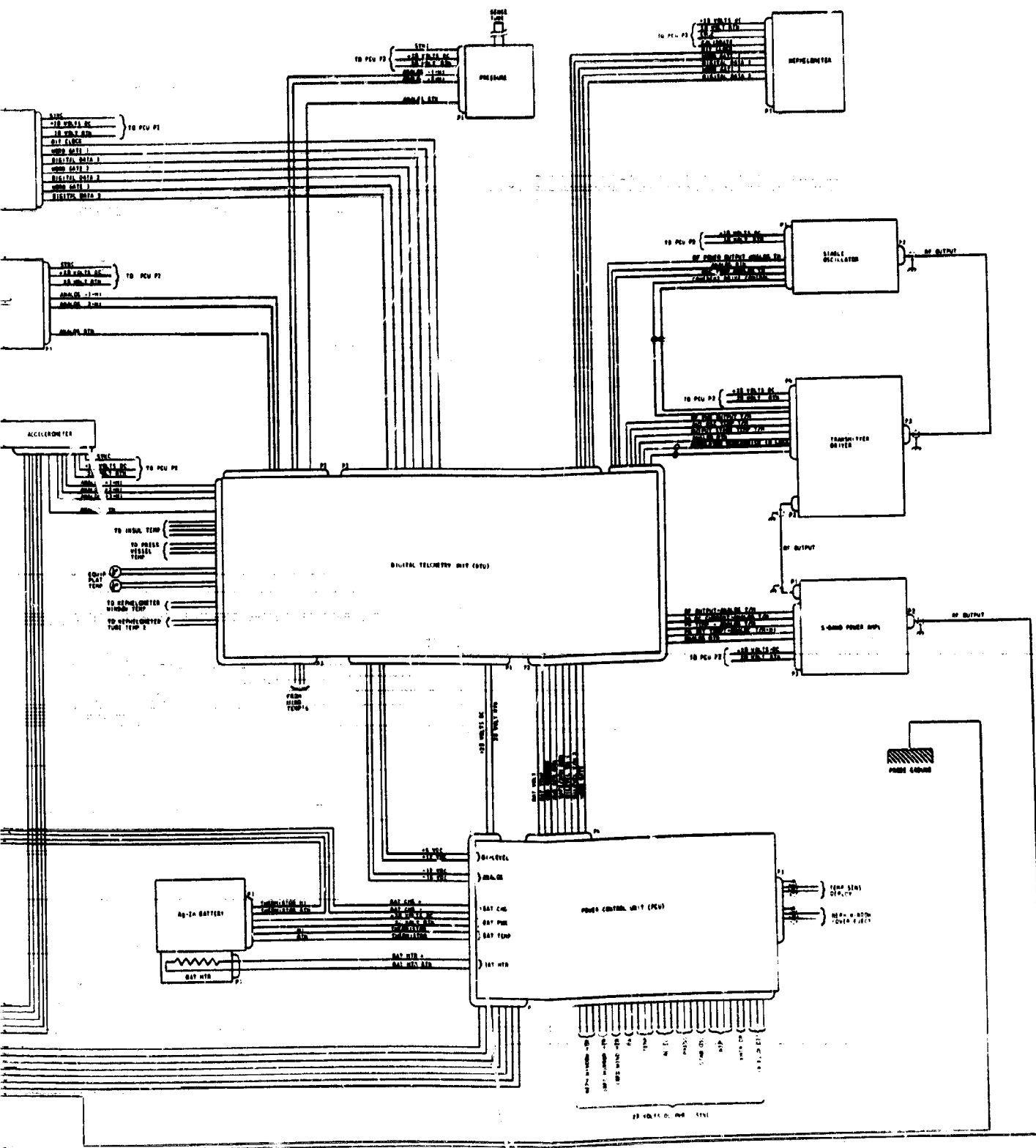
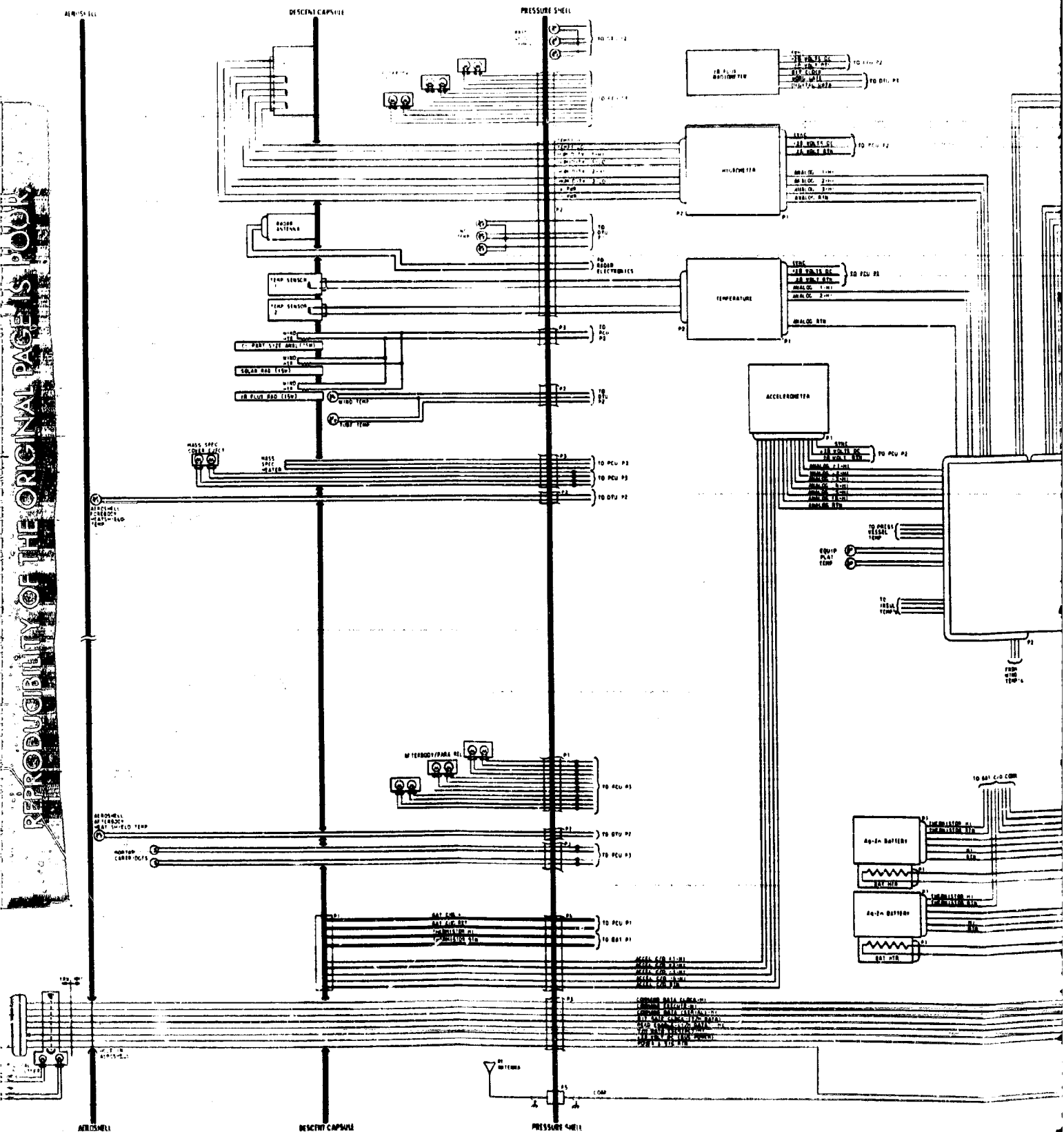


Figure 7.9-1. Atlas/Centaur Small Probe System Interface Connections

7.9-3



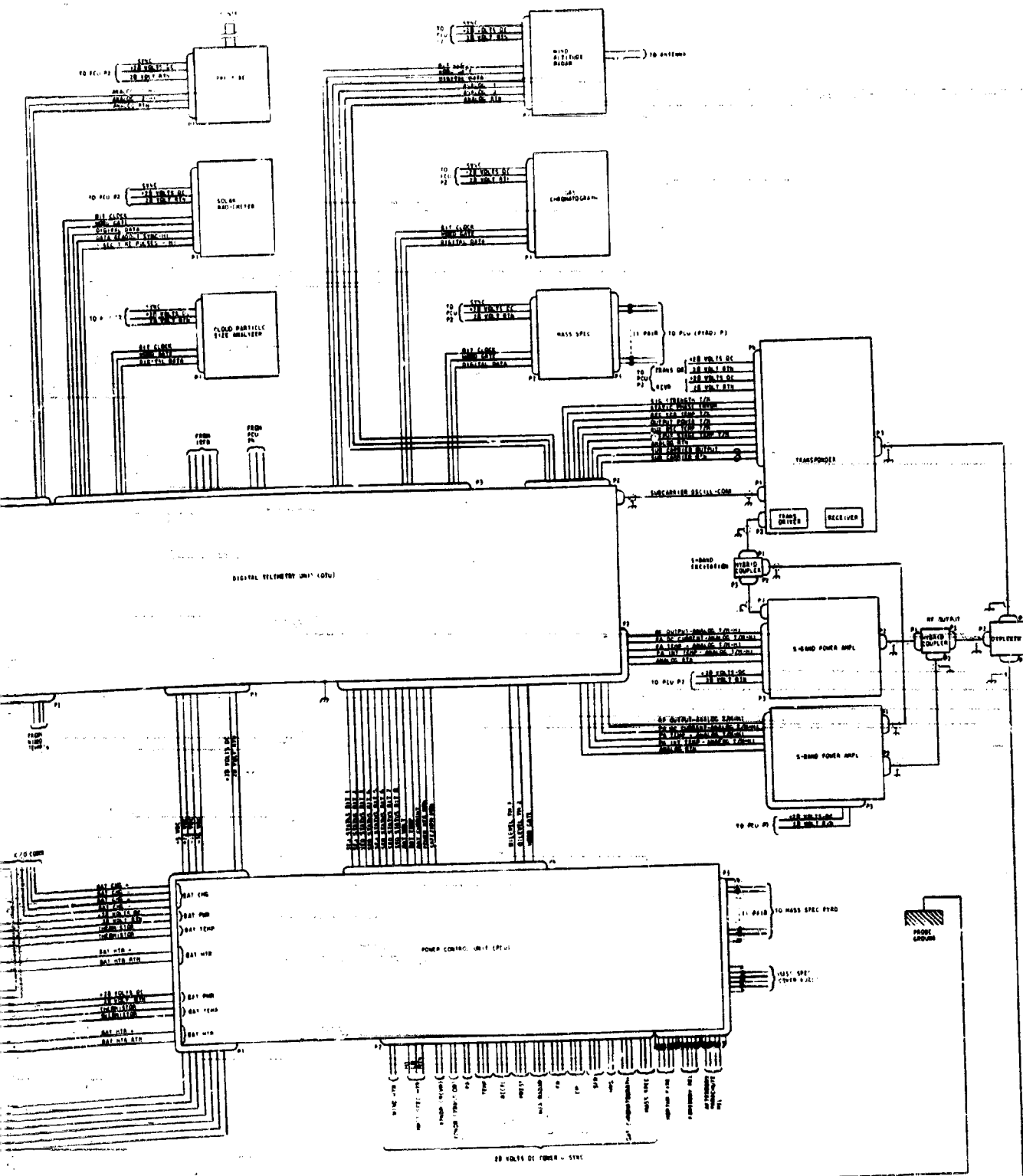


Figure 7.9-2. Atlas/Centaur Large Probe System Interface Connections

7.9-4

FOLDOUT FRA. 2

the shroud is installed. Figures 7.9-1 and 7.9-2 show the interface connections. Connector P-1 is the battery charge and accelerometer calibration connector. The interconnecting harness and connectors were selected for minimum weight and volume characteristics. The harness is a conventional bundle of high-strength insulated lightweight copper wire (STME742) developed for the Viking project. The harness set consists of several separate assemblies designed to minimize fabrication efforts, separate unrelated classes of electrical signals, and allow maximum compliance with EMC requirements. Number 24 AWG is planned for all unit interconnections except for power circuits where 20 or 22 AWG will be used. Cabling and connectors will be positioned and clamped to withstand the high g decelerations of entry. Hermetic Seal corporation feedthrough connectors will be used for descent capsule electrical penetration.

The RF circuits will have the low side grounded at the equipment connectors or coaxial outer conductors. The coaxial connector and cable diagram is shown in Figures 7.9-3 and 7.9-4. Equipment that intentionally operates above 150 kHz may have secondary power circuit ties to the unit case, provided that a minimum resistance of 10,000 ohms exists between all low frequency (0 to 150 kHz) input or output leads and the unit case prior to external electrical connection. System test and checkout equipment will have their low side tied to the bus single point ground when using a separate power source.

All metallic parts making up the primary and secondary structure (including those that support electrical and electronic circuitry) will be designed to provide continuous electrical contact. The direct current resistance across each joint will not exceed 10 milliohms.

Individual experiment units are provided with fault isolation via a fuse located in the PCU. Fuses were selected on the basis of low weight and volume over the more sophisticated fault isolation voltage and current monitors.

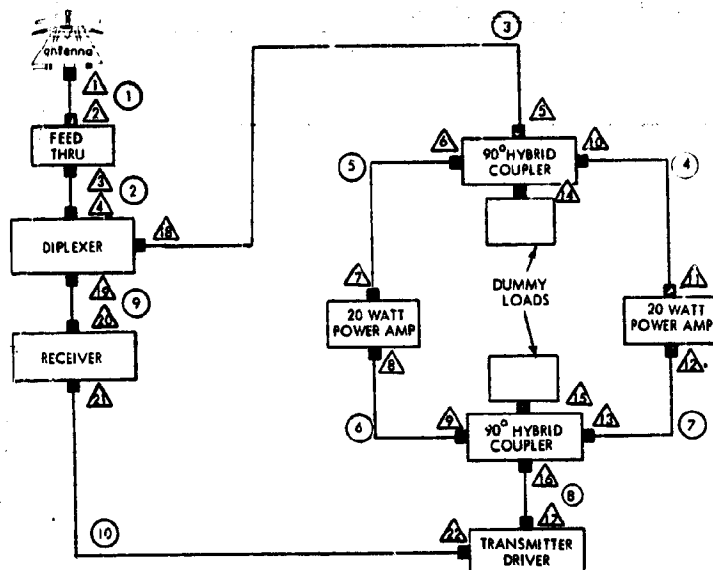


Figure 7.9-3. RF Cable, Large Probe

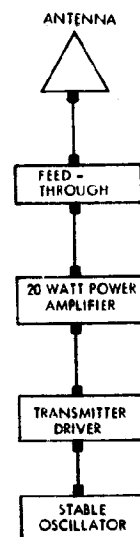


Figure 7.9-4. RF Cable, Small Probe

EMI considerations are heavily influenced by the fact that essentially all of the probe electronics are enclosed in the thick, metallic pressure shell. The shell effectively shields the electronics from external fields and prevents radiation to outside receivers. Thus, careful attention to filtering or isolating all electrical penetrations of the pressure shell should adequately isolate the probes. Internally, cable routing, filtering, and shielding in conjunction with the previously described grounding method should control conducted as well as radiated interference. The wind drift radar in the large probe should not present a significant problem, although it will require close attention. The radar antenna and communications antennas are at opposite ends of the spin axis so they are separated by the body of the probe itself. Both antennas are directional with relatively low back lobe radiation and the frequencies are quite different (S-band and X-band). The filtering specified for the S-band power amplifiers, together with the items discussed above, should effectively prevent the communications signals from interfering with the radar. If similar control is maintained on the radar, there should be no major problem.

7.9.4 Electrical Integration, Thor/Delta

Electrical integration of the Thor/Delta large probe is very similar to that for the Atlas/Centaur probes. The exception is that there is no

wind drift radar. However, there are other instruments, such as the shock layer radiometer and the aureole/extinction detector mounted outside the pressure shell. Therefore special attention to filtering and shielding is necessary, along with an additional electrical separation device.

The Thor/Delta small probe presents a somewhat different problem. Because of the limited payload capability, probe weight had to be minimized. This led to an extreme volume constraint on the small probes. The efficient utilization of allotted volume resulted in a cylindrical housing and an integrated electronics assembly which contains the DHC, PCU, accelerometer, pressure, temperature, and magnetometer electronics. This housing also acts as the equipment mounting shelf for the battery pack, stable oscillator, transmitter driver, nephelometer, and the power amplifier (Figure 7.9-5.) Using this approach, all of the equipment is mounted to the pressure shell separation plane at three locations. Thermal isolators are used at these locations to minimize heat transfer from the pressure shell to the electronic assemblies. With removal of the jam nut on the pressure transducer fitting, and the lower pressure shell, all electrical connectors are accessible for disconnection and removal of the entire electronics assembly, excluding the antenna and its coax cable, which are mounted to the upper pressure shell (Figure 7.9-6). Cannon Series DMA subminiature crimp snap in contact connectors are used for interface connections between the battery pack and the DHC, from the DHC to the transmitter driver, and from the electrical feedthroughs to the DHC.

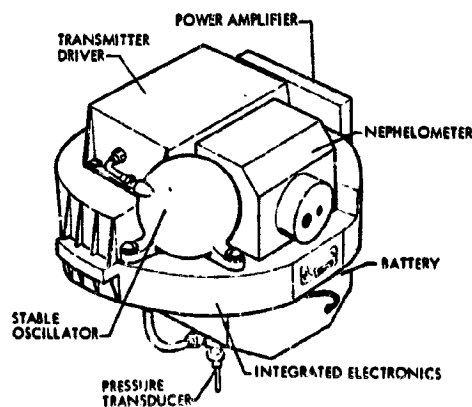


Figure 7.9-5. Equipment Mounting Shelf, Thor/Delta Small Probe

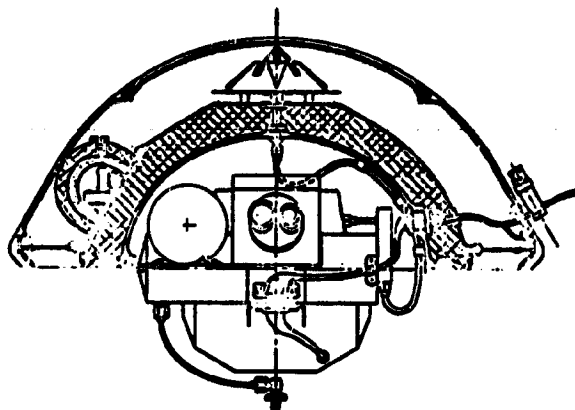


Figure 7.9-6. Cut Away View of Thor/Delta Small Probe

Experiment electronics (pressure, temperature, acceleration, and magnetometer) and the power control circuitry will be packaged in individual cavities located in the bottom half of the integrated electronics housing. Interconnections from board to board is accomplished using flat cable. The integrated housing will be machined from magnesium.